



Universiteit  
Leiden  
The Netherlands

## Novel insights into old anticancer drugs

Zanden, S.Y. van der

### Citation

Zanden, S. Y. van der. (2021, March 2). *Novel insights into old anticancer drugs*. Retrieved from <https://hdl.handle.net/1887/3135058>

Version: Publisher's Version

License: [Licence agreement concerning inclusion of doctoral thesis in the Institutional Repository of the University of Leiden](#)

Downloaded from: <https://hdl.handle.net/1887/3135058>

**Note:** To cite this publication please use the final published version (if applicable).

Cover Page



Universiteit Leiden



The handle <http://hdl.handle.net/1887/3135058> holds various files of this Leiden University dissertation.

**Author:** Zanden, S.Y. van der

**Title:** Novel insights into old anticancer drugs

**Issue date:** 2021-03-02

# **Novel insights into old anticancer drugs**

Sabina Yasmin van der Zanden

ISBN: 978-94-6416-386-5

Coverdesign: M.L.M. Jongsma

Layout: M.L.M. Jongsma and S.Y. van der Zanden

Financial support for printing of this thesis was provided by The Netherlands Cancer Institute and Leiden University Medical Center.

Print: Ridderprint | [www.ridderprint.nl](http://www.ridderprint.nl)

The research described in this thesis was performed at the Department of Cell Biology at the Netherlands Cancer Institute in Amsterdam, The Netherlands, as well as at the Department of Chemical Immunology and the Department of Cell and Chemical Biology at Leiden University Medical Center in Leiden, The Netherlands. The work was financially supported by the Institute for Chemical Immunology and Oncode Institute.

Copyright © 2021 by Sabina Y. van der Zanden. All rights reserved. No part of this publication may be reproduced or transmitted in any form or by any means without prior written permission of the authors, or where appropriate, of the publisher of the articles.



# **Novel insights into old anticancer drugs**

Proefschrift

ter verkrijging van  
de graad van Doctor aan de Universiteit Leiden,  
op gezag van Rector Magnificus prof. dr. ir. H. Bijl,  
volgens besluit van het College voor Promoties  
te verdedigen op dinsdag 2 maart 2021  
klokke 15:00 uur

door

**Sabina Yasmin van der Zanden**

Geboren te Haarlem  
op 15 oktober 1989

**Promotor**

Prof. dr. J.J.C. Neeftjes

**Co-promotor**

Prof. dr. H.S. Overkleeft

**Promotiecommissie**

Prof. dr. P. Baas – *Nederlands Kanker Instituut*

Prof. dr. J.G. Borst

Prof. dr. R.C. Hoeben

Prof. dr. C.L. Mummery

Prof. dr. E.A.J. Reits – *Universiteit van Amsterdam*

Prof. dr. W.T. Zwart – *Nederlands Kanker Instituut*

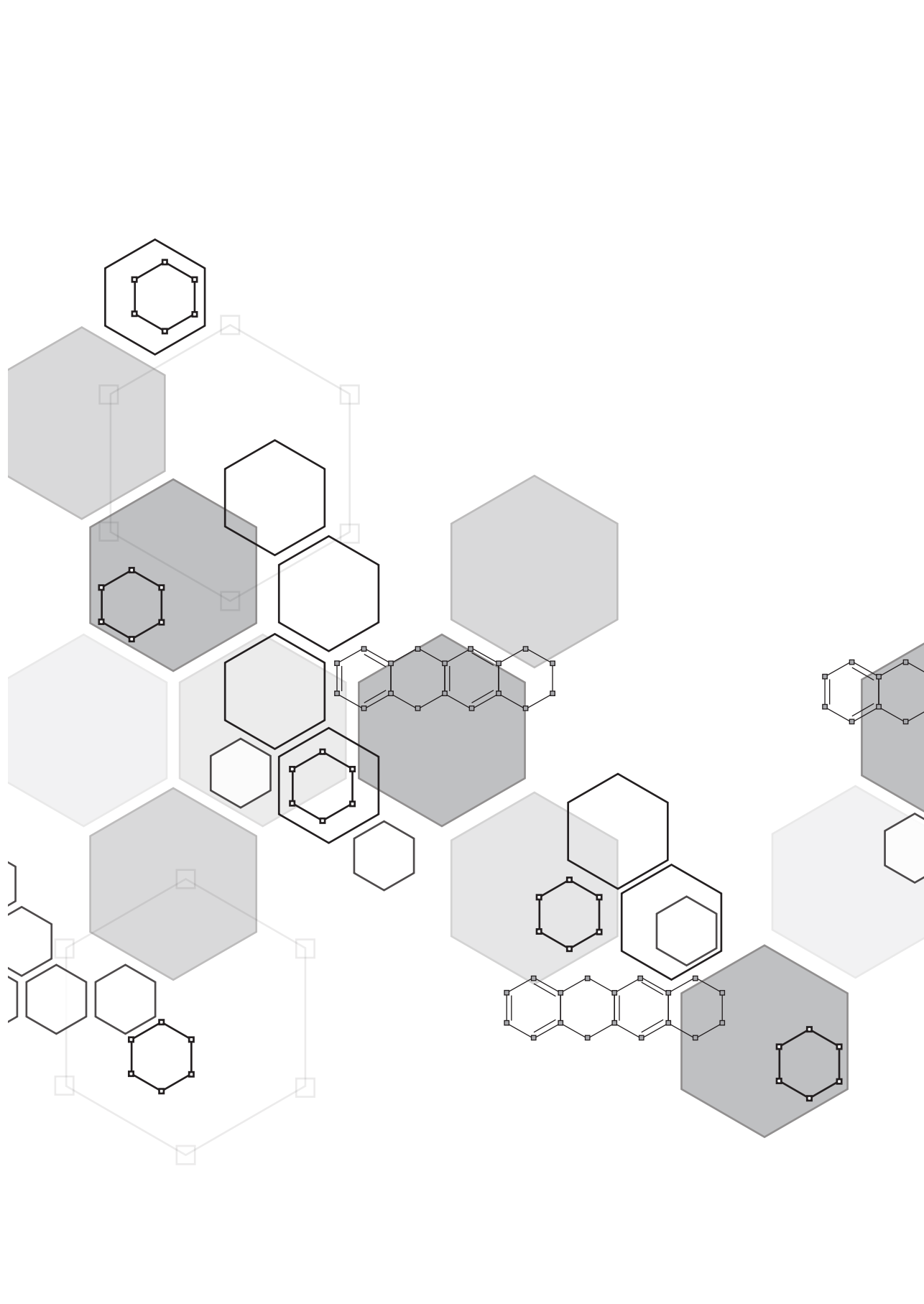
“what we know is a drop,  
what we don't know is an ocean”

- *Isaac Newton* -



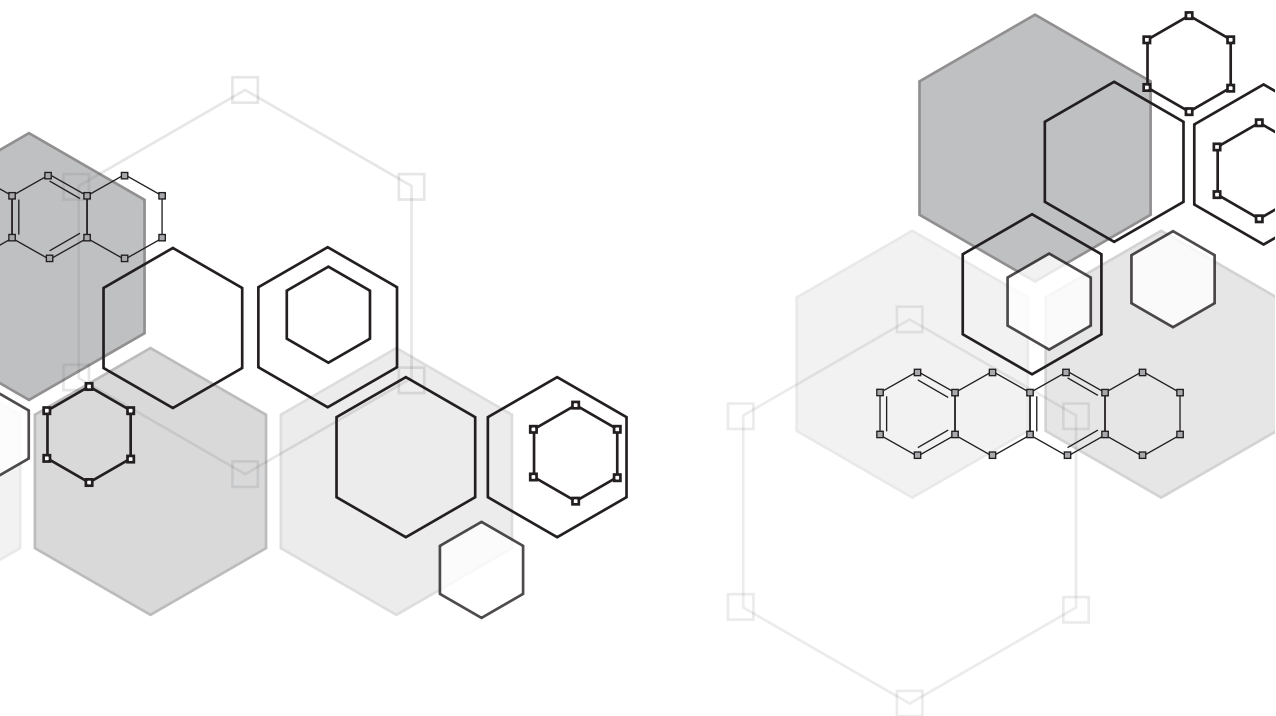
## TABLE OF CONTENTS

<b>Chapter 1</b>	New insights into the activities and toxicities of the old anti-cancer drugs doxorubicin <i>FEBS Journal (2020)</i>	9
<b>Chapter 2</b>	Genome-wide identification and characterization of novel factors conferring resistance to topoisomerase II poisons in cancer <i>Cancer Research (2015)</i>	35
<b>Chapter 3</b>	Uncoupling DNA damage from chromatin damage to detoxify doxorubicin <i>PNAS (2020)</i>	63
<b>Chapter 4</b>	Doxorubicin and aclarubicin: shuffling anthracycline glycans for improved anticancer agents <i>Journal of Medicinal Chemistry (2020)</i>	103
<b>Chapter 5</b>	Synthetic ( <i>N,N</i> -dimethyl)doxorubicin glycosyl diastereomers to dissect modes of action of anthracycline anticancer drugs	141
<b>Chapter 6</b>	Exploring the chemical space around the 3' amine of doxorubicin for improved cytotoxic drugs with different genomic specificity	163
<b>Chapter 7</b>	Nuclear DNA sensors re-localize upon chromatin damage; do they play a role in anthracycline induced cell death?	185
<b>Chapter 8</b>	Opportunities for small molecules in cancer immunotherapy <i>Trends in Immunology (2020)</i>	205
<b>Chapter 9</b>	Summary and future prospects	235
<b>Appendices</b>	Nederlandse samenvatting	245
	List of publications	256
	Curriculum vitae	258
	Acknowledgements	259



# New insights into the activities and toxicities of the old anticancer drug doxorubicin

# 1



Sabina Y. van der Zanden<sup>#</sup>, Xiaohang Qiao<sup>#</sup> and Jacques Neefjes

<sup>#</sup>These authors contributed equally

*FEBS Journal* (2020)

## ABSTRACT

The anthracycline drug doxorubicin is among the most used—and useful—chemotherapeutics. While doxorubicin is highly effective in the treatment of various hematopoietic malignancies and solid tumours, its application is limited by severe adverse effects, including irreversible cardiotoxicity, therapy-related malignancies and gonadotoxicity. This continues to motivate investigation into the mechanisms of anthracycline activities and toxicities, with the aim to overcome the latter without sacrificing the former. It has long been appreciated that doxorubicin causes DNA double-strand breaks due to poisoning topoisomerase II. More recently, it became clear that doxorubicin also leads to chromatin damage achieved through eviction of histones from select sites in the genome. Evaluation of these activities in various anthracycline analogues has revealed that chromatin damage makes a major contribution to the efficacy of anthracycline drugs. Furthermore, the DNA-damaging effect conspires with chromatin damage to cause a number of adverse effects. Structure-activity relationships within the anthracycline family offer opportunities for chemical separation of these activities toward development of effective analogues with limited adverse effects. In this review, we elaborate on our current understanding of the different activities of doxorubicin and their contributions to drug efficacy and side effects. We then offer our perspective on how the activities of this old anticancer drug can be amended in new ways to benefit cancer patients, by providing effective treatment with improved quality of life.

## INTRODUCTION

Doxorubicin, also known as adriamycin, is a member of the anthracycline anticancer drug family (Figure 1). The first anthracycline drug, daunorubicin, was isolated from

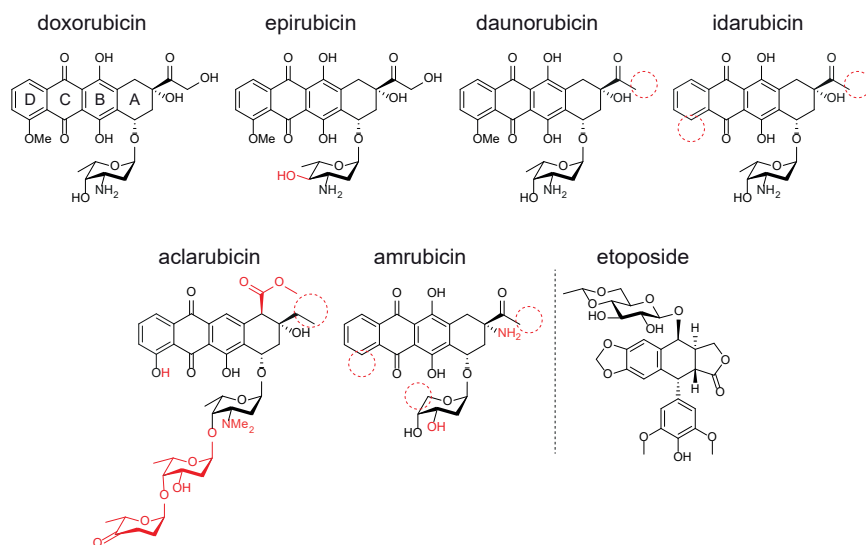


**Figure 1. Structures of different anthracycline drugs and the structurally unrelated Topo II poison etoposide. Aglycon rings are numbered in doxorubicin. Structural differences compared to doxorubicin are indicated in red.**



a soil sample found in Italy in 1960 [1, 2]. Daunorubicin is a pigmented antibiotic produced by the actinobacterium strain *Streptomyces peucetius* [2]. Soon, it was discovered that daunorubicin displayed anticancer activity in mice, which spurred its clinical use for the treatment of leukaemia, lymphoma and solid tumours in the late 1960s [3, 4]. In 1969, a daunorubicin homologue, doxorubicin, was isolated from a culture of chemically mutated *Streptomyces peucetius* [5]. Doxorubicin showed an even broader anticancer activity than daunorubicin, especially against solid tumours [6, 7]. However, quickly a major side effect of both otherwise highly potent anticancer drugs was noted — cardiotoxicity [8]. Cardiotoxicity incited by anthracyclines develops in a dose-dependent manner and can be lethal [9, 10]. As a result, treatment has to be stopped once the maximal tolerated cumulative dose is reached, while patients with poor heart function are excluded from chemo regimens containing anthracyclines. In addition to treatment-limiting cardiotoxicity, therapy-related malignancies and gonadotoxicity are also associated with anthracycline treatment [9, 11]. With latest improvements in cancer therapy, the emphasis in cancer management has changed from 'cure at any cost' to giving quality of life after treatment more consideration. In this light, quests to understand and alleviate the side effects incurred by anthracyclines have been revived. Here, we provide an overview of the mechanisms of action and toxicity of anthracycline drugs and discuss different attempts that have been made to improve them. This is followed by our perspective on how to detoxify doxorubicin for effective anticancer treatment with limited adverse effects.

## MECHANISMS OF ACTION OF ANTHRACYCLINE DRUGS

### Topoisomerase II poison

The classical mechanism of action by which anthracyclines function is inhibition or poisoning of Topoisomerase II (Topo II) [12]. This enzyme plays a critical role in chromosome condensation, decatenation of intertwined DNA strands, and relaxation of tension in the DNA strand in front of the replication fork [13, 14]. Topo II acts by introducing a transient double-strand break (DSB) in one DNA strand (the G-segment), allowing another DNA strand (the T-segment) to pass through and subsequently closing the initial break by re-ligation of the two DNA ends (Figure 2) [13-18]. Most anthracyclines (e.g. doxorubicin, epirubicin, daunorubicin, idarubicin, and amrubicin) intercalate into DNA and poison Topo II in its catalytic step following initial break induction by forming Topo II-DNA complexes. These anthracyclines interfere at the interface of Topo II-DNA with their sugar moieties and the cyclohexane ring A [19]. In essence, the interfacial positioning makes these anthracyclines act as molecular doorstops and prevent Topo II from re-ligating the broken strand, which ultimately results in enzyme-mediated DNA damage in the form of DSB [12, 20, 21]. Although the protein structure of a Topo II-DNA-doxorubicin complex is not available (reason will be discussed in the latter part), the door-stopping act of doxorubicin can be deduced from the structure of a counterpart complex with the non-anthracycline Topo II poison, etoposide [22-24]. As a consequence of DSBs, DNA-damage response (DDR) and TP53 pathways are activated, which lead to cell cycle arrest and cell death [25]. Some anthracyclines interrupt Topo II at other steps of the catalytic cycle, such as preventing the enzyme binding to the DNA (e.g. aclarubicin) or inhibiting ATP binding [13]. Topo II is essential for the survival of rapidly dividing cells, such as cancer cells that are more sensitive to DNA breaks than normal quiescent cells; hence, anthracyclines create a chemotherapeutic window by hijacking the essential enzyme function in cells [26]. For the same reason, anthracyclines also cause side effects, such as hair loss, bone marrow suppression and gastrointestinal complications.

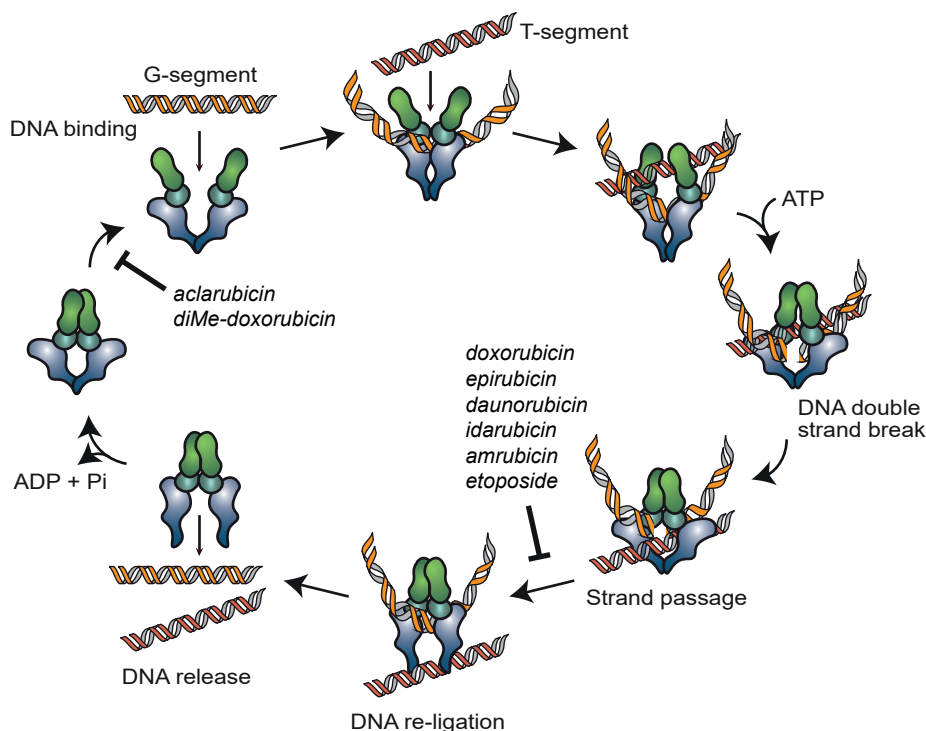


**Figure 2. Schematic representation of the Topo II poisoning mechanism of anthracyclines.** To entangle DNA or to remove DNA supercoils Topo II binds to DNA, introduce a transient double-strand break in one of the DNA strands (the G-segment), allowing the second DNA strand (the T-segment) to pass through. After re-ligation of the G-segment, the Topo II is released from DNA [15-18]. The majority of Topo II poisons, including most anthracyclines (doxorubicin, daunorubicin, epirubicin, idarubicin and amrubicin) and etoposide, stabilize the Topo II complex after it has introduced the DNA double-strand break and prevent the DNA break from being resealed [13, 26]. Anthracycline variants aclarubicin and diMe-doxorubicin inhibit the enzymatic activity by preventing Topo II from loading onto the DNA [13, 44]. Figure is inspired by [13].

### DNA intercalation

Anthracyclines intercalate into the DNA helix with their anthraquinone moiety. While ring B and C of the tetracycline moiety overlap with adjacent DNA base pairs, and ring D passes through the intercalation site, the sugar moiety is pointed into the minor groove, which may compete for space with histones [19, 27]. In addition to stabilizing the Topo II-DNA complex, DNA intercalation of anthracyclines has additional effects, such as inhibiting DNA and RNA synthesis [28, 29].

### Oxidative stress

The quinone moiety in ring C of anthracyclines can be transformed into a semiquinone by a number of oxidoreductases, including cytochrome P450 reductases, xanthine oxidase and NADH dehydrogenase (complex I) of the mitochondrial electron transport chain [30, 31]. Subsequently, this semiquinone quickly regenerates and thereby converts oxygen into reactive oxygen species (ROS), such as superoxide

anion ( $O_2^{\cdot-}$ ) and hydrogen peroxide ( $H_2O_2$ ), or oxidize the bond between the sugar and the aglycon resulting in reductive deglycosylation. Eventually,  $O_2^{\cdot-}$  and  $H_2O_2$  are converted into more reactive hydroxyl radicals ( $\cdot OH$ ) via the iron-catalysed Haber-Weiss reaction [32, 33]. In addition, anthracyclines can also mediate ROS production by directly interfering with iron metabolism. They can increase cellular levels of iron by interacting with iron regulatory proteins (IRP1 and/or IRP2) or accelerate the release of iron from ferritin, which then further amplifies iron-mediated oxidative stress [34–36]. The excessive ROS production can lead to lipid oxidation, genomic and mitochondrial DNA damage, which are toxic to cells. Nevertheless, the contribution of ROS formation to the anticancer activity of anthracyclines is still unclear and heavily discussed. It is worth noting that excessive ROS production is often observed when cells were exposed to anthracycline doses that are much higher than clinical relevant concentrations. Yet, at physiological concentrations, significant ROS formation was observed at late time points after drug removal, indicating this might be a secondary effect of anthracycline treatment rather than a direct mode of action [37]. Notwithstanding, it cannot be excluded that ROS formation may reinforce other mechanisms of anthracyclines.

### Chromatin damage

To organize two meters of DNA in the nucleus of a single cell, DNA is compacted at several levels. One level of organization is the formation of nucleosomes, where a segment of 146 base pairs of DNA is wrapped around eight histone proteins [38]. As mentioned above, when an anthracycline intercalates into DNA, the sugar moiety emanates into the DNA minor groove and competes with histones for space, resulting in the collapse of nucleosomes. As a result, histones are evicted from chromatin (Figure 3) [27, 39]. *In vitro* experiments with reconstituted single nucleosomes showed that doxorubicin causes nucleosome dissociation in an ATP-, transcription-, and histone chaperone-independent manner, which may explain why the structure of Topo II-DNA-doxorubicin complex is not available [27]. Moreover, the doxorubicin metabolite doxorubicinone, which lacks the sugar moiety of doxorubicin, was not able to dissociate nucleosomes under the same condition, suggesting a critical contribution of the sugar moiety to histone eviction [27, 40]. These data indicate that histone eviction induced by anthracyclines is a drug intrinsic process, which is cooperatively mediated by DNA intercalation of the anthraquinone group and nucleosome destabilization by the sugar moiety. This unique activity is not observed for other DNA intercalators (e.g. ethidium bromide [27]) or other chemotherapeutics (e.g. am-sacrine or proflavin, data not published).

The dynamic structure of chromatin is essential for many nuclear processes, including transcription and replication. Therefore, the assembly, spatial organizing, and compactization of chromatin is tightly regulated by various histone chaperones, ATP-dependent chromatin remodelling complexes and histone-modifying enzymes [41, 42]. Being the building blocks of chromatin, histones are directly involved in the regulation of these processes via different epigenetic modifications. Upon eviction, these modified histones are replaced by new/nascent ones with less or different epigenetic marks. This results in DDR delay, epigenetic and transcriptomic alterations, collectively termed as chromatin damage [43]. With the aid of next-generation sequencing, unbiased (epi)genomic analysis revealed that each anthracycline evicts histones at select (epi)genomic regions [27, 43]. More specifically, doxorubicin evicts histones at open genomic regions marked by H3K36me3; while aclarubicin, whose sugar moiety is different from doxorubicin, induces histone eviction in a wider range,

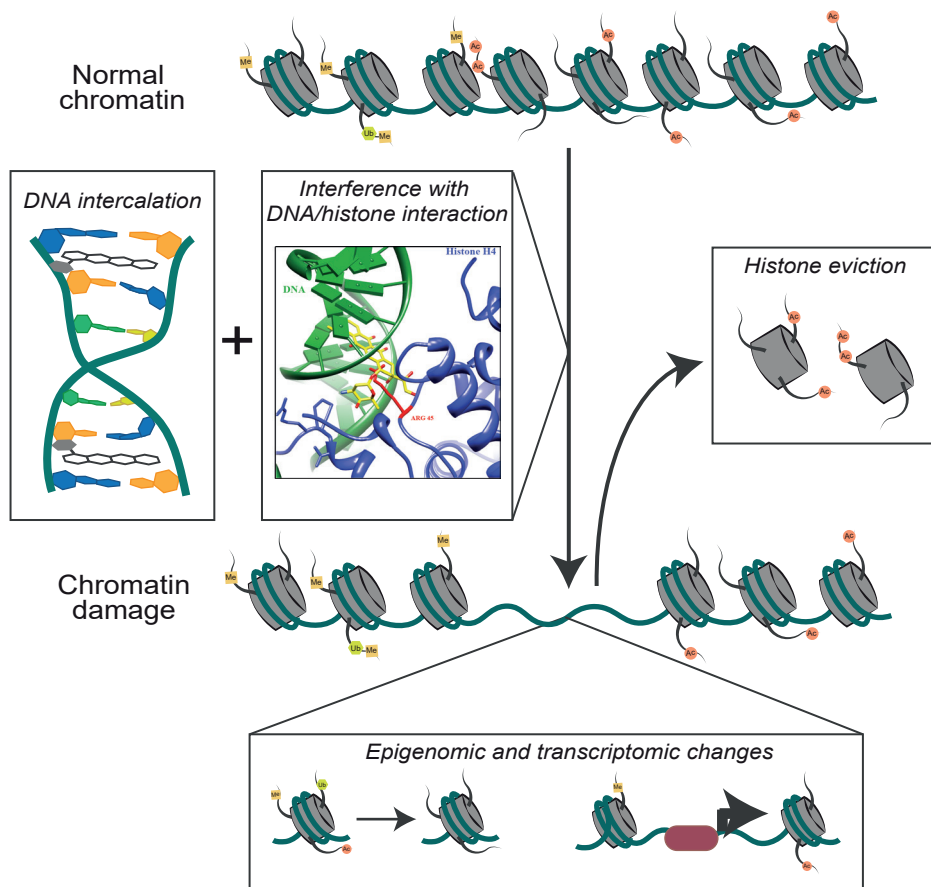


**Figure 3. Schematic representation of chromatin damage induced by doxorubicin.** Besides DNA intercalation by its anthraquinone group, doxorubicin's sugar moiety destabilizes nucleosome by competing for space with histones. Histone eviction caused by doxorubicin is shown to be ATP-, transcription-, and histone chaperone-independent [27]. Histone eviction results in epigenetic and transcriptomic alterations and DSB repair attenuation, collectively referred to as chromatin damage. Part of the figure is reproduced from [27].

including compacted chromatin regions decorated by H3K27me3. As a matter of fact, anthracyclines could therefore be considered as epigenetic modifiers with defined (epi)genomic selectivity.

How histone eviction exactly causes cell death remains unclear, but it is likely to play a major contribution to the anticancer activity of the anthracycline drugs. This is illustrated by the anthracycline drugs aclarubicin and *N,N*-dimethyl-doxorubicin (diMe-doxorubicin), which induce histone eviction without generating DNA damage [44]. Aclarubicin is prescribed mainly for the treatment of acute myeloid leukaemia (AML), showing similar efficacy as doxorubicin [27, 39, 44]. While aclarubicin was once used worldwide, it is currently only used in Japan and China. The specific reason behind this is not clear, and there is no clinical data that can explain the halt of usage. On the other hand, the doxorubicin analogue diMe-doxorubicin was first reported in the 1980s [45]. It exhibited similar anticancer activity compared to doxorubicin in tis-

sue culture experiments and in mice [27, 39, 44]. Further, its pharmacokinetics was tested in mice and rabbits [46], but no further follow-up was reported. Surprisingly, it was recently shown by our lab that diMe-doxorubicin only induces chromatin damage but no DSB, suggesting that chromatin damage rather than DNA breaks may be the dominant cytotoxic mechanism [44]. This is further substantiated by the anthracycline variant amrubicin, which only induces DSBs. Amrubicin is much less effective than doxorubicin, aclarubicin and diMe-doxorubicin in killing cancer cells, thus did not enter clinic. Taken together, this implies that chromatin damage rather than DSB formation constitutes the major anticancer activity of anthracyclines.

### **Immune modulation**

Besides the direct effect on eliminating tumour cells, anthracyclines can also promote antitumour immunity. During cell death, cell contents can be released into the tumour microenvironment, including tumour antigens and danger signals (also known as damage-associated molecular patterns, DAMPs) [47]. These DAMPs can initiate inflammatory response, recruit immune cells and facilitate recognition of tumour cells. This process is known as immunogenic cell death (ICD) [48-50]. It has been shown that anthracyclines such as doxorubicin can induce ICD and thereby elicit a dendritic-cell-mediated tumour-specific CD8<sup>+</sup> T cell response in a colon carcinoma mouse model [51]. Moreover, doxorubicin was reported to selectively deplete myeloid-derived suppressor cells from the tumour microenvironment, which relieved the immunosuppressive impact of these cells in a murine breast cancer model [52]. Recently, it is observed that the C-type lectin receptor Clec2d is activated by binding histones to induce inflammation and tissue damage responses [53]. So it would be interesting to test whether histones can be externalized by doxorubicin, detected by the Clec2d receptor and cause an inflammation response. The immune stimulatory activity of doxorubicin, in the context of immune checkpoint blockade, was confirmed in a multi-arm non-comparative phase II trial. Treatment of triple negative breast cancer patients with doxorubicin followed by PD1 blockade resulted in an overall response rate of 35%, compared to 17% for PD1 blockade alone [54]. Although this finding needs to be confirmed in larger cohorts, it suggests that the immune modulating function of anthracyclines may have a synergistic role in the overall anticancer activity in patients.

### **ANTHRACYCLINE-ASSOCIATED SEVERE SIDE EFFECTS AND PREVENTIVE SOLUTIONS**

Although doxorubicin has been a cornerstone in cancer treatment for nearly five decades, its use is plagued with severe and treatment-limiting side effects. Next to common generally acute and reversible chemo-related adverse effects, such as nausea, vomiting, diarrhoea and bone marrow suppression, anthracycline treatment is associated with long-term side effects, namely cardiotoxicity, therapy-related malignancies and gonadotoxicity. These long-term adverse effects severely impact the quality of life of cancer survivors, which limit the further application of anthracyclines. Therefore, extensive research has been performed to understand and reduce the anthracycline-induced long-term side effects.

### **Cardiotoxicity**

The most treatment-limiting and therefore probably the best studied side effect of anthracyclines is cardiotoxicity. Anthracycline-induced cardiotoxicity presents as cardiomyopathy, ventricular dysfunction, pericarditis-myocarditis syndrome or arrhyth-

mias, and is dose-dependent and irreversible [10, 55, 56]. As a result, doxorubicin treatment is limited to a cumulative dose of 450 – 550 mg/m<sup>2</sup> [9, 10]. Besides cumulative dose, the risk of cardiotoxicity is also associated with treatment schedule, age extremes, and combinations with other drugs or radiotherapy in the heart region [57, 58]. Currently, there is no management or medication to relieve anthracycline-induced cardiotoxicity, and the only option for patients with severe symptoms is a heart transplantation. Therefore, doxorubicin is excluded from treating patients with a poor heart function, usually old patients. Thus, alleviating cardiotoxicity would greatly improve cancer treatment with anthracyclines.

Multiple mechanisms have been proposed, including mitochondrial dysfunction and/or lipid peroxidation as a result of ROS formation, targeting topoisomerase II $\beta$  (Topo II $\beta$ ) in cardiomyocytes, and effects on calcium homeostasis [59-62]. To reduce anthracycline-induced cardiotoxicity, several attempts to manipulate these pathways have been made. In the following sections we will discuss these in detail, and propose a possible solution based on recent data.

### **ROS alleviation**

The most intensely studied mechanism of anthracycline-induced cardiotoxicity is ROS production through interference with redox cycling and mitochondrial function [63]. To meet the high demand of ATP supply, cardiomyocytes have a greater density of mitochondria compared to other tissues, which could explain why the heart is more affected by anthracycline-induced ROS production than other tissues [59, 64]. Green et al. showed that doxorubicin-induced mitochondrial dysfunction coincided with the production of ROS and cytochrome C release, which in turn activated caspase-3 and initiate apoptosis in H9C2 cardiac cells [65]. It was reported that pre-treatment with the free radical scavenger tocopherol reduced the cardiotoxicity of doxorubicin in a lymphoma mouse model, without affecting its antitumour efficacy [60]. Although similar results were observed in an AML animal model, the cardiac protective effects of radical quenchers in clinical trials were disappointing [66, 67].

Similar to ROS scavengers, most iron-chelating agents can reduce ROS formation and alleviate doxorubicin-induced cardiotoxicity in preclinical models. However, such benefits were not observed in patients [68, 69]. The iron chelator dexrazoxane is an exceptional case. It was reported to reduce anthracycline-induced cardiotoxicity in some clinical studies, albeit not in all [70, 71]. However, this reduced toxicity is likely mediated by mechanisms different from ROS quenching, since other iron chelators are not cardiac protective [72]. Several alternative mechanisms of dexrazoxane function have been proposed, including inhibition of both apoptosis and necroptosis of cardiomyocytes [73] and antagonizing doxorubicin-induced DNA damage by interfering with Topo II $\beta$  [74].

Although it is convincingly shown that anthracyclines can induce ROS formation in *in vitro* studies, the discrepancy between the effectivity of ROS scavengers and iron chelators in preclinical studies and patients challenges the contribution of ROS production in anthracycline-induced heart damage. Using appropriate preclinical cardiotoxicity models and treatment with anthracyclines at clinical relevant concentrations and schedules may help clarifying this issue.

### **Precluding from targeting topoisomerase II $\beta$ in cardiomyocytes**

In human, Topo II enzymes are expressed in two isoforms, Topo II $\alpha$  and Topo II $\beta$  [75]. Although these two isoforms are encoded by different genes, they share substantial amino acid sequence identity and exhibit almost identical enzymological properties



[76]. Notwithstanding their similarities, the expression patterns of Topo II $\alpha$  and Topo II $\beta$  are different. Topo II $\alpha$  is mainly expressed in proliferating cells, and almost absent in quiescent and differentiated tissues. Topo II $\alpha$  is associated with replication forks and stays bound to chromosomes during mitosis, which makes its expression essential for proliferation. On the contrary, Topo II $\beta$  expression is independent of proliferation status and is high in most cell types [76]. In line with this notion, adult mammalian cardiomyocytes express Topo II $\beta$ , but no detectable Topo II $\alpha$ . Zhang et. al. reported that targeting Topo II $\beta$  in cardiomyocytes by doxorubicin is important for the initiation of cardiotoxicity [61]. It was shown that mice with cardiomyocytes-selective conditional Topo II $\beta$  knockout (Topo II $\beta^{+/Δ}$  and Topo II $\beta^{Δ/Δ}$ ) were not susceptible to the cardiac impairment caused by doxorubicin as observed in Topo II $\beta^{+/+}$  mice. Further, Lyu et. al. reported that dexrazoxane reduced doxorubicin-induced DNA damage in cardiomyocytes *in vitro* by rapid proteasomal degradation of Topo II $\beta$  [74]. These studies indicate that the DSBs mediated by Topo II $\beta$  poisoning is a major cause of doxorubicin-induced cardiotoxicity. Nevertheless, DSB cannot be the only reason, since the structurally non-related Topo II poison etoposide does not cause cardiotoxicity. From a clinical point of view, it suggests that Topo II $\alpha$ -specific anthracycline would prevent cardiotoxicity in patients and that Topo II $\beta$  expression could be used as a prognostic marker for cardiotoxicity. Unfortunately, no genuine Topo II $\alpha$ - or Topo II $\beta$ -specific drugs are available in clinic at present.

### **Novel delivery strategies to reduce anthracycline-induced toxicity**

Due to the unsatisfactory effects of ROS scavengers and iron chelators in the clinic, tumour-specific drug delivery systems were introduced in 1990s to reduce doxorubicin-induced toxicities. These delivery strategies included nanoparticle encapsulated liposomal doxorubicin (LD) and pegylated liposomal doxorubicin (PLD). LD and PLD both show prolonged serum half-life and a smaller volume of distribution compared to conventional doxorubicin [77]. LD and PLD can extravasate into the tumour via gaps in the micro vessels, whereas other tissues are much less permeable through tight junctions. Therefore, the long serum circulation of LD and PLD results in more specific tumour accumulation. Various animal models, as well as clinical trials, showed that these particles significantly decreased cardiotoxicity compared to conventional doxorubicin, without compromising antitumour efficacy [78-80]. Therefore, both LD and PLD are approved by the FDA for treating AIDS-related Kaposi's sarcoma, multiple myeloma, breast- and ovarian cancer, but their clinical application is limited by drug leakage and higher costs.

### **Separating chromatin damage from DNA damage**

With the aim to identify more effective anthracyclines with fewer side-effects, thousands of doxorubicin analogues, either isolated from natural sources, produced by mutant enzymes or prepared by organic (semi)synthesis, have been evaluated in the past decades. However, only few variant drugs showed reduced cardiotoxicity without loss of anticancer activity. One such analogue which entered the clinic is epirubicin. In a meta-analysis, epirubicin treatment showed significantly less cardiotoxicity compared to doxorubicin (OR 0.39, 95% confidence interval: 0.20 – 0.78,  $p=0.008$ ) and subclinical cardiotoxicity (OR 0.30, 0.16 – 0.57,  $p<0.001$ ) without compromising antitumour efficacy [81]. Therefore, epirubicin can be used at higher cumulative dose (900 – 1000 mg/m<sup>2</sup>) compared to doxorubicin (450 – 550 mg/m<sup>2</sup>). Although epirubicin can be used at higher cumulative dose, its application is still limited by cardiotoxicity. The key question for the development of analogues with reduced toxicity is whether

these toxic effects and anticancer activities are mediated by the same mechanism(s), which determines whether it is theoretically feasible to eliminate the cardiotoxicity of anthracycline without compromising its therapeutic efficacy. Recent work of our group provides some insight. We observed that aclarubicin, as well as the doxorubicin analogue diMe-doxorubicin, showed strongly reduced cardiotoxicity in various mouse models and human induced pluripotent stem cells-derived cardiomyocyte microtissues, without compromising anticancer activity [44]. *N,N*-dimethylation of the amino sugar eliminated the DNA-damaging capacity of these compounds, while retaining effective histone eviction activity (Figure 4). On the other hand, etoposide and amrubicin, with only DNA-damaging activity, are also not cardiotoxic in mouse models and patients, but display much lower anticancer activity. These observations indicate that the combination of DNA- with chromatin damage, as for doxorubicin and other clinically used anthracyclines, is responsible for the cardiotoxicity of these drugs [44]. Therefore, variants with only chromatin-damaging activity would be a promising direction for the development of next-generation anthracyclines. Furthermore, the identification of the structure-activity relationship of the sugar moiety and cardiotoxicity provides a new strategy for anthracycline development.

### **Therapy-related malignant neoplasms**

Attributing to the increased survival of cancer patients which modern anticancer therapy has made possible, the long-term side effects, such as tumorigenicity, have become an issue. Currently, 17–19% of all new primary malignancies occur in cancer survivors [82, 83]. Among all the long-term adverse effects caused by chemotherapy, therapy-related malignant neoplasms (t-MNs) are one of the most deleterious, because of substantial morbidity and considerable mortality. Soon after discovery, anthracyclines (excluding aclarubicin hereafter in this section) has been found to cause transformation and mutagenesis *in vitro* and tumorigenic *in vivo* [84–90], and anthracycline exposure is associated with increased risks of t-MNs in cancer survivors. The t-MNs most often ascribed to anthracyclines are AML [91–93], sarcoma [94–96] and female breast cancer [96, 97]. Thyroid cancer [98] and acute promyelocytic leukaemia (APL) [99, 100] have also been linked to antecedent anthracycline treatment. The anthracycline therapy-related AMLs (t-AMLs) frequently exhibit balanced chromosomal translocations at 11q23 (involving MLL1 gene) or 21q22 (involving AML1/RUNX1/CBFA2 gene), however occurring at unique breakpoints than de novo AML with the same cytogenetics [101–104]. In contrast to alkylating agent-associated t-AMLs, these leukaemias are rarely preceded by a myelodysplastic phase [105]. They develop with a shorter latency, often within 1–3 years after the initial anthracycline-based chemotherapy and, in some cases, within 1 year [106]. Due to unfavourable, complex or monosomal karyotypes, these t-AMLs often present as aggressive diseases and are associated with poor prognosis compared to de novo AML [106, 107]. Anthracyclines are also involved in the development of therapy-related acute promyelocytic leukaemia (t-APL) featured with balanced translocation of t(15;17) [99], which results in a double dominant-negative fusion protein, PML-RAR $\alpha$  [100]. Anthracycline-associated t-APL also arises after a short latency period, usually without a preleukemic phase [99, 100]. After a peak at 2 years following primary anthracycline treatment, the incidence of t-APL quickly decreases with time. Although the chromosomal breakpoints induced by anthracyclines are distinct from those observed in de novo t(15;17) APL, the clinical outcomes of t-APL and de novo APL are similar after all-trans retinoic acid- and anthracycline-based treatments, for which the 5-year survival rate is about 80% [99, 100]. Anthracycline-associated solid tumours



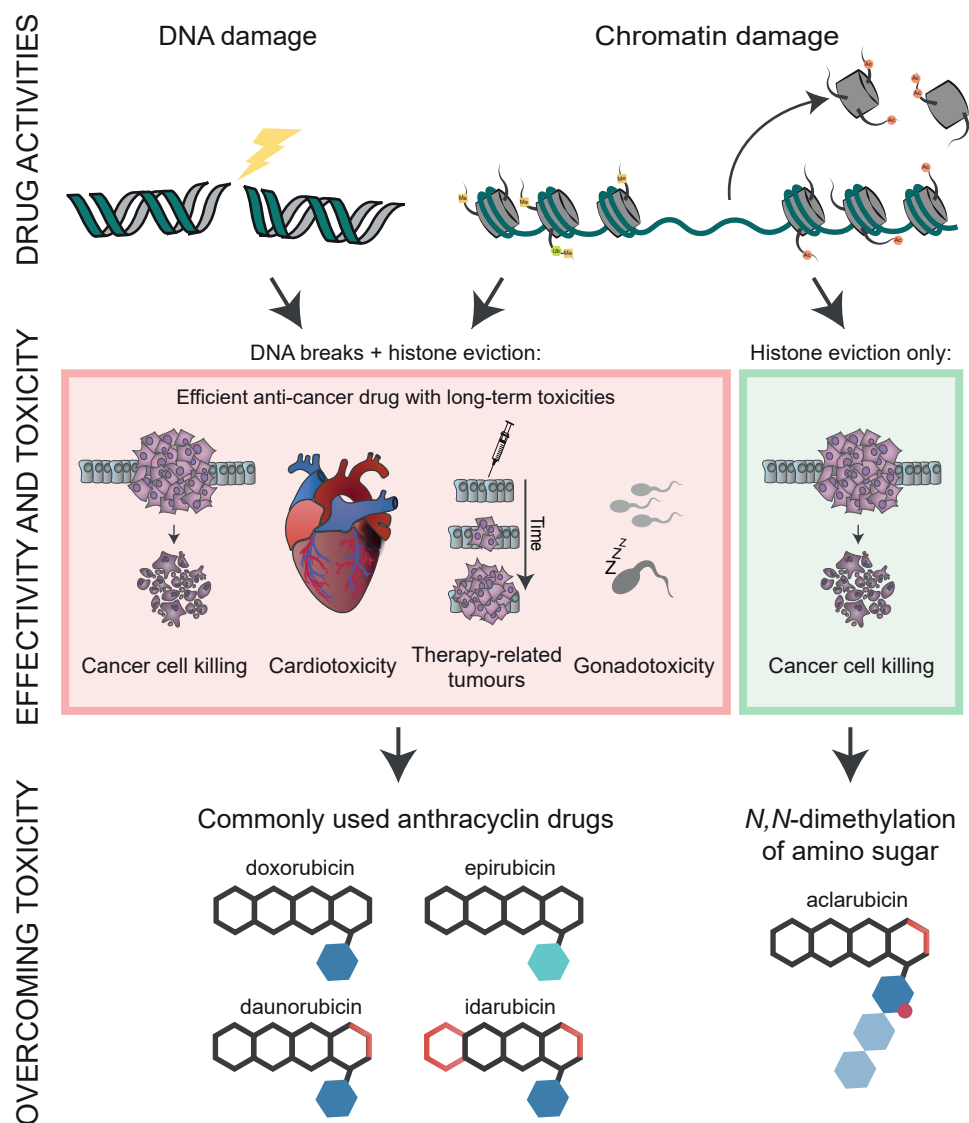


**Figure 4. Schematic overview of the activities and toxicities of the clinically used anthracyclines and their underlying mechanisms.** Most commonly used anthracyclines, including doxorubicin, epirubicin, daunorubicin and idarubicin, possess both DNA- and chromatin-damaging activities. As a consequence, these drugs are associated with cardiotoxicity, therapy-related malignancies and gonadotoxicity. *N,N*-dimethylation of the sugar moiety, as for aclarubicin (and diMe-doxorubicin), results in anthracycline variants with only chromatin-damaging activity, which are effective anticancer drugs with limited toxicities.

typically occur >10 years after exposure and in a dose-dependent manner [94-98]. There is not much known about the genetic alterations of anthracycline-related solid tumours, though a strong dose response correlation with doxorubicin was found in survivors of Li-Fraumeni syndrome-associated cancer types compared with other

childhood cancer survivors [96]. Furthermore, we recently reported that doxorubicin single drug treatment induced breast cancer development in Trp53<sup>+/-</sup> female mice, indicating the direct contribution of doxorubicin treatment to tumour development [44]. Besides the tumorigenicity of anthracyclines, cancer survivors may be especially susceptible to developing t-MNs due to a variety of other risk factors. These include genetic predisposition (such as the abovementioned Li-Fraumeni syndrome), carcinogenic exposures in common (such as tobacco use or alcohol abuse), host effects (age, gender, immunodeficiency or obesity), and combination therapy with other mutagenic chemotherapeutics (alkylating agents, etoposide or radiotherapy) [82, 83, 95-97]. Therefore, the exact mechanisms how anthracyclines contribute to t-MN development remains unclear. One option follows reports showing that leukaemia-associated translocation t(8;21) can be detected in hematopoietic cells of healthy individuals with no overt leukaemia [108, 109], and anthracycline-related t(8;21) t-AMLs were found to be positive for JAK2 V617F mutation [110], which suggests that t-AML is the consequence of a series of genetic alterations. Anthracyclines may facilitate the complete transformation of preleukemic cells by introducing additional mutations. On the other hand, anthracyclines can cause chromosomal translocations through an indirect mechanism mediated by apoptotic nucleases [111-113]. Nevertheless, accumulating evidence suggests that anthracyclines play a direct role in causing t-MN associated genetic aberrations. Anthracyclines generate DSBs by hijacking Topo II, particularly at breakpoint hotspot regions of leukemic translocations [103]. Unfaithful repair by error-prone DNA repair pathways can then result in mutagenesis or chromosomal translocations [114]. Through a similar mechanism of action, the structurally unrelated Topo II poison etoposide was also found to be associated with t-MNs of similar karyotypes in a dose-dependent manner, albeit less potent than anthracyclines [95, 115, 116]. The inferior potency of etoposide in transformation is also observed in a Trp53<sup>+/-</sup> mouse model treated with single agents of comparable dose and schedule, which excluded the influence of genetic predisposition of host and concurrent anticancer therapies [44]. This tumorigenic difference can be explained by the strongly delayed DNA repair of anthracycline due to eviction of histone variant H2AX [27].

H2AX is an important histone variant for DNA damage repair, which is phosphorylated at DNA damage sites and responsible for repair machinery recruitment. Eviction of H2AX by doxorubicin greatly attenuates DNA damage repair, consequently results in enhanced cell death and more transformation compared to etoposide [27, 43]. In line with this hypothesis, the same Trp53<sup>+/-</sup> mouse experiment and *in vitro* data showed that aclarubicin and diMe-doxorubicin without DNA-damaging activity are not tumorigenic [44, 117, 118]. Collectively, DNA damage induced by Topo II poisons is a main cause of t-MNs.

As above mentioned, anthracyclines evict histones with different epigenomic selectivity. It is interesting to notice that t(11q23) AML with MLL1 translocation is also associated with epigenetic changes, since MLL1 is an H3K4 methyltransferase [119]. The C-terminal SET domain of MLL1, which is responsible for methylating H3K4, is missing in the fusion oncoprotein of 5'-MLL1-partner-3' rearrangement. Epigenetic profiling after MLL1 deletion or with MLL1 fusion proteins revealed reduced H3K4 methylation at promotor region of target genes [120, 121]. Considering the selectivity of doxorubicin for H3K4me3 at active promoters, this coincidence may provide another explanation for the development of t(11q23) AML and its resistance to doxorubicin-based regimens [122, 123]. As a result, anthracyclines with different histone eviction profiles, such as aclarubicin and diMe-doxorubicin, could provide alternative

treatment options for doxorubicin-resistant AMLs, and vice versa [45, 124-128]. Due to limited understanding of the mechanisms of action, t-MN was previously considered as the original sin of anthracycline treatment because of resulted DNA damage. Hence, hope was laid on early detection of t-MNs by intense follow-up screening in susceptible cancer survivors or restraint of high cumulative dose of anthracyclines. However, the discovery of histone eviction activity of anthracyclines not only offers a new anticancer mechanism, but also provides a strategy to prevent t-MNs, which is experimentally illustrated by aclarubicin [44, 117]. The recent understanding on the structure-activity relationship of anthracyclines makes it possible to eliminate the DNA-damaging activity of anthracycline and related toxicities, while remaining their anticancer efficacy.

### Gonadotoxicity

Owing to its mechanisms, doxorubicin also targets healthy tissues with high proliferating rates, such as myeloid and lymphoid tissues, gastrointestinal mucosa and gonads. Since the survival rates of cancer patients improved spectacularly in the last two decades, the number of cancer survivors suffering from doxorubicin-induced gonadotoxicity also strongly increased [129]. Gonadotoxicity not only causes psychosocial distress, but also increases the risk of subsequent complications, such as osteoporosis, infertility, and cardiovascular disease [130]. Gonadal damage caused by doxorubicin treatments happens to patients at all stages of life. Although many of the cancer survivors could regain gonadal functions in a few months or years after doxorubicin treatment [131], they may have a shortened reproductive lifespan or late effects on pregnancy than the age-matched normal population [132-134]. Currently, cryopreservation of gametes or embryos is the only option to preserve fertility in patients receiving doxorubicin-containing therapy. However, this approach is only applicable to patients in a reproductive age and can be problematic in adolescent patients. For patients who have not yet commenced puberty, there is no clinically approved method for fertility preservation at present [135], despite that previous doxorubicin treatment during prepubertal period can lead to severe injury of the adult fertility [136].

Several classes of compounds have been proposed to protect gonads from doxorubicin insult in mouse models, including hormone agonists [137], antioxidants [138, 139], proteasome inhibitors [140], tyrosine kinase- and DDR inhibitors [141]. Before validating these drugs in a patient cohort, it is more important to test whether these inhibitors alleviate the gonadotoxicity without compromising the anticancer activity of doxorubicin *in vivo*. Nevertheless, development of active anthracycline variants with limited gonadotoxicity would be a preferable strategy, if possible. The depletion of follicular reserve in females and depletion of spermatogenesis in males caused by doxorubicin treatment can be attributed to the DSBs generated by the drug and subsequent cell death of germ cells [134, 142-144]. Besides direct germ cell destruction, doxorubicin also causes DSBs in somatic cells, vasculature and apoptosis of the stromal compartments in gonads [136, 143, 145-147]. The latter then further impairs the development of fertile germ cells. Similar effects were also observed for the non-anthracycline Topo II poison etoposide, which also causes DSBs and destruction of gonads [148, 149]. These data suggest that the DNA-damaging activity of doxorubicin plays an important role in mediating gonadotoxicity. This observation is further strengthened by our recent study showing that aclarubicin and diMe-doxorubicin, both lacking DNA-damaging activity but with comparable antitumour capacity as doxorubicin, did not cause apoptosis of developing follicles in female mice [44].

However, diMe-doxorubicin, with different histone eviction profile than aclarubicin and doxorubicin (unpublished results) still induced depletion of spermatogenesis in male mice, albeit at a lower degree than doxorubicin.

Oxidative stress has also been proposed as a mechanism of doxorubicin-induced gonadotoxicity [150]. However, some work using spermatogonia and immature Sertoli cell lines has shown no increase of ROS formation before the onset of cytotoxicity [151]. In line with this observation, co-administration of antioxidants showed no protective effect on doxorubicin-induced testicular toxicity *in vivo* [139, 152]. Collectively, these data suggest that DNA-damaging activity of doxorubicin is a major cause for gonadotoxicity, especially in females, with perhaps some contribution of specific histone eviction in the case of diMe-doxorubicin in male gonadotoxicity.

## PERSPECTIVES

Since the discovery of daunorubicin and doxorubicin in the 1960s, a search for less toxic yet effective alternatives to doxorubicin was initiated in the 1980s. Out of thousands of anthracycline variants tested, only a few entered the clinic, most notably epirubicin, idarubicin and aclarubicin. One reason for this limited number of successful compounds might be the lack of consensus on the mechanism of action of anthracyclines for their anticancer activity and toxicities. Furthermore, whether the severe toxicities of these drugs are intimately connected with their anticancer activity has been a lingering topic in the field. For a long time, DSB induction was considered as the main anticancer activity of anthracyclines. While only recently, a second activity –chromatin damage as a result of histone eviction– was proposed [27, 39]. Chromatin damage is not only a novel activity of anthracyclines, but also a new anticancer mechanism, which is not found in other types of chemotherapeutics. The ground-breaking discovery of chromatin damage is granted by modern molecular technologies, such as time-lapse confocal imaging, photoactivation and various next-generation sequencing techniques. Hence, it is still meaningful to re-investigate old drugs with modern technology. This may yield new mechanisms of action that can be explored to arrive at active and detoxified doxorubicin and other drug variants. Additionally, this resulted in the rediscovery of an anthracycline variant, aclarubicin, as a less toxic but very active drug in (relapsed) AML treatment.

While the potential cardiotoxicity-low/free anthracyclines need to be tested in clinic, some improvements of current anthracycline-containing chemotherapy regimen should be considered. For instance, it would be debatable to combine anthracyclines with etoposide in the same treatment regimen concerning the contribution of DNA-damaging activity to multiple toxicities, although this is frequently used in AML treatment. Likewise, specific anthracycline variant should be carefully selected for children cancer patients or patients with predisposal genetic disorder to avoid toxicities. The new mechanism, histone eviction with certain (epi)genomic selectivity, indicates that anthracyclines are in fact also epigenetic drugs. Preliminary data showed that diffuse large B-cell lymphoma cells with elevated levels of H3K27me3 were more susceptible to aclarubicin than daunorubicin [43], indicating anthracycline variant selection can be personalized for cancer treatment based on their histone eviction profiles.

The recent understanding on anthracycline anticancer activity and toxicities suggests that anthracycline development should focus on depleting DNA-damaging activity from chromatin-damaging activity. Such drugs should allow effective anthracycline-based therapies devoid of the major treatment-limiting adverse effects: cardiotoxicity, therapy-related malignancies and gonadotoxicity. This would especially

benefit cancer patients with a poor heart function, which are currently excluded from anthracycline-based chemotherapy. In addition, drug variants lacking these side effects could be used in more intense and/or longer therapy, and could be used for relapsed patients with a history of anthracyclines-based therapies.

In conclusion, despite the long history of anthracyclines, the novel discovery of chromatin damage as the major antitumour activity and its collective contribution with DNA-damaging activity to toxicities, allows the development of potentially new treatment strategies to improve cancer therapy and the quality of life of cancer survivors.

## AUTHOR CONTRIBUTIONS

SvdZ and XQ conceived the manuscript and constructed the text under supervision of JN.

## ACKNOWLEDGMENT

We thank I. Berlin for critical reading of the manuscript and F.L. Hamoen for input on the figures. This work was supported by ERC Adv. Grant and KWF grants to JN and the Institute for Chemical Immunology, an NWO Gravitation project funded by the Ministry of Education, Culture and Science of the Netherlands to JN.

## REFERENCES

1. Camerino B, P. G. (1960) Derivati della parazina II. Sulfonamdoipir (in Italian). , *Gazz Chim Ital* 90: 1802–1815.
2. Di Marco, A., Cassinelli, G. & Arcamone, F. (1981) The discovery of daunorubicin, *Cancer Treat Rep.* 65 Suppl 4, 3-8.
3. C. Tan, H. T., K.-P. Yu, M. L. Murphy and D. A. Karnofsky (1967) Daunomycin, an antitumor antibiotic, in the treatment of neoplastic disease, *Cancer.* 20, 333–353.
4. drugs.com, (2000). Drugs.com/daunorubicin. <https://www.drugs.com/pro/daunorubicin.html>. Accessed at april 8th 2020.
5. Arcamone, F., Cassinelli, G., Fantini, G., Grein, A., Orezzi, P., Pol, C. & Spalla, C. (1969) Adriamycin, 14-hydroxydaunomycin, a new antitumor antibiotic from *S. peucetius* var. *caesius*, *Biotechnol Bioeng.* 11, 1101-10.
6. A.D., H. (1996) New anthracyclines—a comparative analysis of efficacy and toxicity. , In: Hiddemann, W, Büchner T, Wörmann B, Ritter J, Creutzig U, Plunkett W, Keating M, editors *Acute Leukemias V Experimental approaches and management of refractory disease* p. 591–4.
7. drugs.com, (2000). Drugs.com/doxorubicin. <https://www.drugs.com/pro/doxorubicin.html>. Accessed at april 8th 2020.
8. Tan, C., Tasaka, H., Yu, K. P., Murphy, M. L. & Karnofsky, D. A. (1967) Daunomycin an Antitumor Antibiotic in Treatmentt of Neoplastic Disease - Clinical Evaluation with Special Reference to Childhood Leukemia, *Cancer.* 20, 333-+.
9. Lotrionte, M., Biondi-Zoccai, G., Abbate, A., Lanzetta, G., D'Ascenzo, F., Malavasi, V., Peruzzi, M., Frati, G. & Palazzoni, G. (2013) Review and meta-analysis of incidence and clinical predictors of anthracycline cardiotoxicity, *Am J Cardiol.* 112, 1980-4.
10. Jones, R. L., Swanton, C. & Ewer, M. S. (2006) Anthracycline cardiotoxicity, *Expert Opin Drug Saf.* 5, 791-809.
11. Mistry, A. R., Felix, C. A., Whitmarsh, R. J., Mason, A., Reiter, A., Cassinat, B., Parry, A., Walz, C., Wiemels, J. L., Segal, M. R., Ades, L., Blair, I. A., Osheroff, N., Peniket, A. J., Lafage-Pochitaloff, M., Cross, N. C., Chomienne, C., Solomon, E.,

- Fenaux, P. & Grimwade, D. (2005) DNA topoisomerase II in therapy-related acute promyelocytic leukemia, *N Engl J Med.* 352, 1529-38.
12. Tewey, K. M., Rowe, T. C., Yang, L., Halligan, B. D. & Liu, L. F. (1984) Adriamycin-Induced DNA Damage Mediated by Mammalian DNA Topoisomerase-II, *Science.* 226, 466-468.
13. Nitiss, J. L. (2009) Targeting DNA topoisomerase II in cancer chemotherapy, *Nat Rev Cancer.* 9, 338-50.
14. Nitiss, J. L. (2009) DNA topoisomerase II and its growing repertoire of biological functions, *Nature Reviews Cancer.* 9, 327-337.
15. Roca, J. & Wang, J. C. (1992) The Capture of a DNA Double Helix by an Atp-Dependent Protein Clamp - a Key Step in DNA Transport by Type-II DNA Topoisomerases, *Cell.* 71, 833-840.
16. Roca, J. & Wang, J. C. (1994) DNA Transport by a Type-II DNA Topoisomerase - Evidence in Favor of a 2-Gate Mechanism, *Cell.* 77, 609-616.
17. Pommier, Y., Sung, Y. L., Huang, S. Y. N. & Nitiss, J. L. (2016) Roles of eukaryotic topoisomerases in transcription, replication and genomic stability, *Nat Rev Mol Cell Bio.* 17, 703-721.
18. Dong, K. C. & Berger, J. M. (2007) Structural basis for gate-DNA recognition and bending by type IIA topoisomerases, *Nature.* 450, 1201-U4.
19. Wang, A. H. J., Ughetto, G., Quigley, G. J. & Rich, A. (1987) Interactions between an Anthracycline Antibiotic and DNA - Molecular-Structure of Daunomycin Complexed to D(Cpgtppapcpg) at 1.2-Å Resolution, *Biochemistry-U.S.* 26, 1152-1163.
20. Pommier, Y., Schwartz, R. E., Zwelling, L. A. & Kohn, K. W. (1985) Effects of DNA Intercalating Agents on Topoisomerase-II Induced DNA Strand Cleavage in Isolated Mammalian-Cell Nuclei, *Biochemistry-U.S.* 24, 6406-6410.
21. Tewey, K. M., Chen, G. L., Nelson, E. M. & Liu, L. F. (1984) Intercalative Antitumor Drugs Interfere with the Breakage-Reunion Reaction of Mammalian DNA Topoisomerase-II, *Journal of Biological Chemistry.* 259, 9182-9187.
22. Wu, C. C., Li, T. K., Farh, L., Lin, L. Y., Lin, T. S., Yu, Y. J., Yen, T. J., Chiang, C. W. & Chan, N. L. (2011) Structural Basis of Type II Topoisomerase Inhibition by the Anticancer Drug Etoposide, *Science.* 333, 459-462.
23. Wilstermann, A. M., Bender, R. P., Godfrey, M., Choi, S., Anklin, C., Berkowitz, D. B., Osheroff, N. & Graves, D. E. (2007) Topoisomerase II-drug interaction domains: Identification of substituents on etoposide that interact with the enzyme, *Biochemistry-U.S.* 46, 8217-8225.
24. Bender, R. P., Jablonksy, M. J., Shadid, M., Romaine, I., Dunlap, N., Anklin, C., Graves, D. E. & Osheroff, N. (2008) Substituents on etoposide that interact with human topoisomerase II alpha in the binary enzyme-drug complex: Contributions to etoposide binding and activity, *Biochemistry-U.S.* 47, 4501-4509.
25. Perego, P., Corna, E., De Cesare, M., Gatti, L., Polizzi, D., Pratesi, G., Supino, R. & Zunino, F. (2001) Role of apoptosis and apoptosis-related genes in cellular response and antitumor efficacy of anthracyclines, *Curr Med Chem.* 8, 31-7.
26. Liu, L. F. (1989) DNA Topoisomerase Poisons as Antitumor Drugs, *Annu Rev Biochem.* 58, 351-375.
27. Pang, B., Qiao, X., Janssen, L., Velds, A., Groothuis, T., Kerkhoven, R., Nieuwland, M., Ovaa, H., Rottenberg, S., van Tellingen, O., Janssen, J., Huijgens, P., Zwart, W. & Neefjes, J. (2013) Drug-induced histone eviction from open chromatin contributes to the chemotherapeutic effects of doxorubicin, *Nature communications.* 4, 1908.
28. Di Marco, A., Silvestrini, R., Di Marco, S. & Dasdia, T. (1965) Inhibiting effect of



the new cytotoxic antibiotic daunomycin on nucleic acids and mitotic activity of HeLa cells, *J Cell Biol.* 27, 545-50.

29. Munger, C., Ellis, A., Woods, K., Randolph, J., Yanovich, S. & Gewirtz, D. (1988) Evidence for inhibition of growth related to compromised DNA synthesis in the interaction of daunorubicin with H-35 rat hepatoma, *Cancer Res.* 48, 2404-11.

30. Davies, K. J. & Doroshow, J. H. (1986) Redox cycling of anthracyclines by cardiac mitochondria. I. Anthracycline radical formation by NADH dehydrogenase, *J Biol Chem.* 261, 3060-7.

31. Doroshow, J. H. & Davies, K. J. (1986) Redox cycling of anthracyclines by cardiac mitochondria. II. Formation of superoxide anion, hydrogen peroxide, and hydroxyl radical, *J Biol Chem.* 261, 3068-74.

32. Licata, S., Saponiero, A., Mordente, A. & Minotti, G. (2000) Doxorubicin metabolism and toxicity in human myocardium: role of cytoplasmic deglycosidation and carbonyl reduction, *Chem Res Toxicol.* 13, 414-20.

33. Minotti, G., Cairo, G. & Monti, E. (1999) Role of iron in anthracycline cardiotoxicity: new tunes for an old song?, *FASEB J.* 13, 199-212.

34. Gammella, E., Maccarinelli, F., Buratti, P., Recalcatti, S. & Cairo, G. (2014) The role of iron in anthracycline cardiotoxicity, *Front Pharmacol.* 5, 25.

35. Demant, E. J. F. (1984) Transfer of Ferritin-Bound Iron to Adriamycin, *Febs Letters.* 176, 97-100.

36. Hasinoff, B. B. & Kala, S. V. (1993) The Removal of Metal-Ions from Transferrin, Ferritin and Ceruloplasmin by the Cardioprotective Agent Icrf-187 [(+)-1,2-Bis(3,5-Dioxopiperazinyl-1-YI)Propane] and Its Hydrolysis Product Adr-925, *Agents Actions.* 39, 72-81.

37. Minotti, G., Menna, P., Salvatorelli, E., Cairo, G. & Gianni, L. (2004) Anthracyclines: molecular advances and pharmacologic developments in antitumor activity and cardiotoxicity, *Pharmacol Rev.* 56, 185-229.

38. Luger, K., Mader, A. W., Richmond, R. K., Sargent, D. F. & Richmond, T. J. (1997) Crystal structure of the nucleosome core particle at 2.8 angstrom resolution, *Nature.* 389, 251-260.

39. Yang, F., Kemp, C. J. & Henikoff, S. (2013) Doxorubicin enhances nucleosome turnover around promoters, *Curr Biol.* 23, 782-7.

40. Jawad, B., Poudel, L., Podgornik, R., Steinmetz, N. F. & Ching, W. Y. (2019) Molecular mechanism and binding free energy of doxorubicin intercalation in DNA, *Phys Chem Chem Phys.* 21, 3877-3893.

41. Talbert, P. B. & Henikoff, S. (2017) Histone variants on the move: substrates for chromatin dynamics, *Nat Rev Mol Cell Bio.* 18, 115-126.

42. Alabert, C., Jasencakova, Z. & Groth, A. (2017) Chromatin Replication and Histone Dynamics, *Adv Exp Med Biol.* 1042, 311-333.

43. Pang, B., de Jong, J., Qiao, X., Wessels, L. F. & Neefjes, J. (2015) Chemical profiling of the genome with anti-cancer drugs defines target specificities, *Nature chemical biology.* 11, 472-80.

44. Qiao, X., van der Zanden, S. Y., Wander, D. P. A., Borrás, D. M., Song, J. Y., Li, X., van Duikeren, S., van Gils, N., Rutten, A., van Herwaarden, T., van Tellingen, O., Giacomelli, E., Bellin, M., Orlova, V., Tertoolen, L. G. J., Gerhardt, S., Akkermans, J. J., Bakker, J. M., Zuur, C. L., Pang, B., Smits, A. M., Mummery, C. L., Smit, L., Arens, R., Li, J., Overkleeft, H. S. & Neefjes, J. (2020) Uncoupling DNA damage from chromatin damage to detoxify doxorubicin, *Proc Natl Acad Sci U S A.*

45. Schaefer, A., Westendorf, J., Lingelbach, K., Schmidt, C. A., Mihalache, D. L., Reymann, A. & Marquardt, H. (1993) Decreased resistance to N,N-dimethylated an-

thracyclines in multidrug-resistant Friend erythroleukemia cells, *Cancer Chemother Pharmacol.* 31, 301-7.

46. Egorin, M. J., Clawson, R. E., Ross, L. A., Chou, F. T. E., Andrews, P. A. & Bachur, N. R. (1980) Disposition and Metabolism of N,N-Dimethyl-daunorubicin and N,N-Dimethyladriamycin in Rabbits and Mice, *Drug Metab Dispos.* 8, 353-362.

47. Galluzzi, L., Buque, A., Kepp, O., Zitvogel, L. & Kroemer, G. (2015) Immunological Effects of Conventional Chemotherapy and Targeted Anticancer Agents, *Cancer Cell.* 28, 690-714.

48. Obeid, M., Tesniere, A., Ghiringhelli, F., Fimia, G. M., Apetoh, L., Perfettini, J. L., Castedo, M., Mignot, G., Panaretakis, T., Casares, N., Metivier, D., Larochette, N., van Endert, P., Ciccocanti, F., Piacentini, M., Zitvogel, L. & Kroemer, G. (2007) Calreticulin exposure dictates the immunogenicity of cancer cell death, *Nat Med.* 13, 54-61.

49. Martins, I., Wang, Y., Michaud, M., Ma, Y., Sukkurwala, A. Q., Shen, S., Kepp, O., Metivier, D., Galluzzi, L., Perfettini, J. L., Zitvogel, L. & Kroemer, G. (2014) Molecular mechanisms of ATP secretion during immunogenic cell death, *Cell Death Differ.* 21, 79-91.

50. Yamazaki, T., Hannani, D., Poirier-Colame, V., Ladoire, S., Locher, C., Sistigu, A., Prada, N., Adjemian, S., Catani, J. P., Freudenberg, M., Galanos, C., Andre, F., Kroemer, G. & Zitvogel, L. (2014) Defective immunogenic cell death of HMGB1-deficient tumors: compensatory therapy with TLR4 agonists, *Cell Death Differ.* 21, 69-78.

51. Casares, N., Pequignot, M. O., Tesniere, A., Ghiringhelli, F., Roux, S., Chaput, N., Schmitt, E., Hamai, A., Hervas-Stubbs, S., Obeid, M., Coutant, F., Metivier, D., Pichard, E., Aucouturier, P., Pierron, G., Garrido, C., Zitvogel, L. & Kroemer, G. (2005) Caspase-dependent immunogenicity of doxorubicin-induced tumor cell death, *J Exp Med.* 202, 1691-701.

52. Alizadeh, D., Trad, M., Hanke, N. T., Larmonier, C. B., Janikashvili, N., Bonnotte, B., Katsanis, E. & Larmonier, N. (2014) Doxorubicin Eliminates Myeloid-Derived Suppressor Cells and Enhances the Efficacy of Adoptive T-Cell Transfer in Breast Cancer, *Cancer Research.* 74, 104-118.

53. Lai, J. J., Cruz, F. M. & Rock, K. L. (2020) Immune Sensing of Cell Death through Recognition of Histone Sequences by C-Type Lectin-Receptor-2d Causes Inflammation and Tissue Injury, *Immunity.* 52, 123-+.

54. Voorwerk, L., Slagter, M., Horlings, H. M., Sikorska, K., van de Vijver, K. K., de Maaker, M., Nederlof, I., Kluin, R. J. C., Warren, S., Ong, S., Wiersma, T. G., Russell, N. S., Lalezari, F., Schouten, P. C., Bakker, N. A. M., Ketelaars, S. L. C., Peters, D., Lange, C. A. H., van Werkhoven, E., van Tinteren, H., Mandjes, I. A. M., Kemper, I., Onderwater, S., Chalabi, M., Wilgenhof, S., Haanen, J., Salgado, R., de Visser, K. E., Sonke, G. S., Wessels, L. F. A., Linn, S. C., Schumacher, T. N., Blank, C. U. & Kok, M. (2019) Immune induction strategies in metastatic triple-negative breast cancer to enhance the sensitivity to PD-1 blockade: the TONIC trial, *Nat Med.* 25, 920-928.

55. Lefrak, E. A., Pitha, J., Rosenheim, S. & Gottlieb, J. A. (1973) A clinicopathologic analysis of adriamycin cardiotoxicity, *Cancer.* 32, 302-14.

56. Shan, K., Lincoff, A. M. & Young, J. B. (1996) Anthracycline-induced cardiotoxicity, *Ann Intern Med.* 125, 47-58.

57. Swain, S. M., Whaley, F. S. & Ewer, M. S. (2003) Congestive heart failure in patients treated with doxorubicin: a retrospective analysis of three trials, *Cancer.* 97, 2869-79.



58. Von Hoff, D. D., Layard, M. W., Basa, P., Davis, H. L., Jr., Von Hoff, A. L., Rozencweig, M. & Muggia, F. M. (1979) Risk factors for doxorubicin-induced congestive heart failure, *Ann Intern Med.* 91, 710-7.
59. Berthiaume, J. M. & Wallace, K. B. (2007) Adriamycin-induced oxidative mitochondrial cardiotoxicity, *Cell Biol Toxicol.* 23, 15-25.
60. Myers, C. E., McGuire, W. P., Liss, R. H., Ifrim, I., Grotzinger, K. & Young, R. C. (1977) Adriamycin: the role of lipid peroxidation in cardiac toxicity and tumor response, *Science.* 197, 165-7.
61. Zhang, S., Liu, X. B., Bawa-Khalfe, T., Lu, L. S., Lyu, Y. L., Liu, L. F. & Yeh, E. T. H. (2012) Identification of the molecular basis of doxorubicin-induced cardiotoxicity, *Nature Medicine.* 18, 1639-+.
62. Wallace, K. B. (2007) Adriamycin-induced interference with cardiac mitochondrial calcium homeostasis, *Cardiovasc Toxicol.* 7, 101-7.
63. Mei, S. B., Hong, L., Cai, X. Y., Xiao, B., Zhang, P. & Shao, L. (2019) Oxidative stress injury in doxorubicin-induced cardiotoxicity, *Toxicol Lett.* 307, 41-48.
64. Barth, E., Stammeler, G., Speiser, B. & Schaper, J. (1992) Ultrastructural quantitation of mitochondria and myofilaments in cardiac muscle from 10 different animal species including man, *J Mol Cell Cardiol.* 24, 669-81.
65. Green, P. S. & Leeuwenburgh, C. (2002) Mitochondrial dysfunction is an early indicator of doxorubicin-induced apoptosis, *Biochim Biophys Acta.* 1588, 94-101.
66. Sonneveld, P. (1978) Effect of alpha-tocopherol on the cardiotoxicity of adriamycin in the rat, *Cancer Treat Rep.* 62, 1033-6.
67. Legha, S. S., Wang, Y. M., Mackay, B., Ewer, M., Hortobagyi, G. N., Benjamin, R. S. & Ali, M. K. (1982) Clinical and Pharmacologic Investigation of the Effects of Alpha-Tocopherol on Adriamycin Cardiotoxicity, *Ann Ny Acad Sci.* 393, 411-418.
68. Dresdale, A. R., Barr, L. H., Bonow, R. O., Mathisen, D. J., Myers, C. E., Schwartz, D. E., Dangelo, T. & Rosenberg, S. A. (1982) Prospective Randomized Study of the Role of N-Acetyl Cysteine in Reversing Doxorubicin-Induced Cardiomyopathy, *Am J Clin Oncol-Canc.* 5, 657-663.
69. Ladas, E. J., Jacobson, J. S., Kennedy, D. D., Teel, K., Fleischauer, A. & Kelly, K. M. (2004) Antioxidants and cancer therapy: A systematic review, *Journal of Clinical Oncology.* 22, 517-528.
70. Speyer, J. L., Green, M. D., Sanger, J., Zeleniuchjacquotte, A., Kramer, E., Rey, M., Wernz, J. C., Blum, R. H., Hochster, H., Meyers, M. & Muggia, F. M. (1990) A Prospective Randomized Trial of lcrf-187 for Prevention of Cumulative Doxorubicin-Induced Cardiac Toxicity in Women with Breast-Cancer, *Cancer Treat Rev.* 17, 161-163.
71. Lipshultz, S. E., Scully, R. E., Lipsitz, S. R., Sallan, S. E., Silverman, L. B., Miller, T. L., Borry, E. V., Asselin, B. L., Athale, U., Clavell, L. A., Larsen, E., Moghrabi, A., Samson, Y., Michon, B., Schorin, M. A., Cohen, H. J., Neuberg, D. S., Orav, E. J. & Colan, S. D. (2010) Assessment of dexrazoxane as a cardioprotectant in doxorubicin-treated children with high-risk acute lymphoblastic leukaemia: long-term follow-up of a prospective, randomised, multicentre trial, *Lancet Oncol.* 11, 950-961.
72. Hasinoff, B. B., Patel, D. & Wu, X. (2003) The oral iron chelator ICL670A (deferasirox) does not protect myocytes against doxorubicin, *Free Radical Bio Med.* 35, 1469-1479.
73. Yu, X. X., Ruan, Y., Huang, X. Q., Dou, L., Lan, M., Cui, J., Chen, B. D., Gong, H., Wang, Q., Yan, M. J., Sun, S. H., Qiu, Q., Zhang, X. Y., Man, Y., Tang, W. Q., Li, J. & Shen, T. (2020) Dexrazoxane ameliorates doxorubicin-induced cardiotoxicity by inhibiting both apoptosis and necroptosis in cardiomyocytes, *Biochem Bioph Res*

Co. 523, 140-146.

74. Lyu, Y. L., Kerrigan, J. E., Lin, C. P., Azarova, A. M., Tsai, Y. C., Ban, Y. & Liu, L. F. (2007) Topoisomerase II beta-Mediated DNA double-strand breaks: Implications in doxorubicin cardiotoxicity and prevention by dexrazoxane, *Cancer Research*. 67, 8839-8846.
75. Drake, F. H., Zimmerman, J. P., McCabe, F. L., Bartus, H. F., Per, S. R., Sullivan, D. M., Ross, W. E., Mattern, M. R., Johnson, R. K., Crooke, S. T. & Mirabelli, C. K. (1987) Purification of Topoisomerase-II from Amsacrine-Resistant P388 Leukemia-Cells - Evidence for 2 Forms of the Enzyme, *Journal of Biological Chemistry*. 262, 16739-16747.
76. Austin, C. A. & Marsh, K. L. (1998) Eukaryotic DNA topoisomerase II beta, *Bioessays*. 20, 215-226.
77. Gabizon, A., Shmeeda, H. & Barenholz, Y. (2003) Pharmacokinetics of pegylated liposomal doxorubicin - Review of animal and human studies, *Clin Pharmacokinetics*. 42, 419-436.
78. Vaage, J., Barberaguillem, E., Abra, R., Huang, A. & Working, P. (1994) Tissue Distribution and Therapeutic Effect of Intravenous Free or Encapsulated Liposomal Doxorubicin on Human Prostate Carcinoma Xenografts, *Cancer*. 73, 1478-1484.
79. Cabanes, A., Tzemach, D., Goren, D., Horowitz, A. T. & Gabizon, A. (1998) Comparative study of the antitumor activity of free doxorubicin and polyethylene glycol-coated liposomal doxorubicin in a mouse lymphoma model, *Clin Cancer Res*. 4, 499-505.
80. Harris, L., Batist, G., Belt, R., Rovira, D., Navari, R., Azarnia, N., Welles, L., Winer, E. & Group, T. D. S. (2002) Liposome-encapsulated doxorubicin compared with conventional doxorubicin in a randomized multicenter trial as first-line therapy of metastatic breast carcinoma, *Cancer*. 94, 25-36.
81. Smith, L. A., Cornelius, V. R., Plummer, C. J., Levitt, G., Verrill, M., Canney, P. & Jones, A. (2010) Cardiotoxicity of anthracycline agents for the treatment of cancer: Systematic review and meta-analysis of randomised controlled trials, *Bmc Cancer*. 10.
82. Travis, L. B., Demark Wahnefried, W., Allan, J. M., Wood, M. E. & Ng, A. K. (2013) Aetiology, genetics and prevention of secondary neoplasms in adult cancer survivors, *Nat Rev Clin Oncol*. 10, 289-301.
83. Morton, L. M., Swerdlow, A. J., Schaapveld, M., Ramadan, S., Hodgson, D. C., Radford, J. & van Leeuwen, F. E. (2014) Current knowledge and future research directions in treatment-related second primary malignancies, *EJC Suppl*. 12, 5-17.
84. Bertazzoli, C., Chieli, T. & Solcia, E. (1971) Different incidence of breast carcinomas or fibroadenomas in daunomycin or adriamycin treated rats, *Experientia*. 27, 1209-10.
85. Sternberg, S. S., Philips, F. S. & Cronin, A. P. (1972) Renal tumors and other lesions in rats following a single intravenous injection of daunomycin, *Cancer Res*. 32, 1029-36.
86. Price, P. J., Suk, W. A., Skeen, P. C., Chirigos, M. A. & Huebner, R. J. (1975) Transforming potential of the anticancer drug adriamycin, *Science*. 187, 1200-1.
87. Philips, F. S., Gilladoga, A., Marquardt, H., Sternberg, S. S. & Vidal, P. R. (1975) Some Observations on the Toxicity of Adriamycin.
88. Marquardt, H., Philips, F. S. & Sternberg, S. S. (1976) Tumorigenicity in vivo and induction of malignant transformation and mutagenesis in cell cultures by adriamycin and daunomycin, *Cancer Res*. 36, 2065-9.
89. Solcia, E., Ballerini, L., Bellini, O., Sala, L. & Bertazzoli, C. (1978) Mammary

- tumors induced in rats by adriamycin and daunomycin, *Cancer Res.* 38, 1444-6.
90. (1987) Overall evaluations of carcinogenicity: an updating of IARC Monographs volumes 1 to 42, *IARC Monogr Eval Carcinog Risks Hum Suppl.* 7, 1-440.
91. Diamandidou, E., Buzdar, A. U., Smith, T. L., Frye, D., Witjaksono, M. & Hortobagyi, G. N. (1996) Treatment-related leukemia in breast cancer patients treated with fluorouracil-doxorubicin-cyclophosphamide combination adjuvant chemotherapy: the University of Texas M.D. Anderson Cancer Center experience, *J Clin Oncol.* 14, 2722-30.
92. Praga, C., Bergh, J., Bliss, J., Bonnetterre, J., Cesana, B., Coombes, R. C., Fargeot, P., Folin, A., Fumoleau, P., Giuliani, R., Kerbrat, P., Hery, M., Nilsson, J., Onida, F., Piccart, M., Shepherd, L., Therasse, P., Wils, J. & Rogers, D. (2005) Risk of acute myeloid leukemia and myelodysplastic syndrome in trials of adjuvant epirubicin for early breast cancer: correlation with doses of epirubicin and cyclophosphamide, *J Clin Oncol.* 23, 4179-91.
93. Le Deley, M. C., Suzan, F., Cutuli, B., Delaloge, S., Shamsaldin, A., Linassier, C., Clisant, S., de Vathaire, F., Fenau, P. & Hill, C. (2007) Anthracyclines, mitoxantrone, radiotherapy, and granulocyte colony-stimulating factor: risk factors for leukemia and myelodysplastic syndrome after breast cancer, *J Clin Oncol.* 25, 292-300.
94. Henderson, T. O., Whitton, J., Stovall, M., Mertens, A. C., Mitby, P., Friedman, D., Strong, L. C., Hammond, S., Neglia, J. P., Meadows, A. T., Robison, L. & Diller, L. (2007) Secondary sarcomas in childhood cancer survivors: a report from the Childhood Cancer Survivor Study, *J Natl Cancer Inst.* 99, 300-8.
95. Henderson, T. O., Rajaraman, P., Stovall, M., Constine, L. S., Olive, A., Smith, S. A., Mertens, A., Meadows, A., Neglia, J. P., Hammond, S., Whitton, J., Inskip, P. D., Robison, L. L. & Diller, L. (2012) Risk factors associated with secondary sarcomas in childhood cancer survivors: a report from the childhood cancer survivor study, *Int J Radiat Oncol Biol Phys.* 84, 224-30.
96. Teepen, J. C., van Leeuwen, F. E., Tissing, W. J., van Dulmen-den Broeder, E., van den Heuvel-Eibrink, M. M., van der Pal, H. J., Loonen, J. J., Bresters, D., Versluys, B., Neggers, S., Jaspers, M. W. M., Hauptmann, M., van der Heiden-van der Loo, M., Visser, O., Kremer, L. C. M., Ronckers, C. M. & Group, D. L. S. (2017) Long-Term Risk of Subsequent Malignant Neoplasms After Treatment of Childhood Cancer in the DCOG LATER Study Cohort: Role of Chemotherapy, *J Clin Oncol.* 35, 2288-2298.
97. van Leeuwen, F. E. & Ronckers, C. M. (2016) Anthracyclines and Alkylating Agents: New Risk Factors for Breast Cancer in Childhood Cancer Survivors?, *J Clin Oncol.* 34, 891-4.
98. Veiga, L. H., Bhatti, P., Ronckers, C. M., Sigurdson, A. J., Stovall, M., Smith, S. A., Weathers, R., Leisenring, W., Mertens, A. C., Hammond, S., Neglia, J. P., Meadows, A. T., Donaldson, S. S., Sklar, C. A., Friedman, D. L., Robison, L. L. & Inskip, P. D. (2012) Chemotherapy and thyroid cancer risk: a report from the childhood cancer survivor study, *Cancer Epidemiol Biomarkers Prev.* 21, 92-101.
99. Beaumont, M., Sanz, M., Carli, P. M., Maloisel, F., Thomas, X., Detourmignies, L., Guerci, A., Gratecos, N., Rayon, C., San Miguel, J., Odriozola, J., Cahn, J. Y., Huguet, F., Vekhof, A., Stamatoulas, A., Dombret, H., Capote, F., Esteve, J., Stoppa, A. M. & Fenau, P. (2003) Therapy-related acute promyelocytic leukemia, *J Clin Oncol.* 21, 2123-37.
100. Rashidi, A. & Fisher, S. I. (2013) Therapy-related acute promyelocytic leukemia: a systematic review, *Med Oncol.* 30, 625.
101. Pedersen-Bjergaard, J. & Philip, P. (1991) Balanced translocations involving

chromosome bands 11q23 and 21q22 are highly characteristic of myelodysplasia and leukemia following therapy with cytostatic agents targeting at DNA-topoisomerase II, *Blood*. 78, 1147-8.

102. Larson, R. A., Le Beau, M. M., Ratain, M. J. & Rowley, J. D. (1992) Balanced translocations involving chromosome bands 11q23 and 21q22 in therapy-related leukemia, *Blood*. 79, 1892-3.

103. Felix, C. A., Kolaris, C. P. & Osheroff, N. (2006) Topoisomerase II and the etiology of chromosomal translocations, *DNA Repair (Amst)*. 5, 1093-108.

104. Cowell, I. G. & Austin, C. A. (2012) Mechanism of generation of therapy related leukemia in response to anti-topoisomerase II agents, *Int J Environ Res Public Health*. 9, 2075-91.

105. Pendleton, M., Lindsey, R. H., Jr., Felix, C. A., Grimwade, D. & Osheroff, N. (2014) Topoisomerase II and leukemia, *Ann N Y Acad Sci*. 1310, 98-110.

106. Park, S. H., Chi, H. S., Cho, Y. U., Jang, S. & Park, C. J. (2013) Evaluation of prognostic factors in patients with therapy-related acute myeloid leukemia, *Blood Res*. 48, 185-92.

107. Kayser, S., Dohner, K., Krauter, J., Kohne, C. H., Horst, H. A., Held, G., von Lilienfeld-Toal, M., Wilhelm, S., Kundgen, A., Gotze, K., Rummel, M., Nachbaur, D., Schlegelberger, B., Gohring, G., Spath, D., Morlok, C., Zucknick, M., Ganser, A., Dohner, H., Schlenk, R. F. & German-Austrian, A. (2011) The impact of therapy-related acute myeloid leukemia (AML) on outcome in 2853 adult patients with newly diagnosed AML, *Blood*. 117, 2137-45.

108. Basecke, J., Cepek, L., Mannhalter, C., Krauter, J., Hildenhausen, S., Brittinger, G., Trumper, L. & Griesinger, F. (2002) Transcription of AML1/ETO in bone marrow and cord blood of individuals without acute myelogenous leukemia, *Blood*. 100, 2267-8.

109. Mori, H., Colman, S. M., Xiao, Z., Ford, A. M., Healy, L. E., Donaldson, C., Hows, J. M., Navarrete, C. & Greaves, M. (2002) Chromosome translocations and covert leukemic clones are generated during normal fetal development, *Proc Natl Acad Sci U S A*. 99, 8242-7.

110. Schnittger, S., Bacher, U., Kern, W., Haferlach, C. & Haferlach, T. (2007) JAK2 seems to be a typical cooperating mutation in therapy-related t(8;21)/AML1-ETO-positive AML, *Leukemia*. 21, 183-4.

111. Stanulla, M., Wang, J., Chervinsky, D. S., Thandla, S. & Aplan, P. D. (1997) DNA cleavage within the MLL breakpoint cluster region is a specific event which occurs as part of higher-order chromatin fragmentation during the initial stages of apoptosis, *Mol Cell Biol*. 17, 4070-9.

112. Betti, C. J., Villalobos, M. J., Diaz, M. O. & Vaughan, A. T. (2001) Apoptotic triggers initiate translocations within the MLL gene involving the nonhomologous end joining repair system, *Cancer Res*. 61, 4550-5.

113. Betti, C. J., Villalobos, M. J., Diaz, M. O. & Vaughan, A. T. (2003) Apoptotic stimuli initiate MLL-AF9 translocations that are transcribed in cells capable of division, *Cancer Res*. 63, 1377-81.

114. Mays, A. N., Osheroff, N., Xiao, Y., Wiemels, J. L., Felix, C. A., Byl, J. A., Saravanamuttu, K., Peniket, A., Corser, R., Chang, C., Hoyle, C., Parker, A. N., Hasan, S. K., Lo-Coco, F., Solomon, E. & Grimwade, D. (2010) Evidence for direct involvement of epirubicin in the formation of chromosomal translocations in t(15;17) therapy-related acute promyelocytic leukemia, *Blood*. 115, 326-30.

115. Kudo, K., Yoshida, H., Kiyoi, H., Numata, S., Horibe, K. & Naoe, T. (1998) Etoposide-related acute promyelocytic leukemia, *Leukemia*. 12, 1171-5.

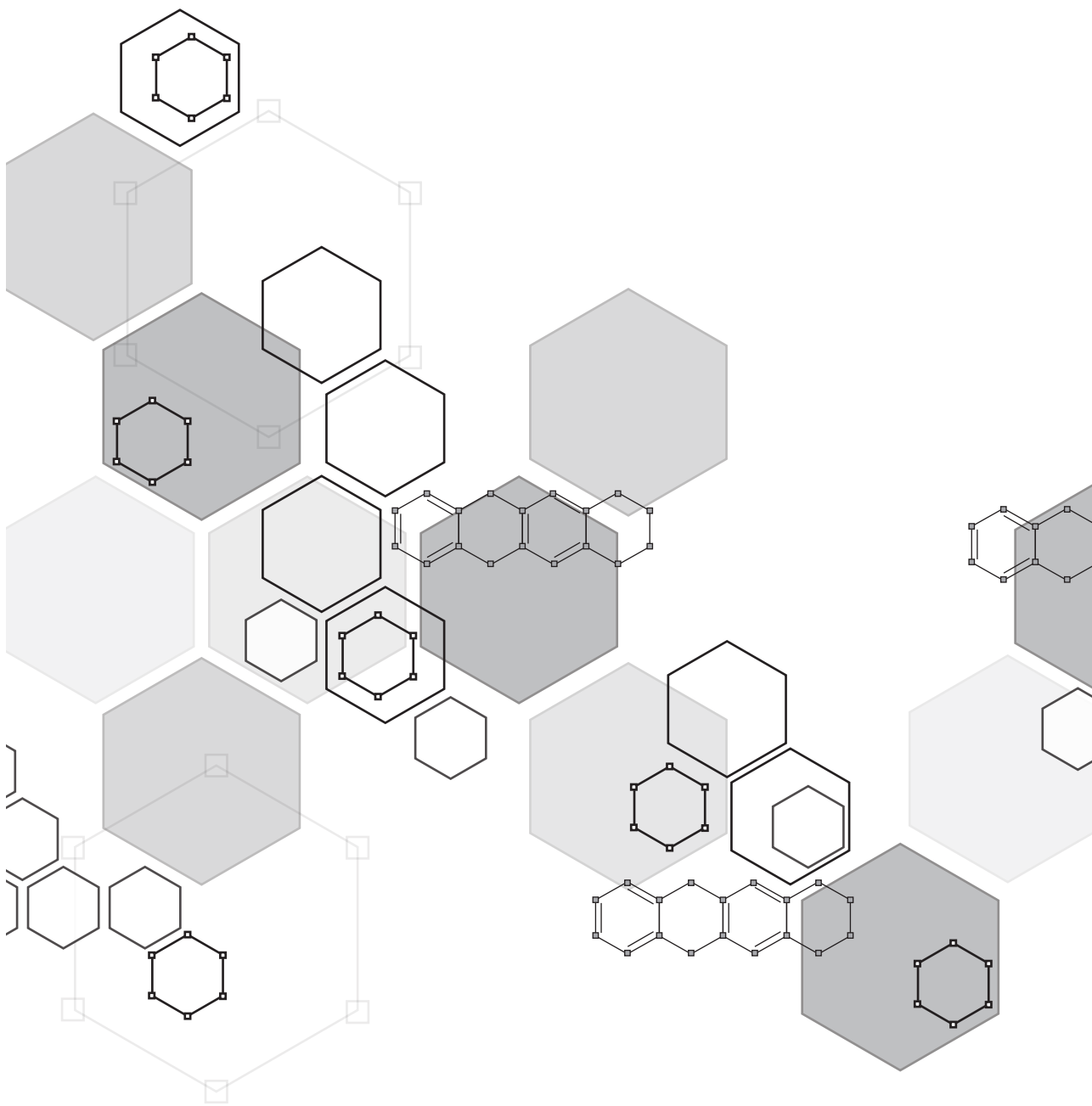
116. Le Deley, M. C., Leblanc, T., Shamsaldin, A., Raquin, M. A., Lacour, B., Sommelet, D., Chompret, A., Cayuela, J. M., Bayle, C., Bernheim, A., de Vathaire, F., Vassal, G., Hill, C. & Societe Francaise d'Oncologie, P. (2003) Risk of secondary leukemia after a solid tumor in childhood according to the dose of epipodophyllotoxins and anthracyclines: a case-control study by the Societe Francaise d'Oncologie Pediatrique, *J Clin Oncol.* 21, 1074-81.
117. Westendorf, J., Marquardt, H., Ketkar, M. B., Mohr, U. & Marquardt, H. (1983) Tumorigenicity in vivo and induction of mutagenesis and DNA repair in vitro by aclacinomycin A and marcellomycin: structure-activity relationship and predictive value of short-term tests, *Cancer Res.* 43, 5248-51.
118. Westendorf, J., Marquardt, H. & Marquardt, H. (1984) Structure-activity relationship of anthracycline-induced genotoxicity in vitro, *Cancer Res.* 44, 5599-604.
119. Del Rizzo, P. A. & Trievel, R. C. (2011) Substrate and product specificities of SET domain methyltransferases, *Epigenetics.* 6, 1059-67.
120. Jakovcevski, M., Ruan, H., Shen, E. Y., Dincer, A., Javidfar, B., Ma, Q., Peter, C. J., Cheung, I., Mitchell, A. C., Jiang, Y., Lin, C. L., Pothula, V., Stewart, A. F., Ernst, P., Yao, W. D. & Akbarian, S. (2015) Neuronal Kmt2a/Mll1 histone methyltransferase is essential for prefrontal synaptic plasticity and working memory, *J Neurosci.* 35, 5097-108.
121. Xu, J., Li, L., Xiong, J., denDekker, A., Ye, A., Karatas, H., Liu, L., Wang, H., Qin, Z. S., Wang, S. & Dou, Y. (2016) MLL1 and MLL1 fusion proteins have distinct functions in regulating leukemic transcription program, *Cell Discov.* 2, 16008.
122. Zuber, J., Radtke, I., Pardee, T. S., Zhao, Z., Rappaport, A. R., Luo, W., McCurrach, M. E., Yang, M. M., Dolan, M. E., Kogan, S. C., Downing, J. R. & Lowe, S. W. (2009) Mouse models of human AML accurately predict chemotherapy response, *Genes Dev.* 23, 877-89.
123. Estey, E. & Dohner, H. (2006) Acute myeloid leukaemia, *Lancet.* 368, 1894-907.
124. Erttmann, R., Munchmeyer, M., Looft, G. & Winkler, K. (1991) Conserved cytostatic activity of aclarubicin in a doxorubicin selected Friend leukaemia cell line with multifactorial multidrug resistance, *Eur J Cancer.* 27, 1064.
125. Natale, R. B., Cody, R. L., Simon, M. S. & Wheeler, R. H. (1993) An in vivo and in vitro trial of aclarubicin in metastatic breast cancer: a novel approach to the study of analogs, *Cancer Chemother Pharmacol.* 31, 485-8.
126. Lehne, G., De Angelis, P., Clausen, O. P. & Rugstad, H. E. (1996) Human hepatoma cells rich in P-glycoprotein are sensitive to aclarubicin and resistant to three other anthracyclines, *Br J Cancer.* 74, 1719-29.
127. Liu, L., Qu, Q., Jiao, W., Zhang, Y., Li, X., Ding, C. & Wu, D. (2015) Increasing aclarubicin dose in low-dose cytarabine and aclarubicin in combination with granulocyte colony-stimulating factor (CAG regimen) is efficacious as salvage chemotherapy for relapsed/refractory mixed-phenotype acute leukemia, *Leukemia research.* 39, 805-11.
128. Qu, Q., Liu, L., Zhang, Y., Li, X. & Wu, D. (2015) Increasing aclarubicin dosage of the conventional CAG (low-dose cytarabine and aclarubicin in combination with granulocyte colony-stimulating factor) regimen is more efficacious as a salvage therapy than CAG for relapsed/refractory acute myeloid leukemia, *Leukemia research.* 39, 1353-9.
129. Delessard, M., Saulnier, J., Rives, A., Dumont, L., Rondanino, C. & Rives, N. (2020) Exposure to Chemotherapy During Childhood or Adulthood and Consequences on Spermatogenesis and Male Fertility, *International journal of molecular*



sciences. 21.

130. European Society for Human, R., Embryology Guideline Group on, P. O. I., Webber, L., Davies, M., Anderson, R., Bartlett, J., Braat, D., Cartwright, B., Cifkova, R., de Muinck Keizer-Schrama, S., Hogervorst, E., Janse, F., Liao, L., Vlasisavljevic, V., Zillikens, C. & Vermeulen, N. (2016) ESHRE Guideline: management of women with premature ovarian insufficiency, *Hum Reprod.* 31, 926-37.
131. Viviani, S., Santoro, A., Ragni, G., Bonfante, V., Bestetti, O. & Bonadonna, G. (1985) Gonadal toxicity after combination chemotherapy for Hodgkin's disease. Comparative results of MOPP vs ABVD, *Eur J Cancer Clin Oncol.* 21, 601-5.
132. Byrne, J., Fears, T. R., Gail, M. H., Pee, D., Connelly, R. R., Austin, D. F., Holmes, G. F., Holmes, F. F., Latourette, H. B., Meigs, J. W. & et al. (1992) Early menopause in long-term survivors of cancer during adolescence, *Am J Obstet Gynecol.* 166, 788-93.
133. Green, D. M., Whitton, J. A., Stovall, M., Mertens, A. C., Donaldson, S. S., Ruymann, F. B., Pendergrass, T. W. & Robison, L. L. (2002) Pregnancy outcome of female survivors of childhood cancer: a report from the Childhood Cancer Survivor Study, *Am J Obstet Gynecol.* 187, 1070-80.
134. Ben-Aharon, I., Bar-Joseph, H., Tzarfaty, G., Kuchinsky, L., Rizel, S., Stemmer, S. M. & Shalgi, R. (2010) Doxorubicin-induced ovarian toxicity, *Reprod Biol Endocrinol.* 8, 20.
135. Anderson, R. A., Mitchell, R. T., Kelsey, T. W., Spears, N., Telfer, E. E. & Wallace, W. H. (2015) Cancer treatment and gonadal function: experimental and established strategies for fertility preservation in children and young adults, *Lancet Diabetes Endocrinol.* 3, 556-67.
136. Brilhante, O., Stumpp, T. & Miraglia, S. J. I. J. M. S. (2011) Long-term testicular toxicity caused by doxorubicin treatment during pre-pubertal phase. 3, 52-60.
137. Manabe, F., Takeshima, H. & Akaza, H. (1997) Protecting spermatogenesis from damage induced by doxorubicin using the luteinizing hormone-releasing hormone agonist leuporelin: an image analysis study of a rat experimental model, *Cancer.* 79, 1014-21.
138. Kropp, J., Roti Roti, E. C., Ringelstetter, A., Khatib, H., Abbott, D. H. & Salih, S. M. (2015) Dexrazoxane Diminishes Doxorubicin-Induced Acute Ovarian Damage and Preserves Ovarian Function and Fecundity in Mice, *PloS one.* 10, e0142588.
139. Levi, M., Tzabari, M., Savion, N., Stemmer, S. M., Shalgi, R. & Ben-Aharon, I. (2015) Dexrazoxane exacerbates doxorubicin-induced testicular toxicity, *Reproduction.* 150, 357-66.
140. Roti Roti, E. C., Ringelstetter, A. K., Kropp, J., Abbott, D. H. & Salih, S. M. (2014) Bortezomib prevents acute doxorubicin ovarian insult and follicle demise, improving the fertility window and pup birth weight in mice, *PloS one.* 9, e108174.
141. Tuppi, M., Kehrloesser, S., Coutandin, D. W., Rossi, V., Luh, L. M., Strubel, A., Hotte, K., Hoffmeister, M., Schafer, B., De Oliveira, T., Greten, F., Stelzer, E. H. K., Knapp, S., De Felici, M., Behrends, C., Klinger, F. G. & Dotsch, V. (2018) Oocyte DNA damage quality control requires consecutive interplay of CHK2 and CK1 to activate p63, *Nat Struct Mol Biol.* 25, 261-269.
142. Perez, G. I., Knudson, C. M., Leykin, L., Korsmeyer, S. J. & Tilly, J. L. (1997) Apoptosis-associated signaling pathways are required for chemotherapy-mediated female germ cell destruction, *Nature medicine.* 3, 1228-32.
143. Roti Roti, E. C., Leisman, S. K., Abbott, D. H. & Salih, S. M. (2012) Acute doxorubicin insult in the mouse ovary is cell- and follicle-type dependent, *PloS one.* 7, e42293.

144. Beaud, H., van Pelt, A. & Delbes, G. (2017) Doxorubicin and vincristine affect undifferentiated rat spermatogonia, *Reproduction*. 153, 725-735.
145. Marcello, M. F., Nuciforo, G., Romeo, R., Di Dino, G., Russo, I., Russo, A., Palumbo, G. & Schiliro, G. (1990) Structural and ultrastructural study of the ovary in childhood leukemia after successful treatment, *Cancer*. 66, 2099-104.
146. Kobayashi, H., Urashima, M., Hoshi, Y., Uchiyama, H., Fujisawa, K., Akatsuka, J., Maekawa, K. & Hurusato, M. (1996) Testicular morphological changes in children with acute lymphoblastic leukemia following chemotherapy, *Acta Paediatr Jpn*. 38, 640-3.
147. Brilhante, O., Okada, F. K., Sasso-Cerri, E., Stumpp, T. & Miraglia, S. M. (2012) Late morfofunctional alterations of the Sertoli cell caused by doxorubicin administered to prepubertal rats, *Reprod Biol Endocrinol*. 10, 79.
148. Stumpp, T., Sasso-Cerri, E., Freymuller, E. & Miraglia, S. M. (2004) Apoptosis and testicular alterations in albino rats treated with etoposide during the prepubertal phase, *Anat Rec A Discov Mol Cell Evol Biol*. 279, 611-22.
149. Ortiz, R. J., Lizama, C., Codelia, V. A. & Moreno, R. D. (2009) A molecular evaluation of germ cell death induced by etoposide in pubertal rat testes, *Mol Hum Reprod*. 15, 363-71.
150. Bar-Joseph, H., Ben-Aharon, I., Rizel, S., Stemmer, S. M., Tzabari, M. & Shalgi, R. (2010) Doxorubicin-induced apoptosis in germinal vesicle (GV) oocytes, *Reprod Toxicol*. 30, 566-72.
151. Tremblay, A. R. & Delbes, G. (2018) In vitro study of doxorubicin-induced oxidative stress in spermatogonia and immature Sertoli cells, *Toxicol Appl Pharmacol*. 348, 32-42.
152. Hou, M., Chrysis, D., Nurmio, M., Parvinen, M., Eksborg, S., Soder, O. & Jahnukainen, K. (2005) Doxorubicin induces apoptosis in germ line stem cells in the immature rat testis and amifostine cannot protect against this cytotoxicity, *Cancer research*. 65, 9999-10005.





# Genome-wide identification and characterization of novel factors conferring resistance to topoisomerase II poisons in cancer

# 2



Ruud H. Wijdeven<sup>#</sup>, Baoxu Pang<sup>#</sup>, Sabina Y. van der Zanden, Xiaohang Qiao, Vincent Blomen, Marlous Hoogstraat, Esther H. Lips, Lennert Janssen, Lodewyk Wessels, Thijn R. Brummelkamp and Jacques Neefjes

<sup>#</sup>These authors contributed equally

*Cancer Research* (2015)

**ABSTRACT**

The Topoisomerase II poisons doxorubicin and etoposide constitute longstanding cornerstones of chemotherapy. Despite their extensive clinical use, many patients do not respond to these drugs. Using a genome-wide gene knockout approach, we identified Keap1, the SWI/SNF complex, and C9orf82 as independent factors capable of driving drug resistance through diverse molecular mechanisms, all converging on the DNA double-strand break (DSB) and repair pathway. Loss of Keap1 or the SWI/SNF complex inhibits generation of DSB by attenuating expression and activity of topoisomerase II $\alpha$ , respectively, while deletion of C9orf82 augments subsequent DSB repair. Their corresponding genes, frequently mutated or deleted in human tumors, may impact drug sensitivity, as exemplified by triple-negative breast cancer patients with diminished SWI/SNF core member expression who exhibit reduced responsiveness to chemotherapy regimens containing doxorubicin. Collectively, our work identifies genes that may predict the response of cancer patients to the broadly used topoisomerase II poisons and defines alternative pathways that could be therapeutically exploited in treatment-resistant patients.

**INTRODUCTION**

Topoisomerase II (Topo II) poisons, including those of the anthracycline and podophyllotoxin families, are among the major classes of chemotherapeutics used to treat a wide spectrum of tumors. These drugs trap Topo II onto the DNA and inhibit DNA re-ligation, hereby ‘poisoning’ the enzyme and generating DNA double-strand breaks [1]. Despite their broad applicability, resistance constitutes a frequent clinical limitation [2]. Given the serious side effects associated with their administration, development of a comprehensive panel of treatment predicting factors could provide a useful clinical tool for matching chemotherapy to individual patients [1].

Anthracyclines, with doxorubicin (Doxo) as their prominent example, constitute an especially effective class of anti-cancer drugs, as they intercalate into the DNA and evict histones from the chromatin, concomitant to inhibiting Topo II after the formation of a DNA double-strand break [3, 4]. As a result, the DNA damage response is attenuated and the epigenome becomes deregulated at defined regions in the genome [3, 5]. The cellular pathways contributing to Doxo resistance have been interrogated extensively, and the drug transporter ABCB1 (MDR1), capable of exporting Doxo from cells [2], has emerged as a major player in this context. Despite its role in drug removal at the blood-brain barrier, inhibition of ABCB1 failed to satisfactorily revert unresponsiveness to Doxo in the clinic [6]. Other factors, acting either alone or in combination with proteins such as ABCB1, have been implicated in Doxo resistance through the downregulation of either Topo II or other DNA damage response (DDR) pathway constituents [7, 8]. Thus far, none of the above factors have been shown to individually account for the observed variability in patients’ responses to Doxo [1, 9]. Taken together, the findings reported to date suggest the existence of other as of yet undefined molecular determinants instrumental in the conversion to a Doxo-resistant state.

Herein we report on a genome-wide screen for factors driving resistance to Doxo using a knockout approach in haploid cells [10]. With the aim of approximating the physiological situation of patient drug exposure—and by extension drug resistance—in the tissue culture environment, we iteratively subjected cells to Doxo for three brief periods as a means of selecting for relative drug resistance. Our screening methodology yielded two previously described contributors to drug resistance: the afore-

mentioned transporter ABCB1 [2] and the stress response gene Keap1 [11]. We also identified several novel factors: the gene product of C9orf82 that appears to function as an inhibitor of DNA damage repair and the chromatin remodeling SWI/SNF complex subunits SMARCB1 and SMARCE1. Depletion of either Keap1, C9orf82 or SMARCB1 was found to induce cellular resistance to Topo II poisons, without significantly affecting sensitivity to either Topo I inhibitors or aclarubicin (Acla), an analog of Doxo that does not induce DNA damage [3, 5]. All genes identified in the resistance screen were found to regulate Topo II-induced DNA break formation or subsequent DNA repair. In the clinic, tumors frequently harbor mutations or deletions in Keap1, C9orf82 or components of the SWI/SNF complex [12-14]. These may be relevant for patient stratification to Doxo-based therapies, as illustrated by the correlation between expression levels of Keap1 and the SWI/SNF complex subunits and the response of triple negative breast cancer patients to Doxo-based treatment. Our data provide a molecular basis for patient selection in the clinic with regards to the broadly used Topo II poisons in cancer therapy.

## RESULTS

### Identification and validation of doxorubicin-resistance factors Keap1, C9orf82 and the SWI/SNF complex

To identify genetic determinants involved in resistance to Doxo, we performed a genome-wide insertional mutagenesis screen in haploid cells using a gene trap retrovirus [10]. A genomic insertion of the virus into the sense direction of a gene disrupts its expression and often results in a complete knockout of the gene. HAP1 cells were infected with a gene trap retrovirus to generate a pool of randomly mutagenized cells and briefly passaged prior to drug exposure. To recapitulate the normal pharmacokinetics of Doxo in a tissue culture setting, we exposed these cells for 2 hours to 1  $\mu$ M Doxo, which is within the peak plasma dose of standard treatment of cancer patients [15]. Cells were treated weekly for three weeks, after which surviving cells were grown out and insertions were mapped and aligned to the human genome (Figure 1A). Disruptions of six genes were significantly enriched ( $p < 0.00005$ ) in the surviving population compared to the untreated control (Figure 1B and Table S1). Among these were two previously reported factors, ABCB1 [6] and Keap1 [16], as well as novel factors, including the SWI/SNF subunits, SMARCB1 and SMARCE1, the C9orf82 gene, and the translation initiation factor Eif4a1. Canonical Doxo-target Topo II $\alpha$  appeared just below the threshold, with an adjusted p-value of 0.01. ABCB1 contained mostly anti-sense mutations following selection, which could enhance its expression (unpublished observation). All other enriched genes contained at least five independent insertions in the sense direction, leading to their inactivation. Identification of Keap1 provided validation of the screening methodology, as it has already been associated with resistance to several anti-cancer drugs, including Doxo [11, 12, 17]. To validate the screen hits, we generated HAP1 cells stably expressing either control shRNA or two independent shRNAs targeting Keap1, which reduced Keap1 expression by 50-80% (Figure 1C and S1A). These knockdown cell lines were subsequently exposed to Doxo for two hours, followed by drug wash out and outgrowth. As expected, Keap1 depletion conferred Doxo resistance as illustrated in both colony formation and viability assays (Figure 1D and S1B).

We then proceeded to validate the novel screen hits. Two independent CRISPR/Cas9 constructs targeting the SMARCB1 gene (Figure 1E) rendered the cells more resistant to Doxo, both in colony formation and viability assays (Figure 1F and S1C).

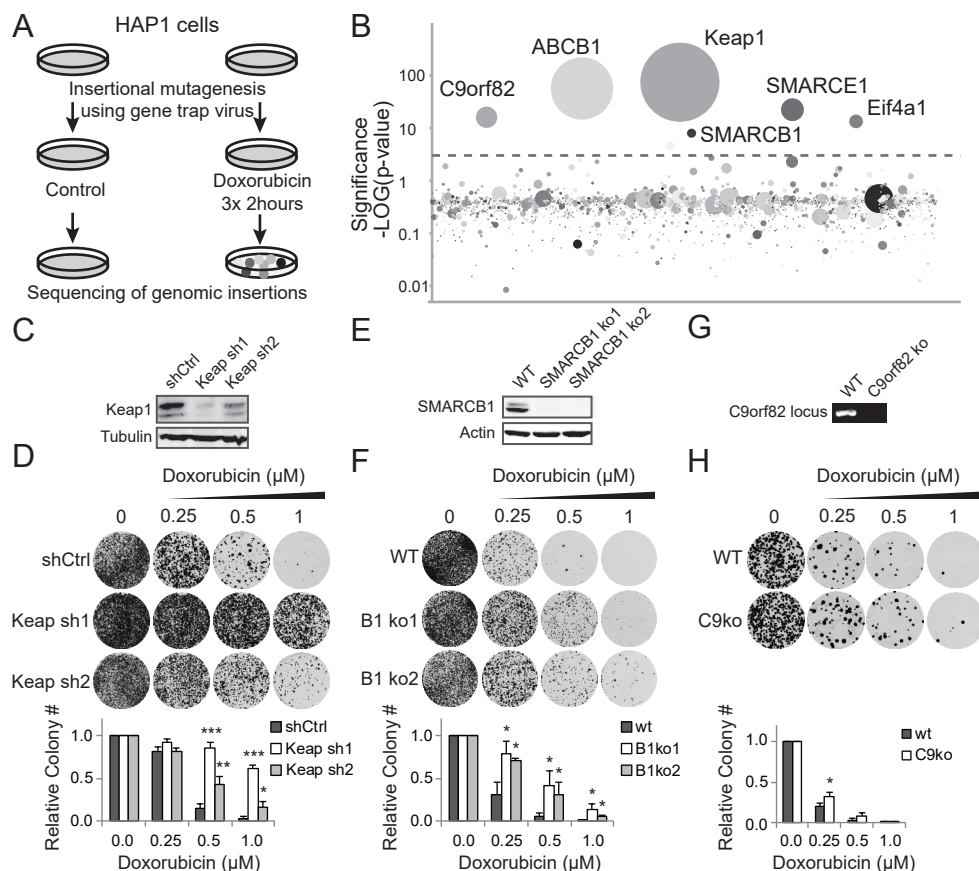


**Figure 1. Genome-wide mutagenesis screen identifies Keap1, the SWI/SNF complex and C9orf82 as regulators of doxorubicin resistance.** (A) Schematic set-up of the haploid genetics screen to identify genes involved in Doxo resistance. (B) Screening results. The y axis indicates the significance of enrichment of gene-trap insertions in Doxo-treated compared to non-treated control cells. The circles represent genes and their size corresponds to the number of independent insertions mapped in the gene. For more hits, see Table S1. (C) Keap1 silencing was determined by Western blotting analysis. (D) Long-term colony formation assay with HAP1 cells transduced with shRNAs targeting Keap1 or a control shRNA. Cells were treated with the indicated concentration Doxo for 2h and left to grow out. After 9 days, cells were fixed, stained and imaged. Quantification of colony numbers per plate and condition from three independent experiments ( $\pm$  SD) are shown below the images. (E) Western blotting showing depletion of SmarCB1 by two independent CRISPR-targeting sequences. (F) Long term colony formation assays for wild-type and SMARCB1-depleted cells. Results from three independent experiments ( $\pm$  SD) were quantified and are shown below the images. (G) Genomic PCR showing the knockout of C9orf82. (H) Long-term colony formation assay for wild-type and C9orf82-depleted cells. Results from three independent experiments ( $\pm$  SD) were quantified and are shown below the images. Statistical significance was calculated compared to control (\*  $p < 0.05$ , \*\*  $p < 0.01$ , \*\*\*  $p < 0.001$ ).

Independent identification of two members of the SWI/SNF chromatin-remodeling complex [18], SMARCB1 and SMARCE1, suggested that deregulation of the complex as a whole may drive resistance to Doxo. Although we could not validate a role

for SMARCE1 in resistance to Doxo, shRNA-mediated depletion of the SWI/SNF core members SMARCA4 and ARID1A, alongside SMARCB1, induced resistance to Doxo (Figure S1D and S1E), supporting the notion that loss of the SWI/SNF complex functionality confers resistance to Doxo.

While we did not further pursue the translational elongation complex subunit Eif4a1, we tested the contribution of the open reading frame 82 on chromosome 9 (C9orf82) to Doxo sensitivity. A small but significant growth advantage was observed in response to Doxo treatment in C9orf82 knockout cells using a colony formation assay (Figure 1G and 1H). Collectively, our genome-wide screen identified multiple novel factors capable of incurring resistance to Doxo in a cell culture setting.

### Cross-resistance to other DNA-damaging drugs

Doxo is known to act on cells by a combination of Topo II poisoning, eviction of histones from the chromatin and the generation of reactive oxygen species (ROS) [3, 4, 19]. To establish which of these mechanisms are affected by Keap1, the SWI/SNF complex and C9orf82, we treated the respective knockdown or knockout cell lines with either the different Topo II poisons daunorubicin (Daun; an anthracycline with a structure and activity similar to Doxo) or etoposide (Etop; a Topo II poison structurally unrelated to Doxo and incapable of evicting histones), or with aclarubicin (Acla; an anthracycline family member that evicts histones, induces ROS and inhibits Topo II but does not induce DNA damage [20]). Silencing Keap1 or eliminating SMARCB1 or C9orf82 rendered cells more resistant to both Etop and Daun, but not Acla (Figure 2A-2C) as indicated by viability as well as colony formation assays. Given the properties of the three drugs, these observations provide hints as to the molecular mechanisms underlying Doxo resistance via these genes – through the DNA damage arm. Interestingly, C9orf82 depletion rendered cells more resistant to Etop than to Doxo or Daun, suggesting that fast DNA repair may be critical for this gene's mode of action, as Doxo and Daun attenuate DNA repair by eviction of H2AX [5].

Importantly, depletion of none of our hits induced measurable resistance to the topoisomerase I poison topotecan (TPT) that induces single-strand DNA breaks (Figure 2C and 2D), suggesting that Keap1, the SWI/SNF complex and C9orf82 are involved in the Topo II-dependent DDR pathway.

### Keap1 controls the expression of Topo IIa independently of Nrf2

Of the three validated resistance factors from the screen, Keap1 has been previously linked to chemoresistance [11, 16, 21]. Keap1 functions as an E3 ligase adaptor and is known to mediate the degradation of Nrf2, a transcription factor for oxidative stress response genes [22]. Upregulation of Nrf2 desensitizes cells to several anti-cancer drugs, including alkylating and anti-mitotic agents, which suggests that downregulation of Keap1 may induce drug resistance by stabilizing Nrf2 [12, 16, 17]. To test this, we used CRISPR/Cas9 technology to generate Nrf2 knockout cells (Figure 3A), functionally validated by a drastic reduction of expression of Nrf2 target gene NQO1 (Figure S2A). Unexpectedly, silencing of Keap1 in the Nrf2 null background still endowed cells more resistance to Doxo and Etop (Figure 3A), implying the existence of an Nrf2-independent mechanism for Keap1 in modulating cellular responsiveness to Topo II dependent DNA-damage inducers.

Double-strand DNA break analysis indicated that loss of Keap1 significantly decreases the amount of such breaks induced by either Etop or Doxo treatment (Figure 3B). These results were corroborated by the observed reduction in the DNA damage response as measured by  $\gamma$ -H2AX following exposure to Etop (Doxo evicts H2AX

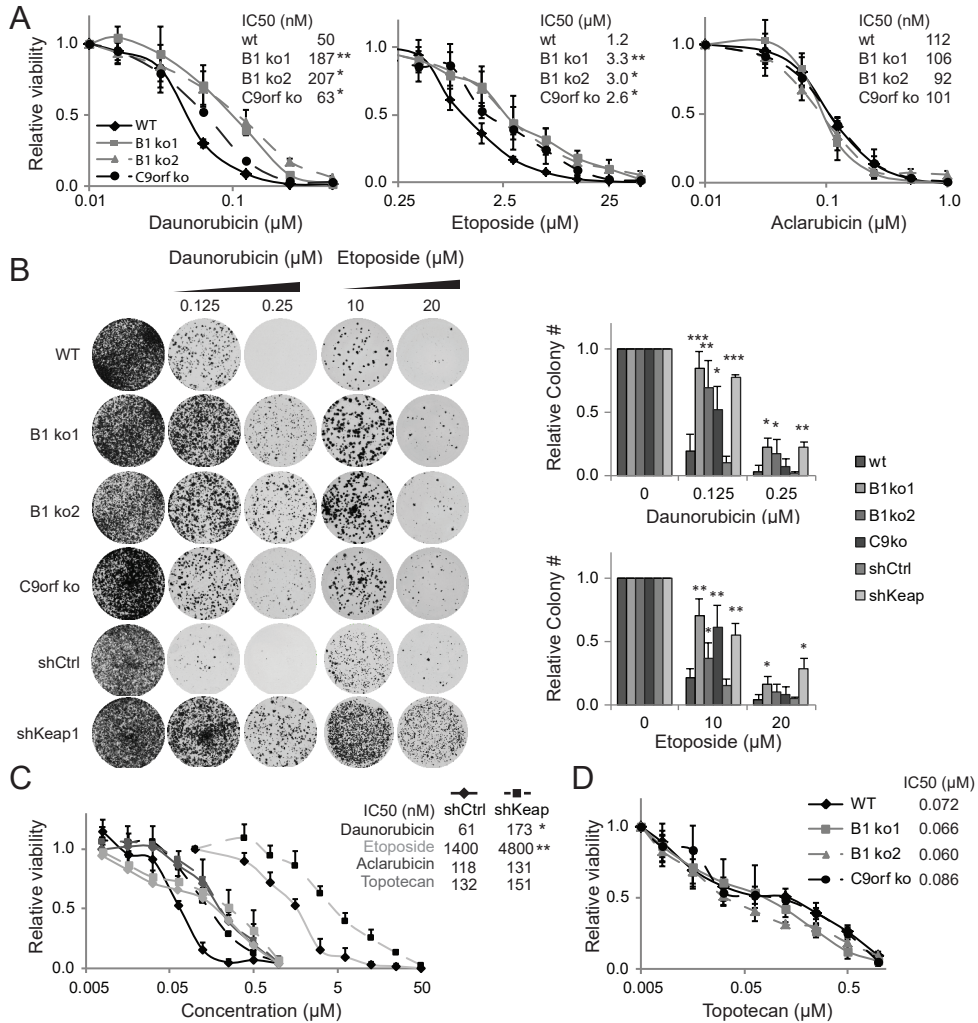


**Figure 2. Keap1, SWI/SNF and C9orf82 control to sensitivity to TopoII but not the TopoI inhibitor or Acla.** (A) HAP1 cells depleted for SMARCB1 or C9orf82 were treated for 2h with Daun, Etop or Acla and cell viability was analyzed 72h later by a cell titer blue (CTB) assay. (B) Long term colony formation assay with HAP1 cells depleted for SMARCB1, C9orf82 or Keap1 that were treated for 2h with the indicated drug at different concentrations. (C) HAP1 cells stably expressing shCtrl or shKeap1 were treated for 2h with Daun, Etop, Acla or topotecan and cell viability was analyzed 72h later by a CTB assay. (D) HAP1 cells depleted for SMARCB1 or C9orf82 were treated for 2h with TPT and cell viability was analyzed 72h later by a CTB assay. All experiments shown are representatives of at least three independent experiments. Statistical significance was calculated as compared to control cells (\*  $p < 0.05$ , \*\*  $p < 0.01$ , \*\*\*  $p < 0.001$ ).

from the DNA and was therefore not used to measure the DDR after drug exposure) (Figure 3C). Keap1 silencing did not affect uptake of Doxo (monitored by intrinsic fluorescence of the drug by flow cytometry, Figure 3D), suggesting that Keap1 may control either the levels or activity of the drug target, Topo II $\alpha$ . Cells depleted of



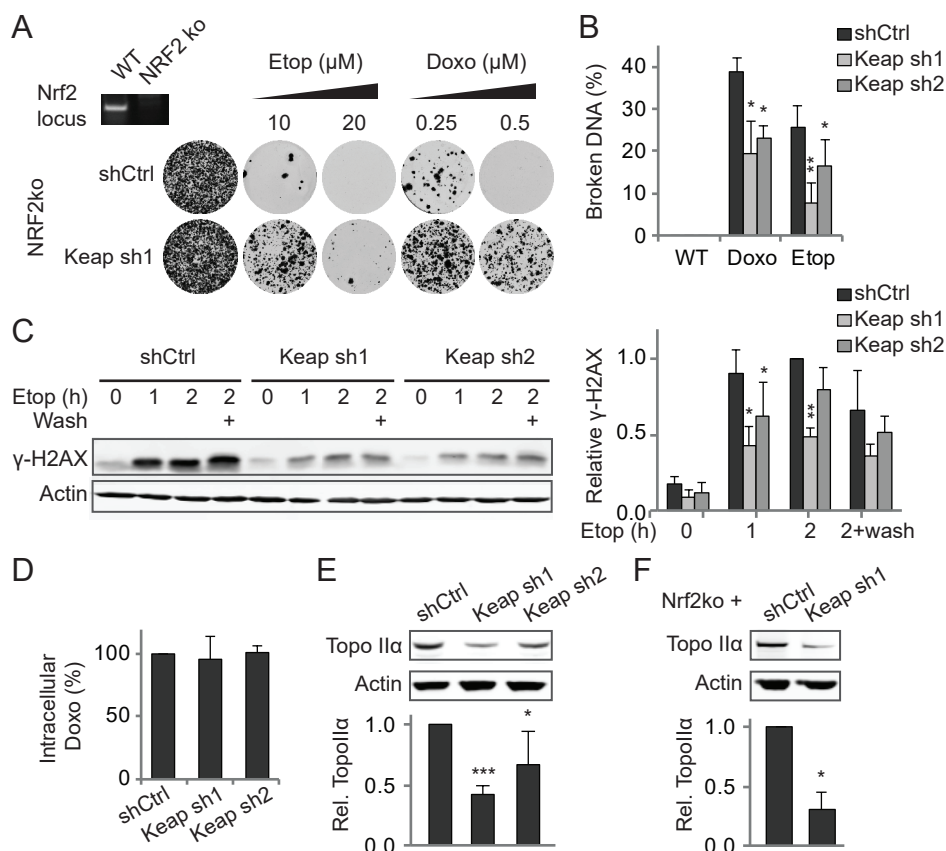


**Figure 3. Keap1 controls Topo IIα expression independently of Nrf2.** (A) Long-term colony growth assay for HAP1 cells depleted for Nrf2 and further stably transduced with shKeap1 or shCtrl. Cells were treated for 2h with Doxo or Etop at the indicated concentrations and left to grow out for 9 days. Insert: the DNA gel shows loss of the genomic Nrf2 locus in the knock-out cells. (B) Analysis of the amount of Etop- or Doxo-induced DNA breaks using constant field gel electrophoresis. HAP1 cells were treated for 2h with 1μM Etop or Doxo, lysed and analyzed. Shown is the quantification of the broken DNA relative to input. (C) HAP1 cells were treated with 5μM Etop for the indicated time points, or the drug was washed out after 2h and cells were left to recover for another 2h (lanes '+'), lysed and analyzed by SDS-PAGE and Western blotting. Right: quantification of the γ-H2AX signal normalized to actin. The signal of wild-type cells treated for 2h was set at 1. (D) Cells were treated with 2μM Doxo for 1h and Doxo levels were analyzed using flow cytometry. Control shRNA was set at 1. (E) Western blotting analysis for expression of Topo IIα in HAP1 cells silenced for Keap1. For quantification, the signal is normalized to actin and the shCtrl was set at 1. (F) Western blotting analysis for expression of Topo IIα in HAP1 Nrf2ko cells stably depleted or not for Keap1. All results are mean ± SD of biological triplicates, except for (E), which are biological quadruplicates. Statistical significance was calculated compared to control (\*  $p < 0.05$ , \*\*  $p < 0.01$ , \*\*\*  $p < 0.001$ ).

Keap1 had lower Topo IIα expression levels relative to the control (Figure 3E), which was independent of Nrf2 activity (Figure 3F). A link between Topo IIα expression levels and resistance against Topo II poisons has been previously suggested [7, 23, 24]. These observations indicate that Keap1 can control resistance to Topo II poisons by two distinct mechanisms—regulating Nrf2 expression to control a series

of stress-response genes and by mediating the expression of the canonical target Topo II $\alpha$ .

### C9orf82 regulates repair of DNA damage induced by TopoII poisons

By contrast to the previously studied role of Keap1 in drug resistance, the role of C9orf82 in this context has not been addressed, with its only function thus far assigned being negative regulation of apoptosis [25]. We began by addressing the effect of this gene on Topo II induced DSB formation and repair as pertaining to Topo II function. Monitoring the DNA DSBs and the resulting DNA damage response following exposure to either Doxo or Etop revealed no difference in the initial levels of DNA damage incurred between the control and C9orf82 knockout cells (Figure 4A and 4B). Strikingly, the resolution of the DNA damage response signal following Etop treatment (as visualized by  $\gamma$ -H2AX) was significantly accelerated in C9orf82 knockout cells (Figure 4B). Similar results were obtained with another independently

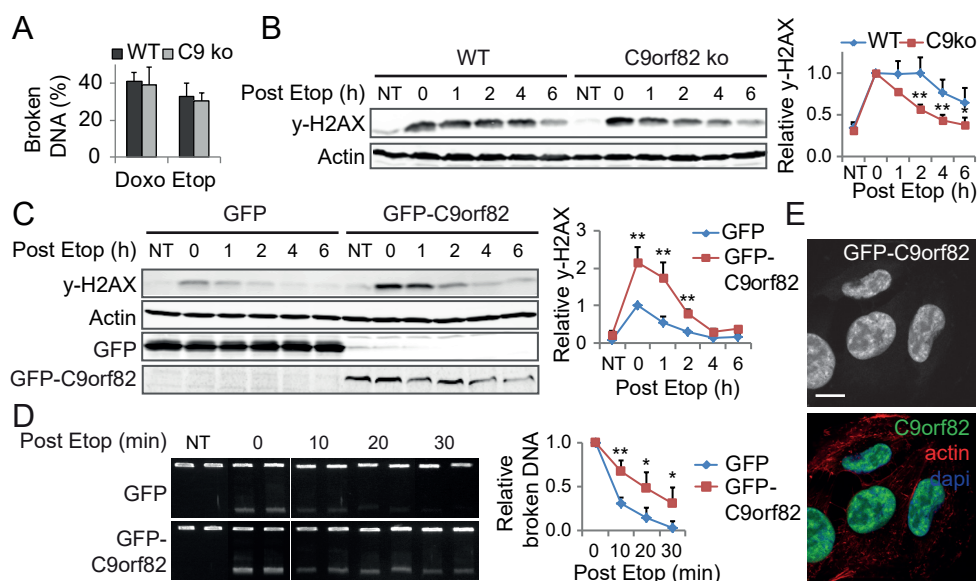


**Figure 4. C9orf82 regulates DNA double-strand break repair.** (A) Analysis of the amount of Etop- or Doxo-induced DNA breaks using constant field gel electrophoresis. HAP1 cells were treated for 2h with 1  $\mu$ M Etop or Doxo, lysed and analyzed. Shown is the quantification of broken DNA relative to input. (B) Western blotting analysis for  $\gamma$ -H2AX. Cells were treated with 1  $\mu$ M Etop for 1h, washed and lysed at the indicated time points. Right panel: quantification of the signals detected on the WB. Signals were normalized to actin and t=0 was set at 1. (C) GFP or GFP-C9orf82 over-expressing MelJuSo cells were exposed to 5  $\mu$ M Etop and analyzed for  $\gamma$ -H2AX as in (B). (D) MelJuSo cells stably over-expressing GFP or GFP-C9orf82 were treated with 1  $\mu$ M Etop for 2h. Drugs were removed before further culture. Cells were lysed at the indicated time points post drug removal. DNA break repair was analyzed using constant field gel electrophoresis. Lower band represents the broken DNA and the top band the intact DNA. Separate panels are different cut-outs from the same gel. For quantification, t=0 of the GFP or GFP-C9orf82 cells was set at 1. (E) Cellular localization of C9orf82 by confocal imaging of MelJuSo cells stably expressing GFP-C9orf82 and stained for DAPI (blue) and actin (red). Scale bar: 10  $\mu$ m. All experiments shown are mean  $\pm$  SD of three independent experiments. Statistical significance compared to control (\*  $p < 0.05$ , \*\*  $p < 0.01$ ). NT = non-treated.



generated C9orf82 knockout clone (Figure S3A-C). Conversely, ectopic expression of GFP-tagged C9orf82 in MelJuSo melanoma cells (a cell line with fast DNA repair kinetics) led to a stronger and more persistent  $\gamma$ -H2AX DNA damage response upon Etop treatment (Figure 4C). Since DNA repair already takes place during the first hour of Etop treatment, these data indicate that C9orf82 influences the kinetics of  $\gamma$ -H2AX resolution and hereby the DNA damage response. To assess whether C9orf82 regulates DSB repair itself, we determined the DSB repair kinetics in cells overexpressing either GFP or GFP-C9orf82 (Figure 4D), with the latter resulting in decreased Etop-induced DNA DSB repair. This suggests that C9orf82 decreases the rate of DNA repair.

Although C9orf82 localizes primarily in the nucleus (Figure 4E), it is unlikely to directly inhibit DNA repair, since it is not recruited to Etop-induced  $\gamma$ -H2AX foci (Figure S3D). On this basis, C9orf82 appears to attenuate DNA double-strand break repair induced by Topo II poisons, for its loss serves to accelerate DNA damage repair, thereby promoting resistance to DNA double-strand break inducers such as Doxo and Etop. The exact molecular mechanism of DNA repair modulation by this novel protein is at present unclear.

### **The SWI/SNF complex controls chromatin loading of Topo II to confer drug resistance**

In addition to the resistance factors described above, we also identified two subunits of the SWI/SNF complex involved in the resistance to Topo II poisons. The SWI/SNF complex is known to modulate transcription through chromatin remodeling [18]. Additionally, it has recently been shown to mediate decatenation of chromatids during mitosis by loading Topo II $\alpha$  onto the DNA [26]. The latter suggests a possible means by which the SWI/SNF complex may affect the susceptibility of cells to Topo II poisons, by reducing the chromatin loading and activity of Topo II $\alpha$ . To address this, HAP1 cells either proficient in or depleted of the SWI/SNF subunit SMARCB1 were exposed to Etop or Doxo, and the resulting DNA double-strand breaks were quantified. The SMARCB1-depleted cells exhibited significantly lower levels of such DNA breaks (Figure 5A), as well as reduced DNA damage response signaling, as visualized by  $\gamma$ -H2AX analysis (Figure 5B and 5C). These changes were not a result of drug uptake deficiency (Figure 5D) or altered expression levels of Topo II $\alpha$  (Figure 5E). Given that SMARCB1 interacts with Topo II $\alpha$  (Figure 5F) [26], the expected reduction in loading of Topo II $\alpha$  onto the DNA in cells compromised for SMARCB1 presents a likely explanation for the diminished efficacy of Topo II poisons in these cells. To confirm this, we assessed the association of Topo II $\alpha$  to the chromatin using a chromatin binding assay as described in [26]. Treatment of cells with Etop yielded more Topo II $\alpha$  loaded onto chromatin (Figure 4G), indicating this assay can be used to assess Topo II $\alpha$  activity and arrest. In line with our hypothesis, SMARCB1 depletion resulted in a decreased amount of Topo II $\alpha$  loaded onto chromatin after Etop exposure (Figure 4G), indicating that loss of SMARCB1 reduces the level of Topo II $\alpha$  that is poisoned on the chromatin. These results suggest that the SWI/SNF complex modulates resistance to TopoII poisons by controlling the loading of Topo II $\alpha$  onto the DNA.

### **Expression of SWI/SNF subunits in epithelioid sarcoma and triple negative breast cancers correlate to doxorubicin response**

Although mutations in the SWI/SNF members are frequently observed in human tumors [14], their relationship to clinical outcome is lacking. Epithelioid sarcomas

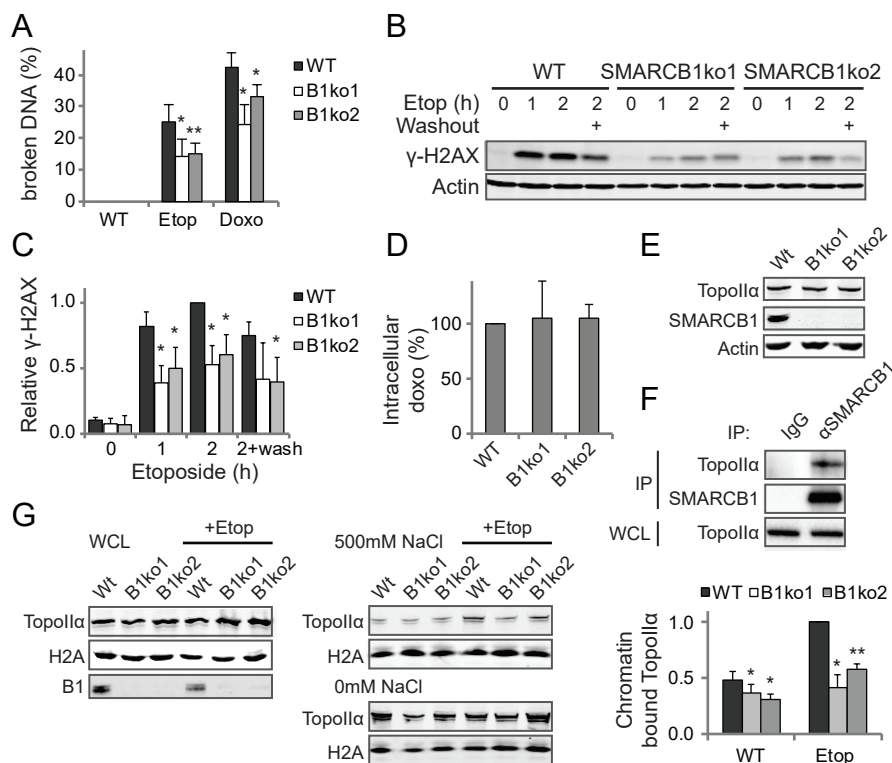


**Figure 5. The SWI/SNF complex regulates Topo IIα chromatin loading and activity.** (A) The amount of Etop- or Doxo-induced DNA breaks was quantified by constant field gel electrophoresis. HAP1 WT and SMARCB1 knockout cells were treated for 2h with 1μM Etop or Doxo. Shown is the quantification of the relative amount of broken DNA. (B) Western blot analysis for γ-H2AX after exposing cells to 5μM Etop for the indicated time points, or first treated for 2h and lysed 2h (lanes '+') after Etop removal. Actin is probed as a loading control. (C) Quantification of (B). The γ-H2AX signal is normalized to the actin signal and t=2 hours for WT is set at 1. (D) Quantification of Doxo uptake levels by flow cytometry. The different cells were incubated for 1h with 2μM Doxo before analysis. (E) Western blot analysis of Topo IIα expression levels in HAP1 cells either or not depleted for SMARCB1, as indicated. Actin is shown as loading control. (F) Co-immunoprecipitation (IP) of SMARCB1 and Topo IIα in HAP1 cells followed by SDS-PAGE and Western blotting. IgG IP is used as control. WCL: Topo II in total lysates are shown as loading control. (G) Chromatin association assay for TopoIIα. Chromatin pellets of indicated HAP1 cells untreated or treated with 1μM Etop for 15min were lysed directly (WCL), or treated with the indicated salt concentration (0mM or 500mM) before lysis. For quantification, the 500mM NaCl Topo IIα signal was corrected for loading (H2A) and WCL input signal. WT Etop 15 min was set at 1. All experiments shown are mean ± SD of independent triplicates. Statistical significance was calculated compared to control (\*  $p < 0.05$ , \*\*  $p < 0.01$ ).

are known to harbor deletions of the SMARCB1 gene in 60-90% of the cases [27, 28] and are commonly treated with Doxo-containing regimens. Re-analysis of a previously reported dataset [28] revealed that patients with a deletion for SMARCB1 experienced more relapses after treatment (Figure 6A), suggesting a relationship between SMARCB1 expression and treatment outcome. To further assess whether SWI/SNF status correlates directly with patient responses to treatment with Topo II

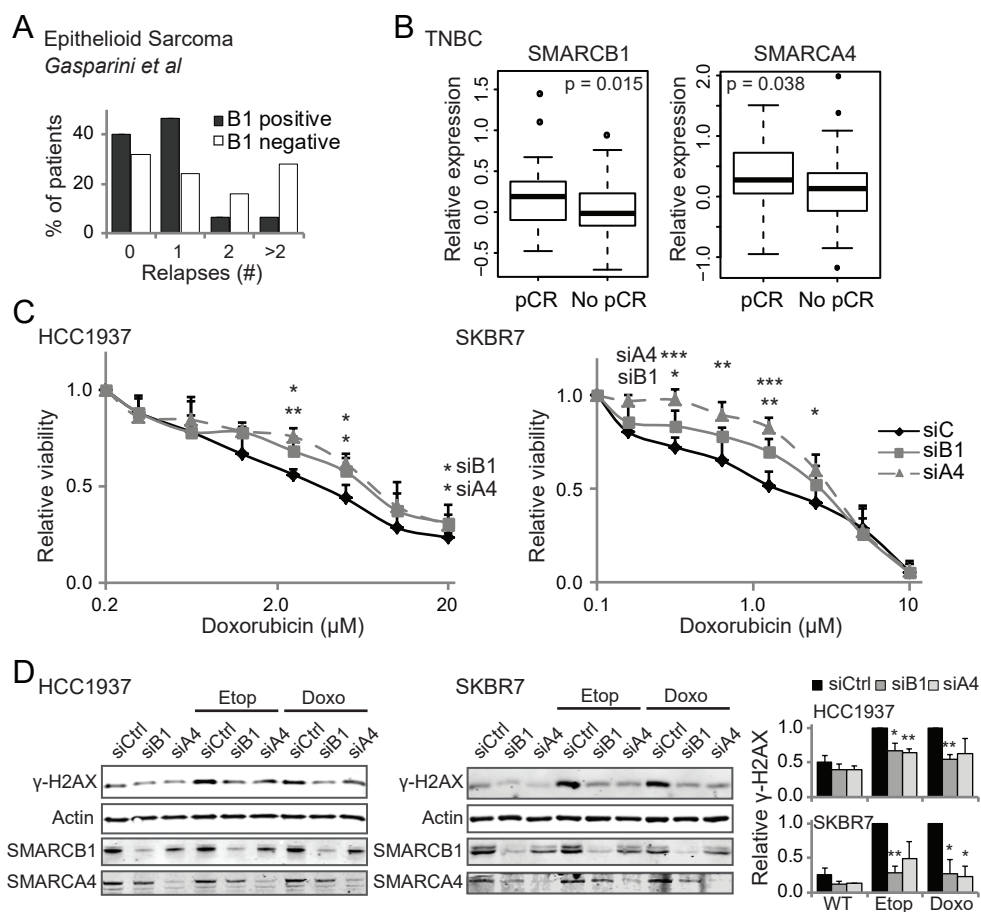


**Figure 6. SMARCB1 and SMARCA4 expression correlates to responses to Doxo in triple negative breast cancer cells and patients.** (A) Re-analysis of the number of relapses in 25 SMARCB1 negative and 15 SMARCB1 positive epithelioid sarcoma patients, as described in [28]. (B) Box plot representing the expression of SMARCB1 and SMARCA4 in 113 triple-negative breast cancer patients with a pathological complete response (pCR, 46 patients) or not (no pCR, 67 patients) following a Doxo containing regimen. Statistical significance was calculated using a Student's T-test. (C) HCC1937 or SKBR7 cells were transfected with control siRNAs or siRNAs targeting SMARCB1 or SMARCA4. 72h after transfection, cells were treated with the indicated doses of Doxo for 2h and cell viability was analyzed 72h after drug exposure. (D) HCC1937 or SKBR7 cells were transfected with siRNAs as in (C) and treated 72h later with 5 $\mu\text{M}$  Etop or Doxo for 1h, lysed and analyzed with SDS-PAGE and western blotting analysis. Quantifications in (C-D) are mean  $\pm$  SD of independent triplicate experiments. Statistical significance was calculated compared to control (\*  $p < 0.05$ , \*\*  $p < 0.01$ , \*\*\*  $p < 0.001$ ).

poisons, we used an expression dataset of 116 human triple-negative breast cancer (TNBC) patients treated at our cancer center with a regimen of Doxo and cyclophosphamide. We compared the expression of the SWI/SNF complex subunits SMARCB1, SMARCA4, SMARCE1 and ARID1a with the clinical response to this treatment. Our analysis showed that patients with a pathological complete response had a significantly higher expression of SMARCB1 and SMARCA4 (Figure 6B), but

not ARID1a or SMARCE1 (Figure S4A). Furthermore, by analyzing the other genes identified from the screen, we found a significant correlation between response and expression for Keap1, but not C9orf82 (Figure S4A). These data suggest that in triple-negative breast cancer patients, low expression of SMARCB1 and SMARCA4 is associated with poor response to a Doxo-containing regimen.

To validate that SMARCB1 and SMARCA4 causally regulate sensitivity to Doxo in TNBC settings, we silenced both genes in two TNBC cell lines, HCC1937 and SKBR7 (Keap1 silencing was toxic for these cells and could not be tested). Silencing of both genes rendered cells more resistant to Doxo (Figure 6C) and led to a reduced induction of DNA damage signaling (Figure 6D). Taken together, loss or reduced expression of SMARCB1 and SMARCA4 negatively impacts Doxo-induced DNA double-strand break formation and leads to drug resistance in triple negative breast cancer cell lines and patients.

## DISCUSSION

Annually, nearly 1 million cancer patients are treated with Topo II poisons such as Doxo, Daun or Etop. Yet, resistance to these drugs persists as a major complication in cancer treatment. Because the molecular basis for this resistance is not fully understood, many patients receive ineffective treatments accompanied by adverse side effects in the absence of the corresponding clinical benefit [1]. To facilitate treatment outcome predictions for Doxo relative to other available alternative drugs, improved insights into the mechanisms of drug resistance are necessary. Using a genome-wide screening approach, we identified and characterized several novel factors involved in resistance to Topo II poisons. In addition to the previously described factors, including the drug transporter ABCB1 and adaptor Keap1, we identified C9orf82 and the SWI/SNF complex as novel regulators of Doxo resistance. Keap1, C9orf82 and SWI/SNF can all be placed in the pathway involving Topo II-induced DNA double-strand break formation and the subsequent DDR (Figure 7). Consequently, depletion

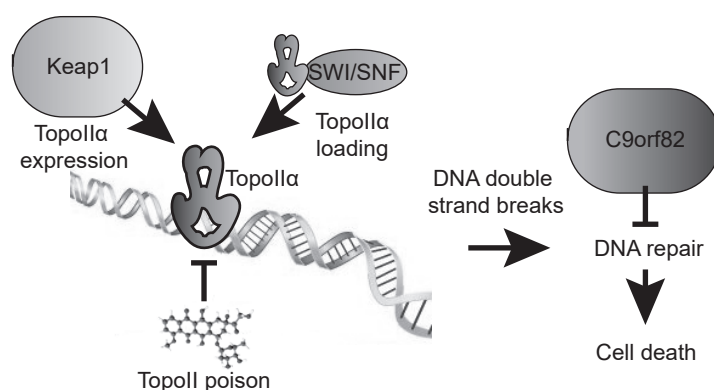


**Figure 7. Model of SWI/SNF, Keap1 and C9orf82 regulating different phases of Topo II poison-induced DNA break formation and DDR.** *Topo II poisons like Doxo induce DNA double-strand breaks by trapping Topo II on the DNA. If not sufficiently repaired, this leads to cell death. Keap1 controls the expression of Topo II $\alpha$ , while SWI/SNF regulates the loading and hereby activity of Topo II $\alpha$ . Loss of these genes therefore attenuates DNA double-strand break formation by Topo II poisons. In the next phase of the DNA breaks and repair cycle, C9orf82 controls DNA repair. Loss of C9orf82 accelerates DNA repair, reducing cell death induced by Topo II poisons.*

of these genes does not confer resistance to either the Topo I inhibitor TPT, or Acla, an anthracycline that does not induce DNA double-strand breaks [3].

Keap1 has already been studied in the context of chemosensitivity to several classes of anti-cancer drugs, including alkylating agents, anti-mitotic agents and Topo II poisons [11, 17, 21]. Inhibition of its cognate substrate Nrf2 sensitizes cells to a number of these drugs, suggesting that Keap1 influences sensitivity by virtue of Nrf2 destabilization [11, 17]. However, Keap1 controls several other signaling pathways [29-31], and could thus affect drug resistance in other ways. We interrogated these two options by depleting Nrf2 and found that besides from regulating Nrf2, Keap1 induces resistance to Topo II poisons by controlling the expression levels of Topo II $\alpha$ . Clinically, we show that the expression of Keap1 is correlated to the response of triple negative breast cancer patients to Doxo and cyclophosphamide. Keap1 inactivating mutations and deletions are frequently observed in human tumors [32, 33]. For example, 12-15% of lung tumors have inactivated Keap1 [32] and since these tumors are frequently treated with combinations of Etop and cisplatin, it may be beneficial to determine patients' Keap1 mutational status to assess the proper treatment protocol. We also defined C9orf82 as a novel factor involved in resistance to Topo II poisons, most notably Etop. A previous study has identified C9orf82 as a negative regulator of caspase-mediated apoptosis [25], which is not in line with our observations that C9orf82 depletion desensitizes cells to Etop. Our data indicate that C9orf82 is a nuclear protein that controls the rate of DNA double-strand break repair after exposure to Topo II poisons. Doxo itself slows down DNA repair, which might explain why the resistance is most prominent following Etop exposure. Given that most Etop-induced DNA double-strand breaks are repaired by non-homologous end-joining (NHEJ) [34], C9orf82 may impinge on this arm of the DNA repair pathway, but how is currently unclear. C9orf82 is found mutated in 7-11% of glioblastoma tumors [13, 35], which makes it a potential prognostic factor in the treatment of such patients with Etop. However, further studies integrating clinical response data with mutational analyses are required to substantiate this possibility.

Besides this relatively unknown protein, we characterized the role of the SWI/SNF complex in the resistance to Topo II poisons. The SWI/SNF complex is mutated in around 20% of human tumors [14] and has been linked to tumor suppression [26]. SWI/SNF complex subunits like SMARCB1 control the loading of Topo II $\alpha$  onto the DNA and hereby determine the extent of DNA damage induced following exposure to Topo II poisons. SMARCB1 depleted cells therefore have less DNA breaks when exposed to Topo II poisons and thus a growth advantage. As many of the tumors that harbor mutations in the SWI/SNF complex are treated with Topo II poisons, drug-resistance could arise even when Topo II $\alpha$  is expressed.

Several lines of evidence support this notion in patients. For example, SMARCB1 is mutated in 90-100% of the rhabdoid tumors [36, 37], a very aggressive childhood tumor that is unresponsive to Doxo [38]. Also, epithelioid sarcoma patients harboring deletions for SMARCB1 have a higher chance of relapse following treatment protocols that usually includes Topo II poisons [28]. Furthermore, we explored a data set of triple negative breast cancer patients where both gene expression and treatment responses were documented. A correlation between treatment response and expression of SWI/SNF subunits SMARCB1 and SMARCA4 was observed within patients treated with Doxo and cyclophosphamide. No correlation was observed for SMARCE1 and ARID1a, which could be because SMARCE1 is not a part of the core complex essential for activity and ARID1a has redundancy with ARID1b [18], or because the expression of these factors is not the limiting factor for the complex



to function. Given the resistance to Doxo observed in our cell culture experiments, these data suggest that patients with low or depleted SWI/SNF expression should not be treated with Doxo, but rather with Acla or TPT, which are drugs that work through a different mechanism and that do not show any cross-resistance in our experiments.

In conclusion, we identified and characterized three factors controlling sensitivity to the frequently used anti-cancer drugs Doxo and Etop. Keap1, C9orf82 and the SWI/SNF chromatin remodeling complex all act by affecting DNA double-strand break formation or repair following exposure to these drugs. Mutations in these genes are frequently observed in human tumors and expected to yield tumors that are resistant to these drugs, as we show for triple negative breast cancer patients. Profiling patients for mutations in these genes can further stratify treatment options as non-responding patients can be selected for other treatments rather than given ineffective treatment containing Topo II poisons.

## **MATERIALS AND METHODS**

### **Cell culture and constructs**

HAP1 and MelJuSo cells were grown in IMDM supplemented with 8% FCS. SKBR7 and HCC1937 cells were grown in RPMI with 8% FCS. HAP1 cells were generated as described in [39], sequence verified during the screen and kept under low passage afterwards. MelJuSo cells were initially described in [40] and sequence verified in 2013 [3], since then identity was confirmed by staining for marker MHCII. HCC1937 cells were obtained from ATCC ([www.ATCC.org](http://www.ATCC.org)), where they were validated using STR profiling, and kept under low passage after receipt. SKBR7 cells were a kind gift from Klaas de Lint (Netherlands Cancer Institute, division of Molecular Carcinogenesis) and analyzed using STR profiling in 2015. Keap1 knockdown cells were generated by transduction with lentiviral vectors containing an shRNA sequence targeting Keap1. Keap1 sh1 targeted the 5'-GCGAATGATCACAGCAAT-GAA-3' sequence of Keap1 and Keap1 sh2 the 5'-CGGGAGTACATCTACATGCAT-3' sequence. Cells were maintained under puromycin (2.5 µg/ml) selection to generate stable knockdown cells. For GFP-C9orf82, the sequence of full length C9orf82 was cloned from an Image clone (#4648932) into the mGFP-C1 vector (Clontech) using the primers 5'-CCCAAAGCTTCCATGACGGGGAAAAAGTCCTC-3' and 5'-CCCAG-GTACCCTAGGCTGGCTTTTTTATATC-3'. MelJuSo cells were transfected using effectene (Qiagen) and cells expressing GFP or GFP-C9orf82 were maintained under continuous selection with G418 (200 µg/ml).

### **Haploid genetic screen**

The haploid genetics screen was performed as described [10]. In brief, gene trap virus was produced by transfecting the gene-trap plasmid together with packaging plasmids in HEK 293T cells. Virus was harvested, concentrated, and used to infect  $1 \times 10^8$  HAP1 cells. After brief passaging to allow for protein turnover, mutagenized cells were exposed to the doxorubicin regimen described below. Drug resistant cells were expanded, genomic DNA was isolated and subsequently retroviral insertion sites were amplified by inverse PCR and mapped by parallel sequencing (Illumina HiSeq2000) of the genomic inserts. The enrichment of insertions in the drug-treated group was calculated by comparing the number of insertions between the doxorubicin-treated group and an unselected population [39] using a one-sided Fisher's exact test. These values were corrected for false discovery rate using the Benjamini and Hochberg method [10].

### Generation of null alleles using CRISPR-Cas9

CRISPR targeting sequences were designed based on the tool from [crispr.mit.edu](http://crispr.mit.edu) [41]. Oligo's were cloned into the pX330 backbone [42] and transfected using electroporation (Qiagen) together with a vector containing a guide RNA to the zebrafish TIA gene (5'-ggatgtcgggaacctctcc-3') and a blasticidin resistance gene with a 2A sequence that is flanked by two TIA target sites. Cells positive for both vectors excise the blasticidin resistance gene from the vector and will sporadically incorporate it into the targeted genomic locus by non-homologous end-joining [43]. Successful integration of the cassette into the targeted gene disrupts the allele and renders cells resistant to blasticidin. The targeting sequences were: SMARCB1: KO1, 5'-TG-GCGCTGAGCAAGACCTTC-3' and KO2, 5'-TGGCGCTGAGCAAGACCTTC-3', C9orf82: KO1, 5'-CAACGCGGGTACGATGTCCG-3' and KO2, 5'-TGACGGG-GAAAAAGTCCTCC-3', and Nrf2: 5'-TGGAGGCAAGATATAGATCT-3'. Cells were selected on blasticidin (10 µg/ml) for two days and knockout clones were validated by sequencing the genomic DNA. The following primers were used to detect deletion at the genomic level: SMARCB1 fw: 5'-CATTTGCGCTTCCGGCTTCGG-3', SMARCB1 rv: 5'-CTCGGAGCCGATCATGTAGAACTC-3', C9orf82 fw: 5'-GGAAGTGACG-CATAACCTGCGAC-3', C9orf82 rv: 5'-CTGCAAGGAGCCCCGAGACG-3', Nrf2 fw: 5'-GACATGGATTGATTGACATACTTTGGAGGC-3', Nrf2 rv: 5'-CTGACTGGAT-GTGCTGGGCTGG-3'.

### Reagents and siRNA transfections

Doxorubicin, etoposide and topotecan were obtained from Pharmachemie and daunorubicin was obtained from Sanofi-Aventis. Aclarubicin was obtained from Santa Cruz. Antibodies used for IP, Western blot and microscopy: mouse anti-Keap1, mouse anti-tubulin, mouse anti-actin (all from Sigma), rabbit anti-Topoisomerase II, rabbit anti-SMARCB1, rabbit anti-SmarcA4, rabbit anti-SMARCE1, rabbit anti-ARID1a (all from Bethyl laboratories), mouse anti-γH2AX, rabbit anti-H2A (Millipore). For siRNA mediated depletion of SMARCA4 and SMARCB1, cells were reverse transfected with DharmaFECT transfection reagent #1 and 50 nM siRNA (Human siGenome SMARTpool, Dharmacon) according to the manufacturing protocol. Briefly, siRNAs and DharmaFECT were mixed and incubated for 20 minutes, after which cells were added and left to adhere. Three days later, cells were treated and lysed for SDS-PAGE and Western blotting analysis or left to grow out for three more days for the cell viability assay.

### Long-term proliferation assays

Cells were seeded into 12-well plates (5000 cells per well). The next day, drugs were added at concentrations indicated and cultured for two hours. Subsequently, drugs were removed and cells were left to grow for 7-9 days, fixed using 3.7% formaldehyde and stained using 0.1% Crystal violet solution (Sigma). Quantification of colonies was done by Image J.

### Short-term growth inhibition assays

Cells were seeded into 96-well plates (2000 cells per well) and exposed the next day to the indicated drugs (for siRNA knockdowns, cells were seeded three days before treatment). Drugs were removed two hours later and cultured for an additional 72 hours. Cell viability was measured using the Cell Titer Blue viability assay (Promega). Relative survival was normalized to the untreated control and corrected for background signal.

**Co-immunoprecipitation and Western blotting**

For co-immunoprecipitation experiments of nuclear proteins, cells were trypsinized, counted and lysed (25mM HEPES pH7.6, 5mM MgCl<sub>2</sub>, 25mM KCl, 0.05mM EDTA, 10% glycerol and 0.1% NP-40 supplemented with complete EDTA-free Protease Inhibitor Cocktail (Roche)). Nuclei were isolated by spinning at 1,300 g and subsequently sonicated for 30 minutes in lysis buffer (50 mM Tris-HCl, pH8.0, 150mM NaCl, 0.1% NP-40 supplemented with Protease Inhibitor Cocktail (Roche)). Chromatin was removed by centrifugation (5 min at 12,000 g) and the supernatant was pre-cleared with protein G dynabeads (Life Technologies). Lysate was incubated overnight with 3µg antibody and 20µl protein G Dynabeads. Beads were washed extensively and re-suspended in SDS-sample buffer (2% SDS, 10% glycerol, 5% β-mercaptoethanol, 60mM Tris-HCl pH 6.8 and 0.01% bromophenol blue) before analysis by SDS-PAGE.

For whole cell lysate analyses, cells were lysed directly in SDS sample buffer (2% SDS, 10% glycerol, 5% β-mercaptoethanol, 60mM Tris-HCl pH 6.8 and 0.01% bromophenol blue). Samples were analyzed by SDS-PAGE and Western blotting. Blocking of the filter and antibody incubations were done in PBS supplemented with 0.1 (v/v)% Tween and 5% (w/v) bovine milk powder.

**Constant-field gel electrophoresis**

DNA double-strand breaks were quantified by constant-field gel electrophoresis as described [44]. In short, HAP1 cells were treated with Doxo or Etop for two hours. Drugs were removed and cells were lysed and processed immediately to isolate the DNA. Samples were separated on a 0.8% agarose gel to separate faster migrating broken DNA from intact DNA and fragments of over >1 MB. Images were analyzed by ImageJ.

**Flow cytometry**

Cells were treated with Doxo (2µM) for one hour and trypsinized and fixed with 3.7% formaldehyde. Fluorescence of Doxo was measured directly using a FACSCalibur flow cytometer (BD Bioscience) and further analyzed by FlowJo software.

**cDNA synthesis and qPCR**

RNA isolation, cDNA synthesis and quantitative RT-PCR were performed as described previously [45]. The primers for detection of Keap1, NQO1 and GAPDH expression were: Keap1 fw: 5'-CTGGAGGATCATACCAAGCAGG-3', Keap1 rv: 5'-GAACATGGCCTTGAAGACAGG-3', NQO1 fw: 5'-GGGCAAGTCCATCCCAACTG-3', NQO1 rv: 5'-GCAAGTCAGGGAAGCCTGGA-3', GAPDH fw: 5'-TGTTGCCATCAATGACCCTT-3', GAPDH rv: 5'-CTCCACGACGTACTCAGCG-3'.

**Confocal microscopy**

MelJuSo cells were seeded on coverslips and treated as indicated in the respective experiments. Cells were fixed in 3.7% formaldehyde for 10 min and permeabilized by 0.1% Triton X-100. Staining was performed with the antibodies mentioned above or with phalloidin (Invitrogen) to stain F-actin and DAPI (Invitrogen) to stain DNA. Images were acquired using a Leica TCS SP5 confocal microscope.

**Chromatin association assay**

HAP1 cells were seeded and treated with Etop for 15 min before lysis when indicated. Cells were lysed in lysis buffer (25 mM HEPES pH7.6, 5mM MgCl<sub>2</sub>, 25mM



KCl, 0.05mM EDTA, 10% glycerol, 0.1% NP-40) and nuclei were spun down and re-suspended at a concentration of 60 million/ml in buffer (20mM Tris-HCl pH 7.6, 3mM EDTA). 25ul samples were adjusted to the indicated NaCl concentrations to a total volume of 50ul. After mixing and incubation on ice for 20 min, chromatin was spun down and re-suspended in sample buffer. After sonication, samples were analyzed by SDS-PAGE and Western blotting.

### Gene expression analysis of the neoadjuvant breast cancer cohort

Gene expression data was obtained from 113 pre-treatment biopsies of triple negative breast cancer patients treated at the Antoni van Leeuwenhoek hospital (associated to the NKI) and scheduled to receive neoadjuvant chemotherapy. All patients had a breast carcinoma with either a primary tumor size of at least 3 cm, or the presence of axillary lymph node metastases. A treatment regimen was assigned to each patient, consisting of six courses of dose-dense doxorubicin/cyclophosphamide (ddAC). If the therapy response was considered unfavorable by MRI evaluation after three courses, ddAC was changed to capecitabine/docetaxel (XD). Response to therapy was defined as pathological complete response (pCR) or no pathological complete response at the time of surgery. 63 samples were labeled and hybridized to Illumina 6v3 arrays (Illumina, La Jolla, CA). Data were log2 transformed and between-array normalized using simple scaling. When a single gene was represented by multiple probes, the probe with the highest variance was chosen. The data is made available through the GEO database, accession GSE34138 (<http://www.ncbi.nlm.nih.gov/geo/query/acc.cgi?acc=GSE34138>) [46]. 50 samples were profiled using RNAseq. Strand-specific sequencing libraries were generated using the TruSeq Stranded mRNA sample preparation guide (Illumina Part # 15031047 Rev. E) according to the manufacturer's instructions. Deep Sequencing was done with a HiSeq2000 machine (Illumina Inc). The reads are mapped against the human reference (hg19) using Tophat (version 2.0.6) [47]. Tophat was supplied with a known set of genemodels using a GTF file (Ensembl version 66). HTSeq-count [48] was used to define gene expressions. This tool generates a list of the total number of uniquely mapped reads for each gene that was provided in the GTF. These data were normalized based on the relative library size using the DESeq2 R package [49] and subsequently log transformed.

### Statistical methods

All experiments were performed at least three times in an independent manner. All data are presented as means  $\pm$  SD. The results were analyzed by using a paired two-tailed Student's T-test (unpaired for the data in Figure 6B). Significance was calculated using Excel and defined as  $p < 0.05$ .

### ACKNOWLEDGMENTS

We thank the NKI Genomics Core Facility for help with the sequencing data and the NKI Flow Cytometry Facility and the NKI Digital Microscopy Facility for support. We thank Piet Borst and Ilana Berlin for critically reading the manuscript and Jelle Weseling and members of the Neefjes lab for fruitful discussions. This work was supported by the Institute for Chemical Immunology, an NWO Gravitation project funded by the Ministry of Education, Culture and Science of the government of the Netherlands. This work was further supported by grants from the Netherlands Organization of Scientific Research NWO and an ERC Advanced Grant.

## AUTHOR CONTRIBUTIONS

R.W., B.P., S.v.d.Z., X.Q. and J.N. designed and performed the experiments. V.B. and T.B. analyzed the screening data. M.H., E.L. and L.W. performed the expression analyses on the clinical samples. L.J. made constructs. R.W., B.P. and J.N. wrote the manuscript with input from all authors.

## REFERENCES

1. Pommier, Y. (2013) Drugging topoisomerases: lessons and challenges, *ACS chemical biology*. 8, 82-95.
2. Borst, P. (2012) Cancer drug pan-resistance: pumps, cancer stem cells, quiescence, epithelial to mesenchymal transition, blocked cell death pathways, persists or what?, *Open biology*. 2, 120066.
3. Pang, B., Qiao, X., Janssen, L., Velds, A., Groothuis, T., Kerkhoven, R., Nieuwland, M., Ovaa, H., Rottenberg, S., van Tellingen, O., Janssen, J., Huijgens, P., Zwart, W. & Neefjes, J. (2013) Drug-induced histone eviction from open chromatin contributes to the chemotherapeutic effects of doxorubicin, *Nat Commun*. 4, 1908.
4. Yang, F., Kemp, Christopher A. J. & Henikoff, S. (2013) Doxorubicin Enhances Nucleosome Turnover around Promoters, *Current Biology*. 23, 782-787.
5. Pang, B., de Jong, J., Qiao, X., Wessels, L. F. & Neefjes, J. (2015) Chemical profiling of the genome with anti-cancer drugs defines target specificities, *Nature chemical biology*.
6. Callaghan, R., Luk, F. & Bebaawy, M. (2014) Inhibition of the multidrug resistance P-glycoprotein: time for a change of strategy?, *Drug metabolism and disposition: the biological fate of chemicals*. 42, 623-31.
7. Burgess, D. J., Doles, J., Zender, L., Xue, W., Ma, B., McCombie, W. R., Hannon, G. J., Lowe, S. W. & Hemann, M. T. (2008) Topoisomerase levels determine chemotherapy response in vitro and in vivo, *Proceedings of the National Academy of Sciences of the United States of America*. 105, 9053-8.
8. Bouwman, P. & Jonkers, J. (2012) The effects of deregulated DNA damage signalling on cancer chemotherapy response and resistance, *Nature reviews Cancer*. 12, 587-98.
9. Zoppi, G., Regairaz, M., Leo, E., Reinhold, W. C., Varma, S., Ballestrero, A., Doroshow, J. H. & Pommier, Y. (2012) Putative DNA/RNA helicase Schlafen-11 (SLFN11) sensitizes cancer cells to DNA-damaging agents, *Proceedings of the National Academy of Sciences of the United States of America*. 109, 15030-5.
10. Carette, J. E., Guimaraes, C. P., Wuethrich, I., Blomen, V. A., Varadarajan, M., Sun, C., Bell, G., Yuan, B., Muellner, M. K., Nijman, S. M., Ploegh, H. L. & Brummelkamp, T. R. (2011) Global gene disruption in human cells to assign genes to phenotypes by deep sequencing, *Nature biotechnology*. 29, 542-6.
11. Shibata, T., Kokubu, A., Gotoh, M., Ojima, H., Ohta, T., Yamamoto, M. & Hirohashi, S. (2008) Genetic alteration of Keap1 confers constitutive Nrf2 activation and resistance to chemotherapy in gallbladder cancer, *Gastroenterology*. 135, 1358-1368.e1-4.
12. Singh, A., Misra, V., Thimmulappa, R. K., Lee, H., Ames, S., Hoque, M. O., Herman, J. G., Baylin, S. B., Sidransky, D., Gabrielson, E., Brock, M. V. & Biswal, S. (2006) Dysfunctional KEAP1-NRF2 interaction in non-small-cell lung cancer, *PLoS medicine*. 3, e420.
13. Network, C. G. A. R. (2008) Comprehensive genomic characterization defines human glioblastoma genes and core pathways, *Nature*. 455, 1061-8.

14. Kadoch, C., Hargreaves, D. C., Hodges, C., Elias, L., Ho, L., Ranish, J. & Crabtree, G. R. (2013) Proteomic and bioinformatic analysis of mammalian SWI/SNF complexes identifies extensive roles in human malignancy, *Nature genetics*. 45, 592-601.
15. Benjamin, R. S., Riggs, C. E., Jr. & Bachur, N. R. (1977) Plasma pharmacokinetics of adriamycin and its metabolites in humans with normal hepatic and renal function, *Cancer research*. 37, 1416-20.
16. Ohta, T., Iijima, K., Miyamoto, M., Nakahara, I., Tanaka, H., Ohtsui, M., Suzuki, T., Kobayashi, A., Yokota, J., Sakiyama, T., Shibata, T., Yamamoto, M. & Hirohashi, S. (2008) Loss of Keap1 function activates Nrf2 and provides advantages for lung cancer cell growth, *Cancer research*. 68, 1303-9.
17. Wang, X. J., Sun, Z., Villeneuve, N. F., Zhang, S., Zhao, F., Li, Y., Chen, W., Yi, X., Zheng, W., Wondrak, G. T., Wong, P. K. & Zhang, D. D. (2008) Nrf2 enhances resistance of cancer cells to chemotherapeutic drugs, the dark side of Nrf2, *Carcinogenesis*. 29, 1235-43.
18. Hohmann, A. F. & Vakoc, C. R. (2014) A rationale to target the SWI/SNF complex for cancer therapy, *Trends in genetics : TIG*. 30, 356-63.
19. Tsang, W. P., Chau, S. P., Kong, S. K., Fung, K. P. & Kwok, T. T. (2003) Reactive oxygen species mediate doxorubicin induced p53-independent apoptosis, *Life sciences*. 73, 2047-58.
20. Rogalska, A., Koceva-Chyla, A. & Jozwiak, Z. (2008) Aclarubicin-induced ROS generation and collapse of mitochondrial membrane potential in human cancer cell lines, *Chemico-biological interactions*. 176, 58-70.
21. Konstantinopoulos, P. A., Spentzos, D., Fountzilas, E., Francoeur, N., Sanisetty, S., Grammatikos, A. P., Hecht, J. L. & Cannistra, S. A. (2011) Keap1 mutations and Nrf2 pathway activation in epithelial ovarian cancer, *Cancer research*. 71, 5081-9.
22. Sporn, M. B. & Liby, K. T. (2012) NRF2 and cancer: the good, the bad and the importance of context, *Nature reviews Cancer*. 12, 564-71.
23. Miyoshi, Y., Kurosumi, M., Kurebayashi, J., Matsuura, N., Takahashi, M., Tokunaga, E., Egawa, C., Masuda, N., Kono, S., Morimoto, K., Kim, S. J., Okishiro, M., Yanagisawa, T., Ueda, S., Taguchi, T., Tamaki, Y. & Noguchi, S. (2010) Predictive factors for anthracycline-based chemotherapy for human breast cancer, *Breast cancer (Tokyo, Japan)*. 17, 103-9.
24. Sinha, B. K., Haim, N., Dusre, L., Kerrigan, D. & Pommier, Y. (1988) DNA strand breaks produced by etoposide (VP-16,213) in sensitive and resistant human breast tumor cells: implications for the mechanism of action, *Cancer research*. 48, 5096-100.
25. Zhang, Y., Johansson, E., Miller, M. L., Janicke, R. U., Ferguson, D. J., Plas, D., Meller, J. & Anderson, M. W. (2011) Identification of a conserved anti-apoptotic protein that modulates the mitochondrial apoptosis pathway, *PloS one*. 6, e25284.
26. Dykhuizen, E. C., Hargreaves, D. C., Miller, E. L., Cui, K., Korshunov, A., Kool, M., Pfister, S., Cho, Y. J., Zhao, K. & Crabtree, G. R. (2013) BAF complexes facilitate decatenation of DNA by topoisomerase IIalpha, *Nature*. 497, 624-7.
27. Hornick, J. L., Dal Cin, P. & Fletcher, C. D. (2009) Loss of INI1 expression is characteristic of both conventional and proximal-type epithelioid sarcoma, *The American journal of surgical pathology*. 33, 542-50.
28. Gasparini, P., Facchinetti, F., Boeri, M., Lorenzetto, E., Livio, A., Gronchi, A., Ferrari, A., Massimino, M., Spreafico, F., Giangaspero, F., Forni, M., Maestro, R., Alaggio, R., Pilotti, S., Collini, P., Modena, P. & Sozzi, G. (2011) Prognostic determinants in epithelioid sarcoma, *European journal of cancer (Oxford, England : 1990)*.

47, 287-95.

29. Lee, D. F., Kuo, H. P., Liu, M., Chou, C. K., Xia, W., Du, Y., Shen, J., Chen, C. T., Huo, L., Hsu, M. C., Li, C. W., Ding, Q., Liao, T. L., Lai, C. C., Lin, A. C., Chang, Y. H., Tsai, S. F., Li, L. Y. & Hung, M. C. (2009) KEAP1 E3 ligase-mediated downregulation of NF-kappaB signaling by targeting IKKbeta, *Molecular cell*. 36, 131-40.

30. Fan, W., Tang, Z., Chen, D., Moughon, D., Ding, X., Chen, S., Zhu, M. & Zhong, Q. (2010) Keap1 facilitates p62-mediated ubiquitin aggregate clearance via autophagy, *Autophagy*. 6, 614-21.

31. Zhan, L., Zhang, H., Zhang, Q., Woods, C. G., Chen, Y., Xue, P., Dong, J., Tokar, E. J., Xu, Y., Hou, Y., Fu, J., Yarborough, K., Wang, A., Qu, W., Waalkes, M. P., Andersen, M. E. & Pi, J. (2012) Regulatory role of KEAP1 and NRF2 in PPAR-gamma expression and chemoresistance in human non-small-cell lung carcinoma cells, *Free radical biology & medicine*. 53, 758-68.

32. Lawrence, M. S., Stojanov, P., Mermel, C. H., Robinson, J. T., Garraway, L. A., Golub, T. R., Meyerson, M., Gabriel, S. B., Lander, E. S. & Getz, G. (2014) Discovery and saturation analysis of cancer genes across 21 tumour types, *Nature*. 505, 495-501.

33. Barbano, R., Muscarella, L. A., Pasculli, B., Valori, V. M., Fontana, A., Coco, M., la Torre, A., Balsamo, T., Poeta, M. L., Marangi, G. F., Maiello, E., Castelvete, M., Pellegrini, F., Murgo, R., Fazio, V. M. & Parrella, P. (2013) Aberrant Keap1 methylation in breast cancer and association with clinicopathological features, *Epigenetics : official journal of the DNA Methylation Society*. 8, 105-12.

34. Quennet, V., Beucher, A., Barton, O., Takeda, S. & Lobrich, M. (2011) CtIP and MRN promote non-homologous end-joining of etoposide-induced DNA double-strand breaks in G1, *Nucleic acids research*. 39, 2144-52.

35. Brennan, C. W., Verhaak, R. G., McKenna, A., Campos, B., Nounshmehr, H., Salama, S. R., Zheng, S., Chakravarty, D., Sanborn, J. Z., Berman, S. H., Beroukhi, R., Bernard, B., Wu, C. J., Genovese, G., Shmulevich, I., Barnholtz-Sloan, J., Zou, L., Vegesna, R., Shukla, S. A., Ciriello, G., Yung, W. K., Zhang, W., Sougnez, C., Mikkelsen, T., Aldape, K., Bigner, D. D., Van Meir, E. G., Prados, M., Sloan, A., Black, K. L., Eschbacher, J., Finocchiaro, G., Friedman, W., Andrews, D. W., Guha, A., Iacocca, M., O'Neill, B. P., Foltz, G., Myers, J., Weisenberger, D. J., Penny, R., Kucherlapati, R., Perou, C. M., Hayes, D. N., Gibbs, R., Marra, M., Mills, G. B., Lander, E., Spellman, P., Wilson, R., Sander, C., Weinstein, J., Meyerson, M., Gabriel, S., Laird, P. W., Haussler, D., Getz, G. & Chin, L. (2013) The somatic genomic landscape of glioblastoma, *Cell*. 155, 462-77.

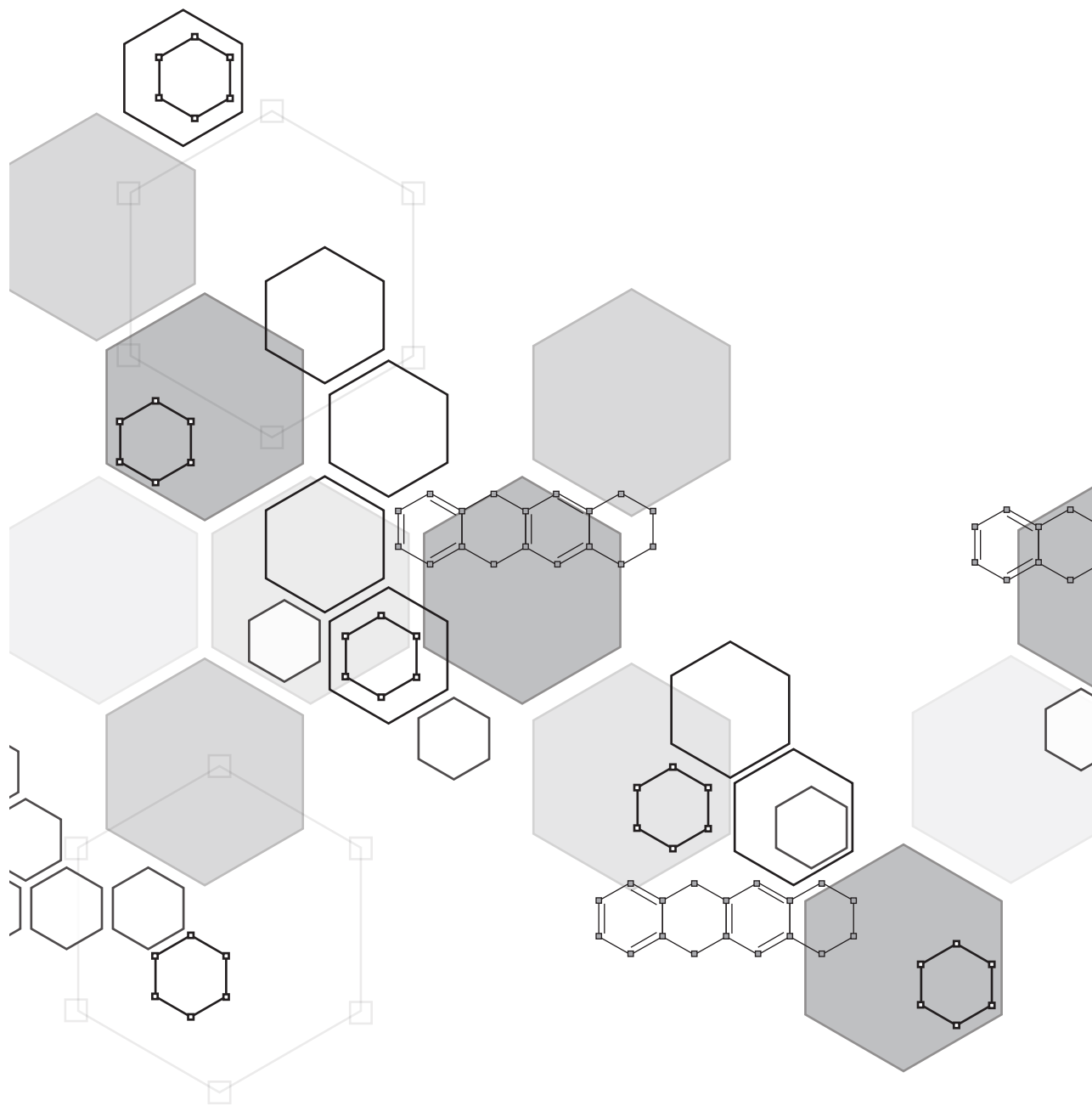
36. Versteeg, I., Sevenet, N., Lange, J., Rousseau-Merck, M. F., Ambros, P., Handgretinger, R., Aurias, A. & Delattre, O. (1998) Truncating mutations of hSNF5/INI1 in aggressive paediatric cancer, *Nature*. 394, 203-6.

37. Margol, A. S. & Judkins, A. R. (2014) Pathology and diagnosis of SMARCB1-deficient tumors, *Cancer genetics*.

38. Tomlinson, G. E., Breslow, N. E., Dome, J., Guthrie, K. A., Norkool, P., Li, S., Thomas, P. R., Perlman, E., Beckwith, J. B., D'Angio, G. J. & Green, D. M. (2005) Rhabdoid tumor of the kidney in the National Wilms' Tumor Study: age at diagnosis as a prognostic factor, *Journal of clinical oncology : official journal of the American Society of Clinical Oncology*. 23, 7641-5.

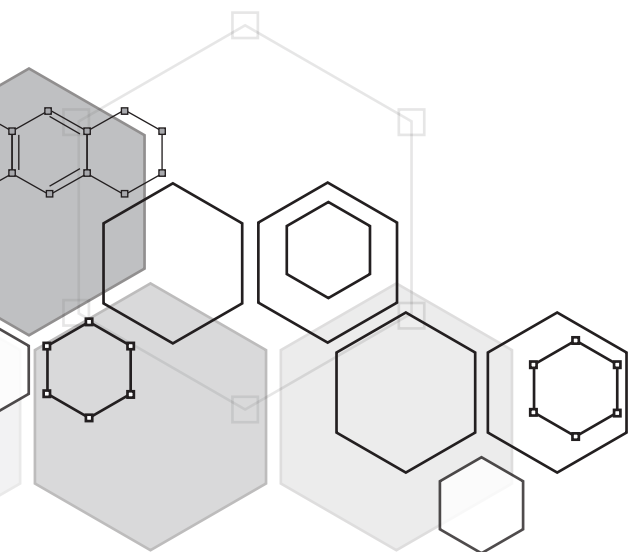
39. Carette, J. E., Raaben, M., Wong, A. C., Herbert, A. S., Obernosterer, G., Mulherkar, N., Kuehne, A. I., Kranzusch, P. J., Griffin, A. M., Ruthel, G., Dal Cin, P., Dye, J. M., Whelan, S. P., Chandran, K. & Brummelkamp, T. R. (2011) Ebola virus entry requires the cholesterol transporter Niemann-Pick C1, *Nature*. 477, 340-3.

40. Johnson, J. P., Demmer-Dieckmann, M., Meo, T., Hadam, M. R. & Riethmuller, G. (1981) Surface antigens of human melanoma cells defined by monoclonal antibodies. I. Biochemical characterization of two antigens found on cell lines and fresh tumors of diverse tissue origin, *European journal of immunology*. 11, 825-31.
41. Hsu, P. D., Scott, D. A., Weinstein, J. A., Ran, F. A., Konermann, S., Agarwala, V., Li, Y., Fine, E. J., Wu, X., Shalem, O., Cradick, T. J., Marraffini, L. A., Bao, G. & Zhang, F. (2013) DNA targeting specificity of RNA-guided Cas9 nucleases, *Nature biotechnology*. 31, 827-32.
42. Wang, H., Yang, H., Shivalila, C. S., Dawlaty, M. M., Cheng, A. W., Zhang, F. & Jaenisch, R. (2013) One-step generation of mice carrying mutations in multiple genes by CRISPR/Cas-mediated genome engineering, *Cell*. 153, 910-8.
43. Auer, T. O., Durore, K., De Cian, A., Concordet, J. P. & Del Bene, F. (2014) Highly efficient CRISPR/Cas9-mediated knock-in in zebrafish by homology-independent DNA repair, *Genome research*. 24, 142-53.
44. Neijenhuis, S., Verwijs-Janssen, M., Kasten-Pisula, U., Rumping, G., Borgmann, K., Dikomey, E., Begg, A. C. & Vens, C. (2009) Mechanism of cell killing after ionizing radiation by a dominant negative DNA polymerase beta, *DNA repair*. 8, 336-46.
45. Paul, P., van den Hoorn, T., Jongsma, M. L., Bakker, M. J., Hengeveld, R., Jansen, L., Cresswell, P., Egan, D. A., van Ham, M., Ten Brinke, A., Ovaa, H., Beijersbergen, R. L., Kuijl, C. & Neefjes, J. (2011) A Genome-wide multidimensional RNAi screen reveals pathways controlling MHC class II antigen presentation, *Cell*. 145, 268-83.
46. de Ronde, J. J., Lips, E. H., Mulder, L., Vincent, A. D., Wesseling, J., Nieuwland, M., Kerkhoven, R., Vrancken Peeters, M. J., Sonke, G. S., Rodenhuis, S. & Wessels, L. F. (2013) SERPINA6, BEX1, AGTR1, SLC26A3, and LAPTM4B are markers of resistance to neoadjuvant chemotherapy in HER2-negative breast cancer, *Breast cancer research and treatment*. 137, 213-23.
47. Trapnell, C., Pachter, L. & Salzberg, S. L. (2009) TopHat: discovering splice junctions with RNA-Seq, *Bioinformatics (Oxford, England)*. 25, 1105-11.
48. Anders, S., Pyl, P. T. & Huber, W. (2014) HTSeq-a Python framework to work with high-throughput sequencing data, *Bioinformatics (Oxford, England)*.
49. Love, M. I., Huber, W. & Anders, S. (2014) Moderated estimation of fold change and dispersion for RNA-Seq data with DESeq2.



# SUPPLEMENTAL INFORMATION

2





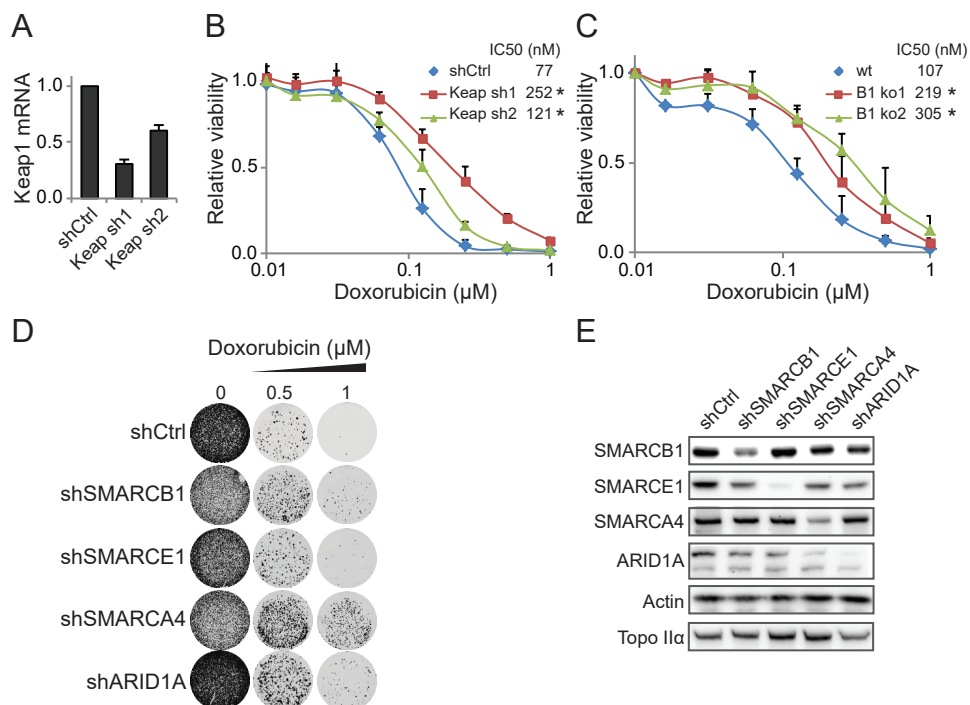


**Figure S1. Keap1, SMARCB1, SMARCA4 and ARID1A regulate resistance to doxorubicin.** (A) Silencing of Keap1 by shRNAs was measured by qPCR. Keap1 mRNA signal was normalized to GAPDH and shCtrl was set at 1. Shown is the mean  $\pm$  SD of biological triplicates. (B) Short term growth assay of Keap1-silenced cells incubated with Doxo for 2h at the indicated concentration. Cell viability was analyzed 72 hours after drug removal and extensive washing. Data shown are mean  $\pm$  SD of biological triplicate experiments. (C) Short-term growth assay as in (B) for wild-type and SmarCB1-depleted cells. Data shown are mean  $\pm$  SD of biological triplicate experiments. (D) HAP1 cells stably expressing shCtrl or shRNAs targeting SMARCB1, SMARCA4 or ARID1a were treated with Doxo for 2h at the indicated concentrations. Doxo was removed and cells were left to grow out. 9 days later, cells were fixed, stained and imaged. (E) Western blot analysis showing silencing of the respective SWI/SNF complex subunits. Actin is shown as the loading control.

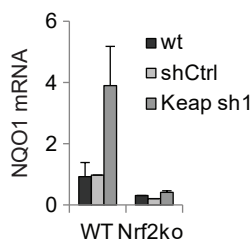


**Figure S2. Keap1 controls expression of NQO1 through Nrf2.** mRNA expression analysis of Nrf2 target gene NQO1 using qPCR in cells either or not expressing Nrf2. Expression of NQO1 was calculated relative to GAPDH and data were normalized to WT shCtrl. Results are mean  $\pm$  SD of biological triplicate experiments.



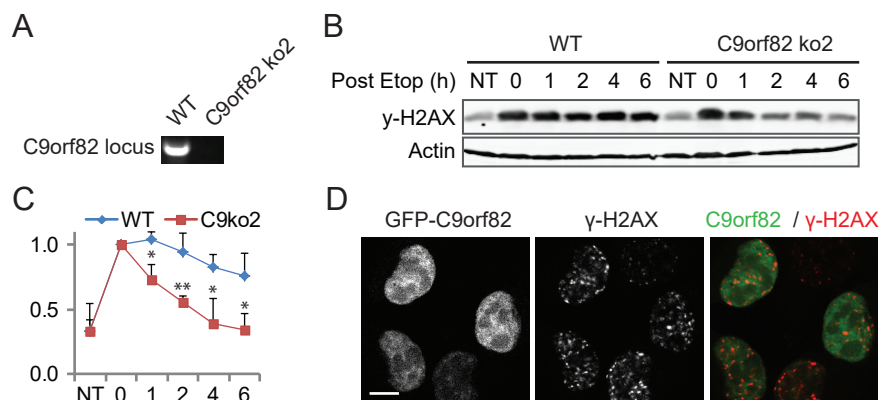


**Figure S3. C9orf82 regulates DNA double strand break repair.** (A) DNA gel showing loss of C9orf82 by targeting its locus with a second CRISPR guide RNA. (B) Cells with C9orf82 inactivated were treated with  $1\mu\text{M}$  Etop for 1hr, washed and lysed at the indicated time points post drug removal. Lysates were analyzed by SDS-PAGE and Western blotting analysis for  $\gamma\text{-H2AX}$  (upper panel) and actin as the loading control (lower panel). (C) quantification of the  $\gamma\text{-H2AX}$  signals from (B), normalized to actin.  $t=0$  was set at 1. Quantification was done from three independent experiments. For all time-points, shown are mean  $\pm$  SD. (D) MelJuSo cells expressing GFP-C9orf82 were treated for 1 hr with  $1\mu\text{M}$  Etop. Cells were fixed and stained for  $\gamma\text{-H2AX}$  before analyses by confocal laser scanning microscope. Bar:  $10\mu\text{m}$ . NT are non-treated cells.

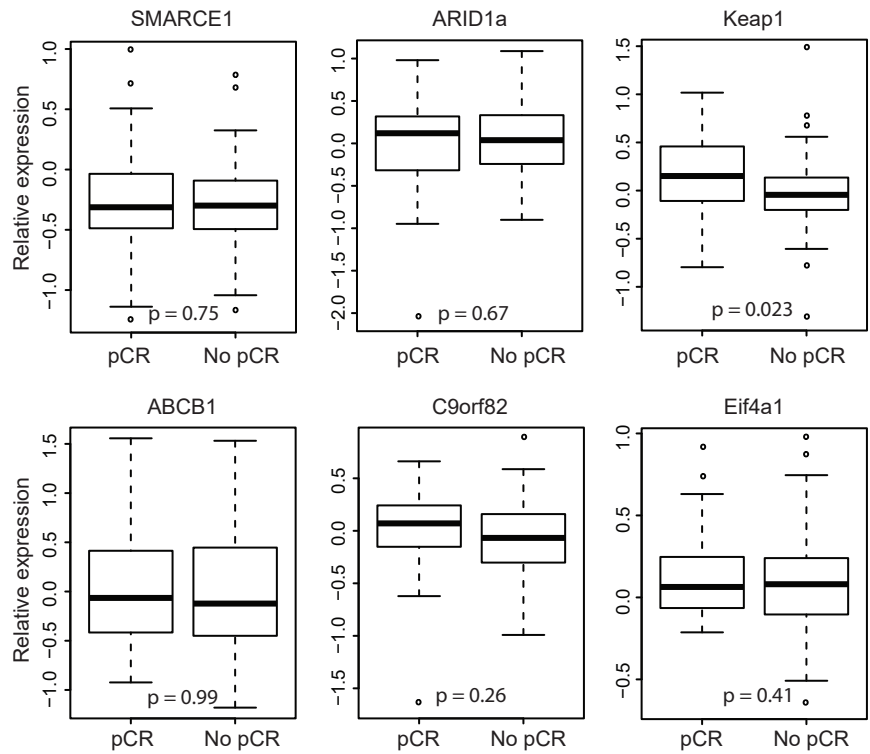
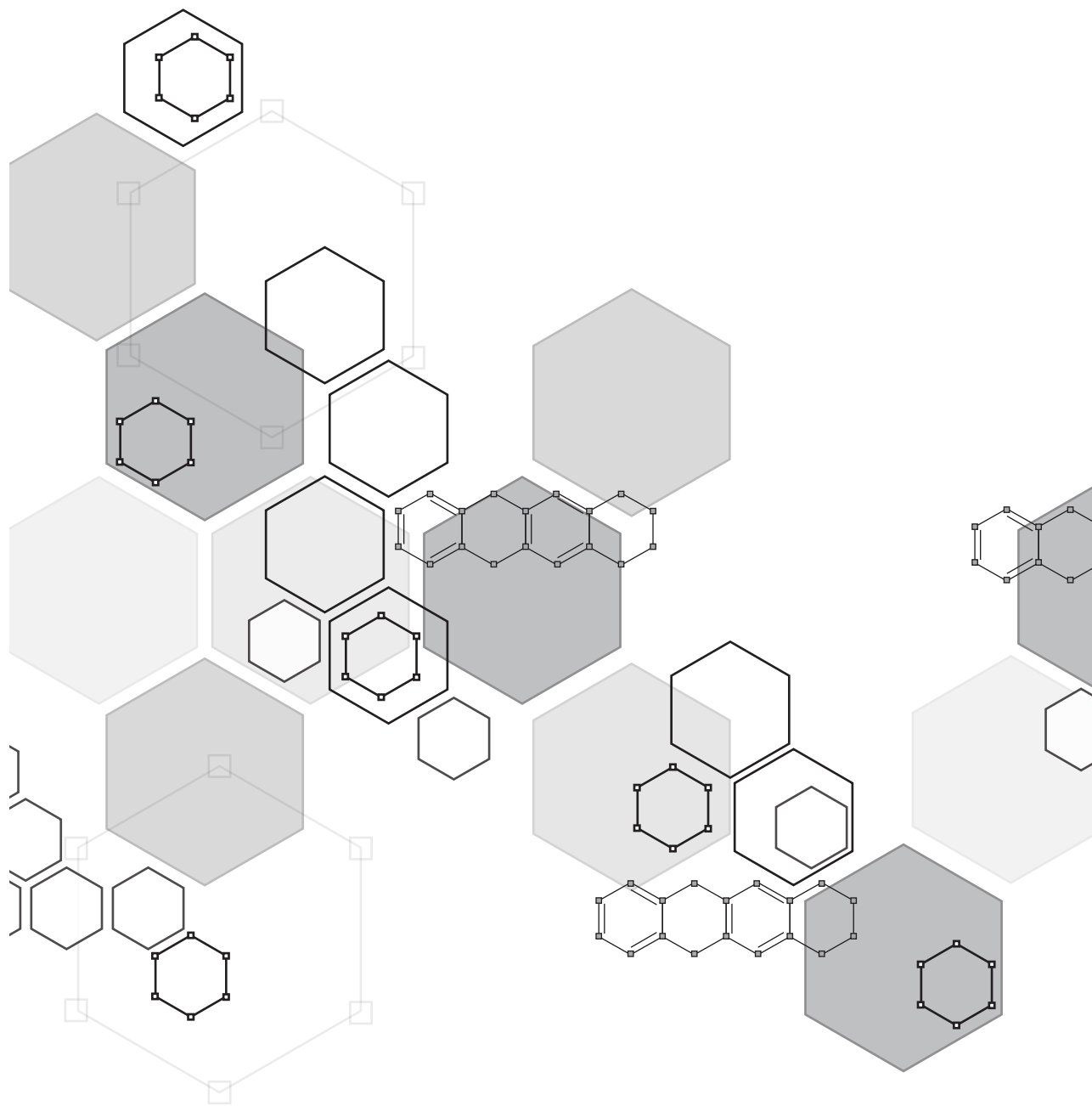


**Figure S4. Expression of some SWI/SNF complex subunits correlates to clinical outcome.** Box plot of normalized expression of the indicated genes in 113 triple-negative breast cancer patients that showed pathological complete response (pCR, 46 patients) or not (no pCR, 67 patients) to the treatment with a Doxo containing regimen. p-values were calculated using a Student's T-test.

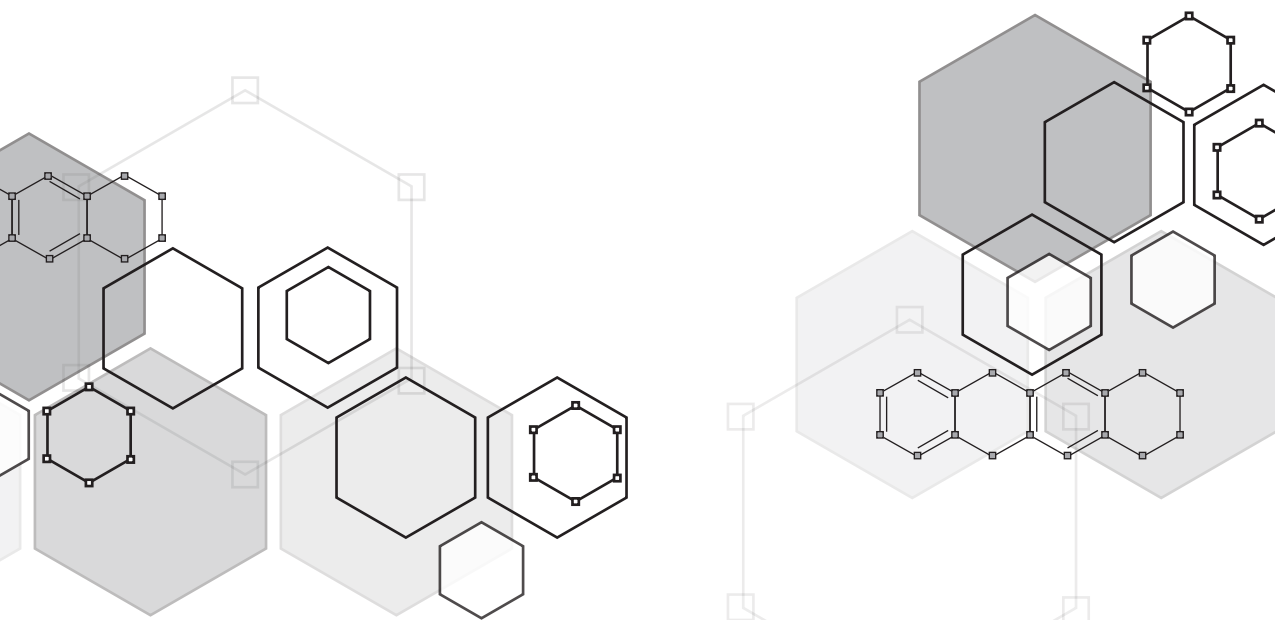
**Table S1. Overview of all screening hits.** Table can be found online: <https://cancerres.aacr-journals.org/content/75/19/4176>





# Uncoupling DNA damage from chromatin damage to detoxify doxorubicin

# 3



Sabina Y. van der Zanden<sup>#</sup>, Xiaohang Qiao<sup>#</sup>, Dennis P.A. Wander, Daniel M. Borràs, Ji-Ying Song, Xiaoyang Li, Suzanne van Duikeren, Noortje van Gils, Arjo Rutten, Tessa van Hewarden, Olaf van Tellingen, Elisa Giacomelli, Milena Bellin, Valeria Orlova, Leon G.J. Tertoolen, Sophie Gerhardt, Jimmy J. Akkermans, Jeroen M. Bakker, Charlotte L. Zuur, Baoxu Pang, Anke M. Smits, Christine L. Mummery, Linda Smit, Ramon Arens, Junmin Li, Herman S. Overkleeft and Jacques Neefjes

<sup>#</sup>These authors contributed equally

*PNAS* (2020)

**ABSTRACT**

The anthracycline doxorubicin (Doxo) and its analogs daunorubicin (Daun), epirubicin (Epi), and idarubicin (Ida) have been cornerstones of anticancer therapy for nearly five decades. However, their clinical application is limited by severe side effects, especially dose-dependent irreversible cardiotoxicity. Other detrimental side effects of anthracyclines include therapy-related malignancies and infertility. It is unclear whether these side effects are coupled to the chemotherapeutic efficacy. Doxo, Daun, Epi, and Ida execute two cellular activities: DNA damage, causing double-strand breaks (DSBs) following poisoning of topoisomerase II (Topo II), and chromatin damage, mediated through histone eviction at selected sites in the genome. Here we report that anthracycline-induced cardiotoxicity requires the combination of both cellular activities. Topo II poisons with either one of the activities fail to induce cardiotoxicity in mice and human cardiac microtissues, as observed for aclarubicin (Acla) and etoposide (Etop). Further, we show that Doxo can be detoxified by chemically separating these two activities. Anthracycline variants that induce chromatin damage without causing DSBs maintain similar anticancer potency in cell lines, mice, and human acute myeloid leukemia patients, implying that chromatin damage constitutes a major cytotoxic mechanism of anthracyclines. With these anthracyclines abstained from cardiotoxicity and therapy-related tumors, we thus uncoupled the side effects from anticancer efficacy. These results suggest that anthracycline variants acting primarily via chromatin damage may allow prolonged treatment of cancer patients and will improve the quality of life of cancer survivors.

**SIGNIFICANCE**

Anthracyclines like doxorubicin are anticancer drugs, used by over 1 million cancer patients annually. However, they cause severe side effects, most notably cardiotoxicity and therapy-related malignancies. It is unclear whether these side effects are directly linked to their anticancer activity. Doxorubicin exerts two activities: DNA damage and chromatin damage. Here, we show that both activities conspire the cardiotoxicity, while doxorubicin variants with only chromatin-damaging activity remain active anticancer drugs devoid of side effects. This challenges the concept that doxorubicin works primarily by inducing DNA double-strand breaks and reveals another major anticancer activity, chromatin damage. Translating these observations will yield anticancer drugs for patients that are currently excluded from doxorubicin treatment and improve the quality of life of cancer survivors.

**INTRODUCTION**

The anthracycline doxorubicin (also known as Adriamycin, Doxo) and its analogs daunorubicin (Daun), epirubicin (Epi), and idarubicin (Ida) are widely used in the treatment of various hematologic malignancies and solid tumors, as monotherapies or main ingredients in combination therapies with other drugs or antibodies [1, 2]. As many other chemotherapeutics, anthracyclines can cause severe side effects in patients, most notably dose-dependent irreversible cardiotoxicity, which can be lethal. Upon reaching the maximal cumulative dose, alternative treatment strategies are needed if any are available [3-5]. The risk of cardiotoxicity increases with age extremes [6] and also limits anthracycline treatment of recurring tumors, even if these drugs could still be effective [7-10]. As a result, elderly cancer patients with a 'weak heart' are often excluded from chemotherapy regimens containing anthracyclines

[11, 12]. Moreover, combination with other drugs or radiotherapy in the heart region further increases the incidence of anthracycline-related cardiotoxicity [13].

Besides cardiotoxicity, Doxo causes other serious side effects. Particularly devastating are therapy-related tumors [14, 15]. Roughly 1 to 3% of juvenile patients and 0.2 to 1% of breast cancer patients develop therapy-related tumors within 5 years after the initial anthracycline-containing treatment [16, 17]. Therapy-related tumors are frequently associated with high-risk cytogenetics with a significantly lower rate of complete remissions (CRs) than *de novo* tumors [18–20]. The third major side effect impacting quality of life is infertility [21]. Therefore, sperm or ova of young cancer patients are frequently collected and preserved prior to anthracycline-based chemotherapy for later fertility treatment.

It is unclear whether the anticancer activities of anthracyclines are intimately coupled to their various side effects. The anthracyclines are topoisomerase II (Topo II) poisons, whereby they induce DNA double-strand breaks (DSBs) [22]. While Doxo and related anthracyclines show high efficacy in the clinic, etoposide (Etop), a structurally unrelated Topo II poison which also generates DSBs [23], is significantly less potent in tumor control [24, 25] and less cardiotoxic [26]. This suggests that DNA damage as a result of Topo II poisoning does not fully account for the clinical effects and cardiotoxicity. More recently, anthracyclines unlike Etop have been shown to evict histones from particular regions in the genome [24, 27, 28]. Histone eviction by anthracyclines has multiple consequences, including epigenomic and transcriptional alterations and attenuated DSB repair, collectively referred to as chromatin damage [24, 29]. These studies identified a variant anthracycline, aclarubicin (Acla), that evicts histones but fails to induce DSBs [24, 29]. This drug is an effective anticancer drug, particularly for the treatment of acute myeloid leukemia (AML) [7, 30, 31].

Here, we reveal that the combination of DNA and chromatin damage assembled in Doxo and its variants is responsible for the different side effects. By understanding the effective chemical structure of each activity, we synthesized and identified analogs that failed to induce DSBs, but maintained histone eviction activity. These analogs abstained from causing therapy-related tumors and cardiotoxicity in mice and human cardiac microtissues, while retaining significant anticancer activity. It suggests that chromatin damage is apparently an important chemotherapeutic activity of anthracyclines, which—when separated from DSB formation—can ameliorate treatment-limiting side effects in mice. Consequently, anthracyclines can be detoxified by chemically removing the DNA-damaging effect while maintaining their chromatin-damaging activity. This provides different strategies for anthracycline development and a rationale for a more intense and broader application of anthracycline variants in the clinic.

## RESULTS

### The combination of DNA- and chromatin-damaging activities accelerates tumor formation and causes tissue toxicities in mice.

In addition to treatment-limiting cardiotoxicity, Doxo-containing chemotherapy induces treatment-related tumors in close to 1% of cancer survivors [16, 17]. To explore the molecular basis of the different side effects of anthracyclines, we tested the *in vivo* carcinogenicity and cardiotoxicity of Doxo, in parallel with its analog Acla, capable only of chromatin damage, and Etop—a nonanthracycline drug proficient in DSB induction via Topo II but incapable of chromatin damage [24]. Trp53<sup>+/-</sup> FVB mice [a spontaneous mouse tumor model [32–34]] were treated six times at two-week

intervals with Doxo, Acla, Etop, or saline at a drug dosage and treatment schedule corresponding to standard patient therapy [24, 35]. As in clinic practice, animals recovered from drug treatment within the two-week intervals, and no death was caused by acute toxicities. These mice were then followed for tumor development and long-term toxicities up to 72 weeks (Figure 1A). Doxo-treated mice presented accelerated death due to tumor formation, excluding 10 out of 32 Doxo-treated mice, who died from cardiotoxicity prior to development of detectable tumors. In contrast, Acla-treated mice showed attenuated spontaneous tumor formation, while Etop treatment moderately accelerated this process (Figure 1B and C). Since DNA mutations are a major driver of cancer [36], the difference in tumor formation for the three drugs could be a dose-dependent result of DNA errors introduced during inaccurate damage repair. Although Doxo and Etop both induce DSB, the damage is further exacerbated by the chromatin-damaging activity of Doxo [24]. Detailed histopathological analysis revealed that, among a variety of tumor types developed in Trp53<sup>-/-</sup> mice, high incidence of breast cancer was observed in 65% (11 out of 17) of Doxo-treated female mice, while the tumor spectra of Etop- and Acla-treated mice were comparable to that of saline-treated mice (SI Appendix, Table S1, Figure S1A and B). This observation may explain the increased risk for breast cancer observed in juvenile cancer survivors with a history of anthracycline-based therapies [37, 38]. Hence, the combination of DSB formation with chromatin damage induction, as for Doxo, enhances tumor formation, while removal of this, as for Acla, alleviates induction of therapy-related tumors.

Similar to human patients [3, 39], cumulative dose and male gender were also risk factors for Doxo-induced cardiotoxicity in mice (SI Appendix, Figure S1C–G). Histopathological analysis revealed substantial and exclusive heart damage in 78.1% of Doxo-treated mice, commonly presented as thrombus formation in the left atrium and auricle of the heart accompanied by inflammation and fibrosis [40, 41] (Figure 1D–F and SI Appendix, Figure S1H). Sirius Red staining highlights these lesion areas showing increased levels of collagen (Figure 1G and H), while further staining for desmin, vimentin and periostin showed impairment of myocytes (SI Appendix, Figure S2A and B) and increased fibrous stroma (SI Appendix, Figure S2C–I). Up-regulation of periostin was also observed in the myocardium of ventricles in Doxo-treated mice, particularly in the left ventricles and septums (SI Appendix, Figure S2F and I). These alterations are known to be associated with anthracycline-induced chronic cardiotoxicity [42, 43]. Postmortem histopathological analysis of all other major organs revealed severe dose-dependent effects on spermatogenesis in Doxo-treated male mice only (Figure 1I and SI Appendix, Figure S2J–P), another known side effect of anthracyclines. These mouse experiments recapitulate three foremost long-term side effects of Doxo known in human patients and other animal models, suggesting that uncoupling DNA- from chromatin-damaging activity of anthracyclines could alleviate side effects, as this combination is absent in Etop and Acla.

### **Chromatin- and DNA-damaging activities can be uncoupled in anthracyclines.**

The anthracyclines Doxo, Daun, Epi and Ida all combine DNA-damaging and chromatin-damaging activities [24]. A recently developed anthracycline analog, amrubicin (Amr), was reported with limited cardiotoxicity [44]. We tested the DNA- and chromatin-damaging activities of Amr at physiologically relevant concentrations [24, 45]. DNA damage was visualized by constant-field gel electrophoresis (CFGE) [46, 47], comet assay [48] and phosphorylation of H2AX at Ser139 (γH2AX) [49]. Amr, Doxo, Daun, Epi, Ida and Etop all induced DSBs, unlike Acla (Figure 2A–E and



SI Appendix, Figure S3A–C). Subsequently, chromatin damage was detected after photo-activation of green fluorescent protein-labeled histone H2A (PAGFP-H2A) in living cells [24]. Only Amr and Etop failed to evict histones (Figure 2F and G and SI Appendix, Figure S3D and Movie S1). The anthracycline Amr thus mimicked Etop, which only induces DSBs. Amr and Etop both have limited cardiotoxicity [26, 44, 50],

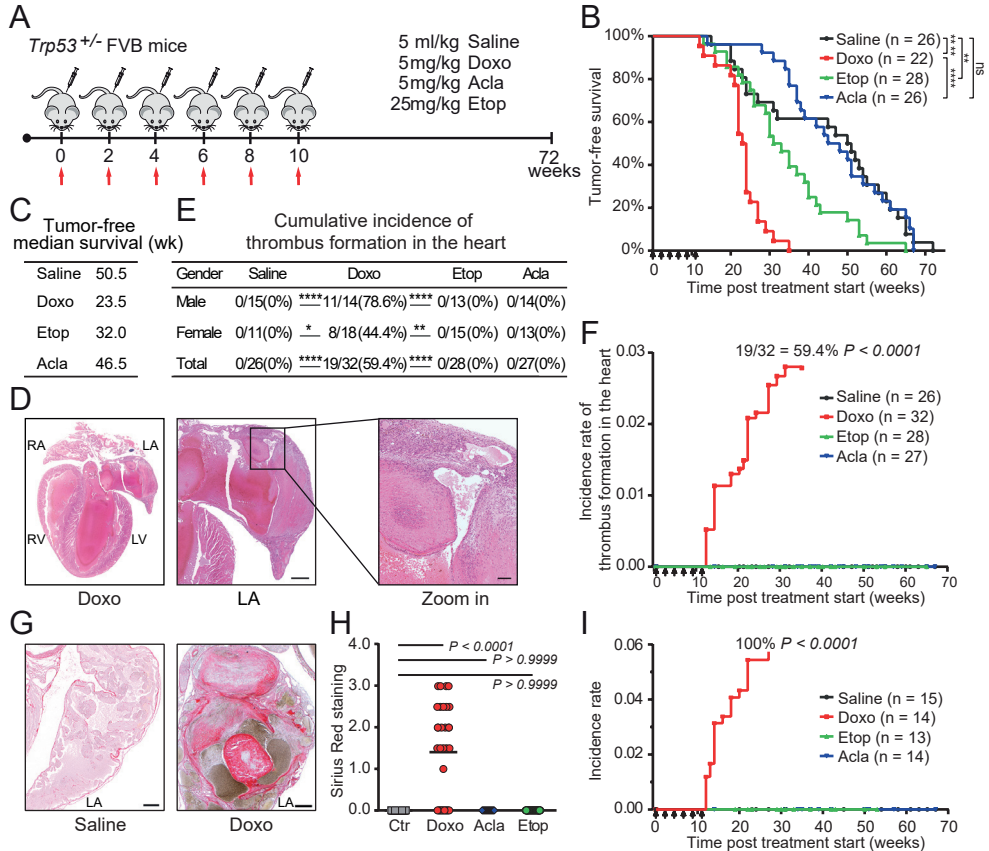


**Figure 1. Doxo and Etop but not Acla accelerates tumor formation and causes tissue toxicities in *Trp53*<sup>+/-</sup> FVB mice.** (A) *Trp53*<sup>+/-</sup> FVB mice were i.v. injected with Doxo, Acla, Etop, or saline every two weeks for six times. Drug injections are indicated by arrows. (B) Tumor-free survival is plotted in a Kaplan-Meier curve. Log-rank test, ns, not significant; \*\*\*\* $P < 0.0001$ ; \*\* $P = 0.0093$ . (C) Tumor-free median survival of mice. (D) Representative microscopic images of the heart from Doxo-treated mouse with thrombosis formation in the left atrium/auricle. Higher magnifications shows thrombi and inflammatory lesions including fibrosis in the left auricle. LA = left atrium, RA = right atrium, LV = left ventricle, RV = right ventricle. Scale bars, 500  $\mu$ m and 100  $\mu$ m, respectively. (E) Cumulative incidence of thrombosis was analyzed for gender effect. Fisher's exact test, two-sided. \* $P < 0.05$ ; \*\* $P < 0.01$ ; \*\*\* $P < 0.001$ ; \*\*\*\* $P < 0.0001$ . (F) The incidence rate of thrombus formation in the heart. Cumulative incidence is indicated next to the curve. Two-way ANOVA with RM, \*\*\*\* $P < 0.0001$ . (G) Representative Sirius Red staining of the LA from saline- or Doxo-treated mouse. Scale bars, 100  $\mu$ m. (H) Quantification of Sirius Red staining. Kruskal-Wallis test, \*\*\*\* $P < 0.0001$ , Ctr vs Acla or Etop is ns. (I) Incidence rate of depletion of spermatogenesis in male mice. Cumulative incidence is indicated next to the curve. Two-way ANOVA with RM, \*\*\*\* $P < 0.0001$ .

again suggesting that DNA damage alone is insufficient to induce cardiotoxicity. Relocation of the amine group from the sugar (as found in Doxo) to the tetracycline moiety in Amr disabled histone eviction (Figure 2A), but still allowed induction of DSBs, suggesting that the amine on the sugar of Doxo is crucial for evicting histones. Furthermore, Acla whose amine group is present at the same position but in a dimethylated form exhibited only histone eviction activity without DSB induction (Figure 2A–G). To identify the structural basis of these two cellular activities of Doxo, we synthesized and tested *N,N*-dimethyldoxorubicin (diMe-Doxo) (Materials and Methods and SI Appendix, Method S1). *N,N*-dimethylation of the amine group in Doxo abolished DNA-damaging activity at various concentrations (Figure 2A–E and SI Appendix, Figure S3A–C), while still allowing histone eviction (Figure 2F and G and SI Appendix, Figure S3E–I and Movie S2). Further, the evicted H2B accumulated in the cytosolic fraction upon treatment of Doxo, diMe-Doxo and Acla but not for Amr and Etop (Figure 2H and I and SI Appendix, Figure S4A and B). The diMe-Doxo still relocated Topo II $\alpha$ -GFP to chromatin (SI Appendix, Figure S4C), indicating that Topo II $\alpha$  was trapped by the drug before the generation of DSB. These data suggest that manipulating the position and modification of the amine group in Doxo allows separation of the DNA-damaging and chromatin-damaging activities.

We then tested the relative contributions of DNA damage and chromatin damage to the anticancer effects of Doxo by assaying the cytotoxicity of these variants in different cancer cell lines (Figure 2J and K and SI Appendix, Figure S5A). The diMe-Doxo showed comparable or even superior effects in most cell lines tested compared to Doxo (14 out of 20), while Amr was poorly cytotoxic (Figure 2J). This increased potency of diMe-Doxo in these cell lines was unexpected, given that this compound lost its DNA-damaging activity. This enhanced potency could not be attributed to the rate of drug uptake as analyzed by flow cytometry following the autofluorescence of the anthracycline drugs (SI Appendix, Figure S5B). Reactive oxygen species (ROS) induced by anthracyclines was observed to be dose-dependent but only at late time point after drug removal (SI Appendix, Figure S6A and B), indicating that it could be a secondary effect of drug action. ROS can cause many vicious damages, which might be responsible for the cell death induced by anthracyclines. Although the different anthracyclines induced some increase in total ubiquitinated proteins, there was no significant difference observed for the different drugs (SI Appendix, Figure S6C and D). Besides ROS induction, chromatin damage induced cell death is probably executed by classical caspase-dependent apoptosis, as shown by PARP cleavage following exposure to these drugs (SI Appendix, Figure S6E and F).

### **Anthracyclines that only evict histones are effective in cancer treatment.**

To assess the importance of chromatin damage for the clinical activity of anthracyclines, we performed a retrospective analysis in *de novo* geriatric AML patients, who were treated with either Ida-based (that induces both DSBs and chromatin damage) or Acla-based regimens (with chromatin damage only). Acla is reported to be equipotent to Daun for AML patients [30, 31], likewise Acla-based regimen resulted in comparable overall survival as Ida-based regimen (Figure 3A and SI Appendix, Figure S7A and Table S2 and S3), indicating that anthracycline drugs lacking DNA-damaging activity are effective in cancer treatment. The direct anticancer activity of diMe-Doxo compared to Doxo was evaluated *ex vivo* in primary human AML blasts (Figure 3B and C and SI Appendix, Figure S7B–H). Although some patient-to-patient variation existed, Doxo and diMe-Doxo were equally effective, while Acla appeared more cytotoxic in these dose-response experiments (Figure 3B and C and SI Ap-

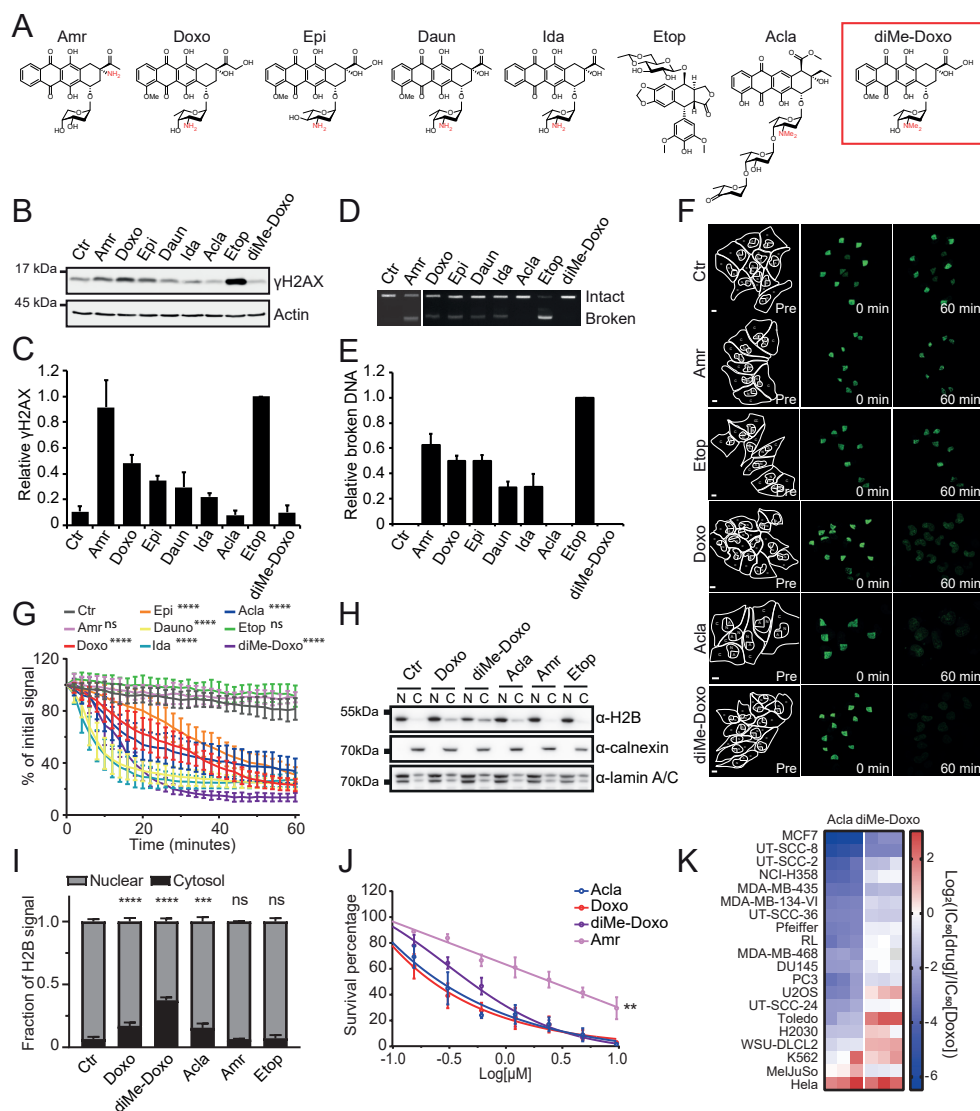


**Figure 2. Evaluation of the DNA- and chromatin-damaging activities of anthracyclines.** (A) Structures of Topo II poisons used in this study, the critical amine group in red. (B) K562 cells were treated for 2 hours with 10 μM of indicated drug. γH2AX levels were examined by Western blot. (C) Quantification of the γH2AX signal normalized to actin. (D) DSBs were analysed by CFGE. (E) Quantification of relative broken DNA in (D). (F) Part of the nucleus from MelJuSo-PAGFP-H2A cells was photo-activated. Photo-activated PAGFP-H2A was monitored by time-lapse confocal microscopy for 1 hour in the absence or presence of indicated drug at 10 μM. Lines in the left panel define the region of cytoplasm (C), nucleus (N) and activated area (A). Scale bar, 10 μm. (G) Quantification of the release of fluorescent PAGFP-H2A from the photo-activated region after drug administration. Two-way ANOVA, \*\*\*\*P < 0.0001. (H) Endogenously tagged scarlet-H2B U2Os cells were treated with 10 μM of the indicated drugs. Cells were fractionated and the nuclear versus cytosolic fraction of H2B was examined by Western blot. Calnexin was used as cytosolic, and lamin A/C as nuclear marker.

**Figure 2. Continued.** (I) The fraction of cytosolic versus nuclear H2B upon histone eviction by the drugs indicated is plotted. Two-way ANOVA, \*\*\* $P < 0.001$ ; \*\*\*\* $P < 0.0001$ ; ns, not significant. (J) Cell viability in K562 cells. Two-way ANOVA, Amr vs Doxo, diMe-Doxo or Acla, \*\* $P < 0.01$ . (K) Relative  $IC_{50}$  values of each drug compared to Doxo in different cell lines.

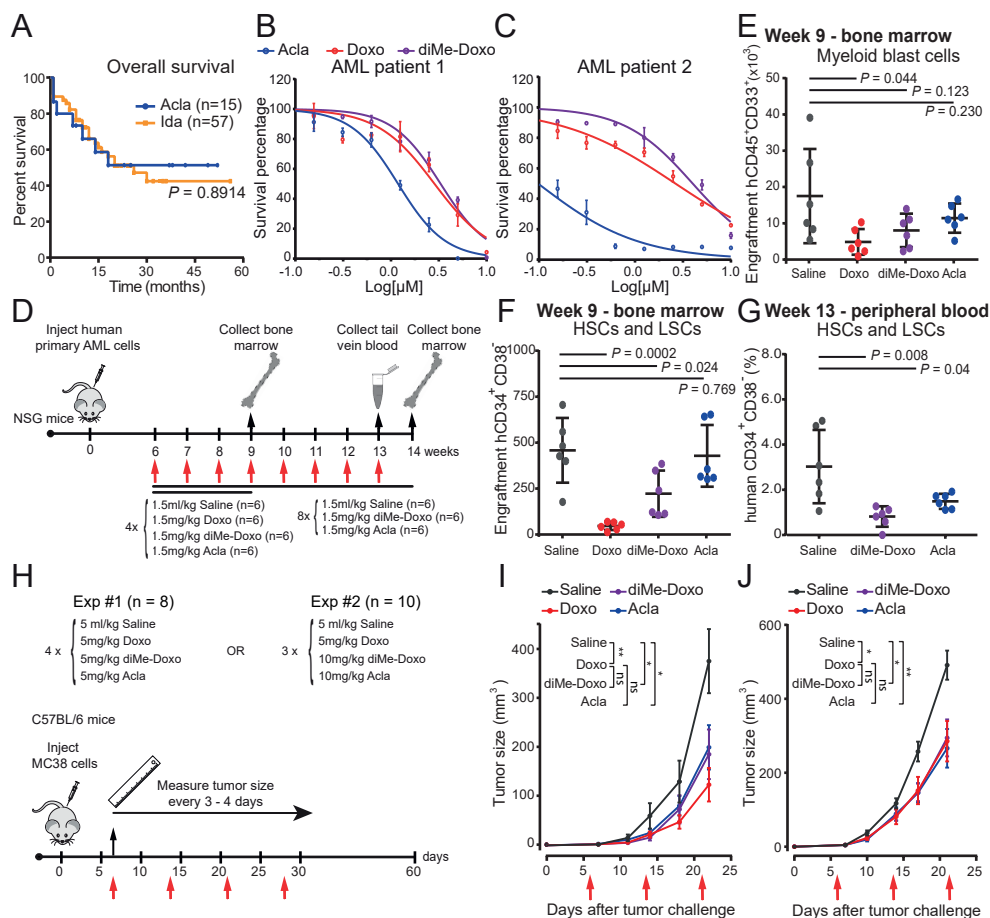


**Figure 3. diMe-Doxo and Acla are effective anticancer drugs.** (A) Overall survival of *de novo* geriatric AML patients treated with a drug regimen including Acla or Ida. Log-rank (Mantel-Cox) test. (B) and (C) Dose-dependent cell viability of human AML samples, shown as mean  $\pm$  SD of technical duplicates. (D) Schematic overview of AML PDX mouse experiment. (E) and (F) The engraftment of human AML cells in the bone marrow of the first cohort at week 9: absolute counts of myeloid blast cells (CD45<sup>+</sup>CD33<sup>+</sup> blasts) (E) and HSCs and LSCs (CD34<sup>+</sup>CD38<sup>+</sup> blasts) (F). Each symbol represents one mouse. Students' *t*-test. (G) The engraftment of human AML cells of the second cohort: the percentage of human HSCs and LSCs in peripheral blood at week 13. Students' *t*-test. (H) C57BL/6 mice were subcutaneously injected with MC38 cells. One week after tumor challenge, mice were treated with indicated drugs every week. Drug injections are indicated by arrows. (I) and (J) MC38 tumor growth following Exp #1 procedure (I) or Exp #2 procedure (J). One-way ANOVA, saline vs treatment, \* $P < 0.05$ ; \*\* $P < 0.01$ .

pendix, Figure S7B–H). Chromatin-damaging activity apparently contributes significantly to the cytotoxicity of Doxo in treating AML.

The anticancer activity of diMe-Doxo *in vivo* was tested in an AML patient-derived xenograft (PDX) mouse model [51] in comparison to Doxo and Acla (Figure 3D). Due to severe toxicity, mice treated with Doxo had to be killed after four courses of treatment at week nine, unlike mice treated with Acla or diMe-Doxo (SI Appendix, Figure S8A), which then received another four courses of treatment without any signs of toxicity (Figure 3D and SI Appendix, Figure S8B). At week nine, four courses of Doxo treatment significantly depleted human AML blast cells, hematopoietic stem cells (HSCs) and leukemic stem cells (LSCs) (Figure 3E and F and SI Appendix, Figure S8C), and it showed modest but not significant impact on normal mouse leukocytes (SI Appendix, Figure S8D). The diMe-Doxo and Acla did reduce the leukemic burden, albeit less efficient than Doxo (Figure 3E and F). With extended treatment of diMe-Doxo and Acla, most proliferating fractions of human hematopoietic cells were significantly reduced in mice (Figure 3G and SI Appendix, Figure S8E–H). The PDX experiment suggests that diMe-Doxo has the capacity to reduce the leukemic burden, the immature LSCs and leukemic progenitors *in vivo* with less hematopoietic toxicity compared to Doxo. Subsequently, we tested a solid colon carcinoma tumor mouse model for the efficacy of the different anthracyclines that either or not induce DSBs (Figure 3H). Both diMe-Doxo and Acla showed significant tumor control, although Doxo was slightly but not significantly better in reducing the tumor growth at equal dose (Figure 3I). A higher dose of diMe-Doxo and Acla resulted in equal tumor control (Figure 3J). Taken together, Acla or diMe-Doxo (with chromatin-damaging activity only) are effective anticancer drugs *in vitro* and *in vivo*, suggesting that chromatin damage could have a major contribution to the mechanism of anthracycline cytotoxicity.

### ***N,N*-dimethylation of Doxo prevents cardiotoxicity.**

Since diMe-Doxo resembles the activity of Acla in terms of evicting histones while not causing DSBs (SI Appendix, Figure S9A), we wondered whether this also translates into reduced side effects. To address this, wild-type FVB mice were intravenously (i.v.) injected with Acla, Doxo or diMe-Doxo every two weeks (Figure 4A). Mouse body weight was monitored as a representative parameter of general toxicity prior to each injection [35]. While Doxo-treated mice significantly lost body weight and died from cardiotoxicity after eight injections, mice treated with diMe-Doxo remained healthy, with no weight loss or discomfort, even after 15 doses (Figure 4B and C and SI Appendix, Figure S9B). Histopathology demonstrated Doxo treatment induced severe cardiotoxicity as observed in Trp53<sup>+/-</sup> FVB mice (Figure 1 and SI Appendix, Figure S1 and S2). None of the mice treated with either diMe-Doxo or Acla showed abnormalities in the heart (Figure 4C and SI Appendix, Figure S9C–J). The effects on cardiac function of mice was further evaluated by echocardiography. Doxo treatment resulted in a serious expansion of the left atrium with reduced fractional shortening (FS), left ventricular ejection fraction (EF), and cardiac output unlike any of the other treatments (Figure 4D–G and Movie S3). More direct (acute) cardiac cell damage and function impairment were assessed using human induced pluripotent stem cell (hiPSC)-derived cardiac microtissues [52–55]. Doxo unlike Acla or diMe-Doxo significantly affected contraction amplitude and contraction duration 24 hours posttreatment (Figure 4H and SI Appendix, Figure S9K–N and Movie S4). This suggested that cardiotoxicity can be the result from combining DNA and chromatin damage. This was directly tested by the combination of Amr (DNA damage only) and Acla (chromatin damage only) which reduced the contraction amplitude to some extent and significantly impaired the velocity of the microtissues, which reconstituted the



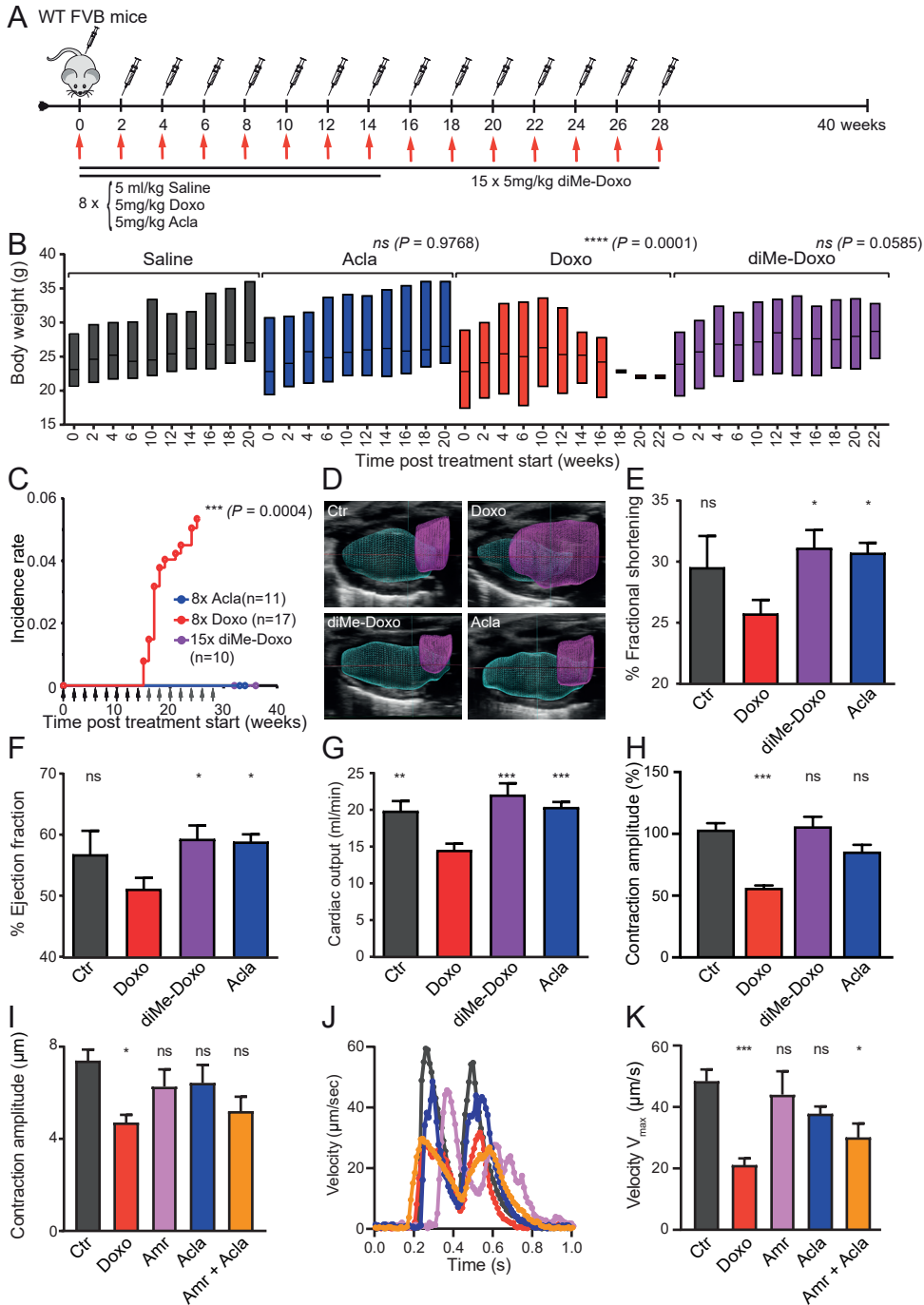


**Figure 4. *N,N*-dimethylation of Doxo prevents cardiotoxicity in mice and hiPSC-derived cardiac microtissues. (A–C), Wild-type FVB mice were i.v. injected with indicated drug every two weeks: Doxo or Acla for 8 times and diMe-Doxo for 15 times.**

**Figure 4. Continued.** (B) The body weight of mice, shown as floating bars with maximum-median-minimum values. Two-way ANOVA with RM. (C) The incidence rate of cardiotoxicity. Arrows indicate drugs injections. Two-way ANOVA. (D–G) Cardiac function assessed by echocardiography 12 weeks post treatment start. FVB mice were treated for 8 times with saline (5 ml/kg,  $n = 5$ ), Doxo (5 mg/kg,  $n = 8$ ), diMe-Doxo (5 mg/kg,  $n = 6$ ) or Acla (5 mg/kg,  $n = 9$ ). (D) 3D reconstruction of the diastole heart by echocardiography. In the sagittal section the left ventricle (cyan) and left atrium (magenta) are highlighted. (E–G) Quantification of echocardiography, fractional shortening (E), left ventricular ejection fraction (F) and cardiac output (G). For (E–G) ordinary one-way ANOVA, Doxo vs saline, diMe-Doxo or Acla,  $*P < 0.05$ ;  $**P < 0.01$ ;  $***P < 0.001$ ; ns, not significant. (H) Drug toxicity on cardiac microtissues 24 hour post treatment. Contraction amplitude of microtissues treated with 20  $\mu\text{M}$  of the different drugs. Krushal-Wallis test,  $***P < 0.0002$ . (I–K) Drug toxicity on cardiac microtissues treated with single drugs or a combination of Amr and Acla, (I) Contraction amplitude of microtissues treated with the indicated single (20  $\mu\text{M}$ ) or combination drugs (10  $\mu\text{M}$  + 10  $\mu\text{M}$ ). (J) Maximum velocity in  $\mu\text{m}/\text{sec}$  is indicated for a represented microtissue for the different treatments. (K) Quantification of the maximum velocity. For (I and K) ordinary one-way ANOVA, Ctr vs treatments;  $*P < 0.05$ ;  $***P < 0.001$ ; ns, not significant.

cardiotoxicity of Doxo in hiPSC-derived cardiac microtissues (Figure 4I–K). These differences in toxicity of the heart cannot be caused by a different biodistribution of the drugs, which was comparable for Doxo and diMe-Doxo (SI Appendix, Figure S9K and O). Unlike Acla, diMe-Doxo affected the male reproductive organs. The diMe-Doxo depleted spermatogenesis in all male mice and caused some Leydig cell hyperplasia but to a lesser extent than its parental drug Doxo, even at higher cumulative dose (SI Appendix, Figure S9P and Q). Significant toxicity in ovaries in young mice at early time points was observed only for Doxo-treated mice, shown as increased apoptosis in secondary and tertiary follicles (SI Appendix, Figure S9R–T). These results indicated that diMe-Doxo or Acla (with chromatin-damaging activity only) are less toxic than anthracyclines that induce both DNA and chromatin damage (such as Doxo), while remaining effective anticancer drugs.

## DISCUSSION

About one million cancer patients annually receive treatment with Doxo or its analogs Daun, Epi, or Ida. Unfortunately, anthracyclines cause severe side effects, particularly cardiotoxicity [3, 4]. This side effect excludes (often elderly) patients with compromised heart function from receiving effective cancer treatments [56]. Understanding and ultimately eliminating the root causes of this and other side effects of anthracyclines would thus greatly expand the application of these drugs in cancer treatment.

It has been suggested that ROS formation may be responsible for cardiotoxicity induced by anthracyclines [57, 58]. However, co-administration of radical quenchers during anthracycline treatment did not ameliorate cardiotoxicity in clinical studies [59, 60]. Moreover, high redox potential of Acla relative to that of Doxo or Daun [61] does not match Acla's lack of cardiotoxic effects. Our data also show that Acla and diMe-Doxo produce more ROS compared to Doxo (SI Appendix, Figure S6A), rather suggesting that ROS induction cannot explain the differences in cardiotoxicity of anthracyclines studied here. Mechanistically, cardiotoxic anthracyclines, such as Doxo, Daun, Epi, and Ida, constitute multifunctional agents capable of DNA damage (by poisoning Topo II and DSB formation) combined with chromatin damage (via histone eviction). The anticancer effects have been attributed to DNA damage, but the variants unable to induce DNA damage show equal anticancer potency in AML treatment. While therapy-related tumors can be understood as the consequence



of delayed and unfaithful DNA damage repair [24], the cause of cardiotoxicity by anthracyclines is still unsolved. Failure of removing cardiotoxicity by chemical modification in the past led to different delivery strategies such as liposome-encapsulated Doxo, but with modest improvement and limited use in clinical practice [62]. Here we show that cardiotoxicity associated with Doxo is alleviated in mice treated with drugs that either induce DSBs (Etop) or evict histones (Acla, diMe-Doxo). This effect is further confirmed in hiPSC-derived cardiac microtissues and by echocardiography, collectively implying that the combination of DNA and chromatin damage induces cardiotoxicity. Although Doxo is an exceptional drug that shows very similar pharmacokinetics in human and mouse [63], there remain some distance between our mouse models and humans. However, the long-term toxicities of Doxo, cardiotoxicity, infertility and therapy-related tumorigenesis, observed in our mouse models do correlate very well with clinical observations. With this promising result from mice, effort will be made to test this concept in other animal models and clinical trial.

Many chemical variations of anthracyclines have been synthesized before, including diMe-Doxo [64, 65]. However, these drugs were only tested for their ability to induce DNA damage, which was considered the main mechanism of therapeutic efficacy for anthracyclines [66]. Since chromatin damage was unknown at that time [24], many of the variants lacking DNA-damaging activity were not further developed. We propose that, by further understanding the cellular activities of anthracyclines, detoxification of Doxo is possible, which only requires a minimal chemical modification to remove the DNA-damaging activity. Such drugs would allow more intense treatment of primary tumors and continuous anthracycline treatment of relapsed tumors. Additionally, patients with higher cardiotoxicity risk, who are now excluded from anthracycline-based cancer treatments, may benefit from the detoxified anthracyclines. Evaluating old anticancer drugs with modern technologies may lead to better understanding of drug activities (such as chromatin damage) that could then provide new strategies for improvement of cancer therapies as exemplified—in this case—by diMe-Doxo. Chemical dissection of the cellular activities of Doxo uncovered a new mechanism of action for anthracyclines—chromatin damage—an effective anticancer drugs devoid of the most critical side effects of anthracyclines.

## MATERIALS AND METHODS

### Reagents

Doxo and Etop were obtained from Pharmachemie (the Netherlands). Daun was obtained from Sanofi-Aventis (the Netherlands). Epi was obtained from Accord Healthcare Limited (UK). Acla for *in vivo* mouse experiment was purchased from Shenzhen Main Luck Pharmaceuticals Inc. (China). All the drugs were dissolved according to the manufacturer's formulation. Amr (sc-207289), Acla (sc-200160, for *in vitro* experiments), and Ida (sc-204774) were purchased from Santa Cruz Biotechnology (USA), dissolved in dimethylsulfoxide at 5 mg/ml concentration, aliquoted and stored at  $-20^{\circ}\text{C}$  for further use.

### Synthesis of *N,N*-dimethyldoxorubicin

All chemicals were used as received unless stated otherwise.  $^1\text{H}$  and  $^{13}\text{C}$  NMR spectra were recorded on a 400/100 or 500/125 NMR spectrometer. Chemical shifts ( $\delta$ ) are given in parts per million relative to tetramethylsilane (TMS) as internal standard. Coupling constants are given in hertz. All given  $^{13}\text{C}$  spectra are proton decoupled. Spin multiplicities are given as s (singlet), d (doublet), dd (doublet of doublets), ddd (doublet of doublet of doublets), dt (doublets of triplets), t (triplet), td (triplet

of doublets), q (quartet), dq (doublet of quartets), qd (quartet of doublets), h (heptet), and m (multiplet). All individual signals were assigned using two-dimensional (2D) NMR spectroscopy, HH-COSY (proton-proton correlated spectroscopy), and heteronuclear single quantum correlation. Flash chromatography was performed on Screening Device B.V. silica gel 60 (0.04–0.063mm). TLC analysis (on Merck silica gel F254 plates) was followed by detection by ultraviolet absorption (254nm) where applicable and by spraying with a solution of  $(\text{NH}_4)_6\text{Mo}_7\text{O}_{24}\cdot\text{H}_2\text{O}$  (25 g/L) and  $(\text{NH}_4)_4\text{Ce}(\text{SO}_4)_4\cdot 2\text{H}_2\text{O}$  (10 g/L) in 10% sulfuric acid in water followed by charring at 275°C. Liquid chromatography-mass spectrometry (LC-MS) standard eluents used were A: 100%  $\text{H}_2\text{O}$ , B: 100% acetonitrile, and C: 1% TFA in  $\text{H}_2\text{O}$ . A C18 column (4.6 mm D×50 mm L, 3  $\mu$  particle size) was used. All analyses were 13 minutes, at a flow-rate of 1 mL/min. High-resolution mass spectra were recorded on a LTQ-Orbitrap equipped with an electrospray ion source in positive mode (source voltage 3.5 kV, sheath gas flow 10, capillary temperature 275°C) with resolution  $R = 60,000$   $m/z = 400$  (mass range = 150–4000) and dioctylphthalate ( $m/z = 391.28428$ ) as “lock mass”. Size exclusion chromatography was performed on Sephadex LH20 (eluent MeOH/DCM, 1:1). Detailed synthesis schemes can be found in the SI Appendix, Methods S1.

### Cell culture

K562 (B. Pang, Stanford University, Stanford, CA), THP-1 (ATCC, Manassas, VA), DU145 (C. Robson, Newcastle University, Newcastle, United Kingdom), NCI-H358, MBA-MD-468 (R. Bernards, Netherlands Cancer Institute [NKI], Amsterdam, The Netherlands), and Pfeiffer cells (ATCC, Manassas, VA) were maintained in RPMI-1640 medium supplemented with 8% FCS. MCF-7 (W. Zwart, NKI, Amsterdam, The Netherlands), U2OS cells (M. Innocenti, NKI, Amsterdam, The Netherlands) and MC38 cells (M. Colonna, Washington University School of Medicine, St. Louis, MO) were cultured in Dulbecco's Modified Eagle's medium (DMEM) supplemented with 8% FCS. MelJuSo cells were cultured in Iscove's Modified Dulbecco's medium (IMDM) supplemented with 8% FCS. UT-SCC-8 cells (R. Grenman, University of Turku, Turku, Finland) were cultured in DMEM medium supplemented with 8% FCS and 1% non-essential amino acid. MelJuSo cells stably expressing PAGFP-H2A, PAGFP-H3 or PAGFP-H4 were maintained in IMDM supplemented with 8% FCS and G-418, as described [24]. MelJuSo cells were transiently transfected with a construct encoding Topo II $\alpha$ -GFP [24]. Endogenous tagged scarlet-H2B cells were generated using homology repair scarlet constructs, which was designed 250 base pairs upstream and downstream of the genomic H2BC11 region. The guide RNA (gRNA) target sequence was designed by the CRISPOR tool and cloned into the pX330 Cas9 vector. Primers used for the homologous recombination (HR) construct: H2B homology arm left fwd: CCCACATATGCAAGGTTCTGAAGCAGGTCCAC; H2B homology arm left rev: CCCAGCTAGCCTTAGCGCTGGTGTACTTGG; H2B homology arm right fwd: CCCAGGTACCACAGTGAGTTGGTTGCAAAC; H2B homology arm right rev: CCCAGGATCCAACCTATAATAGAAAATTTCCCATCTCC. Primers used for the pX330 Cas9 vector: H2B gRNA fwd: CACCGACTCACTGTTTACT-TAGCGC; H2B gRNA rev: AAACGCGCTAAGTAAACAGTGAGTC. All cell lines were maintained in a humidified atmosphere of 5%  $\text{CO}_2$  at 37°C and regularly tested for the absence of mycoplasma.

### Primary human AML cells isolation and culture

All studies were conducted in accordance with the Declaration of Helsinki, and the

full study protocol was approved by the Ethics Committee of the Vrije Universiteit Medical Center (VUmc). At diagnosis, bone marrow (BM) or peripheral blood (PB) from AML patients hospitalized at the VUmc in Amsterdam, The Netherlands was collected with informed consent and according to protocols approved by the Ethics Committee of the VUmc. Mononuclear cells were isolated using Ficoll-Paque Plus (Amersham Biosciences, Uppsala, Sweden). Primary AML cells were kept in IMDM supplemented with 15% BIT9500 (Stemcell Technologies), Pen-Strep, 50 ng/ml human FLT3 ligand, 20 ng/ml human IL3 and 100 ng/ml human stem cell factor (PeproTech).

### **Mouse experiments for assessing drug toxicities**

Mice were housed in individually ventilated cages (IVC) under specific pathogen-free (SPF) conditions in the animal facility of the NKI (Amsterdam, The Netherlands). All mouse experiments were performed according to institutional and national guidelines and were approved by the Animal Ethics Committee of the NKI (Amsterdam, The Netherlands). Trp53<sup>+/-</sup> or wild-type FVB mice were bred by the NKI mouse facility. Trp53<sup>+/-</sup> FVB mouse strain and genotyping protocol were as described [32]. Mice (10 wk to 11 wk old) were i.v. injected with 5 mg/kg of Doxo, 5 mg/kg of Acla, 5 mg/kg of diMe-doxo, 25 mg/kg of Etop or 5 mL/kg of saline every two weeks for the indicated times. Then tumor formation and animal welfare (weight loss, lethargy, hunched posture, poor grooming [rough hair coat]) were monitored every other day. When the tumor diameter exceeded 1 cm or the body-weight loss was more than 20%, the animal was euthanized by CO<sub>2</sub>. Subsequently all organs and tumors were collected, fixed in EAF fixative (ethanol/acetic acid/formaldehyde/saline at 40:5:10:45 v/v), and embedded in paraffin. Sections were cut at 2 µm from the paraffin blocks and stained with hematoxylin and eosin, Sirius Red or indicated antibodies according to standard procedures. Primary antibodies were: Desmin (1:200, M 0760, DakoCytomation), Vimentin (1:100, #5741, Cell Signaling) and Periostin (1:100, ab215199, Abcam). The pathology slides were reviewed by an expert mouse pathologist who was blind to the treatment. Incidence rate (IR = [number of mice with specific side effect over a time period] / [sum of mice x time at risk during the same time period]) and cumulative incidence (CI = [number of mice with specific side effect at end time point] / [total number of mice at start]) were calculated for indicated side effects.

### **Pharmacokinetics of anthracyclines in FVB mice**

Mice were housed in individually ventilated cages (IVC) under specific pathogen-free (SPF) conditions in the animal facility of the NKI (Amsterdam, The Netherlands). All mouse experiments were performed according to institutional and national guidelines and were approved by the Animal Ethics Committee of the NKI (Amsterdam, The Netherlands). Wild-type FVB mice were bred by the NKI mouse facility. Female mice (8 wk old) were i.v. injected with 5 mg/kg of Doxo, 5 mg/kg of Acla or 5 mg/kg of diMe-doxo, with five mice per group. Four hours post injection, animals were killed, and then heart, liver, kidney, spleen, reproductive organ, and plasma was collected. Hearts were cut into two pieces with coronal section. One piece was fixed in EAF for yH2AX staining. The other half of the heart and the rest of organs were weighed and frozen for the pharmacokinetics study. Doxo was measured by high performance liquid chromatography fluorescence detection as described before [67]. Acla and diMe-Doxo were analysed by LC-MS/MS. Sample pretreatment involved protein precipitation with acetonitrile: formic acid (99:1) containing 500 nM of Doxo as internal standard, followed by centrifugation (5 min, 20,000 g) and dilution of the supernatant

with water (1:3). Samples were centrifuged again and an aliquot of 50  $\mu$ l was injected into the LC-MS/MS system. Separation was done using an Extend C18 column (100 x 2.1 mm). Mobile phase A (0.1% formic acid in water) and B (methanol) was delivered at 0.4 ml/min at 20% B. Following injection, a linear gradient to 95% B in 2.5 min was applied, kept at 95% for 2 min and then returned to 20% B. The API4000 MS (Sciex) was used in MRM mode; Acla: 812.5/333.1; diMe-Doxo: 571.9/99.9; and Doxo: 544.4/86.1).

### **PDX mouse model for AML**

Mice were housed in IVC under SPF conditions in the animal facility of the VUmc (Amsterdam, The Netherlands). PDX mouse experiments were performed according to institutional and national guidelines and were approved by the Animal Ethics Committee of the VUmc (Amsterdam, The Netherlands). NOD/SCID/IL2r gamma null (NSG) mice (Jackson Laboratory) (6 wk to 8 wk old) were i.v. injected with  $0.7 \times 10^6$  primary human AML cells per mouse 24 hours post 200-cGy total irradiation. PB was taken via the tail vein and analyzed by flow cytometry for human AML cells, defined by  $> 0.7\%$  of hCD45<sup>+</sup> cells. Six weeks after AML injection, mice were i.v. injected with 1.5 mg/kg of drug or saline weekly for the indicated times. Animals were monitored every other day. PB was taken from the tail vein and analyzed by flow cytometry at week 13. After killing, the hearts were collected for histopathological analysis, and BM was analyzed by flow cytometry.

### **MC38 colon carcinoma mouse model**

Mice were housed in IVC under SPF conditions in the animal facility of Leiden University Medical Center (LUMC, Leiden, The Netherlands). Experiments were performed according to institutional and national guidelines and approved by the Animal Ethics Committee of the LUMC (Leiden, The Netherlands). C57BL/6 female mice obtained from Charles River Laboratories, 8 wk to 10 wk old, were subcutaneously (s.c.) injected with  $3 \times 10^5$  MC38 cells in the right flank of the mice. Tumor size was measured every 3 to 4 days using a caliper. Mice were i.v. or retro-orbitally injected with indicated doses of Doxo, Acla, diMe-doxo or 5 mL/kg of saline every week for the indicated times. Mice were monitored twice per week. When the tumor exceeded 500 mm<sup>3</sup> or the body-weight loss was more than 20%, the animal was killed by CO<sub>2</sub>. Then the heart, reproductive organ, and tumor were collected, fixed in EAF fixative (ethanol/acetic acid/formaldehyde/saline at 40:5:10:45 v/v) and embedded in paraffin for histopathological analysis.

### **Echocardiography**

Mice were housed in IVC under SPF conditions in the animal facility of the LUMC (Leiden, The Netherlands). Experiment was performed according to institutional and national guidelines and approved by the Animal Ethics Committee of the LUMC (Leiden, The Netherlands). Both male and female FVB N/ctr mice (8 wk old), were i.v. injected with 5 mg/kg of Doxo, 5 mg/kg of Acla, 5 mg/kg of diMe-doxo or 5 mL/kg of saline every week for eight times. Animal welfare was monitored every other day. *In vivo* cardiac function was assessed by transthoracic echocardiograph. Mice were anesthetized with 2% isoflurane, depilated, and imaged in a supine position using a Vevo 3100 high-resolution ultrasound system, equipped with a 40-MHz center frequency linear array transducer (MX550D, FUJIFILM VisualSonics Inc., Toronto, Canada). Body temperature was kept at 37°C, cardiac frequency was monitored with ECG and maintained between 400-600bpm. B-mode and M-mode echocardiography

graphic images were obtained in short-axis (SAX) view at the mid-papillary muscle level. Data were analyzed offline using VevoLAB software (FUIJIFILM VisualSonics, Toronto, Canada) and left-ventricular function was assessed using ejection fraction (EF) and fractional shortening (FS) of at least 3 cardiac cycles on SAX M-mode. To reconstruct the dimensions of the left ventricle and left atrium, 4D ultrasound imaging was performed by clamping the probe on a linearly translating step motor and positioning it parallel to the short axis of the left ventricle. System-integrated triggering between the motor and the probe resulted in automatically acquired high frame rate (300 fps) cardiac- and respiratory-gated cine loops with a 200  $\mu$ m step size covering apex to base, that were spatiotemporally compiled into 4D data. 3D images of the left ventricle and atrium were constructed by manual tracing offline using VevoLAB software (FUIJIFILM VisualSonics, Toronto, Canada).

### **Western blot and CFGE**

Cells were treated with drugs at indicated doses for 2 hours. Subsequently, drugs were removed by extensive washing, and cells were collected at indicated time points after drug removal and processed immediately for the assay. Cells were lysed directly in SDS-sample buffer (2% SDS, 10% glycerol, 5%  $\beta$ -mercaptoethanol, 60 mM Tris-HCl pH 6.8 and 0.01% bromophenol blue). Lysates were resolved by SDS/polyacrylamide gel electrophoresis followed by Western blotting. Primary antibodies used for blotting:  $\gamma$ H2AX (1:1000, 05-036, Millipore),  $\beta$ -actin (1:10000, A5441, Sigma), ubiquitin (1:500, P4D1, sc-8017, Santa Cruz),  $\alpha$ -tubulin (1:5000, 11223-1-AP, Protein tech). DNA double-strand breaks were quantified by constant-field gel electrophoresis, as described [46]. Images were quantified with ImageJ.

### **Fractionation assay**

Endogenously tagged scarlet-H2B cells were treated for 1 hour with 10  $\mu$ M of the indicated drugs. Cells were washed and lysed directly in lysis buffer (50mM Tris-HCl pH 8.0, 150 mM NaCl, 5 mM  $MgCl_2$ , 0.5% NP40, 2.5% glycerol supplemented with protease inhibitors, 10 mM NMM and 10  $\mu$ M MG132), collected, vortexed and incubated for 10 min on ice. To collect the cytosolic fraction samples were centrifuged for 10 minutes, 15000g, 4°C. Both nuclear (pellet) and cytosolic (supernatant) fractions were washed and prepared for Western blot analysis. Primary antibodies used for blotting: RFP (1:2000, 6G6, Chromotek), Lamin A/C (1:500, sc-20681, Santa Cruz), Calnexin (1:1000, C5C9, Cell signaling).

### **Comet assay**

Neutral comet assays were performed as described by Olive and Banath [48]. Pictures of individual cells were taken with a Zeiss AxioObserver Z1 inverted microscope equipped with a cooled Hamamatsu ORCAAG Black and White CCD camera and analyzed with CASP software 1.2.3b2 (<http://casplab.com/>).

### **Microscopy**

Cells stably expressing PAGFP-H2A, PAGFP-H3, or PAGFP-H4 were used for histone eviction experiments. Photoactivation and time-lapse confocal imaging were performed as described [24]. All live cell imaging experiments were analyzed by a Leica SP8 confocal microscope system, 63x lens, equipped with a climate chamber. Loss of fluorescence from the photoactivated region after different treatments was quantified using ImageJ software. For cytosolic H2B detection, endogenous tagged scarlet-H2B cells were seeded on coverslips. Upon treatment with 10  $\mu$ M



of the indicated drugs for 1 hour, cells were fixed in paraformaldehyde (PFA) 4%, permeabilized with 0.1% Triton, and stained with anti-RFP (1:100, 6G6, Chomotek), goat-anti-mouse-Alexa Fluor 488 (1:400, Thermo fisher Scientific) and Alexa Fluor 647 phalloidin (1:125, A22287, Thermo fisher Scientific). Cells were analyzed by a Leica SP8 confocal microscope system, 63x lens. Cells were quantified using ImageJ software.

### Cell viability assay

Indicated tumor cells or AML patient cells were seeded into 96-well plates. Twenty-four hours after seeding, cells were treated with indicated drugs for 2 hours at concentrations corresponding to physiological levels of cancer patients at standard treatment [24]. Subsequently, drugs were removed and cells were left to grow for an additional 72 hours. Cell viability was measured using the CellTiter-Blue viability assay (Promega). Relative survival was normalized to the untreated control and corrected for background signals.

### Flow cytometry for measuring drug uptake in cells

Cells were treated with 1  $\mu$ M of drug for the indicated time points. Samples were washed, collected, and fixed with paraformaldehyde. Samples were analyzed by flow cytometry using BD FACS aria II, with 561 nm laser and 610/20 nm detector. Drug uptake was quantified using FlowJo software.

### Detection of ROS

MelJuSo cells were treated with indicated drugs for 2 hours followed by drug removal. Cells were collected immediately or 1 day after drug removal for analysis. Cells were then incubated with 10  $\mu$ M of 2',7'-dichlorodihydrofluorescein diacetate (H2DCFDA) (Invitrogen, D399) for 30 min at 37 °C in the dark, and fluorescence was analyzed with an LSRFortessa™ flow cytometer (BD Biosciences). Mean fluorescence intensity of H2DCFDA was quantified using FlowJo software.

### Flow cytometry for phenotyping AML cells

Human AML cells were treated with indicated drug for 2 hours, followed by extensive washing. Three days later, the cells were stained with anti-CD45-V500 (2D1, BD Bioscience, 1:20), anti-CD34-BV421 (581, BD Bioscience, 1:20), anti-CD38-APC (HB7, BD Bioscience, 1:50), anti-CD33-PE-Cy7 (p67.6, BD Bioscience, 1:20), anti-CD3-PE (SK7, BD Bioscience, 1:50), anti-CD19-APC-H7 (SJ25C1, BD Bioscience, 1:10), 7AAD (BD Bioscience, 1:10) and anti-CD11b-FITC (Bear1, BD Bioscience, 1:10) or anti-CD7-FITC (M-T701, BD Bioscience, 1:20) for 30 minutes. 15  $\mu$ l of well-suspended flow count fluorospheres (Beckman Coulter) were added right before analyzed by flow cytometry with BD Fortessa™.

### Assessing drug toxicity on hiPSC-derived cardiac microtissues

hiPSC-derived cardiac microtissues composed of hiPSC-derived cardiomyocytes and hiPSC-derived cardiac endothelial cells were generated as described [52, 53], with addition of stromal cells derived from hiPSC-epicardial cells, differentiated in monolayer as described [54]. For contraction analysis, microtissues were seeded on a Matrigel-coated 96-well plate (plastic, Black/Clear tissue culture treated plate) and imaged 24 hour post drug treatment with 20 or 30  $\mu$ M of the indicated drugs. The Horn-Schunck Vector Flow analysis method was used to detect changes in pixel displacements during contraction of the microtissues. The analysis package was

developed with LabVIEW Motion and Vision (National Instruments). Images were collected at 100 frames per second with a Thor Labs camera DCC3260M (Thorlabs GmbH 85221) and a 10x objective phase contrast objective (Leica Inverted microscope IBDE). Microtissues were perfused with Tyrode's solution at 37 °C and paced at 1 Hz. Tyrode's solution contains: 140 mM NaCl, 5.4 mM KCl, 1.8 mM CaCl<sub>2</sub>, 1.0 mM MgCl<sub>2</sub>, 5.5 mM glucose and 5.0 mM HEPES; pH 7.4 (NaOH).

### AML patient data analysis

Patients with de novo geriatric AML treated between January 2014 and January 2019 in Ruijin Hospitals were enrolled in this retrospectively study. This study was approved by the ethics committee of Ruijin Hospital, and all patients provided written informed consent. Patients in the Acla group were treated with CAG regimen (Ara-C 15–25 mg/m<sup>2</sup> injected subcutaneously every 12 hours on day 1–14, Acla 20 mg/day infused intravenously on day 1–4, and granulocyte stimulating factor (G-CSF) 200 µg/m<sup>2</sup> administered s.c. daily on day 1 to 14). G-CSF was reduced, or temporarily stopped when neutrophilia was >5×10<sup>9</sup>/L. Patients of Ida group were treated with IA regimen (Ida 6–10 mg/m<sup>2</sup>/day infused i.v. on day 1 to 3 and Ara-C 100–200 mg/m<sup>2</sup> per day on day 1 to 7). Cytogenetic risk was classified according to the modified Southwest Oncology Group criteria [68]: 1) favorable risk, including t(8;21) and inv(16) or t(16;16)(p13;q22); 2) unfavorable risk, including del(5q) or monosomy 5, monosomy 7 or del(7q), abnormal 3q, 9q, 11q, 21q, or 17p, t(6;9), t(9;22), and complex karyotypes (three or more unrelated chromosomes abnormal); and 3) intermediate risk, including normal karyotypes and all other anomalies. Mutations in the NPM1 and CEBPA, and for FLT3 internal tandem duplication (FLT3-ITD), were tested. Integrated risk was classified according to ref. [69]. Complete remission (CR) was defined <5% blast cells in normocellular BM, PB counts showing neutrophils ≥1×10<sup>9</sup>/L and platelet count ≥100×10<sup>9</sup>/L, and the disappearance of all clinical signs of leukemia. Partial remission (PR) was defined as having <15% (and a 50% decrease in BM blasts) but >5% blasts or with <5% blasts but not reaching the CR criteria for blood cell count or clinical manifestation. For analysis of CR, missing data were imputed as no CR. The baseline characteristics and clinical outcomes of the patients are summarized in SI Appendix Table S2 and S3, respectively.

### Quantification and statistical analysis

Each sample was assayed in biological triplicate, unless stated otherwise. All error bars denote SD. Statistical analyses were performed using Prism 7 and 8 software (Graphpad Inc.). Student's t-test was used to compare two groups of independent samples. One-way ANOVA was used to compare more than two groups of independent samples. Two-way ANOVA with repeated measure analysis was used if the response of two drugs was compared over time. Kaplan-Meier analysis and Log-rank (Mantel-Cox) test were used to evaluate the statistical significance for comparison of survival curves. Western blot and confocal data were quantified using ImageJ software. Significance is represented on the graphs as follow: ns, not significant; \*p < 0.05; \*\*p < 0.01; \*\*\*p < 0.001; \*\*\*\*p < 0.0001. No statistical methods were used to predetermine sample size.

### Data availability

All data support the findings of this study are included in the main text and SI appendix. All procedures of experiments are described in detail in the Materials and Methods and SI appendix.



## ACKNOWLEDGEMENTS

We thank the animal facility at the NKI and the LUMC for support, Jos Jonkers for Trp53 heterozygous mice, Ilana Berlin for critical reading the manuscript, Berend van Meer for help with contraction data analysis, Cun Wang and Wenxin Qin for helpful discussion on AML patient data and Lennert Janssen for movie editing. This work was supported by European Research Council (ERC) advance grant and Koningin Wilhelmina Fonds (KWF) grants to J.N. and to C.L.M., RIKI foundation (C.L.Z.), the Institute for Chemical Immunology, and a Nederlandse Organisatie voor Wetenschappelijk Onderzoek (NWO) Gravitation project funded by the Ministry of Education, Culture and Science of the Netherlands (H.O. and J.N.).

## AUTHOR CONTRIBUTIONS

JN, XQ and SvdZ conceived the experiments. SvdZ with help of XQ performed all biochemical experiments. diMe-Doxo was made by DW under supervision of HO. XQ with help of SvdZ, CZ, JB and OvT performed the mouse experiments in FVB mice. AML PDX experiments were performed by NvG and AR under supervision of LS. Analysis of AML patient data is done by XL and XQ under supervision of JL. MC38 mouse experiments were performed by SD under supervision of RA. JYS performed mouse pathology. For the echocardiography mice experiment, treatment of the mice was performed by SvdZ, SG and XQ, echography was performed by TvH under supervision of AS. JA made the endogenous scarlet-H2B cell line. Human cardiac microtissues were generated, tested and analysed by EG, MB, VO and LT under supervision of CM. The manuscript was written by XQ, SvdZ and JN with input of all authors.

## DECLARATION OF INTERESTS

J. Neefjes is a shareholder in NIHM that aims to produce Acla for clinical use.

## REFERENCES

1. Weiss, R. B. (1992) The anthracyclines: will we ever find a better doxorubicin?, *Seminars in oncology*. 19, 670-86.
2. Rayson, D., Richel, D., Chia, S., Jackisch, C., van der Vegt, S. & Suter, T. (2008) Anthracycline-trastuzumab regimens for HER2/neu-overexpressing breast cancer: current experience and future strategies, *Annals of oncology : official journal of the European Society for Medical Oncology*. 19, 1530-9.
3. Lotrionte, M., Biondi-Zoccai, G., Abbate, A., Lanzetta, G., D'Ascenzo, F., Malavasi, V., Peruzzi, M., Frati, G. & Palazzoni, G. (2013) Review and meta-analysis of incidence and clinical predictors of anthracycline cardiotoxicity, *Am J Cardiol*. 112, 1980-4.
4. Shan, K., Lincoff, A. M. & Young, J. B. (1996) Anthracycline-induced cardiotoxicity, *Ann Intern Med*. 125, 47-58.
5. Chatterjee, K., Zhang, J., Honbo, N. & Karliner, J. S. (2010) Doxorubicin cardiomyopathy, *Cardiology*. 115, 155-62.
6. Swain, S. M., Whaley, F. S. & Ewer, M. S. (2003) Congestive heart failure in patients treated with doxorubicin: a retrospective analysis of three trials, *Cancer*. 97, 2869-79.
7. Liu, L., Qu, Q., Jiao, W., Zhang, Y., Li, X., Ding, C. & Wu, D. (2015) Increasing aclarubicin dose in low-dose cytarabine and aclarubicin in combination with granulocyte colony-stimulating factor (CAG regimen) is efficacious as salvage chemother-

- apy for relapsed/refractory mixed-phenotype acute leukemia, *Leuk Res.* 39, 805-11.
8. Qu, Q., Liu, L., Zhang, Y., Li, X. & Wu, D. (2015) Increasing aclarubicin dosage of the conventional CAG (low-dose cytarabine and aclarubicin in combination with granulocyte colony-stimulating factor) regimen is more efficacious as a salvage therapy than CAG for relapsed/refractory acute myeloid leukemia, *Leuk Res.* 39, 1353-9.
  9. Sadurska, E. (2015) Current Views on Anthracycline Cardiotoxicity in Childhood Cancer Survivors, *Pediatric cardiology.* 36, 1112-9.
  10. Mulrooney, D. A., Yeazel, M. W., Kawashima, T., Mertens, A. C., Mitby, P., Stovall, M., Donaldson, S. S., Green, D. M., Sklar, C. A., Robison, L. L. & Leisenring, W. M. (2009) Cardiac outcomes in a cohort of adult survivors of childhood and adolescent cancer: retrospective analysis of the Childhood Cancer Survivor Study cohort, *Bmj.* 339, b4606.
  11. Grenier, M. A. & Lipshultz, S. E. (1998) Epidemiology of anthracycline cardiotoxicity in children and adults, *Seminars in oncology.* 25, 72-85.
  12. Volkova, M. & Russell, R., 3rd (2011) Anthracycline cardiotoxicity: prevalence, pathogenesis and treatment, *Current cardiology reviews.* 7, 214-20.
  13. Shakir, D. K. & Rasul, K. I. (2009) Chemotherapy induced cardiomyopathy: pathogenesis, monitoring and management, *Journal of clinical medicine research.* 1, 8-12.
  14. Mistry, A. R., Felix, C. A., Whitmarsh, R. J., Mason, A., Reiter, A., Cassinat, B., Parry, A., Walz, C., Wiemels, J. L., Segal, M. R., Ades, L., Blair, I. A., Osheroff, N., Peniket, A. J., Lafage-Pochitaloff, M., Cross, N. C., Chomienne, C., Solomon, E., Fenaux, P. & Grimwade, D. (2005) DNA topoisomerase II in therapy-related acute promyelocytic leukemia, *N Engl J Med.* 352, 1529-38.
  15. Ratain, M. J. & Rowley, J. D. (1992) Therapy-related acute myeloid leukemia secondary to inhibitors of topoisomerase II: from the bedside to the target genes, *Annals of oncology : official journal of the European Society for Medical Oncology.* 3, 107-11.
  16. Smith, R. E., Bryant, J., DeCillis, A., Anderson, S., National Surgical Adjuvant, B. & Bowel Project, E. (2003) Acute myeloid leukemia and myelodysplastic syndrome after doxorubicin-cyclophosphamide adjuvant therapy for operable breast cancer: the National Surgical Adjuvant Breast and Bowel Project Experience, *Journal of clinical oncology : official journal of the American Society of Clinical Oncology.* 21, 1195-204.
  17. Andre, M., Mounier, N., Leleu, X., Sonet, A., Brice, P., Henry-Amar, M., Tilly, H., Coiffier, B., Bosly, A., Morel, P., Haioun, C., Gaulard, P., Reyes, F., Gisselbrecht, C. & Groupe D'Etude Des Lymphomes De, L. A. (2004) Second cancers and late toxicities after treatment of aggressive non-Hodgkin lymphoma with the ACVBP regimen: a GELA cohort study on 2837 patients, *Blood.* 103, 1222-8.
  18. Kayser, S., Dohner, K., Krauter, J., Kohne, C. H., Horst, H. A., Held, G., von Lilienfeld-Toal, M., Wilhelm, S., Kundgen, A., Gotze, K., Rummel, M., Nachbaur, D., Schlegelberger, B., Gohring, G., Spath, D., Morlok, C., Zucknick, M., Ganser, A., Dohner, H., Schlenk, R. F. & German-Austrian, A. (2011) The impact of therapy-related acute myeloid leukemia (AML) on outcome in 2853 adult patients with newly diagnosed AML, *Blood.* 117, 2137-45.
  19. Hulegardh, E., Nilsson, C., Lazarevic, V., Garelius, H., Antunovic, P., Rangert Derolf, A., Mollgard, L., Uggla, B., Wennstrom, L., Wahlin, A., Hoglund, M., Juliusson, G., Stockelberg, D. & Lehmann, S. (2015) Characterization and prognostic features of secondary acute myeloid leukemia in a population-based setting: a report from

- the Swedish Acute Leukemia Registry, *American journal of hematology*. 90, 208-14.
20. Felix, C. A. (1998) Secondary leukemias induced by topoisomerase-targeted drugs, *Biochim Biophys Acta*. 1400, 233-55.
  21. Govindan, R. & Morgensztern, D. (2012) *Devita, Hellman, and Rosenberg's Cancer: Principles and Practice of Oncology Review*, Wolters Kluwer Health.
  22. Tewey, K. M., Rowe, T. C., Yang, L., Halligan, B. D. & Liu, L. F. (1984) Adriamycin-induced DNA damage mediated by mammalian DNA topoisomerase II, *Science*. 226, 466-8.
  23. Chen, G. L., Yang, L., Rowe, T. C., Halligan, B. D., Tewey, K. M. & Liu, L. F. (1984) Nonintercalative antitumor drugs interfere with the breakage-reunion reaction of mammalian DNA topoisomerase II, *The Journal of biological chemistry*. 259, 13560-6.
  24. Pang, B., Qiao, X., Janssen, L., Velds, A., Groothuis, T., Kerkhoven, R., Nieuwland, M., Ova, H., Rottenberg, S., van Tellingen, O., Janssen, J., Huijgens, P., Zwart, W. & Neefjes, J. (2013) Drug-induced histone eviction from open chromatin contributes to the chemotherapeutic effects of doxorubicin, *Nature communications*. 4, 1908.
  25. Girling, D. J. (1996) Comparison of oral etoposide and standard intravenous multidrug chemotherapy for small-cell lung cancer: a stopped multicentre randomised trial. Medical Research Council Lung Cancer Working Party, *Lancet*. 348, 563-6.
  26. Hong, W. K., Nicaise, C., Lawson, R., Maroun, J. A., Comis, R., Speer, J., Luedke, D., Hurtubise, M., Lanzotti, V., Goodlow, J. & et al. (1989) Etoposide combined with cyclophosphamide plus vincristine compared with doxorubicin plus cyclophosphamide plus vincristine and with high-dose cyclophosphamide plus vincristine in the treatment of small-cell carcinoma of the lung: a randomized trial of the Bristol Lung Cancer Study Group, *Journal of clinical oncology : official journal of the American Society of Clinical Oncology*. 7, 450-6.
  27. Yang, F., Kemp, C. J. & Henikoff, S. (2013) Doxorubicin enhances nucleosome turnover around promoters, *Curr Biol*. 23, 782-7.
  28. Neshet, E., Safina, A., Aljhdali, I., Portwood, S., Wang, E. S., Koman, I., Wang, J. & Gurova, K. V. (2018) Role of Chromatin Damage and Chromatin Trapping of FACT in Mediating the Anticancer Cytotoxicity of DNA-Binding Small-Molecule Drugs, *Cancer research*. 78, 1431-1443.
  29. Pang, B., de Jong, J., Qiao, X., Wessels, L. F. & Neefjes, J. (2015) Chemical profiling of the genome with anti-cancer drugs defines target specificities, *Nat Chem Biol*. 11, 472-80.
  30. Wei, G., Ni, W., Chiao, J. W., Cai, Z., Huang, H. & Liu, D. (2011) A meta-analysis of CAG (cytarabine, aclarubicin, G-CSF) regimen for the treatment of 1029 patients with acute myeloid leukemia and myelodysplastic syndrome, *Journal of hematology & oncology*. 4, 46.
  31. Jin, J., Wang, J. X., Chen, F. F., Wu, D. P., Hu, J., Zhou, J. F., Hu, J. D., Wang, J. M., Li, J. Y., Huang, X. J., Ma, J., Ji, C. Y., Xu, X. P., Yu, K., Ren, H. Y., Zhou, Y. H., Tong, Y., Lou, Y. J., Ni, W. M., Tong, H. Y., Wang, H. F., Mi, Y. C., Du, X., Chen, B. A., Shen, Y., Chen, Z. & Chen, S. J. (2013) Homoharringtonine-based induction regimens for patients with de-novo acute myeloid leukaemia: a multicentre, open-label, randomised, controlled phase 3 trial, *The Lancet Oncology*. 14, 599-608.
  32. Jonkers, J., Meuwissen, R., van der Gulden, H., Peterse, H., van der Valk, M. & Berns, A. (2001) Synergistic tumor suppressor activity of BRCA2 and p53 in a conditional mouse model for breast cancer, *Nature genetics*. 29, 418-25.
  33. Ben-Yehuda, D., Krichevsky, S., Caspi, O., Rund, D., Polliack, A., Abeliovich,

- D., Zelig, O., Yahalom, V., Paltiel, O., Or, R., Peretz, T., Ben-Neriah, S., Yehuda, O. & Rachmilewitz, E. A. (1996) Microsatellite instability and p53 mutations in therapy-related leukemia suggest mutator phenotype, *Blood*. 88, 4296-303.
34. Wong, T. N., Ramsingh, G., Young, A. L., Miller, C. A., Touma, W., Welch, J. S., Lamprecht, T. L., Shen, D., Hundal, J., Fulton, R. S., Heath, S., Baty, J. D., Kico, J. M., Ding, L., Mardis, E. R., Westervelt, P., DiPersio, J. F., Walter, M. J., Graubert, T. A., Ley, T. J., Druley, T., Link, D. C. & Wilson, R. K. (2015) Role of TP53 mutations in the origin and evolution of therapy-related acute myeloid leukaemia, *Nature*. 518, 552-555.
35. Gabizon, A., Meshorer, A. & Barenholz, Y. (1986) Comparative long-term study of the toxicities of free and liposome-associated doxorubicin in mice after intravenous administration, *J Natl Cancer Inst*. 77, 459-69.
36. Hanahan, D. & Weinberg, R. A. (2011) Hallmarks of cancer: the next generation, *Cell*. 144, 646-74.
37. Teepen, J. C., van Leeuwen, F. E., Tissing, W. J., van Dulmen-den Broeder, E., van den Heuvel-Eibrink, M. M., van der Pal, H. J., Loonen, J. J., Bresters, D., Versluys, B., Neggers, S., Jaspers, M. W. M., Hauptmann, M., van der Heiden-van der Loo, M., Visser, O., Kremer, L. C. M., Ronckers, C. M. & Group, D. L. S. (2017) Long-Term Risk of Subsequent Malignant Neoplasms After Treatment of Childhood Cancer in the DCOG LATER Study Cohort: Role of Chemotherapy, *J Clin Oncol*. 35, 2288-2298.
38. Henderson, T. O., Moskowitz, C. S., Chou, J. F., Bradbury, A. R., Neglia, J. P., Dang, C. T., Onel, K., Novetsky Friedman, D., Bhatia, S., Strong, L. C., Stovall, M., Kenney, L. B., Barnea, D., Lorenzi, E., Hammond, S., Leisenring, W. M., Robison, L. L., Armstrong, G. T., Diller, L. R. & Oeffinger, K. C. (2016) Breast Cancer Risk in Childhood Cancer Survivors Without a History of Chest Radiotherapy: A Report From the Childhood Cancer Survivor Study, *Journal of clinical oncology : official journal of the American Society of Clinical Oncology*. 34, 910-8.
39. Hequet, O., Le, Q. H., Moullet, I., Pauli, E., Salles, G., Espinouse, D., Dumontet, C., Thieblemont, C., Arnaud, P., Antal, D., Bouafia, F. & Coiffier, B. (2004) Subclinical late cardiomyopathy after doxorubicin therapy for lymphoma in adults, *Journal of clinical oncology : official journal of the American Society of Clinical Oncology*. 22, 1864-71.
40. Fujihira, S., Yamamoto, T., Matsumoto, M., Yoshizawa, K., Oishi, Y., Fujii, T., Noguchi, H. & Mori, H. (1993) The high incidence of atrial thrombosis in mice given doxorubicin, *Toxicol Pathol*. 21, 362-8.
41. Lefrak, E. A., Pitha, J., Rosenheim, S. & Gottlieb, J. A. (1973) A clinicopathologic analysis of adriamycin cardiotoxicity, *Cancer*. 32, 302-14.
42. Zhao, S., Wu, H., Xia, W., Chen, X., Zhu, S., Zhang, S., Shao, Y., Ma, W., Yang, D. & Zhang, J. (2014) Periostin expression is upregulated and associated with myocardial fibrosis in human failing hearts, *J Cardiol*. 63, 373-8.
43. Lencova-Popelova, O., Jirkovsky, E., Mazurova, Y., Lenco, J., Adamcova, M., Simunek, T., Gersl, V. & Sterba, M. (2014) Molecular remodeling of left and right ventricular myocardium in chronic anthracycline cardiotoxicity and post-treatment follow up, *PloS one*. 9, e96055.
44. Ogawara, D., Fukuda, M., Nakamura, Y. & Kohno, S. (2010) Efficacy and safety of amrubicin hydrochloride for treatment of relapsed small cell lung cancer, *Cancer management and research*. 2, 191-5.
45. Speth, P. A., van Hoesel, Q. G. & Haanen, C. (1988) Clinical pharmacokinetics of doxorubicin, *Clin Pharmacokinet*. 15, 15-31.

46. Wlodek, D., Banath, J. & Olive, P. L. (1991) Comparison between pulsed-field and constant-field gel electrophoresis for measurement of DNA double-strand breaks in irradiated Chinese hamster ovary cells, *International journal of radiation biology*. 60, 779-90.
47. Neijenhuis, S., Verwijs-Janssen, M., Kasten-Pisula, U., Rumping, G., Borgmann, K., Dikomey, E., Begg, A. C. & Vens, C. (2009) Mechanism of cell killing after ionizing radiation by a dominant negative DNA polymerase beta, *DNA Repair (Amst)*. 8, 336-46.
48. Olive, P. L. & Banath, J. P. (2006) The comet assay: a method to measure DNA damage in individual cells, *Nat Protoc*. 1, 23-9.
49. Kuo, L. J. & Yang, L. X. (2008) Gamma-H2AX - a novel biomarker for DNA double-strand breaks, *In vivo*. 22, 305-9.
50. Suzuki, T., Minamide, S., Iwasaki, T., Yamamoto, H. & Kanda, H. (1997) Cardiotoxicity of a new anthracycline derivative (SM-5887) following intravenous administration to rabbits: comparative study with doxorubicin, *Investigational new drugs*. 15, 219-25.
51. Sanchez, P. V., Perry, R. L., Sarry, J. E., Perl, A. E., Murphy, K., Swider, C. R., Bagg, A., Choi, J. K., Biegel, J. A., Danet-Desnoyers, G. & Carroll, M. (2009) A robust xenotransplantation model for acute myeloid leukemia, *Leukemia*. 23, 2109-17.
52. Giacomelli, E., Bellin, M., Orlova, V. V. & Mummery, C. L. (2017) Co-Differentiation of Human Pluripotent Stem Cells-Derived Cardiomyocytes and Endothelial Cells from Cardiac Mesoderm Provides a Three-Dimensional Model of Cardiac Microtissue, *Curr Protoc Hum Genet*. 95, 21 9 1-21 9 22.
53. Giacomelli, E., Bellin, M., Sala, L., van Meer, B. J., Tertoolen, L. G., Orlova, V. V. & Mummery, C. L. (2017) Three-dimensional cardiac microtissues composed of cardiomyocytes and endothelial cells co-differentiated from human pluripotent stem cells, *Development*. 144, 1008-1017.
54. Guadix, J. A., Orlova, V. V., Giacomelli, E., Bellin, M., Ribeiro, M. C., Mummery, C. L., Perez-Pomares, J. M. & Passier, R. (2017) Human Pluripotent Stem Cell Differentiation into Functional Epicardial Progenitor Cells, *Stem Cell Reports*. 9, 1754-1764.
55. Sala, L., van Meer, B. J., Tertoolen, L. G. J., Bakkers, J., Bellin, M., Davis, R. P., Denning, C., Dieben, M. A. E., Eschenhagen, T., Giacomelli, E., Grandela, C., Hansen, A., Holman, E. R., Jongbloed, M. R. M., Kamel, S. M., Koopman, C. D., Lachaud, Q., Mannhardt, I., Mol, M. P. H., Mosqueira, D., Orlova, V. V., Passier, R., Ribeiro, M. C., Saleem, U., Smith, G. L., Burton, F. L. & Mummery, C. L. (2018) MUSCLEMOTION: A Versatile Open Software Tool to Quantify Cardiomyocyte and Cardiac Muscle Contraction In Vitro and In Vivo, *Circ Res*. 122, e5-e16.
56. Aapro, M., Bernard-Marty, C., Brain, E. G., Batist, G., Erdkamp, F., Krzemieniecki, K., Leonard, R., Lluch, A., Monfardini, S., Ryberg, M., Soubeyran, P. & Wedding, U. (2011) Anthracycline cardiotoxicity in the elderly cancer patient: a SIOG expert position paper, *Annals of oncology : official journal of the European Society for Medical Oncology*. 22, 257-67.
57. Myers, C. E., McGuire, W. P., Liss, R. H., Ifrim, I., Grotzinger, K. & Young, R. C. (1977) Adriamycin: the role of lipid peroxidation in cardiac toxicity and tumor response, *Science*. 197, 165-7.
58. Swain, S. M., Whaley, F. S., Gerber, M. C., Weisberg, S., York, M., Spicer, D., Jones, S. E., Wadler, S., Desai, A., Vogel, C., Speyer, J., Mittelman, A., Reddy, S., Pendergrass, K., Velez-Garcia, E., Ewer, M. S., Bianchini, J. R. & Gams, R. A. (1997) Cardioprotection with dexrazoxane for doxorubicin-containing therapy in ad-



- vanced breast cancer, *Journal of clinical oncology : official journal of the American Society of Clinical Oncology*. 15, 1318-32.
59. Martin, E., Thougard, A. V., Grauslund, M., Jensen, P. B., Bjorkling, F., Hasinoff, B. B., Tjornelund, J., Sehested, M. & Jensen, L. H. (2009) Evaluation of the topoisomerase II-inactive bisdioxopiperazine ICRF-161 as a protectant against doxorubicin-induced cardiomyopathy, *Toxicology*. 255, 72-9.
60. Myers, C., Bonow, R., Palmeri, S., Jenkins, J., Corden, B., Locker, G., Doroshow, J. & Epstein, S. (1983) A randomized controlled trial assessing the prevention of doxorubicin cardiomyopathy by N-acetylcysteine, *Seminars in oncology*. 10, 53-5.
61. Hashimoto, K., Ito, K. & Ishimori, Y. (1994) Novel DNA Sensor for Electrochemical Gene Detection, *Analytica Chimica Acta*. 286, 219-224.
62. Gabizon, A. A., Patil, Y. & La-Beck, N. M. (2016) New insights and evolving role of pegylated liposomal doxorubicin in cancer therapy, *Drug resistance updates : reviews and commentaries in antimicrobial and anticancer chemotherapy*. 29, 90-106.
63. van Asperen, J., van Tellingen, O., Tijssen, F., Schinkel, A. H. & Beijnen, J. H. (1999) Increased accumulation of doxorubicin and doxorubicinol in cardiac tissue of mice lacking *mdr1a* P-glycoprotein, *British journal of cancer*. 79, 108-13.
64. Steinhorst, U. H., Chen, E. P., Freedman, S. F., Machemer, R. & Hatchell, D. L. (1994) Growth inhibition of human Tenon's capsule fibroblasts and rabbit dermal fibroblasts with non-carcinogenic N-alkylated anthracyclines, *Graefes Arch Clin Exp Ophthalmol*. 232, 347-54.
65. Schaefer, A., Westendorf, J., Lingelbach, K., Schmidt, C. A., Mihalache, D. L., Reymann, A. & Marquardt, H. (1993) Decreased resistance to N,N-dimethylated anthracyclines in multidrug-resistant Friend erythroleukemia cells, *Cancer Chemother Pharmacol*. 31, 301-7.
66. Binaschi, M., Capranico, G., Dal Bo, L. & Zunino, F. (1997) Relationship between lethal effects and topoisomerase II-mediated double-stranded DNA breaks produced by anthracyclines with different sequence specificity, *Molecular pharmacology*. 51, 1053-9.
67. van Asperen, J., van Tellingen, O. & Beijnen, J. H. (1998) Determination of doxorubicin and metabolites in murine specimens by high-performance liquid chromatography, *J Chromatogr B Biomed Sci Appl*. 712, 129-43.
68. Slovak, M. L., Kopecky, K. J., Cassileth, P. A., Harrington, D. H., Theil, K. S., Mohamed, A., Paietta, E., Willman, C. L., Head, D. R., Rowe, J. M., Forman, S. J. & Appelbaum, F. R. (2000) Karyotypic analysis predicts outcome of preremission and postremission therapy in adult acute myeloid leukemia: a Southwest Oncology Group/Eastern Cooperative Oncology Group Study, *Blood*. 96, 4075-83.
69. Dohner, H., Estey, E. H., Amadori, S., Appelbaum, F. R., Buchner, T., Burnett, A. K., Dombret, H., Fenau, P., Grimwade, D., Larson, R. A., Lo-Coco, F., Naoe, T., Niederwieser, D., Ossenkoppele, G. J., Sanz, M. A., Sierra, J., Tallman, M. S., Lowenberg, B., Bloomfield, C. D. & European, L. (2010) Diagnosis and management of acute myeloid leukemia in adults: recommendations from an international expert panel, on behalf of the European LeukemiaNet, *Blood*. 115, 453-74.

# SUPPLEMENTAL INFORMATION

3





Tumor types	Saline (n=26)	Doxo (n=22)	Etop (n=28)	Acla (n=26)	Chi-square test <i>P</i> value
Thymic lymphoma	4 (15%)	1 (4.5%)	2 (7.1%)	2 (7.7%)	0,5571
Spindle cell sarcoma/ rhabdomyosarcoma	9 (35%)	8 (36%)	10 (36%)	13 (50%)	0,7168
Histiocytic sarcoma	3 (12%)	0 (0%)	2 (7.1%)	2 (7.7%)	0,4666
Fibrosarcoma	0 (0%)	0 (0%)	2 (7.1%)	0 (0%)	0,1409
Hemangiosarcoma	1 (3.8%)	0 (0%)	0 (0%)	1 (3.8%)	0,5880
Osteosarcoma	2 (7.7%)	1 (4.5%)	0 (0%)	3 (12%)	0,3424
Harderian gland adenoma	1 (3.8%)	0 (0%)	1 (3.6%)	2 (7.7%)	0,6161
Lung carcinoma/adenoma	6 (23%)	1 (4.5%)	4 (14%)	5 (19%)	0,3382
Adenocarcinoma/carcinosarcoma/ sarcoma of mammary gland	1 (3.8%) (9.1%)	11 (50%)*** (65%)**	3 (11%)^ (20%)	3 (12%)^ (23%)	<b>&lt;0.0001</b> <b>0,0060</b>
Squamous cell carcinoma	1 (3.8%)	4 (18%)	2 (7.1%)	0 (0%)^	0,0774
Others	4 (15%)	1 (4.5%)	8 (29%)	3 (12%)	0,1090

**Table S1. The spectrum and incidence of tumors observed in Trp53<sup>+/-</sup> FVB mice after drug treatments.** The isolated tumors were histopathologically analyzed for diagnosis. The number of animals appearing with a defined tumor type is listed in the table for each group. Of note, some mice suffered from two types of tumors at the same time. The corresponding cumulative incidence is indicated in brackets. *Italic characters indicate the cumulative incidence in females*, \*\* *P* = 0.008. Fisher's exact test, two-sided. Saline vs treatment, \*\*\**P* = 0.0004; \*\**P* = 0.0060; Doxo vs other treatment, ^*P* = 0.0376, ^^*P* < 0.01. Not significant results are not marked by symbols.

**Figure S1. Continued (E).** Two-way ANOVA with RM, \*\**P* < 0.01; \*\*\**P* < 0.001. (F) Cumulative incidence of cardiotoxicity including all observed alterations in the heart: thrombosis formation, degenerative changes of the myocytes, inflammatory infiltration and edematous changes in the myocardium or epicardium. (G) Median survival time for each group in weeks following different doses of Doxo treatment. Log-rank (Mantel-Cox) test, \**P* = 0.0439; \*\**P* = 0.0022. (H) Incidence rate of cardiotoxicity including all observed alterations in the Trp53<sup>+/-</sup> FVB mouse hearts. Cumulative incidence is indicated next to the curve. Two-way ANOVA with RM, \*\*\*\**P* < 0.0001.

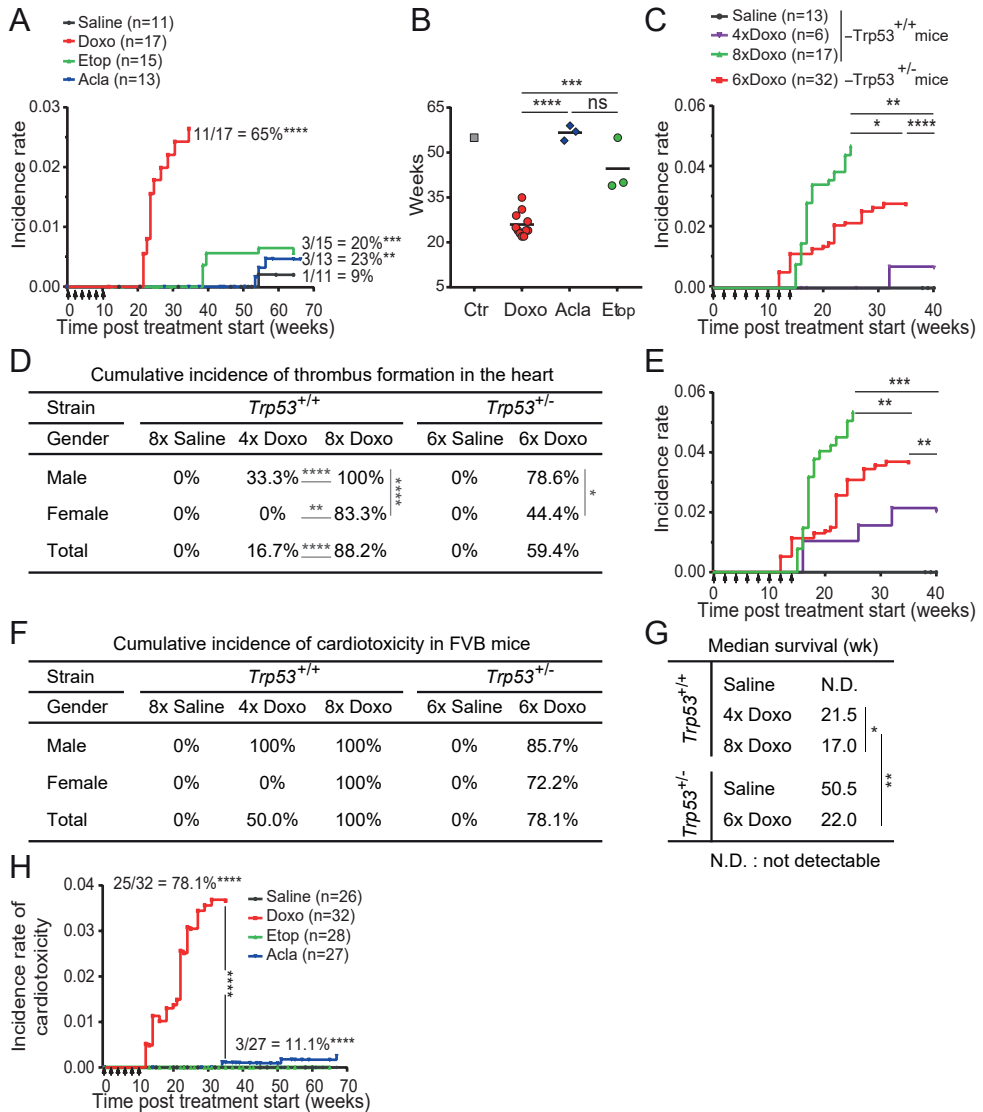


**Figure S1. Side effects induced by Doxo treatment in FVB mice.** *Trp53*<sup>+/-</sup> FVB mice were i.v. injected with 5 mg/kg of Doxo, 5 mg/kg of Acla, 25 mg/kg of Etop, or 5 ml/kg of saline every two weeks for six times, whereas *Trp53*<sup>+/+</sup> FVB mice were i.v. injected with 5 mg/kg of Doxo or 5 ml/kg of saline every two weeks for indicated times. Injections were indicated by arrows. (A) The incidence rate of breast cancer in *Trp53*<sup>+/-</sup> FVB mice. The cumulative incidence of each group is indicated next to the line. Two-way ANOVA with RM, \*\**P* < 0.01; \*\*\**P* < 0.001; \*\*\*\**P* < 0.0001. (B) The latency for breast cancer development. Unpaired *t* test, \*\*\**P* < 0.0001; \*\*\*\**P* < 0.0001. (C) Incidence rate of thrombus formation in the heart related to various doses of Doxo. Two-way ANOVA with RM, \**P* < 0.05; \*\**P* < 0.01; \*\*\**P* < 0.0001. (D) Cumulative incidence of thrombus formation. Fisher's exact test, two-sided: \**P* < 0.05; \*\**P* < 0.01; \*\*\*\**P* < 0.0001. (E) Incidence rate of cardiotoxicity including all observed alterations in the heart: thrombosis formation, degenerative changes of the myocytes, inflammatory infiltration and edematous changes in the myocardium or epicardium.

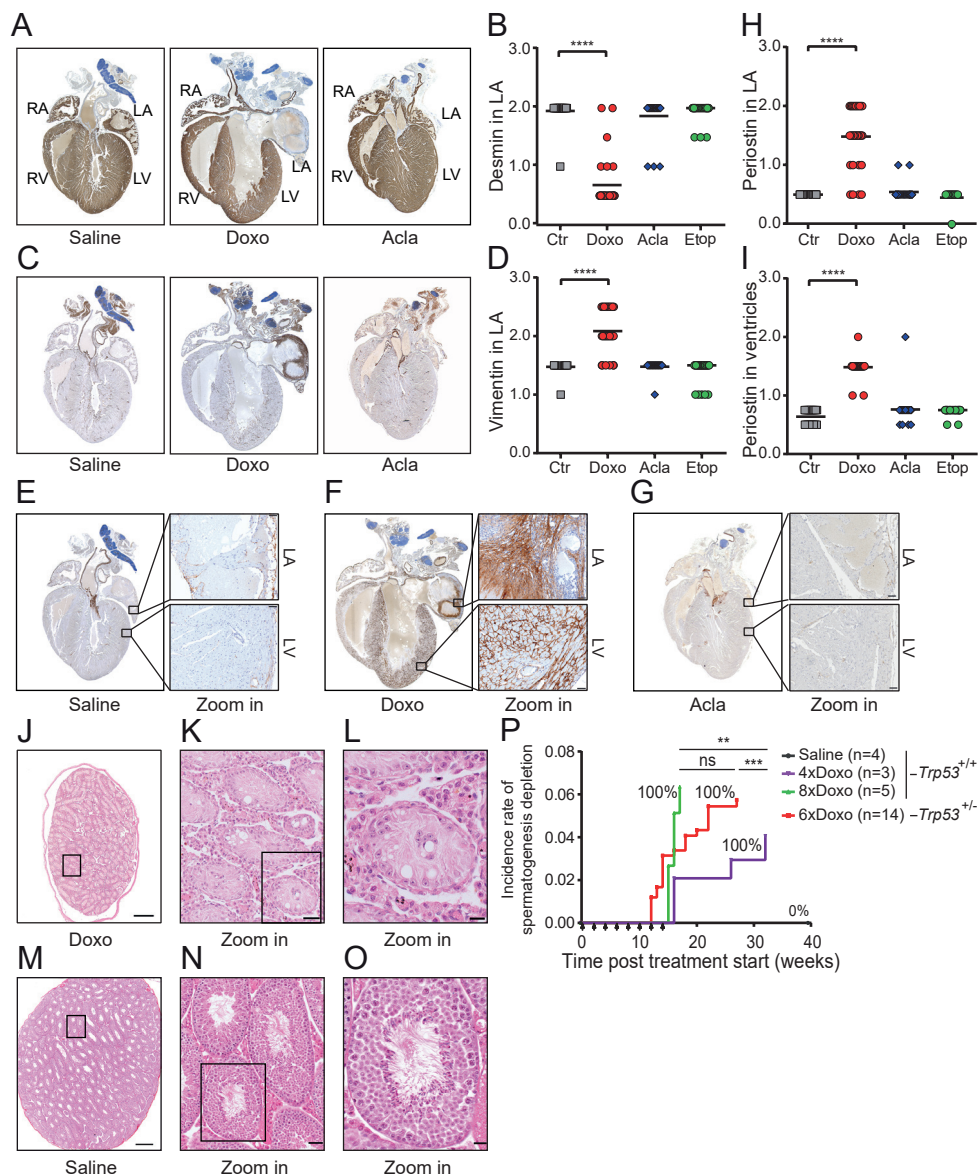


**Figure S2. Cardiotoxicity and depletion of spermatogenesis by Doxo treatment in  $Trp53^{+/-}$  FVB mice.** (A) Representative Desmin staining of the hearts from saline-, Doxo- or Acla-treated mouse. RA = right atrium, RV = right ventricle, LA = left atrium, LV = left ventricle. (B) Quantification of Desmin staining in the LA. Kruskal-Wallis test, \*\*\*\* $P < 0.0001$ . Ctr vs Acla or Etop is ns. (C) Representative Vimentin staining of the hearts from saline-, Doxo- or Acla-treated mouse. (D) Quantification of Vimentin staining in the LA. Kruskal-Wallis test, \*\*\*\* $P < 0.0001$ . Ctr vs Acla or Etop is ns. (E) Representative Periostin staining of the heart from a saline-treated mouse. Scale bars, 50  $\mu$ m. (F) Representative Periostin staining of the heart from a Doxo-treated mouse. Scale bars, 50  $\mu$ m. (G) Representative Periostin staining of the heart from an Acla-treated mouse. Scale bars, 50  $\mu$ m.

**Figure S2. continued.** (H) Quantification of Periostin staining in the LA. Kruskal-Wallis test, \*\*\*\* $P < 0.0001$ . Ctr vs Acla or Etop is ns. (I) Quantification of Periostin staining in the ventricles. Kruskal-Wallis test, \*\*\*\* $P < 0.0001$ . Ctr vs Acla or Etop is ns. (J) An overview of a section of the testis from a Doxo-treated mouse. Scale bar, 500  $\mu$ m. (K) and (L) Higher magnifications from the same testis showing depletion of spermatogenesis. Scale bars, 50  $\mu$ m, 20  $\mu$ m, respectively. (M) An overview of a section of the testis from a saline-treated mouse. Scale bar, 500  $\mu$ m. (N) and (O) Higher magnification from the same testis showing no abnormalities and normal spermatogenesis. Scale bars, 50  $\mu$ m, 20  $\mu$ m, respectively. (P) Depletion of spermatogenesis related to cumulative dose of Doxo. Incidence rate of spermatogenesis depletion is plotted for all groups. Cumulative incidence of spermatogenesis depletion is listed next to the line. Two-way ANOVA with RM, \*\* $P < 0.01$ ; \*\*\* $P < 0.001$ .

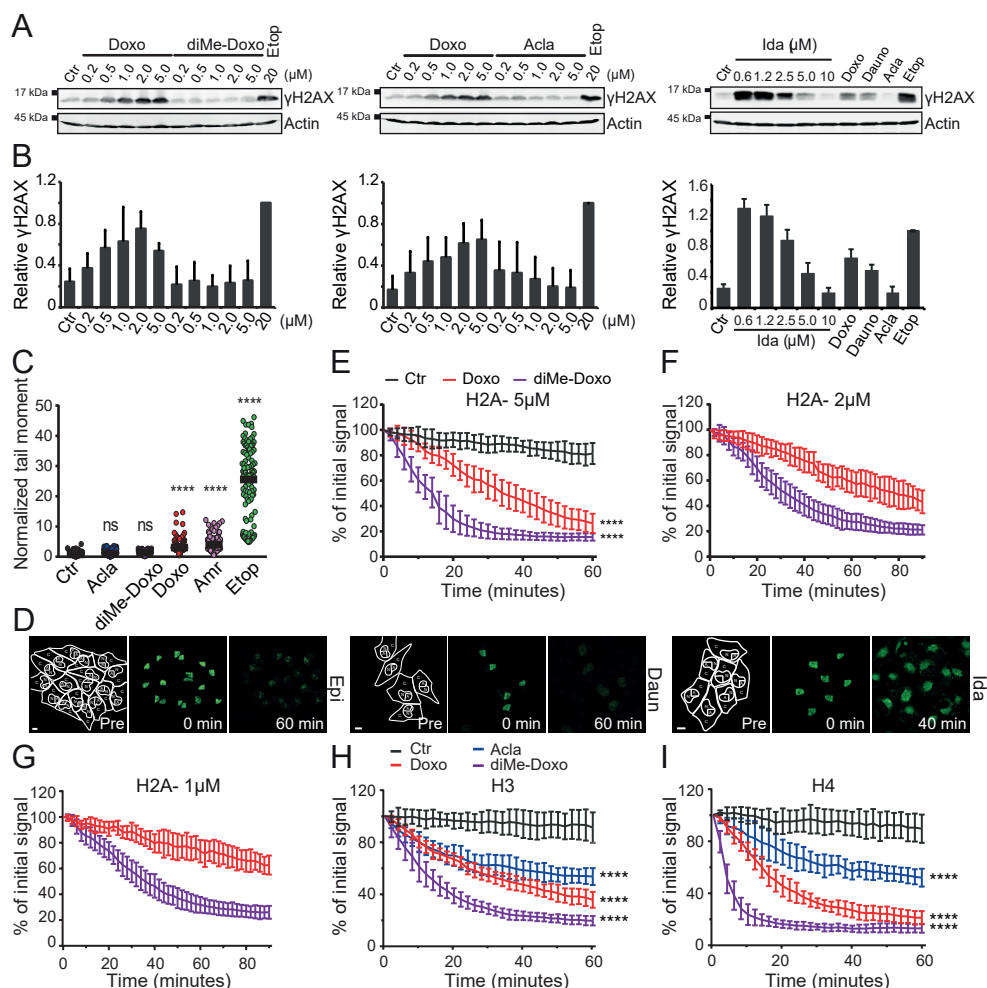


**Figure S3. DNA- and chromatin-damaging activities of Topo II poisons.** (A) K562 cells were treated for 2 hours with indicated drugs and concentrations; subsequently  $\gamma$ H2AX levels were detected by Western blot. (B) Quantification of  $\gamma$ H2AX signal as for Figure 2C. (C) MeJuSo cells were treated for 2 hour with 10  $\mu$ M of anthracyclines or 50  $\mu$ M of Etop and DNA damage was examined using a neutral comet assay, normalized tail moment is plotted. Kruskal-Wallis test, \*\*\*\* $P < 0.0001$ , ns, not significant.

**Figure S3. Continued.** (D) Part of the nucleus from MelJuSo PAGFP-H2A cells were photo-activated. The photo-activated PAGFP-H2A was monitored by time-lapse confocal microscopy for 1 hour either or not in the presence of 10  $\mu$ M of drugs indicated. Lines in the left panel define the cytoplasmic compartment (C), the nuclear compartment (N) and the activated area (A). Scale bar, 10  $\mu$ m. (E-G) Quantification of the release of PAGFP-H2A from the photo-activated regions after the administration of different concentrations of Doxo and diMe-Doxo. Two-way ANOVA, Ctr vs Doxo or diMe-Doxo, \*\*\*\* $P < 0.0001$ . (H and I) Quantification of release of PAGFP-H3 (H) and H4 (I). Two-way ANOVA, ctr vs Doxo, diMe-Doxo or Acla, \*\*\*\* $P < 0.0001$ .

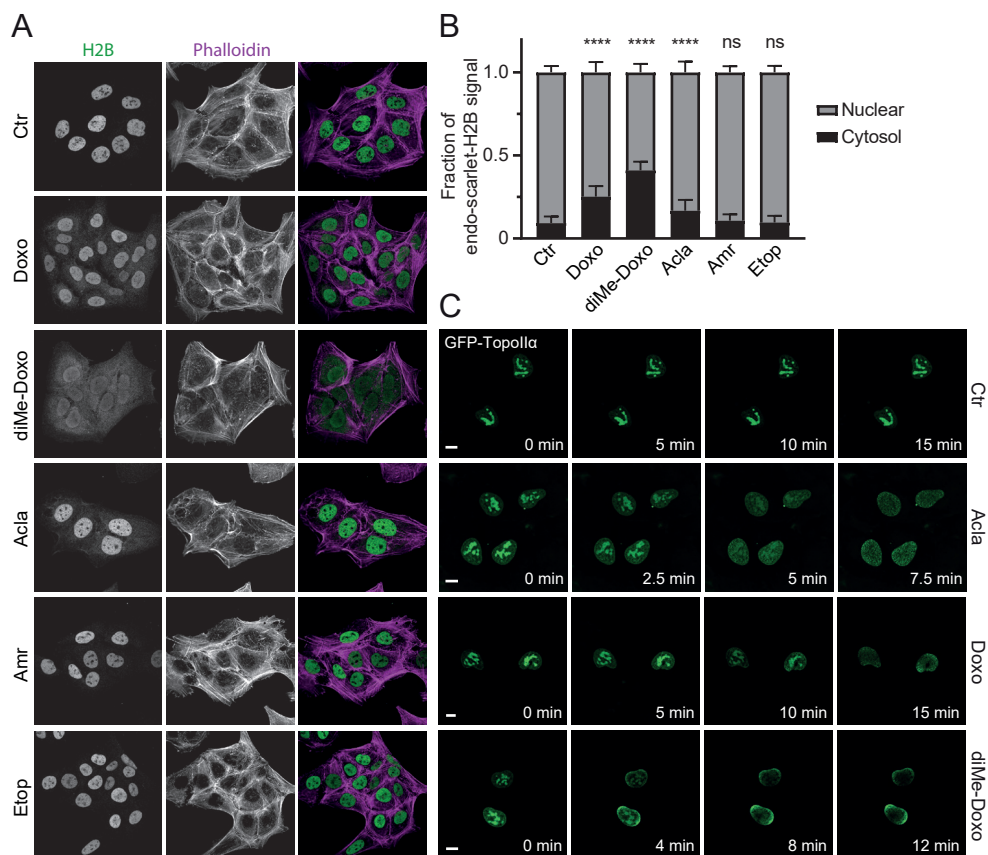


**Figure S4. Chromatin damage activity by Topo II poisons causing cytosolic histone accumulation.** (A) Endogenously tagged scarlet-H2B U2OS cells were treated for 1 hour with 10  $\mu$ M of the indicated drugs. (B) Quantification of the nuclear versus cytosolic signal of H2B upon treatment. Two-way ANOVA, Ctr versus drug treatments, \*\*\*\* $P < 0.0001$ ; ns, not significant. (C) Acla, Doxo as well as diMe-Doxo relocated Topo II $\alpha$  from nucleoli to chromatin. The localization of the GFP-tagged Topo II $\alpha$  in MelJuSo cells was followed upon treatment with 10  $\mu$ M Doxo, 10  $\mu$ M diMe-Doxo or 5  $\mu$ M Acla. Snapshots from movies at indicated time points. Scale bar, 10  $\mu$ m.

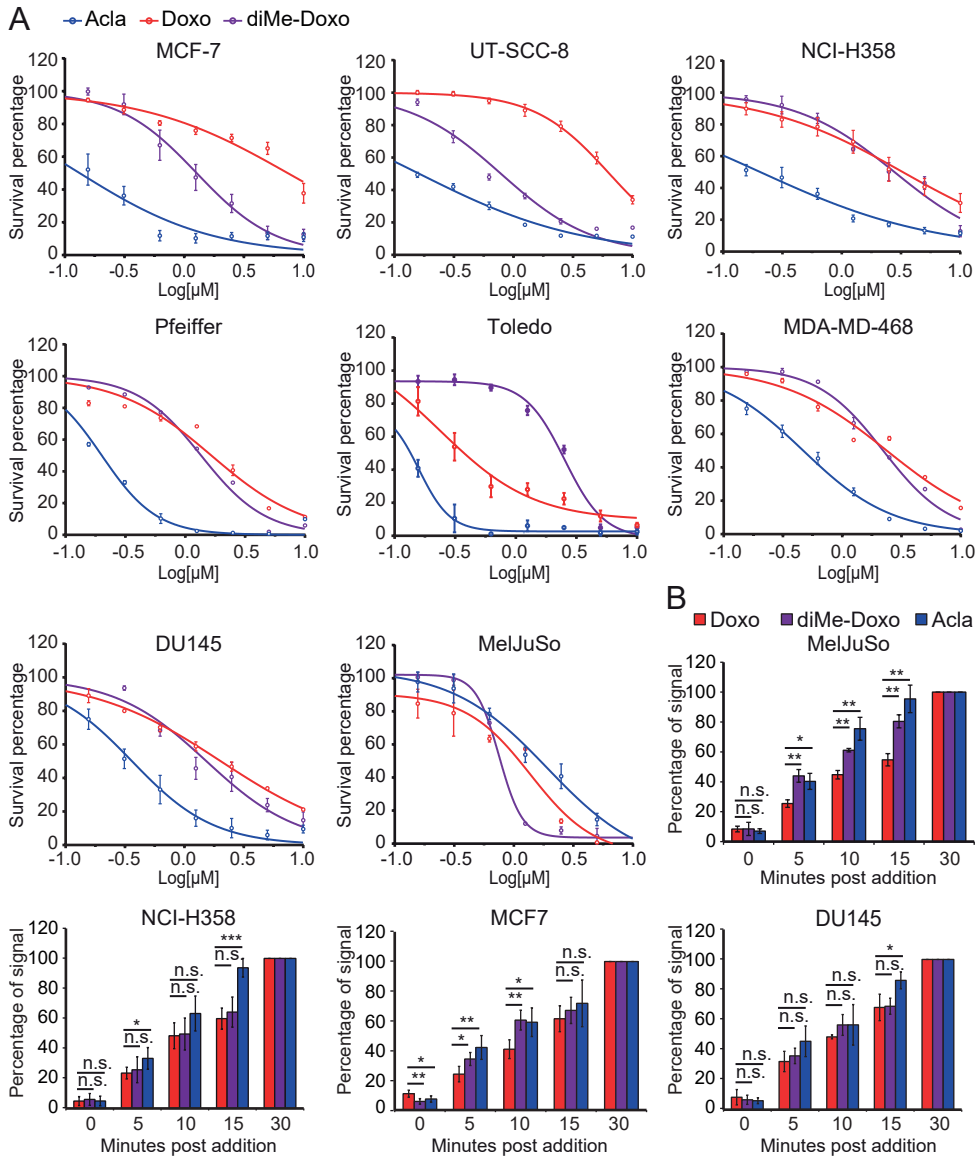


**Figure S5. Cytotoxicity and cellular uptake of diMe-Doxo *in vitro*.** (A) Cell viability of different cell lines. (B) The cellular uptake of drugs, measured by flow cytometry. Signal is normalized to that of the last time point. Two-tailed t-test, ns, not significant, \* $P < 0.05$ ; \*\* $P < 0.01$ ; \*\*\* $P < 0.001$ .

**Figure S6. ROS formation and subsequent protein damage by the different Topo II poisons.** (A) ROS formation 24 hours post treatment with different concentrations of the indicated drugs was examined by flow cytometry. Two-way ANOVA, \* $P < 0.05$ ; \*\* $P < 0.01$ ; \*\*\* $P < 0.001$ ; \*\*\*\* $P < 0.0001$ ; ns, not significant. (B) ROS formation upon 2 hour treatment with 10 μM of anthracyclines or 50 μM of Etop. Two-way ANOVA, \* $P < 0.05$ ; \*\* $P < 0.01$ .



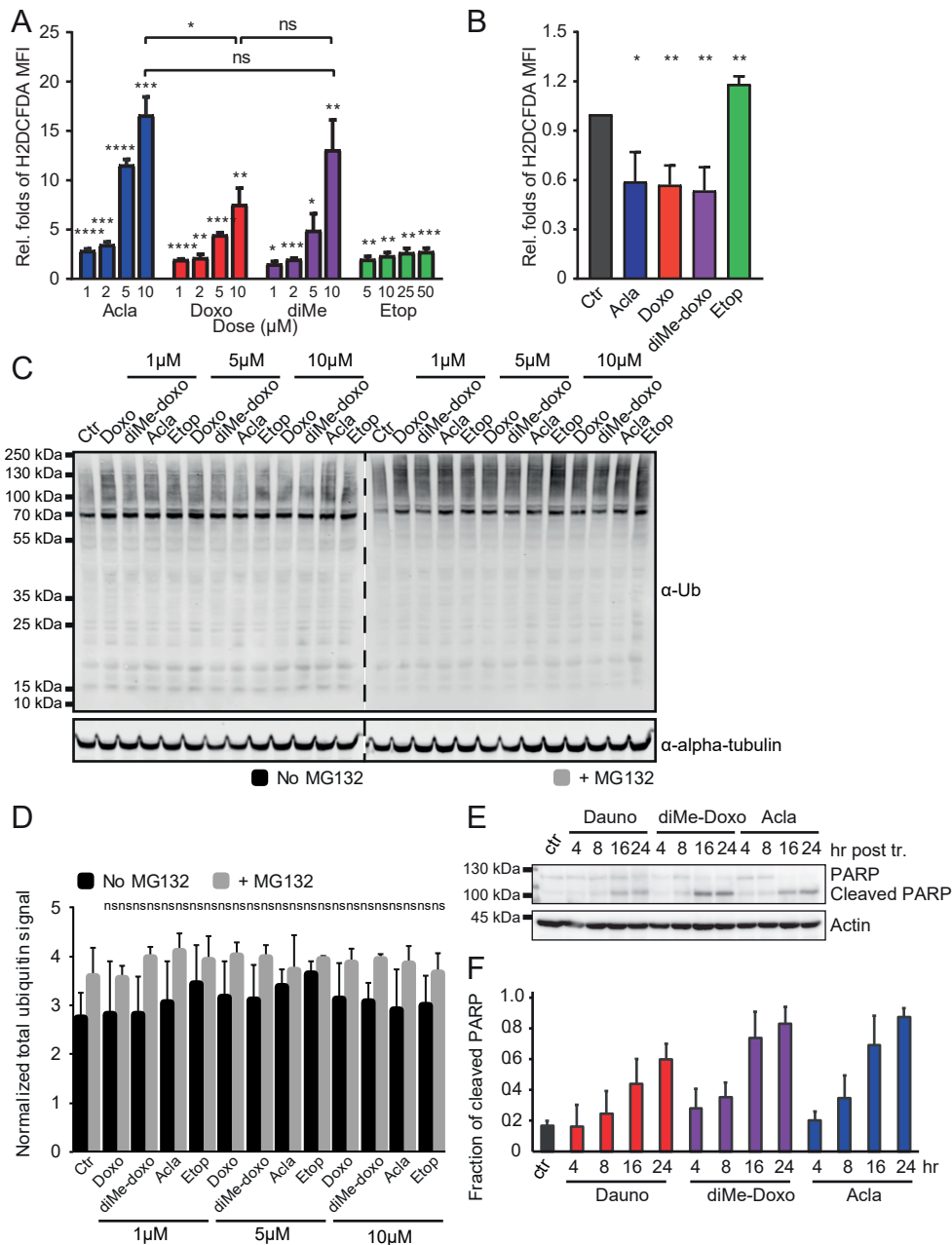


**Figure S6. Continued.** (C) Total protein ubiquitination of MeJuSo cells treated for 2 hour with the indicated drugs and concentrations were examined by Western blot. Alpha-tubulin was used as a loading control. (D) Quantification of (C), total ubiquitin signal was normalized to alpha-tubulin. Ordinary one-way ANOVA, ns, not significant. (E) PARP cleavage in K562 cells analyzed by Western blot. Position of PARP and its cleaved form is indicated. Actin is used as a loading control. (F) Quantification of the fraction of cleaved PARP.



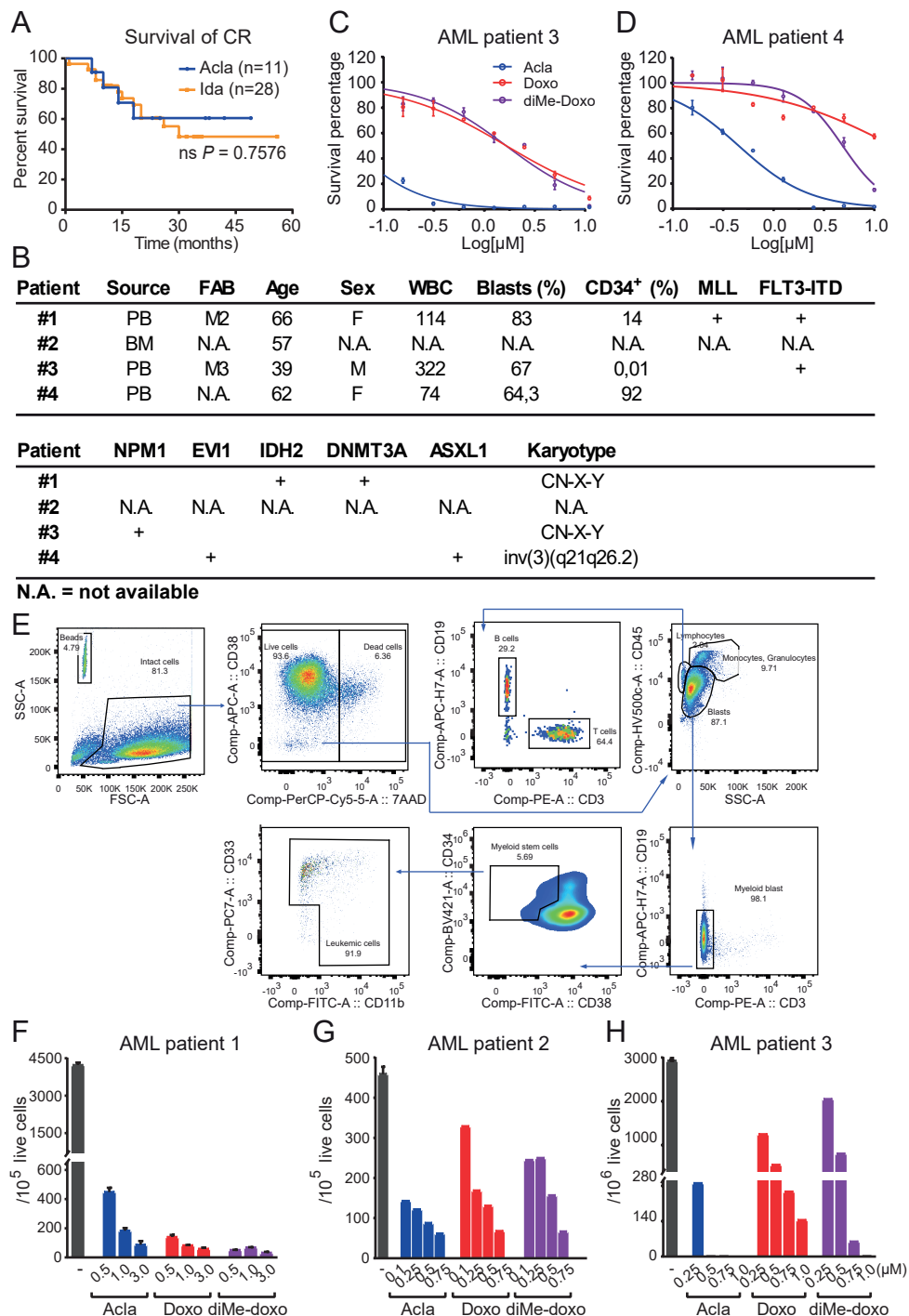


Figure S7. See legend on next page.

**Figure S7. diMe-Doxo and Acla are effective in human AML.** (A) Overall survival of *de novo* geriatric AML patients, who showed complete response after first cycle of Acla- or Ida-based treatment. Log-rank (Mantel-Cox) test. For more information on characteristics and clinical outcomes of patients, see Table S2 and S3. (B) Patient information of the four tested primary human AML samples. PB, peripheral blood; BM, bone marrow as source of the tumor materials; NA, not available. (C) and (D) Dose-dependent cell viability of human AML samples, shown as mean  $\pm$  SD of technical duplicates. (E) Gating strategy of flow cytometry for immune composition analysis of the human primary AML samples. (F–H) The toxicity of drugs on leukemic cells. The data are shown as mean  $\pm$  SD of technical duplicates.

**Characteristics of geriatric AML patients**

Characteristics	Acla group (n = 15)	Ida group (n = 56)	p value
Median Age, years (range)	66 (63-71)	64 (59-70)	0.0361*
Sex			ns†
Male	6 (40%)	31 (55%)	
Female	9 (60%)	25 (45%)	
FAB subtype			ns‡
M0	0 (0%)	0 (0%)	
M1	1 (7%)	1 (2%)	
M2	0 (0%)	8 (14%)	
M4	2 (13%)	11 (20%)	
M5	2 (13%)	14 (25%)	
M6	1 (7%)	0 (0%)	
Not established	9 (60%)	22 (39%)	
Cytogenetic risk			ns‡
Favourable	2 (13%)	6 (11%)	
Intermediate	6 (40%)	19 (34%)	
Not favourable	2 (13%)	16 (28%)	
Unknown	5 (33%)	15 (27%)	
CEBPA mutation			ns‡
Mutated	2 (13%)	11 (19%)	
Wild-type	11 (73%)	44 (77%)	
Unknown	2 (13%)	2 (4%)	
FLT3-ITD mutation			ns‡
Mutated	1 (7%)	5 (9%)	
Wild-type	12 (80%)	49 (88%)	
Unknown	2 (13%)	2 (3%)	
NPM1 mutation			ns‡
Mutated	2 (13%)	19 (33%)	
Wild-type	11 (73%)	36 (63%)	
Unknown	2 (13%)	2 (4%)	
Integrated risk			0.0371‡
Favourable	3 (20%)	20 (36%)	
Intermediate	5 (33%)	4 (7%)	
Not favourable	2 (13%)	16 (28.5%)	
Unknown	5 (33%)	16 (28.5%)	

**Table S2. Characteristics of *de novo* geriatric AML patients at baseline.** Data are n (%) unless otherwise stated. FAB, French–American–British. \* Mann-Whitney test. † Fisher's exact test. ‡ Chi-square test. ns, not significant.

## Clinical outcomes of geriatric AML patients

Clinical outcomes	Acla group	Ida group	p value
Clinical response after one cycle			
Complete remission	11/15 (73%)	28/56 (50%)	0.1468†
Partial remission	0/15 (0%)	3/56 (5%)	>0.9999†
Non-response	4/15 (13%)	25/56 (45%)	0.2494†
Complete remission after one cycle			
Favourable cytogenetics	2/2 (100%)	3/6 (50%)	0.4643†
Intermediate cytogenetics	5/6 (83%)	10/19 (53%)	0.3449†
Unfavourable cytogenetics	2/2 (100%)	6/16 (38%)	0.1830†
Unknown cytogenetics	2/5 (40%)	9/15 (60%)	0.6169†
Overall survival			
Deaths	7/15 (47%)	25/56 (45%)	>0.9999†
Median time (95% CI; months)	18 (11.9-31.7)	14 (13.5-19.9)	0.4152‡
Cumulative dose (mg/m <sup>2</sup> ) (median, range)	63,9 (32.8-572.9)	28,5 (16.7-120.9)	<0.0001‡
TnI increase			
Events	6/8 (75%)	15/39 (38%)	0.1152†
Median time (95% CI; days)*	45 (4-194)	21 (13-25)	0.1476‡
Cumulative dose (mg/m <sup>2</sup> ) (median, range)*	84,4 (32.8-229.2)	19,2 (18-27.9)	<0.0001‡
>10% LVEF decrease			
Events	1/9 (11%)	6/33 (18%)	>0.9999†
Median time (95% CI; days)*	55	131 (48-321)	-
Cumulative dose (mg/m <sup>2</sup> ) (median, range)*	52,5	19,2 (18-27.9)	-
Adverse effects in the heart			
Events	7/11 (64%)	20/56 (36%)	0.1029†
Median time (95% CI; days)*	55 (4-194)	24 (17-56)	0.4891‡
Cumulative dose (mg/m <sup>2</sup> ) (median, range)*	58,4 (32.8-229.2)	19,3 (18.1-28.4)	0.0012‡

**Table S3. Clinical outcomes of *de novo* geriatric AML patients after treatment.** Data are n/N (%) unless otherwise stated. TnI, Troponin I; LVEF, left ventricular ejection fraction; \* from administration till the event happened. Adverse effects in the heart: showing either TnI increase or >10% LVEF decrease, or both. † Fisher's exact test. ‡ Mann Whitney test.

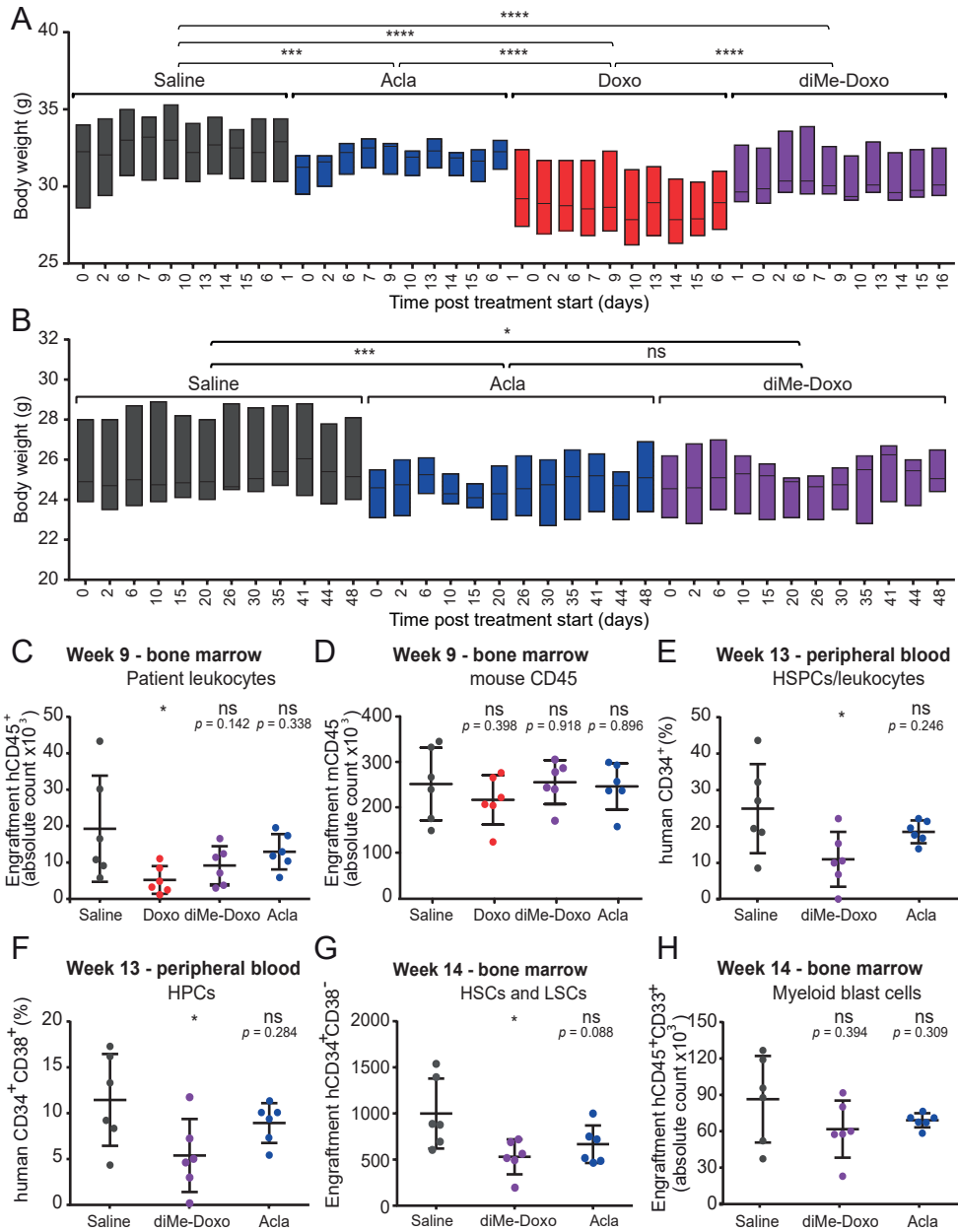


**Figure S8. diMe-Doxo and Acla are effective in an AML PDX model.** (A) and (B) NSG mice were inoculated with primary human AML cells and treated as in Figure 3D. Body weight of the first cohort of mice (A) and the second cohort of mice (B). Shown as floating bars with maximum-median-minimum values. Two-way ANOVA with RM, \* $P < 0.05$ ; \*\*\* $P < 0.001$ ; \*\*\*\* $P < 0.0001$ . (C) The engraftment of human AML cells in the bone marrow of first cohort of mice at week 9, shown as absolute counts of patient leukocytes (hCD45<sup>+</sup>). Students' *t*-test, \* $P < 0.05$ ; ns, not significant. (D) Toxicity on normal mouse leukocytes (mCD45<sup>+</sup>) in bone marrow.

**Figure S8. Continued (D).** Students' *t*-test, ns, not significant. (E) and (F) the percentage of human HSPCs ( $hCD34^+$  leukocytes) and HPCs ( $hCD34^+CD38^+$  leukocytes) in peripheral blood of second cohort of mice at week 13. Students' *t*-test,  $*P < 0.05$ ; ns, not significant. (G) The engraftment of human AML cells of the second cohort, the absolute counts of human HSCs and LSCs in bone marrow at week 14. Students' *t*-test,  $*P < 0.05$ ; ns, not significant. (H) The absolute number of human myeloid blasts ( $hCD45^+CD33^+$  blasts) in the bone marrow of the second cohort of mice at week 14. Students' *t*-test, ns, not significant.

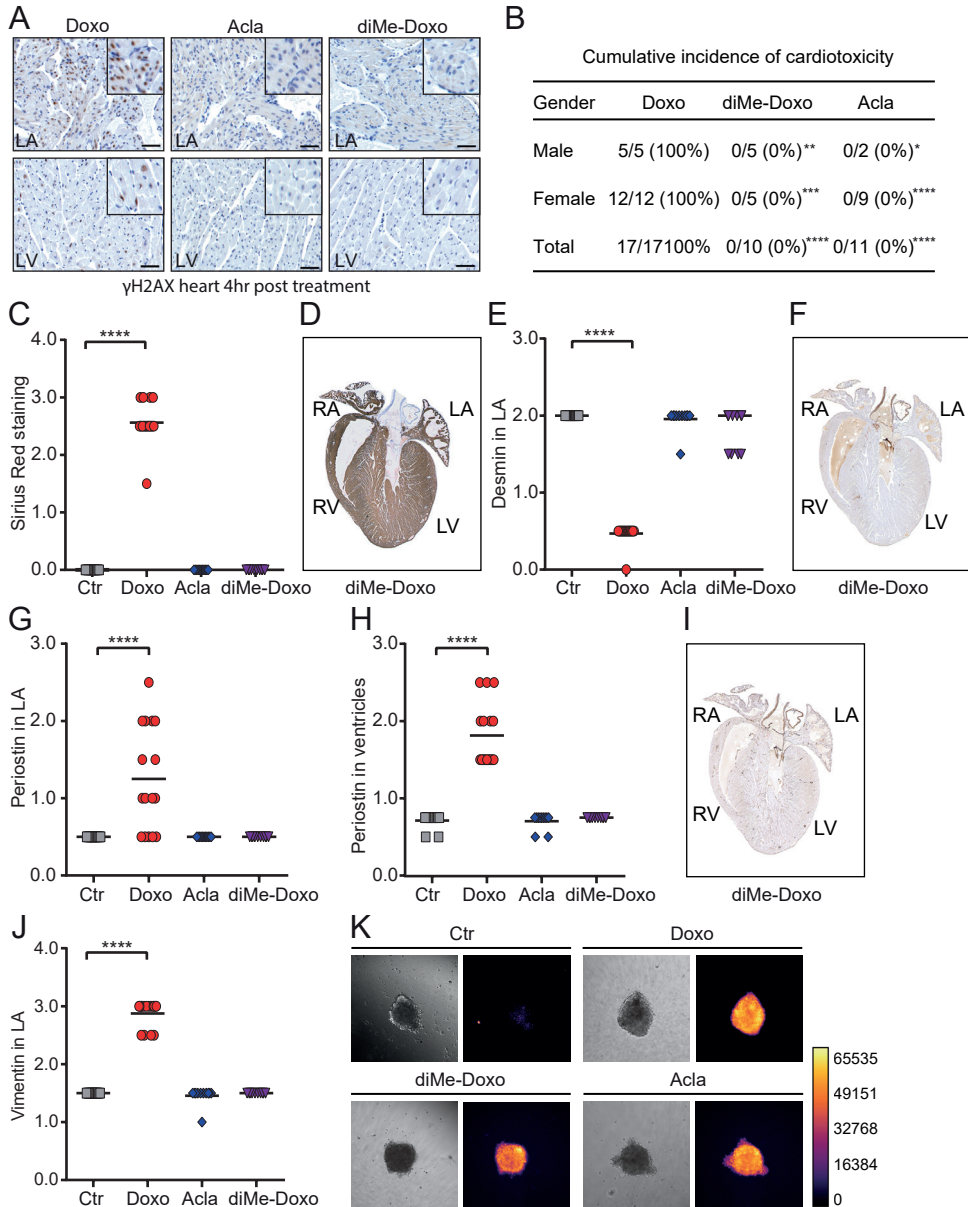


**Figure S9.** See legend on next page.

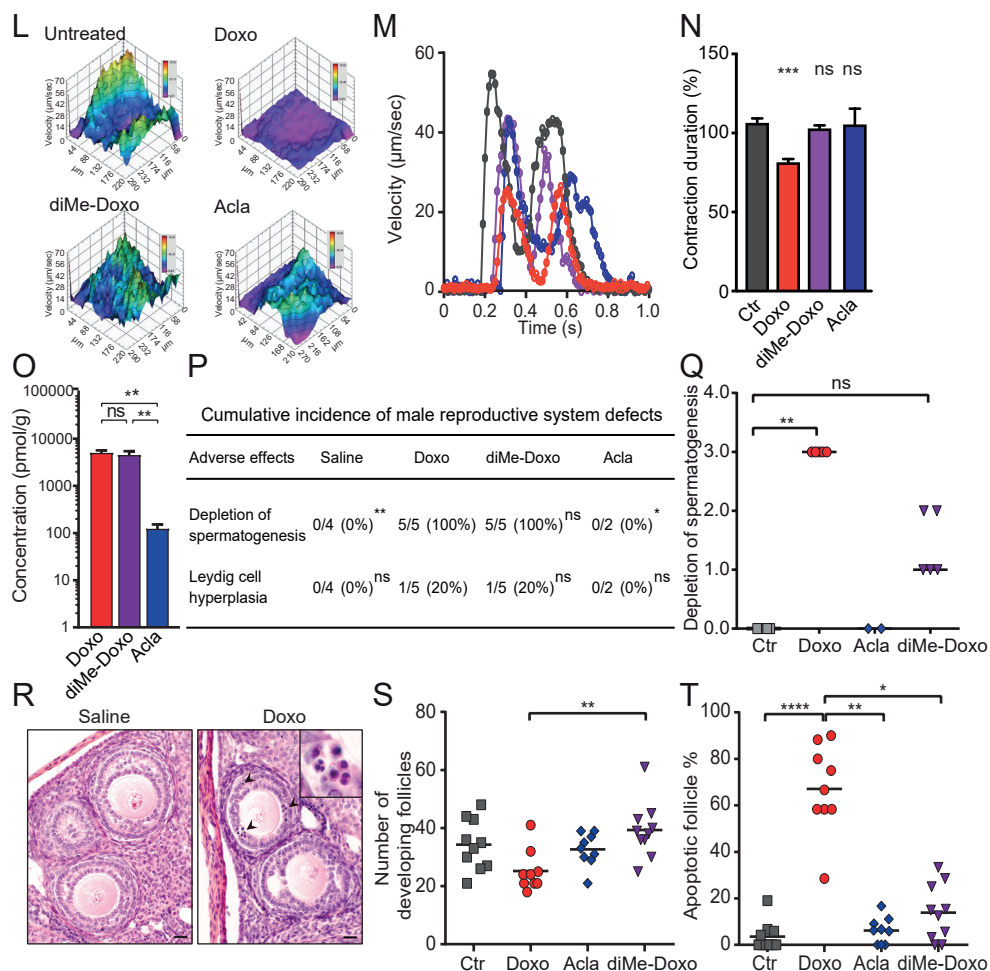


**Figure S9. *N,N*-dimethylation of Doxo reduces cardiotoxicity as observed for Doxo.** (A) Wild-type FVB mice were *i.v.* injected with a single dose of 5 mg/kg of the indicated drugs ( $n = 5$  per group).  $\gamma$ H2AX staining of the heart isolated from mice 4 hours after indicated drug administration. LA = left atrium, LV = left ventricle. (B–J), Wild-type FVB mice were *i.v.* injected every two weeks with 5 mg/kg of Doxo or 5 mg/kg of Acla for 8 times, or with 5 mg/kg of diMe-Doxo for 15 times. The same batch of mice as in Figure 4A–C. (B) The cumulative incidence of cardiotoxicity. Fisher's exact test, Doxo vs diMe-Doxo or Acla,  $^*P < 0.05$ ;  $^{**}P < 0.01$ ;  $^{***}P < 0.001$ ;  $^{****}P < 0.0001$ . (C) Quantification of Sirius Red staining. Kruskal-Wallis test,  $^{****}P < 0.0001$ . Ctr vs Acla or diMe-Doxo is ns. (D–J), Representative IHC staining of a heart from a diMe-Doxo-treated mouse. Desmin (D), Periostin (F), Vimentin (I). (E) Quantification of Desmin staining in the LA. Kruskal-Wallis test,  $^{****}P < 0.0001$ . Ctr vs Acla or diMe-Doxo is ns. (G) and (H), Quantification of Periostin staining in the LA (G) and ventricles (H). Kruskal-Wallis test,  $^{****}P < 0.0001$ . Ctr vs Acla or diMe-Doxo is ns. (J) Quantification of vimentin staining in the LA. Kruskal-Wallis test,  $^{****}P < 0.0001$ . Ctr vs Acla or diMe-Doxo is ns. (K–N), hiPSC-derived cardiac microtissues were paced at 1Hz and contraction velocity was measured 24 hours post treatment. (K) Uptake of the anthracyclines is equal in hiPSC-derived cardiac microtissues. Bright field (left panels) and fluorescent image in G-LUT (right panels).

**Figure S9. Continued.** (L) Maximum velocity in  $\mu\text{m}/\text{sec}$  is indicated for a represented microtissue for the different treatment. (M) Quantification of (L). (N) Drug toxicity on cardiac microtissues. Contraction duration was measured 24 hours post treatment with  $20 \mu\text{M}$  of the indicated drugs. Kruskal-Wallis test,  $***P < 0.0002$ . (O) Bio-distribution of drugs was determined in the heart 4 hours after administration. Same mice as A. One-way ANOVA,  $**P < 0.01$ . (P) The cumulative incidence of defects in male reproductive system. Fisher's exact test, all compared to Doxo group,  $*P < 0.05$ ;  $**P < 0.01$ . (Q) Degree of the spermatogenesis depletion revealed by histopathological analysis. Kruskal-Wallis test,  $**P < 0.01$ . Ctr vs Acla is ns. (R) Representative sections of HE stained ovaries from Saline- or Doxo-treated mice. Scale bar,  $20 \mu\text{m}$ . Arrows indicate apoptotic cells. (S) Quantification of the number of developing follicles in MC38-bearing mice of Exp #2. Except for primordial follicles and primary follicles, all follicles of secondary follicles, tertiary follicles (antral follicles), pre-ovulatory follicles, and large atretic follicles are regarded as developing follicles. Kruskal-Wallis test,  $**P < 0.01$ . Ctr vs Doxo, Acla or diMe-Doxo is ns. (T) Percentage of apoptotic follicles in the secondary and tertiary follicles of Exp #2. Kruskal-Wallis test,  $*P < 0.05$ ;  $**P < 0.01$ ;  $****P < 0.0001$ . Ctr vs Acla or diMe-Doxo is ns.

**Movie S1:** Time-lapse confocal imaging of histone eviction upon treatment with Doxo, Amr or Etop. Cells were treated with the indicated drugs and histone eviction was followed for 1 hour after photoactivation of the indicated region by time lapse confocal microscopy. Related to Figure 2.

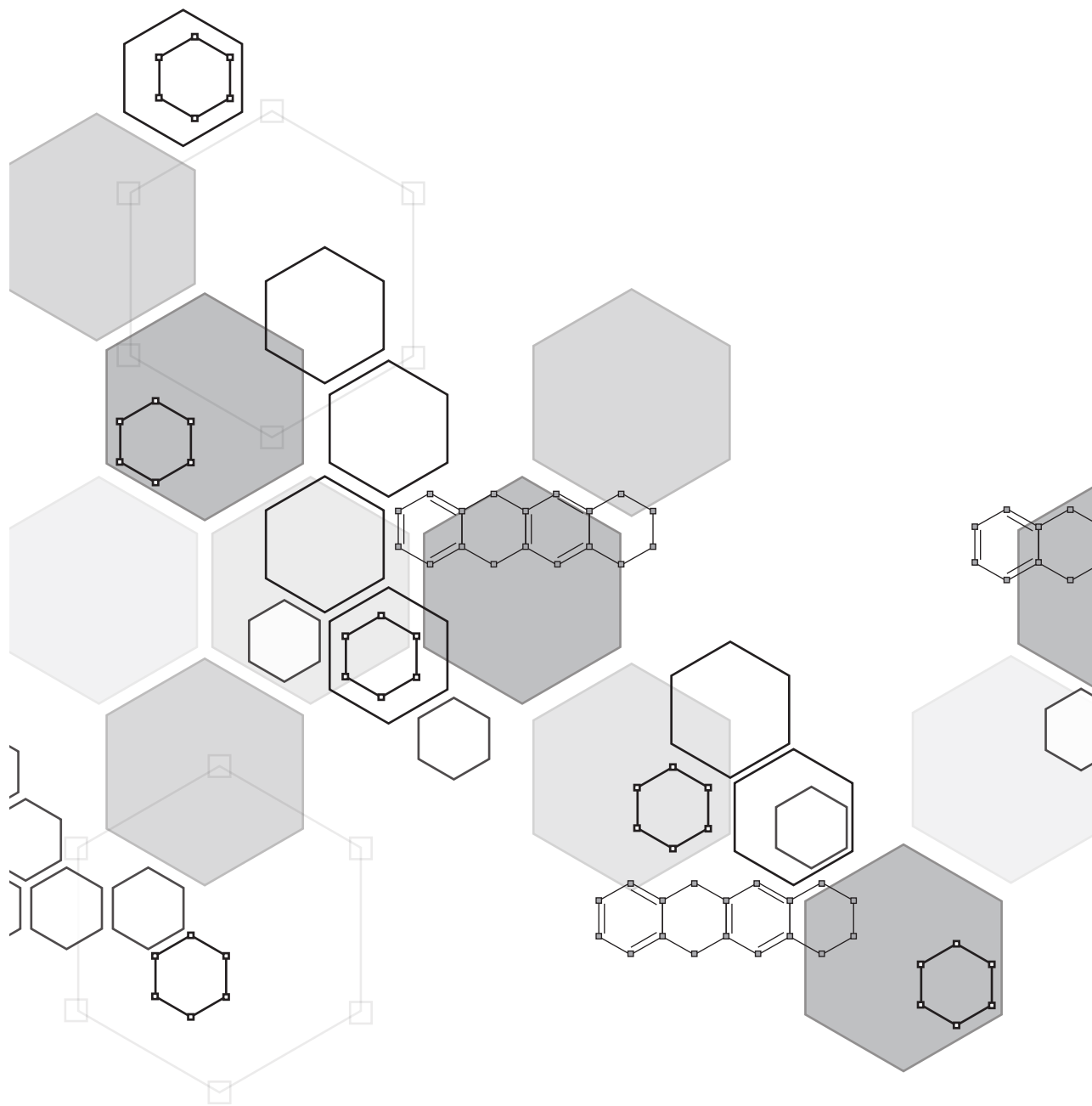
**Movie S2:** Time-lapse confocal imaging of histone eviction upon treatment with Doxo, diMe-Doxo or Acla. Cells were treated with the indicated drugs and histone eviction was followed for 1 hour after photoactivation of the indicated region by time lapse confocal microscopy. Related to Figure 2.

**Movie S3:** Assessment of drug toxicity by echocardiography. Wild-type FVB mice were i.v. injected with the indicated drugs for 8 times every week. Echocardiography was performed 12 weeks post start of the treatment. 3D reconstructions are shown of the heart in diastole of mice treated with the indicated drugs with the left ventricle in cyan and the left atrium in magenta. Related to Figure 4.

**Movie S4:** Drug toxicity on hiPSC-derived cardiac microtissues. hiPSC-derived cardiac microtissues were stimulated at 1Hz, and velocity of microtissue-contraction was analysed after 24 hours exposure to indicated drugs. The Horn-Schunck Vector Flow analysis method was used to detect changes in pixel displacements during contraction of the microtissues in 3D. Related to Figure 4.

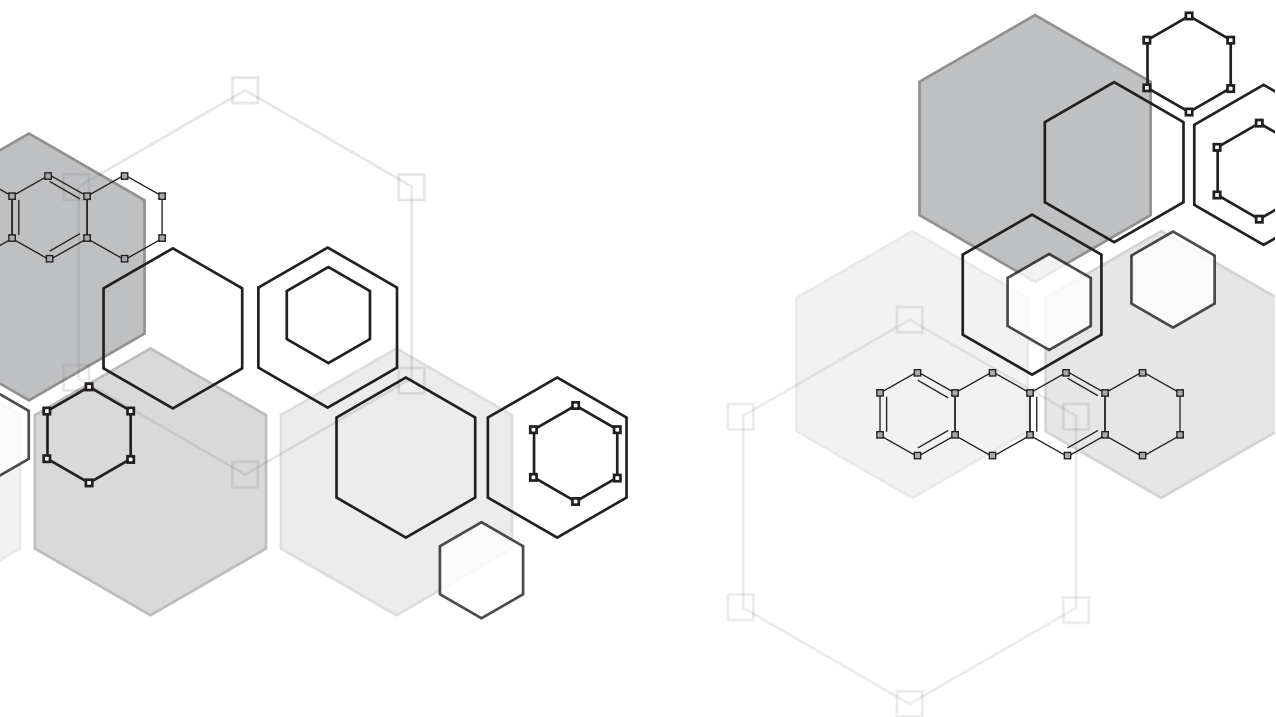
Supplemental Movies S1 - S4 can be found online: <https://www.pnas.org/content/117/26/15182>





# Doxorubicin and aclarubicin: shuffling anthracycline glycans for improved anticancer agents

# 4



Sabina Y. van der Zanden<sup>#</sup>, Dennis P.A. Wander<sup>#</sup>, Gijsbert A. van der Marel, Herman S. Ovekleef, Jacques Neefjes and Jeroen D.C. Codee

<sup>#</sup>These authors contributed equally

*Journal of Medicinal Chemistry* (2020)

## ABSTRACT

Anthracycline anticancer drugs doxorubicin and aclarubicin have been used in the clinic for several decades to treat various cancers. Although closely related structures, their molecular mode of action diverges, which is reflected in their biological activity profile. For a better understanding of the structure-function relationship of these drugs, we synthesized ten doxorubicin/aclarubicin hybrids varying in three distinct features: aglycon, glycan and the amine substitution pattern. We continued to evaluate their capacity to induce DNA breaks, histone eviction, and relocated topoisomerase II $\alpha$  in living cells. Furthermore, we assessed their cytotoxicity in various human tumor cell lines. Our findings underscore that histone eviction alone, rather than DNA breaks contributes strongly to the overall cytotoxicity of anthracyclines, and structures containing an *N,N*-dimethylamine at the reducing sugar are proven more cytotoxic than their non-methylated counterparts. This structural information will support further development of novel anthracycline variants with improved anticancer activity.

## INTRODUCTION

Anthracyclines comprise one of the most successful classes of natural product chemotherapeutic agents. Two archetypal anthracyclines are doxorubicin (**1**) and aclarubicin (**12**, Figure 1), both effective anticancer agents isolated from nature [1,2]. Doxorubicin has been in use in the clinic for more than five decades and is prescribed worldwide to about a million patients annually for the treatment of a variety of cancers [3–5]. Aclarubicin in contrast is prescribed exclusively in Japan and China, mainly for the treatment of acute myeloid leukemia (AML). Although doxorubicin is very effective, its use coincides with cardiotoxicity, the formation of secondary tumors, and infertility [6–9]. Therefore, clinical use with doxorubicin is generally limited to a cumulative dose of 450 – 550 mg/m<sup>2</sup> [7,10,11]. The formation of reactive oxygen species (ROS) by these drugs has been considered as a major mechanism mediating anthracycline-induced cardiotoxicity [12,13]. However, aclarubicin, which has a higher redox potential than doxorubicin [14], displays fewer cardiotoxic side effects, and recent findings in our labs suggested that this difference in cardiotoxicity relates to significant differences in the mode of action of these two compounds [15]. Doxorubicin causes chromatin damage by inducing histone eviction, as well as the formation of DNA double strand breaks by poisoning topoisomerase II $\alpha$  (TopoII $\alpha$ ) [16,17]. Aclarubicin is capable of evicting histones as well, but targets TopoII $\alpha$  without inducing DNA double strand breaks [17–19]. In addition, it has been shown that aclarubicin affects cell viability by reducing the mitochondrial respiratory activity [20]. Histone eviction induced by anthracycline drugs results in epigenetic and transcriptional changes, which are thought to then induce apoptosis [17]. We recently showed that anthracyclines that induce both DNA double strand break formation and histone eviction are cardiotoxic. Aclarubicin and *N,N*-dimethyldoxorubicin (**3**) both lack DNA damage activity but are able to induce histone eviction, and can thus be used as effective anticancer drugs without cardiotoxicity [15]. The structural basis causing this difference in biological activities, however, is still lacking. Therefore, better insight into the structure-function relationship of these molecules is needed.

In addition to the treatment-limiting side effects, development of resistance constitutes to be a frequent clinical limitation for the treatment of patients with anthracycline drugs [21,22]. Common mechanisms of resistance toward anthracycline drugs are reduced expression or activity of TopoII $\alpha$  and overexpression of mem-

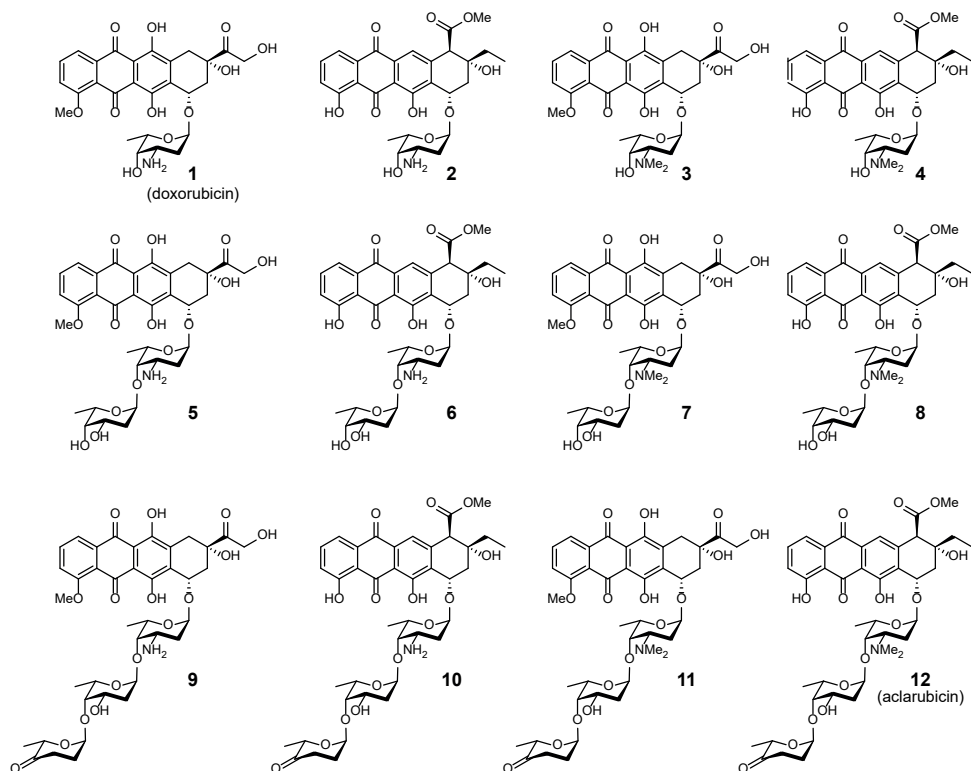


**Figure 1.** Chemical structures of doxorubicin (**1**), aclarubicin (**12**) and hybrid structures **2** – **11**, subject of the here-presented studie.

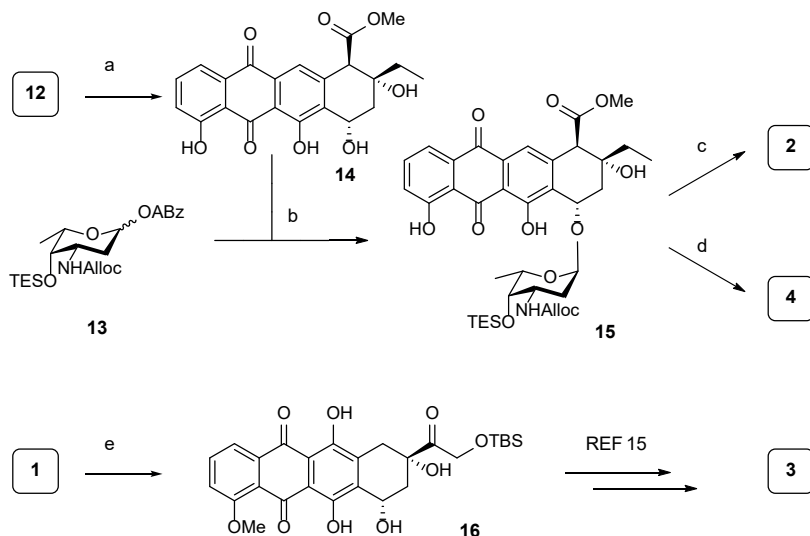
brane transporters such as P-glycoprotein (P-gp) and multidrug resistance associated protein (MRP), which both decrease the cellular accumulation of the drugs via increased drug export [23–25]. Although the structures of doxorubicin (**1**) and aclarubicin (**12**) are quite similar (they both contain an anthraquinone and a sugar containing a basic amine), three differences can be identified: (i) variation in the substitution and oxidation pattern of the anthraquinone aglycon, (ii) variation in the size of the carbohydrate part and (iii) the methylation pattern of the amine of the first sugar attached to the anthraquinone. Doxorubicin features an  $\alpha$ -L-daunosamine as the single monosaccharidic carbohydrate appendage, while aclarubicin features an  $\alpha$ -L-rhodosamine (*N,N*-dimethyldaunosamine), that is further glycosylated at the 4-hydroxyl with a disaccharide composed of  $\alpha$ -L-oliose and  $\alpha$ -L-cinerulose A. Thousands of analogues of doxorubicin and aclarubicin have been isolated from bacterial sources or prepared through organic synthesis [26]. In spite of this, the chemical space between doxorubicin and aclarubicin has not been fully explored. Although some doxorubicin/aclarubicin hybrids have been prepared (including compounds **2** [27], **3** [15,28], **4** [29], **8** [30], **10** [31], and **11** [32]) the reported methods of synthesis are fragmented and the complete set, as shown in Figure 1, has not been evaluated in the context of the different modes of action described above. We therefore set out to generate a comprehensive set of doxorubicin/aclarubicin hybrid structures, systematically varying the structural elements in which the two anthracyclines dif-

fer. Based on these structural differences between doxorubicin and aclarubicin, we envisaged the set of doxorubicin/aclarubicin hybrids **2** – **11** (Figure 1) that comprises anthracyclines composed of either of the two aglycons, additionally featuring either a monosaccharide, a disaccharide, or a trisaccharide glycan composed of the sugar configurations also found in the parent structures, and bearing either no or two *N*-methyl substituents. Altogether, they fill the chemical space between doxorubicin (**1**) and aclarubicin (**12**). Furthermore, we probed this coherent set of anthracycline hybrid structures for their DNA damaging, TopoII $\alpha$  relocalization, histone evicting, and cytotoxic activities to get a better understanding of the structural basis underlying the observed difference for the anticancer activity of these compounds. These new insights could ultimately lead to the development of new anthracycline variants with improved anticancer activity.

## RESULTS

### Synthesis of doxorubicin/aclarubicin hybrid monosaccharides **2** and **4**

For the assembly of the set of anthracyclines, we used Biao Yu's gold(I)-mediated condensation [33] of the glycans and aglycons, as these mild glycosylation conditions are compatible with the lability and reactivity of the deoxy sugars that are to be appended to the anthraquinones. The anthraquinone aglycons were readily obtained by acidic hydrolysis of the drugs doxorubicin (**1**) and aclarubicin (**12**). This yielded aklavinone (**14**) [34] and, following protection of the primary alcohol in doxorubicinone as the tert-butyldimethylsilyl (TBS) ether, 14-O-TBS-doxorubicinone **16** [35] (Scheme 1). Condensation of daunosaminyl alkynylbenzoate **13** (see supplemental information, Scheme S1) for a complete description of the syntheses of the building



**Scheme 1. Synthesis of hybrid monosaccharide anthracyclines **2**, **3** and **4**.** Reagents and conditions: (a) 0.2M aqueous (aq) HCl, 90°C, quant.; (b)  $PPh_3AuNTf_2$  (10 mol%), dichloromethane (DCM), -20°C, 73% (>20:1  $\alpha/\beta$ ); (c) (i)  $Pd(PPh_3)_4$ , NDMBA, DCM, (ii) HF·pyridine, pyr., 40% over two steps; (d) (i)  $Pd(PPh_3)_4$ , NDMBA, DCM, (ii) aq.  $CH_2O$ ,  $NaBH(OAc)_3$ , EtOH, (iii) HF·pyridine, pyr., 43% over three steps; (e) (i) aq. HCl, 90°C; (ii) TBS-Cl, imidazole, dimethylformamide (DMF), 97% over two steps.

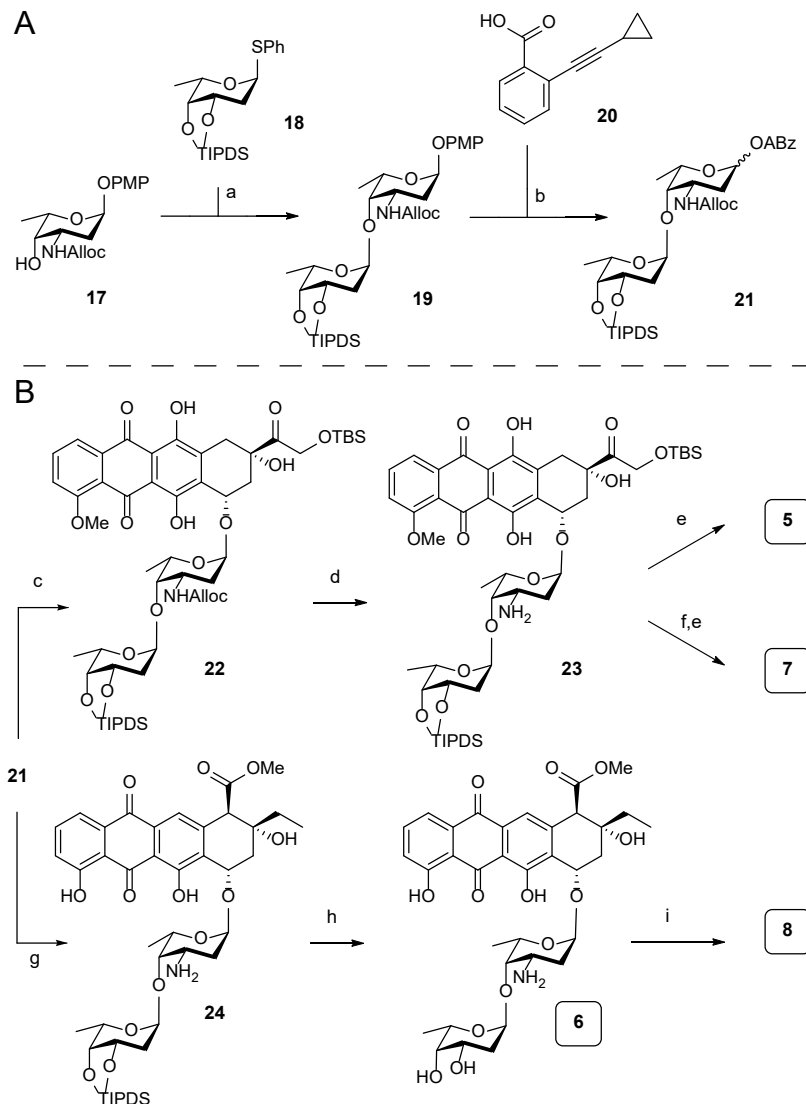
blocks) and aklavinone (**14**) under Yu's conditions provided anthracycline **15** in a stereoselective manner (Scheme 1). The stereoselectivity of this glycosylation can be accounted for by long-range participation [36,37] of the allyl carbamate, as well as the conformation of the intermediate oxocarbenium ion that can be substituted in a stereoselective manner on the  $\alpha$ -face [38]. The yield of this glycosylation reaction (73%) compares favorably to the yields (50-60%) reported by Pearlman et. al., who used glycal donors in combination with Brønsted acid catalysis [39]. The *N*-Alloc group in **15** was then removed using a catalytic amount of  $\text{Pd}(\text{PPh}_3)_4$  and *N,N*-dimethylbarbituric acid (NDMBA) as the allyl scavenger [40]. This was followed by desilylation using an  $\text{HF} \cdot \text{pyr}$  complex to give the first hybrid structure **2** [41]. The corresponding dimethylamine **4** could be prepared by performing reductive alkylation with formaldehyde and  $\text{NaBH}(\text{OAc})_3$  after the removal of the Alloc functionality, and finally a desilylation. The third monosaccharide anthracycline **3** was obtained as we previously described.[15]

### Synthesis of hybrid disaccharides 5 - 8

We then turned our attention to the four disaccharidic antracyclines **5** - **8**. This required the synthesis of disaccharide donor **21**, which is depicted in Scheme 2A. Compound **21** was constructed through an iodonium di-collidinium perchlorate (IDCP)-mediated glycosylation of L-olioside thioglycoside donor **18** [42], protected as the tetraisopropylidisiloxane ether, which effectively shields the  $\beta$ -face to facilitate the stereoselective introduction of the desired  $\alpha$ -linkage. The reaction between donor **18** and acceptor **17** delivered the desired disaccharide **19** in excellent yield and stereoselectivity. Triphenylphosphine was added to the reaction mixture to reduce the in situ formed sulfenamide that was formed from the Alloc carbamate and the generated phenylsulfenyl iodide [43,44]. The chemoselective removal of the anomeric *p*-methoxyphenolate (PMP) protective group in **19** was achieved using silver(II) hydrogen dipicolinate ( $\text{Ag}(\text{DPAH})_2$ ) [45,46], and the anomeric alcohol thus liberated was then condensed with carboxylic acid **20** under Steglich conditions [47], to deliver the disaccharide alkynylbenzoate donor **21**. The coupling to the two aglycone acceptors **14** and **16** is outlined in Scheme 2B. Treatment of a mixture of donor **21** and doxorubicinone acceptor **16** with  $\text{PPh}_3\text{AuNTf}_2$  proceeded stereoselectively to give **22** in 64% yield. Ensuing Alloc removal proceeded quantitatively to give **23**, after which  $\text{HF} \cdot \text{pyridine}$ -mediated desilylation yielded the first disaccharide anthracycline **5**. To introduce the dimethylamino functionality, amine **23** was treated with formaldehyde and a substoichiometric amount of  $\text{NaBH}(\text{OAc})_3$  to prevent reduction of the hydroxyketone function on the aglycone [28]. A final desilylation resulted in dimethylated **7**. Subjecting donor **21** and aklavinone **14** to gold(I)-mediated glycosylation also provided stereoselectively to give the protected disaccharide anthracycline, of which the Alloc group was removed to give **24** in 87% yield over the two steps. Removal of the disiloxane moiety with  $\text{HF} \cdot \text{pyridine}$  then gave disaccharide anthracycline **6**. A double-reductive *N*-methylation was performed on fully deprotected **6** to give **8**.

### Synthesis of hybrid trisaccharides 9 - 11

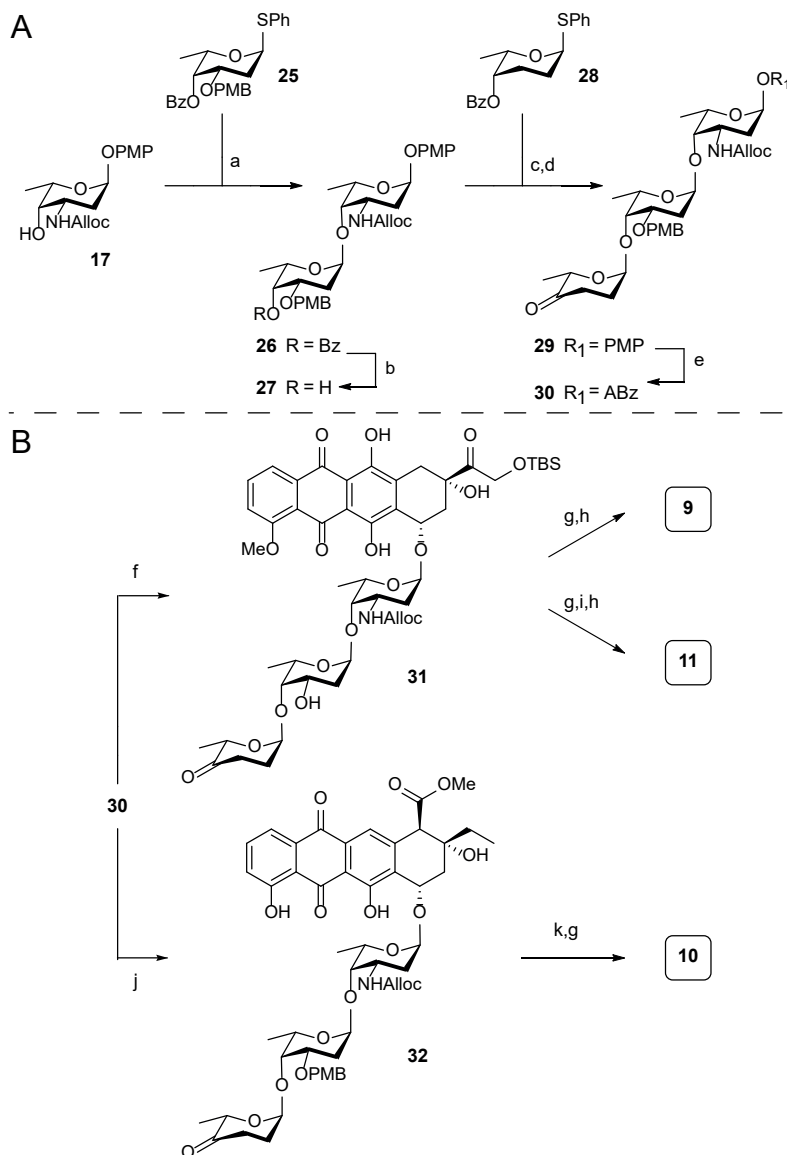
To complete the set of target compounds, trisaccharide anthracyclines **9** - **11** were prepared. These required trisaccharide alkynylbenzoate donor **30**, the synthesis of which is shown in Scheme 3A. First, protected daunosaminyl acceptor **17** and olisosyl donor **25** were condensed using the conditions described for the synthesis of disaccharide **18** to provide disaccharide **26**. This glycosylation proceeded with excellent stereoselectivity, which can be attributed to the structure of the intermediate oxocar-



**Scheme 2. (A) Synthesis of disaccharide alkynylbenzoate donor 21<sup>a</sup>; (B) Synthesis of hybrid disaccharide anthracyclines 5-8<sup>b</sup>** <sup>a</sup>Reagents and conditions: (a) IDCP, Et<sub>2</sub>O, DCE (4:1 v/v), then PPh<sub>3</sub>, 89%; (b) (i) Ag(II)(hydrogen dipicolinate)<sub>2</sub>, NaOAc, MeCN, H<sub>2</sub>O, 0°C; (ii) 20, EDCI·HCl, DIPEA, DMAP, DCM, 84% over two steps (1:8 α:β). <sup>b</sup>Reagents and conditions: (c) 16, PPh<sub>3</sub>AuNTf<sub>2</sub> (10 mol%), DCM, 64% (>20:1 α:β); (d) Pd(PPh<sub>3</sub>)<sub>4</sub>, NDMBA, DCM, quant.; (e) HF·pyridine, pyr., 76% for 5, 81% for 7; (f) aq. CH<sub>2</sub>O, NaBH(OAc)<sub>3</sub>, EtOH, 71%; (g) (i) 14, PPh<sub>3</sub>AuNTf<sub>2</sub> (10 mol%), -20°C, DCM; (ii) Pd(PPh<sub>3</sub>)<sub>4</sub>, NDMBA, DCM, 87% over two steps (>20:1 α:β); (h) HF·pyridine, pyr., 41%; (i) aq. CH<sub>2</sub>O, NaBH(OAc)<sub>3</sub>, EtOH, 34%.

benium ion [38]. Removal of the benzoyl protective group in **26** gave acceptor **27**. Elongation of this disaccharide was achieved using an IDCP-mediated glycosylation using L-rhodinoside donor **28** to stereoselectively provide the protected trisaccha-





**Scheme 3. (A) Synthesis of trisaccharide alkynylbenzoate donor 30<sup>a</sup>. (B) Synthesis of hybrid anthracycline trisaccharides 9-11<sup>b</sup>.** <sup>a</sup>Reagents and conditions: (a) IDCP, Et<sub>2</sub>O:DCE (4:1 v/v), then PPh<sub>3</sub>; (b) NaOMe, MeOH, 78% over two steps (>20:1 α/β); (c) IDCP, Et<sub>2</sub>O:DCE (4:1 v/v), then PPh<sub>3</sub>, 100% (>20:1 α/β); (d) (i) NaOMe, MeOH, 85%; (ii) Dess-Martin periodinane, NaHCO<sub>3</sub>, CH<sub>2</sub>Cl<sub>2</sub>, 97%; (e) (i) Ag(II) (hydrogen dipicolinate)<sub>2</sub>, NaOAc, MeCN/H<sub>2</sub>O (1:1, v/v), 0°C, (ii) 20, EDCI·HCl, DIPEA, DMAP, CH<sub>2</sub>Cl<sub>2</sub>, 75% over the two steps (1:7 α/β). <sup>b</sup>Reagents and conditions: (f) (i) 16, PPh<sub>3</sub>AuNTf<sub>2</sub> (10 mol%), DCM; (ii) 2,3-dichloro-5,6-dicyano-1,4-benzoquinone (DDQ), DCM, pH 7 phosphate buffer (18:1, v/v), 57% over two steps (>20:1 α/β); (g) Pd(PPh<sub>3</sub>)<sub>4</sub>, NDMBA, DCM, 81% from 31, 61% for 10; (h) HF·pyridine, pyr., 73% for 9, 73% for 11; (i) aq. CH<sub>2</sub>O, NaBH(OAc)<sub>3</sub>, EtOH, 52%; (j) 14, PPh<sub>3</sub>AuNTf<sub>2</sub> (10 mol%), DCM, -20°C, 71% (>20:1 α/β); (k) DDQ, DCM/pH 7 phosphate buffer (18:1, v/v), 90%.

ride. Removal of the benzoyl ester gave the alcohol, which was oxidized using a Dess-Martin oxidation to install the required ketone functionality in **29**. The trisaccharide was converted to the corresponding Yu donor with the oxidation-Steglich esterification sequence, as described earlier, to give **30**. Of note, the silver(II) reagent used to remove the anomeric para-methoxyphenol moiety left the para-methoxybenzyl-protecting group unscathed. Treatment of aglycon **16** and donor **30** with  $\text{PPh}_3\text{AuNTf}_2$  led to the stereoselective formation of the first protected trisaccharide anthracycline, of which the para-methylbenzyl (PMB) group was removed to give partially protected anthracycline **31** in 57% yield, over two steps (Scheme 3B). This represents a significant improvement over a previous synthesis, reported by Tanaka et. al. [32], who combined a trisaccharide bromide and the aglycone acceptor in a TBABr/collidine-mediated glycosylation to give the trisaccharide anthracycline in 22% yield. Removal of the Alloc group and desilylation of **31** then afforded **9**. A double-reductive amination on **31** followed by desilylation provided hybrid anthracycline **11**. For the synthesis of **10**, a mixture of **30** and **14** was treated with  $\text{PPh}_3\text{AuNTf}_2$  at  $-20^\circ\text{C}$  to afford **32** as a single diastereoisomer in 71% yield. Removal of the Alloc and PMB groups finally gave **10**. The analytical data for the compounds described previously in the literature (**2** [27], **3** [28], **4** [29], **8** [30], **10** [31], **11** [32]) were in good agreement with the reported data.

### DNA double-strand breakage and histone eviction

Since the main difference in biological activity between doxorubicin and aclarubicin is their capacity to induce DNA double-strand breaks, we tested the ability of hybrid structures **2** - **11** in comparison to their parental drugs **1** and **12** to induce DNA damage. Anthracyclines are often used in the treatment of acute myeloid leukemia; therefore, human chronic myelogenous leukemia cells (K562 cells) were incubated for 2 h with  $10\mu\text{M}$  **1** - **12**, and etoposide as a positive control for DNA double-strand break formation [48,49]. These concentrations are corresponding to physiological serum peak levels of cancer patients at standard treatment [17,50]. DNA break formation was analyzed by measuring phosphorylation of H2AX ( $\gamma\text{H2AX}$ ), a well-known marker for DNA double-strand breaks, by Western blot (Figure 2A and B) as well as by constant-field gel electrophoresis (Figure 2C) [51]. Only doxorubicin (**1**) and hybrid structure **9** induced DNA double-strand breaks, as is evident from both assays (supplemental information Figure S1A-C). None of the other compounds induced phosphorylated H2AX and thus resemble the activity of aclarubicin (**12**). Subsequently, compounds **1** - **12** were tested for their ability to induce histone eviction. To visualize histone eviction, the release of photoactivated green fluorescent protein-labeled histone H2A (PAGFP-H2A) was followed in the adherent human melanoma MelJu-So cell line using time-lapse confocal microscopy, as previously described [15,17]. Compounds **3**, **8**, and **11** are equally potent at evicting histones to their parent structures doxorubicin (**1**) and aclarubicin (**12**). Compounds **4**, **6**, and **7** are able to evict histones, but do so less efficiently than **1** and **12**, while compounds **2**, **5**, **9** and **10** fail to evict histones (Figures 2D and supplemental information Figure S2).

### Cytotoxicity and cellular uptake

To test the cell cytotoxicity of the panel of hybrid anthracyclines, K562 cells were treated for 2 h with compounds **1** - **12** at physiological relevant concentrations, and cell survival was measured 72 h post-treatment using a CellTiter-Blue assay (Figure 3A and B) [17,50]. Compounds **3**, **8**, and **11** were effectively killing K562 cells. While compounds **3** and **8** showed cytotoxicity in the same range as their parental drugs

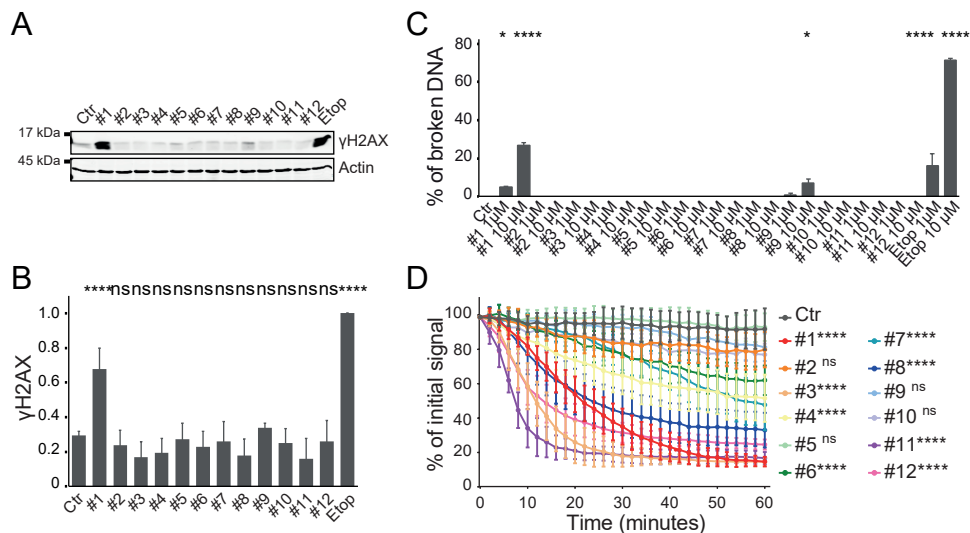


**Figure 2. Evaluation of DNA break capacity and histone evicting activity of hybrid structures 2-11 and parent compounds doxorubicin (1) and aclarubicin (12).** (A) K562 cells were treated for 2 h with 10  $\mu$ M of the indicated drugs, etoposide was used as a positive control for DNA double-strand breaks.  $\gamma$ H2AX levels were examined by Western blot. Actin was used as a loading control, and molecular weight markers are as indicated. (B) Quantification of the  $\gamma$ H2AX signal normalized to actin. Results are presented as mean  $\pm$  SD of three independent experiments. Ordinary one-way ANOVA with Dunnett's multiple comparison test; ns, not significant; \*\*\*\* $P$  < 0.0001. (C) Quantification of broken DNA relative to intact DNA as analyzed by CFGE. Etoposide was used as a positive control for DNA double-strand breaks. Results are presented as mean  $\pm$  SD of three independent experiments. Ordinary one-way ANOVA with Dunnett's multiple comparison test; \* $P$  < 0.05, \*\*\*\* $P$  < 0.0001 is indicated, all others are not significant. (D) Quantification of the release of fluorescent PAGFP-H2A from the photoactivated nuclear regions after administration of 10  $\mu$ M of the indicated drugs. Results are shown as mean  $\pm$  SD of 10–20 cells from at least three independent experiments. Ordinary two-way ANOVA with Dunnett's multiple comparison test; ns, not significant; \*\*\*\* $P$  < 0.0001. See also Figures S1 and S2.

doxorubicin (1) and aclarubicin (12), respectively, compound 11 was ~13 times more cytotoxic than doxorubicin and 2.5 times more than aclarubicin. Compounds 4, 7, 9 and 10 were only effective at higher concentrations, while compounds 2, 5 and 6 did not show any cytotoxicity (Figure 3A, B, and S3A). The observed cytotoxicity is not specific for this acute myeloid leukemia cell line (K562) because similar toxicity profiles were observed for these compounds when tested in the melanoma cell line MelJuSo, the colorectal carcinoma cell line HCT116, the two prostate cancer cell lines PC3 and DU145, and the glioblastoma cell line U87 (Figure 3C-G).

To validate that the differences in DNA damage, chromatin damage induction, and effective cytotoxicity are not caused by differences in cellular uptake of the different hybrid structures, we performed drug uptake experiments for compounds 1–12 utilizing the inherent fluorescent property of the anthraquinone moieties found in the anthracycline drugs [52]. K562 and MelJuSo cells were treated with 1  $\mu$ M of the indicated compounds for 2 h and fluorescence was then measured by flow cytometry (supplemental information, Figure S3B-E). The fractional increase/decrease in fluorescence was compared to the parental drugs with that of the corresponding

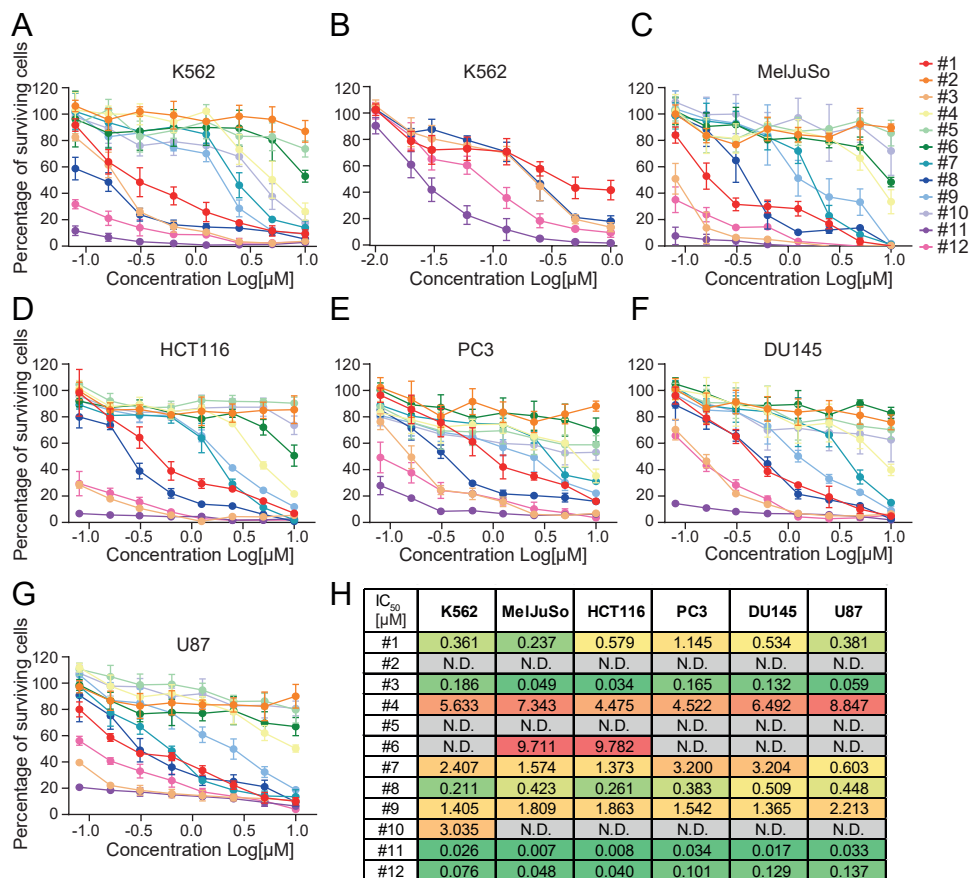


**Figure 3. Cytotoxicity of Compounds 1-12.** (A, B) K562 cells were treated for 2 h at the indicated doses (higher doses in (A), lower doses in (B)) of the various hybrid compounds followed by drug removal. (C – G) Cell survival in MelJuSo (C), human colorectal carcinoma cell line HCT116 (D), human prostate tumor cell line PC3 (E) and DU145 (F), and human glioblastoma cell line U87 (G). Cells were treated for 2 h at indicated dose followed by drug removal. Cell viability was measured by a CellTiter-Blue assay 72 h post-treatment. Data are shown as mean  $\pm$  SD from three different experiments. (H) Table showing the  $IC_{50}$  values for the different doxorubicin/aclarubicin hybrid compounds for the indicated cell lines. See also Figure S3.

anthraquinone aglycon—the fluorophore within the anthracyclines. Significant differences in uptake of the different hybrid structures were observed. Compounds **3** and **11** are taken up  $\sim 6$  and 4 times more efficiently than doxorubicin (**1**), respectively, while compounds **5**, **7** and **9** were more poorly taken up by K562 cells compared to doxorubicin (**1**). A similar observation is made for compounds **4**, **6**, **8** and **10**, which were taken up more efficiently than aclarubicin (**12**), whereas uptake of compound **2** is significantly less compared to aclarubicin (**12**). Nevertheless, when drug uptake is plotted against the  $IC_{50}$  in K562 cells or drug uptake in MelJuSo cells against histone eviction speed, no correlation between uptake of the hybrid structures with cytotoxicity or histone eviction was observed (supplemental information, Figure S3F and G). Of note, while the uptake of compound **5** is similar to that of doxorubicin (**1**),

this compound is not able to induce DNA double-strand breaks or evict histones. Consequently, this compound is one of the least cytotoxic hybrids from this set of compounds (Figure 3H). As anthracycline drugs target TopoII, we decided to validate if the lack of cytotoxicity of compound **5** can be caused by the loss of ability to interfere with the catalytic cycle of TopoII. Therefore, we transiently overexpressed GFP-tagged TopoII $\alpha$  in MelJuSo cells and followed the protein localization over time upon treatment with 10  $\mu$ M of the different doxorubicin/aclarubicin hybrid compounds. At steady state, TopoII $\alpha$  is localized in the nucleus where it accumulates in nucleoli, but upon treatment with the hybrid anthracyclines, the protein rapidly relocates (supplemental information, Figure S4A and B). While most of the hybrid compounds are able to relocate TopoII $\alpha$ , compound **5** does not. Furthermore, relocation of TopoII $\alpha$  by compounds **2**, **6** and **10** was less efficient than by the other compounds, which might explain why these four in total are the least cytotoxic hybrid variants from this set of compounds.

### Correlation between *N,N*-dimethylation and cytotoxicity

Although no clear correlation is observed between the structural features of the compounds and their IC<sub>50</sub>-values (supplemental information, Figure S5A-C), there is a strong relationship between the rate of histone eviction and cell toxicity (Figure 4A and B). In general, *N,N*-dimethylation of the sugar attached to the anthraquinone strongly improves histone eviction and enhances cytotoxicity of these compounds (Figure 4C). This observation could be very useful in the development of more effective anthracycline drugs, since (with the exception of aclarubicin) all anthracycline drugs currently used in the clinic (doxorubicin, daunorubicin, epirubicin, and idarubicin) contain a primary amine on their sugar moiety.

## DISCUSSION AND CONCLUSIONS

Although anthracycline anticancer drugs are known to induce severe side effects, these effective chemotherapeutic drugs have been one of the cornerstones in oncol-

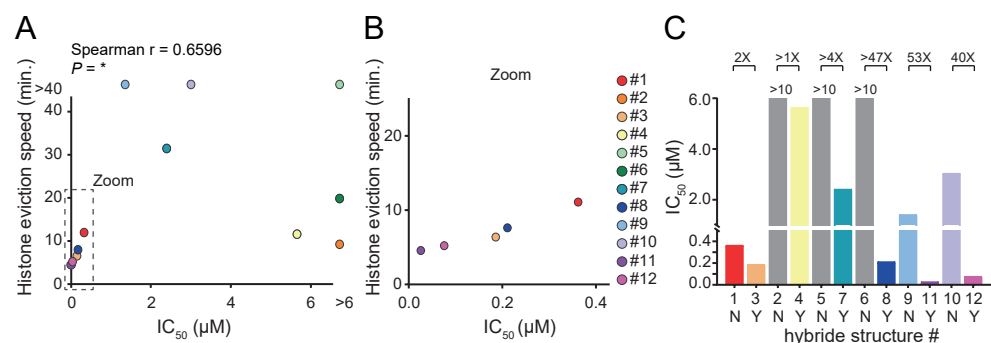


**Figure 4. Cytotoxicity correlates with *N,N*-dimethylation and efficiency of histone eviction.** (A) Histone eviction speed (time at which 25% of the initial signal is reduced) versus IC<sub>50</sub> of the various hybrid compounds is plotted. Two-tailed Spearman  $r$  correlation,  $*P < 0.05$ . (B) Zoom-in of data plotted in (A). (C) *N,N*-dimethylation of the first sugar over no methylation gives improved IC<sub>50</sub> in K562 cells (1 versus 3 / 2 versus 4 / 5 versus 7 / 6 versus 8 / 9 versus 11 / 10 versus 12). IC<sub>50</sub> is plotted for the corresponding hybrid structures without (no; N) and with (yes; Y) *N,N*-dimethylation. The fold change of IC<sub>50</sub> improvement as a result of the *N,N*-dimethylation is indicated above the bars. IC<sub>50</sub> could not be determined for compounds 2, 5, and 6 (gray bars), and was therefore depicted as the highest concentration tested (10 μM).

ogy for over five decades. Following the discovery of doxorubicin (**1**), many anthracycline variants have been evaluated with the aim of reducing their toxicity, but this has not led to any effective and less cardiotoxic variants to enter clinical practice other than aclarubicin (**12**). Remarkably, this drug is only used in Japan and China [3]. It has long been thought that the cytotoxic activity of anthracyclines was due to their DNA double-strand breaking capacity [53]; however, we have previously shown that histone eviction activity is likely the main mechanism of cytotoxicity [15,17–19]. Here, we have developed synthetic chemistry to assemble a complete set of doxorubicin/aclarubicin hybrid structures varying at the anthraquinone aglycon, the nature of the carbohydrate portion, and the alkylation pattern of the amine on the first sugar moiety. The set of doxorubicin/aclarubicin hybrids was assembled using Yu's gold-catalyzed glycosylation of the anthracycline aglycons, which in all cases proceeded with excellent stereoselectivity. The required di- and trisaccharides were generated using fully stereoselective IDCP-mediated glycosylations. Overall, the developed synthetic strategy proved to be broadly applicable and delivered the set of anthracyclines in a highly efficient manner. Furthermore, we have subjected these hybrid structures to a detailed biological evaluation, including cellular uptake, TopoII $\alpha$  re-localization capacity, DNA damage, and histone eviction assays. Although no clear correlation was found between the anthraquinone aglycon moiety and the number of carbohydrate fragments with the observed cytotoxicity of the compounds, a clear relationship between histone eviction efficiency and cytotoxicity was revealed. The coherent set of hybrid structures yielded three compounds that were more cytotoxic than doxorubicin (**3**, **8**, and **11**). Across the board, *N,N*-dimethylation of the carbohydrate appended to the anthraquinone aglycon considerably improved cytotoxicity (**3** and **4** outperform **1** and **2**; **7** and **8** outperform **5** and **6**, and **11** and **12** outperform **9** and **10**). How exactly *N,N*-dimethylation of the amino sugar improves cytotoxicity is not yet fully understood, but the addition of the methyl groups makes those compounds slightly more hydrophobic, which might influence their uptake. Furthermore, it has been shown that *N*-methylation of anthracyclines modulates their transport by the membrane transporter P-glycoprotein (P-gp) [54]. It has been suggested that the steric hindrance created by the methyl groups can impair the interaction between the positively charged amino group with the active site of the P-gp exporter, which leads to better intracellular drug accumulation. This would also indicate that the various *N,N*-dimethylated hybrid variants might be effective drugs for the treatment of multidrug-resistant tumors, in which elevated expression of the P-gp exporter is often observed [23,55]. A third option for the enhanced effectivity of the *N,N*-dimethylation amino sugar variants might be a change in the interaction dynamics of the anthracycline drugs with the DNA. It is known that doxorubicin–DNA aminor adducts can form between the 3'-NH<sub>2</sub> of the doxorubicin sugar, the N<sub>2</sub> of the guanine base, and formaldehyde [56–59]. The addition of two methyl groups to the critical amino sugar might convert these drugs from a covalent DNA intercalator into a reversible DNA intercalator, affecting the dynamics by which these drugs perturb the DNA-histone organization.

In addition to *N,N*-dimethylation of the sugar moiety, the doxorubicin anthraquinone aglycon appears to be slightly better than the aclarubicin anthraquinone aglycon and the aclarubicin trisaccharide improves cytotoxicity over the doxorubicin monosaccharide. A combination of these structural features is found in compound **11**, the most cytotoxic compound in the focused library, being 13 times more cytotoxic than doxorubicin and 2.5 times more than aclarubicin in K562 cells. Histone eviction by compound **11** is approximately three times as fast as doxorubicin and twice as fast



as for aclarubicin. The subsequent difference in cytotoxicity between compound **11** and doxorubicin or aclarubicin can therefore only partially be explained by the enhanced histone eviction efficacy. However, besides the difference in histone eviction efficacy, it has been shown that various anthracycline drug can have selectivity for distinct (epi-)genomic regions (and can therefore be considered different drugs because of different genomic targets) [18]. The different targeted (epi-)genomic regions by these drugs can subsequently have divergent downstream effects, which may explain the improved cytotoxicity for compound **11**.

In summary, in this study, we have developed highly effective and broadly applicable synthetic chemistry, which was used to prepare a set of ten doxorubicin/aclarubicin hybrid structures and studied their specific biological activities in cells. This has given us better insights into the structure-activity relationship for this extensively used group of chemotherapeutics, which can help to direct the development of new effective anticancer drugs. Interestingly, the most potent compounds identified from the systematic library of compounds (**3**, **8**, and **11**) do not exert their activity through the induction of DNA double-strand break formation following inhibition of TopoII $\alpha$ , but rather through the induction of histone eviction, indicating that histone eviction by anthracyclines could be the dominant factor for the cytotoxicity of this class of anticancer drugs.

## EXPERIMENTAL SECTION

### Chemistry

Doxorubicin was obtained from Accord Healthcare Limited, U.K., aclarubicin from Santa Cruz Biotech, and etoposide from Pharmachemie, Haarlem, The Netherlands. For the synthesis of the aclarubicin/ doxorubicin hybrid compounds, all reagents were of commercial grade and used as received. Traces of water from reagents were removed by coevaporation with toluene in reactions that required anhydrous conditions. All moisture/oxygen sensitive reactions were performed under an argon atmosphere. DCM used in the glycosylation reactions was dried with flamed 4 Å molecular sieves before being used. Reactions were monitored by thin-layer chromatography (TLC) analysis with detection by UV (254 nm) and, where applicable, by spraying with 20% sulfuric acid in EtOH or with a solution of  $(\text{NH}_4)_6\text{Mo}_7\text{O}_{24}\cdot 4\text{H}_2\text{O}$  (25 g/L) and  $(\text{NH}_4)_4\text{Ce}(\text{SO}_4)_4\cdot 2\text{H}_2\text{O}$  (10 g/L) in 10% sulfuric acid (aq.) followed by charring at  $\sim 150^\circ\text{C}$ . Flash column chromatography was performed on silica gel (40–63  $\mu\text{m}$ ).  $^1\text{H}$  and  $^{13}\text{C}$  spectra were recorded on a Bruker AV 400 and Bruker AV 500 spectrometers in  $\text{CDCl}_3$ ,  $\text{CD}_3\text{OD}$ , pyridine- $d_5$  or  $\text{D}_2\text{O}$ . Chemical shifts ( $\delta$ ) are given in parts per million (ppm) relative to tetramethylsilane (TMS) as internal standard ( $^1\text{H}$  NMR in  $\text{CDCl}_3$ ) or the residual signal of the deuterated solvent. Coupling constants (J) are given in hertz. All  $^{13}\text{C}$  spectra are proton-decoupled. Column chromatography was carried out using silica gel (0.040–0.063 mm). Size-exclusion chromatography was carried out using a Sephadex LH-20, using DCM/MeOH (1:1, v/v) as the eluent. Neutral silica was prepared by stirring regular silica gel in aqueous ammonia, followed by filtration, washing with water, and heating at  $150^\circ\text{C}$  overnight. High-resolution mass spectrometry (HRMS) analysis was performed with an LTQ Orbitrap mass spectrometer (Thermo Finnigan), equipped with an electrospray ion source in positive mode (source voltage, 3.5 kV; sheath gas flow, 10 mL/min; capillary temperature,  $250^\circ\text{C}$ ) with resolution  $R = 60000$  at  $m/z$  400 (mass range  $m/z = 150 - 2000$ ) and dioctyl phthalate ( $m/z = 391.28428$ ) as a “lock mass”, or with a Synapt G2-Si (Waters), equipped with an electrospray ion source in positive mode (electrospray



ionization time-of-flight (ESI-TOF)), injection via NanoEquity system (Waters), with LeuEnk ( $m/z = 556.2771$ ) as “lock mass”. Eluents used: MeCN/H<sub>2</sub>O (1:1 v/v) supplemented with 0.1% formic acid. The high-resolution mass spectrometers were calibrated prior to measurements with a calibration mixture (Thermo Finnigan). Purity of all compounds is >95% as determined by <sup>1</sup>H NMR. Syntheses of the monosaccharide donors/acceptors are described in the supplemental information.

### General procedure A: *p*-methoxyphenolate oxidative deprotection

To a solution of *p*-methoxyphenyl glycoside in 1:1 MeCN/H<sub>2</sub>O (0.02M, v/v) were added NaOAc (10 equiv) and then Ag(DPAH)<sub>2</sub>·H<sub>2</sub>O [60] (2.1 equiv for trisaccharides, 4 equiv for monosaccharides) portionwise over 30 min at 0°C. The mixture was stirred until disappearance of the starting material, after which it was poured into sat. aq. NaHCO<sub>3</sub>. This was then extracted with DCM thrice, dried over MgSO<sub>4</sub> and concentrated in vacuo to give the crude lactols.

### General procedure B: alkynylbenzoate esterification

A solution of ortho-cyclopropylethynylbenzoic acid methyl ester [47] in tetrahydrofuran (THF) (5 mL/mmol) and 1M NaOH (5 mL/mmol) was stirred at 50°C for at least 5 h. It was then poured into 1M HCl (6 mL/mmol) and extracted with DCM thrice. The combined organic layers were then dried over MgSO<sub>4</sub> and concentrated in vacuo. The resultant acid was then used without further purification. To a solution of the above crude lactol in DCM (0.1M) were added DIPEA (9 equiv), DMAP (1 equiv), EDCI·HCl (3.2 equiv) and the above carboxylic acid (3 equiv). After stirring overnight, the mixture was diluted with DCM and washed with sat. aq. NaHCO<sub>3</sub> and brine. Drying over MgSO<sub>4</sub>, concentration in vacuo and column chromatography of the residue (EtOAc/pentane) gave the alkynylbenzoates.

### General procedure C: Au(I)-catalyzed glycosylation

To a solution of the glycosyl donor and the required anthracycline acceptor (1-2 equiv) in DCM (0.05M), activated molecular sieves (4 Å) were added. The mixture was stirred for 30 min. Subsequently, a freshly prepared 0.1M DCM solution of PPh<sub>3</sub>AuNTf<sub>2</sub> (prepared by stirring 1:1 PPh<sub>3</sub>AuCl and AgNTf<sub>2</sub> in DCM for 30 min) (0.1 equiv) in DCM was added dropwise at the designated temperature. After stirring for 30 min (at room temperature (RT)) or overnight (-20°C or lower), the mixture was filtered and concentrated in vacuo. Column chromatography (EtOAc/pentane or Et<sub>2</sub>O/pentane and then acetone/toluene) followed by (if required) size-exclusion chromatography (Sephadex LH-20, 1:1 DCM/MeOH v/v) gave the glycosides.

### Synthesis of anthracycline monosaccharides 2, 3 and 4

The synthesis of **3** is described in ref. 15.

### 7-[3-*N*-allyloxycarbonyl-2,3-dideoxy- $\alpha$ -L-fucopyranoside]-aklavinone (**15**)

Prepared according to General Procedure C from donor **13** and aklavinone **14** (2 equiv) at RT to give after column chromatography (4:96 Et<sub>2</sub>O/pentane and then 1.5:98.5 acetone/toluene) the title compound as a yellow solid (149 mg, 0.201 mmol, 73%). <sup>1</sup>H NMR (400 MHz, chloroform-*d*)  $\delta$  12.66 (s, 1H), 12.04 (s, 1H), 7.83 (dd, *J* = 7.5, 1.2 Hz, 1H), 7.77 – 7.64 (m, 2H), 7.31 (dd, *J* = 8.4, 1.2 Hz, 1H), 5.86 (ddt, *J* = 16.3, 10.8, 5.6 Hz, 1H), 5.46 (d, *J* = 3.8 Hz, 1H), 5.28 – 5.12 (m, 3H), 4.63 (d, *J* = 8.8 Hz, 1H), 4.58 – 4.41 (m, 2H), 4.21 (s, 1H), 4.15 – 4.01 (m, 2H), 3.86 (dq, *J* = 8.7, 4.1 Hz, 1H), 3.78 (s, 1H), 3.69 (s, 3H), 2.50 (dd, *J* = 15.0, 4.4 Hz, 1H), 2.34 (d, *J* =

15.0 Hz, 1H), 1.92 (td,  $J = 12.8, 4.1$  Hz, 1H), 1.81 – 1.68 (m, 2H), 1.49 (dq,  $J = 14.3, 7.3$  Hz, 1H), 1.36 – 1.18 (m, 3H), 1.08 (t,  $J = 7.3$  Hz, 3H), 0.99 (t,  $J = 7.9$  Hz, 9H), 0.66 (qd,  $J = 7.9, 2.1$  Hz, 6H).  $^{13}\text{C}$  NMR (101 MHz,  $\text{CDCl}_3$ )  $\delta$  192.9, 181.5, 171.6, 162.7, 162.3, 155.2, 142.9, 137.5, 133.7, 133.0, 132.9, 131.3, 124.9, 121.1, 120.3, 117.8, 115.9, 114.8, 101.6, 71.5, 71.4, 71.1, 67.6, 65.6, 57.2, 52.6, 47.4, 34.0, 32.2, 30.4, 17.6, 7.2, 6.8, 5.4. HRMS:  $[\text{M} + \text{Na}]^+$  calculated for  $\text{C}_{38}\text{H}_{49}\text{NO}_{12}\text{SiNa}$  774.2533; found 774.2525.

#### 7-[ $\alpha$ -L-rhodosamino]-aklavinone (4)

To a solution of 15 (23.7 mg, 0.032 mmol) in DCM (3.2 mL) were added *N,N*-dimethylbarbituric acid (15 mg, 0.096 mmol, 3 equiv) and tetrakis(triphenylphosphine)palladium(0) (1.8 mg, 1.6  $\mu\text{mol}$ , 0.05 eq). After stirring for 2.5 h, the mixture was concentrated in vacuo. Column chromatography (DCM; 2:98 MeOH/DCM) gave the crude amine. This was then redissolved in EtOH (7.7 mL) and 37% aquiv.  $\text{CH}_2\text{O}$  (79  $\mu\text{L}$ , 30 equiv) was added  $\text{NaBH}(\text{OAc})_3$  (67 mg, 0.32 mmol, 10 equiv). The mixture was stirred for 2.5 h before being quenched by addition of sat. aq.  $\text{NaHCO}_3$ . It was then poured into  $\text{H}_2\text{O}$  and extracted with DCM, dried over  $\text{Na}_2\text{SO}_4$  and concentrated in vacuo to give the crude dimethylated amine. This was then redissolved in pyridine (3.2 mL) in a poly(tetrafluoroethylene) (PTFE) tube, after which HF.pyr complex (70 wt% HF, 125  $\mu\text{L}$ ) was added at  $0^\circ\text{C}$ . Over the course of 4 h, additional HF.pyr complex (70 wt% HF, 125  $\mu\text{L}$  each time) was added five times. Solid  $\text{NaHCO}_3$  was added to quench, and the mixture was stirred until cessation of effervescence. It was then filtered off, and the filtrate was partitioned between DCM and  $\text{H}_2\text{O}$ . The organic layer was dried over  $\text{Na}_2\text{SO}_4$  and concentrated in vacuo. Column chromatography on neutral silica (DCM; 20:80 MeOH/DCM) gave the title compound as a yellow solid (7.9 mg, 13.9  $\mu\text{mol}$ , 43% over three steps).  $^1\text{H}$  NMR (500 MHz, chloroform- $d$ )  $\delta$  12.70 (s, 1H), 12.01 (s, 1H), 7.83 (dd,  $J = 7.5, 1.1$  Hz, 1H), 7.77 – 7.66 (m, 2H), 7.31 (dd,  $J = 8.4, 1.2$  Hz, 1H), 5.55 (d,  $J = 3.9$  Hz, 1H), 5.29 – 5.20 (m, 1H), 4.27 (s, 1H), 4.16 – 4.03 (m, 2H), 3.87 (s, 1H), 3.70 (s, 3H), 2.54 (dd,  $J = 15.2, 4.5$  Hz, 1H), 2.45 (s, 6H), 2.33 (d,  $J = 15.2$  Hz, 1H), 2.05 (td,  $J = 13.1, 12.6, 4.2$  Hz, 1H), 1.89 (dd,  $J = 12.9, 4.6$  Hz, 1H), 1.76 (dq,  $J = 14.6, 7.3$  Hz, 1H), 1.52 (dq,  $J = 14.5, 7.3$  Hz, 1H), 1.38 (dd,  $J = 6.5, 2.1$  Hz, 3H), 1.09 (t,  $J = 7.3$  Hz, 3H).  $^{13}\text{C}$  NMR (126 MHz,  $\text{CDCl}_3$ )  $\delta$  192.9, 181.4, 171.3, 162.8, 162.3, 142.8, 137.6, 133.6, 133.1, 131.2, 125.0, 121.1, 120.4, 115.9, 114.9, 101.1, 71.9, 71.4, 67.0, 65.8, 61.1, 57.2, 52.7, 42.0, 34.0, 32.2, 27.8, 17.0, 6.8. HRMS:  $[\text{M} + \text{H}]^+$  calculated for  $\text{C}_{30}\text{H}_{36}\text{NO}_{10}$  570.2339; found 570.2921.

#### 7-[ $\alpha$ -L-Daunosamino]-aklavinone (2)

To a solution of 15 (60 mg, 0.081 mmol) in DCM (8.1 mL) were added *N,N*-dimethylbarbituric acid (38 mg, 0.24 mmol, 3 equiv) and tetrakis(triphenylphosphine)palladium(0) (4.6 mg, 4.1  $\mu\text{mol}$ , 0.05 equiv). After stirring for 2.5 h, the mixture was concentrated in vacuo. Column chromatography (DCM; 2:98 MeOH/DCM) gave the crude amine. This was then redissolved in pyridine (6 mL) in a PTFE tube, after which HF.pyr complex (70 wt% HF, 710  $\mu\text{L}$ ) was added at  $0^\circ\text{C}$ . After 3.5 h and 5.5 h, additional HF.pyr complex (70 wt% HF, 355  $\mu\text{L}$  each time) was added. After stirring for a total of 6.5 h, solid  $\text{NaHCO}_3$  was added to quench, and the mixture was stirred until cessation of effervescence. It was then filtered off, and the filter cake was rinsed thoroughly with MeOH/DCM (9:1 v/v). The combined filtrates were then concentrated in vacuo. Column chromatography (DCM; 20:80 MeOH/DCM) gave the title compound as a yellow solid (18 mg, 33  $\mu\text{mol}$ , 41% over two steps).  $^1\text{H}$  NMR (500 MHz, methanol- $d_4$ )  $\delta$  7.77 – 7.61 (m, 2H), 7.53 (s, 1H), 7.31 – 7.20 (m, 1H), 5.49

(s, 1H), 5.14 (d,  $J = 4.7$  Hz, 1H), 4.27 (q,  $J = 6.5$  Hz, 1H), 4.08 (s, 1H), 3.73 (s, 2H), 3.67 (d,  $J = 2.8$  Hz, 1H), 3.57 – 3.47 (m, 1H), 2.52 (dd,  $J = 15.0, 5.2$  Hz, 1H), 2.32 (d,  $J = 15.0$  Hz, 1H), 2.03 (td,  $J = 12.9, 4.0$  Hz, 1H), 1.99 – 1.90 (m, 1H), 1.76 (dq,  $J = 14.7, 7.4$  Hz, 1H), 1.56 (dq,  $J = 13.9, 7.1$  Hz, 1H), 1.31 (d,  $J = 6.6$  Hz, 3H), 1.11 (t,  $J = 7.4$  Hz, 3H).  $^{13}\text{C}$  NMR (126 MHz, MeOD)  $\delta$  193.6, 182.3, 172.6, 163.7, 143.8, 138.5, 134.7, 134.0, 125.8, 121.2, 120.8, 117.0, 115.8, 101.7, 72.5, 72.1, 68.4, 68.1, 58.2, 53.0, 49.8, 48.4, 35.8, 33.3, 30.1, 17.0, 7.1. HRMS:  $[\text{M} + \text{H}]^+$  calculated for  $\text{C}_{28}\text{H}_{32}\text{NO}_{10}$  542.2026; found 542.2031.

### Synthesis of Anthracycline Disaccharides 5-8

#### ***p*-Methoxyphenyl-2-deoxy-3,4-tetraisopropylidisiloxy- $\alpha$ -L-fucopyranosyl-(1 $\rightarrow$ 4)-3-N-allyloxycarbonyl-2,3-dideoxy- $\alpha$ -L-fucopyranoside (19)**

To a solution of the glycosyl acceptor 17 (901 mg, 2.67 mmol, 1 equiv) and the glycosyl donor 18 (1.80 g, 3.73 mmol, 1.3 equiv) in  $\text{Et}_2\text{O}/\text{DCE}$  (70 mL, 4:1 v/v), activated molecular sieves (4 Å) were added. The mixture was stirred for 30 min, and then, at 10°C, iodonium dicollidine perchlorate (5.00 g, 10.7 mmol, 4 equiv) was added. After 30 min, triphenylphosphine (1.40 g, 5.34 mmol, 2 equiv) was added, and the mixture was stirred for an additional hour. It was then diluted with EtOAc and filtered; washed with 10% aq.  $\text{Na}_2\text{S}_2\text{O}_3$ , 1M  $\text{CuSO}_4$  solution twice, and  $\text{H}_2\text{O}$ ; and then dried over  $\text{MgSO}_4$ . Concentration in vacuo and column chromatography (5:95 – 10:90 EtOAc/pentane) of the residue gave the title compound as a white foam (1.69 g, 2.38 mmol, 89%).  $^1\text{H}$  NMR (500 MHz, chloroform-*d*)  $\delta$  7.05 – 6.93 (m, 2H), 6.93 – 6.70 (m, 2H), 6.16 (d,  $J = 7.9$  Hz, 1H), 5.92 (ddt,  $J = 16.1, 10.9, 5.6$  Hz, 1H), 5.52 (d,  $J = 3.2$  Hz, 1H), 5.30 (dq,  $J = 17.2, 1.6$  Hz, 1H), 5.20 (dq,  $J = 10.5, 1.4$  Hz, 1H), 4.93 (d,  $J = 3.7$  Hz, 1H), 4.58 (qdt,  $J = 13.3, 5.6, 1.4$  Hz, 2H), 4.41 (ddd,  $J = 12.2, 4.6, 2.5$  Hz, 1H), 4.37 – 4.25 (m, 1H), 4.14 – 4.04 (m, 2H), 4.01 (s, 1H), 3.77 (s, 3H), 3.54 (s, 1H), 2.19 – 2.05 (m, 2H), 1.99 (dd,  $J = 12.6, 4.6$  Hz, 1H), 1.89 (td,  $J = 12.7, 3.5$  Hz, 1H), 1.34 (d,  $J = 6.4$  Hz, 3H), 1.18 (d,  $J = 6.5$  Hz, 3H), 1.14 – 0.83 (m, 28H).  $^{13}\text{C}$  NMR (126 MHz,  $\text{CDCl}_3$ )  $\delta$  155.6, 154.4, 150.9, 132.8, 117.4, 117.2, 114.4, 101.8, 96.2, 81.2, 73.0, 69.8, 68.0, 67.4, 65.4, 55.5, 46.4, 33.1, 31.5, 17.6, 17.5, 17.4, 17.3, 17.3, 17.2, 17.2, 17.2, 17.1, 17.1, 14.1, 13.9, 13.0, 12.4. HRMS:  $[\text{M} + \text{Na}]^+$  calculated for  $\text{C}_{35}\text{H}_{59}\text{NO}_{10}\text{Si}_2\text{Na}$  732.35752; found 732.3587.

#### ***o*-Cyclopropylethynylbenzoyl-2-deoxy-3,4-tetraisopropylidisiloxane- $\alpha$ -L-fucopyranosyl-(1 $\rightarrow$ 4)-3-N-allyloxycarbonyl-2,3-dideoxy-L-fucopyranoside (21)**

Prepared according to General Procedure A and B from 19 (1.69 g, 2.38 mmol) to give after column chromatography (10:90 – 20:80 EtOAc/pentane) the title compound as a white foam (1.54 g, 1.99 mmol, 84% over two steps,  $\alpha:\beta$  1:8).  $^1\text{H}$  NMR (500 MHz, chloroform-*d*)  $\delta$  8.00 – 7.85 (m, 1H), 7.47 (dd,  $J = 7.8, 1.4$  Hz, 1H), 7.41 (ddd,  $J = 9.1, 6.0, 1.4$  Hz, 1H), 7.35 – 7.24 (m, 1H), 6.35 (d,  $J = 7.6$  Hz, 1H), 5.99 (dd,  $J = 10.0, 2.3$  Hz, 1H), 5.96 – 5.84 (m, 1H), 5.36 – 5.15 (m, 2H), 4.93 (d,  $J = 3.9$  Hz, 1H), 4.56 (qdt,  $J = 13.3, 5.6, 1.5$  Hz, 2H), 4.45 (ddd,  $J = 12.1, 4.5, 2.5$  Hz, 1H), 4.11 – 4.06 (m, 1H), 4.01 (d,  $J = 2.5$  Hz, 1H), 3.87 (dddd,  $J = 12.1, 7.1, 4.1, 2.6$  Hz, 1H), 3.85 – 3.79 (m, 1H), 3.48 – 3.44 (m, 1H), 2.22 (ddd,  $J = 11.9, 4.1, 2.2$  Hz, 1H), 2.14 (td,  $J = 12.4, 4.0$  Hz, 1H), 1.99 (dd,  $J = 12.4, 4.6$  Hz, 1H), 1.85 (td,  $J = 12.3, 10.0$  Hz, 1H), 1.51 (tt,  $J = 7.2, 5.7$  Hz, 1H), 1.36 – 1.30 (m, 6H), 1.13 – 0.81 (m, 28H).  $^{13}\text{C}$  NMR (126 MHz,  $\text{CDCl}_3$ )  $\delta$  164.3, 155.8, 134.2, 133.0, 132.0, 131.1, 130.8, 127.0, 125.1, 117.7, 102.3, 99.8, 93.2, 80.6, 74.5, 73.3, 73.0, 69.9, 68.4, 65.7, 50.1, 33.3, 32.2, 17.8, 17.8, 17.6, 17.5, 17.5, 17.5, 17.4, 17.3, 14.3, 14.2, 13.2, 12.7, 9.0, 8.9, 0.8. HRMS:  $[\text{M} + \text{Na}]^+$  calculated for  $\text{C}_{40}\text{H}_{61}\text{NO}_{10}\text{Si}_2\text{Na}$  794.37317; found 794.3749.

**7-[2-Deoxy-3,4-tetraisopropylidisiloxy- $\alpha$ -L-fucopyranosyl-(1 $\rightarrow$ 4)-3-N-allyloxycarbonyl-2,3-dideoxy- $\alpha$ -L-fucopyranoside]-14-O-tert-butylidimethylsilyl-doxorubicinone (22)**

Prepared according to General Procedure C from donor 21 (722 mg, 1.00 mmol) and 14-O-tert-butylidimethylsilyl-doxorubicinone 16 (793 mg, 1.50 mmol, 1.5 equiv) to give after column chromatography (5:95 – 20:80 EtOAc/pentane – 4:96 acetone/toluene) the title compound as a red solid (714 mg, 0.640 mmol, 64%).  $^1\text{H}$  NMR (500 MHz, chloroform-*d*)  $\delta$  13.83 (s, 1H), 13.09 (s, 1H), 7.93 (dd, *J* = 7.7, 1.0 Hz, 1H), 7.72 (t, *J* = 8.1 Hz, 1H), 7.43 – 7.32 (m, 1H), 6.07 (d, *J* = 7.8 Hz, 1H), 5.91 – 5.78 (m, 1H), 5.50 (d, *J* = 3.8 Hz, 1H), 5.27 – 5.18 (m, 2H), 5.13 (dq, *J* = 10.5, 1.4 Hz, 1H), 4.98 – 4.86 (m, 3H), 4.61 – 4.37 (m, 4H), 4.13 (q, *J* = 6.5 Hz, 1H), 4.05 (d, *J* = 24.2 Hz, 6H), 3.90 – 3.77 (m, 1H), 3.55 (s, 1H), 3.09 (dd, *J* = 18.8, 2.0 Hz, 1H), 2.81 (d, *J* = 18.7 Hz, 1H), 2.29 (d, *J* = 14.6 Hz, 1H), 2.22 – 2.05 (m, 2H), 2.05 – 1.95 (m, 1H), 1.92 (dd, *J* = 13.1, 4.5 Hz, 1H), 1.78 (td, *J* = 12.9, 4.0 Hz, 1H), 1.30 (dd, *J* = 16.4, 6.4 Hz, 6H), 1.16 – 0.82 (m, 37H), 0.15 (d, *J* = 2.7 Hz, 6H).  $^{13}\text{C}$  NMR (126 MHz,  $\text{CDCl}_3$ )  $\delta$  211.4, 186.8, 186.4, 161.0, 156.3, 155.7, 135.7, 135.3, 134.0, 133.9, 132.9, 120.7, 119.8, 118.5, 117.5, 111.3, 111.2, 101.9, 101.0, 81.0, 73.2, 69.9, 69.7, 68.2, 68.0, 66.7, 65.5, 56.7, 46.6, 35.7, 34.0, 33.3, 31.3, 26.0, 18.7, 17.8, 17.7, 17.6, 17.5, 17.5, 17.5, 17.4, 17.3, 17.2, 14.3, 14.1, 13.1, 12.6, -5.2, -5.3. HRMS:  $[\text{M} + \text{Na}]^+$  calculated for  $\text{C}_{55}\text{H}_{83}\text{NO}_{17}\text{Si}_3\text{Na}$  1136.48665; found 1136.4866.

**7-[2-Deoxy-3,4-tetraisopropylidisiloxy- $\alpha$ -L-fucopyranosyl-(1 $\rightarrow$ 4)-3-amino-2,3-dideoxy- $\alpha$ -L-fucopyranoside]-14-O-tert-butylidimethylsilyl-doxorubicinone (23)**

A solution of 22 (704 mg, 0.631 mmol) and *N,N*-dimethylbarbituric acid (440 mg, 2.84 mmol, 4.5 equiv) in DCM (63 mL) was degassed for 5 min. Then,  $\text{Pd}(\text{PPh}_3)_4$  (36.5 mg, 0.032 mmol, 0.05 equiv) was added and the mixture was allowed to stir for 20 min. It was then directly subjected to column chromatography (pentane, then 0:100 – 50:50 acetone/toluene) to give the title compound as a red solid (650 mg, 0.631 mmol, 100%).  $^1\text{H}$  NMR (500 MHz, chloroform-*d*)  $\delta$  7.93 (dd, *J* = 7.8, 1.0 Hz, 1H), 7.73 (t, *J* = 8.1 Hz, 1H), 7.42 – 7.33 (m, 1H), 5.53 – 5.41 (m, 1H), 5.21 (dd, *J* = 4.1, 2.2 Hz, 1H), 4.98 (d, *J* = 3.7 Hz, 1H), 4.96 – 4.81 (m, 2H), 4.65 (s, 1H), 4.42 (ddd, *J* = 12.1, 4.6, 2.5 Hz, 1H), 4.15 (q, *J* = 6.5 Hz, 1H), 4.10 – 3.93 (m, 5H), 3.53 (s, 1H), 3.40 – 3.20 (m, 3H), 3.18 – 3.00 (m, 2H), 2.82 (d, *J* = 18.7 Hz, 1H), 2.29 (dt, *J* = 14.8, 2.2 Hz, 1H), 2.21 – 2.09 (m, 2H), 2.05 – 1.93 (m, 1H), 1.76 (ddd, *J* = 27.6, 14.0, 4.2 Hz, 1H), 1.29 (d, *J* = 6.5 Hz, 3H), 1.23 (d, *J* = 6.5 Hz, 3H), 1.13 – 0.75 (m, 36H), 0.15 (d, *J* = 1.4 Hz, 6H).  $^{13}\text{C}$  NMR (126 MHz,  $\text{CDCl}_3$ )  $\delta$  211.2, 186.7, 186.4, 161.0, 156.3, 155.6, 135.7, 135.3, 134.0, 132.1, 132.1, 128.6, 120.7, 119.7, 118.5, 111.3, 101.3, 101.1, 81.5, 73.3, 70.1, 69.6, 68.3, 67.8, 66.6, 56.7, 46.8, 35.6, 33.8, 33.4, 25.9, 18.7, 17.7, 17.7, 17.6, 17.6, 17.5, 17.5, 17.4, 17.3, 17.2, 14.2, 14.1, 13.1, 12.6. HRMS:  $[\text{M} + \text{H}]^+$  calculated for  $\text{C}_{51}\text{H}_{80}\text{NO}_{15}\text{Si}_3$  1030.48358; found 1030.4855.

**7-[2-Deoxy- $\alpha$ -L-fucopyranosyl-(1 $\rightarrow$ 4)-3-amino-2,3-dideoxy- $\alpha$ -L-fucopyranoside]-doxorubicinone (5)**

To a solution of 23 (30.5 mg, 29.6  $\mu\text{mol}$ ) in pyridine (3.0 mL) in a PTFE tube, was added HF.pyr complex (70 wt% HF, 232  $\mu\text{L}$ ) at 0°C. Over the course of 4 hours, 2 additional such portions of HF.pyr complex were added. Then, solid  $\text{NaHCO}_3$  was added to quench, and the mixture was stirred until cessation of effervescence. It was then filtered off and concentrated in vacuo. Column chromatography on neutral silica (0:100 – 20:80 MeOH/DCM) gave the title compound as a red solid (15.1 mg, 22.4

$\mu\text{mol}$ , 76%).  $^1\text{H}$  NMR (500 MHz, pyridine- $d_5$ )  $\delta$  7.78 (d,  $J$  = 7.7 Hz, 1H), 7.46 (t,  $J$  = 8.1 Hz, 1H), 7.14 (d,  $J$  = 8.4 Hz, 1H), 5.52 (d,  $J$  = 3.0 Hz, 1H), 5.17 (d,  $J$  = 3.9 Hz, 1H), 5.12 (d,  $J$  = 2.3 Hz, 2H), 5.06 (d,  $J$  = 3.8 Hz, 1H), 4.36 (dt,  $J$  = 12.1, 3.9 Hz, 1H), 4.33 – 4.19 (m, 2H), 3.80 (d,  $J$  = 2.9 Hz, 1H), 3.68 (s, 3H), 3.54 (s, 1H), 3.41 (t,  $J$  = 8.7 Hz, 1H), 3.34 – 3.12 (m, 2H), 2.51 (d,  $J$  = 14.4 Hz, 1H), 2.30 (td,  $J$  = 12.2, 3.9 Hz, 1H), 2.22 (dd,  $J$  = 14.3, 5.1 Hz, 1H), 2.08 (dd,  $J$  = 12.3, 4.9 Hz, 1H), 1.97 (dd,  $J$  = 9.2, 2.8 Hz, 2H), 1.27 (d,  $J$  = 6.4 Hz, 3H), 1.06 (d,  $J$  = 6.4 Hz, 3H).  $^{13}\text{C}$  NMR (126 MHz, Pyr)  $\delta$  215.4, 187.5, 161.9, 157.5, 156.2, 135.2, 121.6, 120.1, 119.9, 112.3, 112.0, 101.9, 101.9, 81.6, 77.1, 72.4, 70.9, 69.0, 68.8, 66.7, 66.2, 57.1, 48.0, 37.9, 34.6, 34.4, 34.2, 18.1. HRMS:  $[\text{M} + \text{H}]^+$  calculated for  $\text{C}_{33}\text{H}_{40}\text{NO}_{14}$  674.24488; found 674.2456.

### 7-[2-Deoxy- $\alpha$ -L-fucopyranosyl-(1 $\rightarrow$ 4)-3-dimethylamino-2,3-dideoxy- $\alpha$ -L-fucopyranoside]-doxorubicinone (7)

To a solution of 23 (102 mg, 99  $\mu\text{mol}$ ) in EtOH (20 mL) and 37% aq.  $\text{CH}_3\text{O}$  (245  $\mu\text{L}$ , 30 equiv) was added  $\text{NaBH}(\text{OAc})_3$  (40 mg, 0.193 mmol, 1.95 equiv). The mixture was stirred for 1.5 h before being poured into sat. aq.  $\text{NaHCO}_3$ . This was extracted with DCM, dried over  $\text{Na}_2\text{SO}_4$  and concentrated in vacuo. Column chromatography (3:97 acetone/toluene) gave the dimethylated amine as a red solid (75 mg, 70.9  $\mu\text{mol}$ , 71%).  $^1\text{H}$  NMR (500 MHz, chloroform- $d$ )  $\delta$  13.92 (s, 1H), 13.24 (s, 1H), 8.01 (dd,  $J$  = 7.7, 1.0 Hz, 1H), 7.77 (t,  $J$  = 8.1 Hz, 1H), 7.43 – 7.37 (m, 1H), 5.54 (d,  $J$  = 3.8 Hz, 1H), 5.25 (dd,  $J$  = 4.1, 2.1 Hz, 1H), 5.01 (d,  $J$  = 3.4 Hz, 1H), 4.98 – 4.84 (m, 2H), 4.79 (s, 1H), 4.49 – 4.34 (m, 2H), 4.09 (s, 3H), 3.95 (t,  $J$  = 1.8 Hz, 1H), 3.91 (q,  $J$  = 6.5 Hz, 1H), 3.75 (s, 1H), 3.38 – 3.35 (m, 1H), 3.18 (dd,  $J$  = 18.9, 1.9 Hz, 1H), 2.98 (d,  $J$  = 18.8 Hz, 1H), 2.32 (dt,  $J$  = 14.7, 2.3 Hz, 1H), 2.19 (s, 6H), 2.17 – 2.06 (m, 3H), 2.06 – 1.96 (m, 2H), 1.89 (td,  $J$  = 12.8, 4.0 Hz, 1H), 1.80 (dd,  $J$  = 13.0, 4.1 Hz, 1H), 1.26 (d,  $J$  = 6.6 Hz, 3H), 1.19 (d,  $J$  = 6.4 Hz, 3H), 1.07 (ddt,  $J$  = 9.4, 7.4, 4.6 Hz, 24H), 0.96 (s, 9H), 0.14 (d,  $J$  = 2.9 Hz, 6H).  $^{13}\text{C}$  NMR (126 MHz,  $\text{CDCl}_3$ )  $\delta$  211.4, 187.2, 186.8, 161.1, 156.6, 156.0, 135.8, 135.6, 134.3, 134.2, 121.0, 119.9, 118.5, 111.5, 111.4, 101.5, 99.9, 74.1, 73.8, 70.6, 69.6, 68.8, 67.3, 66.7, 61.8, 56.8, 43.5, 35.7, 34.1, 33.4, 26.0, 18.1, 17.8, 17.8, 17.7, 17.6, 17.6, 17.5, 17.5, 17.4, 17.4, 14.4, 14.3, 13.2, 12.7. HRMS:  $[\text{M} + \text{H}]^+$  calculated for  $\text{C}_{53}\text{H}_{84}\text{NO}_{15}\text{Si}_3$  1058.51488; found 1058.51488. To a solution of the above compound (38 mg, 35.9  $\mu\text{mol}$ ) in pyridine (3.6 mL) in a PTFE tube, was added HF.pyr complex (70 wt% HF, 282  $\mu\text{L}$ ) at 0°C. Over the course of 4.5 h, three additional such portions of HF.pyr complex were added. Then, solid  $\text{NaHCO}_3$  was added to quench, and the mixture was stirred until cessation of effervescence. It was then filtered off and concentrated in vacuo. Column chromatography on neutral silica (DCM; 10:90 MeOH/DCM) gave the title compound as a red solid (20.3 mg, 28.9  $\mu\text{mol}$ , 81%).  $^1\text{H}$  NMR (500 MHz, chloroform- $d$  + MeOD)  $\delta$  8.02 (d,  $J$  = 7.6 Hz, 1H), 7.81 (t,  $J$  = 8.0 Hz, 1H), 7.42 (t,  $J$  = 7.3 Hz, 1H), 5.55 (d,  $J$  = 4.0 Hz, 1H), 5.28 (s, 1H), 5.05 (d,  $J$  = 3.9 Hz, 1H), 4.76 (d,  $J$  = 5.6 Hz, 2H), 4.41 (q,  $J$  = 6.6 Hz, 1H), 4.14 – 4.03 (m, 4H), 3.97 (q,  $J$  = 6.6 Hz, 1H), 3.83 (d,  $J$  = 6.5 Hz, 1H), 3.24 (dd,  $J$  = 18.9, 5.9 Hz, 1H), 3.02 (dd,  $J$  = 19.2, 6.3 Hz, 1H), 2.39 – 2.08 (m, 8H), 2.07 – 1.80 (m, 4H), 1.29 (d,  $J$  = 6.7 Hz, 3H), 1.21 (d,  $J$  = 6.6 Hz, 3H).  $^{13}\text{C}$  NMR (126 MHz,  $\text{CDCl}_3$  + MeOD)  $\delta$  213.6, 187.2, 186.8, 161.1, 155.9, 155.3, 135.9, 135.4, 133.8, 133.5, 120.8, 119.8, 118.6, 111.6, 111.4, 100.9, 99.2, 73.6, 71.0, 69.2, 68.6, 66.6, 65.4, 65.2, 61.7, 56.6, 43.0, 35.5, 33.8, 32.3, 28.7, 17.9, 16.6. HRMS:  $[\text{M} + \text{H}]^+$  calculated for  $\text{C}_{35}\text{H}_{44}\text{NO}_{14}$  702.27619; found 702.2769.

### 7-[2-Deoxy-3,4-tetraisopropylidisiloxy- $\alpha$ -L-fucopyranosyl-(1 $\rightarrow$ 4)-3-amino-2,3-dideoxy- $\alpha$ -L-fucopyranoside]-aklavinone (24)



Prepared according to General Procedure C from donor 21 (623 mg, 0.806 mmol) and aklavinone 14 (665 mg, 1.61 mmol, 2.00 equiv) at  $-20^{\circ}\text{C}$  to give after column chromatography (10:90 EtOAc/pentane and then 2:98 – 10:90 acetone/toluene) of the residue an inseparable mixture of the disaccharide anthracycline and acceptor, which was continued to the next step. A solution of the above mixture and *N,N*-dimethylbarbituric acid (562 mg, 3.60 mmol, 2.2 equiv) in DCM (81 mL) was degassed for 5 min. Then,  $\text{Pd}(\text{PPh}_3)_4$  (23 mg, 0.040 mmol, 0.025 equiv) was added and the mixture was allowed to stir for 30 min. It was then directly subjected to column chromatography (pentane, then 0:100 – 25:75 acetone/toluene) to give the title compound as a yellow solid (636 mg, 0.700 mmol, 86% over two steps).  $^1\text{H}$  NMR (400 MHz, chloroform-*d*)  $\delta$  7.76 (d, *J* = 7.5 Hz, 1H), 7.70 – 7.58 (m, 2H), 7.25 (d, *J* = 8.4 Hz, 1H), 5.47 (d, *J* = 2.8 Hz, 1H), 5.25 (dd, *J* = 4.1, 1.8 Hz, 1H), 4.97 (d, *J* = 3.6 Hz, 1H), 4.42 (ddd, *J* = 12.0, 4.7, 2.5 Hz, 1H), 4.19 – 4.05 (m, 3H), 4.00 (d, *J* = 2.6 Hz, 1H), 3.70 (s, 3H), 3.51 (d, *J* = 2.5 Hz, 1H), 3.24 (qt, *J* = 9.3, 6.6, 5.6 Hz, 1H), 2.52 (dd, *J* = 15.0, 4.3 Hz, 1H), 2.36 – 2.28 (m, 1H), 2.17 – 2.08 (m, 1H), 2.01 (dd, *J* = 12.3, 4.6 Hz, 1H), 1.86 – 1.68 (m, 3H), 1.49 (dd, *J* = 14.1, 7.0 Hz, 1H), 1.30 (d, *J* = 6.4 Hz, 3H), 1.23 (d, *J* = 6.5 Hz, 3H), 1.17 – 0.85 (m, 31H).  $^{13}\text{C}$  NMR (101 MHz,  $\text{CDCl}_3$ )  $\delta$  192.6, 181.2, 171.4, 162.5, 162.1, 142.7, 137.4, 133.4, 132.9, 131.2, 124.8, 120.9, 120.2, 115.7, 114.6, 101.7, 101.1, 81.7, 73.3, 71.6, 70.9, 70.2, 68.1, 67.8, 57.1, 52.6, 46.8, 33.9, 33.4, 32.2, 17.7, 17.6, 17.5, 17.4, 17.3, 17.3, 14.3, 14.1, 13.1, 12.6, 6.8. HRMS:  $[\text{M} + \text{H}]^+$  calculated for  $\text{C}_{46}\text{H}_{68}\text{NO}_{14}\text{Si}_2$  914.4178; found 914.4173.

#### 7-[2-Deoxy- $\alpha$ -L-fucopyranosyl-(1 $\rightarrow$ 4)-3-amino-2,3-dideoxy- $\alpha$ -L-fucopyranoside]-aklavinone (6)

To a solution of 24 (91 mg, 0.10 mmol) in pyridine (10 mL) in a PTFE tube, was added HF.pyr complex (70 wt% HF, 393  $\mu\text{L}$ ) at  $0^{\circ}\text{C}$ . Over the course of 4.5 h, three additional such portions of HF.pyr complex were added. Then, solid  $\text{NaHCO}_3$  was added to quench and the mixture was stirred until cessation of effervescence. It was then filtered off and partitioned between DCM and  $\text{H}_2\text{O}$ . The organic layer was washed with brine, dried over  $\text{Na}_2\text{SO}_4$  and concentrated in vacuo. Column chromatography on neutral silica (DCM; 20:80 MeOH/DCM) followed by size-exclusion chromatography (Sephadex LH-20; eluent DCM/MeOH, 1:1) gave the title compound as a yellow solid (27.5 mg, 40.9  $\mu\text{mol}$ , 41%).  $^1\text{H}$  NMR (400 MHz, chloroform-*d* + MeOD)  $\delta$  7.79 (dd, *J* = 7.5, 1.3 Hz, 1H), 7.74 – 7.57 (m, 2H), 7.32 – 7.23 (m, 1H), 5.47 (t, *J* = 2.5 Hz, 1H), 5.27 – 5.20 (m, 1H), 4.97 (d, *J* = 3.5 Hz, 1H), 4.20 – 4.01 (m, 4H), 3.70 (s, 3H), 3.64 (d, *J* = 3.0 Hz, 2H), 3.61 – 3.52 (m, 2H), 3.11 (dd, *J* = 10.6, 6.7 Hz, 1H), 2.53 (dd, *J* = 15.0, 4.4 Hz, 1H), 2.27 (d, *J* = 15.0 Hz, 1H), 1.97 (ddd, *J* = 22.5, 12.3, 4.2 Hz, 2H), 1.86 – 1.64 (m, 3H), 1.50 (dt, *J* = 14.6, 7.4 Hz, 1H), 1.28 (d, *J* = 6.4 Hz, 3H), 1.23 (d, *J* = 6.5 Hz, 3H), 1.07 (q, *J* = 7.4 Hz, 3H).  $^{13}\text{C}$  NMR (101 MHz,  $\text{CDCl}_3$ )  $\delta$  192.6, 181.4, 171.4, 162.5, 162.0, 142.6, 137.5, 133.5, 132.9, 131.1, 124.9, 121.0, 120.3, 115.8, 114.7, 101.3, 100.8, 81.1, 71.6, 70.9, 70.8, 68.0, 67.4, 65.4, 57.0, 52.6, 46.7, 34.1, 33.2, 32.7, 32.2, 17.3, 16.9, 6.7. HRMS:  $[\text{M} + \text{H}]^+$  calculated for  $\text{C}_{34}\text{H}_{42}\text{NO}_{13}$  672.2656; found 672.2645.

#### 7-[2-Deoxy- $\alpha$ -L-fucopyranosyl-(1 $\rightarrow$ 4)-3-dimethylamino-2,3-dideoxy- $\alpha$ -L-fucopyranoside]-aklavinone (8)

To a solution of 6 (26.2 mg, 37.4  $\mu\text{mol}$ ) in EtOH (3.7 mL) and 37% aq.  $\text{CH}_2\text{O}$  (200  $\mu\text{L}$ , 60 equiv) was added  $\text{NaBH}(\text{OAc})_3$  (85 mg, 0.374 mmol, 10 equiv). The mixture was stirred for 2.5 h before being poured into sat. aq.  $\text{NaHCO}_3$ . This was extracted with DCM, dried over  $\text{Na}_2\text{SO}_4$  and concentrated in vacuo. Column chromatography on

neutral silica (3:97 – 10:90 MeOH/DCM) gave the title compound as a yellow solid (8.8 mg, 12.6  $\mu$ mol, 34%).  $^1\text{H}$  NMR (500 MHz, chloroform-*d*)  $\delta$  12.69 (s, 1H), 12.04 (s, 1H), 7.83 (dd, *J* = 7.5, 1.2 Hz, 1H), 7.78 – 7.60 (m, 2H), 7.31 (dd, *J* = 8.4, 1.2 Hz, 1H), 5.51 (d, *J* = 3.7 Hz, 1H), 5.27 (dd, *J* = 4.3, 1.9 Hz, 1H), 5.01 (s, 1H), 4.53 (dd, *J* = 14.2, 7.7 Hz, 1H), 4.17 – 4.05 (m, 2H), 4.00 (q, *J* = 6.6 Hz, 1H), 3.74 (d, *J* = 8.5 Hz, 1H), 3.63 (d, *J* = 3.1 Hz, 1H), 2.52 (dd, *J* = 15.0, 4.3 Hz, 1H), 2.29 (dd, *J* = 16.9, 9.2 Hz, 1H), 2.25 – 2.11 (m, 6H), 2.07 (dt, *J* = 10.9, 5.4 Hz, 1H), 1.87 – 1.79 (m, 1H), 1.75 (dq, *J* = 14.6, 7.7, 7.3 Hz, 1H), 1.51 (dq, *J* = 14.3, 7.2 Hz, 1H), 1.28 (d, *J* = 6.5 Hz, 3H), 1.20 (d, *J* = 6.5 Hz, 3H), 1.09 (t, *J* = 7.4 Hz, 3H).  $^{13}\text{C}$  NMR (126 MHz,  $\text{CDCl}_3$ )  $\delta$  192.9, 181.5, 162.7, 162.3, 142.8, 137.5, 133.6, 133.1, 124.9, 121.1, 120.3, 116.0, 114.8, 101.7, 99.2, 71.8, 71.7, 70.8, 68.5, 66.3, 66.0, 61.7, 57.3, 52.7, 43.4, 33.9, 33.2, 32.3, 18.0, 16.8, 6.8. HRMS:  $[\text{M} + \text{H}]^+$  calculated for  $\text{C}_{36}\text{H}_{46}\text{NO}_{13}$  700.2969; found 700.2966.

### Synthesis of Trisaccharides 9 - 11

#### ***p*-Methoxyphenyl-2-deoxy-3-O-*p*-methoxybenzyl- $\alpha$ -L-fucopyranosyl-(1 $\rightarrow$ 4)-3-N-allyloxycarbonyl-2,3-dideoxy- $\alpha$ -L-fucopyranoside (27)**

To a solution of the glycosyl acceptor 17 (169 mg, 0.5 mmol, 1 equiv) and the glycosyl donor 25 (325 mg, 0.7 mmol, 1.4 equiv) in 4:1  $\text{Et}_2\text{O}$ /DCE (15 mL, v/v), activated molecular sieves (4 Å) were added. The mixture was stirred for 30 min and then, at 10°C, iodonium dicollidine perchlorate (937 mg, 2.00 mmol, 4 equiv) was added. After 30 min, triphenylphosphine (262 mg, 1.00 mmol, 2 equiv) was added, and the mixture was stirred for an additional hour. It was then diluted with EtOAc and filtered; washed with 10% aq.  $\text{Na}_2\text{S}_2\text{O}_3$ , 1M  $\text{CuSO}_4$  solution twice,  $\text{H}_2\text{O}$  and then dried over  $\text{MgSO}_4$ . Concentration in vacuo and column chromatography (15:85 – 20:80 EtOAc/pentane) of the residue gave the disaccharide. This was then dissolved in MeOH (8.8 mL) and DCM (8.8 mL), after which NaOMe was added to pH=10. After stirring for a week, it was neutralized by addition of dry ice and concentrated in vacuo. Column chromatography (20:80 – 50:50 EtOAc/pentane) gave the title compound as a clear oil (232 mg, 0.39 mmol, 78% over two steps).  $^1\text{H}$  NMR (400 MHz, chloroform-*d*)  $\delta$  7.28 (d, *J* = 6.7 Hz, 2H), 7.05 – 6.96 (m, 2H), 6.96 – 6.87 (m, 2H), 6.87 – 6.77 (m, 2H), 6.21 (d, *J* = 8.2 Hz, 1H), 5.92 (ddt, *J* = 16.4, 10.9, 5.5 Hz, 1H), 5.51 (d, *J* = 3.1 Hz, 1H), 5.37 – 5.25 (m, 1H), 5.20 (dt, *J* = 10.4, 1.4 Hz, 1H), 5.00 – 4.92 (m, 1H), 4.62 – 4.52 (m, 4H), 4.39 – 4.25 (m, 1H), 4.11 (q, *J* = 7.8, 7.1 Hz, 1H), 4.08 – 4.01 (m, 1H), 3.97 (td, *J* = 8.4, 3.1 Hz, 1H), 3.86 (s, 1H), 3.81 (s, 3H), 3.77 (s, 3H), 3.56 (s, 1H), 2.21 (s, 1H), 2.13 (dd, *J* = 12.6, 4.5 Hz, 1H), 2.08 – 2.00 (m, 2H), 1.86 (td, *J* = 12.7, 3.5 Hz, 1H), 1.38 (d, *J* = 6.6 Hz, 3H), 1.17 (d, *J* = 6.5 Hz, 3H).  $^{13}\text{C}$  NMR (101 MHz,  $\text{CDCl}_3$ )  $\delta$  159.6, 155.9, 154.7, 151.1, 133.0, 130.0, 129.5, 117.6, 117.5, 114.6, 114.1, 101.4, 96.4, 81.5, 72.7, 70.2, 68.2, 67.5, 67.2, 65.7, 55.8, 55.4, 46.6, 31.8, 30.3, 17.4, 16.8. HRMS:  $[\text{M} + \text{Na}]^+$  calculated for  $\text{C}_{31}\text{H}_{41}\text{NO}_{10}\text{Na}$  610.2628; found 610.2632.

#### ***p*-Methoxyphenyl-2,3-dideoxy-4-ulo- $\alpha$ -L-fucopyranosyl-(1 $\rightarrow$ 4)-2-deoxy-3-O-*p*-methoxybenzyl- $\alpha$ -L-fucopyranosyl-(1 $\rightarrow$ 4)-3-azido-2,3-dideoxy- $\alpha$ -L-fucopyranoside (29)**

To a solution of the glycosyl acceptor 27 (120 g, 2.04 mmol) and the glycosyl donor 28 (1.01 g, 2.86 mmol, 1.4 equiv) in 4:1  $\text{Et}_2\text{O}$ /DCE (62.5 mL, v/v), activated molecular sieves (4 Å) were added. The mixture was stirred for 30 min and then, at 10°C, iodonium dicollidine perchlorate (3.82 g, 8.16 mmol, 4 equiv) was added. After 35 min, triphenylphosphine (1.07 g, 4.08 mmol, 2.00 equiv) was added and the mixture



was stirred for an additional hour. It was then diluted with EtOAc and filtered, washed with 10% aq.  $\text{Na}_2\text{S}_2\text{O}_3$ , 1M  $\text{CuSO}_4$  solution twice,  $\text{H}_2\text{O}$  and then dried over  $\text{MgSO}_4$ . Concentration in vacuo and column chromatography (10:90 – 30:70 EtOAc/pentane) of the residue gave the trisaccharide benzoate as a thick clear oil (1.59 g, 1.97 mmol, 97%).  $^1\text{H}$  NMR (400 MHz, chloroform- $d$ )  $\delta$  8.12 – 8.05 (m, 2H), 7.61 – 7.54 (m, 1H), 7.51 – 7.37 (m, 2H), 7.28 (d,  $J$  = 2.2 Hz, 2H), 7.04 – 6.94 (m, 2H), 6.92 – 6.85 (m, 2H), 6.85 – 6.76 (m, 2H), 6.16 (d,  $J$  = 8.3 Hz, 1H), 5.92 (ddt,  $J$  = 16.3, 10.8, 5.6 Hz, 1H), 5.49 (d,  $J$  = 2.7 Hz, 1H), 5.34 – 5.16 (m, 2H), 5.04 (s, 1H), 5.03 – 4.94 (m, 2H), 4.72 – 4.50 (m, 5H), 4.40 – 4.25 (m, 1H), 4.17 – 4.01 (m, 2H), 3.99 – 3.88 (m, 2H), 3.79 (s, 3H), 3.77 (s, 3H), 3.56 (s, 1H), 2.29 – 2.15 (m, 2H), 2.14 – 1.98 (m, 3H), 1.94 (d,  $J$  = 14.0 Hz, 1H), 1.88 – 1.76 (m, 2H), 1.31 (d,  $J$  = 6.5 Hz, 3H), 1.16 (d,  $J$  = 6.5 Hz, 3H), 0.89 (d,  $J$  = 6.5 Hz, 3H).  $^{13}\text{C}$  NMR (101 MHz,  $\text{CDCl}_3$ )  $\delta$  166.3, 159.2, 155.9, 154.7, 151.1, 133.1, 130.6, 130.5, 129.8, 129.0, 128.5, 117.7, 117.6, 114.6, 113.9, 101.5, 98.7, 96.4, 81.1, 77.5, 77.4, 77.2, 76.8, 74.9, 72.7, 70.6, 70.3, 70.3, 68.8, 67.5, 65.7, 65.7, 65.7, 55.8, 55.4, 46.6, 31.8, 31.3, 24.5, 23.1, 17.5, 17.2. HRMS:  $[\text{M} + \text{Na}]^+$  calculated for  $\text{C}_{44}\text{H}_{55}\text{NO}_{13}\text{Na}$  828.3571; found 828.3586.

The above benzoate (1.20 g, 2.04 mmol) was dissolved in MeOH (40 mL) and DCM (40 mL), after which NaOMe was added to pH 10. After stirring for a week, it was neutralized by addition of dry ice and concentrated in vacuo. Column chromatography (50:50 – 75:25 EtOAc/pentane) gave the alcohol as a white foam (1.21 g, 1.72 mmol, 85%).  $^1\text{H}$  NMR (400 MHz, chloroform- $d$ )  $\delta$  7.32 – 7.19 (m, 2H), 7.05 – 6.95 (m, 2H), 6.93 – 6.85 (m, 2H), 6.85 – 6.75 (m, 2H), 6.15 (d,  $J$  = 8.3 Hz, 1H), 5.97 – 5.86 (m, 1H), 5.49 (d,  $J$  = 3.1 Hz, 1H), 5.30 (dq,  $J$  = 17.2, 1.6 Hz, 1H), 5.20 (dq,  $J$  = 10.6, 1.5 Hz, 1H), 4.99 (q,  $J$  = 1.5 Hz, 1H), 4.92 (d,  $J$  = 3.2 Hz, 1H), 4.70 – 4.46 (m, 4H), 4.43 – 4.34 (m, 1H), 4.31 (dt,  $J$  = 7.8, 4.3 Hz, 1H), 4.09 (q,  $J$  = 6.3 Hz, 1H), 4.01 (q,  $J$  = 6.6 Hz, 1H), 3.96 – 3.86 (m, 2H), 3.80 (s, 3H), 3.77 (s, 3H), 3.54 (s, 1H), 3.52 (s, 1H), 2.17 (td,  $J$  = 12.1, 3.7 Hz, 1H), 2.12 – 1.90 (m, 4H), 1.82 (td,  $J$  = 12.6, 3.5 Hz, 1H), 1.78 – 1.66 (m, 3H), 1.29 (d,  $J$  = 6.6 Hz, 3H), 1.14 (d,  $J$  = 6.5 Hz, 3H), 0.91 (d,  $J$  = 6.5 Hz, 3H).  $^{13}\text{C}$  NMR (101 MHz,  $\text{CDCl}_3$ )  $\delta$  159.2, 155.9, 154.6, 151.1, 133.0, 130.6, 129.0, 117.7, 117.5, 114.6, 113.8, 101.4, 98.7, 96.4, 81.0, 74.9, 72.7, 68.9, 67.6, 67.5, 66.6, 55.8, 55.4, 46.6, 31.8, 31.3, 25.8, 23.6, 17.5, 17.1. HRMS:  $[\text{M} + \text{Na}]^+$  calculated for  $\text{C}_{37}\text{H}_{51}\text{NO}_{12}\text{Na}$  724.3309; found 724.3322.

To a solution of the above alcohol (351 mg, 0.500 mmol) in DCM (20 mL) were added  $\text{NaHCO}_3$  (840 mg, 5.00 mmol, 10 equiv) and Dess-Martin periodinane (530 mg, 1.25 mmol, 2.5 equiv). After stirring for 1.5 h, 10% aq.  $\text{Na}_2\text{S}_2\text{O}_3$  (20 mL) was added and the mixture was stirred for a further 30 min. Then, it was washed with sat. aq.  $\text{NaHCO}_3$ , dried over  $\text{MgSO}_4$  and concentrated in vacuo. Size-exclusion chromatography (Sephadex LH-20; eluent 1:1 DCM/MeOH) gave the title compound as a white solid (341 mg, 0.487 mmol, 97%).  $^1\text{H}$  NMR (400 MHz, chloroform- $d$ )  $\delta$  7.32 – 7.20 (m, 2H), 7.06 – 6.99 (m, 2H), 6.92 – 6.85 (m, 2H), 6.85 – 6.76 (m, 2H), 6.16 (d,  $J$  = 8.2 Hz, 1H), 5.92 (ddd,  $J$  = 17.3, 10.6, 5.4 Hz, 1H), 5.50 (d,  $J$  = 3.1 Hz, 1H), 5.36 – 5.15 (m, 2H), 5.10 (t,  $J$  = 4.3 Hz, 1H), 5.00 (dd,  $J$  = 3.7, 1.7 Hz, 1H), 4.72 – 4.45 (m, 5H), 4.38 – 4.25 (m, 1H), 4.08 (dq,  $J$  = 13.3, 6.4 Hz, 2H), 4.03 – 3.88 (m, 2H), 3.79 (s, 3H), 3.76 (s, 3H), 3.56 (s, 1H), 2.60 (ddd,  $J$  = 15.0, 8.9, 5.7 Hz, 1H), 2.41 (ddd,  $J$  = 15.6, 7.6, 5.5 Hz, 1H), 2.30 (ddt,  $J$  = 14.1, 8.9, 5.2 Hz, 1H), 2.25 – 1.99 (m, 4H), 1.84 (td,  $J$  = 12.7, 3.5 Hz, 1H), 1.33 (d,  $J$  = 6.5 Hz, 3H), 1.15 (d,  $J$  = 6.4 Hz, 3H), 0.97 (d,  $J$  = 6.7 Hz, 3H).  $^{13}\text{C}$  NMR (101 MHz,  $\text{CDCl}_3$ )  $\delta$  210.7, 158.9, 155.4, 154.3, 150.7, 132.7, 130.0, 128.7, 117.3, 117.2, 114.2, 113.5, 101.1, 97.6, 96.0, 80.7, 74.7, 72.1, 71.5, 69.9, 68.2, 67.1, 65.3, 55.4, 55.0, 46.2, 33.6, 31.4, 30.7, 29.1, 17.1, 17.0, 14.5. HRMS:  $[\text{M} + \text{Na}]^+$  calculated for  $\text{C}_{37}\text{H}_{49}\text{NO}_{12}\text{Na}$  722.3153; found 722.3165.

**o-Cyclopropylethynylbenzoyl-2,3-dideoxy-4-ulo- $\alpha$ -L-fucopyranosyl-(1 $\rightarrow$ 4)-2-deoxy-3-O-*p*-methoxybenzyl- $\alpha$ -L-fucopyranosyl-(1 $\rightarrow$ 4)-3-azido-2,3-dideoxy-L-fucopyranoside (30)**

Prepared according to General Procedure A and B from 29 (1.06 g, 1.51 mmol) to give the title compound as a white foam (872 mg, 1.14 mmol, 75% over two steps,  $\alpha$ : $\beta$  1:7). Spectral data for the  $\beta$ -anomer:  $^1\text{H}$  NMR (400 MHz, chloroform-*d*)  $\delta$  7.94 (dd,  $J$  = 7.9, 1.4 Hz, 1H), 7.48 (dd,  $J$  = 7.9, 1.4 Hz, 1H), 7.42 (td,  $J$  = 7.5, 1.4 Hz, 1H), 7.37 – 7.16 (m, 3H), 6.93 – 6.79 (m, 2H), 6.36 (d,  $J$  = 8.0 Hz, 1H), 5.98 (dd,  $J$  = 10.0, 2.2 Hz, 1H), 5.90 (ddd,  $J$  = 16.3, 10.7, 5.4 Hz, 1H), 5.37 – 5.15 (m, 2H), 5.10 (t,  $J$  = 4.4 Hz, 1H), 5.03 – 4.97 (m, 1H), 4.75 – 4.45 (m, 5H), 4.08 (q,  $J$  = 6.6 Hz, 1H), 4.03 – 3.95 (m, 2H), 3.90 (ddt,  $J$  = 12.4, 7.4, 4.1 Hz, 1H), 3.85 – 3.78 (m, 2H), 3.76 (s, 3H), 3.49 (s, 1H), 2.60 (ddd,  $J$  = 15.0, 8.8, 5.7 Hz, 1H), 2.42 (ddd,  $J$  = 15.7, 7.7, 5.4 Hz, 1H), 2.31 (ddt,  $J$  = 13.9, 8.8, 5.2 Hz, 1H), 2.24 – 2.15 (m, 2H), 2.10 (tt,  $J$  = 10.4, 5.5 Hz, 2H), 1.81 (td,  $J$  = 12.3, 9.9 Hz, 1H), 1.50 (tt,  $J$  = 7.8, 5.4 Hz, 1H), 1.36 – 1.27 (m, 6H), 0.97 (d,  $J$  = 6.7 Hz, 3H), 0.87 (dd,  $J$  = 7.6, 5.3 Hz, 3H).  $^{13}\text{C}$  NMR (101 MHz,  $\text{CDCl}_3$ )  $\delta$  211.1, 164.3, 159.3, 155.8, 134.3, 132.9, 132.0, 130.3, 129.1, 127.0, 125.2, 117.7, 113.9, 101.8, 99.8, 98.0, 93.2, 80.3, 75.1, 74.5, 72.9, 72.4, 71.9, 70.3, 68.7, 65.7, 55.4, 50.0, 34.0, 32.2, 31.1, 29.5, 17.4, 14.8, 9.0, 0.8. HRMS:  $[\text{M} + \text{Na}]^+$  calculated for  $\text{C}_{42}\text{H}_{51}\text{NO}_{12}\text{Na}$  784.3309; found 784.3322.

**7-[2,3-Dideoxy-4-ulo- $\alpha$ -L-fucopyranosyl-2-deoxy-3-*p*-methoxybenzyl- $\alpha$ -L-fucopyranosyl-(1 $\rightarrow$ 4)-3-amino-2,3-dideoxy- $\alpha$ -L-fucopyranoside]-14-O-*tert*-butyldimethylsilyl-doxorubicinone (31)**

Prepared according to General Procedure C from donor 30 (422 mg, 0.552 mmol) and doxorubicinone acceptor 16 [35] (1.5 equiv) to give after column chromatography (20:80 – 100:0 EtOAc/pentane) the crude anthracycline trisaccharide. To a solution of the above trisaccharide in DCM (93 mL) and phosphate buffer (9.3 mL, pH=7) was added DDQ (1.25 g, 5.52 mmol, 10 equiv) at 0°C after which the mixture was stirred at that temperature for 45 min. It was then stirred at room temperature for an additional 2.5 h, after which it was diluted with DCM and washed with  $\text{H}_2\text{O}$  four times. The organic layer was then dried over  $\text{Na}_2\text{SO}_4$  and concentrated in *vacuo*. Column chromatography (5:95 – 12:88 acetone/toluene) gave the free 3''-hydroxyl anthracycline trisaccharide as a red solid (310 mg, 0.315 mmol, 57% over two steps).  $^1\text{H}$  NMR (400 MHz, chloroform-*d*)  $\delta$  13.93 (s, 1H), 13.24 (s, 1H), 8.03 (dd,  $J$  = 7.8, 1.0 Hz, 1H), 7.78 (t,  $J$  = 8.1 Hz, 1H), 7.39 (dd,  $J$  = 8.6, 1.1 Hz, 1H), 6.02 (d,  $J$  = 7.9 Hz, 1H), 5.84 (ddt,  $J$  = 16.2, 10.8, 5.5 Hz, 1H), 5.51 (d,  $J$  = 3.7 Hz, 1H), 5.26 (td,  $J$  = 3.4, 1.7 Hz, 1H), 5.23 – 5.05 (m, 2H), 4.99 – 4.93 (m, 1H), 4.90 (d,  $J$  = 2.8 Hz, 2H), 4.58 – 4.41 (m, 4H), 4.19 – 4.10 (m, 3H), 4.09 (s, 3H), 3.93 – 3.82 (m, 1H), 3.78 – 3.70 (m, 2H), 3.58 (s, 1H), 3.20 (dd,  $J$  = 18.7, 1.8 Hz, 1H), 2.97 (d,  $J$  = 18.9 Hz, 1H), 2.55 – 2.39 (m, 3H), 2.29 (d,  $J$  = 14.8 Hz, 1H), 2.24 – 2.02 (m, 4H), 1.92 (ddd,  $J$  = 14.0, 10.0, 3.8 Hz, 2H), 1.83 – 1.72 (m, 1H), 1.37 – 1.22 (m, 10H), 0.96 (s, 9H), 0.14 (d,  $J$  = 2.2 Hz, 6H).  $^{13}\text{C}$  NMR (101 MHz,  $\text{CDCl}_3$ )  $\delta$  211.5, 209.9, 187.2, 186.8, 161.1, 156.5, 156.0, 155.6, 135.8, 135.6, 134.2, 134.0, 133.0, 121.0, 119.9, 118.5, 117.6, 111.6, 111.4, 101.6, 100.9, 100.3, 82.2, 81.1, 72.0, 69.8, 67.9, 66.8, 65.6, 65.0, 56.8, 46.6, 35.8, 34.4, 34.2, 33.5, 31.4, 27.6, 26.0, 18.7, 17.5, 16.9, 14.9. HRMS:  $[\text{M} + \text{Na}]^+$  calculated for  $\text{C}_{49}\text{H}_{65}\text{NO}_{18}\text{SiNa}$  1006.3869; found 1006.3876.

**7-[2,3-Dideoxy-4-ulo- $\alpha$ -L-fucopyranosyl-2-deoxy- $\alpha$ -L-fucopyranosyl-(1 $\rightarrow$ 4)-3-amino-2,3-dideoxy- $\alpha$ -L-fucopyranoside]-doxorubicinone (9)**

A solution of 31 (159 mg, 0.162 mmol) and *N,N*-dimethylbarbituric acid (115 mg,

0.729 mmol, 4.5 equiv) in DCM (16.3 mL) was degassed for 5 min. Then, Pd(PPh<sub>3</sub>)<sub>4</sub> (9.0 mg, 81 μmol, 0.05 equiv) was added and the mixture was allowed to stir for 20 min. It was then directly subjected to column chromatography on neutral silica (0:100 – 3:97 MeOH/DCM) to give the free amine as a red solid (118 mg, 0.131 mmol, 81%). <sup>1</sup>H NMR (500 MHz, chloroform-*d*) δ 13.90 (s, 1H), 7.97 (dd, *J* = 7.7, 1.1 Hz, 1H), 7.75 (t, *J* = 8.1 Hz, 1H), 7.38 (dd, *J* = 8.7, 1.1 Hz, 1H), 5.48 (d, *J* = 3.7 Hz, 1H), 5.23 (dd, *J* = 4.1, 2.2 Hz, 1H), 5.10 (t, *J* = 6.1 Hz, 1H), 5.01 (d, *J* = 3.6 Hz, 1H), 4.94 – 4.81 (m, 2H), 4.50 (q, *J* = 6.7 Hz, 1H), 4.25 (q, *J* = 6.6 Hz, 1H), 4.13 (ddd, *J* = 12.2, 4.7, 2.7 Hz, 1H), 4.08 (s, 3H), 4.03 (q, *J* = 6.4 Hz, 1H), 3.73 (s, 1H), 3.52 (d, *J* = 2.5 Hz, 1H), 3.13 (dd, *J* = 18.8, 1.9 Hz, 1H), 3.00 (ddd, *J* = 12.4, 4.7, 2.4 Hz, 1H), 2.89 (d, *J* = 18.7 Hz, 1H), 2.56 – 2.38 (m, 3H), 2.30 (dt, *J* = 14.8, 2.1 Hz, 1H), 2.23 – 2.00 (m, 3H), 1.89 (td, *J* = 12.4, 3.8 Hz, 1H), 1.75 (td, *J* = 12.9, 3.9 Hz, 1H), 1.68 (dd, *J* = 13.1, 4.5 Hz, 1H), 1.33 (d, *J* = 6.8 Hz, 3H), 1.28 (d, *J* = 6.5 Hz, 3H), 1.22 (d, *J* = 6.5 Hz, 3H), 0.96 (s, 9H), 0.14 (d, *J* = 1.2 Hz, 6H). <sup>13</sup>C NMR (126 MHz, CDCl<sub>3</sub>) δ 211.2, 210.0, 186.9, 186.6, 161.1, 156.4, 155.8, 135.7, 135.5, 134.1, 120.8, 119.8, 118.5, 111.4, 101.4, 100.8, 100.2, 82.3, 81.7, 71.9, 69.6, 68.4, 67.4, 66.6, 65.2, 56.7, 46.8, 35.6, 34.4, 33.9, 33.5, 27.7, 26.0, 18.7, 17.7, 17.2, 14.8. HRMS: [M + H]<sup>+</sup> calculated for C<sub>45</sub>H<sub>62</sub>NO<sub>16</sub>Si 900.3838; found 900.3836. To a solution of the above compound (19.7 mg, 21.9 μmol) in pyridine (0.7 mL) and THF (1.4 mL) in a PTFE tube was added HF.pyr complex (70 wt% HF, 86 μL) at 0°C. After 3 h, an additional such portion of HF.pyr complex was added. After stirring one more hour, solid NaHCO<sub>3</sub> was added to quench, and the mixture was stirred until cessation of effervescence. It was then filtered off, and the filtrate was poured into DCM/H<sub>2</sub>O. The organic layer was dried over Na<sub>2</sub>SO<sub>4</sub> and concentrated in vacuo. Column chromatography on neutral silica (DCM; 4:96 MeOH/DCM) gave the title compound as a red solid (12.7 mg, 16.2 μmol, 74%). <sup>1</sup>H NMR (500 MHz, chloroform-*d*) δ 13.94 (s, 1H), 8.13 – 7.89 (m, 1H), 7.78 (t, *J* = 8.1 Hz, 1H), 7.52 – 7.31 (m, 1H), 5.51 (d, *J* = 3.8 Hz, 1H), 5.36 – 5.27 (m, 1H), 5.09 (t, *J* = 6.1 Hz, 1H), 5.01 (d, *J* = 3.7 Hz, 1H), 4.81 – 4.68 (m, 2H), 4.49 (q, *J* = 6.6 Hz, 1H), 4.23 (q, *J* = 6.4 Hz, 1H), 4.16 – 4.05 (m, 4H), 4.01 (q, *J* = 6.5 Hz, 1H), 3.72 (s, 1H), 3.52 (s, 1H), 3.25 (dd, *J* = 18.9, 2.0 Hz, 1H), 3.08 – 2.96 (m, 2H), 2.46 (dt, *J* = 17.8, 10.3, 5.8 Hz, 4H), 2.32 (dt, *J* = 14.5, 2.1 Hz, 1H), 2.25 (t, *J* = 7.6 Hz, 1H), 2.22 – 2.05 (m, 4H), 1.89 (td, *J* = 12.3, 3.7 Hz, 1H), 1.76 (td, *J* = 12.9, 3.9 Hz, 1H), 1.70 (d, *J* = 4.5 Hz, 1H), 1.33 (d, *J* = 6.5 Hz, 3H), 1.28 (d, *J* = 6.4 Hz, 3H), 1.22 (d, *J* = 6.7 Hz, 3H). <sup>13</sup>C NMR (126 MHz, CDCl<sub>3</sub>) δ 213.9, 210.0, 187.2, 186.8, 161.2, 156.4, 155.8, 135.9, 135.6, 134.0, 133.7, 121.0, 120.0, 118.6, 111.7, 111.5, 101.3, 100.9, 100.3, 82.4, 81.7, 72.0, 69.2, 68.5, 67.5, 65.6, 65.3, 56.8, 46.8, 35.6, 34.5, 34.1, 33.6, 27.7, 17.8, 17.2, 14.9. HRMS: [M + H]<sup>+</sup> calculated for C<sub>39</sub>H<sub>48</sub>NO<sub>16</sub>: 786.2973; found 786.2982.

#### 7-[2,3-Dideoxy-4-ulo-α-L-fucopyranosyl-2-deoxy-α-L-fucopyranosyl-(1→4)-3-dimethylamino-2,3-dideoxy-α-L-fucopyranoside]-doxorubicinone (11)

A solution of 31 (159 mg, 0.162 mmol) and *N,N*-dimethylbarbituric acid (115 mg, 0.729 mmol, 4.5 equiv) in DCM (16.3 mL) was degassed for 5 min. Then, Pd(PPh<sub>3</sub>)<sub>4</sub> (9.0 mg, 81 μmol, 0.05 equiv) was added and the mixture was allowed to stir for 20 min. It was then directly subjected to column chromatography on neutral silica (0:100 – 3:97 MeOH/DCM) to give the free amine as a red solid (118 mg, 0.131 mmol, 81%). To a solution of the above amine (48.0 mg, 53.3 μmol) in EtOH (10.8 mL) and 37% aq. CH<sub>2</sub>O (132 μL, 30 equiv) was added NaBH(OAc)<sub>3</sub> (21.5 mg, 0.101 mmol, 1.9 equiv). The mixture was stirred for 1.5 h before being poured into sat. aq. NaHCO<sub>3</sub>. This was repetitively extracted with DCM, dried over Na<sub>2</sub>SO<sub>4</sub> and concentrated in

vacuo. Column chromatography on neutral silica (10:90 – 40:60 acetone/toluene) followed by size-exclusion chromatography (Sephadex LH-20, 1:1 DCM:MeOH v/v) gave the dimethylamine as a red solid (25.8 mg, 27.8  $\mu$ mol, 52%).  $^1\text{H}$  NMR (500 MHz, chloroform-*d*)  $\delta$  13.93 (s, 1H), 13.24 (s, 1H), 8.01 (dt, *J* = 7.7, 1.5 Hz, 1H), 7.83 – 7.70 (m, 1H), 7.45 – 7.36 (m, 1H), 5.53 (d, *J* = 3.8 Hz, 1H), 5.26 (dd, *J* = 4.1, 2.1 Hz, 1H), 5.10 – 5.06 (m, 1H), 5.03 (d, *J* = 3.4 Hz, 1H), 4.97 – 4.82 (m, 2H), 4.77 (s, 1H), 4.55 (q, *J* = 6.4 Hz, 1H), 4.50 (q, *J* = 6.7 Hz, 1H), 4.09 (d, *J* = 3.3 Hz, 4H), 3.92 (q, *J* = 6.6 Hz, 1H), 3.75 (s, 1H), 3.72 – 3.58 (m, 2H), 3.18 (dd, *J* = 18.9, 2.0 Hz, 1H), 2.98 (d, *J* = 18.8 Hz, 1H), 2.53 – 2.38 (m, 3H), 2.32 (dt, *J* = 14.6, 2.2 Hz, 1H), 2.26 – 2.01 (m, 10H), 1.94 – 1.73 (m, 4H), 1.33 (d, *J* = 6.8 Hz, 3H), 1.31 – 1.20 (m, 7H), 1.17 (d, *J* = 6.4 Hz, 3H), 0.96 (s, 9H), 0.14 (d, *J* = 2.8 Hz, 6H).  $^{13}\text{C}$  NMR (126 MHz,  $\text{CDCl}_3$ )  $\delta$  211.4, 210.3, 187.1, 186.7, 161.1, 156.6, 155.9, 135.8, 135.6, 134.3, 134.1, 124.9, 121.0, 119.9, 118.5, 111.5, 111.4, 101.5, 100.3, 99.6, 83.1, 74.1, 71.9, 69.7, 68.6, 66.7, 65.4, 61.7, 56.8, 43.4, 35.6, 34.4, 34.0, 33.6, 30.4, 29.8, 27.7, 26.0, 18.1, 17.1, 14.9. HRMS:  $[\text{M} + \text{H}]^+$  calculated for  $\text{C}_{47}\text{H}_{66}\text{NO}_{16}\text{Si}$ : 928.4151; found 928.4157. To a solution of the above compound (20.6 mg, 22.2  $\mu$ mol) in pyridine (1.4 mL) and THF (1.4 mL) in a PTFE tube, was added HF.pyr complex (70 wt% HF, 87  $\mu$ L) at 0°C. Four more additional such amounts of HF.pyr complex were added over the course of 4.5 h. Then, solid  $\text{NaHCO}_3$  was added to quench, and the mixture was stirred until cessation of effervescence. It was then filtered off, and the filtrate was poured into DCM/ $\text{H}_2\text{O}$ . The organic layer was dried over  $\text{Na}_2\text{SO}_4$  and concentrated in vacuo. Column chromatography on neutral silica (DCM; 10:90 MeOH/DCM) gave the title compound as a red solid (13.3 mg, 16.3  $\mu$ mol, 73%).  $^1\text{H}$  NMR (500 MHz, chloroform-*d*)  $\delta$  13.95 (s, 1H), 13.26 (s, 1H), 8.03 (dd, *J* = 7.7, 1.0 Hz, 1H), 7.79 (dd, *J* = 8.5, 7.7 Hz, 1H), 7.40 (dd, *J* = 8.7, 1.1 Hz, 1H), 5.55 (d, *J* = 3.8 Hz, 1H), 5.32 – 5.28 (m, 1H), 5.08 (dd, *J* = 7.0, 5.6 Hz, 1H), 5.03 (s, 1H), 4.92 (s, 1H), 4.76 (d, *J* = 1.0 Hz, 2H), 4.54 (d, *J* = 6.6 Hz, 1H), 4.49 (q, *J* = 6.7 Hz, 1H), 4.16 – 4.03 (m, 4H), 3.91 (q, *J* = 6.5 Hz, 1H), 3.76 (s, 1H), 3.71 – 3.60 (m, 2H), 3.26 (dd, *J* = 18.8, 2.0 Hz, 1H), 3.03 (d, *J* = 18.8 Hz, 1H), 2.54 – 2.40 (m, 3H), 2.34 (dt, *J* = 14.6, 2.2 Hz, 1H), 2.24 – 2.12 (m, 7H), 2.10 (dd, *J* = 12.1, 4.6 Hz, 1H), 2.03 (d, *J* = 15.0 Hz, 1H), 1.83 (td, *J* = 12.2, 3.8 Hz, 3H), 1.33 (d, *J* = 6.7 Hz, 3H), 1.27 (d, *J* = 6.6 Hz, 3H), 1.17 (d, *J* = 6.4 Hz, 3H).  $^{13}\text{C}$  NMR (126 MHz,  $\text{CDCl}_3$ )  $\delta$  213.9, 210.3, 187.3, 186.9, 161.2, 156.5, 155.9, 135.9, 135.6, 134.2, 133.7, 121.1, 119.9, 118.5, 111.7, 111.5, 101.4, 100.3, 99.6, 83.1, 74.1, 71.9, 69.3, 68.8, 66.9, 65.6, 65.4, 61.8, 56.8, 43.5, 35.6, 34.4, 34.1, 33.7, 27.8, 18.2, 17.1, 14.9. HRMS:  $[\text{M} + \text{H}]^+$  calculated for  $\text{C}_{41}\text{H}_{52}\text{NO}_{16}$ : 814.3286; found 814.3301.

**7-[2,3-Dideoxy-4-ulo- $\alpha$ -L-fucopyranosyl-2-deoxy-3-O-*p*-methoxybenzyl- $\alpha$ -L-fucopyranosyl-(1 $\rightarrow$ 4)-3-*N*-allyloxycarbonyl-2,3-dideoxy- $\alpha$ -L-fucopyranoside]-aklavinone (32)**

Prepared according to General Procedure C from donor 30 (211 mg, 0.276 mmol) and aklavinone 14 [34] (2 equiv) at -20°C to give after column chromatography (10:90 EtOA/pentane and then 2:98 – 20:80 acetone/toluene) the title compound as a yellow solid (210 mg, 0.213 mmol, 77%).  $^1\text{H}$  NMR (400 MHz, chloroform-*d*)  $\delta$  12.66 (s, 1H), 12.01 (s, 1H), 7.82 (dd, *J* = 7.5, 1.1 Hz, 1H), 7.72 – 7.61 (m, 2H), 7.34 – 7.21 (m, 2H), 6.93 – 6.82 (m, 2H), 6.07 (d, *J* = 7.8 Hz, 1H), 5.83 (ddt, *J* = 16.0, 10.8, 5.6 Hz, 1H), 5.46 (d, *J* = 3.8 Hz, 1H), 5.30 – 5.06 (m, 4H), 4.98 (s, 1H), 4.71 – 4.62 (m, 1H), 4.62 – 4.49 (m, 2H), 4.46 (ddt, *J* = 6.9, 5.5, 1.5 Hz, 2H), 4.22 (s, 2H), 4.12 (s, 1H), 4.09 – 3.90 (m, 3H), 3.87 (d, *J* = 7.1 Hz, 1H), 3.82 (s, 3H), 3.70 (s, 3H), 3.55 (s, 1H), 2.66 – 2.47 (m, 2H), 2.42 (ddd, *J* = 15.7, 7.6, 5.5 Hz, 1H), 2.36 – 2.25 (m, 2H), 2.25 – 2.04 (m, 3H), 2.00 (dd, *J* = 12.9, 4.5 Hz, 1H), 1.74 (dq, *J* = 13.5, 6.0, 4.3

Hz, 2H), 1.50 (dq,  $J = 14.6, 7.1$  Hz, 1H), 1.30 (d,  $J = 6.6$  Hz, 3H), 1.28 – 1.24 (m, 3H), 1.08 (t,  $J = 7.3$  Hz, 3H), 0.98 (d,  $J = 6.7$  Hz, 3H).  $^{13}\text{C}$  NMR (101 MHz,  $\text{CDCl}_3$ )  $\delta$  211.1, 192.8, 181.4, 171.5, 162.6, 162.2, 159.3, 155.5, 142.7, 137.4, 133.5, 133.0, 133.0, 131.1, 130.3, 129.1, 124.8, 121.0, 120.3, 117.5, 115.8, 114.8, 113.9, 101.6, 101.5, 98.0, 80.9, 75.0, 72.5, 71.8, 71.4, 70.3, 68.5, 67.7, 65.5, 57.1, 55.4, 52.6, 46.5, 34.0, 32.2, 31.6, 31.1, 29.5, 17.4, 17.3, 14.8, 6.8. HRMS:  $[\text{M} + \text{Na}]^+$  calculated for  $\text{C}_{52}\text{H}_{61}\text{NO}_{18}\text{Na}$  1010.3786; found 1010.3796.

### 3',3'-didesmethyl-aclarubicin (10)

To a biphasic mixture of 32 (210 mg, 0.213 mmol) in DCM (36 mL) and phosphate buffer (3.6 mL, pH=7) was added DDQ (484 mg, 2.13 mmol, 10 equiv) at 0°C after which the mixture was stirred at that temperature for 90 min. It was diluted with DCM, and washed with  $\text{H}_2\text{O}$  four times, after which the organic layer was dried over  $\text{Na}_2\text{SO}_4$  and concentrated in vacuo. Column chromatography (5:95–10:90 acetone/toluene) gave the intermediate free 3"-hydroxyl as a yellow solid (155 mg, 0.179 mmol, 84%).  $^1\text{H}$  NMR (400 MHz, chloroform- $d$ )  $\delta$  12.65 (s, 1H), 12.00 (s, 1H), 7.81 (dd,  $J = 7.5, 1.2$  Hz, 1H), 7.75 – 7.60 (m, 2H), 7.32 – 7.25 (m, 1H), 6.05 (d,  $J = 7.8$  Hz, 1H), 5.83 (ddt,  $J = 16.3, 10.7, 5.5$  Hz, 1H), 5.46 (d,  $J = 3.8$  Hz, 1H), 5.27 – 5.06 (m, 4H), 4.95 (d,  $J = 3.5$  Hz, 1H), 4.53 – 4.38 (m, 3H), 4.28 – 4.18 (m, 2H), 4.18 – 4.06 (m, 3H), 3.86 (dd,  $J = 12.2, 6.5$  Hz, 1H), 3.81 – 3.72 (m, 2H), 3.70 (s, 3H), 3.55 (s, 1H), 2.59 – 2.38 (m, 4H), 2.31 (d,  $J = 15.0$  Hz, 1H), 2.24 – 2.06 (m, 2H), 2.01 (dd,  $J = 12.9, 4.6$  Hz, 1H), 1.92 (td,  $J = 12.4, 3.8$  Hz, 1H), 1.83 – 1.68 (m, 2H), 1.49 (dq,  $J = 14.7, 7.2$  Hz, 1H), 1.36 – 1.24 (m, 9H), 1.08 (t,  $J = 7.2$  Hz, 3H).  $^{13}\text{C}$  NMR (101 MHz,  $\text{CDCl}_3$ )  $\delta$  209.9, 192.8, 181.4, 171.5, 162.6, 162.2, 155.5, 142.7, 137.4, 133.6, 133.0, 133.0, 131.1, 124.8, 121.0, 120.3, 117.5, 115.9, 114.8, 101.6, 101.6, 100.3, 82.1, 81.2, 71.9, 71.5, 71.4, 67.9, 67.7, 65.5, 65.0, 57.1, 52.6, 46.6, 34.4, 34.0, 33.5, 32.2, 31.6, 27.6, 17.3, 16.9, 14.8, 6.8. HRMS:  $[\text{M} + \text{Na}]^+$  calculated for  $\text{C}_{44}\text{H}_{53}\text{NO}_{17}\text{Na}$  890.3211; found 890.3220. A solution of the above compound (155 mg, 0.179 mmol) and *N,N*-dimethylbarbituric acid (125 mg, 0.806 mmol, 4.5 equiv) in DCM (18 mL) was degassed for 5 min. Then,  $\text{Pd}(\text{PPh}_3)_4$  (10.0 mg, 0.0090 mmol, 0.05 equiv) was added and the mixture was allowed to stir for 15 min. It was then directly subjected to column chromatography on neutral silica (0:100 – 3:97 MeOH/DCM), followed by size-exclusion chromatography (Sephadex LH-20; eluent, 1:1 DCM/MeOH) twice and finally column chromatography on neutral silica (3:97 MeOH/DCM) to give the title compound as a yellow solid (86 mg, 0.11 mmol, 61%).  $^1\text{H}$  NMR (500 MHz, chloroform- $d$  + MeOD)  $\delta$  7.81 (dt,  $J = 7.4, 2.0$  Hz, 1H), 7.74 – 7.62 (m, 2H), 7.30 (d,  $J = 1.2$  Hz, 1H), 5.47 (t,  $J = 2.5$  Hz, 1H), 5.26 (dd,  $J = 4.4, 1.8$  Hz, 1H), 5.10 (t,  $J = 6.2$  Hz, 1H), 4.99 (d,  $J = 3.6$  Hz, 1H), 4.52 (q,  $J = 6.7$  Hz, 1H), 4.19 (q,  $J = 6.7$  Hz, 1H), 4.17 – 4.04 (m, 3H), 3.74 (s, 1H), 3.70 (s, 3H), 3.50 (d,  $J = 2.4$  Hz, 1H), 2.99 (ddd,  $J = 10.9, 6.3, 2.4$  Hz, 1H), 2.56 – 2.37 (m, 4H), 2.30 (dt,  $J = 14.9, 1.8$  Hz, 2H), 2.21 – 2.12 (m, 1H), 2.09 (dd,  $J = 12.4, 4.6$  Hz, 1H), 1.91 (td,  $J = 12.4, 3.8$  Hz, 1H), 1.75 (ddd,  $J = 14.1, 9.4, 5.7$  Hz, 3H), 1.50 (dp,  $J = 13.8, 7.0$  Hz, 1H), 1.32 (d,  $J = 6.8$  Hz, 3H), 1.29 (d,  $J = 6.4$  Hz, 3H), 1.23 (d,  $J = 6.5$  Hz, 3H), 1.08 (t,  $J = 7.3$  Hz, 3H).  $^{13}\text{C}$  NMR (126 MHz,  $\text{CDCl}_3$  + MeOD)  $\delta$  210.3, 192.7, 181.4, 171.4, 162.4, 162.0, 142.6, 137.4, 133.5, 133.0, 131.2, 124.8, 120.9, 120.2, 115.8, 114.7, 101.6, 100.9, 100.0, 81.9, 81.8, 71.9, 71.6, 70.9, 68.1, 67.5, 65.1, 57.1, 52.6, 46.6, 34.2, 34.2, 33.8, 33.5, 32.1, 27.6, 17.4, 17.0, 14.7, 6.6. HRMS:  $[\text{M} + \text{H}]^+$  calculated for  $\text{C}_{40}\text{H}_{50}\text{NO}_{15}$  784.3181; found 784.3196.



**Cell culture**

K562 cells (B. Pang, Stanford University, USA), HCT116 cells (T. van Hall, LUMC, The Netherlands), and PC3 and DU145 cells (C. Robson, Newcastle University, U.K.) were maintained in Roswell park Memorial Institute (RPMI)-1640 medium supplemented with 8% fetal bovine serum (FCS). Wild-type MeJuSo cells were maintained in Iscove's Modified Dulbecco's medium (IMDM) supplemented with 8% FCS. MeJuSo cells stably expressing PAGFP-H2A were maintained in IMDM supplemented with 8% FCS and G-418, as described.[17] U87 cells (ATCC® HTB-14) were maintained in Dulbecco's Modified Eagle's medium (DMEM) supplemented with 8% FCS. Cell lines were maintained in a humidified atmosphere of 5% CO<sub>2</sub> at 37°C and regularly tested for the absence of mycoplasma.

**Western blot and constant-field gel electrophoresis (CFGE)**

Cells were treated with drugs at indicated doses for 2 h. These concentrations and treatment times correspond to physiological serum peak concentrations in cancer patients under standard treatment [17,50]. Subsequently, drugs were removed by extensive washing and cells were collected at indicated time points after drug removal and processed immediately for the assay. Cells were lysed directly in sodium dodecyl sulfate (SDS) sample buffer (2% SDS, 10% glycerol, 5% β-mercaptoethanol, 60 mM Tris-HCl pH 6.8, and 0.01% bromophenol blue). Lysates were resolved by SDS-polyacrylamide gel electrophoresis (PAGE) followed by Western blotting. Primary antibodies used for blotting were γH2AX (1:1000, 05-036, Millipore) and β-actin (1:10000, A5441, Sigma). DNA double-strand breaks were visualized by constant-field gel electrophoresis, as described [51]. Images were quantified with ImageJ.

**Microscopy**

PAGFP-H2A photoactivation and time-lapse confocal imaging were performed as described [17] on a Leica SP8 confocal microscope system, 63x lens, equipped with a climate chamber. Loss of fluorescence after different treatments was quantified using ImageJ software. For Topollα live cell imaging, MeJuSo cells were transiently transfected with a construct encoding Topollα-GFP [17]. Fractional distance calculations for the Topollα relocalization were done using LAS X software (Leica).

**Cell viability assay**

Cells were seeded into 96-well plates. Twenty-four hours after seeding, the cells were treated with indicated drugs for 2 h. Subsequently, drugs were removed and cells were left to grow for an additional 72 h. Cell viability was measured using the CellTiter-Blue viability assay (Promega). Relative survival was normalized to the untreated control and corrected for background signal.

**Flow cytometry for measuring drug uptake in cells**

Cells were treated with 1 μM of the indicated drugs for 2 h. The samples were washed, collected, and fixed with paraformaldehyde. Samples were analyzed by flow cytometry using a BD FACS Aria II, with a 561 nm laser and a 610/20 nm detector.

**AUTHOR CONTRIBUTIONS**

D.P.A.W. and S.Y.v.d.Z. contributed equally to this work. D.P.A.W., S.Y.v.d.Z., H.S.O., J.N., and J.D.C.C. conceived the experiments. D.P.A.W. under supervision of H.S.O., G.A.v.d.M. and J.D.C.C. performed the synthesis. S.Y.v.d.Z. under supervision of

J.N. performed all biochemical and cellular experiments. The manuscript was written by D.P.A.W. and S.Y.v.d.Z. with input of all authors.

## FUNDING SOURCES

This work was supported by grants from the Dutch Cancer Society KWF (JN) and by the Institute for Chemical Immunology, an NWO Gravitation project funded by the Ministry of Education, Culture and Science of the Netherlands to HO and JN.

## NOTES

JN is a shareholder in NIHM that aims to produce aclarubicin for clinical use.

## REFERENCES

- 1 Arcamone F, Franceschi G, Penco S & Selva A (1969) Adriamycin (14-hydroxydaunomycin), a novel antitumor antibiotic. *Tetrahedron Lett* 10, 1007–1010.
- 2 Röthig HJ, Kraemer HP & Sedlacek HH (1985) Aclarubicin: experimental and clinical experience. *Drugs Exp Clin Res* 11, 123–5.
- 3 Weiss RB (1992) The anthracyclines: will we ever find a better doxorubicin? *Semin Oncol* 19, 670–686.
- 4 Rizvi SFA, Tariq S & Mehdi M (2018) Anthracyclines: Mechanism of Action, Classification, Pharmacokinetics and Future – A Mini Review. *Int J Biotechnol Bioeng* 4, 81–85.
- 5 Rayson D, Richel D, Chia S, Jackisch C, van der Vegt S & Suter T (2008) Anthracycline–trastuzumab regimens for HER2/neu-overexpressing breast cancer: current experience and future strategies. *Ann Oncol* 19, 1530–1539.
- 6 Sadurska E (2015) Current Views on Anthracycline Cardiotoxicity in Childhood Cancer Survivors. *Pediatr Cardiol* 36, 1112–1119.
- 7 Lotrionte M, Biondi-Zoccai G, Abbate A, Lanzetta G, D'Ascenzo F, Malavasi V, Peruzzi M, Frati G & Palazzoni G (2013) Review and Meta-Analysis of Incidence and Clinical Predictors of Anthracycline Cardiotoxicity. *Am J Cardiol* 112, 1980–1984.
- 8 Felix CA (1998) Secondary leukemias induced by topoisomerase-targeted drugs. *Biochim Biophys Acta - Gene Struct Expr* 1400, 233–255.
- 9 Mistry AR, Felix CA, Whitmarsh RJ, Mason A, Reiter A, Cassinat B, Parry A, Walz C, Wiemels JL, Segal MR, Adès L, Blair IA, Osheroff N, Peniket AJ, Lafage-Pochitaloff M, Cross NCP, Chomienne C, Solomon E, Fenaux P & Grimwade D (2005) DNA Topoisomerase II in Therapy-Related Acute Promyelocytic Leukemia. *N Engl J Med* 352, 1529–1538.
- 10 Lefrak EA, Pit'ha J, Rosenheim S & Gottlieb JA (1973) A clinicopathologic analysis of adriamycin cardiotoxicity. *Cancer* 32, 302–314.
- 11 Jones RL, Swanton C & Ewer MS (2006) Anthracycline cardiotoxicity. *Expert Opin Drug Saf* 5, 791–809.
- 12 Cappetta D, De Angelis A, Sapio L, Prezioso L, Illiano M, Quaini F, Rossi F, Berriño L, Naviglio S & Urbanek K (2017) Oxidative Stress and Cellular Response to Doxorubicin: A Common Factor in the Complex Milieu of Anthracycline Cardiotoxicity. *Oxid Med Cell Longev* 2017, 1–13.
- 13 Songbo M, Lang H, Xinyong C, Bin X, Ping Z & Liang S (2019) Oxidative stress injury in doxorubicin-induced cardiotoxicity. *Toxicol Lett* 307, 41–48.
- 14 Hashimoto K, Ito K & Ishimori Y (1994) Novel DNA sensor for electrochemical gene detection. *Anal Chim Acta* 286, 219–224.
- 15 Qiao X, van der Zanden SY, Wander DPA, Borràs DM, Song J-Y, Li X, van



- Duikeren S, van Gils N, Rutten A, van Herwaarden T, van Tellingen O, Giacomelli E, Bellin M, Orlova V, Tertoolen LGJ, Gerhardt S, Akkermans JJ, Bakker JM, Zuur CL, Pang B, Smits AM, Mummery CL, Smit L, Arens R, Li J, Overkleeft HS & Neefjes J (2020) Uncoupling DNA damage from chromatin damage to detoxify doxorubicin. *Proc Natl Acad Sci* 117, 15182–15192.
- 16 Nitiss JL (2009) Targeting DNA topoisomerase II in cancer chemotherapy. *Nat Rev Cancer* 9, 338–350.
- 17 Pang B, Qiao X, Janssen L, Velds A, Groothuis T, Kerkhoven R, Nieuwland M, Ovaa H, Rottenberg S, van Tellingen O, Janssen J, Huijgens P, Zwart W & Neefjes J (2013) Drug-induced histone eviction from open chromatin contributes to the chemotherapeutic effects of doxorubicin. *Nat Commun* 4, 1–13.
- 18 Pang B, de Jong J, Qiao X, Wessels LFA & Neefjes J (2015) Chemical profiling of the genome with anti-cancer drugs defines target specificities. *Nat Chem Biol* 11, 472–480.
- 19 Yang F, Kemp CJ & Henikoff S (2013) Doxorubicin enhances nucleosome turnover around promoters. *Curr Biol* 23, 782–7.
- 20 Iihoshi H, Ishihara T, Kuroda S, Ishihara N & Saitoh H (2017) Aclarubicin, an anthracycline anti-cancer drug, fluorescently contrasts mitochondria and reduces the oxygen consumption rate in living human cells. *Toxicol Lett* 277, 109–114.
- 21 Wijdeven RH, Pang B, van der Zanden SY, Qiao X, Blomen V, Hoogstraat M, Lips EH, Janssen L, Wessels L, Brummelkamp TR & Neefjes J (2015) Genome-Wide Identification and Characterization of Novel Factors Conferring Resistance to Topoisomerase II Poisons in Cancer. *Cancer Res* 75, 4176–4187.
- 22 Gottesman MM & Ling V (2006) The molecular basis of multidrug resistance in cancer: The early years of P-glycoprotein research. *FEBS Lett* 580, 998–1009.
- 23 Mechetner E, Kyshtoobayeva A, Zonis S, Kim H, Stroup R, Garcia R, Parker RJ & Fruehauf JP (1998) Levels of multidrug resistance (MDR1) P-glycoprotein expression by human breast cancer correlate with in vitro resistance to taxol and doxorubicin. *Clin Cancer Res* 4, 389–398.
- 24 Cox J & Weinman S (2016) Mechanisms of doxorubicin resistance in hepatocellular carcinoma. *Hepatic Oncol* 3, 57–59.
- 25 Pajic M, Iyer JK, Kersbergen A, Van Der Burg E, Nygren AOH, Jonkers J, Borst P & Rottenberg S (2009) Moderate increase in Mdr1a/1b expression causes in vivo resistance to doxorubicin in a mouse model for hereditary breast cancer. *Cancer Res* 69, 6396–6404.
- 26 Krohn K (ed.) (2008) Anthracycline Chemistry and Biology II Springer Berlin Heidelberg, Berlin, Heidelberg.
- 27 Yoshimoto A, Johdo O, Nishida H, Okamoto R & Takeuchi T (1993) Anthracycline metabolites from baumycin-producing *Streptomyces* sp. D788. III. New anthracycline metabolites produced by blocked mutants 4L-660 and YDK-18. *J Antibiot (Tokyo)* 46, 1758–1761.
- 28 Tong GL, Wu HY, Smith TH & Henry DW (1979) Adriamycin analogs. 3. Synthesis of N-alkylated anthracyclines with enhanced efficacy and reduced cardiotoxicity. *J Med Chem* 22, 912–918.
- 29 Kunnari T, Niemi J, Ylihonko K, Mäntsälä P & Hakala J (1997) Hybrid anthracyclines by a genetically engineered *Streptomyces galilaeus* mutant. *Bioorg Med Chem Lett* 7, 725–726.
- 30 Lu W, Leimkuhler C, Oberthür M, Kahne D & Walsh CT (2004) AklK Is An L-2-Deoxyfucosyltransferase in the Biosynthesis of the Anthracycline Aclacinomycin A. *Biochemistry* 43, 4548–4558.

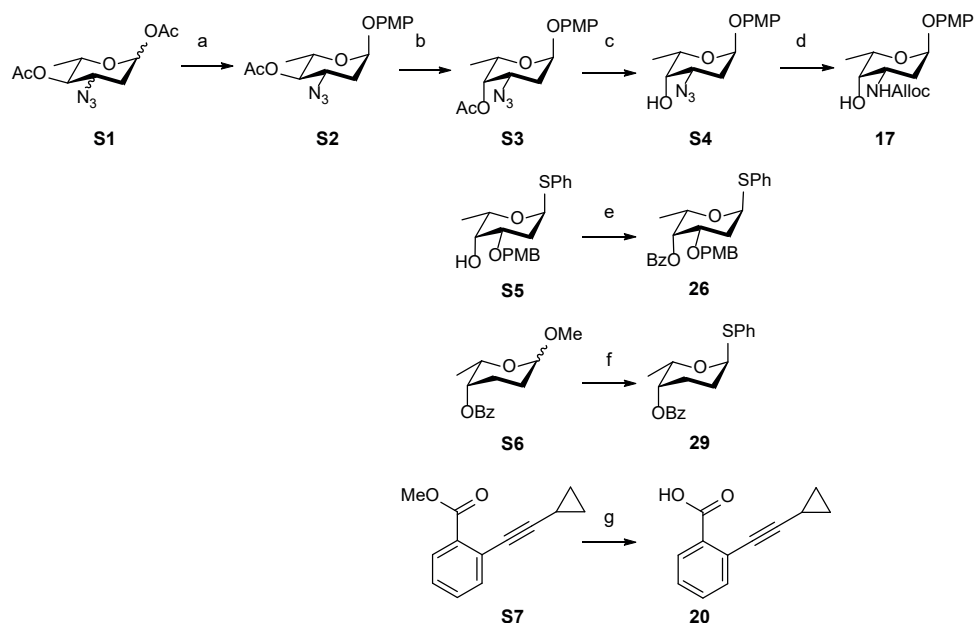
- 31 Oki T, Kitamura I, Matsuzawa Y, Shibamoto N, Ogasawara T, Yoshimoto A, Inui T, Naganawa H, Takeuchi T & Umezawa H (1979) Antitumor anthracycline antibiotics, aclacinomycin A and analogues. II. Structural determination. *J Antibiot (Tokyo)* 32, 801–819.
- 32 Tanaka H, Yoshioka T, Shimauchi Y, Matsushita Y, Matsuzawa Y, Oki T & Ishikura T (1982) Chemical modification of anthracycline antibiotics. IV. Synthesis of new anthracyclines with trisaccharide. *J Antibiot (Tokyo)* 35, 312–320.
- 33 Yu B (2018) Gold(I)-Catalyzed Glycosylation with Glycosyl *o*-Alkynylbenzoates as Donors. *Acc Chem Res* 51, 507–516.
- 34 Smith A (1998) Toward A General Method For The Construction Of Anthracycline Antibiotics. .
- 35 Horton D, Priebe W & Valera O (1984) Synthesis and Antitumour Activity of 3'-deamino-3'-hydroxydoxorubicin. *J Antibiot (Tokyo)* 37, 853–857.
- 36 Hansen T, Elferink H, van Hengst JMA, Houthuijs KJ, Remmerswaal WA, Kromm A, Berden G, van der Vorm S, Rijs AM, Overkleeft HS, Filippov D V, Rutjes FPJT, van der Marel GA, Martens J, Oomens J, Codée JDC & Boltje TJ (2020) Characterization of Glycosyl Dioxolenium Ions and Their Role in Glycosylation Reactions. *Nat Commun* 11, 1–9.
- 37 Komarova BS, Tsvetkov YE & Nifantiev NE (2016) Design of  $\alpha$ -Selective Glycopyranosyl Donors Relying on Remote Anchimeric Assistance. *Chem Rec* 16, 488–506.
- 38 Hansen T, Lebedel L, Remmerswaal WA, van der Vorm S, Wander DPA, Somers M, Overkleeft HS, Filippov D V., Désiré J, Mingot A, Bleriot Y, van der Marel GA, Thibaudeau S & Codée JDC (2019) Defining the SN1 Side of Glycosylation Reactions: Stereoselectivity of Glycopyranosyl Cations. *ACS Cent Sci* 5, 781–788.
- 39 Pearlman BA, McNamara JM, Hasan I, Hatakeyama S, Sekizaki H & Kishi Y (1981) Practical total synthesis of ( $\pm$ )-aklavinone and total synthesis of aklavin. *J Am Chem Soc* 103, 4248–4251.
- 40 Garro-Helion F, Merzouk A & Guibé F (1993) Mild and selective palladium(0)-catalyzed deallylation of allylic amines. Allylamine and diallylamine as very convenient ammonia equivalents for the synthesis of primary amines. *J Org Chem* 58, 6109–6113.
- 41 Johdo O, Nishida H, Okamoto R, Yoshimoto A & Takeuchi T (1995) New Anthracycline Antibiotics 10-epi-Oxaunomycin and 10-epi-11-Deoxyoxaunomycin. *J Antibiot (Tokyo)* 48, 1153–1158.
- 42 Veeneman GH, Van Leeuwen SH, Zuurmond H & Van Boom JH (1990) Synthesis of Carbohydrate-Antigenic Structures of Mycobacterium Tuberculosis using an Iodonium Ion Promoted Glycosidation Approach. *J Carbohydr Chem* 9, 783–796.
- 43 Cipollone A, Berettoni M, Bigioni M, Binaschi M, Cermele C, Monteagudo E, Olivieri L, Palomba D, Animati F, Goso C & Maggi C. (2002) Novel anthracycline oligosaccharides: influence of chemical modifications of the carbohydrate moiety on biological activity. *Bioorg Med Chem* 10, 1459–1470.
- 44 Craine L & Raban M (1989) The chemistry of sulfenamides. *Chem Rev* 89, 689–712.
- 45 Noshita T, Sugiyama T, Kitazumi Y & Oritani T (1994) Phenolic ferrier reaction and its application to the natural product synthesis. *Tetrahedron Lett* 35, 8259–8262.
- 46 Zhang X, Zhou Y, Zuo J & Yu B (2015) Total synthesis of periploside A, a unique pregnane hexasaccharide with potent immunosuppressive effects. *Nat Commun* 6, 1–10.
- 47 Ma Y, Li Z, Shi H, Zhang J & Yu B (2011) Assembly of digitoxin by gold(I)-cat-

- alyzed glycosidation of glycosyl o-alkynylbenzoates. *J Org Chem* 76, 9748–9756.
- 48 Soubeyrand S, Pope L & Haché RJG (2010) Topoisomerase II $\alpha$ -dependent induction of a persistent DNA damage response in response to transient etoposide exposure. *Mol Oncol* 4, 38–51.
- 49 van Maanen JMS, Retel J, de Vries J & Pinedo HM (1988) Mechanism of Action of Antitumor Drug Etoposide: A Review. *JNCI J Natl Cancer Inst* 80, 1526–1533.
- 50 Speth PAJ, van Hoesel QGCM & Haanen C (1988) Clinical Pharmacokinetics of Doxorubicin. *Clin Pharmacokinet* 15, 15–31.
- 51 Olive PL, Wlodek D & Banáth JP (1991) DNA double-strand breaks measured in individual cells subjected to gel electrophoresis. *Cancer Res* 51, 4671–6.
- 52 Dordal MS, Ho AC, Jackson-Stone M, Fu YF, Goolsby CL & Winter JN (1995) Flow cytometric assessment of the cellular pharmacokinetics of fluorescent drugs. *Cytometry* 20, 307–314.
- 53 Capranico G, De Isabella P, Penco S, Tinelli S & Zunino F (1989) Role of DNA breakage in cytotoxicity of doxorubicin, 9-deoxydoxorubicin, and 4-demethyl-6-deoxydoxorubicin in murine leukemia P388 cells. *Cancer Res* 49, 2022–7.
- 54 Gate L, Couvreur P, Nguyen-Ba G & Tapiero H (2003) N-methylation of anthracyclines modulates their cytotoxicity and pharmacokinetic in wild type and multidrug resistant cells. *Biomed Pharmacother* 57, 301–308.
- 55 Gianni L (1997) Anthracycline resistance: the problem and its current definition. *Semin Oncol* 24, S10–17.
- 56 Mansour OC, Evison BJ, Sleebs BE, Watson KG, Nudelman A, Rephaeli A, Buck DP, Collins JG, Bilardi RA, Phillips DR & Cutts SM (2010) New anthracenedione derivatives with improved biological activity by virtue of stable drug-DNA adduct formation. *J Med Chem* 53, 6851–66.
- 57 Liaw YC, Gao YG, Robinson H, Van der Marel GA, Van Boom JH & Wang AHJ (1989) Antitumor drug nogalamycin binds DNA in both grooves simultaneously: molecular structure of nogalamycin-DNA complex. *Biochemistry* 28, 9913–9918.
- 58 Frederick CA, Williams LD, Ughetto G, van der Marel GA, Van Boom JH, Rich A & Wang AHJ (1990) Structural comparison of anticancer drug-DNA complexes: adriamycin and daunomycin. *Biochemistry* 29, 2538–2549.
- 59 Zeman SM, Phillips DR & Crothers DM (1998) Characterization of covalent adriamycin-DNA adducts. *Proc Natl Acad Sci U S A* 95, 11561–11565.
- 60 Kloc K, Mlochowski J & Syper L (1980) Synthesis of Novel Quinones with Silver (II) Dipicolinate as a New Selective Oxidant. *Chem Lett* 9, 725–728.

# SUPPLEMENTAL INFORMATION

4





**Scheme S1. Synthesis of monosaccharide building blocks 17, 26 and 29.** Reagents and conditions: (a) *p*-methoxyphenol, TMSOTf, DCM, 0°C, 50%; (b) 1) NaOMe, MeOH, 100%, 2)  $\text{Ti}_2\text{O}_3$ , pyr., DCM, 0°C; 3) KOAc, 18-crown-6, DMF, 92% over 2 steps; (c) NaOMe, MeOH, 90%; (d) polymer-bound  $\text{PPh}_3$ , THF/ $\text{H}_2\text{O}$ , then Alloc-OSu, 89%; (e) BzCl, pyr., DCM, 82%; (f) PhSH,  $\text{BF}_3 \cdot \text{OEt}_2$ , DCM,  $-78^\circ\text{C} \rightarrow -15^\circ\text{C}$ , 80%, 1.2:1  $\alpha:\beta$ ; (g) NaOH, THF/ $\text{H}_2\text{O}$

Full supplemental information for the synthesis of monosaccharide building blocks and accompanied NMR data can be found online: <https://pubs.acs.org/doi/10.1021/acs.jmedchem.0c01191>

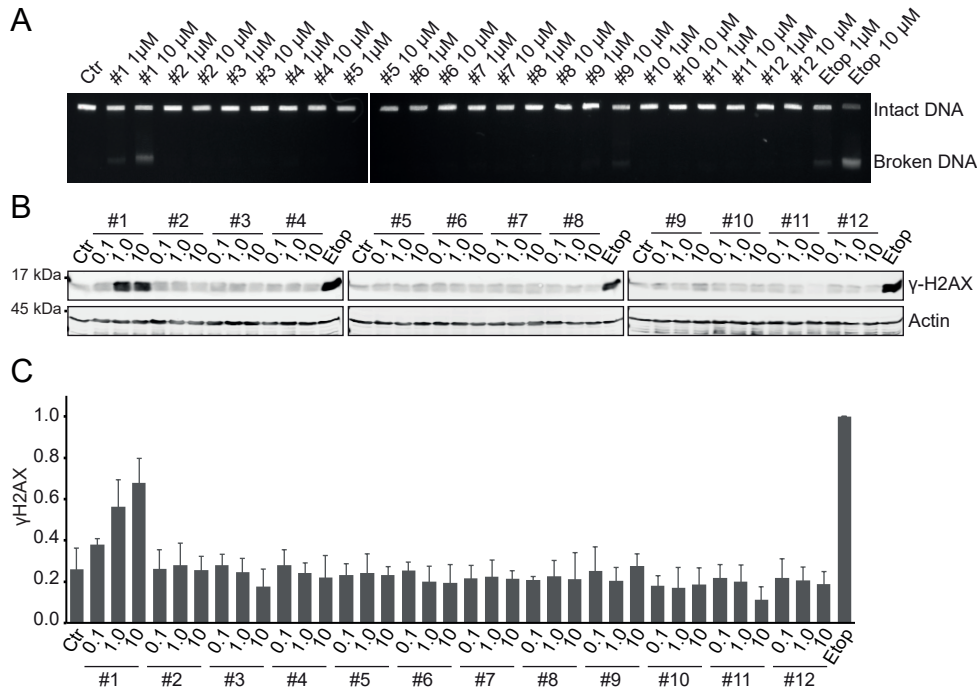


**Figure S1. Evaluation of DNA break capacity of the hybrid structures.** (A) K562 cells were treated for two hours with the indicated compound and concentration and DNA double strand breaks were analysed by CFGE. The position of intact and broken DNA is indicated. (B) K562 cells were treated for two hours with the indicated concentration of the various hybrid structures.  $\gamma$ H2AX levels were visualized by Western blot. Actin was used as a loading control. (C) Quantification of the  $\gamma$ H2AX signal normalized to actin. Results are presented as mean  $\pm$  SD of three independent experiments.



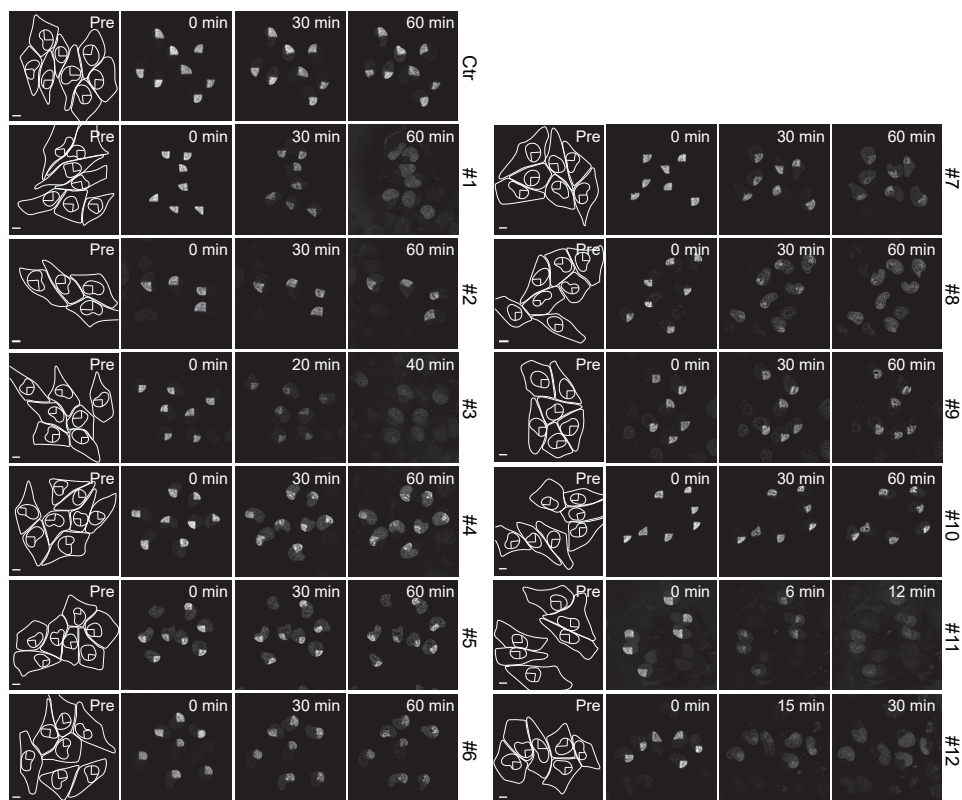


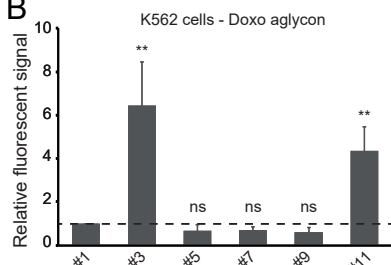
**Figure S2. Chromatin damage activity of the doxorubicin/aclarubicin hybrid structures.** Histone eviction was measured by time-lapse confocal microscopy. Photo-activated GFP-H2A was monitored for one hour after administration of 10uM of the indicated compounds. Lines in the left panel define the cytoplasm, nucleus and the activated region of the nucleus before treatment. Scale bar, 10 $\mu$ m.

**Figure S3. Continued (C and E).** Dotted line indicated the signal of the parental drug doxorubicin and aclarubicin. Two-tailed t-test; ns, not significant; \* $P < 0.05$ ; \*\* $P < 0.01$ ; \*\*\* $P < 0.001$ ; \*\*\*\* $P < 0.0001$ . (F) The drug uptake (normalized fluorescent intensity at two hours) in K562 cells versus the  $IC_{50}$  in K562 cells is plotted. Two-tailed Spearman correlation, ns; not significant. (G) The drug uptake (normalized fluorescent intensity at two hours) in MelJuSo cells versus histone eviction speed (time at which 25% of the initial signal is reduced) in MelJuSo cells is plotted. Two-tailed Spearman correlation, ns; not significant.

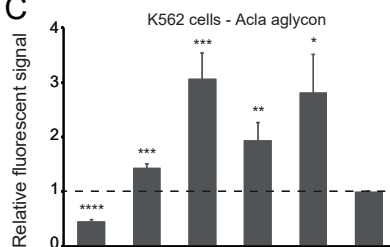
A

Compound	IC <sub>50</sub>	IC <sub>50</sub> [#] IC <sub>50</sub> [Doxo]	IC <sub>50</sub> [#] IC <sub>50</sub> [Acla]
#1	0.362	1.000	4.751
#2	N.D.	N.D.	N.D.
#3	0.186	0.515	2.446
#4	5.633	15.569	73.963
#5	N.D.	N.D.	N.D.
#6	N.D.	N.D.	N.D.
#7	2.407	6.653	31.605
#8	0.211	0.583	2.769
#9	1.405	3.883	18.448
#10	3.035	8.389	39.850
#11	0.026	0.073	0.346
#12	0.076	0.211	1.000

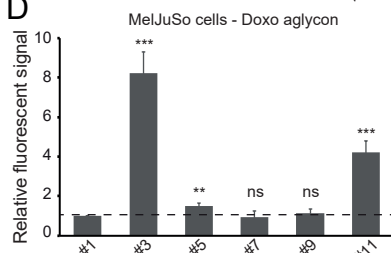
B



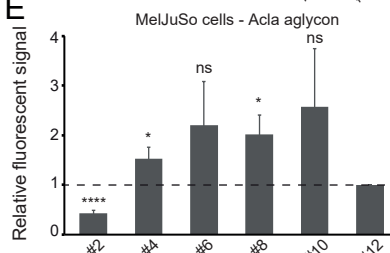
C



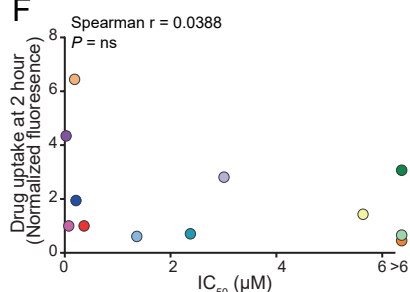
D



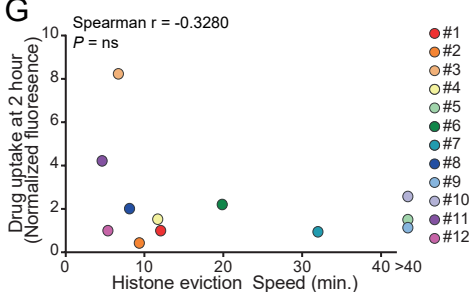
E



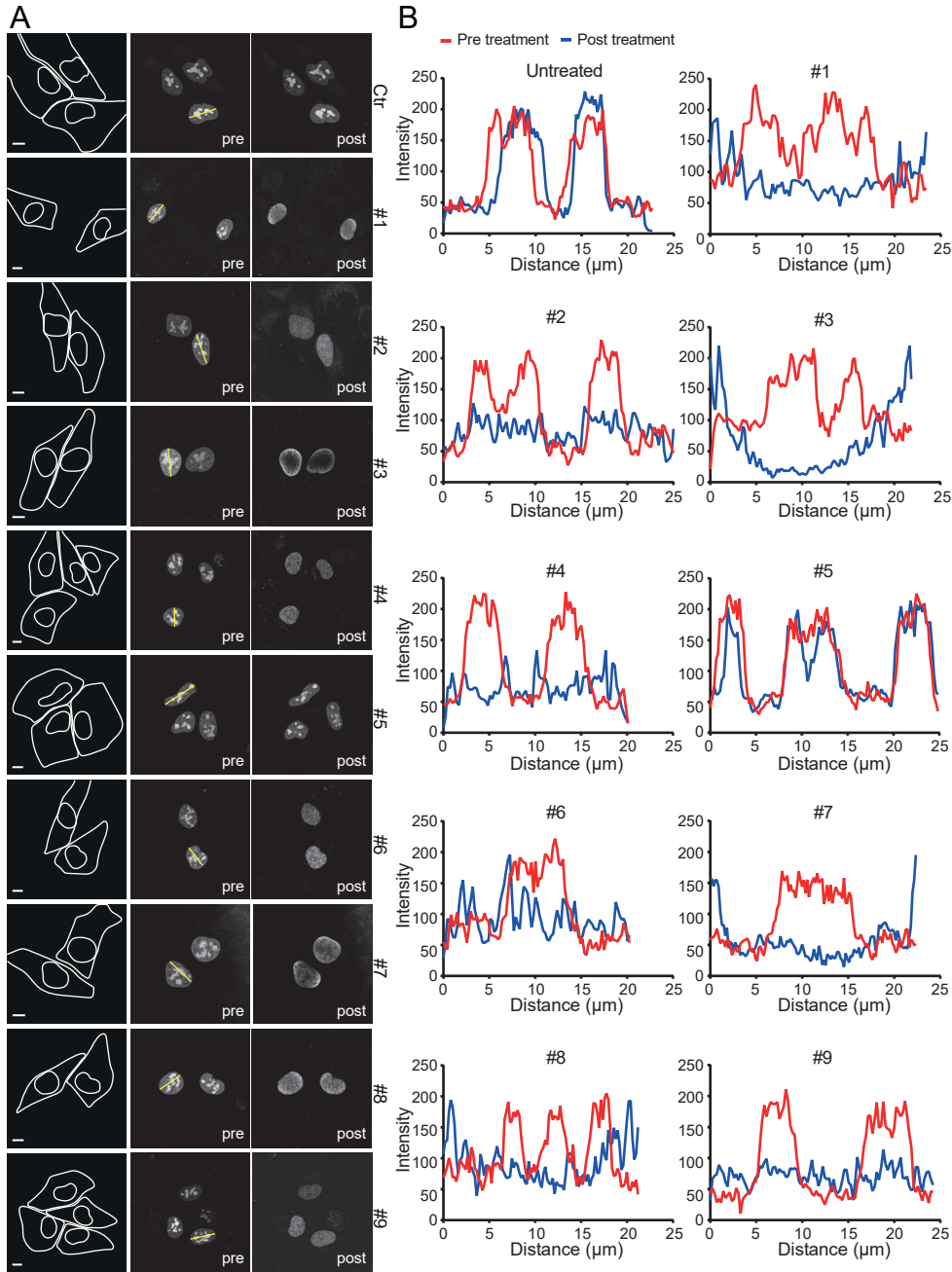
F



G



**Figure S3. Evaluation of various hybrid structures uptake.** (A) IC<sub>50</sub> values in  $\mu\text{M}$  of the various hybrid structures for K562 cells. Last panels list the IC<sub>50</sub> ratio from the indicated compound in relation to doxorubicin (Doxo, 1) or aclarubicin (Acla, 12). N.D. = Not detected. (B - E) The cellular drug uptake was measured. K562 (B and C) or MelJuSo (D and E) cells were treated for two hours with  $1\mu\text{M}$  of the indicated compound. Cells were washed, fixed and the autofluorescence of the compounds were quantified by flow cytometry. Data is shown as mean  $\pm$  SD from three independent experiments. Fluorescent intensity was normalized to doxorubicin (1) for the hybrid structures containing the doxorubicin aglycon (B and D), or to aclarubicin (12) for the structures containing the aclarubicin aglycon (C and E).



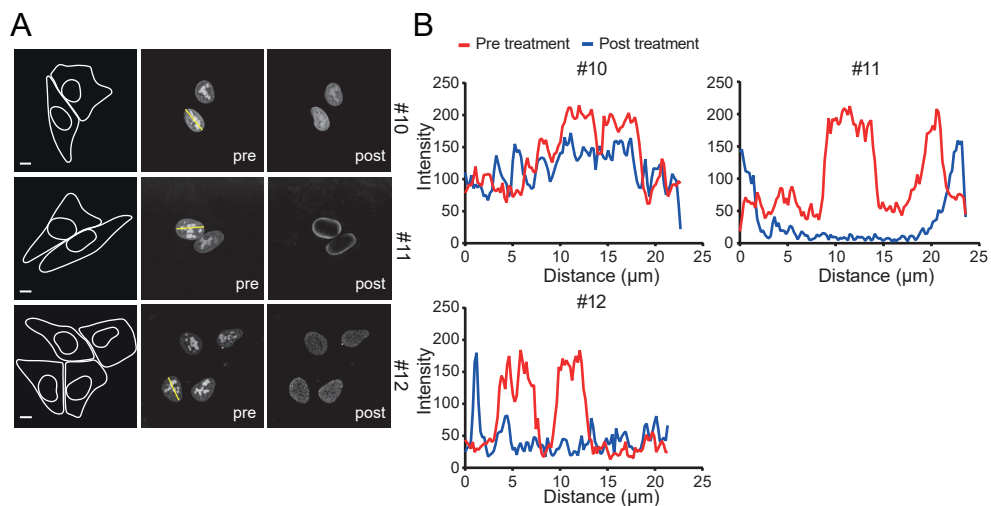
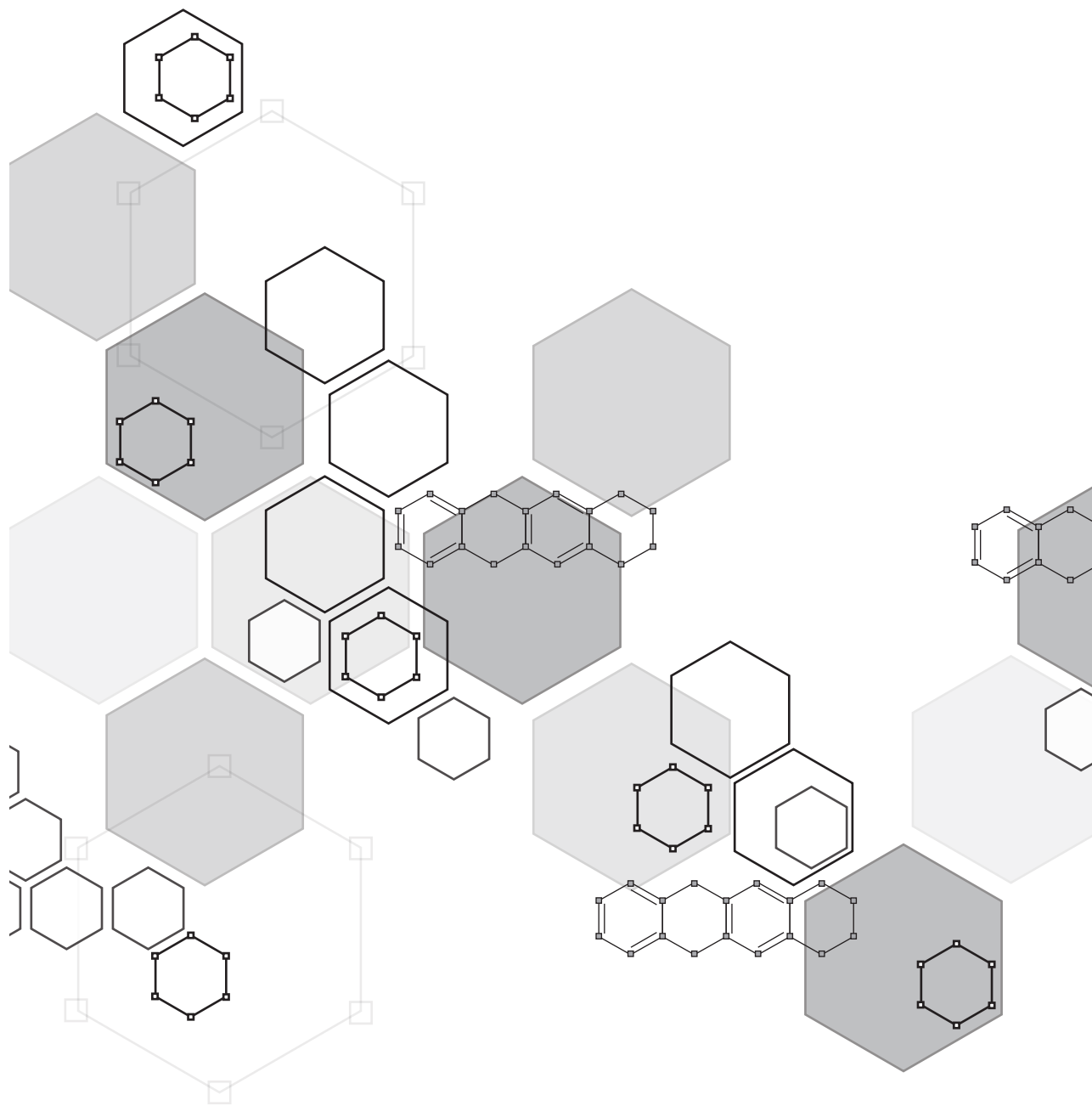
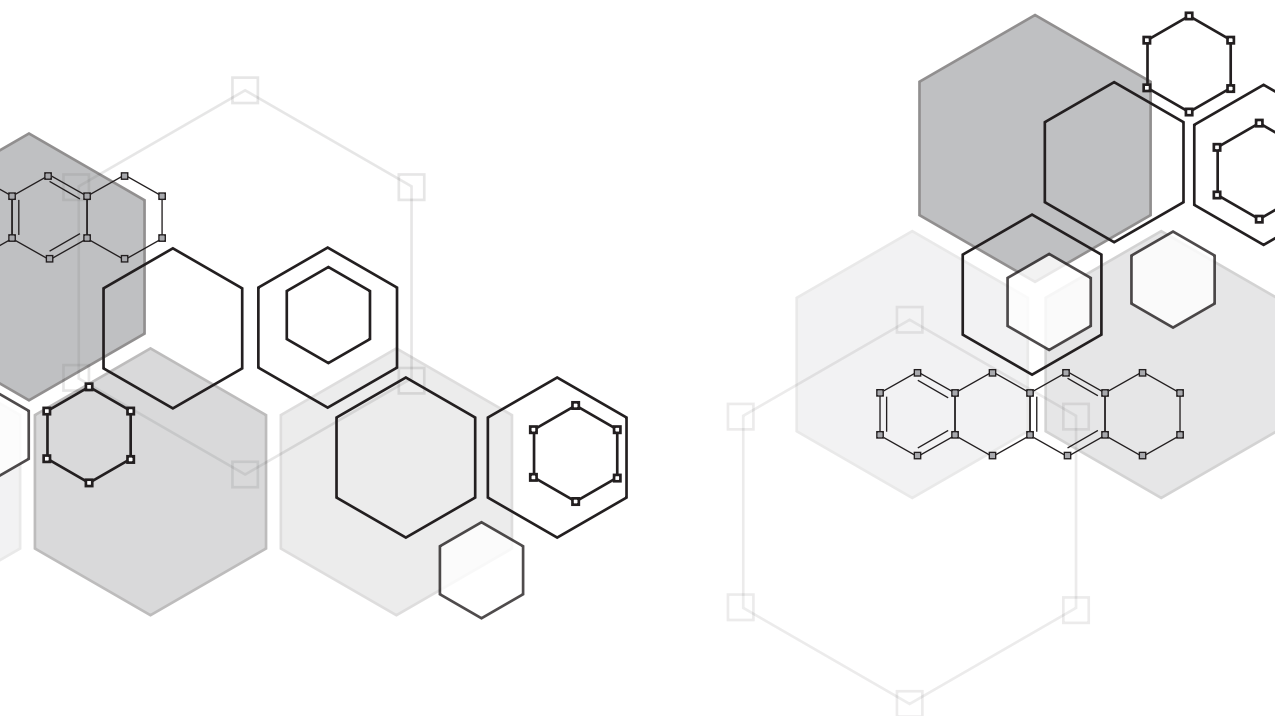


**Figure S4. Topo II $\alpha$  targeting by the doxorubicin/aclarubicin hybrid structures.** *Me/JuSo* cells transiently expressed with GFP-tagged TopoII $\alpha$ . (A) Cells are treated for 15 minutes with  $10\mu\text{M}$  of the indicated compounds and followed over time. Lines in the left panel define the cytoplasm and nucleus. Stills from time-laps experiment, before (pre) and after (post) treatment are shown. Scale bar,  $10\mu\text{m}$ . (B) Pixel plot of the GFP signal pre- and post treatment with the indicated compounds. Fractional distance is plotted as fluorescence over distance of yellow line as marked in (A).



# Synthetic (*N,N*-dimethyl) doxorubicin glycosyl diastereomers to dissect modes of action of anthracycline anticancer drugs

# 5



Sabina Y. van der Zanden<sup>#</sup>, Dennis P.A. Wander<sup>#</sup>, Merijn B.L. Vriends, Branca C. van Veen, Joey G. C. Vlaming, Thomas Bruyning, Gijsbert A. van der Marel, Jeroen D.C. Codee, Heman S. Overkleeft and Jacques Neefjes

<sup>#</sup>These authors contributed equally

*Manuscript in preparation*

## ABSTRACT

Anthracyclines are effective drugs in the treatment of various cancers, but their use coincides with severe side effects. The archetypal anthracycline drug, doxorubicin, displays two molecular modes of action: DNA double strand break formation (through topoisomerase II $\alpha$  poisoning) and chromatin damage (via eviction of histones). These biological activities can be modulated, and toxic side effects reduced by separating these two modes of action, through alteration of the aminoglycoside moiety of doxorubicin. Here, we report on the design, synthesis and evaluation of a coherent set of configurational doxorubicin analogs featuring all possible stereoisomers of the 1,2-amino-alcohol characteristic for the doxorubicin 3-amino-2,3-dideoxyfucoside, each in non-substituted and *N,N*-dimethylated forms. We show that both stereochemistry of the 3-amine carbon and *N*-substitution state are critical for anthracycline cytotoxicity and generally improve cellular uptake. *N,N*-dimethylepirubicin is identified as the most potent anthracycline that does not induce DNA damage while remaining cytotoxic.

## INTRODUCTION

The anthracycline drug doxorubicin (adriamycin, Figure 1A, **1a**) is one of the most used anticancer drugs in history, and is annually subscribed to over one million cancer patients [1]. While doxorubicin is effective against a wide variety of tumors, including leukemia, non-Hodgkin's lymphoma and breast cancer, its use is limited by severe side-effects. Cardiotoxicity, the main treatment-limiting side effect, emerges in a cumulative manner, and for this reason treatment with doxorubicin is restricted to a maximum of six to eight treatment courses [2]. With the aim to identify more effective anthracyclines with limited side-effects, thousands of analogs of doxorubicin, either isolated from natural sources, produced by mutant enzymes or prepared by organic (semi) synthesis, have been evaluated in the past decades [3–5]. Only a handful of these anthracyclines has however entered the clinic. The 4'-epimer of doxorubicin, epirubicin (Figure 1A, **2a**) is one such clinically approved doxorubicin variant, in part because it appears to be effective at lower doses compared to doxorubicin for certain cancers, resulting in reduced cardiotoxicity [6]. Today, epirubicin is used in the treatment of breast-, ovarian-, gastric- and lung tumors, as well as several lymphomas [7]. This illustrates that new effective and less toxic anthracyclines can be developed, which may allow more intense, longer, and more effective treatment with limited long-term side effects for cancer survivors.

Understanding the molecular mode of action of anthracycline drugs is key for the development of new and improved (in terms of efficacy and toxicity) analogs. One key feature of doxorubicin is the formation of DNA double strand breaks due to topoisomerase II $\alpha$  poisoning [8,9]. Doxorubicin inhibits topoisomerase II $\alpha$  after the generation of DNA double stranded breaks and before re-ligation of DNA, thus resulting in DNA damage. For decades, this mode of action has been considered the main mechanism for the remarkable anticancer activity of doxorubicin and its structural analogs. However, aclarubicin (Figure 1B), another anthracycline analog used in Japan and China, is at least equally effective in the treatment of acute myeloid leukemia (AML), but does not produce such DNA double stranded breaks [9]. Moreover, aclarubicin is much less cardiotoxic [10]. We recently showed the existence of a second activity of anthracyclines: eviction of histones from the chromatin [9]. These evicted histones are then replaced by new nascent ones, resulting in epigenetic alterations [11]. Further, we showed that histone eviction combined with



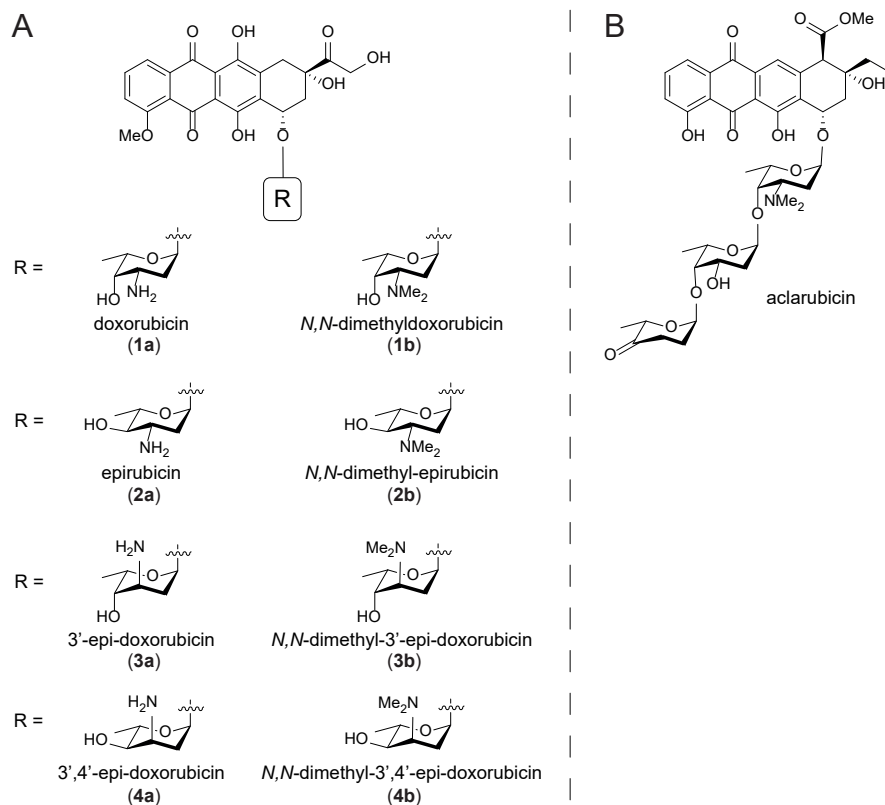


**Figure 1. Chemical structures of doxorubicin and analogs.** (A) doxorubicin (**1a**) and derivatives (**1b–4b**), differing in stereochemistry and *N,N*-dimethylation on the sugar moiety. (B) structure of aclarubicin.

DNA double strand break formation, as for doxorubicin, is responsible for the major side effects of doxorubicin; cardiotoxicity and secondary tumor formation [10]. In this study, we showed that *N,N*-dimethyldoxorubicin (Figure 1, **1b**), a close doxorubicin analog featuring the dimethylamine characteristic for aclarubicin, mirrors the biological activity of aclarubicin, by only inducing histone eviction [10]. Like aclarubicin, *N,N*-dimethyldoxorubicin is an effective anticancer agent and lacks the severe side effects displayed by doxorubicin in various mouse models [10]. These data show that chemically separating DNA- from chromatin damage activities, as found in the anthracyclines currently used in the clinic, results in drugs lacking the major long-term side effects. In addition, chromatin damage appeared to be the major cause for the anticancer activity of these compounds. Our follow-up studies on a series of doxorubicin/aclarubicin hybrid structures, varying in the tetracyclic aglycon, the sugar moiety (from monosaccharide as in doxorubicin up until the aclarubicin trisaccharide) and the *N*-alkylation pattern confirm previous results that dimethylated structures fail to induce DNA double strand breaks while remaining cytotoxic [12]. This work raises the question if there is a structure-activity relationship for stereoisomeric analogs of doxorubicin, and whether this may lead to potential new effective

anticancer drugs. To test this, we synthesized and evaluated a coherent, focused library of epimeric doxorubicin analogs featuring entries of all four stereoisomeric forms of the 1,2-amino alcohol arrangement of the 3-amino-2,3-dideoxy-L-fucoside (daunosamine) characteristic for doxorubicin (**1a**). Each of these entries features the non-substituted as well as the *N,N*-dimethylated compound. Together, this resulted in the synthesis of compounds **1a/b** - **4a/b** (Figure 1), some of which have been reported previously [10,13,14].

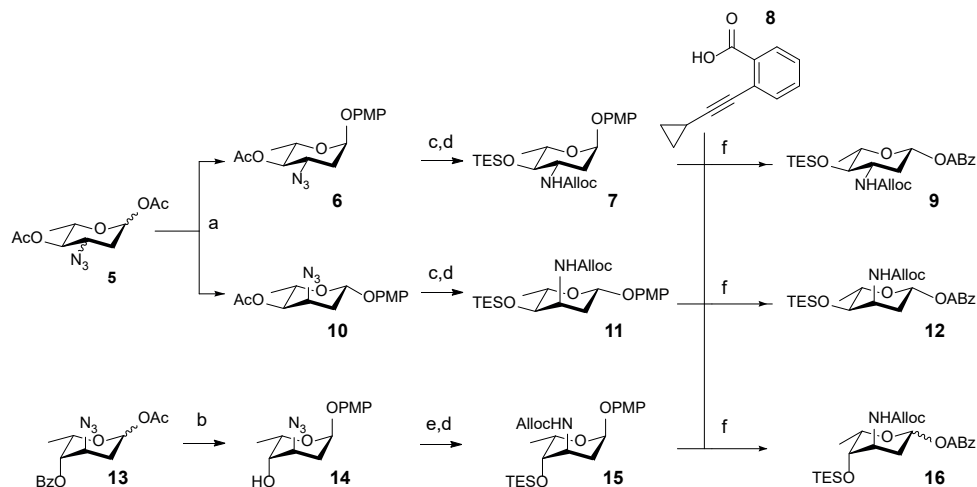
Here we report a general synthesis route for the preparation of these target compounds, based on the use of gold-catalyzed glycosylation reactions of alkynylbenzoate donors. Most of these proceed with excellent stereoselectivity, which can be related to the oxocarbenium ion intermediates formed in these reactions. Subsequently, we evaluated the biological activities of the systematic set of diastereoisomers by dissecting their capacity to induce DNA damage, histone eviction, their cellular uptake and cytotoxicity. Dimethylation of the sugar amine and an equatorial orientation of this moiety are required for cytotoxicity of these compounds and generally improve cellular uptake *in vitro*. These features are combined in *N,N*-dimethylepirubicin (**2b**), the most potent anthracycline in this coherent set of epimeric doxorubicin analogs, which has an excellent cytotoxicity profile with only chromatin damage activity.

## RESULTS AND DISCUSSION

### Synthesis of a coherent set of (*N,N*-dimethyl)doxorubicin stereoisomers.

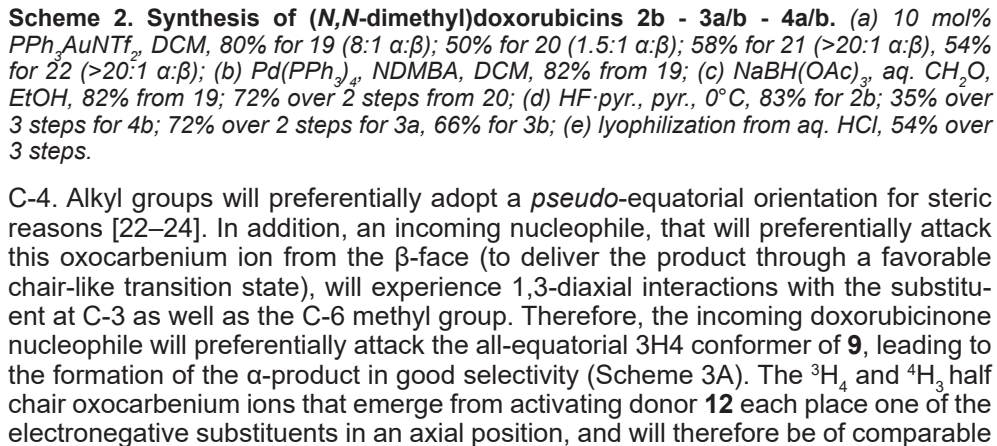
We started with the development of synthetic methodology to prepare the focused library depicted in Figure 1A (compounds **2b**, **3a/b**, **4a/b**). Recently, we reported on the synthesis of *N,N*-dimethyldoxorubicin (**1b**) [10], whereas doxorubicin (**1a**) and epirubicin (**2a**) are both commercially available. Our methodology is rooted in gold(I)-mediated glycosylation chemistry, developed by Yu and coworkers [15], that in our hands has proven effective in the creation of the anthracycline  $\alpha$ -fucosidic linkages [12,16]. In the assembly of doxorubicin/aclarubicin hybrids we found that the use of an allyloxycarbonate to mask the amino group of the 2,3-dideoxy-3-aminofucose in combination with relatively labile silyl ethers to protect the hydroxyl groups proved very effective for the assembly of the anthracycline targets and we therefore adopted this protecting group strategy here as well [12]. Thus, alkynylbenzoate donors **9**, **12** and **16** were designed and assembled as depicted in Scheme 1. *p*-Methoxyphenolates **6** and **10** were prepared from precursor **5** [17] (a mixture of 33 : 67 R/S at C3) by treatment with *p*-methoxyphenol in the presence of catalytic TMSOTf to give  $\alpha$ -configured equatorial azide **6** in 50% yield and  $\beta$ -configured axial azide **10** in 7%. Deacylation under Zemplén conditions was followed by triethylsilylation, and the azide was then converted to the allyloxycarbamate using a Staudinger reduction, after which reaction of the liberated amine with allylchloroformate gave fully protected **7** and **11**. The *p*-methoxyphenolates were then subjected to oxidative hydrolysis of the anomeric *p*-methoxyphenolate using  $\text{Ag}(\text{DPAH})_2$  [18], delivering the lactols which were transformed into the required alkynylbenzoates (ABz) by a Steglich esterification with *o*-cyclopropylethynylbenzoic acid **8** [19], providing donor glycosides **9** and **12**.

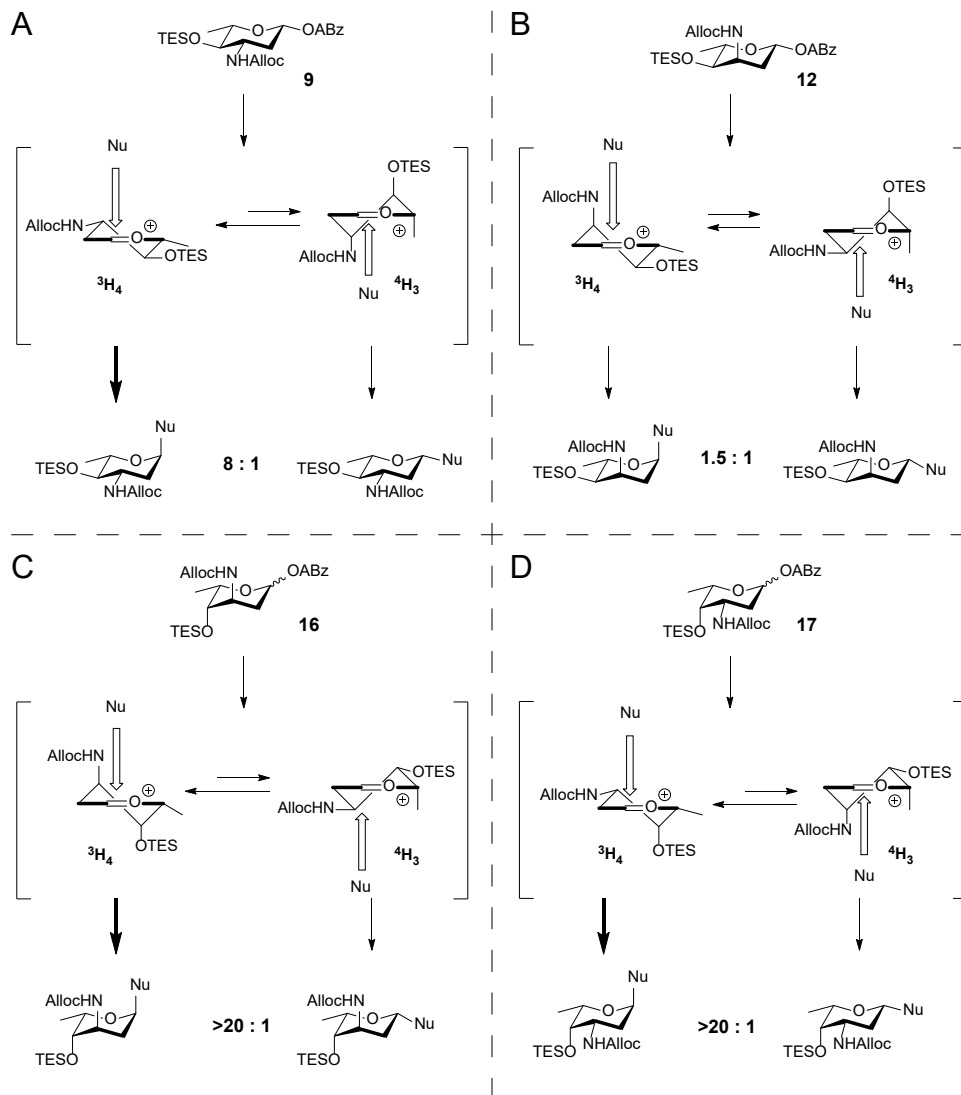
In preparing for the synthesis of the 3-*epi*-daunosamine donor **16**, acetate **13** [20], was converted to the *p*-methoxyphenolate by the action of  $\text{BF}_3 \cdot \text{OEt}_2$  giving, after deacylation, compound **14**. Triethylsilylation of the 4-hydroxyl and conversion of the azide into the allyloxycarbamate yielded **15**. Removal of the anomeric *p*-methoxy-



**Scheme 1. Synthesis of aminosugar alkynylbenzoate donors 9, 12 and 16.** Reagents and conditions: (a) *p*-methoxyphenol, TMSOTf, DCM, 0°C, 50% for **6**, 7% for **10**; (b) i. *p*-methoxyphenol, BF<sub>3</sub>·OEt<sub>2</sub>, DCM, -60°C to -40°C; ii. NaOMe, MeOH, 70% over 2 steps; (c) i. NaOMe, MeOH; ii. TESOTf, pyr., DCM, 95% over 2 steps from **6**, quant. from **10**; (d) i. polymer-bound PPh<sub>3</sub>, THF, H<sub>2</sub>O; ii. allyl chloroformate, pyr., DCM, quant. over 2 steps for **7**; 95% over 2 steps for **11**; quant. over 2 steps for **15**; (e) TESOTf, pyr., quant.; (f) i. Ag(DPAH)<sub>2</sub>, H<sub>2</sub>O, NaOAc, MeCN, H<sub>2</sub>O, 0°C; ii. EDCI·HCl, DMAP, DIPEA, DCM, 49% over 2 steps for **9** (β-anomer only), 57% over 2 steps for **12** (β-anomer only), 79% over 2 steps for **16** (1:3 α:β).

phenol group and installation of the alkynylbenzoate was then achieved as described for donors **9** and **12** to give donor **16**. The three alkynylbenzoate donors **9**, **12** and **16** were used, alongside daunosamine donor **17** that we previously assembled [12], in glycosylation reactions towards doxorubicin analogs **2b** - **3a/b** - **4a/b** (Scheme 2). Treatment of a mixture of donor **9** and protected doxorubicinone acceptor **18** [21], with a catalytic amount of PPh<sub>3</sub>AuNTf<sub>2</sub> in DCM at room temperature led to the formation of anthracycline **19** in 80% yield as an 8:1 α:β-mixture. The desired α-anomer could be readily separated to provide the desired axially linked **19**. The analogous glycosylation of **12** and **18** proceeded with poor stereoselectivity and provided **20** as a 1.5:1 α:β mixture in 50% yield. The condensation of donor **16**, having two axial substituents at C-3 and C-4, led to the formation of the protected doxorubicin analog **21** with excellent stereoselectivity and the desired product was obtained as a single anomer in 58% yield. The glycosylation of daunosamine donor **17** and **18** also delivered the desired α-anomer with excellent stereoselectivity, forming **22** in 54% yield. We suggest that the observed stereoselectivity - or lack thereof - in these glycosylations can be understood upon perusal of the intermediate oxocarbenium ions (or oxocarbenium ion-like species), their conformational behavior and the direction nucleophiles may take towards forming a glycosidic linkage. The dideoxy nature of the used donors makes them relatively reactive ('armed') and the anomeric cation thus readily forms upon activation of the alkynylbenzoate anomeric leaving group.<sup>‡</sup> The intermediate oxocarbenium ion can adopt different conformations (often close to half-chair structures) and preferred conformations are the result of stereoelectronic effects of the substituents on the ring [22]. Electronegative atoms (such as oxygen and nitrogen) prefer to adopt an axial orientation when mounted at C-3 or





**Scheme 3. Mechanistic rationale for the stereoselectivity found in the glycosylations of donors **9**, **12**, **16** and **17** with acceptor **18**.** The equilibria between the  $^3H_4$  and  $^4H_3$  conformers of the oxocarbenium ions are indicated. The bold arrows indicate the most favorable product forming pathways. Nu = acceptor **18**.

stability (Scheme 3B). The trajectories of incoming nucleophiles on these ions will experience similar steric interactions, explaining the poor selectivity observed in the glycosylation of donor **12** and acceptor **18**. Zeng et al. have previously reported that glycosylations of similar ristosaminyl alkynylbenzoate donors to various glycosyl acceptors proceeded with comparably poor selectivity [25]. The excellent stereoselectivity of donor **16** can be traced back to the  $^3H_4$  half chair oxocarbenium ion, which places both the C-3 and C-4 electronegative groups in an axial position, while having the C-6-methyl oriented equatorially (Scheme 3C). This ion is preferentially attacked

from the top face to provide the  $\alpha$ -linked product. Finally, when the half chair ions formed from daunosamine donor **17** are regarded, the  $^3H_4$  one appears the most favorable, because it benefits from the axially oriented C-4-OTES group and lacks unfavorable 1,3-diaxial interactions (Scheme 3D). In addition, the incoming nucleophile will experience little steric interactions when approaching this ion from the top face, explaining the excellent stereoselectivity of donor **17**.

With the fully protected anthracyclines in hand we focused on deprotection of the compounds and the installation of the methyl groups on the amines (Scheme 2). Deblocking of the Alloc carbamate in **19** was achieved by treatment with catalytic  $Pd(PPh_3)_4$  in the presence of *N,N*-dimethylbarbituric acid (NDMBA) [26] as the allyl scavenger to liberate the amine. Reductive amination using formaldehyde and a stoichiometric amount of  $NaBH(OAc)_3$ , was followed by desilylation with HF in pyridine to afford target compound *N,N*-dimethylepirubicin **2b**. Alloc removal of **20** and subsequent desilylation delivered **4a**, which was turned into its HCl salt for solubility. Reductive amination of the amine formed upon Alloc removal from **20** and desilylation delivered **4b**. Using a similar sequence of reactions, **21** was transformed into **3a** and **3b**. Of note, NMR analysis of compound **4b** indicated that the sugar ring adopts a  $^4C_1$  conformation, rather than the  $^1C_4$  conformation, taken up by its non-methylated counterpart **4a** (see supplemental information Figure S4 for annotated NMR spectra). The observed conformation of the L-megosamine sugar moiety in **4b** is consistent with that found in the macrolide megalomycin [27]. As a result, the tertiary amine in **4b** points away from the aglycone, and the overall shape of anthracycline **4b** differs significantly from the other generated compounds.

### Biological evaluation of (*N,N*-dimethyl)doxorubicin stereoisomers

Doxorubicin and its analogs used in the clinic, have two main activities: DNA damage and chromatin damage [9,10]. Modification at the amine can separate these activities, but sugar epimers of doxorubicin have not been evaluated for this. Therefore, we assessed our panel of (*N,N*-dimethyl)doxorubicin isomers for these biological activities. DNA double strand break formation by the various compounds was determined (indirectly) by visualization of  $\gamma$ H2AX (a post-translational modification on histone H2A that occurs as part of the DNA damage response) by western blot analysis (Figure 2A and B) [28]. In addition, DNA breaks were assessed more directly using constant-field gel electrophoresis (CFGE) (Figure 2C and D). The anthracyclines bearing a free amine in their sugar, i.e. doxorubicin (**1a**), epirubicin (**2a**), 3'-epi-doxorubicin (**3a**) and 3',4'-epi-doxorubicin (**4a**) all induced DNA breaks. For the analogs featuring a tertiary amine (**1b**, **2b**, **3b** and **4b**), DNA double strand break formation was absent or reduced, compared to their primary amine counterparts. *N,N*-dimethyldoxorubicin (**1b**) and *N,N*-dimethyl-epi-doxorubicin (**2b**) induced (almost) no DNA breaks, yet *N,N*-dimethyl-3'-epi-doxorubicin (**3b**) and *N,N*-dimethyl-3',4'-epi-doxorubicin (**4b**) did produce DNA breaks, although significantly less so than their non-methylated counterparts (Figure 2B and D). Overall, the orientation of the 4-OH function (**1a** vs **2a**, **1b** vs **2b**, **3a** vs **4a**, **3b** vs **4b**) had little effect on their DNA damaging activity. Since our previous findings indicate that chromatin damage, rather than DNA damage, is the most dominant cytotoxic mechanism of tumor killing by anthracycline drugs [10,11], we investigated the ability of our panel of compounds (**1a/b** - **4a/b**) to induce histone eviction. To do so, part of the nucleus of MeJUSo cells stably expressing PAGFP-H2A was photoactivated, and release of these fluorescent histones was followed over time upon treatment with the different compounds (Figure 3A and supplemental information Figure S1). In all cases, the *N,N*-dimethylated variants (**1b**, **2b**, **3b** and

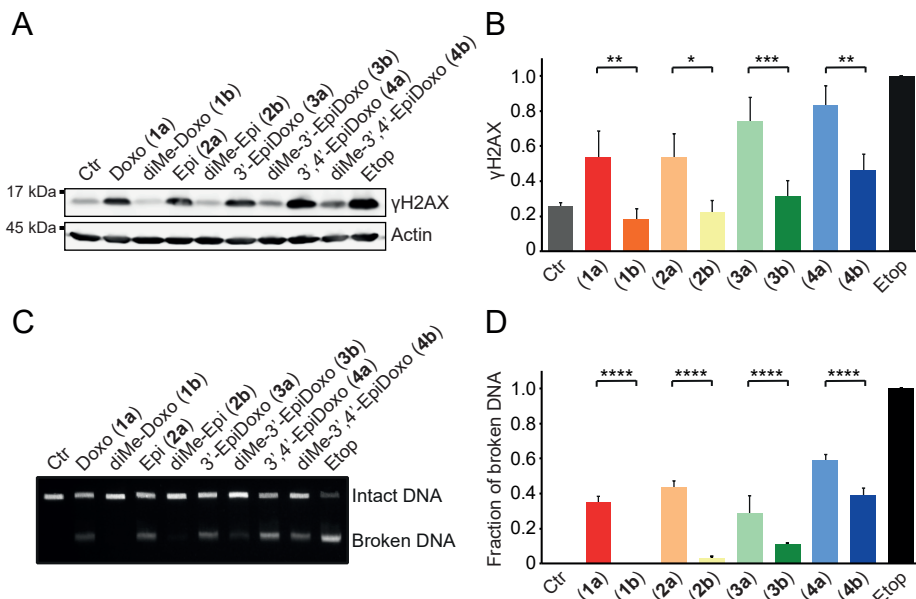


**Figure 2. DNA damage formation by the epimeric doxorubicin analogs (1a/b - 4a/b).** K562 cells were treated for 2 hours with 10  $\mu$ M of the indicated compounds, and etoposide (10  $\mu$ M) was used as a positive control. (A) DNA double strand breaks were measured indirectly by visualization of the  $\gamma$ H2AX levels by Western blot. Actin was used as a loading control and molecular weight markers are indicated. (B) Quantification of the  $\gamma$ H2AX signal normalized to actin, and relative to etoposide. Results are presented as mean  $\pm$  SD of three independent experiments. Ordinary one-way ANOVA; \* $P$  < 0.05, \*\* $P$  < 0.01, \*\*\* $P$  < 0.001. (C) DNA break formation by the various compounds was directly analyzed by CFGE. The position of intact and broken DNA is indicated. (D) Quantification of the fraction of broken DNA relative to etoposide. Results are presented as mean  $\pm$  SD of four independent experiments. Ordinary one-way ANOVA; \*\*\*\* $P$  < 0.0001.

**4b**) were more potent in evicting histones than their free amine counterparts (Figure 3A). Of the dimethylated compounds, *N,N*-dimethyl-3'-epidoxorubicin (**3b**) showed the lowest histone evicting activity and 3'-epidoxorubicin (**3a**) was the only compound that failed to evict histones. Subsequently, the cytotoxicity of the compounds was determined in a panel of 14 different tumor cell lines *in vitro* (Figure 3B and 3C, and supplemental information Figure S2). With the exception of compound **3b**, all compounds with tertiary amines have a lower  $IC_{50}$  value in the tested tumor cell lines than their non-methylated counterparts. Furthermore, the compounds with the amine in an equatorial position (**1a/b**, **2a/b** and **4b**) are effective at killing most of the tumor cell lines, down to nanomolar concentrations, while the compounds with the amine in axial configuration (**3a/b**, **4a**) show poor cytotoxicity. The difference in cytotoxicity between **3a** versus **4a**, and **3b** versus **4b** is remarkable. 3'-Epidoxorubicin (**3a**) and 3',4'-epidoxorubicin (**4a**) both show poor cytotoxicity and the dimethylated variant of **3a**, compound **3b**, is not more effective, while the dimethylated variant of **4a**, being **4b**, is significantly more cytotoxic (Figure 3C). Possibly, this is due to the fact that the sugar in *N,N*-dimethylated **4b** exists in a different conformation than in **4a**, placing the C-3 dimethylamino group in an equatorial orientation (similarly to **1a/b** and **2a/b**), pointing away from the aglycone rather than towards it (as for compounds **3a/b** and



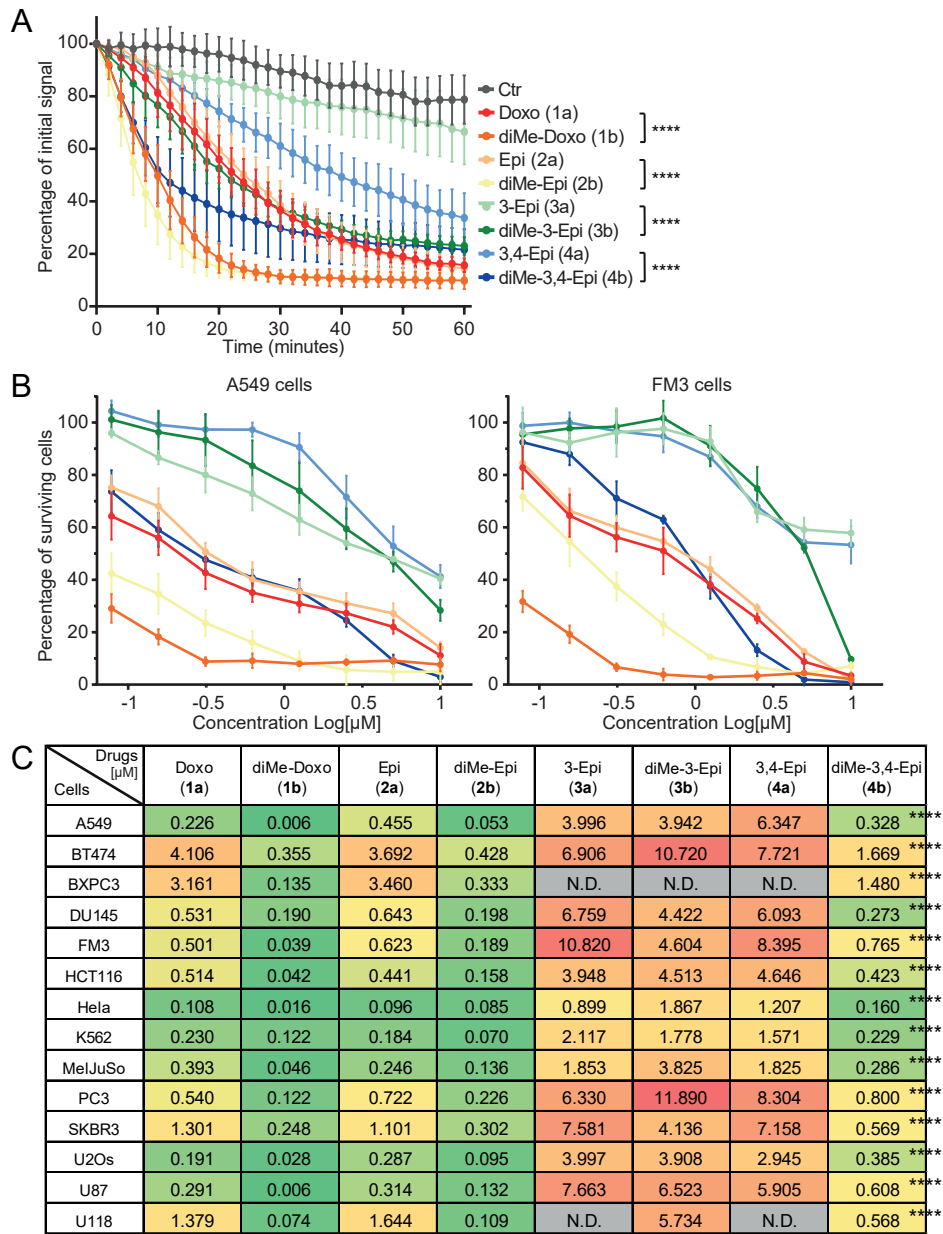


**Figure 3. Chromatin damage capacity and cytotoxicity of epimeric doxorubicin analogs.** (A) Quantification of histone eviction measured as PAGFP-H2A release from photo-activated nuclear regions after administration of 10μM of the indicated doxorubicin isomers (in colors on right). Ordinary two-way ANOVA, Turkey's multiple comparison test; \*\*\*\**P* < 0.0001. (B) Cytotoxicity of 1a/b - 4a/b in A549 and FM3 cells. Cells were treated for 2 hours with different concentration of the indicated isomers followed by drug removal. Cell survival was determined 72 hours post drug removal using CellTiter-Blue. Colors correspond to the drugs shown in Figure 3A. Data is shown as mean ± SD from 4 independent experiments.

**Figure 3. Continued.** (C) Color code table depicting the  $IC_{50}$  for compounds 1a/b - 4a/b determined for the 14 tumor cell lines tested. Red, (high  $IC_{50}$  = low cytotoxicity), to yellow (medium  $IC_{50}$ ), to green (low  $IC_{50}$  = high cytotoxicity).  $IC_{50}$  for 4a vs 4b: Ordinary two-way ANOVA with Sidak's multiple comparison test; \*\*\*\* $P < 0.0001$ .

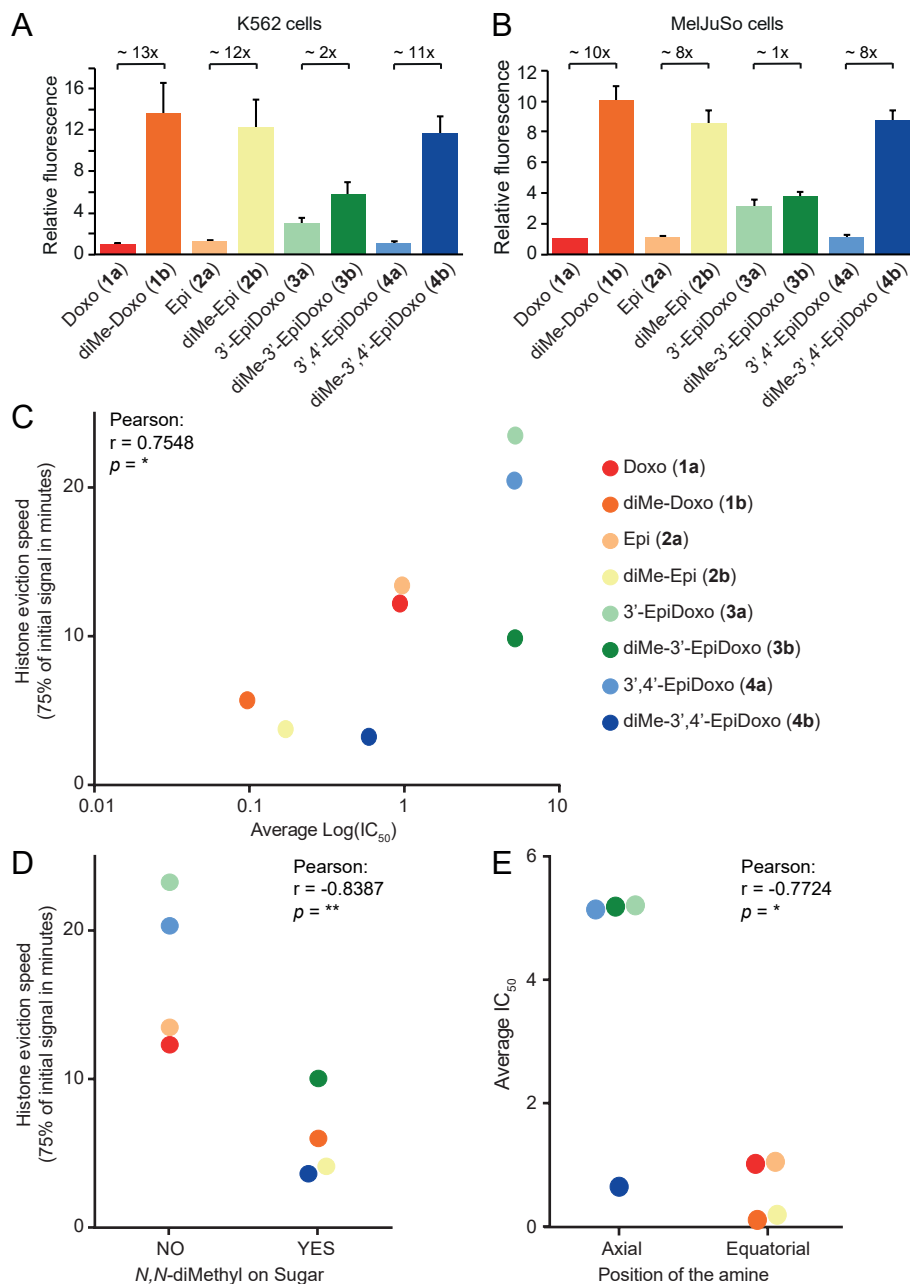


**Figure 4.** See legend on next page.

**Figure 4. Structure-function relationship of our library of (*N,N*)-dimethyldoxorubicin isomers.** (A and B) Uptake of the different isomers 2 hours post treatment with 1  $\mu$ M of the indicated compound for K562 (A) and MelJuSo (B) cells. Relative fluorescence to the parental compound doxorubicin is plotted for K562 and MelJuSo cells. Data is shown as mean  $\pm$  SD. (C) Histone eviction speed (the time at which 25% of the initial signal is reduced) is correlated with  $IC_{50}$  of the various doxorubicin isomers. (D) *N,N*-dimethylation of the sugar of the analogs enhances the histone eviction speed. (E) Equatorial positioning of the amine improves the cytotoxicity of the doxorubicin analogs. Two-tailed Pearson *r* correlation  $p = * < 0.05$ ,  $** < 0.01$ .

**4a).** Another critical factor for the effectiveness of drugs is their ability to enter the cell. Since all variants in this library are fluorescent, this could be easily determined by flow cytometry. K562 and MelJuSo cells were treated with compounds **1a/b** – **4a/b** and intracellular fluorescence was measured 2 hours post treatment (Figure 4A and B). Compounds **1b**, **2b** and **4b** all featuring the *N,N*-dimethyl are taken up much more efficiently than the corresponding primary amines, **1a**, **2a** and **4a**, respectively. This was not the case for **3a**, which was already taken up more efficiently than the other primary amine epimers. The difference in uptake with its dimethylated variant **3b** is small. Overall, it can be concluded that the cytotoxicity of the here studied anthracyclines is mainly determined by their histone eviction effectivity (Figure 4C and supplemental information Figure S3A), which strongly correlates to the rate of uptake of the compounds (Figure 4A and B). Compounds featuring an *N,N*-dimethyl moiety are more effective histone evictors (Figure 4D) and are therefore more cytotoxic than the corresponding compounds having a primary amine, while the orientation of the OH group at the 4' position has very little effect on cytotoxicity (supplemental information Figure S3A and B). Additionally, the stereochemistry of the fucose-carbon (C-3) bearing the amine functionality has a major influence on the  $IC_{50}$  values of the compounds *in vitro*. Compounds featuring an equatorial amine are the most effective (**1a/b**, **2a/b** and **4b**; Figure 4E).

## CONCLUSION

Despite the widespread use of doxorubicin in the clinic for the treatment of various cancers for several decades, its structure-activity relationship is still not fully understood. Although doxorubicin is a very effective anticancer drug, its use is limited by cumulative cardiotoxicity and treatment related secondary tumors. Chromatin damage by eviction of histones is a new mode of action of anthracyclines [9], which brings renewed interest to develop new doxorubicin analogs. We showed that the anthracyclines, *N,N*-dimethyldoxorubicin (**2b**) and aclarubicin, are unable to generate DNA breaks, yet induce chromatin damage via eviction of histones [10]. These compounds remain equally potent as doxorubicin, but without the induction of cardiotoxicity and secondary tumor formation. Here, we synthesized and tested a focused library of stereoisomers with respect to the 1,2-amino-alcohol characteristic for the daunosamine sugar within doxorubicin; and the four possible stereoisomers both as primary and tertiary (dimethylated) amines. Analysis of this focused library showed that doxorubicin isomers with the amine positioned axially have poor histone eviction activity and display limited cytotoxicity compared to their equatorial amine counterparts. The exception to this is **4b**, in which the sugar moiety has shown to undergo a ring-flip in solution. Possibly, this configuration, having an equatorial orientation of the amine as a result, causes the observed activities. Remarkably, the *N,N*-dimethylated variants showed strongly improved cellular uptake, some up to 10-fold, when compared to their non-methylated counterparts. How anthracyclines

are taken up by cells is unclear, but the *N,N*-dimethylation likely increases the basicity of the amine, and also the logP, both of which could influence diffusion over the hydrophobic cell membrane. The rate of histone eviction correlates strongly with the cellular uptake, which influences their cytotoxicity. Further chemical modifications of anthracyclines aimed at improving cellular uptake will help in achieving cytotoxicity at lower concentrations.

We have shown previously that *N,N*-dimethyldoxorubicin (**1b**) completely abolishes DNA double strand break formation while not affecting the ability to kill tumor cells, when compared to doxorubicin (**1a**), which does induce DNA damage [10]. This appears to be a general theme, as *N,N*-dimethylepirubicin (**2b**) also lacks DNA damage capacity and is more cytotoxic than epirubicin (**2a**). Because *N,N*-dimethylepirubicin (**2b**) displays potent anti-tumor activity *in vitro*, lacks DNA damage activity and therefore possibly also lacks cardiotoxicity and second tumor formation [10], it makes us believe this compound could be an attractive lead for further development towards novel, possibly more effective anthracyclines with limited side effects. More generally, we feel our results, based on the synthesis and evaluation of this focused library of close structural and stereochemical analogs, warrants the assessment of more such compound collections. These would feature, for instance, selected variations in the aglycon, in the sugar part (instead of stereoisomers as presented here also regio-isomers and/or glycosylated derivatives) and in the nature of the amine (next to methylation also other alkyl substituents). Evaluating the chemical space around old anticancer drugs can lead to the discovery of new activities and improvement of these drugs, as illustrated in this study.

## MATERIALS AND METHODS

### Chemicals

Doxorubicin and epirubicin were purchased from Accord Healthcare Limited, UK and etoposide from Pharmachemie, NL.

### Cell Culture

K562 cells (B. Pang, Stanford University, USA), HCT116 cells (T. van Hall, LUMC, The Netherlands), BXPC-3 cells (ATCC® CRL-1687), PC3 and DU145 cells (C. Robson, Newcastle University, UK), were maintained in RPMI-1640 medium supplemented with 8% FCS. A549 cells (R. Bernards, NKI, The Netherlands), FM3 cells (D. Peeper, NKI, The Netherlands), U87 MG (ATCC® HTB-14), U118 MG (ATCC® HTB-15), U2Os cells (ATCC® HTB-96), Hela cells (ATCC® CCL-2) and SKBR3 (R. Beijersbergen, NKI, The Netherlands), were maintained in DMEM medium supplemented with 8% FCS. BT474 cells (R. Beijersbergen, NKI, The Netherlands) were maintained in DMEM/F12 medium supplemented with 8% FCS. MelJuSo cells were maintained in IMDM medium supplemented with 8% FCS. MelJuSo cells stably expressing PAGFP-H2A were maintained in IMDM supplemented with 8% FCS and G-418, as described. Cell lines were maintained in a humidified atmosphere of 5% CO<sub>2</sub> at 37°C and regularly tested for the absence of mycoplasma.

### Western blot and constant-field gel electrophoresis (CFGE)

Cells were treated with drugs at indicated dose for 2 hours. Subsequently, drugs were removed by extensive washing and cells were collected and processed immediately for the assays. Cells were lysed directly in SDS-sample buffer (2%SDS, 10% glycerol, 5% β-mercaptoethanol, 60mM Tris-HCl pH 6.8 and 0.01% bromophenol

blue). Lysates were resolved by SDS-PAGE followed by Western blotting. Primary antibodies used for blotting:  $\gamma$ H2AX (1:1000, 05-036, Millipore),  $\beta$ -actin (1:10000, A5441, Sigma). DNA double strand breaks were quantified by constant-field gel electrophoresis as described [29]. Images were quantified using ImageJ software.

### **Microscopy**

PAGFP-H2A photoactivation and time-lapse confocal imaging were performed as described [9] on a Leica SP8 confocal microscope system, 63x lens, equipped with a climate chamber. Loss of fluorescence after different treatments was quantified using ImageJ software.

### **Cell viability assay**

Cells were seeded into 96-well plates. Twenty-four hours after seeding, cells were treated with indicated drugs for 2 hours. Subsequently, drugs were removed by extensive washing and cultured for an additional 72 hours. Cell viability was measured using a CellTiter-Blue viability assay (Promega). Relative survival was normalized to the untreated control and corrected for background signal.

### **Flow cytometry for measuring drug uptake in cells**

Cells were treated with 1  $\mu$ M of the indicated compounds for 2 hours. Samples were washed, collected and fixed with paraformaldehyde. Samples were analyzed by flow cytometry using BD FACS aria II, with 561 nm laser and 610/20nm detector. Data was analyzed using FlowJo software.

### **Quantification and statistical analysis**

Each experiment was assayed in triplicate, unless stated otherwise. All error bars denote SD. Statistical analyses was performed using Prism 8 software (GraphPad Inc.). Two-tailed Pearson analysis was used to determine correlations, ns, not significant, \* $p < 0.05$ , \*\* $p < 0.01$ .

‡ The stereochemical outcome of the glycosylations indicates that long-range participation of the *N*-Alloc group does not play a significant role in the studied glycosylations [30,31].

### **ACKNOWLEDGEMENTS**

This work was supported by grants from the Dutch Cancer Society KWF (JN) and by the Institute for Chemical Immunology, an NWO Gravitation project funded by the Ministry of Education, Culture and Science of the Netherlands to HO and JN.

### **CONFLICTS OF INTEREST**

J. Neefjes is a shareholder in NIHM that aims to produce aclarubicin for clinical use.

### **REFERENCES**

- 1 Grand View Research (2016) Doxorubicin Market By Application (Ovarian, Multiple Myeloma, Kaposi Sarcoma, Leukemia, Bone Sarcoma, Breast, Endometrial, Gastric, Liver, Kidney, Other Cancers) And Segment Forecasts, 2018 - 2024.
- 2 Lefrak EA, Pi'tha J, Rosenheim S & Gottlieb JA (1973) A clinicopathologic analysis of adriamycin cardiotoxicity. *Cancer* 32, 302–314.
- 3 Krohn K (2008) Anthracycline Chemistry and Biology I Biological Occurrence and

Biosynthesis, Synthesis and Chemistry (H. Balzani, V.; de Meijere, A.; Houk, K. N.; Kessler, H.; Lehn, J.-M.; Ley, S.V.; Schreiber, S. L.; Thiem, J.; Trost, B.M.; Vögtle, F.; Yamamoto, ed.) Springer Verlag.

4 Weiss RB (1992) The anthracyclines: will we ever find a better doxorubicin? *Semin Oncol* 19, 670–686.

5 Booser DJ & Hortobagyi GN (1994) Anthracycline Antibiotics in Cancer Therapy. *Drugs* 47, 223–258.

6 Mele D, Nardoza M, Spallarossa P, Frassoldati A, Tocchetti CG, Cadeddu C, Madonna R, Malagù M, Ferrari R & Mercuro G (2016) Current views on anthracycline cardiotoxicity. *Heart Fail Rev* 21, 621–634.

7 Launchbury AP, Habboubi N, Paul Launchbury A, Habboubi N, Launchbury AP & Habboubi N (1993) Epirubicin and doxorubicin: a comparison of their characteristics, therapeutic activity and toxicity. *Cancer Treat Rev* 19, 197–228.

8 Nitiss JL (2009) Targeting DNA topoisomerase II in cancer chemotherapy. *Nat Rev Cancer* 9, 338–350.

9 Pang B, Qiao X, Janssen L, Velds A, Groothuis T, Kerkhoven R, Nieuwland M, Ovaa H, Rottenberg S, van Tellingen O, Janssen J, Huijgens P, Zwart W & Neefjes J (2013) Drug-induced histone eviction from open chromatin contributes to the chemotherapeutic effects of doxorubicin. *Nat Commun* 4, 1–13.

10 Qiao X, van der Zanden SY, Wander DPA, Borràs DM, Song J-Y, Li X, van Duikeren S, van Gils N, Rutten A, van Herwaarden T, van Tellingen O, Giacomelli E, Bellin M, Orlova V, Tertoolen LGJ, Gerhardt S, Akkermans JJ, Bakker JM, Zuur CL, Pang B, Smits AM, Mummery CL, Smit L, Arens R, Li J, Overkleeft HS & Neefjes J (2020) Uncoupling DNA damage from chromatin damage to detoxify doxorubicin. *Proc Natl Acad Sci* 117, 15182–15192.

11 Pang B, de Jong J, Qiao X, Wessels LFA & Neefjes J (2015) Chemical profiling of the genome with anti-cancer drugs defines target specificities. *Nat Chem Biol* 11, 472–480.

12 Wander DPA, van der Zanden SY, van der Marel GA, Overkleeft HS, Neefjes J & Codée JDC (2020) Doxorubicin and Aclarubicin: Shuffling Anthracycline Glycans for Improved Anticancer Agents. *J Med Chem* 63, 12814–12829.

13 Kulikowski T, Bretner M, Najda A & Cova L (2006) New Derivatives of Epirubicin, their Medicinal Application and Pharmaceutically Acceptable Forms of Drugs. .

14 Arlandini, Vigevani & Arcamone (1980) Interaction of new derivatives of daunorubicin and doxorubicin with DNA. Part II. *Farm Ed Sci* 35, 65–78.

15 Yu B (2018) Gold(I)-Catalyzed Glycosylation with Glycosyl o-Alkynylbenzoates as Donors. *Acc Chem Res* 51, 507–516.

16 Wander DPA (2019) Understanding Anthracyclines: Synthesis of a Focused Library of Doxorubicin/Aclarubicin - Inspired Structures. .

17 Fan E, Shi W & Lowary TL (2007) Synthesis of Daunorubicin Analogues Containing Truncated Aromatic Cores and Unnatural Monosaccharide Residues. *J Org Chem* 72, 2917–2928.

18 Noshita T, Sugiyama T, Kitazumi Y & Oritani T (1995) Reinvestigation of Phenolic Ferrier Reaction: Selective Synthesis of Aryl O- $\Delta^2$  -Glycosides. *Biosci Biotechnol Biochem* 59, 2052–2055.

19 Ma Y, Li Z, Shi H, Zhang J & Yu B (2011) Assembly of digitoxin by gold(I)-catalyzed glycosidation of glycosyl o-alkynylbenzoates. *J Org Chem* 76, 9748–9756.

20 Renneberg B, Li Y-M, Laatsch H & Fiebig H-H (2000) A short and efficient transformation of rhamnose into activated daunosamine, acosamine, ristosamine and epi-daunosamine derivatives, and synthesis of an anthracycline antibiotic acosaminyl- $\epsilon$ -



iso-rhodomyacinone. *Carbohydr Res* 329, 861–872.

21 Horton D & Weckerle W (1975) A preparative synthesis of 3-amino-2,3,6-trideoxy-l-lyxo-hexose (daunosamine) hydrochloride from d-mannose. *Carbohydr Res* 44, 227–240.

22 Hansen T, Lebedel L, Remmerswaal WA, van der Vorm S, Wander DPA, Somers M, Overkleeft HS, Filippov D V., Désiré J, Mingot A, Bleriot Y, van der Marel GA, Thibaudeau S & Codée JDC (2019) Defining the SN1 Side of Glycosylation Reactions: Stereoselectivity of Glycopyranosyl Cations. *ACS Cent Sci* 5, 781–788.

23 Romero JAC, Tabacco SA & Woerpel KA (2000) Stereochemical Reversal of Nucleophilic Substitution Reactions Depending upon Substituent: Reactions of Heteroatom-Substituted Six-Membered-Ring Oxocarbenium Ions through Pseudoaxial Conformers. *J Am Chem Soc* 122, 168–169.

24 Ayala L, Lucero CG, Romero JAC, Tabacco SA & Woerpel KA (2003) Stereochemistry of Nucleophilic Substitution Reactions Depending upon Substituent: Evidence for Electrostatic Stabilization of Pseudoaxial Conformers of Oxocarbenium Ions by Heteroatom Substituents. *J Am Chem Soc* 125, 15521–15528.

25 Zeng J, Sun G, Yao W, Zhu Y, Wang R, Cai L, Liu K, Zhang Q, Liu X-W & Wan Q (2017) 3-Aminodeoxypyranoses in Glycosylation: Diversity-Oriented Synthesis and Assembly in Oligosaccharides. *Angew Chemie Int Ed* 56, 5227–5231.

26 Garro-Helion F, Merzouk A & Guibé F (1993) Mild and selective palladium(0)-catalyzed deallylation of allylic amines. Allylamine and diallylamine as very convenient ammonia equivalents for the synthesis of primary amines. *J Org Chem* 58, 6109–6113.

27 Bartner P, Boxler DL, Brambilla R, Mallams AK, Morton JB, Reichert P, Sancilio FD, Surprenant H, Tomalesky G, Lukacs G, Olesker A, Thang TT, Valente L & Omura S (1979) The megalomicins. Part 7. A structural revision by carbon-13 nuclear magnetic resonance and X-ray crystallography. Synthesis and conformational analysis of 3-dimethylamino- and 3-azido- D - and - L -hexopyranosides, and the crystal structure of 4"-O-(4-Iodobenzoyl)megalomicin A. *J Chem Soc, Perkin Trans 1* 0, 1600–1624.

28 Kuo LJ & Yang LX (2008)  $\gamma$ -H2AX- A novel biomarker for DNA double-strand breaks. *In Vivo (Brooklyn)* 22, 305–310.

29 Olive PL, Wlodek D & Banáth JP (1991) DNA double-strand breaks measured in individual cells subjected to gel electrophoresis. *Cancer Res* 51, 4671–6.

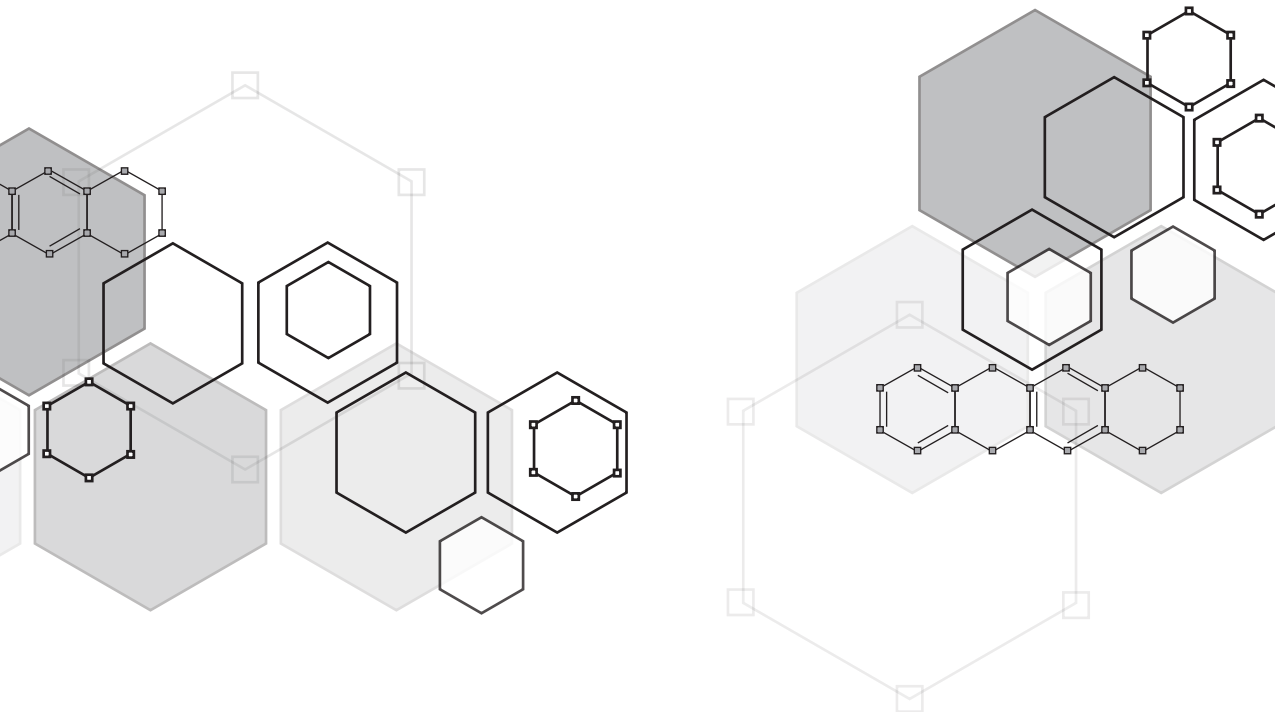
30 Hansen T, Elferink H, van Hengst JMA, Houthuijs KJ, Remmerswaal WA, Kromm A, Berden G, van der Vorm S, Rijs AM, Overkleeft HS, Filippov D V, Rutjes FPJT, van der Marel GA, Martens J, Oomens J, Codée JDC & Boltje TJ (2020) Characterization of Glycosyl Dioxolenium Ions and Their Role in Glycosylation Reactions. *Nat Commun* 11, 1–9.

31 Komarova BS, Tsvetkov YE & Nifantiev NE (2016) Design of  $\alpha$ -Selective Glycopyranosyl Donors Relying on Remote Anchimeric Assistance. *Chem Rec* 16, 488–506.



SUPPLEMENTAL  
INFORMATION

5



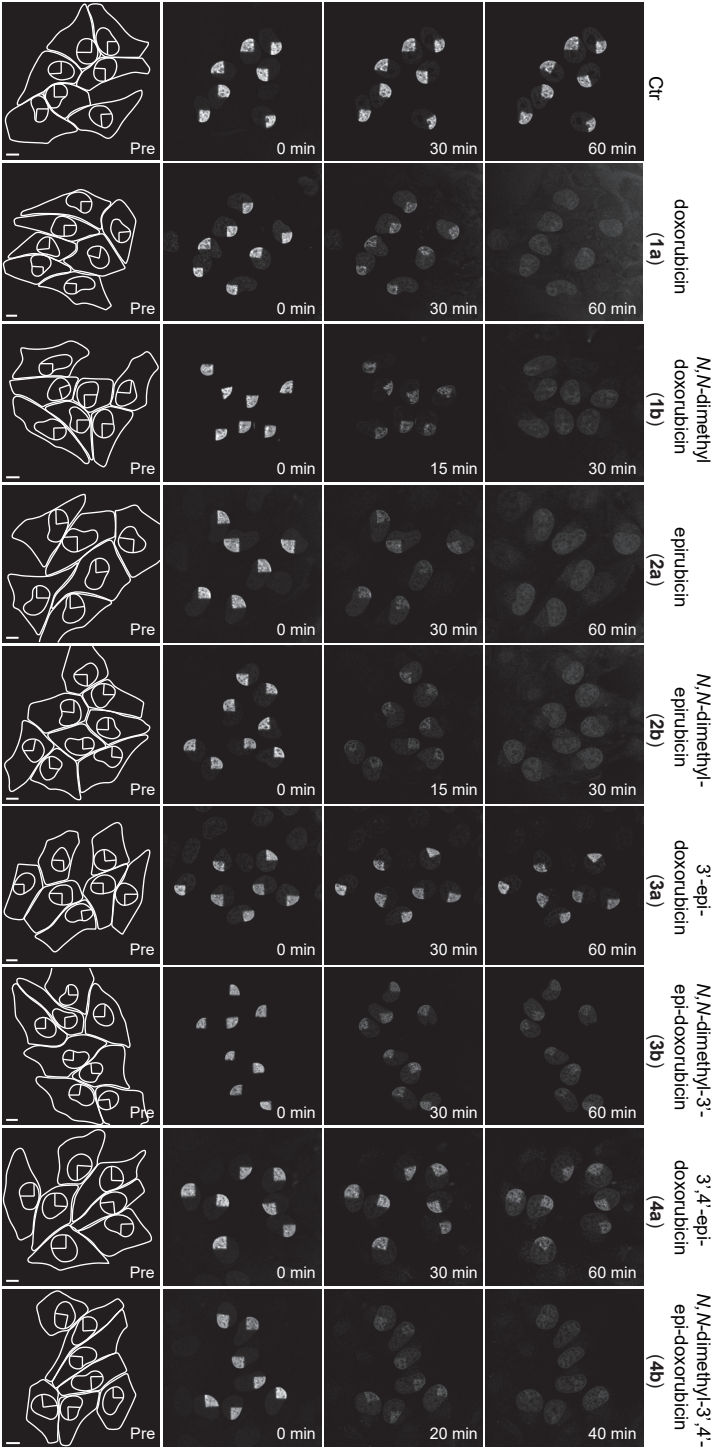


**Figure S1. Chromatin damage is induced by the different doxorubicin isomers.** Part of the nucleus of MelJuSo cells stably expressing PAGFP-H2A was photo-activated and histone eviction was measured by time-lapse confocal microscopy upon administration of 10  $\mu$ M of the indicated compounds. Lines in the left panel define the cytoplasm, nucleus and activated region of the nucleus before treatment. Stills at indicated time points from time-lapse experiment are shown. Scale bar, 10  $\mu$ m

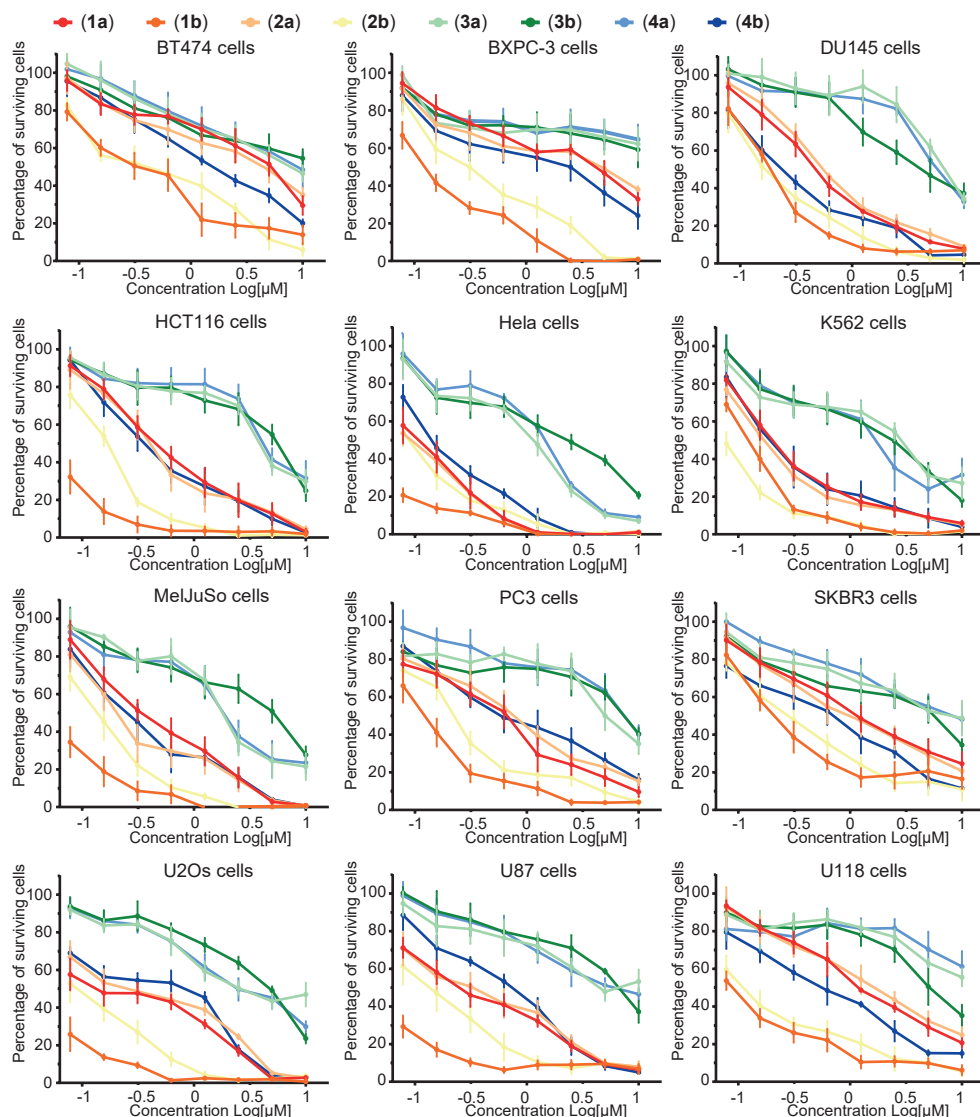


**Figure S2. Cytotoxic effect in different tumor cell lines of the doxorubicin isomers.** Indicated tumor cells were treated for 2 hours with different doses of the indicated doxorubicin isomers followed by drug removal. Cell viability was measured by a CellTiter-Blue assay 72 hours post treatment. Data is shown as mean  $\pm$  SD from four different experiments.

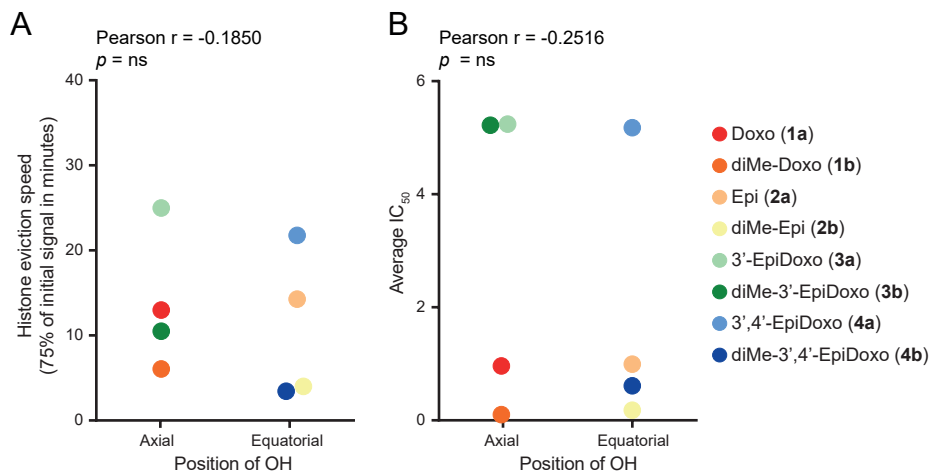
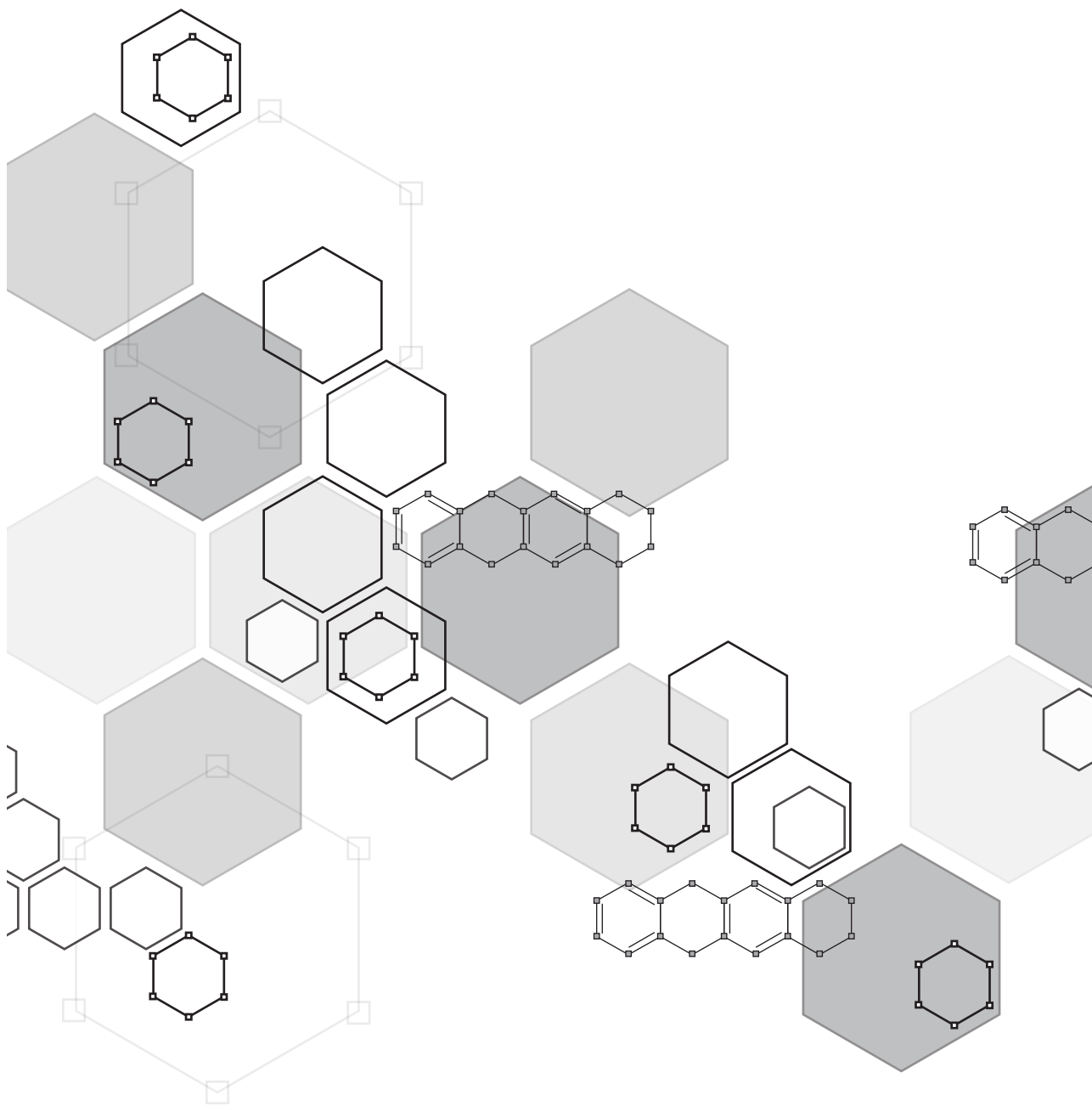


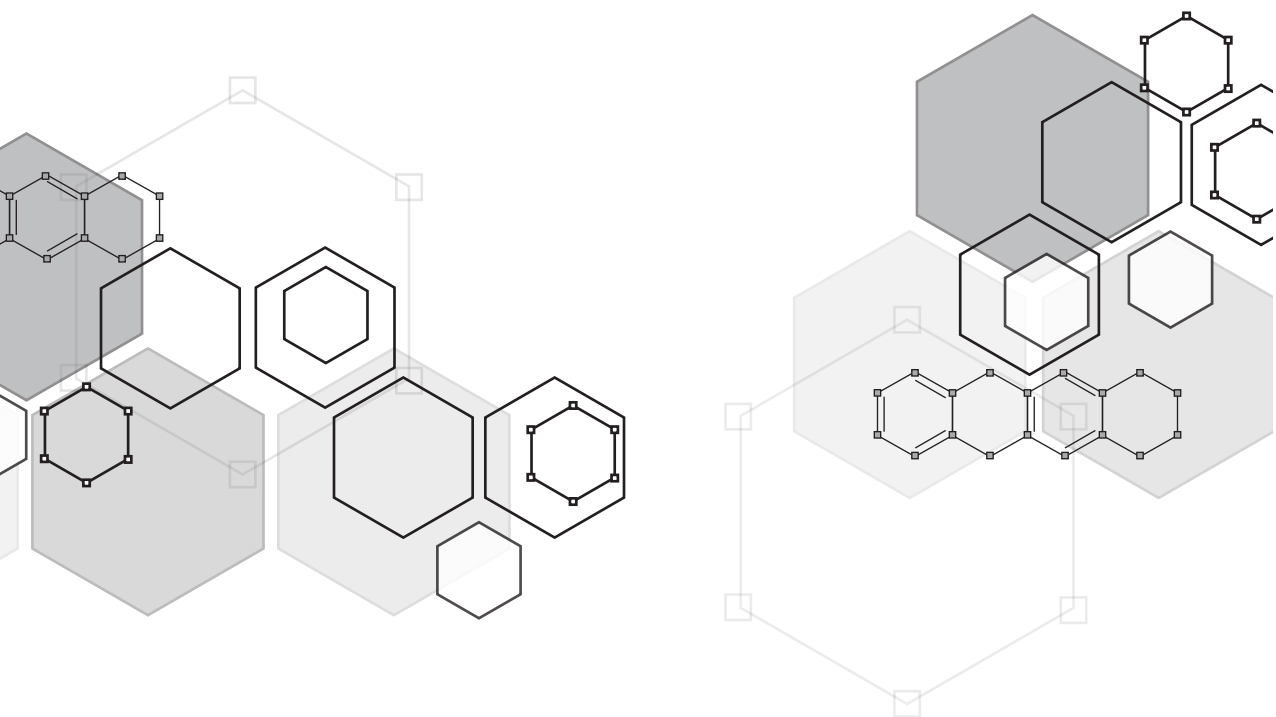
**Figure S3. The position of the OH has little effect on the effectivity of the doxorubicin isomers.** (A and B) The position of the hydroxyl group of the doxorubicin isomers was correlated with the rate of histone eviction (A) and cytotoxicity (B). Two-tailed Pearson  $r$  correlation  $ns$ ; not significant.





Exploring the chemical  
space around the 3' amine  
of doxorubicin for improved  
cytotoxic drugs with  
different genomic specificity

6



Sabina Y. van der Zanden, Feija L. Hamoen, Daniel Borràs, Dennis P. A. Wander, Herman S. Overkleeft, Jeroen D. C. Codée, Baoxu Pang, Jacques Neefjes

*Manuscript in preparation*



**ABSTRACT**

The anthracycline drug doxorubicin is a very effective anticancer drug for different types of solid and hematological tumors. However, treatment coincides with severe adverse effects. Although hundreds of anthracycline analogs are either isolated from natural or mutant sources, or prepared via organic synthesis with the aim to find novel anticancer therapies without toxicities, limited drugs made it into clinic. Therefore, a better understanding of the molecular mechanism of actions, and a clear structure-function relationship for these drugs would benefit the search for new therapies. Recently, chromatin damage via eviction of histones was discovered as a novel mechanism of action, and we have shown that the amino sugar is important for this activity. Based on this new knowledge, we synthesized and evaluated a set of doxorubicin analogs varying at the 3' position, to further investigate the structure-function relationship of the anthracyclines. We show that the bulky tertiary amine at the 3' position is responsible for the effective histone evicting activity, which correlates with low  $IC_{50}$  values in various tumor cell lines. On the contrary, the absence of the amine at this position result in effective DNA damaging compounds without chromatin damage activity. Furthermore, by chemically modifying the amino sugar of doxorubicin, the genomic locations of these drugs, in terms of chromatin damage and/or targeting topoisomerase II $\alpha$ , are also altered. The chemical space around the 3' position of doxorubicin's sugar moiety includes variants with higher cytotoxicity and a different genomic selectivity than their parental drug.

**INTRODUCTION**

Anthracycline drugs, including doxorubicin, belong to the most used and effective anticancer drugs. However, treatment containing these drugs is plagued by severe adverse effect [1, 2]. To overcome these side effects, thousands of anthracycline analogs have been made with the aim to develop effective treatment with limited toxicity, but only few drugs have entered the clinic [3]. For decades, formation of DNA double-strand breaks via interference with the catalytic cycle of topoisomerase II $\alpha$  (Topo II $\alpha$ ) was considered the major mechanism of action of these drugs [4]. Recently, a second mechanism of action was discovered, namely, chromatin damage via eviction of histones [5-7]. We showed that chromatin damage is a major mechanism by which these drugs initiate tumor cell killing, since analogs only able to evict histones are also effective anticancer drugs *in vitro* and *in vivo* [8]. In addition, separation of these two activities resulted in drugs with reduced toxicity. This novel insight can help in the development of new anthracycline analogs for improved cancer therapy. Further data suggest, that the modification, position and orientation of the amine on the sugar moiety of these anthracycline drugs are responsible for its combined biological activity [9, 10]. Methylation and the equatorial position of the amine enhances both cellular uptake and histone eviction efficiency [9, 10]. Having a tertiary amine in the equatorial position thereby significantly enhances the cytotoxicity of these compounds. To further investigate the molecular mode of action of these drugs, we decided to synthesize an extended set of doxorubicin analogs and study their biological activity and function. These analogs can be divided into three subsets: 1. doxorubicin and its dimethylated analogs; 2. non-basic analogs to study the presence of the amine on the 3' position; and 3. cyclic-doxorubicin analogs to extent the variation of the tertiary amine features.

In line with previous data [9, 10], all four cyclic-doxorubicin analogs are very effective histone evictors abstained from the DNA damage capacity, with  $IC_{50}$  values in the

nanomolar range in multiple tumor cell lines. The opposite observation was made for the non-basic analogs, being effective DNA damage inducers without the ability to induce chromatin damage. These compounds are also less effective anticancer drugs *in vitro*. Nevertheless, all doxorubicin variants in this set are capably of re-localizing Topo II $\alpha$ .

An unconsidered feature of anthracycline drugs is the genomic location where they are active. Earlier studies showed that daunorubicin induced histone eviction at distinct genomic areas from those targeted by aclarubicin [5, 7]. Therefore, here we evaluated the genomic selectivity of both the Topo II $\alpha$  targeting and the site of histone eviction of the new set of analogs and identify doxorubicin variants with distinct genome specificity.

In summary, the modification of the sugar moiety at the 3' position is important for the biological activity of the anthracycline drugs. In addition, the different doxorubicin analogs show distinct genomic selectivity for their Topo II $\alpha$  targeting and chromatin damage activity. Exploring the chemical space around doxorubicin leads to novel insights allowing further improvement of this old anticancer drug.

## RESULTS

### Evaluating the biological activity of the doxorubicin analogs

To further understand the molecular mode of action of anthracycline drugs, we synthesized and tested a new set of 3' analogs of doxorubicin (Figure 1). Based on the previous data [8-10], we included three non-basic doxorubicin variants to study the function of the 3' amine, and four cyclic-doxorubicin analogs to determine the role of other tertiary amine variants. To investigate the capacity of these doxorubicin analogs to induce DNA damage, we treated K562 cells for 2 hour with the indicated drugs and visualized DNA double-strand break formation indirectly by detecting  $\gamma$ H2AX by Western Blot (Figure 2A and B), and directly using constant-field gel electrophoresis (Figure 2C and D). Besides dimethylation of the amino sugar, other

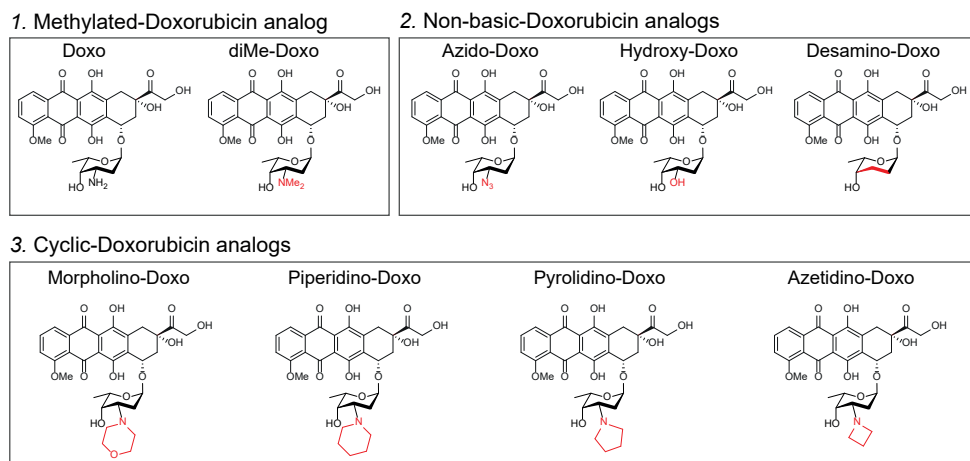


**Figure 1. Structure of doxorubicin analogs.** The different doxorubicin analogs can be subdivided into three groups: 1. Doxorubicin and *N,N*-dimethyl-doxorubicin (*diMe-Doxo*), 2. The non-basic doxorubicin analogs and 3. The cyclic-doxorubicin analogs. In red structural differences compared to doxorubicin are indicated.

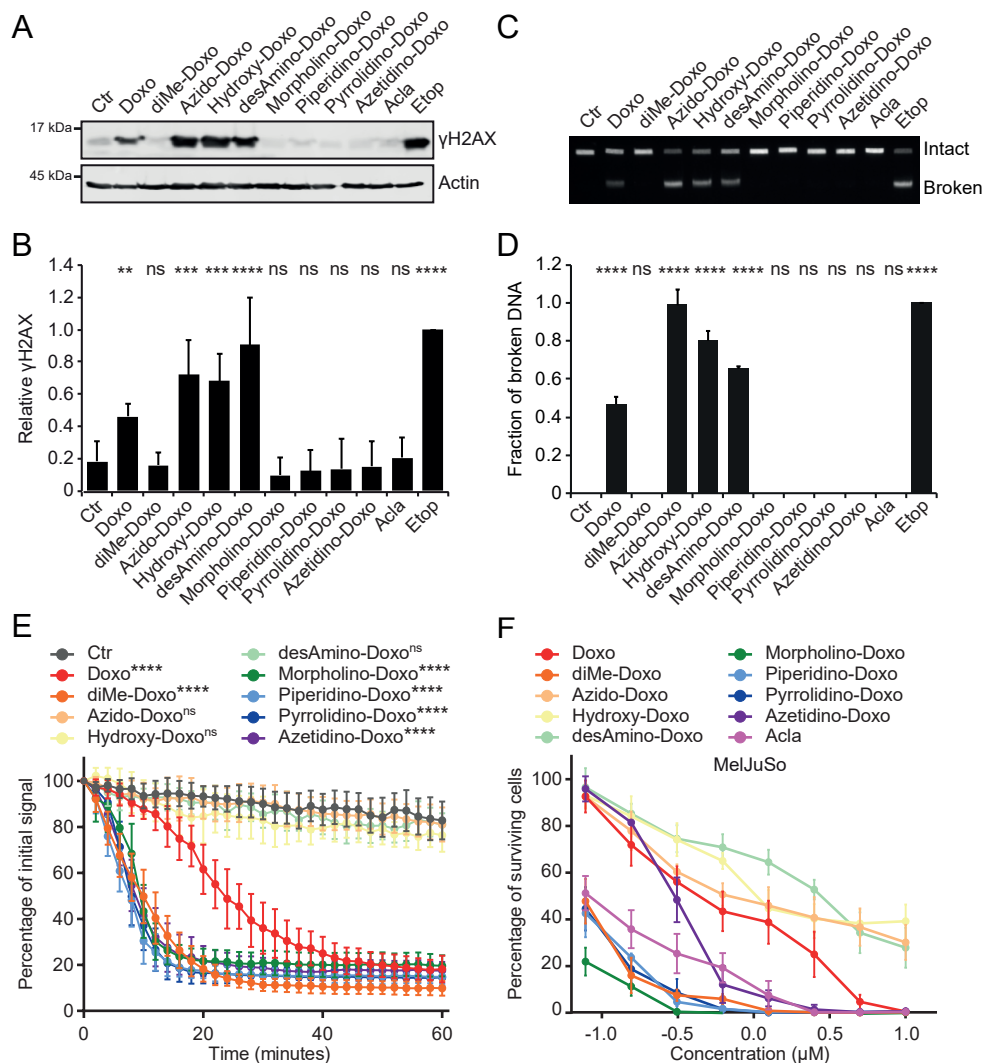


**Figure 2. Biological evaluation of the doxorubicin analogs.** (A) K562 cells are treated for 2 hours with 10 $\mu$ M of the indicated drugs. DNA double strand breaks are visualized by  $\gamma$ H2AX levels by Western Blot. Etoposide (Etop) and aclarubicin (Acla) were used as positive and negative control, respectively. Actin was used as a loading control. (B) Quantification of A. Results are presented as mean  $\pm$  SD of three independent experiments. Ordinary one-way ANOVA with Dunnett's multiple comparison test; ns, not significant, \*\* $P$  < 0.01, \*\*\* $P$  < 0.001, \*\*\*\* $P$  < 0.0001. (C) K562 cells are treated for 2 hours with 10 $\mu$ M of the indicated drugs. DNA break formation by the various analogs was directly analyzed by CFGE. The position of intact and broken DNA is indicated. (D) Quantification of the fraction of broken DNA relative to Etop. Results are presented as mean  $\pm$  SD of three independent experiments. Ordinary one-way ANOVA with Dunnett's multiple comparison test; ns, not significant, \*\*\*\* $P$  < 0.0001. (E) Quantification of histone eviction measured as PAGFP-H2A release from photo-activated nuclear regions after administration of 10 $\mu$ M of the indicated doxorubicin analogs. Ordinary one-way ANOVA with Dunnett's multiple comparison test; ns, not significant, \*\*\*\* $P$  < 0.0001.

**Figure 2. Continued.** (F) Cytotoxicity of the different doxorubicin analogs in MelJuSo cells. Cells were treated for 2 hours with the indicated concentrations followed by drug removal. Cell survival was determined 72 hours post drug removal using CellTiter-Blue assay. Data is shown as mean  $\pm$  SD of three independent experiments.

tertiary amine substitutions, as presented in the cyclic-doxorubicin analogs, are also abolished from their DNA damage activity. The three non-basic variants lacking the 3' amine are effective DNA damaging compounds. We then continued to investigate the histone eviction capacity of the doxorubicin variants. To do so, we followed the fluorescence intensity of photo-activated GFP-H2A histones (PAGFP-H2A) in MelJuSo cells upon treatment with the different drugs (Figure 2E and Figure S1). All analogs containing a tertiary amine at the 3' position were effective histone evicting compounds compared to their parental drug, while the non-basic compounds were unable to evict histones. We have thus generated doxorubicin analogs that either effectively induce DNA damage without evicting histones (Azido-Doxo, Hydroxy-Doxo and Desamino-Doxo), or variants that are unable to induce DNA double-strand breaks while being effective histone evictors (diMe-Doxo, Morpholino-Doxo, Piperidino-Doxo, Pyrolydino-Doxo and Azetidino-Doxo). This indicates that the absence/presence of a tertiary amine at the 3' position determines the DNA- and chromatin damage activities of the doxorubicin analogs.

### Cytotoxicity of the doxorubicin analogs

Earlier, we showed that the effectivity of histone eviction correlated with the cytotoxicity of the compounds *in vitro* [9, 10]. Therefore, we continued to test the anticancer potential of the newly synthesized doxorubicin analogs. MelJuSo cells were treated for 2 hours with different concentrations of the various drugs, and cell viability was determined 72 hours post treatment using CellTiter-Blue. Again, the compounds with chromatin damage activity are more cytotoxic, while the non-basic doxorubicin variants (with DNA damage activity only) are the least effective anticancer drugs (Figure 2F). The cyclic-doxorubicin analogs Morpholino-Doxo, Piperidono-Doxo and Pyrolydino-Doxo were even more cytotoxic than their parental drug doxorubicin or aclarubicin, tested in 14 tumor cell lines (Table 1 and Figure S2A). In line with previous data, the histone eviction effectivity strongly correlates with cytotoxicity for this set of doxorubicin analogs (Figure S2B).

### Genomic selectivity for the chromatin damage activity of the doxorubicin variants

Histone eviction by the anthracyclines daunorubicin and aclarubicin occurs in different epigenomic regions of the genome, effectively defining anthracycline drugs as region-specific epigenetic modifiers [7]. The released histones are degraded and replaced by new nascent histones, resulting in epigenomic and transcriptional changes [5, 7]. We hypothesize that this genomic specificity is determined by features within the anthracycline structure. Therefore, we assessed the different drugs for their genomic location of histone eviction. To address this, we performed ATAC-sequencing (ATAC-seq) on K562 cells treated with doxorubicin, the clinically used doxorubicin homologues daunorubicin and epirubicin, aclarubicin, amrubicin, the most cytotoxic doxorubicin isomeric analog diMe-Epi [10], and the newly synthesized doxorubicin analogs that showed chromatin damage activity (Figure 3A). ATAC-seq identifies open chromatin segments, which include histone-evicted regions [11, 12]. Overall genomic regions showing drug-specific ATAC-seq signals for the different

IC <sub>50</sub> (μM) Cells	Doxo	diMe- Doxo	Azido- Doxo	Hydroxy- Doxo	desAmino- Doxo	Morpholino- Doxo	Piperidino- Doxo	Pyrolidino- Doxo	Azetidino- Doxo	Acla
A549	0.408	< 0.078	0.902	2.927	7.723	0.098	0.070	0.042	0.191	0.048
BT474	5.765	0.516	> 10.0	> 10.0	> 10.0	0.194	0.197	0.221	0.741	0.375
BXPC3	3.818	0.193	7.998	> 10.0	> 10.0	0.099	0.118	0.211	0.591	0.289
DU145	0.566	0.282	0.346	1.295	3.106	0.079	0.187	0.291	0.832	0.350
FM3	0.601	< 0.078	3.022	6.094	9.742	0.119	0.107	0.093	0.136	0.083
HCT116	0.666	0.103	0.872	1.746	5.210	0.079	0.136	0.099	0.300	0.110
HeLa	0.149	0.075	0.405	1.054	3.770	0.065	0.128	0.094	0.239	0.179
K562	0.346	0.122	0.636	0.849	1.049	0.064	0.150	0.100	0.302	0.532
MelJuSo	0.523	0.073	1.224	1.904	2.430	0.051	0.078	0.073	0.297	0.099
PC3	0.829	0.166	0.888	2.786	8.294	0.033	0.120	0.189	0.532	0.225
SKBR3	1.449	0.251	> 10.0	8.892	> 10.0	0.069	0.164	0.215	0.733	0.418
U2Os	0.339	0.056	> 10.0	6.793	> 10.0	0.077	0.105	0.122	0.159	0.209
U87	0.455	< 0.078	2.032	> 10.0	9.468	0.058	0.048	0.041	0.103	0.112
U118	1.152	0.080	1.758	5.217	8.708	0.067	0.080	0.126	0.091	0.188

**Table 1. Cytotoxicity of the different doxorubicin analogs *in vitro*.** Color code table of IC<sub>50</sub> values of the different doxorubicin analogs in various tumor cell lines *in vitro*. Cells were treated for 2 hours with the indicated concentrations followed by drug removal. Cell survival was determined 72 hours post drug removal using CellTiter-Blue assay. Grey bars indicate that IC<sub>50</sub> values are either higher or lower than the concentration tested.

compounds nicely separates the histone evicting drugs from amrubicin (only DNA damage activity) and the untreated sample, which is illustrated by a principle component analysis (PCA; Figure 3B). When we further filter the called peaks for the control peaks (Figure S3A) and plotted the fold change of upregulated peaks compared to untreated samples (Figure 3C) the drugs were separated in three groups; i. no histone eviction (ctr and amrubicin), ii. the analogs capable of both eviction of histones and DNA damage activity (doxorubicin, daunorubicin and epirubicin), and iii. the analogs with effective histone eviction activity only (aclarubicin, diMe-Epi, diMe-Doxo, Morpho-doxo, Piperidino-doxo, Pyrolidino-doxo, Azetidino-doxo). All analogs featuring a tertiary amine at the 3' position of the sugar moiety are clustered by principle component 1, where aclarubicin (which has a different aglycon, and two additional sugar moieties) is most separated from the other doxorubicin analogs by principle component 2 (Figure 3C and S3B). However, the other doxorubicin variants also show some dispersion for principle component 2. A more detailed analyses is required to define the exact regions targeted by the various drugs, but, redirecting the various anthracycline analogs to different genomic regions is possible by modifying the 3' amino sugar.

### Genomic selectivity of topoisomerase IIα targeting

The classical mechanism of action of the anthracycline drugs, is poisoning the catalytic cycle of Topo IIα, and thereby inducing DNA damage. Therefore we wondered whether the new doxorubicin analogs also target Topo IIα in specific regions in the genome; and if so, can we determine the structural features that might be responsible for this function? To test this, the nuclear localization of GFP-tagged Topo IIα was followed using time-laps confocal microscopy upon treatment with the different drugs. At steady state, Topo IIα is localized in the nucleus where it accumulates in nucleoli, but upon treatment the protein rapidly re-localized (Figure 4A and B, and Figure S4). While re-localization was observed for doxorubicin as well as all the other analogs, localizations of Topo IIα was different upon treatment with the doxorubicin variants.

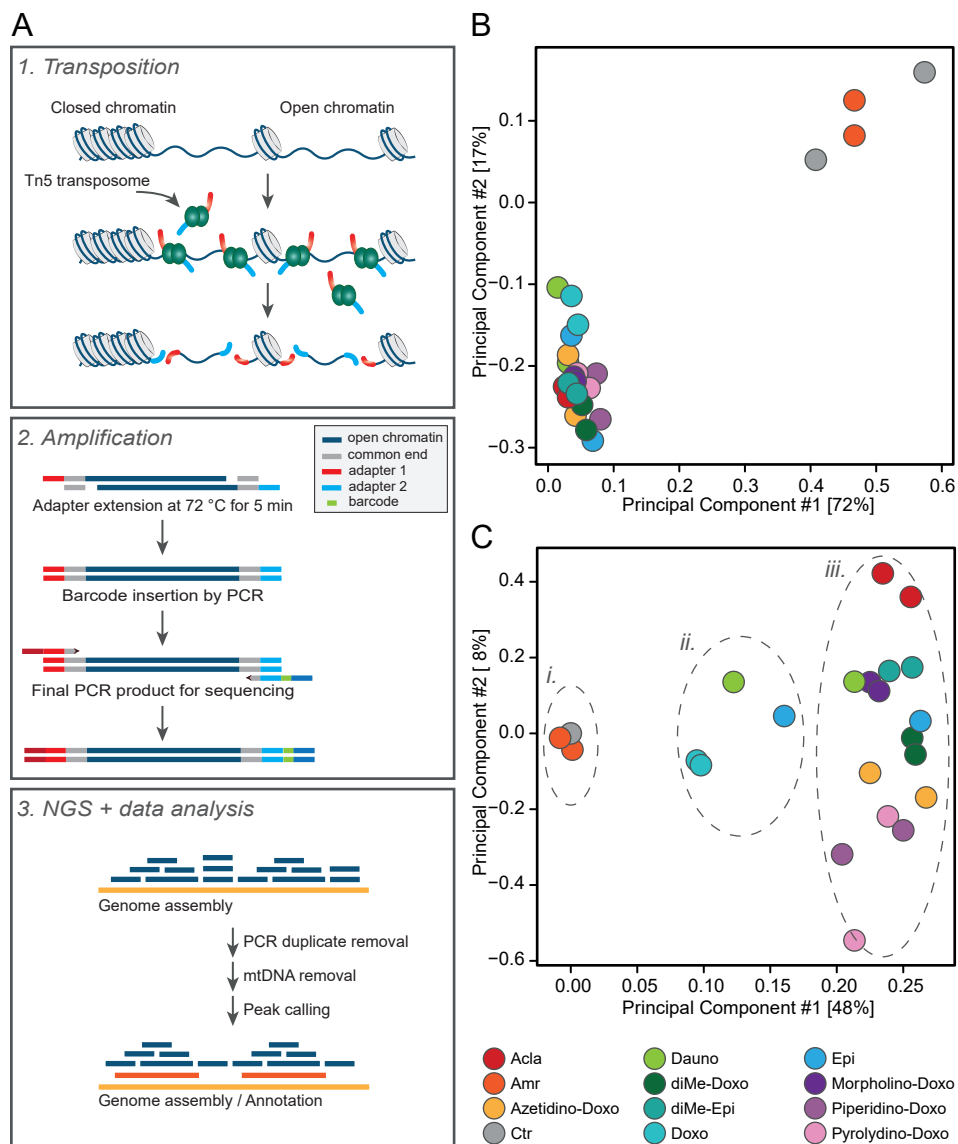


**Figure 3. Doxorubicin analogs evict histones in unique genomic regions.** (A) Schematic representation of the ATAC-seq workflow: 1. The Tn5 transposome is able to access open chromatin regions and introduce its preloaded NGS adapters, thereby generating the ATAC-seq library. 2. After DNA purification, the adapters are extended and barcodes are inserted using PCR to prepare the library for sequencing. 3. The resulting DNA can be analyzed by qPCR and/or next generation sequencing (NGS). PCR duplicates and mitochondrial DNA (mtDNA) were removed using different bioinformatic packages after which the genomic locations of the open chromatin can be identified. (B) Principle Component Analysis (PCA) of total ATAC-seq peak calls, overall signal (RPKM counts) no filters were applied. (C) PCA of the fold change of upregulated peaks compared to ctr. Separation of the drugs in three groups; i. no histone eviction (ctr and amrubicin), ii. the analogs capable of both histone eviction and DNA damage



**Figure 3. Continued (C).** activity (doxorubicin, daunorubicin and epirubicin), iii. the analogs with effective histone evicting activity only (Acla, diMe-Epi, diMe-Doxo, morpho-doxo, piperidino-doxo, pyrrolidino-doxo, azetidino-doxo). ATAC-seq peak calls were extracted with the ENCODE ATAC-seq analysis pipeline.

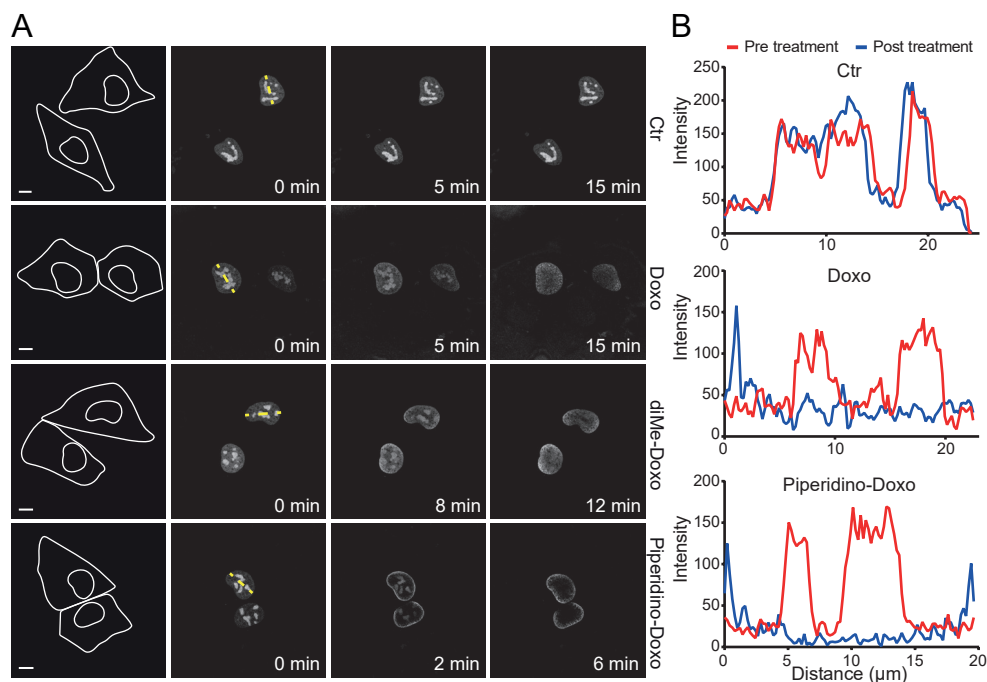


**Figure 4. Topoisomerase II $\alpha$  relocalization.** Relocalization of GFP-Topo II $\alpha$  transiently expressed in MelJuSo cells. (A) Cells are treated with 10  $\mu$ M of the indicated doxorubicin analogs and followed over time. Lines in the left panel define the cytoplasm and nucleus. Stills at indicated time points from time-laps experiment are shown. Scale bar, 10  $\mu$ m. (B) Pixel plot of the GFP signal pre- and post treatment with the drugs. Plotted as fluorescence over distance of dotted yellow line as marked in (A).

Especially the cyclic-doxorubicin analogs targeted the protein to the outer side of the nucleus, compared to the other analogs, which re-mobilized Topo II $\alpha$  more equal over the whole nucleus. To determine, at a higher resolution, the genomic location of Topo II $\alpha$  trapped by the various analogs, we generated an endogenous 3xFLAG-tagged Topo II $\alpha$  K562 cell line (Figure S5). Subsequently, these cells were treated with the different drugs and analyzed by ChIP-sequencing (ChIP-seq; Figure 5A). The overall ChIP-seq signal revealed three main drug clusters, which is illustrated by PCA of the total ChIP-seq peaks called (Figure 5B). The first cluster (*i.*) constitutes mainly of analogs able to induce both DNA- and chromatin damage, and the non-basic doxorubicin analogs with DNA damage activity only. The second group (*ii.*) is formed by aclarubicin and most of the doxorubicin analogs that are very effective histone evictors (all featuring a tertiary amine at the 3' position), while amrubicin, the structurally unrelated Topo II $\alpha$  inhibitor etoposide, and the untreated control sample form the third group (*iii.*). When called peaks are filtered for ctr peaks, the third cluster formed by the untreated cells, etoposide and amrubicin disappeared, indicating that both etoposide and amrubicin target Topo II $\alpha$  at the location where the enzyme



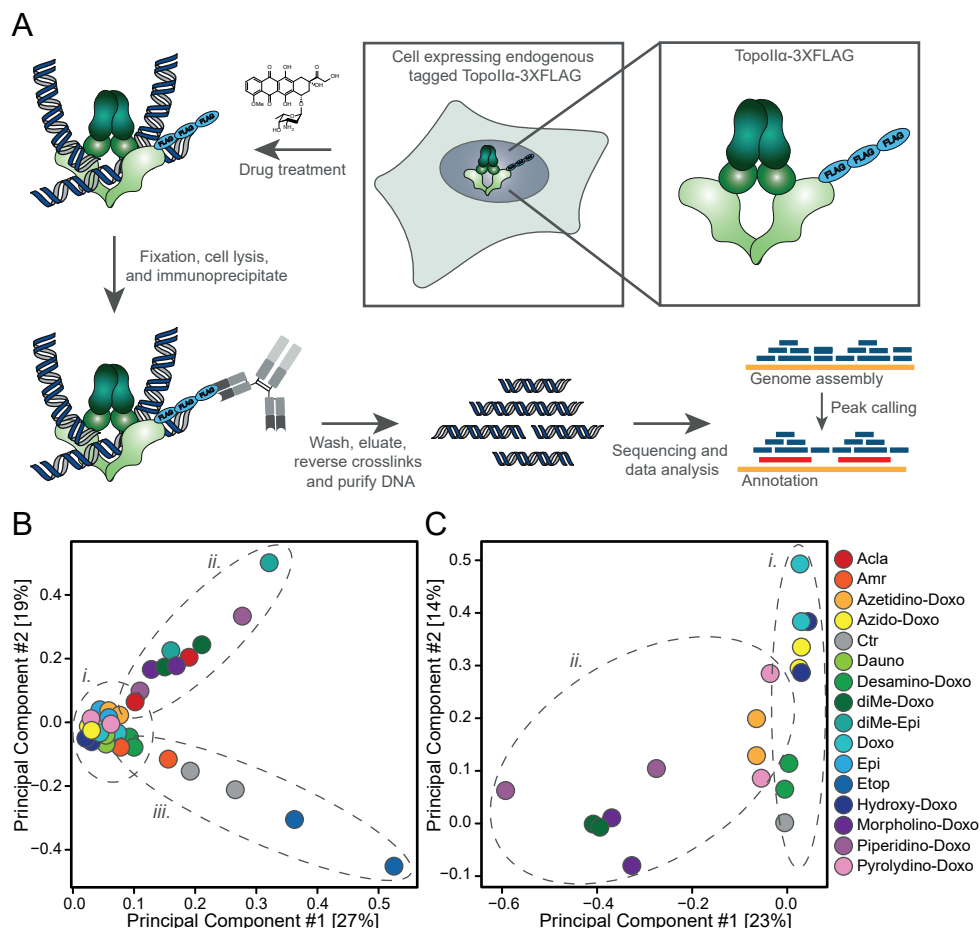


**Figure 5. Doxorubicin analogs alter genomic location of topoisomerase II $\alpha$ .** (A) Schematic representation of Topo II $\alpha$  ChIP-seq experiment. K562 cells endogenously expressing 3xFLAG-tagged Topo II $\alpha$  were treated with the indicated drugs followed by fixation, cell lysis and immunoprecipitation using FLAG antibody. Subsequently, Topo II $\alpha$  bound DNA was isolated, sequenced and analyzed. (B) Principle Component Analysis (PCA) of total ChIP-seq peak calls, overall signal (RPKM counts) no filters were applied. (i.) main cluster of analogs able to both induce DNA- and chromatin damage, the non-basic doxorubicin analogs with DNA damage activity only and pyrolydino-doxorubicin. (ii.) aclarubicin and most of the doxorubicin analogs featuring a tertiary amine at the 3' position. (iii.) ctr, etoposide and amrubicin. (C) PCA of the fold change of upregulated peaks compared to ctr of a selection of the samples (doxorubicin analogs). ChIP-seq peak calls were extracted with the ENCODE ChIP-seq analysis pipeline. (i.) the DNA damaging doxorubicin analogs, featuring a primary amine or non-basic side group (ii.) the histone eviction only doxorubicin analogs with tertiary amine.

performs its biological function (Figure S6A). Further analysis by plotting the normalized data (fold change compared to ctr) separates the DNA damaging compounds (i.) from the histone evicting drugs (ii.) (Figure 5C and S6B). This suggests that the different analogs trap Topo II $\alpha$  at different genomic regions, and that these regions may be determined by their structure and ability to induce DNA- or chromatin damage.

## CONCLUSION AND FUTURE DIRECTIONS

Although the anthracycline drugs are used in the clinic for over five decades to treat various types of cancer, detailed understanding of their structure – function relationship is limited. Therefore, studying the biological consequence of novel analogs can be valuable in understanding their exact molecular mechanism. Based on previous data, the methylation status and orientation of the 3' amine of the compound appeared to be important for the biological function. Therefore, we aimed to further decipher the effects of modifications on this chemical group. To do so, we synthesized various doxorubicin analogs featuring novel side groups at this amino sugar 3' position, resulting in three non-basic and four cyclin-doxorubicin analogs. Biological evaluation of this set of compounds suggests that the tertiary amine on this 3' position is responsible for the chromatin damage capacity of these structures. All four cyclic-doxorubicin analogs were, like diMe-Doxo, equally effective histone evicting compounds and show overall similar cytotoxicity, without inducing DNA double-strand breaks. While the non-basic doxorubicin analogs were unable to evict histones, they still were, similar to their parental drug, effective DNA damaging compounds. Although the compounds differed in their biological activity, all doxorubicin variants remained capable to re-locate Topo II $\alpha$  in the nucleus of living cells. Identification of the genomic regions where Topo II $\alpha$  was trapped by the different compounds, as detected by ChIP-seq, indicate that these drugs can be clustered in two main groups. The anthracycline analogs that poison Topo II $\alpha$  and thereby produce DNA damage likely target Topo II $\alpha$  at the genomic locations where the enzyme performs its biological function, while the other analogs, more specialized in histone eviction, seem to redirect Topo II $\alpha$  to other genomic regions. The microscopy data indicate that the doxorubicin variants containing a tertiary amine relocated Topo II $\alpha$  more to the genomic regions close to the nuclear envelop. However, further detailed evaluation of these genomic regions is necessary to define their genomic selectivity and understand the biological consequence of this difference. Comparable results were obtained for the chromatin damage activity for the doxorubicin analogs by ATAC-seq analysis. Histone eviction is induced at different genomic locations, which can be linked to their chemical structure. The analogs featuring a tertiary amine (aclarubicin, Azetidino-doxo, diMe-Doxo, diMe-Epi, Morpholino-doxo, Pyrolidino-doxo and Piperidino-doxo) are all very effective histone evicting drugs, and seem to induce chromatin damage at a distinct genomic regions from the analogs with a primary amine at the 3' position, which have both DNA damage and chromatin damage activity (doxorubicin, epirubicin and daunorubicin) and from amrubicin, which is unable to evict histones.

A more detailed analysis of the genomic selectivity of these analogs could help to better understand the structure-function relationship of anthracycline drugs, which could help with predicting the effectivity of particular tumors types (with e.g. epigenetic alterations) for specific anthracycline analogs. Exploring the chemical space around doxorubicin resulted in potential novel drug variants with distinct structure-function relationship and genomic selectivity, which can help in the development of improved anthracycline-based cancer therapies.

## MATERIALS AND METHODS

### Reagents and antibodies

Doxorubicin was obtained from Accord Healthcare Limited, UK, etoposide was obtained from Pharmachemie (the Netherlands), aclarubicin (sc-200160) was pur-

chased from Santa Cruz Biotechnology (USA), diMe-doxo was obtained via synthesis as described before [8]. The doxorubicin analogs were synthesized as described [13]. Primary antibodies used for Western blotting:  $\gamma$ H2AX (1:1000, 05-036, Millipore),  $\beta$ -actin (1:10000, A5441, Sigma). Secondary antibody used for blotting: IRDye 800CW goat anti-mouse IgG (H+L) (926-32210, Li-COR, 1:10000).

### Cell culture and constructs

K562 cells (B. Pang, Stanford University, USA), HCT116 cells (T. van Hall, LUMC, The Netherlands), BXPC-3 cells (ATCC® CRL-1687), PC3 and DU145 cells (C. Robson, Newcastle University, UK), were maintained in RPMI-1640 medium supplemented with 8% FCS. A549 cells (R. Bernards, NKI, The Netherlands), FM3 cells (D. Peeper, NKI, The Netherlands), U87 MG (ATCC® HTB-14), U118 MG (ATCC® HTB-15), U2Os cells (ATCC® HTB-96), Hela cells (ATCC® CCL-2) and SKBR3 (R. Beijersbergen, NKI, The Netherlands), were maintained in DMEM medium supplemented with 8% FCS. BT474 cells (R. Beijersbergen, NKI, The Netherlands) were maintained in DMEM/F12 medium supplemented with 8% FCS. MelJuSo cells were maintained in IMDM medium supplemented with 8% FCS. MelJuSo cells stably expressing PAGFP-H2A were maintained in IMDM supplemented with 8% FCS and G-418, as described [5]. Endogenous tagged 3xFLAG-Topo II $\alpha$  K562 cell lines were generated using homology repair 3xFLAG constructs designed at least 40 base pairs up and downstream of the genomic topoisomerase II $\alpha$  stop codon. The gRNA target sequence was designed using the ZANG Lab CRISPR tool (<http://crispr.mit.edu/>) and cloned into the pX330 vector. Primers used for the HR construct: 5' CACCGATGATCTGTTTTAAATGTG 3' and 5' AAACCACATTTTAAACAGATCATC 3'. Co-transfection of ssDNA oligo and CRISPR plasmid (CRISPR sequence into pX459) into K562 cells by electroporation using Lonza SF cell line kit. Primers used for genotyping: Topo II $\alpha$  fwd: TAAGCAGAATTCATGCCACTTATTTGGGCAAT and Topo II $\alpha$  rev: TGCTTAAAGCTTTGCCCATGAGATGGTCACTA. Cell lines were maintained in a humidified atmosphere of 5% CO<sub>2</sub> at 37°C and regularly tested for the absence of mycoplasma. Topo II $\alpha$ -GFP construct was described before [5].

### Confocal microscopy

For PAGFP-H2A photoactivation and time-lapse confocal imaging cells were seeded in a 35mm glass bottom petri dish (Poly-dlysine-Coated, MatTek Corporation), and imaged 16 hours later as described [5]. For live cell imaging of GFP-Topo II $\alpha$ , MelJuSo cells were seeded in a 35mm glass bottom petri dish (Poly-dlysine-Coated, MatTek Corporation), transfected (effectene, Qiagen) 16 hours later and treated as indicated. Time-lapse confocal imaging was performed on a Leica SP8 confocal microscope system, 63x lens, equipped with a climate chamber. Images were quantified using Image J software.

### Western blot and constant-field gel electrophoresis (CFGE)

Cells were treated with drugs at indicated dose for 2 hours. Subsequently, drugs were removed by extensive washing and cells were collected and processed immediately for the assays. For Western blot cells were lysed directly in SDS-sample buffer (2% SDS, 10% glycerol, 5%  $\beta$ -mercaptoethanol, 60mM Tris-HCl pH 6.8 and 0.01% bromophenol blue). Lysates were resolved by SDS/polyacrylamide gel electrophoresis followed by western blotting. Primary antibodies used for blotting:  $\gamma$ H2AX (1:1000, 05-036, Millipore) and  $\beta$ -actin (1:10000, A5441, Sigma). For CFGE: DNA double strand breaks were quantified by constant-field gel electrophoresis as

described [14]. Images were quantified using ImageJ software.

### ***In vitro* cell viability assay**

Cells were seeded into 96-well format. Twenty-four hours after seeding, cells were treated with indicated drugs for 2 hours at various concentrations. Subsequently, drugs were removed and cells were left to grow for an additional 72 hours. Cell viability was measured using the CellTiter-Blue viability assay (Promega). Relative survival was normalized to the untreated control and corrected for background signal.

### **Topo II $\alpha$ ChIP sequencing**

A total of  $5 \times 10^7$  endogenous tagged 3xFLAG-Topo II $\alpha$  K562 cells per sample were treated with 10  $\mu$ M of the indicated drugs for 4 hours. The experiments were performed with biological replicates. Cells were fixed and processed as described [15, 16]. For ChIP-seq, the mouse anti-FLAG M2 (F3165, Sigma) was used. Sequencing was done on a Illumina HiSeq2000 platform (Genome Sequencing Service Center of Stanford Center for Genomics and Personalized Medicine Sequencing Center). All samples were quality controlled and processed identically using the available ChIP-seq peak calling pipeline published by ENCODE, version 0.2.0 (<https://github.com/ENCODE-DCC/chip-seq-pipeline2>). Peak normalization and contrasts to control samples was performed using the package DiffBind for R statistical computing software [17].

### **Epigenomic profiling of histone eviction regions by ATAC-sequencing**

A total of  $5 \times 10^4$  K562 cells per sample were treated with 10  $\mu$ M of the indicated drugs for 4 hours. The experiments were performed with biological replicates. For ATAC-seq, after treatment cells were fixed and processed as described [11, 18]. DNA was processed using a customized library preparation method for ATAC-seq as described and was sequenced using an Illumina HiSeq4000 platform. All samples were quality controlled and processed identically using the available ATAC-seq peak calling pipeline published by ENCODE, version 0.3.0 (DOI: 10.5281/zenodo.156534). Peaks were annotated with epigenomic signatures of K562, downloaded from ENCODE Project [19]. Peak normalization and contrasts to control samples was performed using the package DiffBind for R statistical computing software [17].

### **Quantification and statistical analysis**

Each experiment was assayed in triplicate, unless stated otherwise. All error bars denote  $\pm$ SD. Statistical analyses was performed using Prism 8 software (GraphPad Inc.). ns, not significant, \* $p < 0.05$ , \*\* $p < 0.01$ , \*\*\* $p < 0.001$ , \*\*\*\* $p < 0.0001$ .

## **REFERENCES**

1. Lotrionte, M., Biondi-Zoccai, G., Abbate, A., Lanzetta, G., D'Ascenzo, F., Malavasi, V., Peruzzi, M., Frati, G. & Palazzoni, G. (2013) Review and meta-analysis of incidence and clinical predictors of anthracycline cardiotoxicity, *Am J Cardiol.* 112, 1980-4.
2. Mistry, A. R., Felix, C. A., Whitmarsh, R. J., Mason, A., Reiter, A., Cassinat, B., Parry, A., Walz, C., Wiemels, J. L., Segal, M. R., Ades, L., Blair, I. A., Osherooff, N., Peniket, A. J., Lafage-Pochitaloff, M., Cross, N. C., Chomienne, C., Solomon, E., Fenaux, P. & Grimwade, D. (2005) DNA topoisomerase II in therapy-related acute promyelocytic leukemia, *N Engl J Med.* 352, 1529-38.

3. Weiss, R. B. (1992) The Anthracyclines - Will We Ever Find a Better Doxorubicin, *Semin Oncol.* 19, 670-686.
4. Nitiss, J. L. (2009) Targeting DNA topoisomerase II in cancer chemotherapy, *Nat Rev Cancer.* 9, 338-350.
5. Pang, B., Qiao, X., Janssen, L., Velds, A., Groothuis, T., Kerkhoven, R., Nieuwland, M., Ovaa, H., Rottenberg, S., van Tellingen, O., Janssen, J., Huijgens, P., Zwart, W. & Neefjes, J. (2013) Drug-induced histone eviction from open chromatin contributes to the chemotherapeutic effects of doxorubicin, *Nature communications.* 4, 1908.
6. Yang, F., Kemp, C. J. & Henikoff, S. (2013) Doxorubicin enhances nucleosome turnover around promoters, *Curr Biol.* 23, 782-7.
7. Pang, B., de Jong, J., Qiao, X., Wessels, L. F. & Neefjes, J. (2015) Chemical profiling of the genome with anti-cancer drugs defines target specificities, *Nat Chem Biol.* 11, 472-80.
8. Qiao, X., van der Zanden, S. Y., Wander, D. P. A., Borrás, D. M., Song, J. Y., Li, X., van Duikeren, S., van Gils, N., Rutten, A., van Herwaarden, T., van Tellingen, O., Giacomelli, E., Bellin, M., Orlova, V., Tertoolen, L. G. J., Gerhardt, S., Akkermans, J. J., Bakker, J. M., Zuur, C. L., Pang, B., Smits, A. M., Mummery, C. L., Smit, L., Arens, R., Li, J., Overkleeft, H. S. & Neefjes, J. (2020) Uncoupling DNA damage from chromatin damage to detoxify doxorubicin, *Proc Natl Acad Sci U S A.*
9. Dennis P. A. Wander, S. Y. v. d. Z., Gijsbert A. van der Marel, Herman S. Overkleeft, Jeroen D. C. Codée, Jacques Neefjes (2020) Doxorubicin and Aclarubicin: Shuffling Anthracycline Glycans for Improved Anti-Cancer Agents, Chapter 4.
10. Dennis P. A. Wander, S. Y. v. d. Z., Merijn B. L. Vriends, Branca C. van Veen, Joey G. C. Vlaming, Thomas Bruyning, Gijsbert A. van der Marel, Herman S. Overkleeft, Jacques Neefjes, Jeroen D. C. Codée (2020) Synthetic (N,N-dimethyl)doxorubicin Glycosyl Diastereomers to Dissect Modes of Action of Anthracycline Anticancer Drugs, Chapter 5.
11. Buenrostro, J. D., Giresi, P. G., Zaba, L. C., Chang, H. Y. & Greenleaf, W. J. (2013) Transposition of native chromatin for fast and sensitive epigenomic profiling of open chromatin, DNA-binding proteins and nucleosome position, *Nat Methods.* 10, 1213-+.
12. Giresi, P. G., Kim, J., McDaniel, R. M., Iyer, V. R. & Lieb, J. D. (2007) FAIRE (Formaldehyde-Assisted Isolation of Regulatory Elements) isolates active regulatory elements from human chromatin, *Genome Res.* 17, 877-85.
13. Wander, D. P. A. (2019) Synthesis of a Focused Library of Doxorubicin/Aclarubicin - Inspired Structures.
14. Wlodek, D., Banath, J. & Olive, P. L. (1991) Comparison between Pulsed-Field and Constant-Field Gel-Electrophoresis for Measurement of DNA Double-Strand Breaks in Irradiated Chinese-Hamster Ovary Cells, *Int J Radiat Biol.* 60, 779-790.
15. Schmidt, D., Wilson, M. D., Spyrou, C., Brown, G. D., Hadfield, J. & Odom, D. T. (2009) ChIP-seq: Using high-throughput sequencing to discover protein-DNA interactions, *Methods.* 48, 240-248.
16. Pang, B. X., de Jong, J., Qiao, X. H., Wessels, L. F. A. & Neefjes, J. (2015) Chemical profiling of the genome with anti-cancer drugs defines target specificities, *Nat Chem Biol.* 11, 472-+.
17. Ross-Innes, C. S., Stark, R., Teschendorff, A. E., Holmes, K. A., Ali, H. R., Dunning, M. J., Brown, G. D., Gojis, O., Ellis, I. O., Green, A. R., Ali, S., Chin, S. F., Palmieri, C., Caldas, C. & Carroll, J. S. (2012) Differential oestrogen receptor binding is associated with clinical outcome in breast cancer, *Nature.* 481, 389-U177.

18. Corces, M. R., Trevino, A. E., Hamilton, E. G., Greenside, P. G., Sinnott-Armstrong, N. A., Vesuna, S., Satpathy, A. T., Rubin, A. J., Montine, K. S., Wu, B., Kathiria, A., Cho, S. W., Mumbach, M. R., Carter, A. C., Kasowski, M., Orloff, L. A., Risca, V. I., Kundaje, A., Khavari, P. A., Montine, T. J., Greenleaf, W. J. & Chang, H. Y. (2017) An improved ATAC-seq protocol reduces background and enables interrogation of frozen tissues, *Nat Methods*. 14, 959-+.
19. Pazin, M. J. (2015) Using the ENCODE Resource for Functional Annotation of Genetic Variants., *Cold Spring Harb Protoc*. 2015, 522-536.

# SUPPLEMENTAL INFORMATION

6





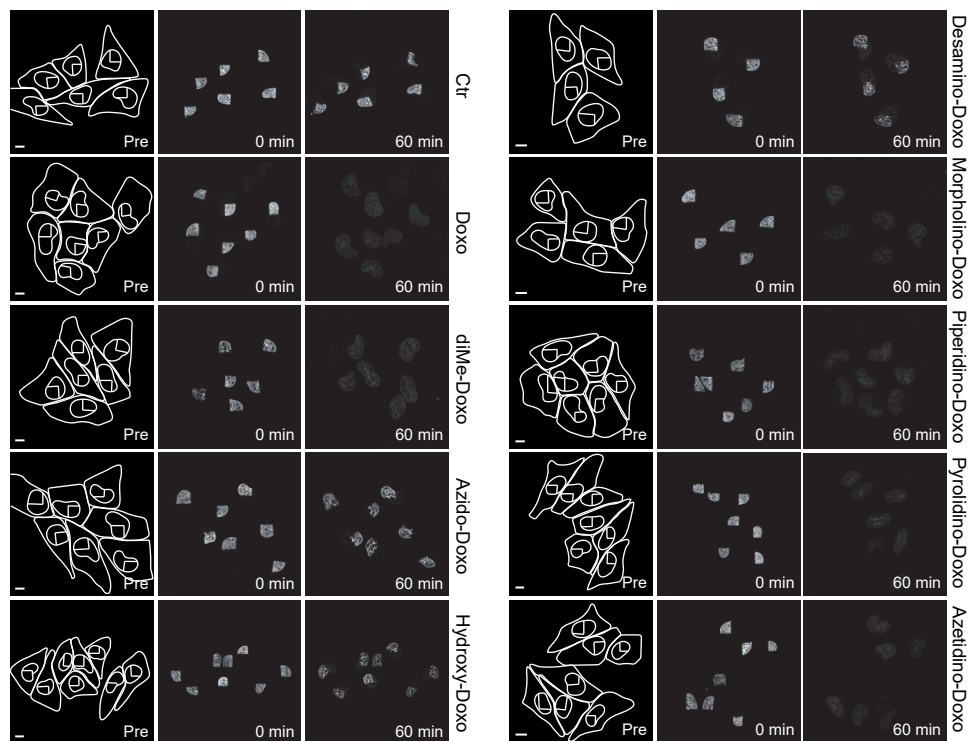


**Figure S1. Chromatin damage via eviction of histone by the various doxorubicin analogs.** Part of the nucleus of MeJuSo cells stably expressing PAGFP-H2A was photo-activated and histone eviction was measured by time-lapse confocal microscopy upon administration of 10  $\mu$ M of the indicated compounds. Lines in the left panel define the cytoplasm, nucleus and activated region of the nucleus before treatment. Stills at indicated time points from time-lapse experiment are shown. Scale bar, 10  $\mu$ m.

**Figure S2. Continued (A).** Cell survival was determined 72 hours post drug removal using CellTiter-Blue assay. Data is shown as mean  $\pm$  SD of three independent experiments. (B) Histone eviction speed (the time at which 25% of the initial signal is reduced) is correlated with  $IC_{50}$  of the various doxorubicin isomers. Two-tailed Pearson  $r$  correlation  $p = ** < 0.01$ .

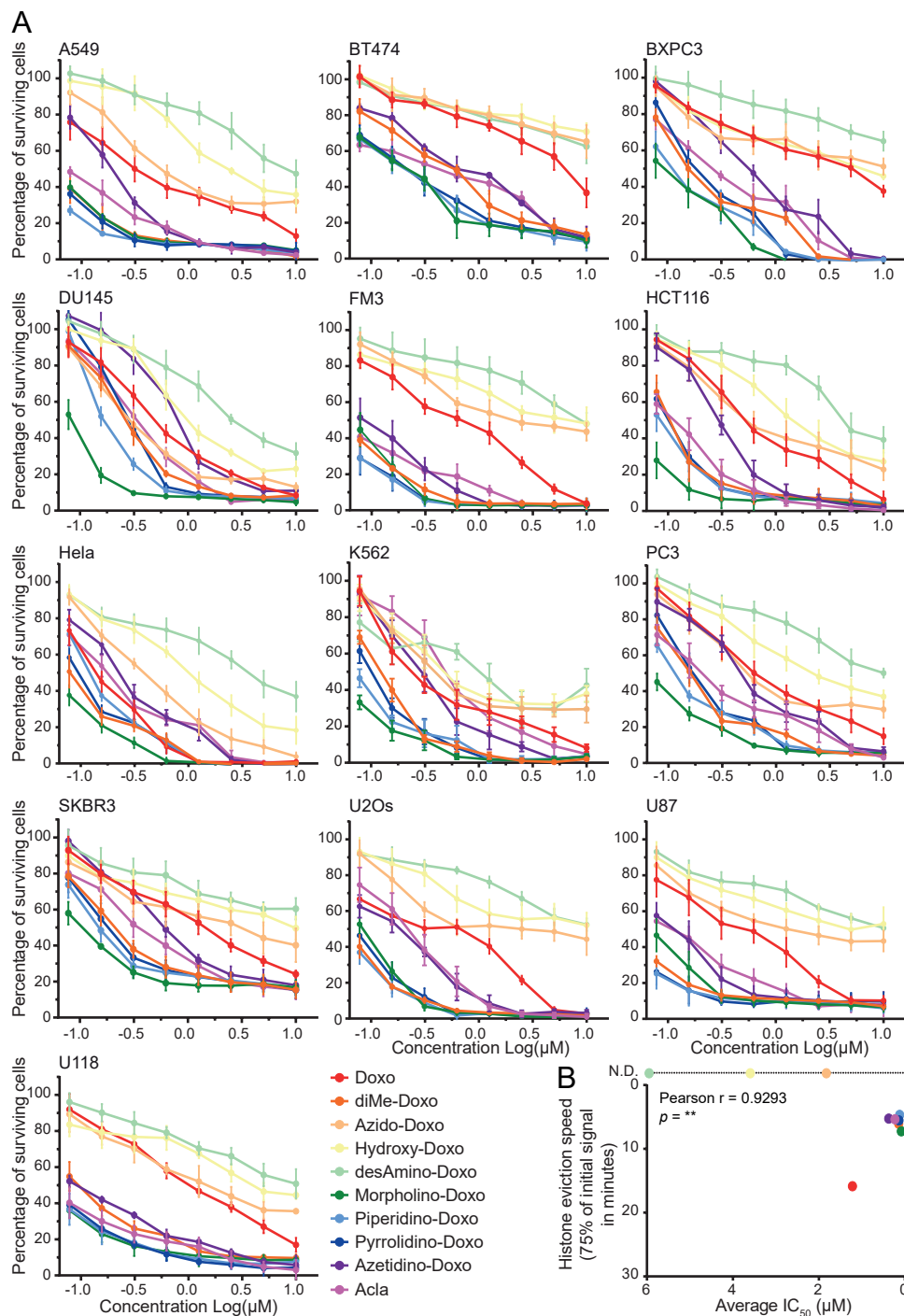


**Figure S2. Cytotoxicity of the different doxorubicin analogs in various tumor cell lines.**  
(A) Cells were treated for 2 hours with the indicated concentrations followed by drug removal.

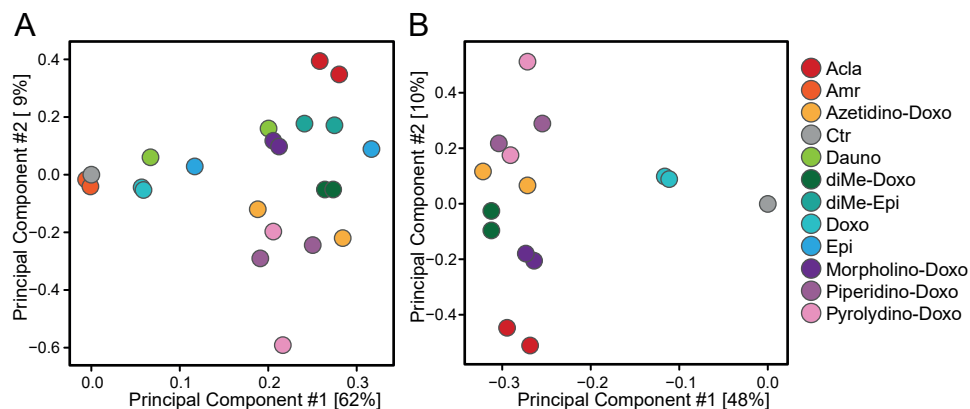


**Figure S3. ATAC-seq analysis of chromatin damage differences.** K562 cells were treated for 4 hours with the indicated drugs and processed for ATAC-seq. (A) Principle Component Analysis (PCA) of total ATAC-seq peak calls, overall signal filtered for ctr peaks. (B) PCA of the fold change of peaks compared to ctr, a selection of the samples plotted in Figure 3C is included. ATAC-seq peak calls were extracted with the ENCODE ATAC-seq analysis pipeline.

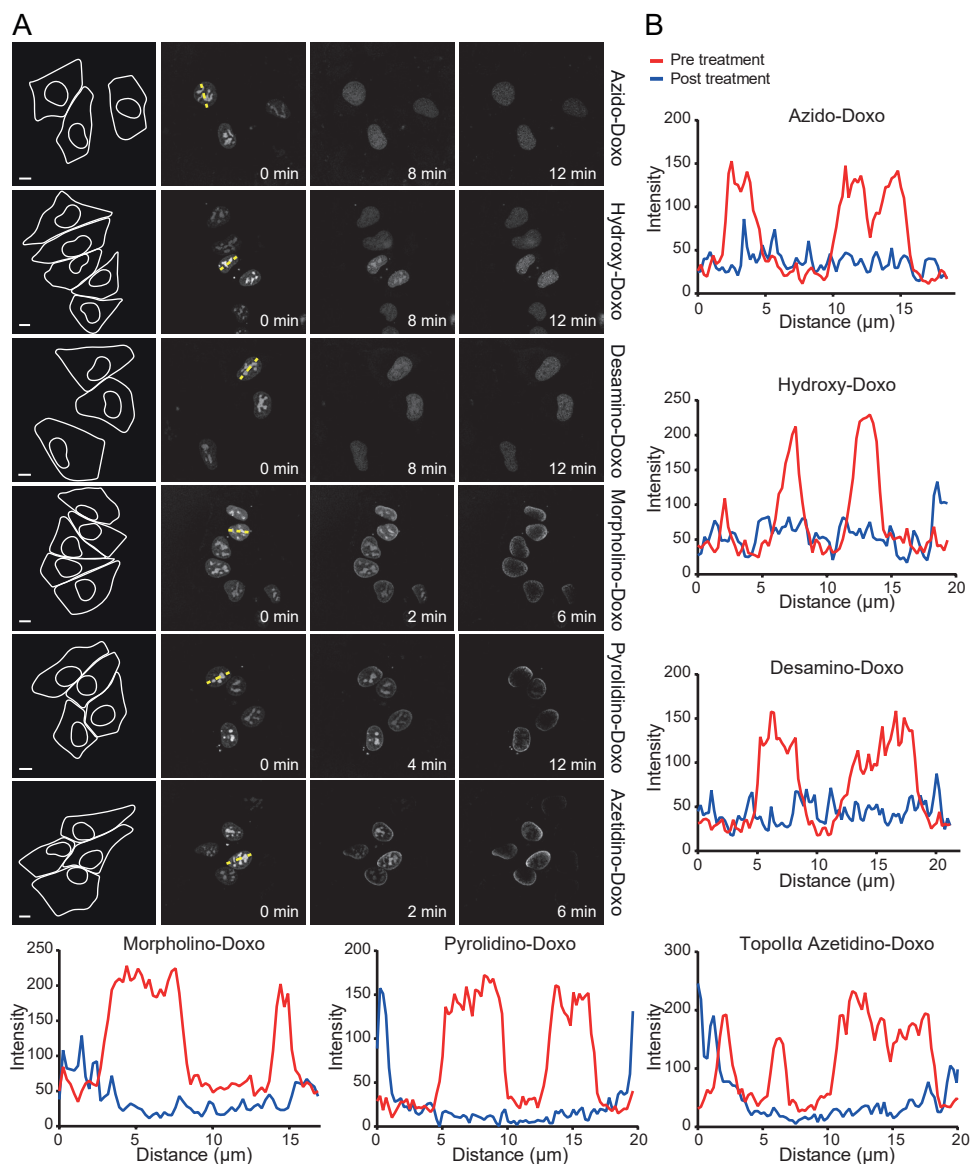


**Figure S4. Topoisomerase IIα relocalization.** Relocalization of GFP-Topo IIα transiently expressed in MeJuSo cells. (A) Cells are treated with 10 μM of the indicated doxorubicin analogs and followed over time. Lines in the left panel define the cytoplasm and nucleus. Stills at indicated time points from time-laps experiment are shown. Scale bar, 10 μm. (B) Pixel plot of the GFP signal pre- and post treatment with the drugs. Plotted as fluorescence over distance of dotted yellow line as marked in (A).

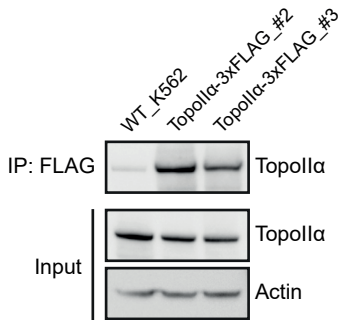


**Figure S5.** Verification of endogenously tagged TopoIIα-3xFLAG K562 cell line. Wild-type and two single cell clones of TopoIIα-3xFLAG K562 cells lines were lysed and immunoprecipitated. Immunoprecipitated TopoIIα is visualized by Western blot.

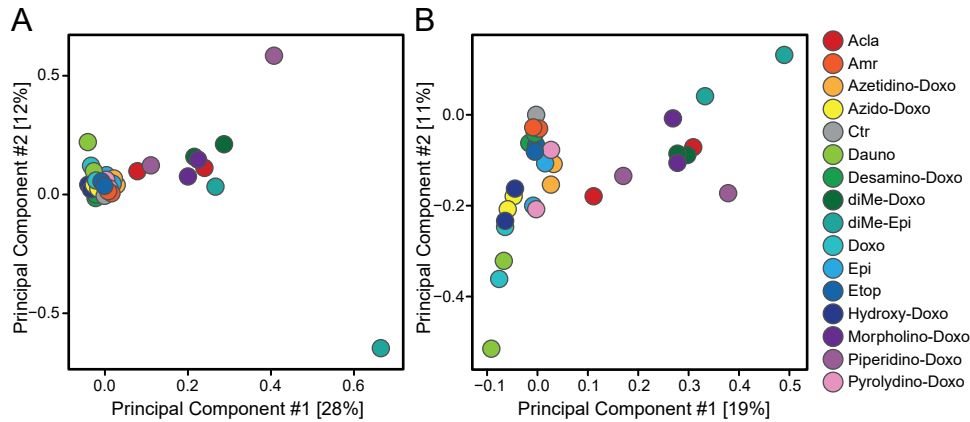
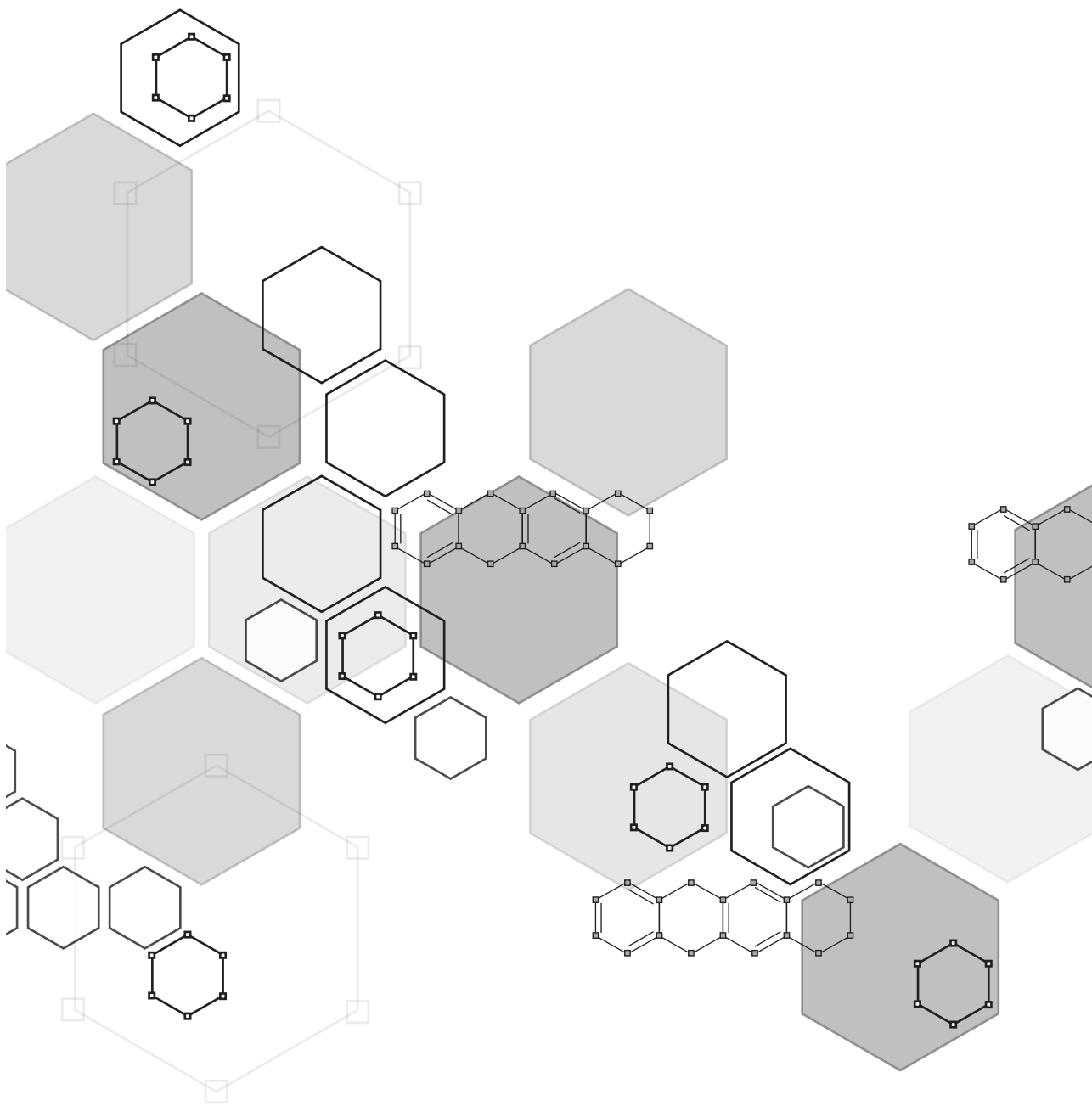


**Figure S6.** Differences in genomic location of TopoIIα targeting by the doxorubicin analogs. Endogenous TopoIIα-3xFLAG K562 cells were treated for 4 hours with the indicated drugs and processes for FLAG-ChIP-seq. (A) Principle Component Analysis (PCA) of ChIP-seq peak calls, filtered for control peaks. (B) PCA of the fold change of peaks compared to ctr, all samples tested are included. ChIP-seq peak calls were extracted with the ENCODE ChIP-seq analysis pipeline.

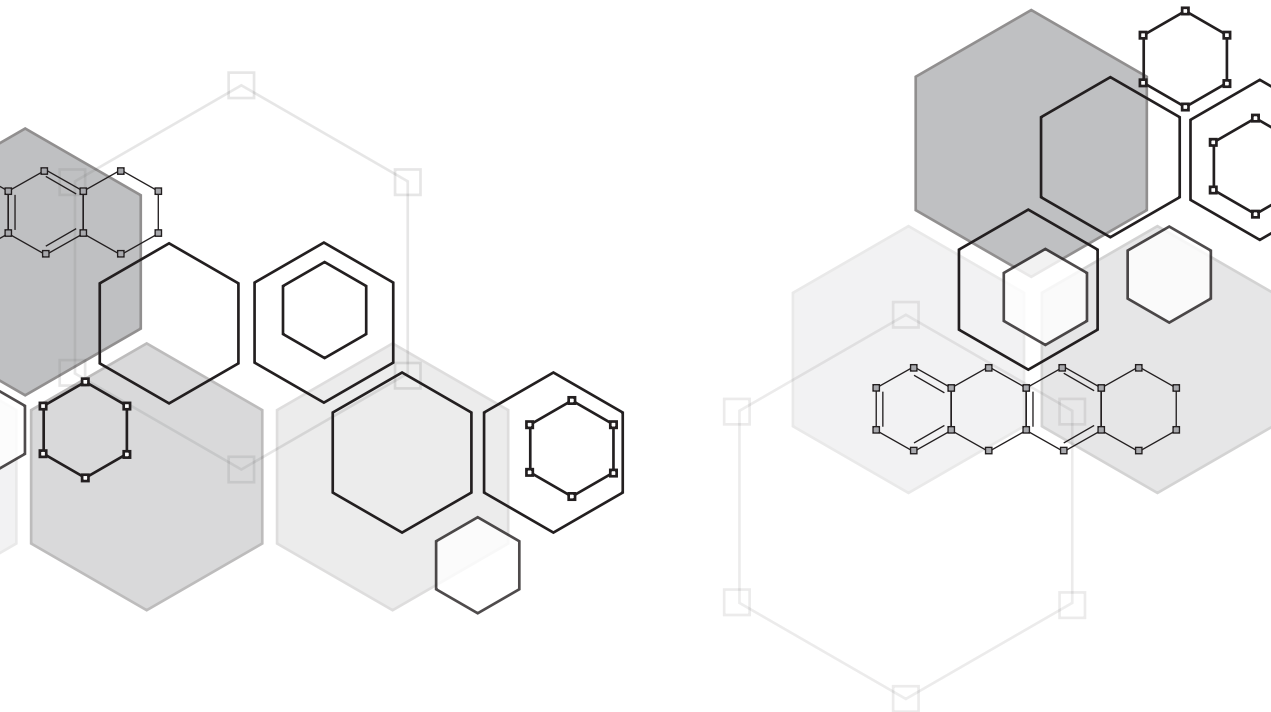






Nuclear DNA sensors  
re-localize upon  
chromatin damage;  
do they play a role in  
anthracycline induced cell  
death?

7



Sabina Y. van der Zanden, Feija L. Hamoen, Jimmy J. Akkermans, Noa Linthorst, Daniel Borràs, Lennert Janssen, George M.C. Janssen, Peter A. van Veelen, Jacques Neeffjes

*Manuscript in preparation*

**ABSTRACT**

Since the 1970s the anthracycline drugs daunorubicin and doxorubicin are extensively used as single drugs or in combination therapies to treat many types of tumors. Even after 50 years of clinical usage, the exact molecular mechanism by which these drugs function is still not fully known. A well accepted mechanism of action is the formation of DNA damage, via interference with the catalytic cycle of topoisomerase II. However, a recently discovered second mechanism – chromatin damage as the result of histone eviction – was shown to be the main cytotoxic mechanism of these drugs. How histone eviction subsequently leads to the induction of cell death is poorly understood. Here, we identified three nuclear DNA sensors (IFI16, IFIX and MND A) active in the innate immune response to DNA viruses that specifically re-localize to DNA upon histone eviction, and novel interaction partners for these sensors that might play a role in anthracycline-induced cytotoxicity.

**INTRODUCTION**

The anthracycline drugs doxorubicin (Doxo) and its analogs epirubicin (Epi) and daunorubicin (Dauno) are cornerstones in the treatment of different types of hematological and solid tumors for half a century [1, 2]. A well accepted mechanism of action for these chemotherapeutic drugs is the induction of DNA double strand breaks, by blocking the catalytic cycle of the enzyme topoisomerase II $\alpha$  (Topo II $\alpha$ ) and thereby forming topoisomerase-DNA adducts [3, 4]. Recently, we and others described that anthracyclines such as Doxo can also induce chromatin damage by eviction of histones. However, how histone eviction then leads to the initiation of cell death remains unclear [5, 6]. The occurrence of large stretches of histone free DNA, as is the case for cells treated with anthracycline drugs, is an unusual situation in eukaryotic cells, where the DNA is usually tightly packed in nucleosomes. The formation of nucleosomes ensures that the long DNA molecules can be condensed to fit into the nucleus, but also controls (tissue-specific) gene expression [7]. We hypothesized that the histone free DNA induced by these anthracycline drugs can be recognized by specific proteins to mask the naked DNA or to initiate a stress response. Potential protein candidates to fulfill this function are the DNA sensing proteins of the PYHIN protein family. This protein family consist of four proteins (PYHIN 1-3 and AIM2), of which three are expressed in the nucleus [8]. All four proteins consist of an N-terminal pyrin (PYD) domain, a death domain DD protein fold that can form homotypic interactions with other PYD-containing proteins. In general, these DD domain protein interactions result in the formation of complexes which are known to play a role in inflammation, cell cycle and apoptosis [9]. In addition to the PYD domain, these DNA sensors consist of one or two DNA binding HIN200 domains. The best studied nuclear DNA sensor of this protein family, PYHIN 2 (also known as IFI16 or interferon inducible protein 16), is described to play a role in the detection and response to double stranded DNA viruses, such as HCMV, KSHV and HIV [10-12]. We wondered whether the histone-free DNA generated by anthracyclines could be sensed by the nuclear DNA sensing proteins PYHIN 1 (IFI16), IFI16 and/or PYHIN 3 (MND A) thereby connecting the innate immune response to anthracycline induced cell death (Figure 1A).

**RESULTS****Histone eviction dependent re-localization of nuclear DNA sensors**

To determine whether nuclear DNA sensors play a role in anthracycline induced cell death, we evaluated the localization of three of these DNA sensors (PYHIN1-3, or

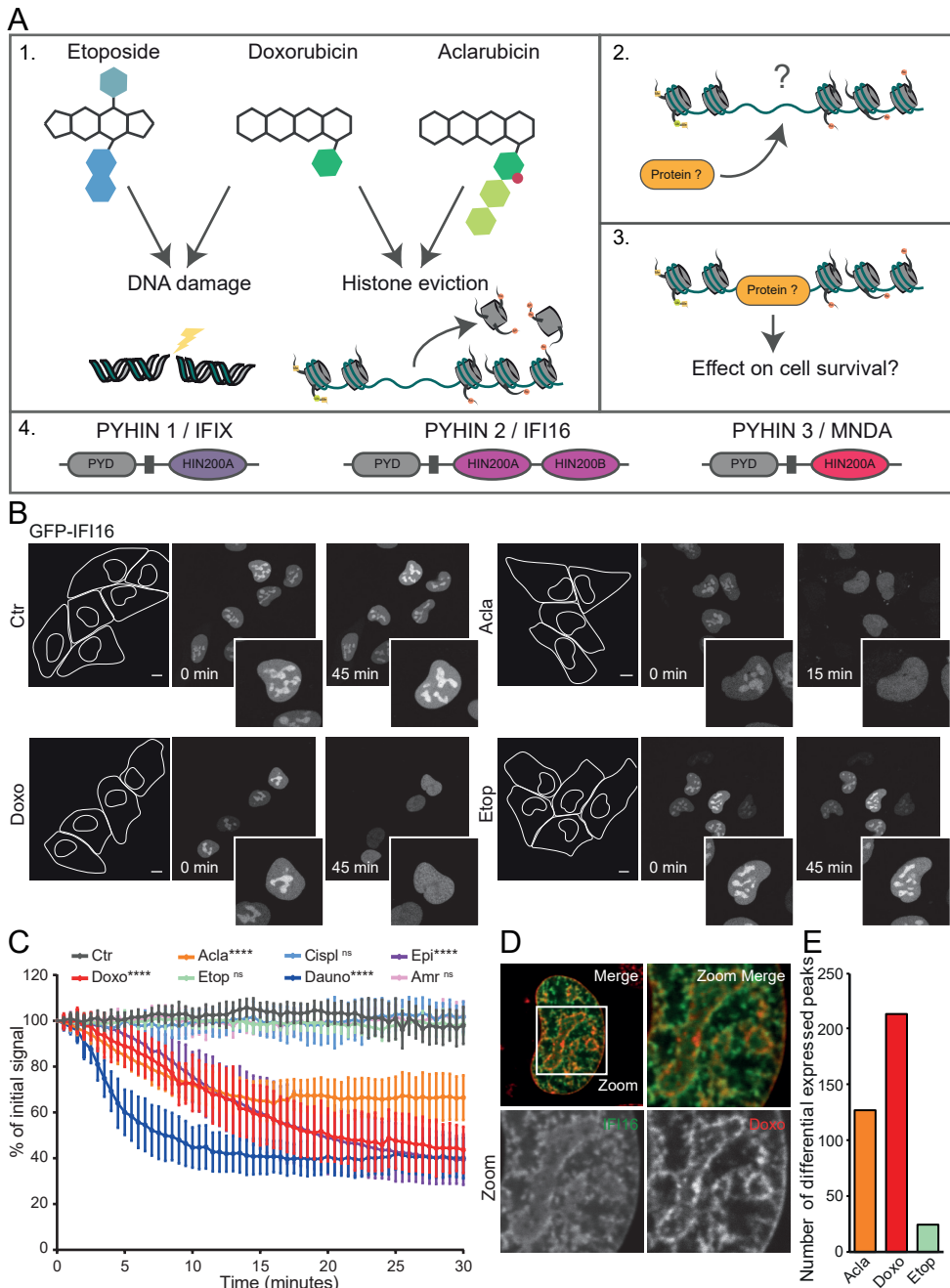


**Figure 1. Nuclear DNA sensors re-localize upon histone eviction.** (A) Schematic representation of anthracycline mechanism of action: 1. Anthracycline drugs can induce DNA damage via the formation of topoisomerase II $\alpha$ -DNA adducts and/or evict histones following intercalation into the DNA resulting in chromatin damage. 2. What happens after histones are evicted? 3. Are there proteins that detect the anthracycline induced 'naked DNA' and do

**Figure 1. Continued (A).** *they play a role in anthracycline induced cytotoxicity? 4. Schematic domain organization of three nuclear DNA sensing proteins of the PYHIN protein family. (B) MelJuSo cells transiently expressing GFP-tagged IFI16 are followed by time-lapse confocal microscopy upon treatment with various drugs: Doxo 10 $\mu$ M, Acla 5 $\mu$ M, Etop 10 $\mu$ M. Scale bar, 10  $\mu$ m. (C) Quantification of the fluorescent intensity in the nucleoli of cells in B. Ordinary Two-way ANOVA with Turkey's multiple comparison test; ns, not significant; \*\*\*\*P < 0,0001. (D) Localization of GFP-tagged IFI16 in MelJuSo cell nucleus treated with Doxo 10 $\mu$ M for 30 minutes. (E) Number of differential expressed reads for endogenous IFI16-ChIP sequencing in MelJuSo cells, upon treatment for 2 hour with the different drugs. Acla 10 $\mu$ M, Doxo 10 $\mu$ M and Etop 10 $\mu$ M.*

IFIX, IFI16 and MNDA respectively) before and after treatment with different anticancer drugs. GFP-tagged IFIX, IFI16 or MNDA were transiently expressed in MelJuSo cells, allowing detection of the fluorescent signal over time upon treatment with different genotoxic stimuli (Figure 1B, 1C and Figure S1-S3). At steady state, the DNA sensors localized in the nuclear where it accumulated in the nucleoli. Upon treatment with histone evicting anthracycline drugs (Doxo, Acla, Epi or Dauno), the DNA sensors rapidly re-localized from the nucleoli to the nucleosol. This re-localization was specific for chromatin damage, since drugs unable to induce histone eviction (Etop, cisplatin; Cispl and amrubicin; Amr) did not change DNA sensor localization upon treatment. To identify whether the DNA sensors were able to detect the histone free DNA upon eviction of histones, we had a closer look at the location of IFI16 upon treatment with Doxo. Thirty minutes post Doxo treatment, IFI16 localization partially overlapped with the Doxo (which is fluorescent) intercalated into the DNA (Figure 1D), indicating that IFI16 indeed sensed the Doxo-induced histone-free DNA. To validate this observation, we immunoprecipitated endogenous IFI16 upon treatment of MelJuSo cells with Doxo, Acla and Etop, and analyzed DNA binding by sequencing (ChIP-seq). Indeed, treatment with histone evicting drugs increased the number of differentially expressed peaks, indicating that histone eviction induces DNA binding of IFI16 (Figure 1E).

### Identification of novel interacting proteins

Upon histone eviction, the nuclear DNA sensors IFIX, IFI16 and MNDA re-localize from the nucleoli to the nucleosol, potentially to detect the histone free DNA regions. However, what happens after these DNA sensors bind the DNA is unclear. In the context of HSV-1 viral infection, IFI16 reduces viral replication via repression of viral gene expression [13]. This suggests that the DNA sensors could affect the transcriptome while binding the DNA following histone eviction induced by the anthracycline drugs (Figure 2A). Alternatively, upon DNA binding they initiate the formation of protein complexes via their PYD-domain, which are known to play a role in the formation and activation of the inflammasome [9]. However, the molecular mechanism for the latter is unknown. To identify novel interactors for the DNA sensors, we performed a Bio-ID proximity labeling assay. BirA-tagged DNA sensors were transiently over-expressed and upon lysis, biotinylated proteins were precipitated and analyzed by mass spectrometry (Figure 2A and Table 1). Novel interactions, which were selected based on their known role in cell death and innate immunity pathways, with the deubiquitinating enzyme USP7, the E3-ligase TRIM26 and the ATP-dependent DNA helicase XRCC6 were validated by co-immunoprecipitation experiments (Figure 2B-D). IFIX preferentially interacted with TRIM26 and XRCC6 while IFI16 and MNDA preferred interactions with USP7. This suggests that the DNA sensors have some specificity in recruiting ligands to the DNA. Interestingly, upon treatment with Doxo,

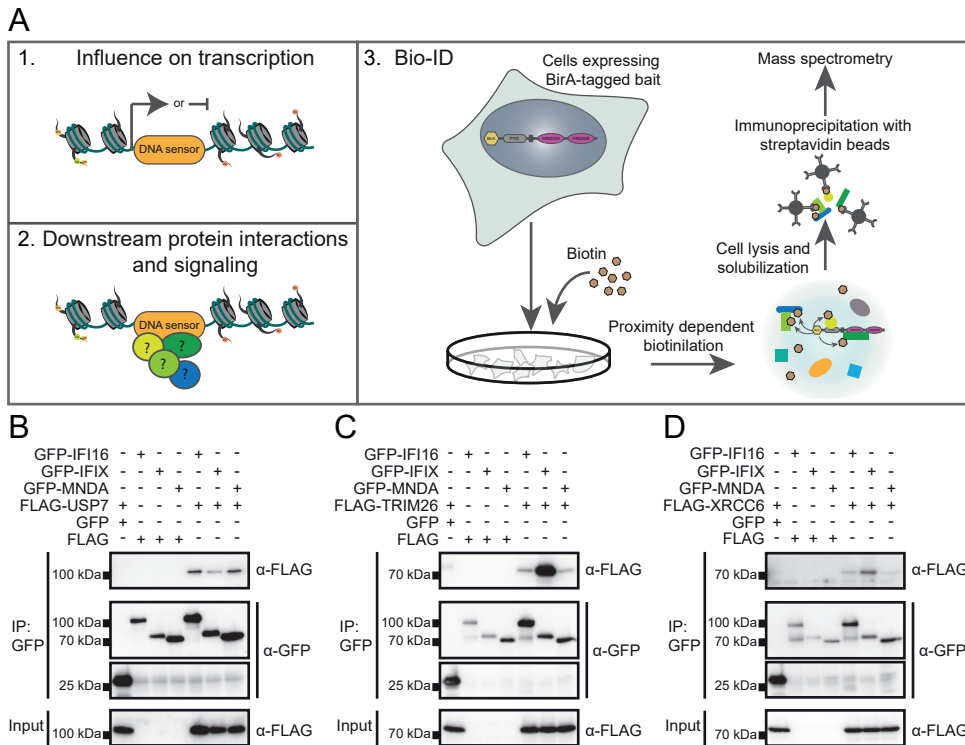


**Figure 2. Identification of nuclear DNA sensor-interacting proteins.** (A) Schematic representation potential consequences of histone eviction. 1. Binding of nuclear DNA sensor to the anthracycline induced histone free DNA might induce or repress transcription. 2. After binding of the histone free DNA the DNA sensor recruit, bind and activate other proteins to initiate downstream signaling. 3. Overview of Bio-ID workflow for DNA sensors interacting protein identification. BirA tagged DNA sensors are transiently expressed in HEK293T cells, upon incubation with biotin protein in close proximity of the bait are biotinylated. Upon lysis, biotinylated proteins were isolated and identified by mass spectrometry. (B – D) Validation of some of the interactions found by Bio-ID: USP7 (B), TRIM26 (C) and XRCC6 (D) with the nuclear DNA sensors.

transiently expressed mTurq-USP7 re-localized in a way similar to the DNA sensors (Figure S4).

### Domain characterization of USP7 and TRIM26

To identify the responsible interacting domain for the hits determined by Bio-ID, we cloned different truncation mutants of USP7 and TRIM26 (Figure 3A and 3C). Subsequently, HEK293T cells were transiently transfected with GFP-IFI16 and the various FLAG-tagged USP7 constructs and interaction were assessed by co-immunoprecipitation. Both full length USP7 and USP7-NTD-CAT interacted with IFI16, indicating that the catalytic domain of USP7 count mediate this interaction (Figure 3B).

To identify which domain of TRIM26 interacts with the DNA sensors, its different domains were immunoprecipitated with IFIX, the strongest interactor according to the Bio-ID and co-immunoprecipitation validation. HEK293T cells were transiently transfected with GFP-IFIX and the different FLAG-TRIM26 constructs (Figure 3C). IFIX

		Exclusive Unique Peptide Count						
Protein ID	MW	GFP-BirA	GFP-BirA-IFI16	Coverage	GFP-BirA-IFIX	Coverage	GFP-BirA-MNDA	Coverage
IFI16	88 kDa	0	99	77%	6	16%		
IFIX	55 kDa	0			49	74%		
MNDA	46 kDa	0					43	78%
DYNC1H1	532 kDa	2	56	18%	67	20%	39	11%
IPO7	120 kDa	8	25	30%				
HUWE1	482 kDa	5	24	9%	30	10%	14	5%
USP7	128 kDa	2	17	22%	9	12%	7	9%
GTF2F2	28 kDa	0	10	33%				
PPM1G	59 kDa	2	7	14%				
ARID3B	61 kDa	2	7	18%				
XRCC6	70 kDa	3	7	8%	11	25%	13	28%
NACC1	57 kDa	0	6	20%				
ZBTB10	95 kDa	0	6	11%				
DDX21	87 kDa	0	5	10%	7	11%	11	18%
WDR70	73 kDa	0	5	9%	6	11%		
CLTC	192 kDa	7			29	24%		
PARP1	113 kDa	13			20	27%	28	36%
EIF3A	167 kDa	4			20	17%	14	11%
MYBBP1A	149 kDa	5			15	15%	27	26%
MSH6	153 kDa	6			14	12%		
PPM1G	59 kDa	2			12	22%		
TRIM26	62 kDa	0			10	24%		
DNMT1	183 kDa	3			10	8%	12	9%
MYH10	229 kDa	2			9	10%		
IQGAP1	189 kDa	2			9	9%		
ESF1	99 kDa	0			8	11%		
MSH2	105 kDa	2			7	10%	6	7%
TPX2	86 kDa	0			7	11%	16	26%
NACC1	57 kDa	0			7	22%		
SMC1A	143 kDa	0			7	6%		
GTF2F2	28 kDa	0			6	22%	10	36%
POLA1	166 kDa	0			6	6%		
ZBTB10	95 kDa	0			4	6%	5	8%
DDX10	101 kDa	0					12	15%
SERPINB3	45 kDa	0					11	33%
NOP14	89 kDa	0					7	10%

**Table 1.** Selection of potential nuclear DNA sensor interacting proteins identified by Bio-ID.

co-immunoprecipitated full length TRIM26, TRIM26- $\Delta$ RING, TRIM26- $\Delta$ RING $\Delta$ Box and TRIM26-PRYSPRY, suggesting that the interaction with IFIX is mediated by the PRYSPRY domain of TRIM26 (Figure 3D). Little is known about TRIM26 interacting proteins, but the interaction described with TBK1, which plays a role in TBK1 activation upon RNA viral infection, is also mediated by this PRYSPRY domain [14].

### Ubiquitination of nuclear DNA sensors

Since the CAT domain could be responsible for the de-ubiquitinating activity of USP7, we wondered whether IFI16 can be ubiquitinated. To test this, GFP-IFI16 and HA-Ub were overexpressed in Hela cells. Indeed, ubiquitinated IFI16 was de-

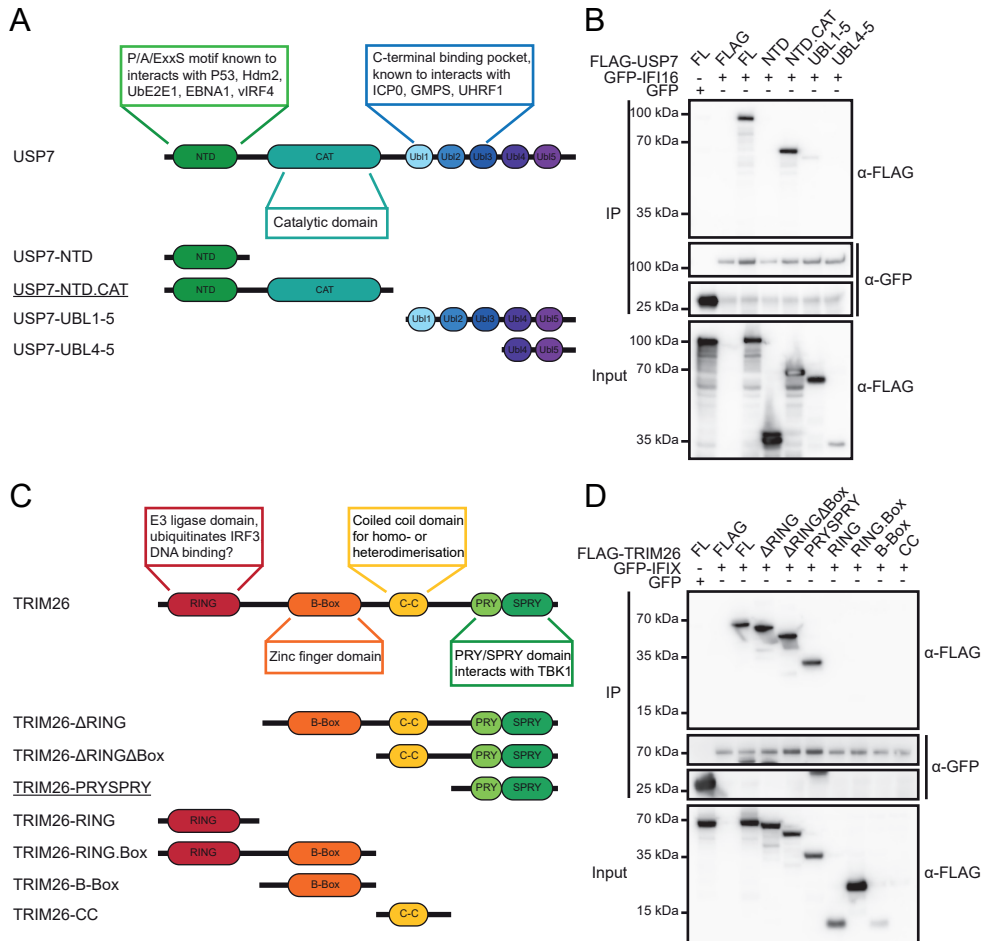


**Figure 3. Domain characterization of USP7 and TRIM26.** (A) Schematic domain organization of USP7. (B) Interactions between IFI16 and USP7 domains assayed by co-immunoprecipitation. (C) Schematic domain organization of TRIM26. (D) Interactions between IFIX and TRIM26 domains assayed by co-immunoprecipitation.

tectable and treatment with Acla slightly increased the amount of IFI16 ubiquitination (Figure 4A). Possibly USP7 could de-ubiquitinate IFI16 and hereby influence its function. Therefore we generated the USP7C223S catalytic mutant, which renders the enzyme catalytically inactive, and assessed its interacting and de-ubiquitination activity towards the DNA sensors compared to wild-type USP7. While the interaction with IFI16 did not change compared to wild-type USP7 (Figure 4B), USP7 partially reduced ubiquitination of the DNA sensors IFI16 (Figure 4C) and MNDA (Figure 4D), but not for IFIX (Figure 4E). Only for MNDA ubiquitination is depended on the catalytic activity of USP7, suggesting MNDA could be a potential substrate for USP7. Since the E3-ligase TRIM26 also interacted with the different DNA sensors, we wondered whether TRIM26 affects their ubiquitination status. Indeed, TRIM26 was found to increase poly-ubiquitination of MNDA whereas IFI16 remained unaffected. While



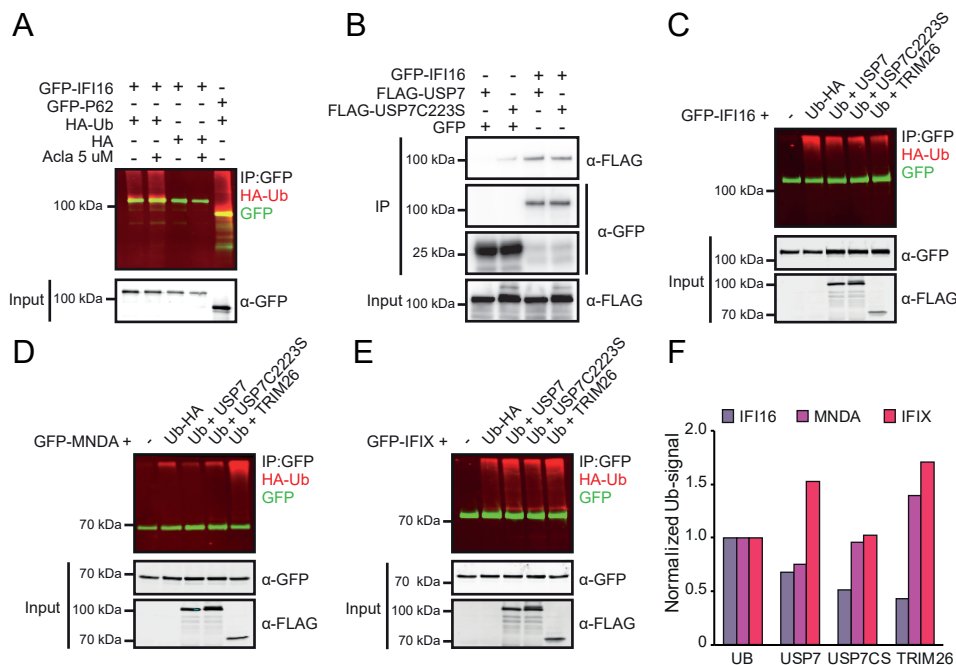


**Figure 4. Ubiquitination of nuclear DNA sensors.** (A) Ubiquitination status of IFI16 expressed in Hela cells. GFP-P62 was expressed as positive control. Ubiquitination status of GFP-substrate (green) was assessed by immunoblots against HA (red). (B) Interaction between wild-type and catalytic death USP7 (USP7C233S) mutant and IFI16. (C – E) Ubiquitination status of IFI16 (C), MND4 (D) and IFIX (E) as a function of catalytic activities of USP7, USP7C233S and TRIM26 co-expressed with HA-Ub in HEK293T cells. (F) Quantification of (C – E), normalized ubiquitin signal of the three nuclear DNA sensor.

IFI16 interact with TRIM26 most efficiently, it was only poorly ubiquitinated (Figure 4C–E). Together, these data suggest that MND4 might be subjected to TRIM26/USP7 controlled ubiquitination unlike its family members IFI16 and IFIX. These two DNA sensors may recruit the ubiquitin machinery for the manipulation of other substrates and/or pathways that are –as yet– unclear.

### Interferon stimulation affects anthracycline sensitivity

Re-localization of the DNA sensors upon histone eviction suggest a role in anthracycline-induced cell death. Interestingly, many tumor cells do not express these DNA sensors. IFI16 for example is mainly expressed in cells of the immune system, as well as fibroblasts, epithelial-, and endothelial cells, and altered expression has been shown to play a role in tumor development [15–17]. However, both type I ( $\alpha$  and  $\beta$ ) and type II ( $\gamma$ ) interferons positively regulate the expression of the PYHIN-family of proteins [18]. Therefore, we decided to investigate whether stimulation with interferons would upregulate the expression of IFI16 in MeJuSo cells, and if this could affect their cell survival upon treatment with the anthracycline drugs. To determine IFI16 expression following stimulation with type I (IFN $\beta$ ) and type II (IFN $\gamma$ ) interferons, we stimulated MeJuSo cells for 8, 24 and 48 hours and visualized protein expression by Western blot (Figure 5A and B). As expected, IFI16 protein levels

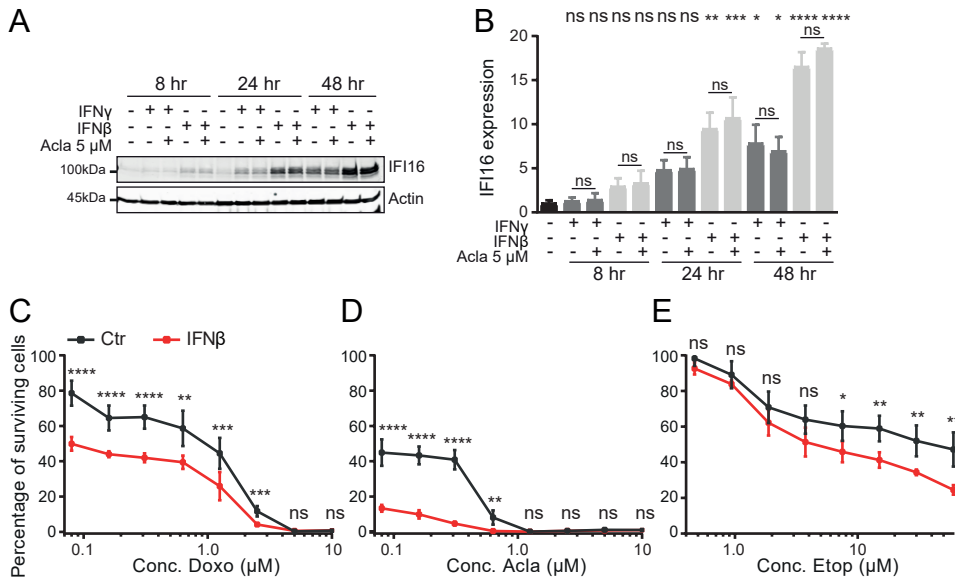


**Figure 5. Interferon stimulation upregulates IFI16 expression and sensitizes cells to anticancer drugs.** (A) IFI16 protein expression upon stimulation with interferon. MelJuSo cells are stimulated with IFN $\gamma$  or IFN $\beta$  (100ng/ml) for the indicated time points. One hour prior to collection, indicated samples were treated with Acla 5  $\mu$ M. (B) Quantification of A. Ordinary One-way ANOVA with Turkey's multiple comparison test; ns, not significant; \* $P < 0.05$ ; \*\* $P < 0.01$ ; \*\*\* $P < 0.001$ ; \*\*\*\* $P < 0.0001$ . (C - E) Cell Titer blue viability assay. MelJuSo cells with or without IFN $\beta$  stimulation (24 hours prior to treatment) were treated with various concentration of Doxo (C), Acla (D) and Etop (E). Multiple unpaired t-test; ns, not significant; \* $P < 0.05$ ; \*\* $P < 0.01$ ; \*\*\* $P < 0.001$ ; \*\*\*\* $P < 0.0001$ .

strongly increased over time by both IFN $\beta$  and IFN $\gamma$  stimulation. Of note, treatment with the histone evicting drug Acla did not affect IFI16 expression levels (Figure 5A and B). To determine the role of elevated IFI16 expression levels on sensitivity towards histone evicting drugs, we determined the cytotoxicity of Doxo, Acla or Etop in MelJuSo cells either pre-stimulated or not with IFN $\beta$ . Interferon stimulation sensitized MelJuSo cells especially for Acla (histone eviction only) and Doxo (histone eviction and DNA damage) treatment and had only marginal effects on Etop (DNA damage only) (Figure 5C-E). These data form preliminary evidence that IFI16 might play a role in detection of histone free DNA induced by the anthracycline drugs, and subsequent initiation of cell death.

## CONCLUSION AND FUTURE DIRECTIONS

Every year over one million patients with different types of cancer receive anthracycline based-treatments. While these drugs are very effective anticancer drugs, their exact mechanism of action is disputed. Since their discovery decades ago, various working mechanism have been suggested. These include; interfering with the catalytic cycle of Topo II $\alpha$  resulting in the induction of DNA double strand breaks, the formation of free radicals, and induction of chromatin damage via eviction of histones [4-6, 19]. Our recent work indicated that the latter mechanism might be the most relevant activity for the anticancer mechanism of these drugs [20]. However,

how chromatin damage then leads to the initiation of cell death remains unclear. We hypothesized that histone free DNA, a consequence of histone eviction, could be sensed by nuclear proteins to either restore this unnatural situation or to initiate cell death. Here, we identify three proteins from the PYHIN protein family (IFI16, IFI16 and MDA5) that re-localized to DNA upon treatment with the anthracyclines Doxo, Acla, Epi or Dauno, but not with drugs that are unable to evict histones (Figure 1A, B and Figure S1, S2 and S3). In addition, DNA binding of IFI16 was increased by the histone eviction drugs Doxo and Acla (Figure 1E). Thus, chromatin damage as a result of anthracycline treatment results in increased DNA binding of DNA sensors, potentially signaling to the cell that undesired naked DNA is present.

But what happens after these DNA sensors detect the histone free DNA? In the context of viral infection Unterholzner et. al. reported that detection by IFI16 induces IFN $\beta$  production via recruitment and activation of the STING-TBK1-IRF3 pathway [21]. Production of IFN $\beta$ , which is a hallmark for a functional innate immune response, via DNA sensing by IFI16 might also play a role in the anti-tumor response of anthracyclines in vivo. Alternatively, IFI16 is involved in transcriptional repression. Johnstone et. al. showed that IFI16 can repress transcription of a GAL4 reporter construct and the HCMV gene UL54 reporter construct via binding of its HIN200 domain [22]. In human embryo lung fibroblasts, IFI16 downregulates viral gene expression and hereby replication of HCMV by preventing the binding of the transcription factor Sp1 [23]. Similarly, IFI16 inhibits HSV-1 viral replication via repression of HSV-1 gene expression [24, 25]. Mechanistically, IFI16 alters the epigenetic state of the viral DNA [24] and likely restricts viral gene expression by inducing a viral heterochromatin (H3K9me3) state [25]. This suggests that IFI16 might repress transcription upon anthracycline-induced histone eviction. Interestingly, it is known that the anthracycline drugs effects the transcriptome [5]. Therefore, studying the role of these different nuclear DNA sensors on altered transcription of anthracycline treated cells would be an interesting next step.

Others have described that IFI16 can interact with p53 via its HIN200A domain to regulate the cell cycle and apoptosis [26]. This interaction does not impact p53 expression or stability, but rather its DNA binding capability. Co-expression of IFI16 and p53 also resulted in a dose-dependent increase of p53-mediated transcription activation of the CAT reporter. In addition, the interaction of IFI16 with p53 modulates p53 function and target gene regulation to control cell cycle regulation via p21 in U2OS cells [27]. In our Bio-ID screen we identified multiple potential interacting proteins for IFIX, IFI16 and MDA5, including the DUB USP7 and the E3-ligase TRIM26 (Table 1 and Figure 2B and C). Since both IFI16 and USP7 are known to interact with p53 [26, 28], USP7 might be recruited to de-ubiquitinate p53 and initiate a stress response upon detection of the histone free DNA by IFI16. In support of this, treatment with Doxo indeed resulted in redistribution of mTurq-tagged USP7 in a manner similar as the DNA sensors (Figure S4). Besides a role for USP7 and p53, sensing of histone free DNA might be linked to activation of the innate immune system via recruitment of TRIM26, since TRIM26 is described to interact with and activate TBK1 [14]. How DNA sensing and binding of USP7 or TRIM26 affects anthracycline induced cell death remains unclear. But p53-mediated apoptosis initiation upon complex formation of the DNA sensors with USP7 and/or TRIM26 would be of interest for further investigation.

The human PYHIN protein family was initially identified as interferon inducible genes due to their sequence similarity to the murine gene cluster [29]. Expression of these proteins is positively regulated by type I and/or type II interferons [18]. We show

that interferon stimulation of MelJuSo cells also resulted in increased expression of IFI16, which increased the sensitivity to treatment with anthracycline drugs (Figure 5). This might indicate that indeed IFI16 plays a role in histone eviction-mediated cell death in these cells, although this should be confirmed in IFI16 depleted cells. If so, our observations are supported by a study of Fujiuchi et. al. who showed that enhanced expression of IFI16 in the breast cancer cell line MCF-7 increased their susceptibility toward ionizing radiation-induced apoptosis [30]. Enhanced IFI16 expression resulted in p53-mediated apoptosis upon irradiation via the known p53 target genes p21, Hdm2 and bax. Together, this argues that IFI16 can initiate p53-mediated apoptosis upon sensing of DNA/genotoxic stress in general. Collectively, our work suggests that the nuclear DNA sensors IFIX, IFI16 and MNDA might function as novel players in anthracycline induced cell death. We defined the interactions between the sensors with the ubiquitin machinery (USP7 and TRIM26) and a DNA helicase (XRCC6) involved in innate immunity. Further research is needed to unravel their exact molecular mechanism and contribution in anthracycline-induced chromatin damage. But this could yield new insights in the cellular response to an old anticancer drug family that employs the innate immune system.

## MATERIALS AND METHODS

### Reagents and antibodies

Doxorubicin, epirubicin, and cisplatin were obtained from Accord Healthcare, UK. Etoposide was obtained from Pharmachemie, the Netherlands. Daunorubicin was obtained from Sanofi-Aventis, the Netherlands. Aclarubicin (sc-200160) and am-rubicin (sc-207289) were purchased from Santa Cruz Biotechnology, USA. All the drugs were dissolved according to the manufacturer's formulation, aliquoted and stored at  $-20^{\circ}\text{C}$  for further use. Rabbit anti-GFP (generated in house, NKL, The Netherlands, 1:1000 [31]), HRP-Protein A (10-1023, Invitrogen, 1:5000), HRP-conjugated anti-FLAG M2 (Mouse, A8592, Sigma, 1:5000), Mouse anti-HA (16B12, Covance, 1:1000), IRDye 680LT goat anti-mouse IgG (H+L) (926-68020, Li-COR, 1:20000), IRDye 800CW goat anti-rabbit IgG (H+L) (926-32211, Li-COR, 1:10000), mouse anti-FLAG M2 (F3165, Sigma, 1:5000), mouse anti- $\beta$ -actin (A5441, Sigma, 1:10000), mouse anti-IFI16 (Santa Cruz, sc-8023, 1:500).

### Cell culture and constructs

MelJuSo cells were cultured in IMDM medium supplemented with 8% FCS. HEK293T and Hela cells were cultured in DMEM medium supplemented with 8% FCS. Cell lines were maintained in a humidified atmosphere of 5%  $\text{CO}_2$  at  $37^{\circ}\text{C}$  and regularly tested for the absence of mycoplasma. IFIX amplified from IMAGE # 40033401 and MNDA amplified from IMAGE # 5223430 were cloned into the mGFP-C1 vector by BglII-Asp718I restriction sites. IFI16 was amplified from Addgene clone #35064 and cloned into the pEGFP-C2 vector by BamHI/Bsp120I restriction sites. USP7 was amplified from addgene clone # 16655 and cloned into the FLAG-C1 and mTurq-C1 vector by Sall/BamHI restriction sites. Inactive mutant of USP7 (C223S) was created by site directed mutagenesis. USP7 truncation mutant constructs (FLAG-C1 vector) were obtained by IVA cloning [32]. TRIM26 was described before and kindly gifted by JL Parsons [33], amplified and cloned into the FLAG-C1 vector by Sall/BamHI restriction sites. TRIM26 truncation mutant constructs (FLAG-C1 vector) were obtained by IVA cloning. XRCC6 was amplified from the pDONR223 library and cloned into the FLAG-C1 vector by Sall/BamHI restriction sites. BirA-GFP constructs were created

by amplification of the gene from the full length constructs (pEGFP-C2-IFI16, mGFP-C1-IFIX and mGFP-C1-MNDA) and cloned into the mGFP-BirA-C1 vector [34] using Sall/BamHI (for IFIX and IFI16) and HindIII/Sall (for MNDA) restriction enzymes. For ubiquitination assays HA-Ub pcDNA3.1, 2xHA-C1 were previously described [35]. All constructs were sequence verified.

### **Confocal microscopy**

For live cell imaging MeJuSo cells were seeded in a 35mm glass bottom petri dish (Poly-dlysine-Coated, MatTek Corporation), transfected (effectene, Qiagen) 16 hours later and treated as indicated. Time-lapse confocal imaging was performed on a Leica SP8 confocal microscope system, 63x lens, equipped with a climate chamber. Images were quantified using Image J software.

### **ChIP-sequencing**

A total of  $5 \times 10^7$  MeJuSo cells were used per sample and treated with 10 $\mu$ M Doxo, 10 $\mu$ M Acla or 10 $\mu$ M Etop for 2 hours. The experiment was performed with biological replicates. Upon treatment cells were fixed and processed as describes [36]. For immunoprecipitation mouse anti-IFI16 (Santa Cruz, sc-8023) was used. DNA was processed to be sequenced following a standard TrueSeq library preparation for the Illumina HiSeq2000 platform. All samples were quality controlled and processed in the same way before further analyzed. ChIP peak calling was measured by a binarized genome with a 500 bp window. Differential expressed peaks were determined using MACS version 2.1.1.20160309 software.

### **Bio-ID and Mass spectrometry**

For Bio-ID, HEK293T cells were seeded in a 10cm dish, transfected 16 hours later with the BirA-GFP constructs using PEI-transfection reagent. Cell were incubated with 50  $\mu$ M biotin for 3 hours and lysed for 30 minutes in lysis buffer (50mM Tris-HCl pH 8.0, 150mM NaCl, 5mM MgCl<sub>2</sub>, 0.5% NP-40 supplemented with protease inhibitors (Roche 7 Diagnostics, EDTA free). Supernatant after spinning (15min. at 12000g) was incubated with High Capacity Neutravidin Agarose Resin beads (Thermo Scientific) for 1 hour. Beads were extensively washed in washing buffer (50mM Tris-HCl pH 8.0, 150mM NaCl, 5mM MgCl<sub>2</sub>, 0.08% NP-40 supplemented with 1% SDS) before addition of Laemmli Sample Buffer (containing 5%  $\beta$ -mercaptoethanol) followed by 10 minutes incubation at 95°C. Immunoprecipitated proteins were separated by SDS-PAGE, lanes were cut from the silver stained (Invitrogen) gel and subjected to reduction by dithiothreitol, alkylation with iodoacetamide and in-gel trypsin digestion using a Proteineer DP digestion robot (Bruker). Tryptic peptides were extracted from the gel, lyophilized, dissolved in 95/3/0.1 v/v/v water/acetonitril/formic acid and subsequently analyzed by on-line nanoHPLC MS/MS using an 1100 HPLC system (Agilent Technologies), as previously described [37]. Peptides were trapped at 10  $\mu$ l/min on a 15-mm column (100- $\mu$ m ID; ReproSil-Pur C18-AQ, 3  $\mu$ m, Dr. Maisch GmbH) and eluted to a 200 mm column (50- $\mu$ m ID; ReproSil-Pur C18-AQ, 3  $\mu$ m) at 150 nl/min. All columns were packed in house. The column was developed with a 30-min gradient from 0 to 50% acetonitrile in 0.1% formic acid. The end of the nanoLC column was drawn to a tip (5- $\mu$ m ID), from which the eluent was sprayed into a 7-tesla LTQ-FT Ultra mass spectrometer (Thermo Electron). The mass spectrometer was operated in data-dependent mode, automatically switching between MS and MS/MS acquisition. Full scan MS spectra were acquired in the FT-ICR with a resolution of 25,000 at a target value of 3,000,000. The two most intense ions were then isolated



for accurate mass measurements by a selected ion-monitoring scan in FT-ICR with a resolution of 50,000 at a target accumulation value of 50,000. Selected ions were fragmented in the linear ion trap using collision-induced dissociation at a target value of 10,000. In a post-analysis process, raw data were first converted to peak lists using Bioworks Browser software v3.2 (Thermo Electron), and then submitted to the Swissprot database version 51.6 (257,964 entries), using Mascot v. 2.2.04 ([www.matrixscience.com](http://www.matrixscience.com)) for protein identification. Mascot searches were with 2 ppm and 0.8 Da deviation for precursor and fragment mass, respectively, and trypsin as enzyme. Protein was finally sorted and compared using Scaffold software version 3.0.1 ([www.proteomesoftware.com](http://www.proteomesoftware.com)).

### Co-immunoprecipitation

For co-immunoprecipitation experiments, HEK293T cells were seeded, transfected 16 hours later using PEI-transfection reagent and lysed for 30 minutes at 4°C in lysis buffer (50mM Tris-HCl pH 8.0, 150mM NaCl, 5mM MgCl<sub>2</sub>, 0.5% NP-40 supplemented with protease inhibitors (Roche 7 Diagnostics, EDTA free). Supernatant after spinning (15min at 12000g) was incubated with GFP-trap agarose beads (ChromoTek) for 1 hour. Beads were washed four times in wash buffer (50mM Tris-HCl pH 8.0, 150mM NaCl, 5mM MgCl<sub>2</sub>, 0.08% NP-40) before addition of Laemmli Sample buffer (containing 5% β-mercaptoethanol) followed by 10 minutes incubation at 95°C. Co-immunoprecipitated proteins were separated by SDS-PAGE for Western blotting and detection by antibody staining. Antibody signals were detected by Chemidoc XRS+ imager (Bio-Rad).

### Ubiquitination assay

HEK293T cells were lysed for 30 min in lysis buffer (50mM Tris-HCl pH7.5, 150mM NaCl, 5mM MgCl<sub>2</sub>, 5mM EDTA, 0.5%TX100, 0.2% SDS, freshly added 10mM NMM (DUB inhibitor diluted in DMSO) and protease inhibitors (Roche Diagnostics, EDTA free). Supernatants were sonicated (Branson Sonifier 250, 3 pulses, 70%) followed by spinning (15 min at 12,000g), and incubated with GFP-trap agarose beads (ChromoTek) for 1 hour. Beads were washed four times in lysis buffer before addition of Laemmli Sample Buffer (containing 5% β-mercaptoethanol) followed by 10 min incubation at 95°C. Proteins were separated by SDS-PAGE, transferred to nitrocellulose membranes and detected by antibodies. Li-Cor fluorescent dyes were used as secondary antibodies and detected by an Odyssey Classic imager (Li-Cor).

### Western blotting

SDS-sample buffer (2% SDS, 10% glycerol, 5% β-mercaptoethanol, 60mM Tris-HCl pH 6.8 and 0.01% bromophenol blue) was added to the samples. Samples were separated by a 10% acrylamide gel followed by western blotting. Primary antibodies used for blotting: anti-GFP (generated in house, NKI, The Netherlands, 1:1000 [31]), HRP-conjugated anti-FLAG M2 (Mouse, A8592, Sigma, 1:5000), mouse anti-FLAG M2 (F3165, Sigma, 1:5000), mouse anti-HA (16B12, Covance, 1:1000), mouse anti-β-actin (A5441, Sigma, 1:10000), mouse anti-β-actin (A5441, Sigma, 1:10000), mouse anti-IFI16 (Santa Cruz, sc-8023, 1:500). Images were quantified using ImageJ software.

### *In vitro* cell viability assay

MelJuSo cells were seeded into 96-well plates in the presence or absence of IFNβ or IFNγ (100ng/ml). Twenty-four hours after seeding, cells were treated with indicated

drugs for 2 hours at various concentrations. Subsequently, drugs were removed and cells were left to grow for an additional 72 hours. Cell viability was measured using the CellTiter-Blue viability assay (Promega). Relative survival was normalized to the untreated control and corrected for background signal

## REFERENCE

1. Weiss, R. B. (1992) The Anthracyclines - Will We Ever Find a Better Doxorubicin, *Semin Oncol.* 19, 670-686.
2. Hortobagyi, G. N. (1997) Anthracyclines in the treatment of cancer - An overview, *Drugs.* 54, 1-7.
3. Pommier, Y. (1993) DNA Topoisomerase-I and Topoisomerase-II in Cancer-Chemotherapy - Update and Perspectives, *Cancer Chemoth Pharm.* 32, 103-108.
4. Nitiss, J. L. (2009) Targeting DNA topoisomerase II in cancer chemotherapy, *Nat Rev Cancer.* 9, 338-350.
5. Pang, B. X., Qiao, X. H., Janssen, L., Velds, A., Groothuis, T., Kerkhoven, R., Nieuwland, M., Ovaa, H., Rottenberg, S., van Tellingen, O., Janssen, J., Huijgens, P., Zwart, W. & Neefjes, J. (2013) Drug-induced histone eviction from open chromatin contributes to the chemotherapeutic effects of doxorubicin, *Nat Commun.* 4.
6. Yang, F., Kemp, C. J. & Henikoff, S. (2013) Doxorubicin Enhances Nucleosome Turnover around Promoters, *Curr Biol.* 23, 782-787.
7. McGinty, R. K. & Tan, S. (2015) Nucleosome Structure and Function, *Chem Rev.* 115, 2255-2273.
8. Ludlow, L. E. A., Johnstone, R. W. & Clarke, C. J. P. (2005) The HIN-200 family: More than interferon-inducible genes?, *Exp Cell Res.* 308, 1-17.
9. Park, H. H., Lo, Y. C., Lin, S. C., Wang, L., Yang, J. K. & Wu, H. (2007) The death domain superfamily in intracellular signaling of apoptosis and inflammation, *Annu Rev Immunol.* 25, 561-586.
10. Monroe, K. M., Yang, Z. Y., Johnson, J. R., Geng, X., Doitsh, G., Krogan, N. J. & Greene, W. C. (2014) IFI16 DNA Sensor Is Required for Death of Lymphoid CD4 T Cells Abortively Infected with HIV, *Science.* 343, 428-432.
11. Kerur, N., Veetil, M. V., Sharma-Walia, N., Bottero, V., Sadagopan, S., Otageri, P. & Chandran, B. (2011) IFI16 Acts as a Nuclear Pathogen Sensor to Induce the Inflammasome in Response to Kaposi Sarcoma-Associated Herpesvirus Infection, *Cell Host Microbe.* 9, 363-375.
12. Dell'Oste, V., Gatti, D., Gugliesi, F., De Andrea, M., Bawadekar, M., Lo Cigno, I., Biolatti, M., Vallino, M., Marschall, M., Gariglio, M. & Landolfo, S. (2014) Innate Nuclear Sensor IFI16 Translocates into the Cytoplasm during the Early Stage of In Vitro Human Cytomegalovirus Infection and Is Entrapped in the Egressing Virions during the Late Stage, *J Virol.* 88, 6970-6982.
13. Johnson, K. E., Bottero, V., Flaherty, S., Dutta, S., Singh, V. V. & Chandran, B. (2014) IFI16 Restricts HSV-1 Replication by Accumulating on the HSV-1 Genome, Repressing HSV-1 Gene Expression, and Directly or Indirectly Modulating Histone Modifications, *Plos Pathog.* 10.
14. Ran, Y., Zhang, J., Liu, L. L., Pan, Z. Y., Nie, Y., Zhang, H. Y. & Wang, Y. Y. (2016) Autoubiquitination of TRIM26 links TBK1 to NEMO in RLR-mediated innate antiviral immune response, *J Mol Cell Biol.* 8, 31-43.
15. Gariglio, M., Azzimonti, B., Pagano, M., Palestro, G., De Andrea, M., Valente, G., Voglino, G., Navino, L. & Landolfo, S. (2002) Immunohistochemical expression analysis of the human interferon-inducible gene IFI16, a member of the HIN200 fam-

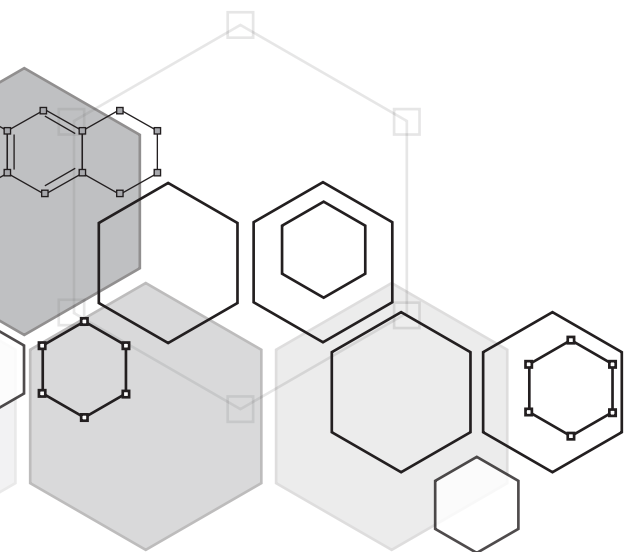


- ily, not restricted to hematopoietic cells, *J Interf Cytok Res.* 22, 815-821.
16. W. Wei, C. J. C., G. R. Somers, K. S. Cresswell, K. A. Loveland, J. A. Trapani & R. W. Johnstone. (2003) Expression of IFI16 in epithelial cells and lymphoid tissues. , *Histochem Cell Biol.* 119, 45-54.
17. Choubey, D., Deka, R. & Ho, S. M. (2008) Interferon-inducible IFI16 protein in human cancers and autoimmune diseases, *Front Biosci.* 13, 598-608.
18. Landolfo, S., Gariglio, M., Gribaudo, G. & Lembo, D. (1998) The Ifi 200 genes: An emerging family of IFN-inducible genes, *Biochimie.* 80, 721-728.
19. Doroshow, J. H. & Davies, K. J. A. (1986) Redox Cycling of Anthracyclines by Cardiac Mitochondria .2. Formation of Superoxide Anion, Hydrogen-Peroxide, and Hydroxyl Radical, *J Biol Chem.* 261, 3068-3074.
20. Qiao, X., van der Zanden, S. Y., Wander, D. P. A., Borrás, D. M., Song, J. Y., Li, X., van Duikeren, S., van Gils, N., Rutten, A., van Herwaarden, T., van Tellingen, O., Giacomelli, E., Bellin, M., Orlova, V., Tertoolen, L. G. J., Gerhardt, S., Akkermans, J. J., Bakker, J. M., Zuur, C. L., Pang, B., Smits, A. M., Mummery, C. L., Smit, L., Arens, R., Li, J., Overkleeft, H. S. & Neefjes, J. (2020) Uncoupling DNA damage from chromatin damage to detoxify doxorubicin, *Proc Natl Acad Sci U S A.*
21. Unterholzner, L., Keating, S. E., Baran, M., Horan, K. A., Jensen, S. B., Sharma, S., Sirois, C. M., Jin, T. C., Latz, E., Xiao, T. S., Fitzgerald, K. A., Paludan, S. R. & Bowie, A. G. (2010) IFI16 is an innate immune sensor for intracellular DNA, *Nat Immunol.* 11, 997-U42.
22. Johnstone, R. W., Kerry, J. A. & Trapani, J. A. (1998) The human interferon-inducible protein, IFI 16, is a repressor of transcription, *J Biol Chem.* 273, 17172-17177.
23. Gariano, G. R., Dell'Oste, V., Bronzini, M., Gatti, D., Luganini, A., De Andrea, M., Gribaudo, G., Gariglio, M. & Landolfo, S. (2012) The Intracellular DNA Sensor IFI16 Gene Acts as Restriction Factor for Human Cytomegalovirus Replication, *Plos Pathog.* 8.
24. Johnson, K. E., Bottero, V., Flaherty, S., Dutta, S., Singh, V. V. & Chandran, B. (2014) IFI16 restricts HSV-1 replication by accumulating on the hsv-1 genome, repressing HSV-1 gene expression, and directly or indirectly modulating histone modifications, *Plos Pathog.* 10, e1004503.
25. Orzalli, M. H., Connell, S. E., Berrios, C., DeCaprio, J. A. & Knipe, D. M. (2013) Nuclear interferon-inducible protein 16 promotes silencing of herpesviral and transfected DNA, *Proc Natl Acad Sci U S A.* 110, E4492-501.
26. Johnstone, R. W., Wei, W., Greenway, A. & Trapani, J. A. (2000) Functional interaction between p53 and the interferon-inducible nucleoprotein IFI 16, *Oncogene.* 19, 6033-6042.
27. Kwak, J. C., Ongusaha, P. P., Ouchi, T. & Lee, S. W. (2003) IFI16 as a negative regulator in the regulation of p53 and p21(Waf1), *J Biol Chem.* 278, 40899-40904.
28. Sheng, Y., Saridakis, V., Sarkari, F., Duan, S. L., Wu, T. N., Arrowsmith, C. H. & Frappier, L. (2006) Molecular recognition of p53 and MDM2 by USP7/HAUSP, *Nat Struct Mol Biol.* 13, 285-291.
29. Trapani, J. A., Browne, K. A., Dawson, M. J., Ramsay, R. G., Eddy, R. L., Shows, T. B., White, P. C. & Dupont, B. (1992) A Novel Gene Constitutively Expressed in Human Lymphoid-Cells Is Inducible with Interferon-Gamma in Myeloid Cells, *Immunogenetics.* 36, 369-376.
30. Fujiuchi, N., Aglipay, J. A., Ohtsuka, T., Maehara, N., Sahin, F., Su, G. H., Lee, S. W. & Ouchi, T. (2004) Requirement of IFI16 for the maximal activation of p53 induced by ionizing radiation, *J Biol Chem.* 279, 20339-20344.

31. van der Kant, R., Fish, A., Janssen, L., Janssen, H., Krom, S., Ho, N., Brummelkamp, T., Carette, J., Rocha, N. & Neefjes, J. (2013) Late endosomal transport and tethering are coupled processes controlled by RILP and the cholesterol sensor ORP1L, *J Cell Sci.* 126, 3462-3474.
32. Garcia-Nafria, J., Watson, J. F. & Greger, I. H. (2016) IVA cloning: A single-tube universal cloning system exploiting bacterial In Vivo Assembly, *Sci Rep-Uk.* 6.
33. Edmonds, M. J., Carter, R. J., Nickson, C. M., Williams, S. C. & Parsons, J. L. (2017) Ubiquitylation-dependent regulation of NEIL1 by Mule and TRIM26 is required for the cellular DNA damage response, *Nucleic Acids Res.* 45, 726-738.
34. Sapmaz, A., Berlin, I., Bos, E., Wijdeven, R. H., Janssen, H., Konietzny, R., Akkermans, J. J., Erson-Bensan, A. E., Koning, R. I., Kessler, B. M., Neefjes, J. & Ovaa, H. (2019) USP32 regulates late endosomal transport and recycling through deubiquitylation of Rab7, *Nat Commun.* 10.
35. Jongsma, M. L. M., Berlin, I., Wijdeven, R. H. M., Janssen, L., Janssen, G. M. C., Garstka, M. A., Janssen, H., Mensink, M., van Veelen, P. A., Spaapen, R. M. & Neefjes, J. (2016) An ER-Associated Pathway Defines Endosomal Architecture for Controlled Cargo Transport, *Cell.* 166, 152-166.
36. Schmidt, D., Wilson, M. D., Spyrou, C., Brown, G. D., Hadfield, J. & Odom, D. T. (2009) ChIP-seq: Using high-throughput sequencing to discover protein-DNA interactions, *Methods.* 48, 240-248.
37. Meiring, H. D., van der Heeft, E., ten Hove, G. J. & de Jong, A. P. J. M. (2002) Nanoscale LC-MS(n): technical design and applications to peptide and protein analysis, *J Sep Sci.* 25, 557-568.

# SUPPLEMENTAL INFORMATION

7



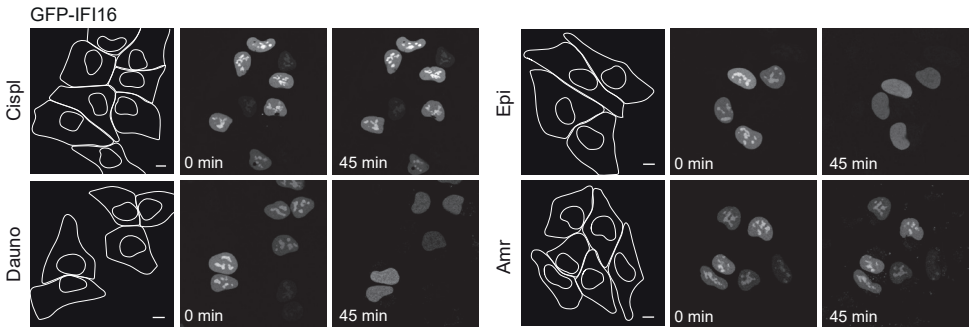


**Figure S1. Nuclear DNA sensor IFI16 re-localize upon histone eviction.** *MelJuSo* cells transiently expressing GFP-tagged IFI16 are followed over time upon treatment with various drugs: Cispl 10 $\mu$ M, Dauno 5 $\mu$ M, Epi 10  $\mu$ M or Amr 10  $\mu$ M. Scale bar, 10  $\mu$ m.

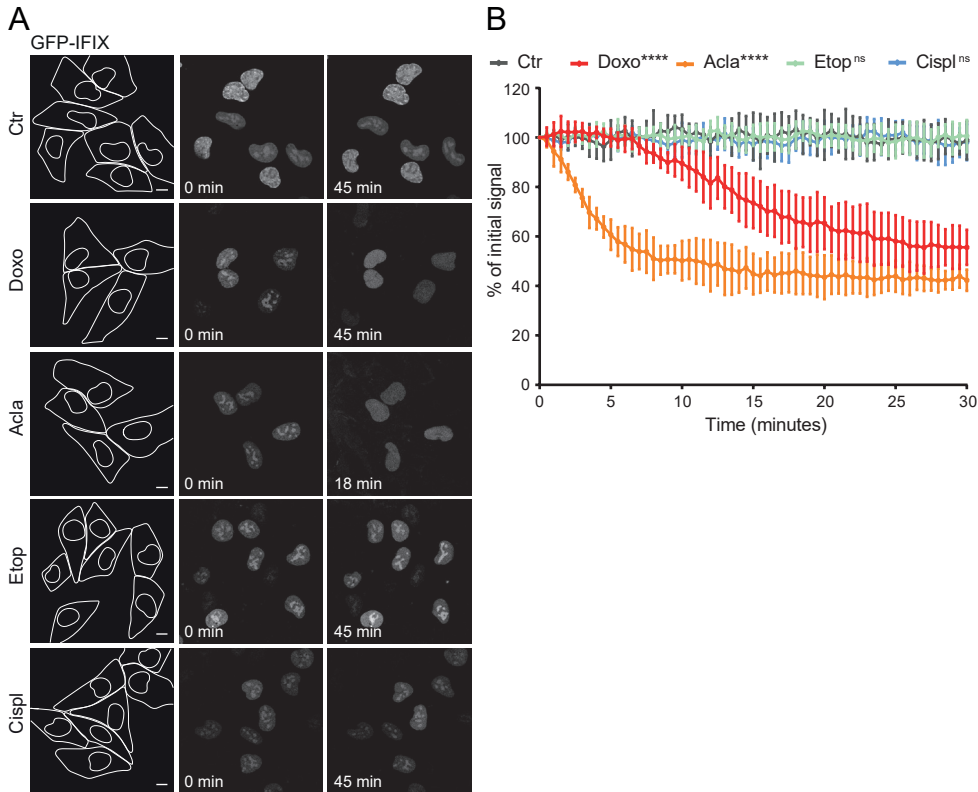


**Figure S2. Nuclear DNA sensor IFIX re-localize upon histone eviction.** (A) *MelJuSo* cells transiently expressing GFP-tagged IFIX are followed over time upon treatment with various drugs: Doxo 10 $\mu$ M, Acla 5 $\mu$ M, Etop 10 $\mu$ M, Cispl 10 $\mu$ M. Scale bar, 10  $\mu$ m. (B) Quantification of the fluorescent intensity in the nucleoli of cells in A. Ordinary Two-way ANOVA with Turkey's multiple comparison test; ns, not significant; \*\*\*\* $P < 0,0001$ .

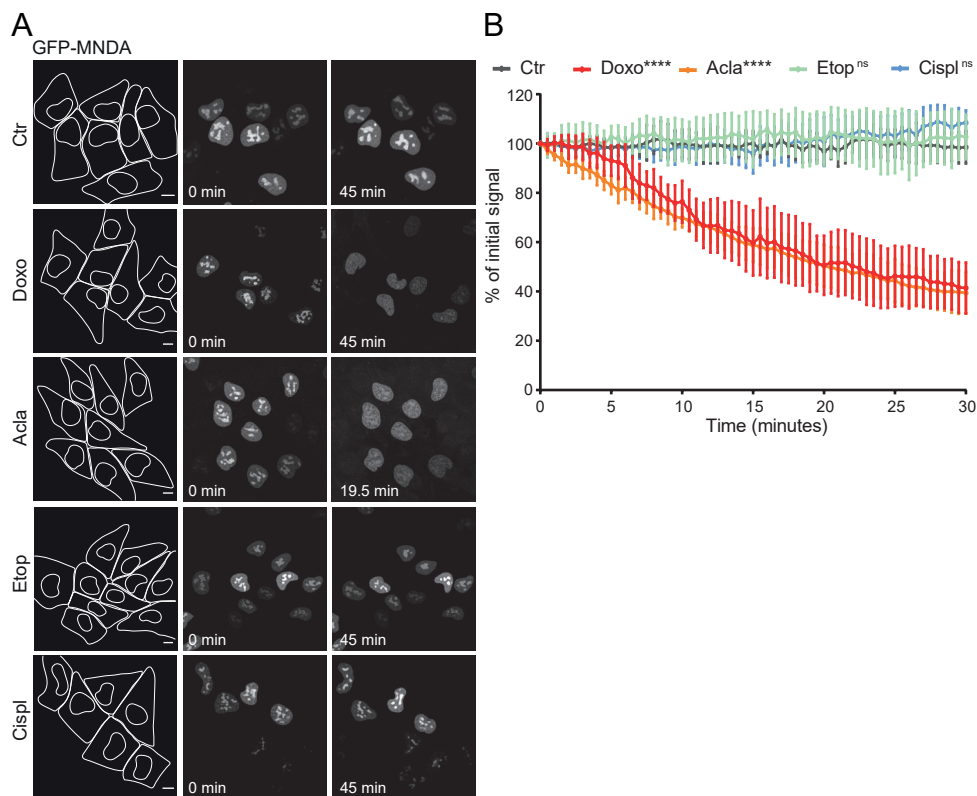


**Figure S3. Nuclear DNA sensor MNDA re-localize upon histone eviction.** (A) *MelJuSo* cells transiently expressing GFP-tagged MNDA are followed over time upon treatment with various drugs: Doxo 10 $\mu$ M, Acla 5 $\mu$ M, Etop 10 $\mu$ M, Cispl 10 $\mu$ M. Scale bar, 10  $\mu$ m. (B) Quantification of the fluorescent intensity in the nucleoli of cells in C. Ordinary Two-way ANOVA with Turkey's multiple comparison test; ns, not significant; \*\*\*\* $P < 0,0001$ .

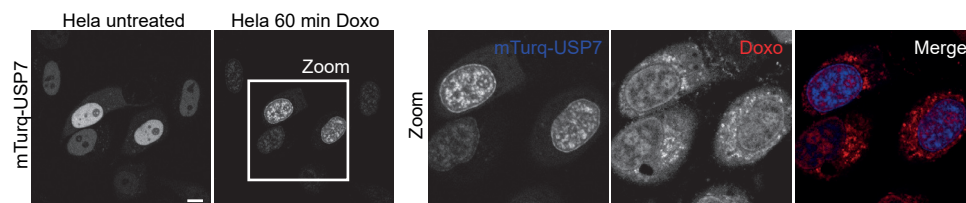
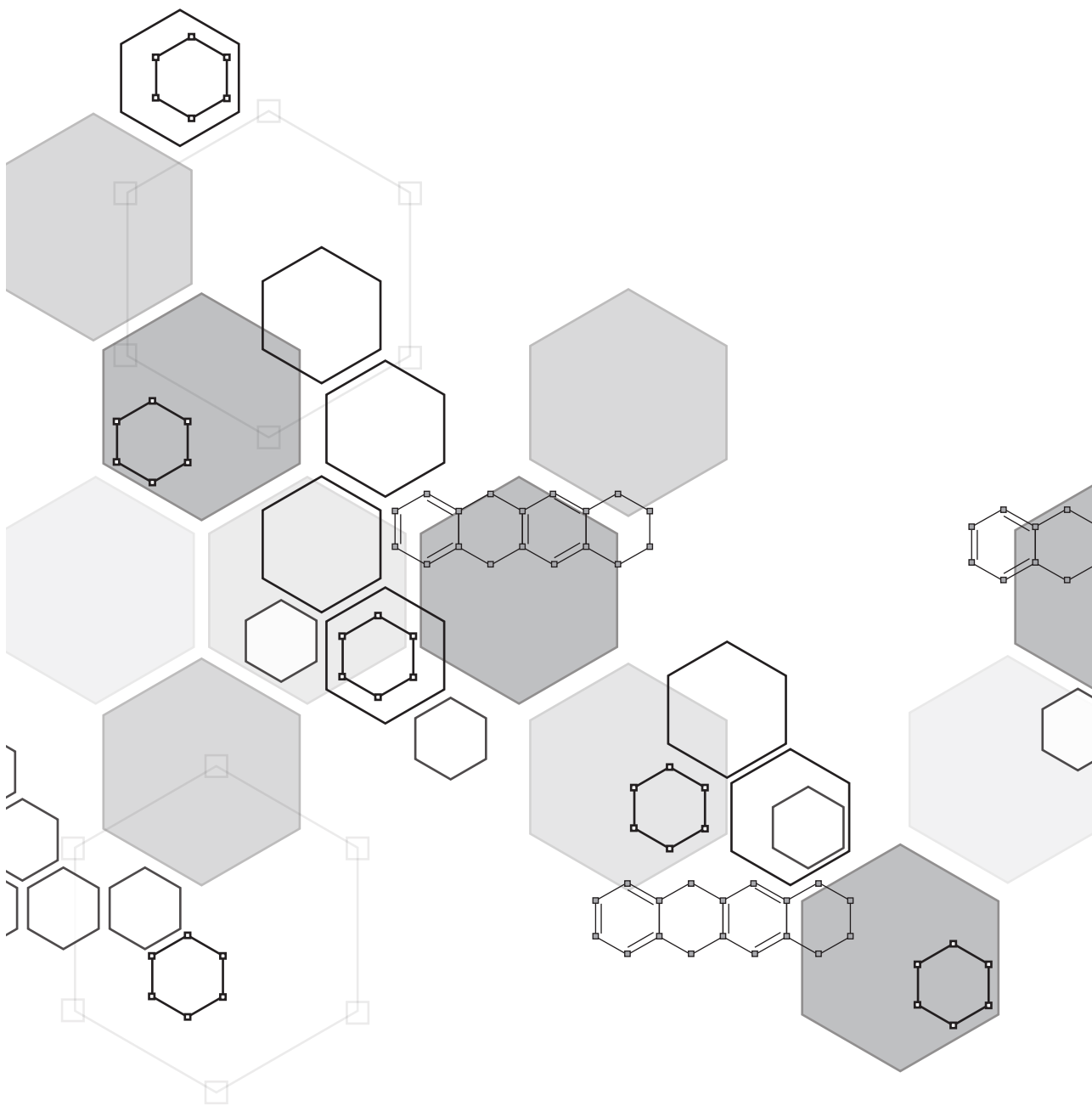
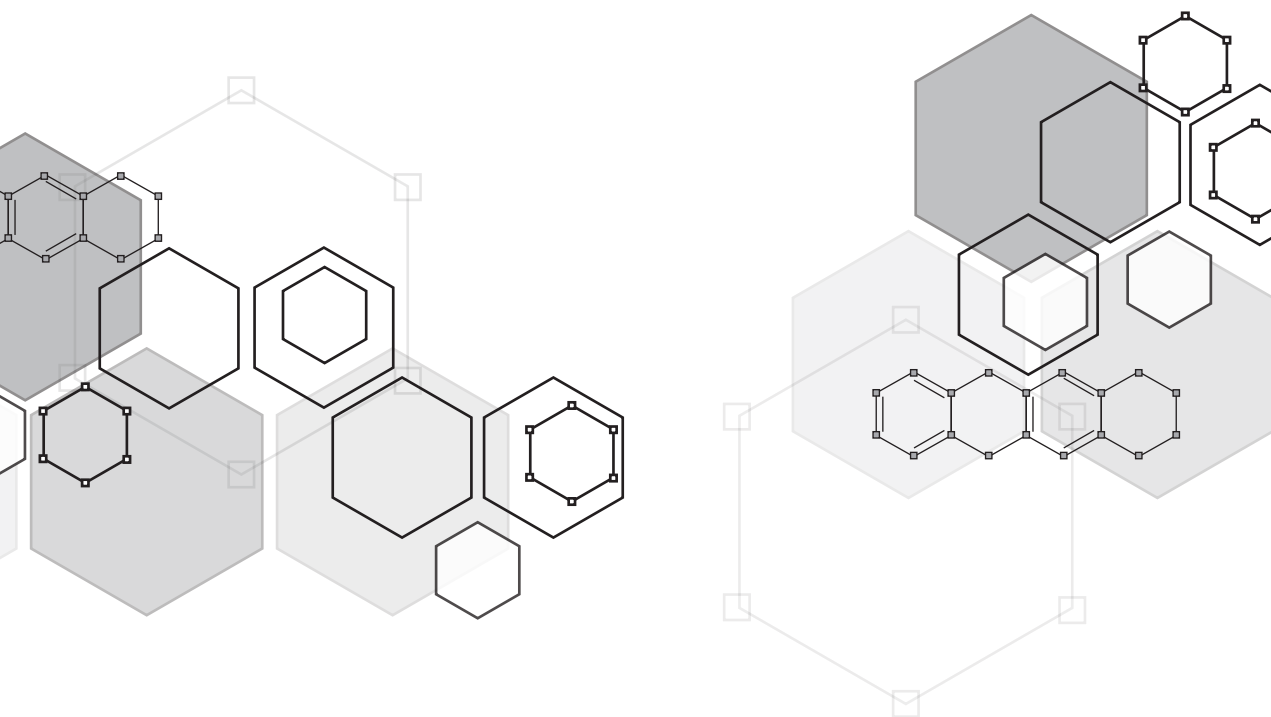


**Figure S4. USP7 re-localize upon Doxo treatment.** USP7 localization in HeLa cells transiently expressing mTurq-USP7 upon treatment with Doxo 10 $\mu$ M for 1 hour. Scale bar, 10  $\mu$ m.



# Opportunities for small molecules in cancer immunotherapy

# 8



Sabina Y. van der Zanden, Jolien J. Luimstra, Jacques Neeffjes, Jannie Borst and Huib Ovaa

*Trends in Immunology (2020)*



**ABSTRACT**

Cancer immunotherapy has proven remarkably successful through instigation of systemic anti-tumor T cell responses. Despite this achievement, further advancements are needed to expand the scope of susceptible cancer types and overcome variation in treatment outcomes between patients. Small-molecule drugs targeting defined pathways and/or cells capable of immune modulation are expected to substantially improve efficacy of cancer immunotherapy. Small-molecule drugs possess unique properties compatible with systemic administration and amenable to both extracellular and intracellular targets. These compounds can modify molecular pathways to overcome immune tolerance and suppression towards effective anti-tumor responses. Here, we provide an overview of how such effects might be achieved by combining immuno-therapy with conventional and/or new small-molecule chemotherapeutics.

**ENGAGING IMMUNE PATHWAYS TO TREAT CANCER**

Immunotherapy is rapidly becoming an established cancer treatment next to surgery, chemotherapy, and radiotherapy. In contrast to targeted cancer therapies, immunotherapy relies on tumor-extrinsic mechanisms, which allow it to act on different cancer types in a manner independent of genetic tumor **heterogeneity** (see Glossary). Its central aim is to activate systemic tumor-specific CD8<sup>+</sup> **cytotoxic T lymphocyte (CTL)** responses against cancer cells. Ideally, a CTL response also eradicates (occult) metastases, even when only the primary tumor has been diagnosed [1]. Immunotherapy strategies include antibody-based ‘checkpoint’ inhibition, adoptive T cell therapy and therapeutic vaccination [2-5]. **Checkpoint blockade** using monoclonal antibodies (mAb) against cytotoxic T lymphocyte-associated protein 4 (CTLA-4), programmed death 1 (PD-1), or programmed death ligand 1 (PD-L1) has led to prominent breakthroughs in cancer immunotherapy. Such antibodies are effective boosters of anti-tumor immune responses, but bear the risk of inducing **immune-related adverse events (irAEs)** (generally most pronounced for anti-CTLA-4) [6, 7]. Despite its advantages, immunotherapy is successful in only a fraction of patients, and biomarkers broadly predictive of its efficacy remain to be defined. Immune responses to cancer are generally limited by three major bottle-necks: (i) recognition of tumor cells as ‘non-self’, (ii) peripheral tolerance, and (iii) **immunosuppression** in the **tumor microenvironment (TME)**. Immunotherapy, on its own or in combination with other strategies, should ideally overcome these bottlenecks. Various combination treatments have been tested to date, with limited success due to lack of synergy or unacceptable toxicity [6]. For instance, combining CTLA-4 and PD-1/PD-L1 blockades results in stronger anti-tumor responses with unique treatment-limiting toxicity profiles in melanoma and colorectal cancer patients [8, 9]. Here, use of small-molecule therapies may prove helpful, as such drugs feature a number of advantages over mAbs. Specifically, shorter half-lives of small molecules favor acute and reversible action, as well as reduce the chance of lasting systemic side-effects [10]. In contrast to antibodies, small molecules typically target intracellular proteins and feature distinct toxicity profiles, making them suitable candidates for combination treatments [11, 12]. Moreover, they can be produced at lower costs compared with antibodies and can often be administered orally [11, 12]. Hence, new strategies based on molecular insights of immunological and oncological processes are needed to advance the potential of small molecules in immunotherapy. Here, we provide our perspective on the future of cancer immunotherapy, with emphasis on

small molecules expected to improve checkpoint blockade success against cancer (Figure 1; Key Figure, Table 1).

### IMPROVING TUMOR-SPECIFIC T CELL PRIMING

In order to evoke a T cell response, tumor-derived proteins need to be proteolytically processed into pep-tides, which are subsequently presented by major histocompatibility complex class I and class II molecules (MHC I and MHC II) on the surface of professional antigen-presenting cells, in particular dendritic cells (DCs). T cells in secondary lymphoid organs can then recognize these peptide-MHC complexes via their T cell anti-gen receptors (TCRs). However, to undergo clonal expansion and effector- and memory-differentiation, T cells require additional signals provided by specific costimulatory molecules and cytokines. DCs provide these signals upon pattern recognition receptor (PRR) activation by **pathogen-associated molecular pat-terns (PAMPs)** or **danger-associated molecular patterns (DAMPs)**, in concert with specific cytokines, such as type I interferons (IFNs). Furthermore, tumor cells must present suitable **(neo)antigens** (peptides to which no **central tolerance** has been developed) for recognition by T cells. Tumors with a high mutational load, including melanoma, smoking-induced lung cancers, **microsatellite-liable** colon cancer, and virus-induced cancers, generally express neoantigens. Hence, these tumors are often immunogenic and raise T cell responses as they develop. Consequently, these cancers can be sensitive to checkpoint blockade [13]. On the other hand, recognition of tumors that are not immunogenic on their own may be facilitated through induction of immunogenic cell death with the help of radiotherapy, certain

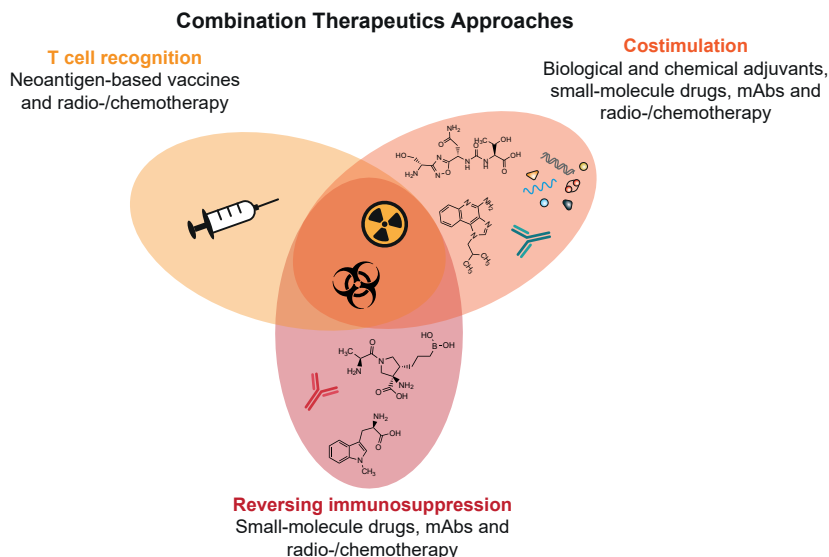


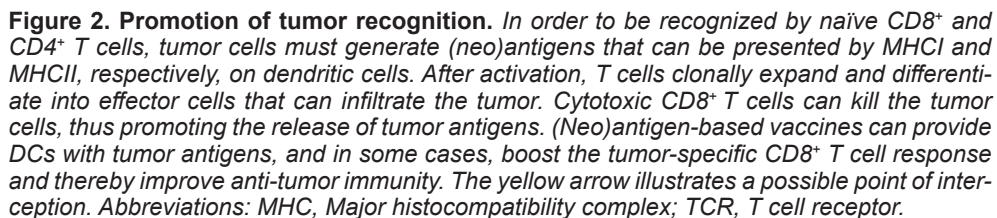
**Figure 1, Key Figure. Combination therapeutic approaches in cancer immunotherapy.** Neoantigen-based vaccines, conventional chemotherapeutic drugs, radiotherapy, adjuvants, monoclonal antibodies (mAbs), and small-molecule drugs may be designed and targeted to work at different stages of impeded anti-tumor immunity. A combination of strategies can be exploited to ideally boost T cell immunity and overcome tumor-associated immunosuppression.

Targeted pathway	Compound	Function	ClinicalTrials.gov	Clinical trial details
Standard-of-care drugs / Immunogenic cell death	Cisplatin	DNA crosslinker	NCT02578680 <sup>III</sup>	<sup>III</sup> Phase 3, randomized, multicenter, double-blind KEYNOTE-189 trial. Combination with anti-PD-1 mAb. First-line treatment of metastatic non-small cell lung cancer (NSCLC).
	Doxorubicin	Topoisomerase I $\alpha$ inhibitor	NCT02499367 <sup>IV</sup>	<sup>IV</sup> Phase 2, randomized, single center, non-blinded TONIC trial. Combination with anti-PD-1 mAb. Triple-negative breast cancer (TNBC).
			NCT02499367 <sup>IV</sup>	<sup>IV</sup> Phase 2, randomized, single center, non-blinded TONIC trial. Combination with anti-PD-1 mAb. TNBC.
	Nab-paclitaxel	Microtubule stabilizer	NCT02425891 <sup>V</sup>	<sup>V</sup> Phase 3, randomized, multicenter, double blind IMpassion130 trial. Combination with anti-PD-L1 mAb. Locally advanced or metastatic TNBC.
	Olaparib	PARP inhibitor	NCT02484404 <sup>VI</sup>	<sup>VI</sup> Phase 1/2, non-randomized trial. Combination with anti-PD-L1 mAb and/or cediranib. Advanced solid tumors and advanced or recurrent ovarian, TNBC, lung, prostate and colorectal cancer.
			NCT02734004 <sup>VII</sup>	<sup>VII</sup> Phase 1/2 trial, single group assignment. Combination with anti-PD-L1 mAb. Advanced solid tumors.
	Talazoparib	PARP inhibitor	NCT03964532 <sup>VIII</sup>	<sup>VIII</sup> Phase 1/2 trial, single group assignment. Combination with anti-PD-L1 mAb. Advanced breast cancer.
			NCT03330405 <sup>IX</sup>	<sup>IX</sup> Phase 1b/2, non-randomized trial. Combination with anti-PD-L1 mAb. Locally advanced and metastatic solid tumors.
	Rucaparib	PARP inhibitor	NCT03639935 <sup>X</sup>	<sup>X</sup> Phase 2, multicenter trial, single group assignment. Combination with anti-PD-1 mAb. Advanced or metastatic biliary tract cancer.
	Veliparib	PARP inhibitor		
	Palbociclib	CDK4/6 inhibitor		
	Abemaciclib	CDK4/6 inhibitor		
	Enzalutamide	Androgen receptor antagonist		
	Bicalutamide	Androgen receptor antagonist	NCT03650894 <sup>XI</sup>	<sup>X</sup> Phase 2 trial, single group assignment. Combination with anti-PD-1 and anti-CTLA-4 mAbs. Advanced breast cancer.
	GTX024	Androgen receptor modulator	NCT02971761 <sup>XII</sup>	<sup>XII</sup> Phase 2 trial, single group assignment. Combination with anti-PD-1 mAb. Androgen receptor positive metastatic TNBC.
	Fulvestrant	Estrogen receptor antagonist	NCT03280563 <sup>XIII</sup>	<sup>XIII</sup> Phase 1b/2, multicenter, randomized trial. Combination with anti-PD-L1 mAb. Locally advanced and metastatic HR-positive/HER2-negative breast cancer.
	BMS-103	PD-L1 antagonist		
	BMS-142	PD-L1 antagonist		
	BMS-200	PD-L1 antagonist		
	BMS-202	PD-L1 antagonist		
	BMS-242	PD-L1 antagonist		
	BMS-1001	PD-L1 antagonist		
	BMS-1166	PD-L1 antagonist		
PD-1/PD-L1	CA-170	PD-L1, PD-L2, VISTA antagonist	NCT02812875 <sup>II</sup>	<sup>II</sup> Phase 1 trial, single group assignment, dose escalation. Advanced tumors and lymphomas.

TLRs	Imiquimod	TLR7 agonist	NCT03276832 <sup>xv</sup>	<sup>xv</sup> Early phase 1 trial, single group assignment. Combination with anti-PD-1. Metastatic melanoma.
	Motolimod (VTX-2337)	TLR8 agonist	NCT03906526 <sup>xv</sup>	<sup>xv</sup> Phase 1b, multicenter, non-randomized trial. Combination with anti-PD-1 mAb. Head and neck squamous cell carcinoma (HNSCC).
	Resiquimod	Dual TLR7/TLR8 agonist	NCT02126579 <sup>xvi</sup>	<sup>xvi</sup> Phase 1/2, randomized trial. Combination with long peptide vaccination. Melanoma.
	DMXAA/Vadimezan	Murine STING agonist	NCT01204684 <sup>xvii</sup>	<sup>xvii</sup> Phase 2, randomized trial. Combination with vaccination. Brain tumors.
cGAS/STING	MK-1454	Human STING agonist	NCT03010176 <sup>xxxvi</sup>	<sup>xxxvi</sup> Phase 1, multicenter, non-randomized trial. Single agent or in combination with anti-PD-1 mAb. Advanced/metastatic solid tumors or lymphomas.
	ADU-S100	Human STING agonist	NCT02675439 <sup>xxxviii</sup>	<sup>xxxviii</sup> Phase 1, multicenter, non-randomized trial. Single agent and in combination with anti-CTLA-4 mAb. Advanced/metastatic solid tumors and lymphomas.
			NCT03172936 <sup>xxxix</sup>	<sup>xxxix</sup> Phase 1b, multicenter, non-randomized trial. Combination with anti-PD-1 mAb. Advanced/metastatic solid tumors or lymphomas.
			NCT03937141 <sup>xxxx</sup>	<sup>xxxx</sup> Phase 2, multicenter trial, single group assignment. Combination with anti-PD-1 mAb. Recurrent or metastatic HNSCC.
IDO1	ABZVABZi analogs	Murine/human STING agonist		
	Indoximod	IDO1 inhibitor	NCT02178722 <sup>xviii</sup>	<sup>xviii</sup> Phase 1/2, multicenter ECHO-202/KEYNOTE-037 trial. Combination with anti-PD-1 mAb. Multiple advanced solid tumors.
	Epacado-stat	IDO1 inhibitor	NCT02752074 <sup>xix</sup>	<sup>xix</sup> Phase 3, randomized, double-blind, placebo-controlled ECHO-301-KEYNOTE-252 trial. Combination with anti-PD-1 mAb. Melanoma.
			NCT02318277 <sup>xx</sup>	<sup>xx</sup> Phase 1/2 trial, single group assignment. ECHO-203. Combination with anti-PD-L1 mAb. Advanced solid tumors.
Prostaglandin pathway	Celecoxib	Dual COX-2/IDO1 inhibitor		
	Melafolone	Dual COX-2/EGFR inhibitor		
	SH-6809	Dual EP <sub>1</sub> /EP <sub>2</sub> antagonist		
	TG4-155	EP <sub>2</sub> antagonist		
	TG6-129	EP <sub>2</sub> antagonist		
	PF-04418948	EP <sub>2</sub> antagonist		
	AH6809	EP <sub>1/2</sub> antagonist		
Arginine metabolism	RQ-07	EP <sub>4</sub> antagonist		
	RQ-15986	EP <sub>4</sub> antagonist		
	AH23848	EP <sub>4</sub> antagonist		
	CB-1158 (NCB001158)	ARG1 antagonist	NCT02903914 <sup>xxi</sup>	<sup>xxi</sup> Phase 1/2, non-randomized trial. As single agent or in combination with anti-PD-1 mAb. Advanced/metastatic solid tumors.
			NCT03910530 <sup>xxii</sup>	<sup>xxii</sup> Phase 1b, non-randomized trial. As single agent or in combination with a small-molecule PD-1 inhibitor. Locally advanced or metastatic solid tumors.
	NCX-4016	Dual ARG-1/INOS antagonist		
	TA38	Dual ARG-1/INOS antagonist		

Adenosine receptor	AZD4635	A2A receptor antagonist	NCT02740985 <sup>xxii</sup> NCT04089553 <sup>xxv</sup>	xxiii Phase 1, multicenter, non-randomized trial. As single agent or in combination with anti-PD-1 mAb. Advanced solid malignancies. xxiv Phase 2, non-randomized trial. Combination with anti-PD-1 or anti-CD73 mAbs. Prostate cancer.
	CPI-444	A2A receptor antagonist	NCT02655822 <sup>xxv</sup> NCT03454451 <sup>xxvi</sup>	xxv Phase 1/1b, multicenter, randomized, dose-selection trial. Combination with anti-PD-1 mAb. Advanced renal cell and prostate cancer. xxvi Phase 1/1b, multicenter, randomized trial. As single agent and in combination with anti-CD73 and anti-PD-1 mAbs. Advanced tumors.
	PBF-509	A2A receptor antagonist	NCT02403193 <sup>xxvii</sup>	xxvii Phase 1/2b, non-randomized trial. Single agent and in combination with anti-PD-1 mAb. Advanced NSCLC.
	Vipadenant	A2A receptor antagonist		
	Preladenant (SCH-420815, MK-3814)	A2A receptor antagonist	NCT02929862 <sup>xxviii</sup> NCT03396497 <sup>xxix</sup>	xxviii Phase 1/2a, multicenter trial. Locally advanced metastatic solid tumors. xxix Phase 1b, multicenter trial. Combination with anti-PD-1 mAb. NSCLC.
	RORγt transcription factor			
	LYC-55716	RORγt agonist		
	Plerixafor (AMD3100)	CXCR4 antagonist		
	AMD070 (AMD11070)	CXCR4 antagonist		
	SX-682	Dual CXCR1/2 inhibitor	NCT03161431 <sup>xxx</sup>	xxx Phase 1/2, non-randomized trial. Single agent or in combination with anti-PD-1 mAb. Melanoma.
Chemokine receptor	AZD5069	CXCR2 antagonist	NCT02583477 <sup>xxxi</sup>	xxxi Phase 1b/2, multicenter, non-randomized trial. Combination with anti-PD-1 mAb and chemotherapy. Metastatic ductal adenocarcinoma.
	X4P-001	CXCR4 antagonist	NCT02923531 <sup>xxxii</sup>	xxxii Phase 1b/2a, single group assignment. Combination with anti-PD-1 mAb. Renal cell carcinoma.
	PF-413609	CCR2 antagonist		
	Maraviroc	CCR5 antagonist	NCT03274804 <sup>xxxiii</sup>	xxxiii Phase 1, single group assignment. Combination with anti-PD-1 mAb. Metastatic colorectal cancer.
	BMS-813160	Dual CCR2/5 antagonist	NCT03496662 <sup>xxxiv</sup>	xxxiv Phase 1/2, non-randomized trial. Combination with anti-PD-1 mAb and chemotherapy. Locally advanced pancreatic ductal adenocarcinoma.
			NCT03184870 <sup>xxxv</sup>	xxxv Phase 1/2 trial. Combination with anti-PD-1 mAb or chemotherapy. Metastatic colorectal and pancreatic cancer.
	FLX475	CCR4 inhibitor	NCT03674567 <sup>xxxvi</sup>	xxxvi Phase 1/2, non-randomized dose-escalation trial. As single agent or in combination with anti-PD-1 mAb. Advanced solid tumors.
	GNF351	AHR antagonist		
	PT2385	HIF-2α antagonist	NCT02293980 <sup>xxxvii</sup>	xxxvii Phase 1, non-randomized, dose-escalation trial. Advanced renal cell carcinoma.

**Table 1. Small-molecule drugs in cancer immunotherapy.** Abbreviations: AHR, Aryl hydrocarbon receptor; ARG 1, arginase 1; CCR, C-C chemokine receptor; CXCR, C-X-C chemokine receptor; CDK, cyclin-dependent kinase; COX-2, cyclo-oxygenase 2; CTLA-4, cytotoxic T lymphocyte-associated antigen 4; HER2, human epidermal growth factor receptor 2; HNSCC, head and neck squamous cell carcinoma, IDO1, in-doleamine-2,3-dioxygenase-1; mAb, monoclonal antibody; NSCLC, non-small cell lung cancer; PARP, poly-ADP-ribose polymerase; PD-1, programmed death 1; PD-L1, programmed death ligand 1; RORγt, retinoic acid receptor-related orphan receptor gamma; TLR, toll-like receptor; TNBC, triple-negative breast cancer; VISTA, V-domain Ig containing suppressor of T cell activation.



211

IC:LC (polyinosinic and polycytidylic acid) or (incomplete) Freund's adjuvant [15]. Here, synthetic approaches could offer ample opportunities for further improvement by boosting therapeutic vaccination (Box 1).

### Small-molecule drugs targeting PD-1 or PD-L1

The PD-1/PDL-1 axis inhibits TCR and CD28 signaling and can thus limit optimal priming of tumor-specific T cells and their anti-tumor activity [16]. Currently, this axis is targeted by antibodies; however, small-molecule PD-1/PD-L1 antagonists may be useful to reduce toxicity. Some of these appear to act via a novel dimer-locking mechanism (e.g., BMS-103, -142, -200, -202, -242, -1001, and -1166; Table 1) with promising results *in vitro* [17-19]. Another small-molecule antagonist for PD-L1, PD-

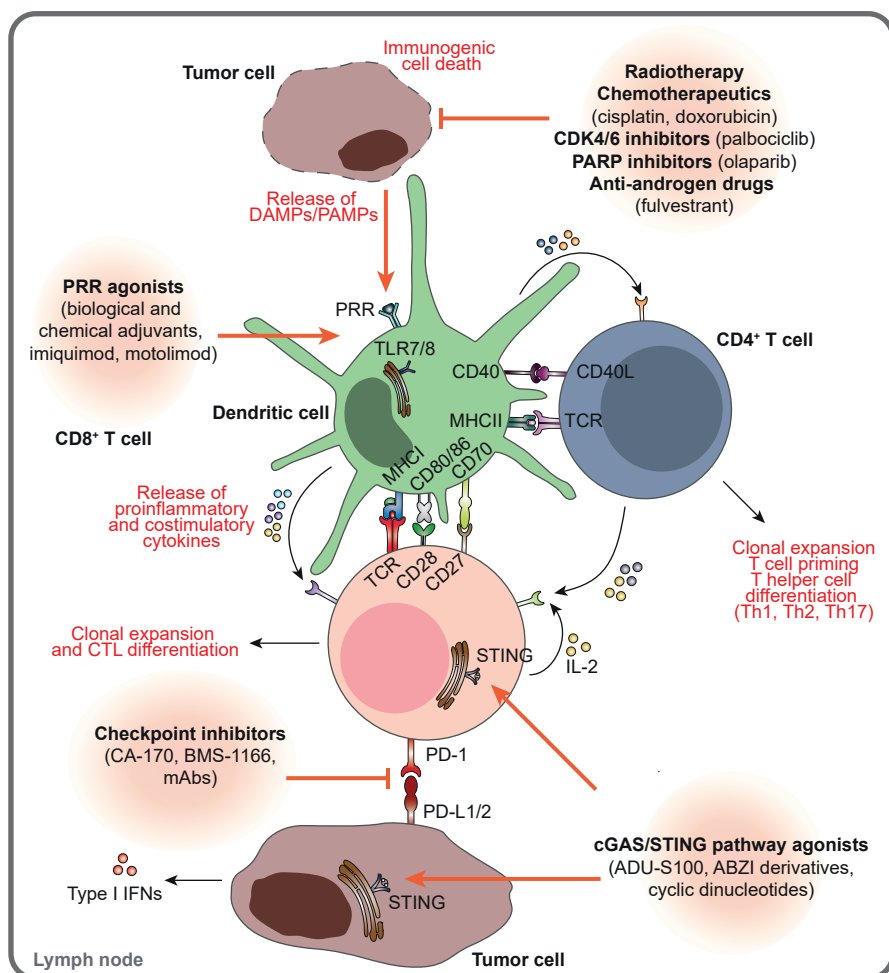


**Figure 3. Overcoming peripheral tolerance.** Dendritic cells must receive activating signals in the form of DAMPs and PAMPs, as well as signals from CD4<sup>+</sup> T cells, in order to supply the costimulatory signals (via CD27 and CD28) and cytokines (primarily IL-12 or IL-15) needed for clonal expansion and differentiation of newly activated CD8<sup>+</sup> T cells. Tumors often do not provide these activating signals, even when their antigens are recognized by T cells.



**BOX 1. Combining chemical adjuvants with antigenic vaccines**

Excellent examples of a vaccines aimed at overcoming peripheral tolerance and promoting recognition of tumor cells as 'non-self' are highlighted by recent studies on synthetic long peptides (SLPs) with both CD4<sup>+</sup> and CD8<sup>+</sup> T cell epitopes covalently linked to synthetic ligands that trigger two PRRs: nucleotide-binding oligomerization domain-containing protein 2 (NOD2) and toll-like receptor 2 (TLR2) [103, 104]. The resulting synergy increases proinflammatory cytokine secretion relative to the free TLR and SLP. Investigation of multiple structural combinations of SLPs conjugated to muramyl-dipeptide (MDP), the minimal peptidoglycan component in Freund's adjuvant activating NOD2, and Pam3CSK4, a synthetic lipopeptide activating TLR1/2, revealed enhanced murine DC activation [103]. This in turn led to elevated secretion of vaccine-specific CD8<sup>+</sup> T cells expressing IFN $\gamma$  and IL-2 *in vitro*, which illustrates the potential of combining chemical adjuvants with antigenic vaccines to boost the anti-tumor response.

L2, and VISTA (CA-170) is currently being evaluated in a Phase I, dose escalation trial (NCT02812875)<sup>l</sup> for patients with advanced tumors and lymphomas (300 participants; primary outcomes measurements were the number of patients with a dose-limiting toxicity in the first treatment cycle, a maximum tolerated dose, and recommended Phase II dose) [20]. However, development of small molecules targeting the PD-1/PD-L1 pathway lags behind that of mAb, due to challenges in designing molecules to occupy the hydrophobic PD-1/PD-L1 interface with high affinity.

**Therapeutic vaccination**

Therapeutic vaccines aim to prime tumor-specific CD8<sup>+</sup> T cells to generate a CTL response. For optimal CTL priming, CD4<sup>+</sup> T cell help is required. Therefore, therapeutic vaccines encompass specific antigens for CD4<sup>+</sup> and CD8<sup>+</sup> T cells, as well as compounds to activate DC [21]. Leading strategies use synthetic long peptides (SLP) (around 20-40 amino acids in length) or antigen-encoding mRNA or DNA, encompassing both MHC I and MHC II epitopes to ensure CD8<sup>+</sup> CTL priming and CD4<sup>+</sup> T cell help for a robust CTL response [5]. These vaccines have shown a degree of therapeutic promise in treating early stage virus-induced cancers [22]. Addi-

**Figure 3. Continued.** Dendritic cell activation can be induced by biological- and small-molecule adjuvants, or by small-molecule PRR agonists targeted at extracellular or intracellular PRRs. Additionally, treatment of the tumor with selected standard-of-care (chemo)therapeutics or radiation can induce immunogenic cell death and thereby stimulate neoantigen release. STING agonists can induce type I IFN production, promoting DC activation and T cell priming. To evade CD8<sup>+</sup> T cell killing, tumor cells can upregulate suppressive molecules such as PD-L1/2. Suboptimally primed CD8<sup>+</sup> T cells that have not experience CD4<sup>+</sup> T cell help express PD-1. To block the PD-1/PD-L1 interaction, different monoclonal antibodies (mAbs) or small-molecule checkpoint inhibitors have and are being developed. Orange arrows indicate possible points of interception; pointed and flat arrowheads indicate activation and inhibition, respectively. Drugs between brackets are examples of small-molecule drugs or biologicals targeting the indicated proteins/cells. Abbreviations: CTL, cytotoxic T lymphocyte; DAMP, danger-associated molecular pattern; IFN, interferon; MHC, major histocompatibility complex; PAMP, pathogen-associated molecular pattern; PD-1, programmed death 1; PD-L1/2, programmed death ligand 1/2; PRR, pattern recognition receptor; STING, stimulator of IFN genes; TCR, T cell receptor; TLR, toll-like receptor.

tionally, a recent Phase Ib randomized glioblastoma trial (NCT02287428)<sup>ii</sup> indicated that vaccination with a multi-epitope, personalized neoantigen successfully induced intratumoral neoantigen-specific CD4<sup>+</sup> and CD8<sup>+</sup> immune responses, according to single-cell T cell receptor analysis [23]. However, all patients included in the study eventually relapsed, suggesting that tumor-associated immunosuppression and/or other challenges represented a significant and persistent bottleneck.

### **Small molecules targeting toll-like receptors (TLRs)**

The first small-molecule immuno-oncology drug approved by the FDA for the treatment of basal cell carcinoma was imiquimod, an imidazoquinoline derivative, commonly used in the treatment of genital warts [24]. Imiquimod targets toll-like receptor 7 (TLR7), a PRR that binds conserved PAMPs, such as double-stranded RNA, lipopolysaccharide, or unmethylated CpG DNA [25]. Most TLRs are expressed on the cell surface, but TLR3, 7, 8, and 9 locate predominantly in endosomes [26]. A small-molecule TLR8 agonist, motolimod (VTX-2337), exhibits anti-tumor activity in recurrent or metastatic head and neck squamous cell carcinomas (HNSCC), by stimulation of natural killer (NK) cells and enhanced antibody-dependent cell-mediated toxicity [27]. Motolimod treatment in combination with cetuximab (an anti-EGFR antibody) or conventional chemo-therapy resulted in a decrease of Tregs in the TME, elevation of circulating EGFR-specific CD8<sup>+</sup> T cells and increase in progression-free and overall survival in a subset of HNSCC patients in, as compared with cetuximab or chemotherapy alone [28, 29]. Imiquimod, motolimod, and resiquimod (relatives of imiquimod targeting TLR7 and TLR8), are currently under investigation in a number of clinical trials (NCT03276832)<sup>xiv</sup>, (NCT03906526)<sup>xv</sup>, (NCT02126579)<sup>xvi</sup>, (NCT01204684)<sup>xvii</sup> for treatment of solid tumors, typically as adjuvants to vaccination. Thus, the search for small molecules targeting other (and preferably multiple) TLRs continues, often using high-throughput screening of drug libraries in cell-based assays [30]. Other PRRs, such as NOD-like receptors (NLRs), C-type lectin receptors (CLRs) or RIG-I-like receptors (RLRs) have been less extensively studied, but agonists targeting these families are likely to enhance immune responsiveness and are currently being developed [31].

### **Small molecules targeting the cyclic-GMP-AMP synthase (cGAS)/stimulator of IFN genes (STING) pathway**

STING is a PRR on the endoplasmatic reticulum membrane that binds cyclic dinucleotides derived from cytosolic DNA converted by cGAS. Activation of the cGAS/STING pathway leads to type I IFN production, which promotes DC activation and T cell priming, as shown in tumor-bearing mice [32], highlighting STING as a putative target for cancer immunotherapy (Box 2). The STING pathway is regulated by ectonucleotide pyrophosphatase/phosphodiesterase-1 (ENPP1) that hydrolyzes cGAMP and thereby controls activation of the signaling cascade. As a consequence, various attempts are made to activate the STING pathway by inhibition of ENPP1 [33-35]. However, other studies report that cGAS/STING signaling can induce indoleamine-2,3-dioxygenase (IDO1; a tryptophan catabolic enzyme found to induce immunosuppression and immunoevasion [36]) and suppress homologous-mediated DNA repair, thus dampening the immune response and promoting tumor growth in a Lewis lung carcinoma mouse model [37, 38]. These studies suggest that more research is needed on the function of the cGAS/STING pathway in cancer immunity before we understand the effects of STING agonist therapies sufficiently.

**BOX 2. STING as a target for cancer immunotherapy**

Intratumoral injection of small-molecule STING agonist DMXAA (5,6-dimethylxantheone-4-acetic acid) in mice showed specificity and efficacy in controlling B16 melanoma tumor outgrowth (of both injected and distant tumors in the same animal) [105]. However, this drug was ineffective in humans because of structural differences with murine STING [106]. Considerable efforts to create derivatives of DMXAA active against human STING are ongoing [107]. For example, among three amidobenzimidazole (ABZI)-based small-molecule STING agonists reported in the same study, the most potent compound was shown to bind several human and one murine isoforms of STING with high affinity, inducing dose dependent activation of STING and secretion of IFN $\beta$  in human PBMCs, and its intravenous delivery strongly reduced subcutaneous CT26 colon tumor growth in mice [108]. Also, in a high-grade serous carcinoma mouse model, a cyclic dinucleotide STING agonist, combined with anti-PD-1 antibodies and chemotherapy, showed increased survival and decreased tumor burden compared to single treatments [109]. Transcriptomic tumor analysis revealed elevated expression of IFN response and antigen-presenting genes for tumors treated with the STING agonist over control samples. Various STING small agonist are currently tested in early phase clinical trials: MK-1454 (NCT03010176)<sup>xxxvii</sup>, ADU-S100 (NCT02675439)<sup>xxxviii</sup>, and (NCT03172936)<sup>xxxix</sup>. However, preliminary results for ADU-S100 presented at the American Society of Clinical Oncology (ASCO) meeting in 2019 showed that only 6 out of 83 patients achieved confirmed responses, with a single complete response (CR), 3 partial responses (PR) among PD-1 naïve TNBC patients, and 2 PRs among previously immunotherapy-treated melanoma patients [110]. A multicenter, Phase II trial combining ADU-S100 and anti-PD-1 antibodies to assess safety and efficacy as first-line treatment of PD-L1-positive recurrent or metastatic HNSCC is ongoing (NCT03937141)<sup>xxxx</sup>.

**Immunogenic capacity of standard-of-care therapy**

Radiotherapy and chemotherapy can directly kill tumor cells, but they may also enhance anti-tumor immunity. The prevailing idea is that these treatments may induce **immunogenic cell death**, characterized by the release of tumor antigens and danger signals (e.g., cytosolic DNA) capable of activating DCs via PRRs, such as **toll like receptors (TLRs)** and cGAS/STING [39, 40]. Remarkable effects were reported when standard-of-care therapy was followed by immunotherapy [41], as illustrated by cisplatin treatment and CTLA-4 inhibition in a lung epithelial tumor mouse model [42]. Furthermore, based on the Phase III KEY-NOTE-189 trial (NCT02578680)<sup>iii</sup>, the combination of pembrolizumab (anti-PD-1 mAb) with cisplatin and **pemetrexed** is now FDA approved as first-line treatment for metastatic non-small cell lung cancer (NSCLC) [43]. Moreover, anthracycline drugs such as **doxorubicin** can induce type I IFN production in a fibrosarcoma mouse model and selectively deplete immunosuppressive **myeloid derived suppressor cells (MDSCs)** in a murine breast cancer model, which impairs tumor development *in vivo* [44, 45]. The recent Phase II, single center TONIC trial (NCT02499367)<sup>iv</sup> showed that the combination of either cisplatin (overall response (OR) 23%) or doxorubicin (OR 35%) with nivolumab (anti-PD-1 mAb) improves treatment outcomes of triple-negative breast cancer (TNBC) patients relative to anti-PD-1 alone [46]. Similarly, atezolizumab (anti-PD-L1 mAb) in combination with paclitaxel, a chemotherapeutic that blocks mitosis via stabilization of microtubules, is now FDA approved for treatment of locally advanced or metastatic

TNBCs. This was based on the Phase II IMpassion130 trial (NCT02425891)<sup>v</sup>, showing improved progression-free survival for the combination therapy over chemotherapy alone. Other chemotherapeutics that have been reported to boost the effects of checkpoint inhibitors in pre-clinical trials and are under evaluation in clinical trials include: cyclophosphamide; platinum drugs, such as **oxaliplatin**; and **PARP inhibitors** olaparib (NCT02484404)<sup>vi</sup>, (NCT02734004)<sup>vii</sup>, talazoparib (NCT03964532)<sup>viii</sup>, (NCT03330405)<sup>ix</sup>, rucaparib (NCT03639935)<sup>x</sup> and veliparib. In addition, various cyclin-dependent kinase 4 and 6 inhibitors (CDK4/6i), including palbociclib and abemaciclib, as well as anti-androgen drugs enzalutamide, bicalutamide (NCT03650894)<sup>xi</sup>, GTX-024 (NCT02971761)<sup>xii</sup>, and fulvestrant (NCT03280563)<sup>xiii</sup>, are also being tested in combination approaches with checkpoint blockade for various cancers in pre-clinical and clinical trials [47-52].

### ENABLING T CELL ACTIVITY IN THE TUMOR MICROENVIRONMENT

The TME and the signals it exudes in concert with the T cell response may lead to a state of immunosuppression. The TME might be hypoxic (Box 3) and it may present physical barriers that exclude T cells or express inhibitory molecules, such as IDO1 and PD-L1, that can directly inhibit effector T cell function [53]. Furthermore, it can express cytokines such as transforming growth factor  $\beta$  (TGF- $\beta$ ) and IL-10 that can alter cellular phenotypes (e.g., macrophages) and modulate the function of CD4<sup>+</sup> T cells and promote Treg generation and expansion, thereby inhibiting effector T cell

#### BOX 3. Targeting the hypoxic environment in many solid tumors

Hypoxia is often observed in solid tumors and can induce a plethora of effects promotive of tumor growth and metastases. A critical signaling molecule in hypoxia is hypoxia-induced factor (HIF-1 $\alpha$  classical helix-loop-helix (HLH) transcription factor. Under oxygen-rich conditions, HIF-1 $\alpha$  interacts with VHL in the cytosol, resulting in its ubiquitination and degradation by the proteasome [111]. Under hypoxic conditions, HIF-1 $\alpha$  translocates into the nucleus and pairs with the aryl hydrocarbon receptor (AhR) nuclear translocator protein (ARNT) [112]. The HIF1 $\alpha$ -ARNT dimer mediates transcription of hypoxia-specific genes that stimulate erythropoiesis, metabolism and angiogenesis, but also induce PD-L1 expression and Treg differentiation [113, 114]. Inhibition of HIF-1 $\alpha$  transcription in these hypoxic tumors could prevent tumor outgrowth, as well as improve immune responses, such as in the case of AhR antagonist GNF351, shown to decrease migration and invasion of HNSCC tumor cell lines *in vitro* [115]. Recently, the first HIF-2 $\alpha$  antagonist PT2385, which inhibits its interaction with ARNT, has been tested in a Phase I, nonrandomized, dose-escalation trial (NCT02293980)<sup>xxxxi</sup> for safety and efficacy in patients with advanced renal cell carcinoma. They show that the drug is well tolerated, with clinical benefit observed in 66% of the patients [116]. Many other HIF-1 inhibitors are currently under development. These drugs have not been tested in combination with immunotherapy, but a synergistic effect on tumor control through modulation of the TME can be expected. One of the adaptive responses of tumor cells to hypoxia involves increased expression of carbonic anhydrase IX (CA IX), an enzyme located at the cell surface of tumors that catalyzes conversion of carbon dioxide to bicarbonate ions and protons. CA IX expression increases adaptation of tumor cells to a hypoxic TME and confers an increased ability to migrate and metastasize [117, 118]. The last years, various CA IX mAbs and small-molecule inhibitors have been developed as potential anti-cancer therapies or for tumor-imaging purposes [119, 120].

responses [54]. Additionally, the TME may attract or create suppressive immune cells, including arbitrarily designated MDSCs, Tregs and certain **tumor-associated macrophages (TAMs)**, which would render T cells dysfunctional and attenuate the efficacy of immunotherapy [55]. Elucidating and targeting immunosuppression and -evasion mechanisms may help improve clinical outcomes. Small-molecule drugs may also be used to specifically target suppressive factors and induce or restore immune reactivity in the TME (Figure 4).

### Targeting IDO1

One such a TME target is IDO1. IDO1 is the most broadly expressed of three enzymes (together with IDO2 and tryptophan 2,3-dioxygenase (TDO)), involved in the first step of the kynurenine pathway. The immuno-suppressive effects of IDO1/kynurenine include Treg cell expansion and recruitment of MDSCs. IDO1 de-prives

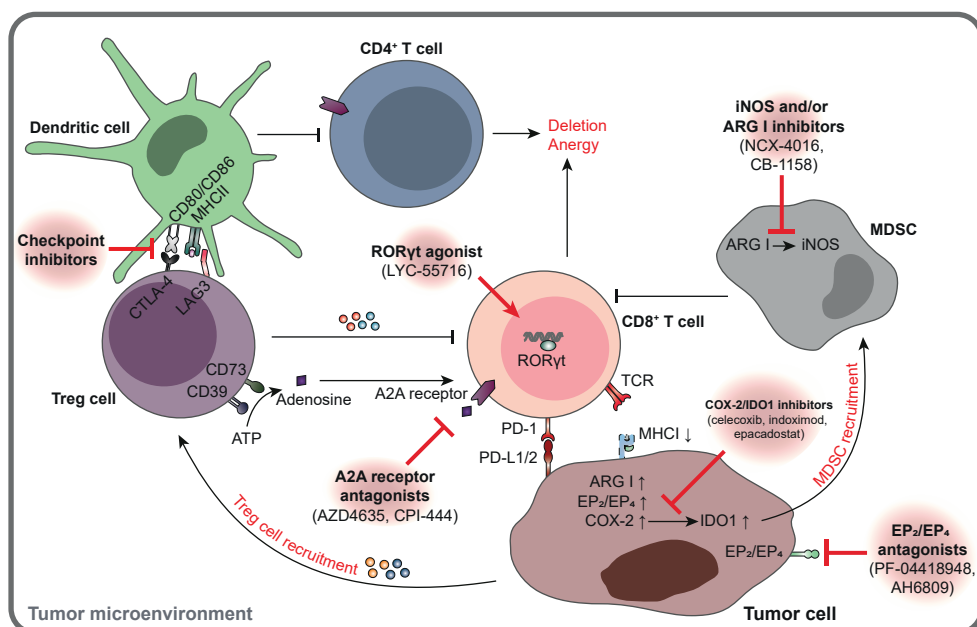


**Figure 4. Reversing immunosuppression in the tumor microenvironment.** Tumor cells, as well as immune- and stromal cells in the tumor microenvironment, can collaborate to establish an immunosuppressive environment, through upregulation of inhibitory molecules, such as PD-L1 and IDO1, conversion of conventional CD4<sup>+</sup> T cells into Tregs, alteration of cytokine profiles, hypoxia, recruitment of suppressive cell types such as myeloid-derived suppressor cells (MDSCs), and the production/upregulation of specific proteins and metabolites. Suppression may be relieved by small-molecule drugs targeted at relevant mechanisms and, in combination with checkpoint blockade this could enhance the anti-tumor response. Red lines indicate possible points of interception; pointed and flat arrowheads indicate activation and inhibition, respectively. Drugs between brackets are examples of small-molecule drugs or biologicals targeting the indicated proteins/cells. Abbreviations: ARG, Arginase; COX-2, cyclooxygenase 2; CTLA-4, cytotoxic T lymphocyte-associated antigen 4; IDO1, indoleamine-2,3-dioxygenase; iNOS, nitric oxide synthase; LAG-3, lymphocyte-activation gene 3; MHC, major histocompatibility complex; PD-1, programmed death 1; PD-L1/2, programmed death ligand 1/2; RORγt, retinoic acid receptor-related orphan receptor gamma; TCR, T cell receptor; Treg, regulatory T cell.



effector T cells of tryptophan, which is required for CTL activation and antagonizes CD8<sup>+</sup> T cell effector function by PD-1 expression [56, 57]. Indoximod was the first IDO1 inhibitor tested in humans, but with confounding results, as this compound might in fact inhibit mTORC1, a downstream effector of IDO1 [58]. Epacadostat, a specific and more potent IDO1 inhibitor, in combination with pembrolizumab (anti-PD-1 mAb) showed promising results in the Phase I/II ECHO-202/KEYNOTE-037 trial (NCT02178722)<sup>xviii</sup> for patients with multiple advanced solid tumors, but did not increase anti-PD-1 efficacy in a Phase III clinical trial in melanoma patients (NCT02752074)<sup>xix</sup> [59]. Likewise, epacadostat was combined safely with anti-PD-L1 in the Phase I/II ECHO-203 trial (NCT02318277)<sup>xx</sup> for advanced solid tumors, but yielded no combined responses in these patients [60]. Consequently, various pharmaceutical companies have stopped or are downsizing the development of IDO1 inhibitors, which significantly curtails the early clinical development of these types of small molecules [61]. Further robust research is needed to optimize the timing of IDO1 inhibitor administration in combination with checkpoint blockade antibodies. In addition, patient selection and testing of other IDO1 inhibitors will be warranted to ideally find a more successful combination regimen. The kynurenine produced in the IDO1 pathway is an endogenous ligand for the aryl hydrocarbon receptor AhR, a transcription factor that regulates immunological responses [62]. Inhibition of AhR may therefore be an alternative for IDO1 inhibitors. Crosstalk was also observed between IDO1 and the amino acid-sensing kinase general control nonderepressible 2 (GCN2), which is important in inflammation and viability of cancer cells in the TME [63, 64]. Therefore, efforts are made to test the potential of GCN2 antagonists as anticancer drugs [64].

### Small molecules targeting the prostaglandin pathway

One of the drivers of IDO1 expression is cyclooxygenase 2 (COX-2), an underexplored target in cancer immunotherapy, but a common target of nonsteroidal anti-inflammatory drugs (NSAIDs) [65]. COX-2 catalyzes the synthesis of prostaglandins, lipid compounds involved in the response to injury and inflammation. This enzyme is expressed in several cancers and therefore, celecoxib, an NSAID that inhibits COX-2 as well as IDO1, is being explored for cancer therapy [66]. One study developed analogs of celecoxib and showed a potent cytostatic effect on melanoma and colon cancer cell lines *in vitro* [67]. Concurrent inhibition of COX-2 and EGFR was previously reported to have a synergistic effect on cell proliferation and apoptosis in NSCLC cell lines *in vitro* [68]. Dual inhibition of COX-2 and EGFR by melafolone (a naturally occurring flavonoid) shows improved effects of PD-1 blockade in a Lewis lung carcinoma and lung carcinoma mouse model through vascular normalization and PD-L1 downregulation [69]. These studies demonstrate the potential of combination therapies targeting multiple tumor-associated molecules simultaneously. Downstream of the COX-2 signaling pathway are the G protein-coupled prostanoid receptors EP2 and EP4, which bind prostaglandin E2 (PGE2). Signaling via the prostaglandin pathway through EP2 and/or EP4 has been implicated in establishment of an immunosuppressive environment by blocking DC activity, redirection of DC differentiation towards suppressive phenotypes and suppression of macrophages [70]. Consequently, interest in small-molecule antagonists targeting these receptors is growing and various EP2 and EP4 antagonists are being developed (e.g., AH6809, AH23848, TG6-129, TG4-155, PF-04418948, RQ-07, and RQ-15986; Table 1) [70-72]. Dual inhibition of EP2 and EP4 in combination with checkpoint inhibitors shows increased production of antigen-specific proinflammatory cytokines by

tumor-derived CTLs in epithelial ovarian cancer *ex vivo* [73]. Thus, manipulating the signaling of prostaglandins in the TME may boost anti-tumor immunity.

### Targeting arginine metabolism to overcome the immunosuppressive function of MDSCs and TAMs

Arginase is another potential therapeutic target in the TME. This ubiquitous manganese-containing enzyme catalyzes the hydrolysis of L-arginine to L-ornithine and urea and plays an important role in various aspects of inflammation [74]. Mammals express two isoforms of the enzyme: the cytoplasmic arginase I (ARG I), predominantly in the liver, and arginase II (ARG II) in the mitochondrial matrix. In the TME, MDSCs and TAMs can release high amounts of ARG I into the extracellular space to locally deplete arginine concentrations and thereby impair TCR signaling and proliferation [75]. In T cell cocultures, ARG I inhibitor CB-1158 (INCB001158) blocks the myeloid cell-mediated immunosuppression of T cell proliferation, reducing tumor growth in different mouse models [76]. Furthermore, profiling the TME shows that CB-1158 treatment increases expression of interferon-inducible genes, inflammatory cytokines, and tumor-infiltrating NK and CD8<sup>+</sup> T cells, compared with controls [76]. This drug is currently being tested as single agent and in combination with anti-PD-1 mAb and small-molecule inhibitors in two early stage clinical trials for advanced/metastatic solid tumors (NCT02903914)<sup>xxi</sup>, (NCT03910530)<sup>xxii</sup>. Another enzyme expressed at high levels in MDSCs and TAM is the nitric oxide synthase (iNOS). iNOS hydrolyzes L-arginine into nitric oxide (NO), which subsequently suppresses T cell function via interference with the JAK3-STAT5 signaling pathway [77]. When ARG-I is inhibited, iNOS has more substrate for NO production, resulting in immunosuppression via the formation of nitrogen species [77]. To overcome this, dual ARG I/iNOS inhibitors, such as NCX-4016 and TA38, have recently been developed and will be tested in the near future [78, 79].

### Targeting Tregs in the TME

Tregs can express extracellular ectonucleotidases CD39 and CD73; membrane molecules that produce adenosine via dephosphorylation of ATP. Adenosine can subsequently bind to A2A or A2B receptors on the surface of conventional T cells and was found to thereby inhibit CD8<sup>+</sup> T cell infiltration in a melanoma tumor mouse model [80]. Adenosine can also bind to A2A receptors on Tregs, resulting in expansion of the Treg population to strengthen their immunosuppressive effects *in vitro* [81]. To relieve Treg-mediated suppression in the TME, small-molecule A2A antagonists, such as CPI-444, AZD4635, vipadenant, preladenant (SCH-420815, MK3814, MSD), and PBF-509, have been developed [82-84]. These compounds are currently tested in Phase I and II clinical trials either alone or in combination with anti-PD-1 or anti-PD-L1 inhibitors for various solid tumors (NCT02740985)<sup>xxiii</sup>, (NCT04089553)<sup>xxiv</sup>, (NCT02655822)<sup>xxv</sup>, (NCT03454451)<sup>xxvi</sup> and (NCT02403193)<sup>xxvii</sup>.

Another Treg target is retinoic acid receptor-related orphan receptor gamma (RORγt), a transcription factor involved in the proinflammatory IL-17 pathway in T cells. RORγt agonists can induce the production of cytokines and chemokines, decrease the proliferation of Tregs, and revoke immunosuppression by tumor cells [85]. Synthetic small-molecule RORγt agonists promote activity, proliferation, and survival of Th17 (CD4<sup>+</sup>) and Tc17 (CD8<sup>+</sup>) cells *in vitro* relative to the endogenous agonist desmosterol, and result in enhanced Th17 effector function in an adoptive T cell therapy mouse model [86, 87]. Two Phase II clinical trials have been designed to test the effects of these agonists, one to test safety and tolerability as a single drug (NCT02929862)



<sup>xxviii</sup> and the other to test safety/tolerability either alone or in combination with anti-PD-1 mAb in NSCLC (NCT03396497)<sup>xxix</sup>. The outcome of these trials is difficult to predict, since Th17 cells have been associated with poor prognosis in a number of cancer types [88-90]. In these cases, RORγt antagonists might provide therapeutic benefit. However, design of inhibitors is complicated because RORγt has a large and lipophilic ligand-binding domain [91]. Furthermore, stimulating RORγt may promote autoimmune disorders, such as inflammatory bowel disease [92]. Thus, considering that the 'classical' checkpoint inhibitors anti-CTLA-4 and anti-PD-1 antibodies can also induce autoimmunity, it is necessary to caution that this type of combination might induce strong side effects.

### Small molecules targeting chemokine receptors

Chemokines and their receptors guide both tumor cells to metastatic locations and immune cells to defined tissues. The chemokine receptor CXCR4 is frequently activated in cancer cells and contributes to epithelial-mesenchymal transition, invasion, metastasis, and tumor vascularization [93, 94]. A series of small-molecule antagonists of chemokine receptors have been developed, of which one of the most well-known, plerixafor (AMD3100), has reported efficacy in acute lymphocytic leukemia and relapsed acute myeloid leukemia [95-97]. Plerixafor reduced primary tumor growth and suppressed metastasis in combination with chemotherapy in a small cell lung cancer xenograft mouse model [98]. CXCR4 inhibition by plerixafor counteracted CXCL12-dependent upregulation of PD-L1 in the TME and recruitment of immunosuppressive Tregs and M2 macrophages [99]. This study in a hepatocellular carcinoma mouse model showed that CXCR4 inhibition in combination with anti-PD-1 mAb and **sorafenib** inhibits tumor growth, reduces lung metastasis, and improves survival [99]. The chemokine receptor CXCR2, overexpressed in various cancers, is correlated with poor prognosis in human pancreatic ductal adenocarcinoma patients [100]. CXCR2 inhibition prevent entry of MDSCs into the TME in pancreatic-, breast- and colorectal cancer mouse models and has therefore been suggested to sensitize tumors to immunotherapy [100-102]. Currently, a Phase I/II, nonrandomized trial is recruiting melanoma patients to test the safety and efficacy of the dual CXCR1/2 inhibitor SX-682, as single drug or in combination with anti-PD-1 mAb (NCT03161431)<sup>xxx</sup>. Other chemokine receptor-targeting small molecules are under evaluation in pre-clinical and clinical trials as single agents or in combination with checkpoint blockade. These include CXCR2 antagonist AZD5069 (NCT02583477)<sup>xxxi</sup>, CXCR4 inhibitor X4P-001 (NCT02923531)<sup>xxxii</sup>, CCR2 inhibitor PF-413609, CCR5 inhibitor maraviroc (NCT03274804)<sup>xxxiii</sup>, dual CCR2/5 antagonist BMS-813160 (NCT03496662)<sup>xxxiv</sup>, (NCT03184870)<sup>xxxv</sup> and CCR4 inhibitor FLX475 (NCT03674567)<sup>xxxvi</sup> [84].

### What will the future bring?

The field of cancer immunotherapy is exploding, and a new phase of directed and specific modulation of immune responses by small molecules is taking hold. There are many exciting developments and it is likely that new small molecules will be explored in combination with anti-PD-1/PD-L1 or anti-CTLA-4 blocking mAbs in the near future. The number of potential targets for small molecules has dramatically increased by a novel therapeutic strategy that induces specific protein degradation by proteolysis-targeting chimeras (PROTACs) (Box 4). We anticipate that these PROTACs will greatly expand the options to manipulate immune responses. These, along with other novel drug developments are expected to further expand the arse-

**BOX 4. Small-molecule-based proteolysis-targeting chimeras (PROTACS) in cancer immunotherapy**

PROTACs are bifunctional hybrid molecules, consisting of two ligands connected by a linker. The first ligand targets a protein of interest, while the second ligand targets an E3 ubiquitin ligase. By bridging a protein of interest to the E3 ubiquitin ligase, PROTACs engage the ubiquitin-proteasome system to degrade the protein of interest [121]. Numerous studies have shown that targeting (onco-)proteins for degradation presents a successful strategy in anti-cancer therapy *in vitro* [122, 123]. This is illustrated by small-molecule-based PROTACs against FKBP12 and BTK, which have shown rapid (24-72 hours) and global knockdown of their targets in different organs of mice and non-human primates, highlighting their potential for further clinical testing in the context of putative cancer therapies in human patients [124]. Meanwhile, development of small-molecule PROTACS is rapidly increasing, and recently, the first orally bioavailable PROTAC drug (ARV-110) targeting the androgen receptor has been approved for a Phase I, single group assignment, dose escalation clinical trial to evaluate its safety, tolerability, pharmacokinetics, and pharmacodynamics in metastatic castration-resistant prostate cancer (NCT03888612)<sup>xxxxii</sup>, which is currently recruiting patients. Although there are numerous issues to solve before broad clinical application of PROTACS is possible, including their cellular permeability and stability, these agents constitute a major focus in drug development, offering a conceptually simple and general approach. Indeed, PROTAC compounds can selectively induce specific peptide presentation by MHC I molecules, indicating that this strategy can promote neoantigen presentation on tumor cells [125]. PROTACS could then inhibit tumor growth and sensitize tumor cells for CTL mediated elimination.

nal of approaches heading into the future of cancer treatment.

**CONCLUDING REMARKS**

Targeting the PD-1/PD-L1 and CTLA-4 signaling pathways in immunotherapy can induce potent anti-tumor CTL responses in patients with various cancer types. However, only a subset of patients responds and available treatment combinations often coincide with severe adverse events. Therefore, novel treatment options are essential for further improvement of cancer immunotherapy efficacy, all while lowering toxicity. We propose that small-molecule drugs provide opportunities for improving treatment success. Small molecules can easily penetrate into tissues compared with most antibodies and can therefore be directed towards both extracellular and intracellular targets to promote anti-tumor immunity. Additionally, their half-lives are generally short, lowering their chance for adverse effects. Because of these features, there is extensive interest in the development of small-molecule-based strategies in the cancer immunotherapy field. The lasting challenge is to rationally select chemo-immunotherapy combinations, that are based on known molecular mechanisms underlying the lack of immune activation against cancer and subvert this state. Also, focus should be on optimizing dose and timing of these combination treatments to maximize their synergistic effect. There are many targets to evaluate in the space of chemo-immunotherapy and only few combinations have been evaluated or are currently tested. Thus, the future of chemo-immunotherapy remains broad and exciting (Figure 1).

## ACKNOWLEDGMENTS

We thank Ilana Berlin for critical reading and editing of the manuscript. This work was supported by grants from the Institute for Chemical Immunology (ICI, to H. Ovaa, J. Borst and J. Neefjes). This work is part of Oncode Institute, which is partly financed by the Dutch Cancer Society.

## GLOSSARY

**Central tolerance:** the absence of self-reactive T cells to avoid autoimmunity. T cells that recognize self-antigens are deleted during negative selection in the thymus.

**Checkpoint blockade:** inhibition of immune checkpoints PD-1/PD-L1 or CTLA4.

**Cisplatin:** platinum-based chemotherapeutic, functions by interfering with DNA replication.

**Cytotoxic T lymphocyte (CTL):** (generally CD8<sup>+</sup>) killer T cell that recognizes intracellular alterations in the context of major histocompatibility class I complexes expressed on all tissues.

**Danger-associated molecular patterns (DAMPs):** danger signals released by damaged or dying cells, such as cytosolic or nuclear proteins, or DNA. Binding of DAMPs to pattern recognition receptors induces innate immunity and DC activation.

**Doxorubicin:** anthracycline chemotherapeutic that induce cell death by DNA double strand break formation via inhibition of topoisomerase II and the induction of chromatin damage.

**Heterogeneity:** here, phenotypical variations between cells of the same cancer in one patient, often of genetic origin, that affect therapy response and hamper treatment design.

**Immune-related adverse events (irAEs):** inflammatory side effects that may occur during immune therapy. Any organ system can be affected, but irAEs most commonly involve the gastrointestinal tract, endocrine glands, skin, and liver.

**Immunogenic cell death:** form of cell death resulting in the release of immune-stimulating factors.

**Immunosuppression:** here, inhibition of immunity induced by tumor cells and their microenvironment that results in escape from elimination.

**Microsatellite instability:** genetic predisposition to mutation caused by the loss of DNA mismatch repair activity.

**Myeloid-derived suppressor cells (MDSCs):** population of immature myeloid cells that are presumed to have a strong immunosuppressive function in the tumor microenvironment.

**Neoantigen:** tumor antigen arising from somatic DNA mutations, so that no central tolerance has been raised. T cells may be able to recognize these antigens and attack tumor cells expressing them.

**Oxaliplatin:** platinum-based chemotherapeutic, functions by interfering with DNA synthesis.

**PARP inhibitors:** pharmacological inhibitors of poly-ADP-ribose polymerase, which plays a role in DNA repair, genomic stability, and programmed cell death.

**Pathogen-associated molecular patterns (PAMPs):** molecules found on/in microorganisms that trigger innate immunity by binding pattern recognition receptors. Classic PAMPs are double-stranded RNA, endotoxins, or bacterial cell wall constituents.

**Pemetrexed:** antifolate chemotherapeutic that interferes with folate-dependent metabolic processes essential for replication.

**Peripheral tolerance:** suppression in the periphery of self-reactive immune cells

that have escaped central tolerance.

**Regulatory T cells (Tregs):** subset of CD4<sup>+</sup> T cells that modulate the immune response by suppressing effector cells.

**Sorafenib:** small-molecule kinase inhibitor for the Raf/Mek/Erk pathway.

**Toll-like receptors:** single-pass membrane-spanning receptors that plays a key role in the innate immune response.

**Tumor-associated macrophages (TAMs):** macrophages present in the tumor microenvironment of solid tumors, usually associated with an unfavorable prognosis due to their immunosuppressive function.

*All clinical trials described in this manuscript are registered with ClinicalTrials.gov, and references to these trials can be found online: [https://www.cell.com/trends/immunology/fulltext/S1471-4906\(20\)30069-7](https://www.cell.com/trends/immunology/fulltext/S1471-4906(20)30069-7)*

## REFERENCES

1. Koebel, C. M., Vermi, W., Swann, J. B., Zerafa, N., Rodig, S. J., Old, L. J., Smyth, M. J. & Schreiber, R. D. (2007) Adaptive immunity maintains occult cancer in an equilibrium state, *Nature*. 450, 903-7.
2. Sharma, P. & Allison, J. P. (2015) The future of immune checkpoint therapy, *Science*. 348, 56-61.
3. Ribas, A. & Wolchok, J. D. (2018) Cancer immunotherapy using checkpoint blockade, *Science*. 359, 1350-1355.
4. Hammerl, D., Rieder, D., Martens, J. W. M., Trajanoski, Z. & Debets, R. (2018) Adoptive T Cell Therapy: New Avenues Leading to Safe Targets and Powerful Allies, *Trends Immunol.* 39, 921-936.
5. Melief, C. J., van Hall, T., Arens, R., Ossendorp, F. & van der Burg, S. H. (2015) Therapeutic cancer vaccines, *J Clin Invest.* 125, 3401-12.
6. Ciccarese, C., Alfieri, S., Santoni, M., Santini, D., Brunelli, M., Bergamini, C., Licitra, L., Montironi, R., Tortora, G. & Massari, F. (2016) New toxicity profile for novel immunotherapy agents: focus on immune-checkpoint inhibitors, *Expert Opin Drug Metab Toxicol.* 12, 57-75.
7. Postow, M. A., Sidlow, R. & Hellmann, M. D. (2018) Immune-Related Adverse Events Associated with Immune Checkpoint Blockade, *N Engl J Med.* 378, 158-168.
8. Larkin, J., Chiarion-Sileni, V., Gonzalez, R., Grob, J. J., Cowey, C. L., Lao, C. D., Schadendorf, D., Dummer, R., Smylie, M., Rutkowski, P., Ferrucci, P. F., Hill, A., Wagstaff, J., Carlino, M. S., Haanen, J. B., Maio, M., Marquez-Rodas, I., McArthur, G. A., Ascierto, P. A., Long, G. V., Callahan, M. K., Postow, M. A., Grossmann, K., Sznol, M., Dreno, B., Bastholt, L., Yang, A., Rollin, L. M., Horak, C., Hodi, F. S. & Wolchok, J. D. (2015) Combined Nivolumab and Ipilimumab or Monotherapy in Untreated Melanoma, *N Engl J Med.* 373, 23-34.
9. Overman, M. J., Lonardi, S., Wong, K. Y. M., Lenz, H. J., Gelsomino, F., Aglietta, M., Morse, M. A., Van Cutsem, E., McDermott, R., Hill, A., Sawyer, M. B., Hendlish, A., Neyns, B., Svrcek, M., Moss, R. A., Ledezine, J. M., Cao, Z. A., Kamble, S., Kopetz, S. & Andre, T. (2018) Durable Clinical Benefit With Nivolumab Plus Ipilimumab in DNA Mismatch Repair-Deficient/Microsatellite Instability-High Metastatic Colorectal Cancer, *J Clin Oncol.* 36, 773-779.
10. Liston, D. R. & Davis, M. (2017) Clinically Relevant Concentrations of Anticancer Drugs: A Guide for Nonclinical Studies, *Clin Cancer Res.* 23, 3489-3498.
11. Sheng, J., Srivastava, S., Sanghavi, K., Lu, Z., Schmidt, B. J., Bello, A. & Gupta,

- M. (2017) Clinical Pharmacology Considerations for the Development of Immune Checkpoint Inhibitors, *J Clin Pharmacol.* 57 Suppl 10, S26-S42.
12. Khera, N. & Rajput, S. (2017) Therapeutic Potential of Small Molecule Inhibitors, *J Cell Biochem.* 118, 959-961.
13. McGranahan, N., Furness, A. J., Rosenthal, R., Ramskov, S., Lyngaa, R., Saini, S. K., Jamal-Hanjani, M., Wilson, G. A., Birkbak, N. J., Hiley, C. T., Watkins, T. B., Shafi, S., Murugaesu, N., Mitter, R., Akarca, A. U., Linares, J., Marafioti, T., Henry, J. Y., Van Allen, E. M., Miao, D., Schilling, B., Schadendorf, D., Garraway, L. A., Makarov, V., Rizvi, N. A., Snyder, A., Hellmann, M. D., Merghoub, T., Wolchok, J. D., Shukla, S. A., Wu, C. J., Peggs, K. S., Chan, T. A., Hadrup, S. R., Quezada, S. A. & Swanton, C. (2016) Clonal neoantigens elicit T cell immunoreactivity and sensitivity to immune checkpoint blockade, *Science.* 351, 1463-9.
14. Borst, J., Ahrends, T., Babala, N., Melief, C. J. M. & Kastenmuller, W. (2018) CD4(+) T cell help in cancer immunology and immunotherapy, *Nat Rev Immunol.* 18, 635-647.
15. Speiser, D. E., Lienard, D., Rufer, N., Rubio-Godoy, V., Rimoldi, D., Lejeune, F., Krieg, A. M., Cerottini, J. C. & Romero, P. (2005) Rapid and strong human CD8+ T cell responses to vaccination with peptide, IFA, and CpG oligodeoxynucleotide 7909, *J Clin Invest.* 115, 739-46.
16. Hui, E., Cheung, J., Zhu, J., Su, X., Taylor, M. J., Wallweber, H. A., Sasmal, D. K., Huang, J., Kim, J. M., Mellman, I. & Vale, R. D. (2017) T cell costimulatory receptor CD28 is a primary target for PD-1-mediated inhibition, *Science.* 355, 1428-1433.
17. Guzik, K., Zak, K. M., Grudnik, P., Magiera, K., Musielak, B., Torner, R., Skalniak, L., Domling, A., Dubin, G. & Holak, T. A. (2017) Small-Molecule Inhibitors of the Programmed Cell Death-1/Programmed Death-Ligand 1 (PD-1/PD-L1) Interaction via Transiently Induced Protein States and Dimerization of PD-L1, *J Med Chem.* 60, 5857-5867.
18. Zak, K. M., Grudnik, P., Guzik, K., Zieba, B. J., Musielak, B., Domling, A., Dubin, G. & Holak, T. A. (2016) Structural basis for small molecule targeting of the programmed death ligand 1 (PD-L1), *Oncotarget.* 7, 30323-35.
19. Ganesan, A. A., Ahmed, M., Okoye, I., Arutyunova, E., Babu, D., Turnbull, W. L., Kundu, J. K., Shields, J., Agopsowicz, K. C., Xu, L., Tabana, Y., Srivastava, N., Zhang, G., Moon, T. C., Belovodskiy, A., Hena, M., Kandada, A. S., Hosseini, S. N., Hitt, M., Walker, J., Smylie, M., West, F. G., Siraki, A. G., Lemieux, M. J., Elahi, S., Nieman, J. A., Tyrrell, D. L., Houghton, M. & Barakat, K. (2019) Comprehensive in vitro characterization of PD-L1 small molecule inhibitors, *Sci Rep.* 9, 12392.
20. Yang, J. & Hu, L. (2019) Immunomodulators targeting the PD-1/PD-L1 protein-protein interaction: From antibodies to small molecules, *Med Res Rev.* 39, 265-301.
21. Tran, E., Ahmadzadeh, M., Lu, Y. C., Gros, A., Turcotte, S., Robbins, P. F., Gartner, J. J., Zheng, Z., Li, Y. F., Ray, S., Wunderlich, J. R., Somerville, R. P. & Rosenberg, S. A. (2015) Immunogenicity of somatic mutations in human gastrointestinal cancers, *Science.* 350, 1387-90.
22. Sahin, U., Derhovanessian, E., Miller, M., Kloke, B. P., Simon, P., Lower, M., Bukur, V., Tadmor, A. D., Luxemburger, U., Schrors, B., Omokoko, T., Vormehr, M., Albrecht, C., Paruzynski, A., Kuhn, A. N., Buck, J., Heesch, S., Schreeb, K. H., Muller, F., Ortseifer, I., Vogler, I., Godehardt, E., Attig, S., Rae, R., Breitkreuz, A., Tolliver, C., Suchan, M., Martic, G., Hohberger, A., Sorn, P., Diekmann, J., Ciesla, J., Waksman, O., Bruck, A. K., Witt, M., Zillgen, M., Rothermel, A., Kasemann, B., Langer, D., Bolte, S., Diken, M., Kreiter, S., Nemecek, R., Gebhardt, C., Grabbe, S., Holler, C., Utikal, J., Huber, C., Loquai, C. & Tureci, O. (2017) Personalized RNA mutanome



vaccines mobilize poly-specific therapeutic immunity against cancer, *Nature*. 547, 222-226.

23. Keskin, D. B., Anandappa, A. J., Sun, J., Tirosh, I., Mathewson, N. D., Li, S., Oliveira, G., Giobbie-Hurder, A., Felt, K., Gjini, E., Shukla, S. A., Hu, Z., Li, L., Le, P. M., Allesoe, R. L., Richman, A. R., Kowalczyk, M. S., Abdelrahman, S., Geduldig, J. E., Charbonneau, S., Pelton, K., Iorgulescu, J. B., Elagina, L., Zhang, W., Olive, O., McCluskey, C., Olsen, L. R., Stevens, J., Lane, W. J., Salazar, A. M., Daley, H., Wen, P. Y., Chiocca, E. A., Harden, M., Lennon, N. J., Gabriel, S., Getz, G., Lander, E. S., Regev, A., Ritz, J., Neuberg, D., Rodig, S. J., Ligon, K. L., Suva, M. L., Wucherpfenig, K. W., Hacohen, N., Fritsch, E. F., Livak, K. J., Ott, P. A., Wu, C. J. & Reardon, D. A. (2019) Neoantigen vaccine generates intratumoral T cell responses in phase Ib glioblastoma trial, *Nature*. 565, 234-239.

24. Smith, M., Garcia-Martinez, E., Pitter, M. R., Fucikova, J., Spisek, R., Zitvogel, L., Kroemer, G. & Galluzzi, L. (2018) Trial Watch: Toll-like receptor agonists in cancer immunotherapy, *Oncoimmunology*. 7, e1526250.

25. Kaczanowska, S., Joseph, A. M. & Davila, E. (2013) TLR agonists: our best frenemy in cancer immunotherapy, *J Leukoc Biol*. 93, 847-63.

26. Mancini, R. J., Stutts, L., Ryu, K. A., Tom, J. K. & Esser-Kahn, A. P. (2014) Directing the immune system with chemical compounds, *ACS Chem Biol*. 9, 1075-85.

27. Dietsch, G. N., Lu, H., Yang, Y., Morishima, C., Chow, L. Q., Disis, M. L. & Hershberg, R. M. (2016) Coordinated Activation of Toll-Like Receptor8 (TLR8) and NLRP3 by the TLR8 Agonist, VTX-2337, Ignites Tumoricidal Natural Killer Cell Activity, *PLoS One*. 11, e0148764.

28. Shayan, G., Kansy, B. A., Gibson, S. P., Srivastava, R. M., Bryan, J. K., Bauman, J. E., Ohr, J., Kim, S., Duvvuri, U., Clump, D. A., Heron, D. E., Johnson, J. T., Hershberg, R. M. & Ferris, R. L. (2018) Phase Ib Study of Immune Biomarker Modulation with Neoadjuvant Cetuximab and TLR8 Stimulation in Head and Neck Cancer to Overcome Suppressive Myeloid Signals, *Clin Cancer Res*. 24, 62-72.

29. Ferris, R. L., Saba, N. F., Gitlitz, B. J., Haddad, R., Sukari, A., Neupane, P., Morris, J. C., Misiukiewicz, K., Bauman, J. E., Fenton, M., Jimeno, A., Adkins, D. R., Schneider, C. J., Sacco, A. G., Shirai, K., Bowles, D. W., Gibson, M., Nwizu, T., Gotardo, R., Manjarrez, K. L., Dietsch, G. N., Bryan, J. K., Hershberg, R. M. & Cohen, E. E. W. (2018) Effect of Adding Motolimod to Standard Combination Chemotherapy and Cetuximab Treatment of Patients With Squamous Cell Carcinoma of the Head and Neck: The Active8 Randomized Clinical Trial, *JAMA Oncol*. 4, 1583-1588.

30. Zhang, L., Dewan, V. & Yin, H. (2017) Discovery of Small Molecules as Multi-Toll-like Receptor Agonists with Proinflammatory and Anticancer Activities, *J Med Chem*. 60, 5029-5044.

31. Zhu, G., Xu, Y., Cen, X., Nandakumar, K. S., Liu, S. & Cheng, K. (2018) Targeting pattern-recognition receptors to discover new small molecule immune modulators, *Eur J Med Chem*. 144, 82-92.

32. Woo, S. R., Fuertes, M. B., Corrales, L., Spranger, S., Furdyna, M. J., Leung, M. Y., Duggan, R., Wang, Y., Barber, G. N., Fitzgerald, K. A., Alegre, M. L. & Gajewski, T. F. (2014) STING-dependent cytosolic DNA sensing mediates innate immune recognition of immunogenic tumors, *Immunity*. 41, 830-42.

33. Li, L., Yin, Q., Kuss, P., Maliga, Z., Millan, J. L., Wu, H. & Mitchison, T. J. (2014) Hydrolysis of 2'3'-cGAMP by ENPP1 and design of nonhydrolyzable analogs, *Nat Chem Biol*. 10, 1043-8.

34. Chang, L., Lee, S. Y., Leonczak, P., Rozenski, J., De Jonghe, S., Hanck, T., Muller, C. E. & Herdewijn, P. (2014) Imidazopyridine- and purine-thioacetamide deriva-

- tives: potent inhibitors of nucleotide pyrophosphatase/phosphodiesterase 1 (NPP1), *J Med Chem.* 57, 10080-100.
35. Zelikman, V., Pelletier, J., Simhaev, L., Sela, A., Gendron, F. P., Arguin, G., Senderowitz, H., Seigny, J. & Fischer, B. (2018) Highly Selective and Potent Ecto-nucleotide Pyrophosphatase-1 (NPP1) Inhibitors Based on Uridine 5'-Palph $\alpha$ , $\alpha$ -Dithiophosphate Analogues, *J Med Chem.* 61, 3939-3951.
36. Zhai, L., Ladomersky, E., Lenzen, A., Nguyen, B., Patel, R., Lauing, K. L., Wu, M. & Wainwright, D. A. (2018) IDO1 in cancer: a Gemini of immune checkpoints, *Cell Mol Immunol.* 15, 447-457.
37. Liu, H., Zhang, H., Wu, X., Ma, D., Wu, J., Wang, L., Jiang, Y., Fei, Y., Zhu, C., Tan, R., Jungblut, P., Pei, G., Dorhoi, A., Yan, Q., Zhang, F., Zheng, R., Liu, S., Liang, H., Liu, Z., Yang, H., Chen, J., Wang, P., Tang, T., Peng, W., Hu, Z., Xu, Z., Huang, X., Wang, J., Li, H., Zhou, Y., Liu, F., Yan, D., Kaufmann, S. H. E., Chen, C., Mao, Z. & Ge, B. (2018) Nuclear cGAS suppresses DNA repair and promotes tumorigenesis, *Nature.* 563, 131-136.
38. Lemos, H., Mohamed, E., Huang, L., Ou, R., Pacholczyk, G., Arbab, A. S., Munn, D. & Mellor, A. L. (2016) STING Promotes the Growth of Tumors Characterized by Low Antigenicity via IDO Activation, *Cancer Res.* 76, 2076-81.
39. Krombach, J., Hennel, R., Brix, N., Orth, M., Schoetz, U., Ernst, A., Schuster, J., Zuchtriegel, G., Reichel, C. A., Bierschenk, S., Sperandio, M., Vogl, T., Unkel, S., Belka, C. & Lauber, K. (2019) Priming anti-tumor immunity by radiotherapy: Dying tumor cell-derived DAMPs trigger endothelial cell activation and recruitment of myeloid cells, *Oncoimmunology.* 8, e1523097.
40. Galluzzi, L., Buque, A., Kepp, O., Zitvogel, L. & Kroemer, G. (2015) Immunological Effects of Conventional Chemotherapy and Targeted Anticancer Agents, *Cancer Cell.* 28, 690-714.
41. Heinhuis, K. M., Ros, W., Kok, M., Steeghs, N., Beijnen, J. H. & Schellens, J. H. M. (2019) Enhancing antitumor response by combining immune checkpoint inhibitors with chemotherapy in solid tumors, *Ann Oncol.* 30, 219-235.
42. Beyranvand Nejad, E., van der Sluis, T. C., van Duikeren, S., Yagita, H., Jansen, G. M., van Veelen, P. A., Melief, C. J., van der Burg, S. H. & Arens, R. (2016) Tumor Eradication by Cisplatin Is Sustained by CD80/86-Mediated Costimulation of CD8<sup>+</sup> T Cells, *Cancer Res.* 76, 6017-6029.
43. Gandhi, L. & Garassino, M. C. (2018) Pembrolizumab plus Chemotherapy in Lung Cancer, *N Engl J Med.* 379, e18.
44. Sistigu, A., Yamazaki, T., Vacchelli, E., Chaba, K., Enot, D. P., Adam, J., Vitale, I., Goubar, A., Baracco, E. E., Remedios, C., Fend, L., Hannani, D., Aymeric, L., Ma, Y., Niso-Santano, M., Kepp, O., Schultze, J. L., Tuting, T., Belardelli, F., Bracci, L., La Sorsa, V., Ziccheddu, G., Sestili, P., Urbani, F., Delorenzi, M., Lacroix-Triki, M., Quidville, V., Conforti, R., Spano, J. P., Puzsai, L., Poirier-Colame, V., Delaloge, S., Penault-Llorca, F., Ladoire, S., Arnould, L., Cyrta, J., Dessoliers, M. C., Eggermont, A., Bianchi, M. E., Pittet, M., Engblom, C., Pfirschke, C., Preville, X., Uze, G., Schreiber, R. D., Chow, M. T., Smyth, M. J., Proietti, E., Andre, F., Kroemer, G. & Zitvogel, L. (2014) Cancer cell-autonomous contribution of type I interferon signaling to the efficacy of chemotherapy, *Nat Med.* 20, 1301-9.
45. Alizadeh, D., Trad, M., Hanke, N. T., Larmonier, C. B., Janikashvili, N., Bonnotte, B., Katsanis, E. & Larmonier, N. (2014) Doxorubicin eliminates myeloid-derived suppressor cells and enhances the efficacy of adoptive T-cell transfer in breast cancer, *Cancer Res.* 74, 104-18.
46. Voorwerk, L., Slagter, M., Horlings, H. M., Sikorska, K., van de Vijver, K. K., de



- Maaker, M., Nederlof, I., Kluin, R. J. C., Warren, S., Ong, S., Wiersma, T. G., Russell, N. S., Lalezari, F., Schouten, P. C., Bakker, N. A. M., Ketelaars, S. L. C., Peters, D., Lange, C. A. H., van Werkhoven, E., van Tinteren, H., Mandjes, I. A. M., Kemper, I., Onderwater, S., Chalabi, M., Wilgenhof, S., Haanen, J., Salgado, R., de Visser, K. E., Sonke, G. S., Wessels, L. F. A., Linn, S. C., Schumacher, T. N., Blank, C. U. & Kok, M. (2019) Immune induction strategies in metastatic triple-negative breast cancer to enhance the sensitivity to PD-1 blockade: the TONIC trial, *Nat Med.* 25, 920-928.
47. Orecchioni, S., Talarico, G., Labanca, V., Calleri, A., Mancuso, P. & Bertolini, F. (2018) Vinorelbine, cyclophosphamide and 5-FU effects on the circulating and intratumoural landscape of immune cells improve anti-PD-L1 efficacy in preclinical models of breast cancer and lymphoma, *Br J Cancer.* 118, 1329-1336.
48. Zhou, J., Yang, T., Liu, L. & Lu, B. (2017) Chemotherapy oxaliplatin sensitizes prostate cancer to immune checkpoint blockade therapies via stimulating tumor immunogenicity, *Mol Med Rep.* 16, 2868-2874.
49. Paz-Ares, L., Luft, A., Vicente, D., Tafreshi, A., Gumus, M., Mazieres, J., Hermes, B., Cay Senler, F., Csoszi, T., Fulop, A., Rodriguez-Cid, J., Wilson, J., Sugawara, S., Kato, T., Lee, K. H., Cheng, Y., Novello, S., Halmos, B., Li, X., Lubiniecki, G. M., Piperdi, B., Kowalski, D. M. & Investigators, K.-. (2018) Pembrolizumab plus Chemotherapy for Squamous Non-Small-Cell Lung Cancer, *N Engl J Med.* 379, 2040-2051.
50. Karzai, F., VanderWeele, D., Madan, R. A., Owens, H., Cordes, L. M., Hankin, A., Couvillon, A., Nichols, E., Bilusic, M., Beshiri, M. L., Kelly, K., Krishnasamy, V., Lee, S., Lee, M. J., Yuno, A., Trepel, J. B., Merino, M. J., Dittamore, R., Marte, J., Donahue, R. N., Schlom, J., Killian, K. J., Meltzer, P. S., Steinberg, S. M., Gulley, J. L., Lee, J. M. & Dahut, W. L. (2018) Activity of durvalumab plus olaparib in metastatic castration-resistant prostate cancer in men with and without DNA damage repair mutations, *J Immunother Cancer.* 6, 141.
51. Jiao, S., Xia, W., Yamaguchi, H., Wei, Y., Chen, M. K., Hsu, J. M., Hsu, J. L., Yu, W. H., Du, Y., Lee, H. H., Li, C. W., Chou, C. K., Lim, S. O., Chang, S. S., Litton, J., Arun, B., Hortobagyi, G. N. & Hung, M. C. (2017) PARP Inhibitor Upregulates PD-L1 Expression and Enhances Cancer-Associated Immunosuppression, *Clin Cancer Res.* 23, 3711-3720.
52. Deng, J., Wang, E. S., Jenkins, R. W., Li, S., Dries, R., Yates, K., Chhabra, S., Huang, W., Liu, H., Aref, A. R., Ivanova, E., Paweletz, C. P., Bowden, M., Zhou, C. W., Herter-Sprie, G. S., Sorrentino, J. A., Bisi, J. E., Lizotte, P. H., Merlino, A. A., Quinn, M. M., Bufo, L. E., Yang, A., Zhang, Y., Zhang, H., Gao, P., Chen, T., Cavanaugh, M. E., Rode, A. J., Haines, E., Roberts, P. J., Strum, J. C., Richards, W. G., Lorch, J. H., Parangi, S., Gunda, V., Boland, G. M., Bueno, R., Palakurthi, S., Freeman, G. J., Ritz, J., Haining, W. N., Sharpless, N. E., Arthanari, H., Shapiro, G. I., Barbie, D. A., Gray, N. S. & Wong, K. K. (2018) CDK4/6 Inhibition Augments Antitumor Immunity by Enhancing T-cell Activation, *Cancer Discov.* 8, 216-233.
53. Uyttenhove, C., Pilotte, L., Theate, I., Stroobant, V., Colau, D., Parmentier, N., Boon, T. & Van den Eynde, B. J. (2003) Evidence for a tumoral immune resistance mechanism based on tryptophan degradation by indoleamine 2,3-dioxygenase, *Nat Med.* 9, 1269-74.
54. Lippitz, B. E. (2013) Cytokine patterns in patients with cancer: a systematic review, *Lancet Oncol.* 14, e218-28.
55. Giraldo, N. A., Sanchez-Salas, R., Peske, J. D., Vano, Y., Becht, E., Petitprez, F., Validire, P., Ingels, A., Cathelineau, X., Fridman, W. H. & Sautès-Fridman, C. (2019) The clinical role of the TME in solid cancer, *Br J Cancer.* 120, 45-53.

56. Prendergast, G. C., Malachowski, W. J., Mondal, A., Scherle, P. & Muller, A. J. (2018) Indoleamine 2,3-Dioxygenase and Its Therapeutic Inhibition in Cancer, *Int Rev Cell Mol Biol.* 336, 175-203.
57. Liu, Y., Liang, X., Dong, W., Fang, Y., Lv, J., Zhang, T., Fiskesund, R., Xie, J., Liu, J., Yin, X., Jin, X., Chen, D., Tang, K., Ma, J., Zhang, H., Yu, J., Yan, J., Liang, H., Mo, S., Cheng, F., Zhou, Y., Zhang, H., Wang, J., Li, J., Chen, Y., Cui, B., Hu, Z. W., Cao, X., Xiao-Feng Qin, F. & Huang, B. (2018) Tumor-Repopulating Cells Induce PD-1 Expression in CD8(+) T Cells by Transferring Kynurenine and AhR Activation, *Cancer Cell.* 33, 480-494 e7.
58. Soliman, H. H., Jackson, E., Neuger, T., Dees, E. C., Harvey, R. D., Han, H., Ismail-Khan, R., Minton, S., Vahanian, N. N., Link, C., Sullivan, D. M. & Antonia, S. (2014) A first in man phase I trial of the oral immunomodulator, indoximod, combined with docetaxel in patients with metastatic solid tumors, *Oncotarget.* 5, 8136-46.
59. Long, G. V., Dummer, R., Hamid, O., Gajewski, T. F., Caglevic, C., Dalle, S., Arance, A., Carlino, M. S., Grob, J. J., Kim, T. M., Demidov, L., Robert, C., Larkin, J., Anderson, J. R., Maleski, J., Jones, M., Diede, S. J. & Mitchell, T. C. (2019) Epacadostat plus pembrolizumab versus placebo plus pembrolizumab in patients with unresectable or metastatic melanoma (ECHO-301/KEYNOTE-252): a phase 3, randomised, double-blind study, *Lancet Oncol.* 20, 1083-1097.
60. Aung Naing, J. D. P., Gerald Falchook, Benjamin Creelan, John Nemunaitis, Jose Lutzky, Adi Diab, Judy S. Wang, Naomi Laing, Michelle Niewood, Xiaohua Gong, Gongfu Zhou and Manish Patel (2018) Abstract CT177: Epacadostat plus durvalumab in patients with advanced solid tumors: preliminary results of the ongoing, open-label, phase I/II ECHO-203 study.
61. Depth, N. i. (2018) Companies Scaling Back IDO1 Inhibitor Trials, *CANCER DISCOVERY.* 8, OF5.
62. Opitz, C. A., Litzenburger, U. M., Sahm, F., Ott, M., Tritschler, I., Trump, S., Schumacher, T., Jestaedt, L., Schrenk, D., Weller, M., Jugold, M., Guillemin, G. J., Miller, C. L., Lutz, C., Radlwimmer, B., Lehmann, I., von Deimling, A., Wick, W. & Platten, M. (2011) An endogenous tumour-promoting ligand of the human aryl hydrocarbon receptor, *Nature.* 478, 197-203.
63. McGaha, T. L. (2015) IDO-GCN2 and autophagy in inflammation, *Oncotarget.* 6, 21771-2.
64. Fujimoto, J., Kurasawa, O., Takagi, T., Liu, X., Banno, H., Kojima, T., Asano, Y., Nakamura, A., Nambu, T., Hata, A., Ishii, T., Sameshima, T., Debori, Y., Miyamoto, M., Klein, M. G., Tjhen, R., Sang, B. C., Levin, I., Lane, S. W., Snell, G. P., Li, K., Kefala, G., Hoffman, I. D., Ding, S. C., Cary, D. R. & Mizojiri, R. (2019) Identification of Novel, Potent, and Orally Available GCN2 Inhibitors with Type I Half Binding Mode, *ACS Med Chem Lett.* 10, 1498-1503.
65. Hennequart, M., Pilotte, L., Cane, S., Hoffmann, D., Stroobant, V., Plaen, E. & Van den Eynde, B. J. (2017) Constitutive IDO1 Expression in Human Tumors Is Driven by Cyclooxygenase-2 and Mediates Intrinsic Immune Resistance, *Cancer Immunol Res.* 5, 695-709.
66. Pang, L. Y., Hurst, E. A. & Argyle, D. J. (2016) Cyclooxygenase-2: A Role in Cancer Stem Cell Survival and Repopulation of Cancer Cells during Therapy, *Stem Cells Int.* 2016, 2048731.
67. Buzharevski, A., Paskas, S., Sarosi, M. B., Laube, M., Lonnecke, P., Neumann, W., Mijatovic, S., Maksimovic-Ivanic, D., Pietzsch, J. & Hey-Hawkins, E. (2019) Carboranyl Analogues of Celecoxib with Potent Cytostatic Activity against Human Melanoma and Colon Cancer Cell Lines, *ChemMedChem.* 14, 315-321.

68. Li, N., Li, H., Su, F., Li, J., Ma, X. & Gong, P. (2015) Relationship between epidermal growth factor receptor (EGFR) mutation and serum cyclooxygenase-2 Level, and the synergistic effect of celecoxib and gefitinib on EGFR expression in non-small cell lung cancer cells, *Int J Clin Exp Pathol.* 8, 9010-20.
69. Tang, H., Liu, Y., Wang, C., Zheng, H., Chen, Y., Liu, W., Chen, X., Zhang, J., Chen, H., Yang, Y. & Yang, J. (2019) Inhibition of COX-2 and EGFR by Melafolone Improves Anti-PD-1 Therapy through Vascular Normalization and PD-L1 Downregulation in Lung Cancer, *J Pharmacol Exp Ther.* 368, 401-413.
70. Sun, X. & Li, Q. (2018) Prostaglandin EP2 receptor: Novel therapeutic target for human cancers (Review), *Int J Mol Med.* 42, 1203-1214.
71. af Forselles, K. J., Root, J., Clarke, T., Davey, D., Aughton, K., Dack, K. & Pullen, N. (2011) In vitro and in vivo characterization of PF-04418948, a novel, potent and selective prostaglandin EP(2) receptor antagonist, *Br J Pharmacol.* 164, 1847-56.
72. Ma, X., Holt, D., Kundu, N., Reader, J., Goloubeva, O., Take, Y. & Fulton, A. M. (2013) A prostaglandin E (PGE) receptor EP4 antagonist protects natural killer cells from PGE2-mediated immunosuppression and inhibits breast cancer metastasis, *Oncoimmunology.* 2, e22647.
73. Miao, J., Lu, X., Hu, Y., Piao, C., Wu, X., Liu, X., Huang, C., Wang, Y., Li, D. & Liu, J. (2017) Prostaglandin E2 and PD-1 mediated inhibition of antitumor CTL responses in the human tumor microenvironment, *Oncotarget.* 8, 89802-89810.
74. Morris, S. M., Jr. (2009) Recent advances in arginine metabolism: roles and regulation of the arginases, *Br J Pharmacol.* 157, 922-30.
75. Rodriguez, P. C., Zea, A. H., Culotta, K. S., Zabaleta, J., Ochoa, J. B. & Ochoa, A. C. (2002) Regulation of T cell receptor CD3zeta chain expression by L-arginine, *J Biol Chem.* 277, 21123-9.
76. Steggerda, S. M., Bennett, M. K., Chen, J., Emberley, E., Huang, T., Janes, J. R., Li, W., MacKinnon, A. L., Makkouk, A., Marguier, G., Murray, P. J., Neou, S., Pan, A., Parlati, F., Rodriguez, M. L. M., Van de Velde, L. A., Wang, T., Works, M., Zhang, J., Zhang, W. & Gross, M. I. (2017) Inhibition of arginase by CB-1158 blocks myeloid cell-mediated immune suppression in the tumor microenvironment, *J Immunother Cancer.* 5, 101.
77. Adams, J. L., Smothers, J., Srinivasan, R. & Hoos, A. (2015) Big opportunities for small molecules in immuno-oncology, *Nat Rev Drug Discov.* 14, 603-22.
78. De Santo, C., Serafini, P., Marigo, I., Dolcetti, L., Bolla, M., Del Soldato, P., Melani, C., Guiducci, C., Colombo, M. P., Iezzi, M., Musiani, P., Zanovello, P. & Bronte, V. (2005) Nitroaspirin corrects immune dysfunction in tumor-bearing hosts and promotes tumor eradication by cancer vaccination, *Proc Natl Acad Sci U S A.* 102, 4185-90.
79. Molon, B., Ugel, S., Del Pozzo, F., Soldani, C., Zilio, S., Avella, D., De Palma, A., Mauri, P., Monegal, A., Rescigno, M., Savino, B., Colombo, P., Jonjic, N., Pecanic, S., Lazzarato, L., Fruttero, R., Gasco, A., Bronte, V. & Viola, A. (2011) Chemokine nitration prevents intratumoral infiltration of antigen-specific T cells, *J Exp Med.* 208, 1949-62.
80. Ohta, A., Gorelik, E., Prasad, S. J., Ronchese, F., Lukashev, D., Wong, M. K., Huang, X., Caldwell, S., Liu, K., Smith, P., Chen, J. F., Jackson, E. K., Apasov, S., Abrams, S. & Sitkovsky, M. (2006) A2A adenosine receptor protects tumors from antitumor T cells, *Proc Natl Acad Sci U S A.* 103, 13132-7.
81. Ohta, A., Kini, R., Ohta, A., Subramanian, M., Madasu, M. & Sitkovsky, M. (2012) The development and immunosuppressive functions of CD4(+) CD25(+) FoxP3(+) regulatory T cells are under influence of the adenosine-A2A adenosine receptor

pathway, *Front Immunol.* 3, 190.

82. Gillespie, R. J., Bamford, S. J., Botting, R., Comer, M., Denny, S., Gaur, S., Griffin, M., Jordan, A. M., Knight, A. R., Lerpiniere, J., Leonardi, S., Lightowler, S., McAteer, S., Merrett, A., Misra, A., Padfield, A., Reece, M., Saadi, M., Selwood, D. L., Stratton, G. C., Surry, D., Todd, R., Tong, X., Ruston, V., Upton, R. & Weiss, S. M. (2009) Antagonists of the human A(2A) adenosine receptor. 4. Design, synthesis, and preclinical evaluation of 7-aryltriazolo[4,5-d]pyrimidines, *J Med Chem.* 52, 33-47.

83. Kerr, W. G. & Chisholm, J. D. (2019) The Next Generation of Immunotherapy for Cancer: Small Molecules Could Make Big Waves, *J Immunol.* 202, 11-19.

84. Huck, B. R., Kotzner, L. & Urbahns, K. (2018) Small Molecules Drive Big Improvements in Immuno-Oncology Therapies, *Angew Chem Int Ed Engl.* 57, 4412-4428.

85. Chang, M. R., Dharmarajan, V., Doebelin, C., Garcia-Ordonez, R. D., Novick, S. J., Kuruvilla, D. S., Kamenecka, T. M. & Griffin, P. R. (2016) Synthetic ROR $\gamma$  Agonists Enhance Protective Immunity, *ACS Chem Biol.* 11, 1012-8.

86. Hu, X., Liu, X., Moisan, J., Wang, Y., Lesch, C. A., Spooner, C., Morgan, R. W., Zawadzka, E. M., Mertz, D., Bousley, D., Majchrzak, K., Kryczek, I., Taylor, C., Van Huis, C., Skalitzy, D., Hurd, A., Aicher, T. D., Toogood, P. L., Glick, G. D., Paulos, C. M., Zou, W. & Carter, L. L. (2016) Synthetic ROR $\gamma$  agonists regulate multiple pathways to enhance antitumor immunity, *Oncoimmunology.* 5, e1254854.

87. Ivanov, II, McKenzie, B. S., Zhou, L., Tadakoro, C. E., Lepelley, A., Lafaille, J. J., Cua, D. J. & Littman, D. R. (2006) The orphan nuclear receptor ROR $\gamma$  directs the differentiation program of proinflammatory IL-17+ T helper cells, *Cell.* 126, 1121-33.

88. Asadzadeh, Z., Mohammadi, H., Safarzadeh, E., Hemmatzadeh, M., Mahdian-Shakib, A., Jadidi-Niaragh, F., Azizi, G. & Baradaran, B. (2017) The paradox of Th17 cell functions in tumor immunity, *Cell Immunol.* 322, 15-25.

89. Wang, R., Yang, L., Zhang, C., Wang, R., Zhang, Z., He, Q., Chen, X., Zhang, B., Qin, Z., Wang, L. & Zhang, Y. (2018) Th17 cell-derived IL-17A promoted tumor progression via STAT3/NF- $\kappa$ B/Notch1 signaling in non-small cell lung cancer, *Oncoimmunology.* 7, e1461303.

90. Lee, M. H., Tung-Chieh Chang, J., Liao, C. T., Chen, Y. S., Kuo, M. L. & Shen, C. R. (2018) Interleukin 17 and peripheral IL-17-expressing T cells are negatively correlated with the overall survival of head and neck cancer patients, *Oncotarget.* 9, 9825-9837.

91. Kono, M., Ochida, A., Oda, T., Imada, T., Banno, Y., Taya, N., Masada, S., Kawamoto, T., Yonemori, K., Nara, Y., Fukase, Y., Yukawa, T., Tokuhara, H., Skene, R., Sang, B. C., Hoffman, I. D., Snell, G. P., Uga, K., Shibata, A., Igaki, K., Nakamura, Y., Nakagawa, H., Tsuchimori, N., Yamasaki, M., Shirai, J. & Yamamoto, S. (2018) Discovery of [ cis-3-((5 R)-5-((7-Fluoro-1,1-dimethyl-2,3-dihydro-1 H-inden-5-yl) carbamoyl)-2-methoxy-7,8-dihydro-1,6-naphthyridin-6(5 H)-yl)carbonyl]cyclobutyl] acetic Acid (TAK-828F) as a Potent, Selective, and Orally Available Novel Retinoic Acid Receptor-Related Orphan Receptor  $\gamma$  Inverse Agonist, *J Med Chem.* 61, 2973-2988.

92. Wang, J., Bhatia, A., Krugliak Cleveland, N., Gupta, N., Dalal, S., Rubin, D. T. & Sakuraba, A. (2018) Rapid Onset of Inflammatory Bowel Disease after Receiving Secukinumab Infusion, *ACG Case Rep J.* 5, e56.

93. Ghosh, M. C., Makena, P. S., Gorantla, V., Sinclair, S. E. & Waters, C. M. (2012) CXCR4 regulates migration of lung alveolar epithelial cells through activation of Rac1

- and matrix metalloproteinase-2, *Am J Physiol Lung Cell Mol Physiol.* 302, L846-56.
94. Onoue, T., Uchida, D., Begum, N. M., Tomizuka, Y., Yoshida, H. & Sato, M. (2006) Epithelial-mesenchymal transition induced by the stromal cell-derived factor-1/CXCR4 system in oral squamous cell carcinoma cells, *Int J Oncol.* 29, 1133-8.
  95. Zhou, W., Guo, S., Liu, M., Burow, M. E. & Wang, G. (2019) Targeting CXCL12/CXCR4 Axis in Tumor Immunotherapy, *Curr Med Chem.* 26, 3026-3041.
  96. Kato, I., Niwa, A., Heike, T., Fujino, H., Saito, M. K., Umeda, K., Hiramatsu, H., Ito, M., Morita, M., Nishinaka, Y., Adachi, S., Ishikawa, F. & Nakahata, T. (2011) Identification of hepatic niche harboring human acute lymphoblastic leukemic cells via the SDF-1/CXCR4 axis, *PLoS One.* 6, e27042.
  97. Uy, G. L., Rettig, M. P., Motabi, I. H., McFarland, K., Trinkaus, K. M., Hladnik, L. M., Kulkarni, S., Abboud, C. N., Cashen, A. F., Stockerl-Goldstein, K. E., Vij, R., Westervelt, P. & DiPersio, J. F. (2012) A phase 1/2 study of chemosensitization with the CXCR4 antagonist plerixafor in relapsed or refractory acute myeloid leukemia, *Blood.* 119, 3917-24.
  98. Taromi, S., Kayser, G., Catusse, J., von Elverfeldt, D., Reichardt, W., Braun, F., Weber, W. A., Zeiser, R. & Burger, M. (2016) CXCR4 antagonists suppress small cell lung cancer progression, *Oncotarget.* 7, 85185-85195.
  99. Chen, Y., Ramjiawan, R. R., Reiberger, T., Ng, M. R., Hato, T., Huang, Y., Ochiai, H., Kitahara, S., Unan, E. C., Reddy, T. P., Fan, C., Huang, P., Bardeesy, N., Zhu, A. X., Jain, R. K. & Duda, D. G. (2015) CXCR4 inhibition in tumor microenvironment facilitates anti-programmed death receptor-1 immunotherapy in sorafenib-treated hepatocellular carcinoma in mice, *Hepatology.* 61, 1591-602.
  100. Steele, C. W., Karim, S. A., Leach, J. D. G., Bailey, P., Upstill-Goddard, R., Rishi, L., Foth, M., Bryson, S., McDaid, K., Wilson, Z., Eberlein, C., Candido, J. B., Clarke, M., Nixon, C., Connelly, J., Jamieson, N., Carter, C. R., Balkwill, F., Chang, D. K., Evans, T. R. J., Strathdee, D., Biankin, A. V., Nibbs, R. J. B., Barry, S. T., Sansom, O. J. & Morton, J. P. (2016) CXCR2 Inhibition Profoundly Suppresses Metastases and Augments Immunotherapy in Pancreatic Ductal Adenocarcinoma, *Cancer Cell.* 29, 832-845.
  101. Katoh, H., Wang, D., Daikoku, T., Sun, H., Dey, S. K. & Dubois, R. N. (2013) CXCR2-expressing myeloid-derived suppressor cells are essential to promote colitis-associated tumorigenesis, *Cancer Cell.* 24, 631-44.
  102. Zhu, H., Gu, Y., Xue, Y., Yuan, M., Cao, X. & Liu, Q. (2017) CXCR2(+) MDSCs promote breast cancer progression by inducing EMT and activated T cell exhaustion, *Oncotarget.* 8, 114554-114567.
  103. Zom, G. G., Khan, S., Britten, C. M., Sommandas, V., Camps, M. G., Loof, N. M., Budden, C. F., Meeuwenoord, N. J., Filippov, D. V., van der Marel, G. A., Overkleeft, H. S., Melief, C. J. & Ossendorp, F. (2014) Efficient induction of antitumor immunity by synthetic toll-like receptor ligand-peptide conjugates, *Cancer Immunol Res.* 2, 756-64.
  104. Zom, G. G., Willems, M., Meeuwenoord, N. J., Reintjens, N. R. M., Tondini, E., Khan, S., Overkleeft, H. S., van der Marel, G. A., Codee, J. D. C., Ossendorp, F. & Filippov, D. V. (2019) Dual Synthetic Peptide Conjugate Vaccine Simultaneously Triggers TLR2 and NOD2 and Activates Human Dendritic Cells, *Bioconjug Chem.* 30, 1150-1161.
  105. Corrales, L., Glickman, L. H., McWhirter, S. M., Kanne, D. B., Sivick, K. E., Katibah, G. E., Woo, S. R., Lemmens, E., Banda, T., Leong, J. J., Metchette, K., Dubensky, T. W., Jr. & Gajewski, T. F. (2015) Direct Activation of STING in the Tumor Microenvironment Leads to Potent and Systemic Tumor Regression and Immunity,



Cell Rep. 11, 1018-30.

106. Shih, A. Y., Damm-Ganamet, K. L. & Mirzadegan, T. (2018) Dynamic Structural Differences between Human and Mouse STING Lead to Differing Sensitivity to DMXAA, *Biophys J.* 114, 32-39.

107. Hwang, J., Kang, T., Lee, J., Choi, B. S. & Han, S. (2019) Design, synthesis, and biological evaluation of C7-functionalized DMXAA derivatives as potential human-STING agonists, *Org Biomol Chem.* 17, 1869-1874.

108. Ramanjulu, J. M., Pesiridis, G. S., Yang, J., Concha, N., Singhaus, R., Zhang, S. Y., Tran, J. L., Moore, P., Lehmann, S., Eberl, H. C., Muelbaier, M., Schneck, J. L., Clemens, J., Adam, M., Mehlmann, J., Romano, J., Morales, A., Kang, J., Leister, L., Graybill, T. L., Charnley, A. K., Ye, G., Nevins, N., Behnia, K., Wolf, A. I., Kasparcova, V., Nurse, K., Wang, L., Puhl, A. C., Li, Y., Klein, M., Hopson, C. B., Guss, J., Bantscheff, M., Bergamini, G., Reilly, M. A., Lian, Y., Duffy, K. J., Adams, J., Foley, K. P., Gough, P. J., Marquis, R. W., Smothers, J., Hoos, A. & Bertin, J. (2018) Design of amidobenzimidazole STING receptor agonists with systemic activity, *Nature.* 564, 439-443.

109. Ghaffari, A., Peterson, N., Khalaj, K., Vitkin, N., Robinson, A., Francis, J. A. & Koti, M. (2018) STING agonist therapy in combination with PD-1 immune checkpoint blockade enhances response to carboplatin chemotherapy in high-grade serous ovarian cancer, *Br J Cancer.* 119, 440-449.

110. Aduro (2019) ([http://investors.aduro.com/news-releases/news-release-details/aduro-biotech-and-novartis-present-results-ongoing-phase-1b?field\\_nir\\_news\\_date\\_value\[min\]=2019](http://investors.aduro.com/news-releases/news-release-details/aduro-biotech-and-novartis-present-results-ongoing-phase-1b?field_nir_news_date_value[min]=2019)) in

111. Wang, G. L., Jiang, B. H., Rue, E. A. & Semenza, G. L. (1995) Hypoxia-inducible factor 1 is a basic-helix-loop-helix-PAS heterodimer regulated by cellular O<sub>2</sub> tension, *Proc Natl Acad Sci U S A.* 92, 5510-4.

112. Hogenesch, J. B., Chan, W. K., Jackiw, V. H., Brown, R. C., Gu, Y. Z., Pray-Grant, M., Perdew, G. H. & Bradfield, C. A. (1997) Characterization of a subset of the basic-helix-loop-helix-PAS superfamily that interacts with components of the dioxin signaling pathway, *J Biol Chem.* 272, 8581-93.

113. Chiu, D. K., Tse, A. P., Xu, I. M., Di Cui, J., Lai, R. K., Li, L. L., Koh, H. Y., Tsang, F. H., Wei, L. L., Wong, C. M., Ng, I. O. & Wong, C. C. (2017) Hypoxia inducible factor HIF-1 promotes myeloid-derived suppressor cells accumulation through EN-TPD2/CD39L1 in hepatocellular carcinoma, *Nat Commun.* 8, 517.

114. Ruf, M., Moch, H. & Schraml, P. (2016) PD-L1 expression is regulated by hypoxia inducible factor in clear cell renal cell carcinoma, *Int J Cancer.* 139, 396-403.

115. DiNatale, B. C., Smith, K., John, K., Krishnegowda, G., Amin, S. G. & Perdew, G. H. (2012) Ah receptor antagonism represses head and neck tumor cell aggressive phenotype, *Mol Cancer Res.* 10, 1369-79.

116. Courtney, K. D., Infante, J. R., Lam, E. T., Figlin, R. A., Rini, B. I., Brugarolas, J., Zojwalla, N. J., Lowe, A. M., Wang, K., Wallace, E. M., Josey, J. A. & Choueiri, T. K. (2018) Phase I Dose-Escalation Trial of PT2385, a First-in-Class Hypoxia-Inducible Factor-2alpha Antagonist in Patients With Previously Treated Advanced Clear Cell Renal Cell Carcinoma, *J Clin Oncol.* 36, 867-874.

117. Chiche, J., Ilc, K., Laferriere, J., Trottier, E., Dayan, F., Mazure, N. M., Brahimi-Horn, M. C. & Pouyssegur, J. (2009) Hypoxia-inducible carbonic anhydrase IX and XII promote tumor cell growth by counteracting acidosis through the regulation of the intracellular pH, *Cancer Res.* 69, 358-68.

118. Radvak, P., Repic, M., Svastova, E., Takacova, M., Csaderova, L., Strnad, H., Pastorek, J., Pastorekova, S. & Kopacek, J. (2013) Suppression of carbonic anhy-

drase IX leads to aberrant focal adhesion and decreased invasion of tumor cells, *Oncol Rep.* 29, 1147-53.

119. Lou, Y., McDonald, P. C., Oloumi, A., Chia, S., Ostlund, C., Ahmadi, A., Kyle, A., Auf dem Keller, U., Leung, S., Huntsman, D., Clarke, B., Sutherland, B. W., Waterhouse, D., Bally, M., Roskelley, C., Overall, C. M., Minchinton, A., Pacchiano, F., Carta, F., Scozzafava, A., Touisni, N., Winum, J. Y., Supuran, C. T. & Dedhar, S. (2011) Targeting tumor hypoxia: suppression of breast tumor growth and metastasis by novel carbonic anhydrase IX inhibitors, *Cancer Res.* 71, 3364-76.

120. Dubois, L., Lieuwes, N. G., Maresca, A., Thiry, A., Supuran, C. T., Scozzafava, A., Wouters, B. G. & Lambin, P. (2009) Imaging of CA IX with fluorescent labelled sulfonamides distinguishes hypoxic and (re)-oxygenated cells in a xenograft tumour model, *Radiother Oncol.* 92, 423-8.

121. Toure, M. & Crews, C. M. (2016) Small-Molecule PROTACS: New Approaches to Protein Degradation, *Angew Chem Int Ed Engl.* 55, 1966-73.

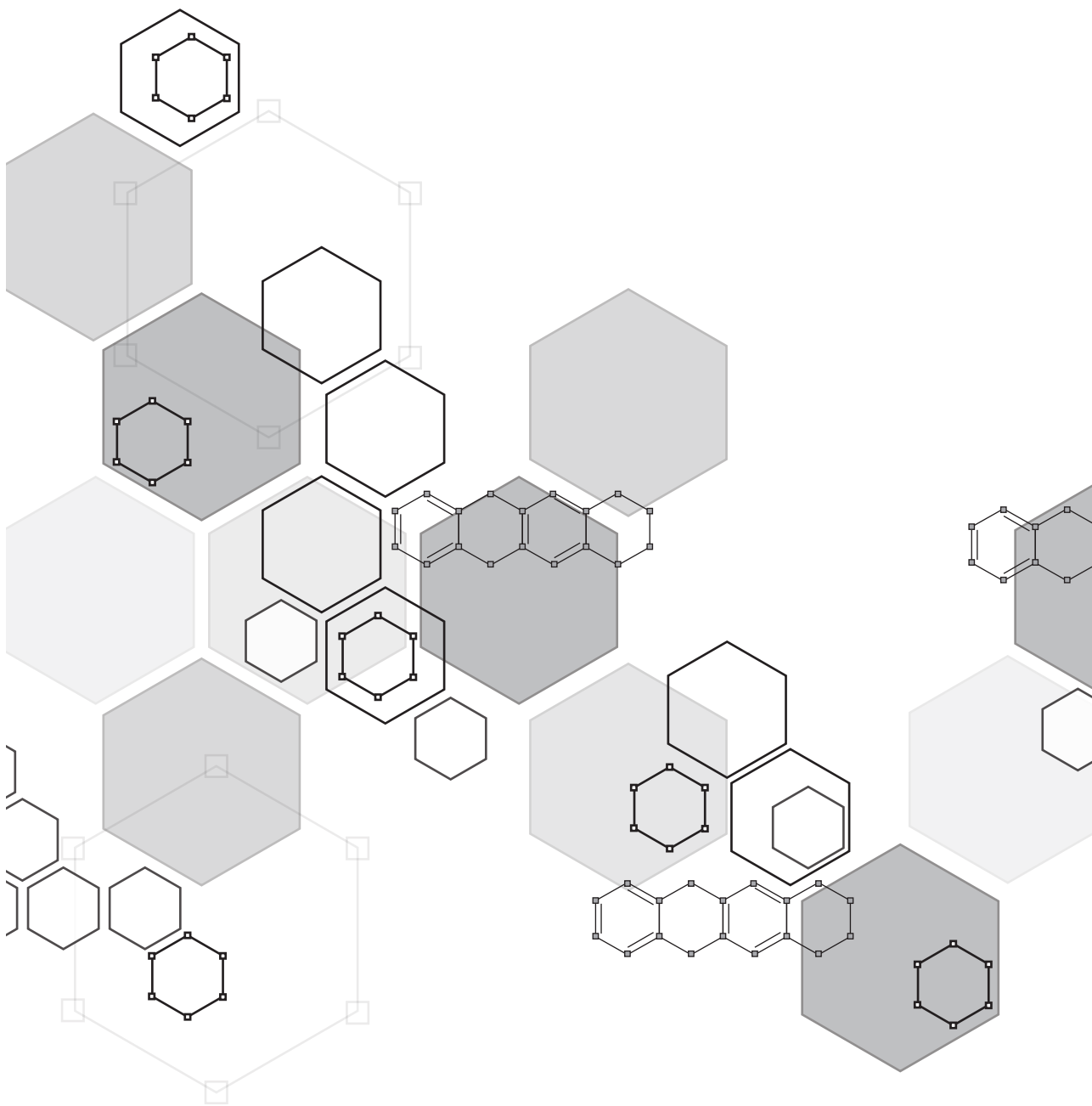
122. Winter, G. E., Buckley, D. L., Paulk, J., Roberts, J. M., Souza, A., Dhe-Paganon, S. & Bradner, J. E. (2015) DRUG DEVELOPMENT. Phthalimide conjugation as a strategy for in vivo target protein degradation, *Science.* 348, 1376-81.

123. Watt, G. F., Scott-Stevens, P. & Gaohua, L. (2019) Targeted protein degradation in vivo with Proteolysis Targeting Chimeras: Current status and future considerations, *Drug Discov Today Technol.* 31, 69-80.

124. Sun, X., Wang, J., Yao, X., Zheng, W., Mao, Y., Lan, T., Wang, L., Sun, Y., Zhang, X., Zhao, Q., Zhao, J., Xiao, R. P., Zhang, X., Ji, G. & Rao, Y. (2019) A chemical approach for global protein knockdown from mice to non-human primates, *Cell Discov.* 5, 10.

125. Jensen, S. M., Potts, G. K., Ready, D. B. & Patterson, M. J. (2018) Specific MHC-I Peptides Are Induced Using PROTACs, *Front Immunol.* 9, 2697.





## Summary and future prospects

# 9



## SUMMARY AND FUTURE PROSPECTS

After infectious diseases, cancer is the leading cause of death worldwide, with about 1 in 5 men and 1 in 6 women diagnosed with cancer during their lifetime [1]. A tumor results intrinsically from tissue growth deregulation and develops when normal cells start dividing in an uncontrolled manner. In order for a normal cell to transform into a cancer cell, genes that tightly control the cell cycle and cell growth get altered, often via mutations in or deletions of so-called oncogenes or tumor suppressor genes [2]. Many therapies exist to treat cancer, and multiple new treatment options are developed and implemented in the clinic as medical research keeps progressing. These treatments include targeted therapies and cancer-immunotherapy, which have shown high efficiency in certain tumor types. Nevertheless, the primary treatment options for most cancers remain surgery, irradiation, and/or chemotherapy. Anthracyclines are one of the most extensively used classes of chemotherapeutics to treat various solid and hematological tumors [3]. The first compound of this class of chemotherapeutic drugs, daunorubicin, was already reported in 1960, after being isolated from a soil bacterial sample in Italy [4, 5]. This compound is a product of the actinobacterium strain *Streptomyces peucetius*. While it was initially studied for its antibiotic properties, its anticancer properties were soon discovered [5]. Shortly after, daunorubicin's close structural homolog doxorubicin was isolated from a slightly different *S. peucetius* culture [6]. Daunorubicin and doxorubicin act by interfering with the catalytic cycle of topoisomerase II $\alpha$  (Topo II $\alpha$ ), resulting in the formation of DNA double-strand breaks [7]. Cells then activate the DNA damage repair pathway to repair the breaks, or to initiate cell death when the damage is too severe [8]. Rapidly replicating cells, such as tumor cells, are in general more sensitive to the resulting DNA damage than normal cells, thus constituting a chemotherapeutic window [8]. A second mechanism by which the anthracycline drugs impose their antitumor effect is via eviction of histones [9, 10]. This has multiple consequences such as epigenetic and transcriptomic changes, which are together referred to as chromatin damage. Nowadays, multiple anthracycline variants are used to treat over one million patients every year. However, the exact molecular mechanism by which these drug kill tumor cells remain unclear. In addition, treatment with anthracyclines coincides with severe adverse effects such as cardiotoxicity, secondary tumor formation and gonadotoxicity. Understanding how these highly effective anticancer drugs function and why they cause these severe toxicities would have tremendous impact on cancer treatment and the quality of life of cancer survivors. Therefore, even today, studying old anticancer drugs has high therapeutic potential and opens new exciting paths to improve currently available treatment options.

### Treatment-limiting side effects of doxorubicin

Although doxorubicin is a very effective anticancer therapeutic, treatment is limited by various adverse effects. These side effects can be categorized into two groups: (i.) acute and generally reversible side effects, such as nausea, vomiting and diarrhea and (ii.) long-term and generally irreversible side effects, including gonadotoxicity, therapy-related tumor formation, and cumulative cardiotoxicity. These long-term side effects are especially treatment limiting and devastating for cancer survivors [11, 12]. To overcome these limitations, extensive research is done to identify the underlying mechanisms by which these drugs induce their anticancer function as well as their side effects. Additionally, hundreds of doxorubicin analogs have been isolated or synthesized in order to find effective treatment with less toxicity, however,

this did not result in new effective anthracyclines variants that entered the clinic. In **Chapter 1**, we describe the various mechanisms proposed by which doxorubicin functions and induces these side effects. Further, we provide several suggestions to overcome these toxicities, and we discuss perspectives on how to improve doxorubicin.

### **Novel factors controlling doxorubicin resistance**

Besides the occurrence of side effects, doxorubicin treatment is hampered by drug resistance. To overcome the lack of knowledge on the molecular basis of doxorubicin resistance, we performed a genome-wide gene knockout screen. In **Chapter 2**, we describe the identification of three novel factors independently controlling doxorubicin resistance by interfering with the DNA double-strand break and repair pathway, namely Keap1, the SWI/SNF complex, and C9orf82 (also known as CAAP1). Both Keap1 and the SWI/SNF complex affect the promotion of DNA damage via Topo II $\alpha$ . While the loss of the SWI/SNF complex limits the activity of Topo II $\alpha$  by preventing the loading of the protein onto chromatin, Keap1 controls the expression of Topo II $\alpha$ . On the other hand, C9orf82, controls the DNA repair pathway. Loss of C9orf82 accelerates  $\gamma$ H2AX resolution and thereby promotes resistance to DNA double-strand break inducers such as the Topo II $\alpha$  poisons doxorubicin and etoposide. Clinically, we showed that the expression of Keap1 and the SWI/SNF complex subunits SMARCB1 and SMARCA4, correlate with the response of triple-negative breast cancer patients to doxorubicin-containing regimes. Collectively, our work provides a molecular basis for doxorubicin resistance. Since mutations in various SWI/SNF complex subunits, as well as in Keap1 and C9orf82, have been found in different tumor types [13-19], profiling patients for mutations in these specific genes would help to predict their response towards doxorubicin-based treatment. This knowledge would prevent people from undergoing ineffective treatment and supports the selection of alternative regimes with drugs that do not target Topo II $\alpha$ , such as the Topo I poison topotecan, or anthracycline analogues that only have chromatin damage activity (such as aclarubicin or diMe-Doxo, see below).

### **Chromatin damage is the main mechanism for the anticancer activity of anthracyclines**

The anthracycline drug doxorubicin and its analogs daunorubicin, epirubicin, and idarubicin are Topo II $\alpha$  poisons [7]. They induce DNA double-strand breaks by interfering with the catalytic cycle of topoisomerase forming DNA-Topo II $\alpha$ -drug tertiary complexes [7]. As a consequence, DNA repair pathways are activated, the cell cycle is arrested, and apoptosis is initiated [20]. For a long time, it was thought that induction of DNA breaks via Topo II $\alpha$  was the main mechanism by which these drugs function. But recently, a second mechanism of action was uncovered: chromatin damage via eviction of histones [9, 21]. **Chapter 3** describe our findings that indicates that histone eviction might be the major anticancer activity of these drugs. We studied the biological activity of doxorubicin (inducing both DNA- and chromatin damage), the structurally unrelated Topo II $\alpha$  poison etoposide (inducing DNA damage only), the anthracycline family member aclarubicin (inducing chromatin damage only) and amrubicin (inducing DNA damage only), and the newly synthesized doxorubicin analog diMe-Doxo (inducing chromatin damage only). Our results demonstrate that drugs abstained from the classical DNA damaging capacity (i.e. aclarubicin and diMe-Doxo) are effective anticancer drugs *in vitro* and *in vivo*. Furthermore, we report that the doxorubicin-induced cardiotoxicity is caused by the combination of these two ac-

tivities, since compounds that either induce DNA damage (etoposide) or chromatin damage (aclarubicin and diMe-Doxo) fail to induce cardiotoxicity in mice and human cardiac microtissues. While treatment of pluripotent stem cell derived human cardiac microtissues with amrubicin (DNA damage only) and aclarubicin (chromatin damage only) had no effect on the contraction amplitude and velocity of the microtissues, the combination treatment resulted in impaired contraction, similar to treatment with doxorubicin where these two activities are combined in one molecule. Also, therapy-related secondary tumors and infertility are absent or reduced for drugs possessing only one of these two activities. We showed that detoxification of doxorubicin is possible by separating the DNA- and chromatin damage activities by introducing a small modification on the 3' amine of the amino sugar moiety. In the different murine models tested, both aclarubicin and diMe-Doxo remain effective anticancer drugs with limited toxicity, suggesting that these drugs could be used for patients which are currently excluded from effective treatment, such as old patients or patients with a recurrent tumor with a history of anthracycline-based therapy.

### Chemical features defining the biological activity of anthracycline drugs

Based on our findings described in **Chapter 3**, we anticipated that finding structural features responsible for chromatin damage activity without inducing DNA damage will advance the discovery of novel anthracycline analogs with limited toxicity. Therefore, we decided to synthesize and test three coherent sets of anthracycline analogs. In **Chapter 4**, we evaluated 10 doxorubicin/aclarubicin hybrid structures for their ability to induce DNA double strand breaks, eviction of histones, and cytotoxicity. These structures diverged by the anthraquinone aglycon, the nature of the carbohydrate portion, and the alkylation pattern of the amine on the first sugar moiety. Comparing these analogs, we observed a clear correlation between the efficiency of histone eviction and cytotoxicity *in vitro*, which is in line with our results described in Chapter 3. We observed that *N,N*-dimethylation of the carbohydrate considerably improved the histone eviction capacity of these compounds and thereby cytotoxicity. Furthermore, the doxorubicin anthraquinone aglycon appeared slightly more efficient in killing tumor cells *in vitro* than the aclarubicin aglycon, and the aclarubicin trisaccharide showed higher cytotoxicity than the doxorubicin monosaccharide. Hence, we yielded three structures, named compound 3, 8 and 11 (**Chapter 4**), that were more cytotoxic than doxorubicin. Remarkably, compound 11 that combines the structural features described above, was the most cytotoxic variant in this focused library. Besides, these three hybrid compounds were unable to produce DNA double-strand breaks but induced cell death via chromatin damage, strengthening our scenario of histone eviction as the main mechanism of action of this class of anticancer drugs. Our findings raised the following broader question: 'Is there a structure-activity relationship for the stereoisomeric analogs of doxorubicin?' To test this, we synthesized and evaluated a targeted library of epimeric doxorubicin analogs (**Chapter 5**). We showed that both the *N*-substitution state and the stereochemistry of the 3' amine were critical for the biological activity of the drugs. While the orientation of the hydroxyl group at the 4' position did not affect cytotoxicity, compounds featuring an *N,N*-dimethylamine in the equatorial position showed improved cellular uptake, histone eviction effectivity, and cytotoxicity.

In **Chapter 6**, we described a third set of doxorubicin analogs designed to further investigate the mode of action of the 3' amine moiety. Next to diMe-Doxo, we synthesized and tested three non-basic 3' variants and four cyclic-doxorubicin analogs and compared their biological activity with doxorubicin. Where all the non-basic

doxorubicin induced effective DNA damage without histone eviction activity, the four cyclic-doxorubicin analogues, on the opposite, evicted histone without inducing DNA damage. Despite this divergence, they were all able to re-locate Topo II $\alpha$ . Using ChIP-sequencing of endogenously tagged Topo II $\alpha$ , we found that Topo II $\alpha$  targeting occurred at distinct genomic locations. This difference appears to be determined by their structure (modification at the amino sugar) and subsequent biologic activity. A similar observations is made for the genomic selectivity of the chromatin damage activity of these drugs. Analogs that are able to induce DNA double-strand breaks affect distinct regions from the variant that are effective histone evicting drugs because of their tertiary amine at the 3' position.

In summary, the side group at the 3' position of the amino sugar determines the biological activity and genomic selectivity of the various analogues. Studying the effectivity and toxicity of the most potent analogs described above in an *in vivo* model, could lead to the development of anthracycline analogs for novel therapeutics. Besides, since these analogs selectivity target genomic locations for Topo II $\alpha$  relocation and/or chromatin damage activity, identifying which exact genomic locations are targeted would shed new light on anthracycline molecular mode of action. Eventually, such information could be used to refine the selection of specific analogs over others for the treatment of different tumor types.

### **A role for nuclear DNA sensors in chromatin damage-induced cell death**

Chromatin damage, via eviction of histones, is the main anticancer activity of the different anthracycline drugs [22]. Yet, the exact mechanism by which histone eviction induces cell death remains unclear. Under physiological circumstances, DNA is closely packed in nucleosomes and the chromatin compaction state tightly controls the regulation of gene expression [23]. Large stretches of histone-free DNA are therefore uncommon in eukaryotic cells, and we predicted that this unnatural situation would induce a cellular response. Hence, we hypothesized that anthracycline-induced histone-free DNA can be sensed by proteins that can restore histone-DNA association, that can initiate an immune response as they 'think' that the cell is infected by a DNA virus and/or that initiate cell death. In **Chapter 7**, we described three nuclear DNA sensors from the PYHIN protein family (IFI16 and MDA5), which are known for their role during viral infection [24-26]. These three sensors specifically re-locate to DNA upon treatment with histone evicting anthracycline drugs. Furthermore, we showed that DNA binding of IFI16 is enhanced upon treatment with doxorubicin and aclarubicin, but not with etoposide. These results indicated that the 'naked DNA' resulting from the chromatin damage activity of these drugs can be sensed and bound by the DNA sensors. Mass spectrometry analyses to identify novel interaction partners for these three nuclear DNA sensors yielded two proteins from the ubiquitin machinery (the de-ubiquitinating enzyme USP7, and the E3-ligase TRIM26) and a DNA helicase (XRCC6), all known to play a role in viral infection and cell death [27-29]. Yet, if and how the interactions of these proteins with the DNA sensors could lead to cell death upon chromatin damage is as of yet unclear. Work by Johnstone and colleagues showed that the DNA sensors IFI16 can interact with p53 to regulate the cell cycle and apoptosis [30]. This interaction enhances the p53-mediated transcription of its target gene p21 in U2Os cells, allowing cell cycle regulation [31]. Since both IFI16 and USP7 are known to interact with p53 [30, 32], we hypothesized that USP7 is recruited to the histone-free DNA via IFI16 to de-ubiquitinate p53 and initiate a stress response. On the other hand, sensing histone-free DNA could activate the innate immune system via the recruitment

of TRIM26. While not much is known about the function of TRIM26, this protein is described to interact and activate TBK1 and thereby regulate IRF3 and NF- $\kappa$ B activation and IFN- $\beta$  induction upon detection of RNA virus infection [28]. Activation of an innate immune response upon TRIM26 recruitment to the DNA might play a role in the anti-tumor response *in vivo*. The molecular mechanism by which the sequential binding of 'naked-DNA', by the DNA sensors, and USP7 and/or TRIM26 leads to anthracycline-induced cell death remains to be explored. In particular, p53-mediated apoptosis upon the complex formation of the DNA sensors with USP7, TRIM26, or other interactors would be a promising lead for further investigations.

Besides, expression of the PYHIN protein family in hematopoietic cells is positively regulated by type I and/or type II interferons [33]. We showed that stimulation with IFN $\beta$  or IFN $\gamma$  upregulates the expression of IFI16 in MelJuSo cells. Consequently, IFN $\beta$  stimulation makes these cells more sensitive to treatment with anthracycline drugs. This observation is supported by a study from Fujiuchi and colleagues, who showed that enhanced expression of IFI16 in MCF-7 cells increased the cellular susceptibility for apoptosis induced by p53-dependent ionizing radiation [34]. Together, this indicates that IFI16 might play a role in DNA/genotoxic stress-induced cell death in general. More experiments need to be done to reveal the consequences of the PYHIN family protein activation in response to anthracycline treatment.

### **Small molecules to improve cancer-immunotherapy**

While chemotherapy has a long history in cancer treatment, cancer-immunotherapy is a relatively new treatment option used in the clinic [35, 36]. Its operating principle is to direct a systemic cytotoxic (CD8<sup>+</sup>) T lymphocyte response toward tumor cells, which ideally also eradicates secondary lesions [37]. Various immunotherapy strategies are known, but especially checkpoint blockade therapies, using monoclonal antibodies against CTLA-4, PD-1, or PD-L1, have led to prominent breakthroughs in the cancer-immunotherapy field. However, despite its impressive achievements, checkpoint blockade therapy is only successful in a fraction of the patients [36]. This limited effectivity generally results from inhibitory immune cells or other mechanisms that counteract the cytotoxic T cell response towards the tumor. To overcome these immunosuppressive mechanisms, various combination treatments have been suggested and tested. Especially the use of small-molecule based combination therapies are promising. They offer valuable opportunities to increase the efficacy of cancer immunotherapy, either by targeting immunosuppressive cells in the tumor microenvironment in a rationale mechanism-guided fashion, or by stimulating tumor immunogenicity. An overview of these novel small-molecule based combination therapies is provided in **Chapter 8**.

In summary, we demonstrated that the combination of DNA- and chromatin damages coinciding with doxorubicin treatment is the underlying mechanism responsible for its severe long-term side effects. Furthermore, we showed that chromatin damage is most likely the major anticancer activity of several anthracycline drugs. We identified specific structural features that are responsible for the biological activity of anthracycline drugs and determined novel analogs with improved cytotoxicity. The exact mechanism by which histone eviction leads to cell death remains unknown, but we anticipate that nuclear DNA sensors may play a role in the detection of histone-free DNA. Together, the findings described in this thesis illustrate that studying an old anticancer drug with novel concepts and techniques can open uncharted paths to improve current cancer treatment.

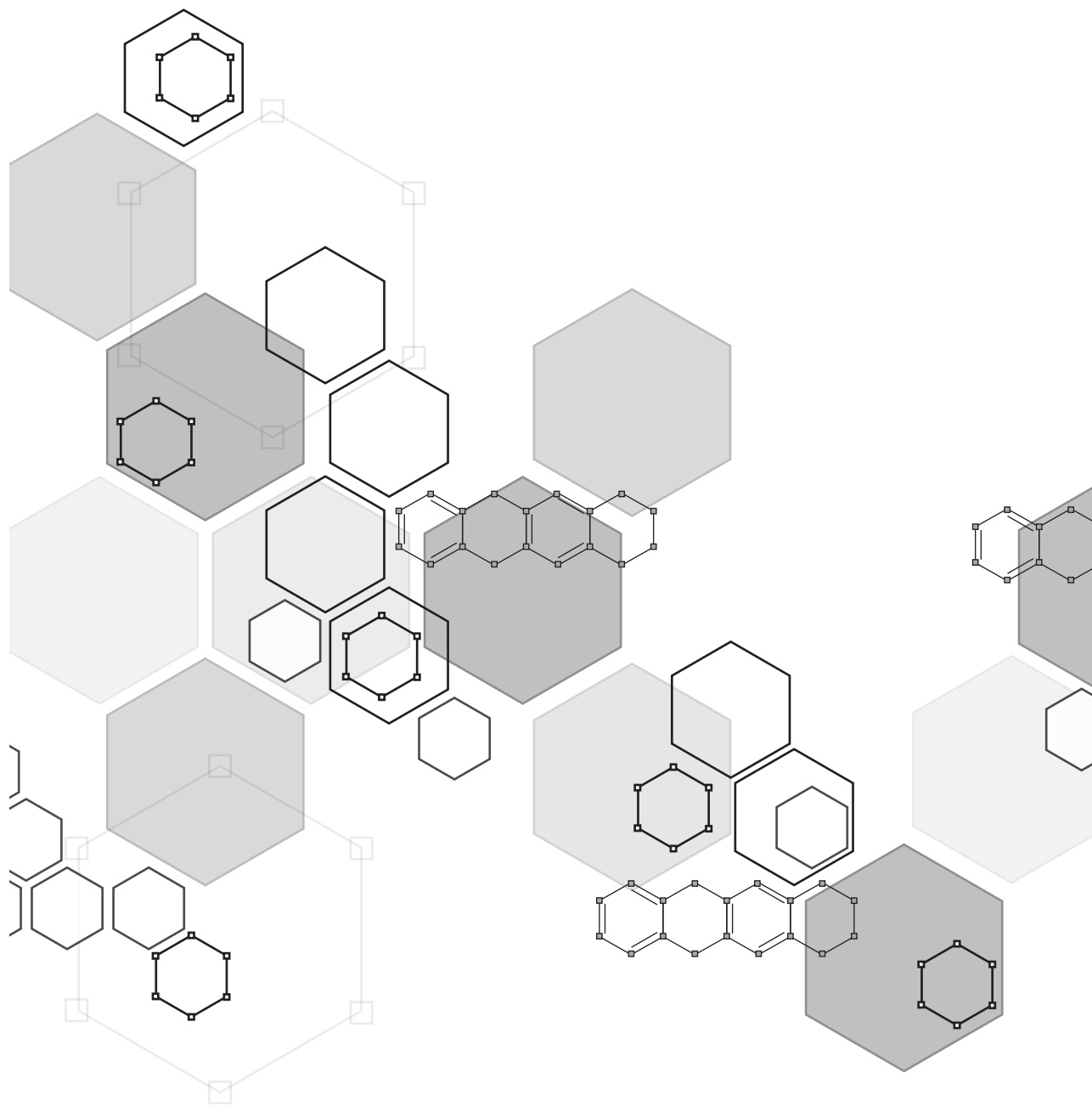


## REFERENCES

1. (2018) Latest global cancer data: Cancer burden rises to 18.1 million new cases and 9.6 million cancer deaths in 2018. [www.iarc.fr](http://www.iarc.fr).
2. Lee, E. Y. H. P. & Muller, W. J. (2010) *Oncogenes and Tumor Suppressor Genes*, Cold Spring Harbor Perspectives in Biology. 2.
3. Hortobagyi, G. N. (1997) Anthracyclines in the treatment of cancer - An overview, *Drugs*. 54, 1-7.
4. Camerino B, P. G. (1960) Derivati della parazina II. Sulfonamdopir (in Italian). , *Gazz Chim Ital* 90: 1802–1815.
5. Di Marco, A., Cassinelli, G. & Arcamone, F. (1981) The discovery of daunorubicin, *Cancer Treat Rep*. 65 Suppl 4, 3-8.
6. Arcamone, F., Cassinelli, G., Fantini, G., Grein, A., Orezzi, P., Pol, C. & Spalla, C. (1969) Adriamycin, 14-hydroxydaunomycin, a new antitumor antibiotic from *S. peucetius* var. *caesius*, *Biotechnol Bioeng*. 11, 1101-10.
7. Nitiss, J. L. (2009) Targeting DNA topoisomerase II in cancer chemotherapy, *Nat Rev Cancer*. 9, 338-50.
8. Misteli, T. & Soutoglou, E. (2009) The emerging role of nuclear architecture in DNA repair and genome maintenance, *Nature Reviews Molecular Cell Biology*. 10, 243-254.
9. Pang, B., Qiao, X., Janssen, L., Velds, A., Groothuis, T., Kerkhoven, R., Nieuwland, M., Ovaa, H., Rottenberg, S., van Tellingen, O., Janssen, J., Huijgens, P., Zwart, W. & Neefjes, J. (2013) Drug-induced histone eviction from open chromatin contributes to the chemotherapeutic effects of doxorubicin, *Nature communications*. 4, 1908.
10. Pang, B., de Jong, J., Qiao, X., Wessels, L. F. & Neefjes, J. (2015) Chemical profiling of the genome with anti-cancer drugs defines target specificities, *Nat Chem Biol*. 11, 472-80.
11. Lotrionte, M., Biondi-Zoccai, G., Abbate, A., Lanzetta, G., D'Ascenzo, F., Malavasi, V., Peruzzi, M., Frati, G. & Palazzoni, G. (2013) Review and meta-analysis of incidence and clinical predictors of anthracycline cardiotoxicity, *Am J Cardiol*. 112, 1980-4.
12. Mistry, A. R., Felix, C. A., Whitmarsh, R. J., Mason, A., Reiter, A., Cassinat, B., Parry, A., Walz, C., Wiemels, J. L., Segal, M. R., Ades, L., Blair, I. A., Osherooff, N., Peniket, A. J., Lafage-Pochitaloff, M., Cross, N. C., Chomienne, C., Solomon, E., Fenaux, P. & Grimwade, D. (2005) DNA topoisomerase II in therapy-related acute promyelocytic leukemia, *N Engl J Med*. 352, 1529-38.
13. Chin, L.Meyerson, M.Aldape, K.Bigner, D.Mikkelsen, T.VandenBerg, S.Kahn, A.Penny, R.Ferguson, M. L.Gerhard, D. S.Getz, G.Brennan, C.Taylor, B. S.Winckler, W.Park, P.Ladanyi, M.Hoadley, K. A.Verhaak, R. G. W.Hayes, D. N.Spellman, P. T.Absher, D.Weir, B. A.Ding, L.Wheeler, D.Lawrence, M. S.Cibulskis, K.Mardis, E.Zhang, J. H.Wilson, R. K.Donehower, L.Wheeler, D. A.Purdum, E.Wallis, J.Laird, P. W.Herman, J. G.Schubel, K. E.Weisenberger, D. J.Baylin, S. B.Schultz, N.Yao, J.Wiedemeyer, R.Weinstein, J.Sander, C.Gibbs, R.A.Gray, J.Kucherlapati, R.Lander, E. S.Myers, R. M.Perou, C. M.McLendon, R.Friedman, A.Van Meir, E. G.Brat, D. J.Mastrogianakis, G. M.Olson, J. J.Lehman, N.Yung, W. K. A.Bogler, O.Berger, M.Prados, M.Muzny, D.Morgan, M.Scherer, S.Sabo, A.Nazareth, L.Lewis, L.Hall, O.Zhu, Y. M.Ren, Y. R.Alvi, O.Yao, J. Q.Hawes, A.Jhangiani, S.Fowler, G.San Lucas, A.Kovar, C.Cree, A.Dinh, H.Santibanez, J.Joshi, V.Gonzalez-Garay, M. L.Miller, C. A.Milosavljevic, A.Sougnuez, C.Fennell, T.Mahan, S.Wilkinson, J.Ziaugra, L.Onofrio, R.Bloom, T.Nicol, R.Ardlie, K.Baldwin, J.Gabriel, S.Fulton, R. S.McLellan, M.

- D.Larson, D. E.Shi, X. Q.Abbott, R.Fulton, L., et al. (2008) Comprehensive genomic characterization defines human glioblastoma genes and core pathways, *Nature*. 455, 1061-1068.
14. Kadoch, C., Hargreaves, D. C., Hodges, C., Elias, L., Ho, L., Ranish, J. & Crabtree, G. R. (2013) Proteomic and bioinformatic analysis of mammalian SWI/SNF complexes identifies extensive roles in human malignancy, *Nature Genetics*. 45, 592-+.
15. Hornick, J. L., Dal Cin, P. & Fletcher, C. D. M. (2009) Loss of INI1 Expression is Characteristic of Both Conventional and Proximal-type Epithelioid Sarcoma, *American Journal of Surgical Pathology*. 33, 542-550.
16. Gasparini, P., Facchinetti, F., Boeri, M., Lorenzetto, E., Livio, A., Gronchi, A., Ferrari, A., Massimino, M., Spreafico, F., Giangaspero, F., Forni, M., Maestro, R., Alaggio, R., Pilotti, S., Collini, P., Modena, P. & Sozzi, G. (2011) Prognostic determinants in epithelioid sarcoma, *European Journal of Cancer*. 47, 287-295.
17. Lawrence, M. S., Stojanov, P., Mermel, C. H., Robinson, J. T., Garraway, L. A., Golub, T. R., Meyerson, M., Gabriel, S. B., Lander, E. S. & Getz, G. (2014) Discovery and saturation analysis of cancer genes across 21 tumour types, *Nature*. 505, 495-+.
18. Barbano, R., Muscarella, L. A., Pasculli, B., Valori, V. M., Fontana, A., Coco, M., la Torre, A., Balsamo, T., Poeta, M. L., Marangi, G. F., Maiello, E., Castelveter, M., Pellegrini, F., Murgo, R., Fazio, V. M. & Parrella, P. (2013) Aberrant Keap1 methylation in breast cancer and association with clinicopathological features, *Epigenetics*. 8, 105-112.
19. Brennan, C. W., Verhaak, R. G. W., McKenna, A., Campos, B., Noushmehr, H., Salama, S. R., Zheng, S. Y., Chakravarty, D., Sanborn, J. Z., Berman, S. H., Beroukhi, R., Bernard, B., Wu, C. J., Genovese, G., Shmulevich, I., Barnholtz-Sloan, J., Zou, L. H., Vegesna, R., Shukla, S. A., Ciriello, G., Yung, W. K., Zhang, W., Sougnez, C., Mikkelsen, T., Aldape, K., Bigner, D. D., Van Meir, E. G., Prados, M., Sloan, A., Black, K. L., Eschbacher, J., Finocchiaro, G., Friedman, W., Andrews, D. W., Guha, A., Iacocca, M., O'Neill, B. P., Foltz, G., Myers, J., Weisenberger, D. J., Penny, R., Kucherlapati, R., Perou, C. M., Hayes, D. N., Gibbs, R., Marra, M., Mills, G. B., Lander, E., Spellman, P., Wilson, R., Sander, C., Weinstein, J., Meyerson, M., Gabriel, S., Laird, P. W., Haussler, D., Getz, G., Chin, L. & Network, T. R. (2013) The Somatic Genomic Landscape of Glioblastoma, *Cell*. 155, 462-477.
20. Perego, P., Corna, E., De Cesare, M., Gatti, L., Polizzi, D., Pratesi, G., Supino, R. & Zunino, F. (2001) Role of apoptosis and apoptosis-related genes in cellular response and antitumor efficacy of anthracyclines, *Curr Med Chem*. 8, 31-7.
21. Yang, F., Kemp, C. J. & Henikoff, S. (2013) Doxorubicin Enhances Nucleosome Turnover around Promoters, *Curr Biol*. 23, 782-787.
22. Qiao, X., van der Zanden, S. Y., Wander, D. P. A., Borrás, D. M., Song, J. Y., Li, X., van Duikeren, S., van Gils, N., Rutten, A., van Herwaarden, T., van Tellingen, O., Giacomelli, E., Bellin, M., Orlova, V., Tertoolen, L. G. J., Gerhardt, S., Akkermans, J. J., Bakker, J. M., Zuur, C. L., Pang, B., Smits, A. M., Mummery, C. L., Smit, L., Arens, R., Li, J., Overkleeft, H. S. & Neefjes, J. (2020) Uncoupling DNA damage from chromatin damage to detoxify doxorubicin, *Proc Natl Acad Sci U S A*.
23. McGinty, R. K. & Tan, S. (2015) Nucleosome Structure and Function, *Chem Rev*. 115, 2255-2273.
24. Monroe, K. M., Yang, Z. Y., Johnson, J. R., Geng, X., Doitsh, G., Krogan, N. J. & Greene, W. C. (2014) IFI16 DNA Sensor Is Required for Death of Lymphoid CD4 T Cells Abortively Infected with HIV, *Science*. 343, 428-432.
25. Kerur, N., Veettil, M. V., Sharma-Walia, N., Bottero, V., Sadagopan, S., Otageri,

- P. & Chandran, B. (2011) IFI16 Acts as a Nuclear Pathogen Sensor to Induce the Inflammasome in Response to Kaposi Sarcoma-Associated Herpesvirus Infection, *Cell Host Microbe*. 9, 363-375.
26. Dell'Oste, V., Gatti, D., Gugliesi, F., De Andrea, M., Bawadekar, M., Lo Cigno, I., Biolatti, M., Vallino, M., Marschall, M., Gariglio, M. & Landolfo, S. (2014) Innate Nuclear Sensor IFI16 Translocates into the Cytoplasm during the Early Stage of In Vitro Human Cytomegalovirus Infection and Is Entrapped in the Egressing Virions during the Late Stage, *J Virol*. 88, 6970-6982.
27. Johnson, K. E., Bottero, V., Flaherty, S., Dutta, S., Singh, V. V. & Chandran, B. (2014) IFI16 Restricts HSV-1 Replication by Accumulating on the HSV-1 Genome, Repressing HSV-1 Gene Expression, and Directly or Indirectly Modulating Histone Modifications, *Plos Pathog*. 10.
28. Ran, Y., Zhang, J., Liu, L. L., Pan, Z. Y., Nie, Y., Zhang, H. Y. & Wang, Y. Y. (2016) Autoubiquitination of TRIM26 links TBK1 to NEMO in RLR-mediated innate antiviral immune response, *J Mol Cell Biol*. 8, 31-43.
29. Frost, J. R., Olanubi, O., Cheng, S. K. H., Soriano, A., Crisostomo, L., Lopez, A. & Pelka, P. (2017) The interaction of adenovirus E1A with the mammalian protein Ku70/XRCC6, *Virology*. 500, 11-21.
30. Johnstone, R. W., Wei, W., Greenway, A. & Trapani, J. A. (2000) Functional interaction between p53 and the interferon-inducible nucleoprotein IFI 16, *Oncogene*. 19, 6033-6042.
31. Kwak, J. C., Ongusaha, P. P., Ouchi, T. & Lee, S. W. (2003) IFI16 as a negative regulator in the regulation of p53 and p21(Waf1), *J Biol Chem*. 278, 40899-40904.
32. Sheng, Y., Saridakis, V., Sarkari, F., Duan, S. L., Wu, T. N., Arrowsmith, C. H. & Frappier, L. (2006) Molecular recognition of p53 and MDM2 by USP7/HAUSP, *Nat Struct Mol Biol*. 13, 285-291.
33. Landolfo, S., Gariglio, M., Gribaudo, G. & Lembo, D. (1998) The Ifi 200 genes: An emerging family of IFN-inducible genes, *Biochimie*. 80, 721-728.
34. Fujiuchi, N., Aglipay, J. A., Ohtsuka, T., Maehara, N., Sahin, F., Su, G. H., Lee, S. W. & Ouchi, T. (2004) Requirement of IFI16 for the maximal activation of p53 induced by ionizing radiation, *J Biol Chem*. 279, 20339-20344.
35. Sharma, P. & Allison, J. P. (2015) The future of immune checkpoint therapy, *Science*. 348, 56-61.
36. Ribas, A. & Wolchok, J. D. (2018) Cancer immunotherapy using checkpoint blockade, *Science*. 359, 1350-1355.
37. Koebel, C. M., Vermi, W., Swann, J. B., Zerafa, N., Rodig, S. J., Old, L. J., Smyth, M. J. & Schreiber, R. D. (2007) Adaptive immunity maintains occult cancer in an equilibrium state, *Nature*. 450, 903-7.



Nederlandse samenvatting  
List of publications  
Curriculum vitae  
Acknowledgements

A



## NEDERLANDSE SAMENVATTING

Na infectieziekten sterven wereldwijd de meeste mensen aan kanker. Eén op de vijf mannen en één op de zes vrouwen krijgt tijdens zijn of haar leven deze diagnose [1]. Een tumor ontstaat wanneer normale cellen ongecontroleerd beginnen te delen, met als gevolg onregelde weefselgroei. Deze ongecontroleerde celdeling kan ontstaan door veranderingen in genen die de celcyclus en celgroei reguleren, als gevolg van mutaties in of deleties van de zogenoemde oncogenen of tumor suppressie genen [2]. Er zijn veel verschillende therapieën om kankerpatiënten te behandelen, en met de groeiende medische kennis worden er voortdurend nieuwe behandelopties ontwikkelend en geïmplementeerd. Tot deze nieuwe behandelingen behoren doelgerichte therapieën en immunotherapie, welke beide erg effectief zijn voor specifieke tumor types. Maar ondanks deze ontwikkelingen zijn radiotherapie, het operatief verwijderen en/of chemotherapie nog steeds de primaire behandelopties voor de meeste tumoren. Een van de meest gebruikte chemotherapieën voor de behandeling van solide en hematologische tumoren zijn moleculen uit de anthracycline klasse. [3]. Daunorubicine was de eerste anthracycline die werd ontdekt in 1960, waar het werd gevonden en geïsoleerd uit een grondmonster [4, 5]. Dit molecuul wordt geproduceerd door de actino-bacterie *Streptomyces peucetius* en wordt gewonnen door middel van fermentatie. Daunorubicine werd in eerste instantie bestudeerd voor zijn antibacteriële werking, maar er werd al snel ontdekt dat het ook antitumor activiteit heeft [5]. Kort na de ontdekking van daunorubicine werd doxorubicine, een anthracycline met vergelijkbare chemische structuur, geïsoleerd uit een andere *S. peucetius* bacteriestam [6]. Daunorubicine en doxorubicine werken door te interfereren met de katalytische cyclus van topoisomerase II $\alpha$  (Topo II $\alpha$ ), met de formatie van DNA dubbelstrengs breuken tot gevolg [7]. Cellen activeren dan hun DNA schade reparatie mechanisme om de breuk te repareren of om celdood te initiëren als de schade te groot is [8]. Snel delende cellen, zoals tumor cellen, zijn over het algemeen gevoeliger voor DNA schade vergeleken met normale cellen, wat zorgt voor een therapeutisch venster [8]. Een tweede antitumor mechanisme van anthracyclines is via de verwijdering van histonen uit het chromatine [9, 10]. Dit heeft verschillende gevolgen, zoals epigenetische en transscriptionele veranderingen, welke samen worden omschreven als chromatine schade.

Tegenwoordig worden er ieder jaar meer dan één miljoen patiënten behandeld met anthracyclines, ondanks dat het exacte mechanisme waarmee deze medicijnen tumorcellen doden nog steeds niet volledig bekend is. Verder geven deze medicijnen hevige bijwerkingen, zoals hartfalen, het vormen van nieuwe tumoren en onvruchtbaarheid. Inzicht hoe deze zeer effectieve antikanker medicijnen werken en wat de hevige bijwerkingen veroorzaakt kan een enorme bijdrage leveren aan de behandeling en algehele gezondheid van veel patiënten. Het bestuderen van oude medicijnen kan daarom, ook tegenwoordig nog, voor nieuwe kennis en inzichten zorgen die een bijdrage leveren aan het verbeteren van de huidige behandelopties voor kankerpatiënten.

### Hevige bijwerkingen door doxorubicine: oorzaken en hoe kunnen deze overkomen worden

Doxorubicine is een zeer effectief medicijn voor de behandeling van kanker, maar patiënten worden geteisterd door zware bijwerkingen. Deze bijwerkingen kunnen verdeeld worden in twee groepen (*i.*) acute bijwerkingen zoals misselijkheid, overgeven, diarree en beenmerg suppressie die over het algemeen tijdelijk zijn, en (*ii.*)

langdurige en onomkeerbare bijwerkingen zoals onvruchtbaarheid, de ontwikkeling van nieuwe tumoren als gevolg van de therapie, en cumulatieve hartschade. Juist deze laatste categorie bijwerkingen beperkt de behandeling en is erg zwaar voor (genezen) patiënten [11, 12]. In de hoop om deze tweede categorie bijwerkingen te verzachten is er in het verleden, en wordt er nog steeds, uitvoerig onderzoek gedaan naar het onderliggende mechanisme. Ook zijn er doxorubicine varianten gemaakt en getest in de hoop dat deze minder bijwerkingen geven. Helaas worden slechts een aantal van deze nieuwe anthracycline varianten op dit moment gebruikt als behandeling, met vergelijkbare bijwerkingen. In **Hoofdstuk 1** wordt een overzicht gegeven van de verschillende werkingsmechanismen van doxorubicine, en de verschillende mogelijke oorzaken voor de bijwerkingen zoals beschreven in de wetenschappelijke literatuur. Verder geven wij ons perspectief op de oorzaak van de verschillende bijwerkingen, en geven wij suggesties hoe de bijwerkingen van deze type medicijnen kunnen worden verminderd om de gezondheid van de patiënten te verbeteren.

### **Identificatie van nieuwe factoren voor doxorubicine resistentie**

Doxorubicine behandeling gaat niet alleen gepaard met hevige bijwerkingen, maar kan ook belemmerd worden doordat er resistentie optreedt. Er is nog veel onbekend over hoe tumoren precies resistentie ontwikkelen tegen doxorubicine. Daarom hebben we een genoom-breed mutagenese-experiment uitgevoerd, waarbij gebruik wordt gemaakt van een virus om willekeurige genen uit te schakelen, om op deze manier mechanisme te identificeren die betrokken zijn bij de ontwikkeling van resistentie tegen doxorubicine. In **Hoofdstuk 2** beschrijven we de identificatie van drie nieuwe factoren (Keap1, het SWI/SNF complex en C9orf82) die onafhankelijk van elkaar een rol spelen in doxorubicine resistentie door te interfereren met het DNA-schade en -reparatiemechanisme. Zowel Keap1 als het SWI/SNF complex hebben een effect op het ontstaan van DNA-breuken door doxorubicine via Topo II $\alpha$ . Keap1 reguleert de expressie van Topo II $\alpha$ , terwijl afwezigheid van een functioneel SWI/SNF complex er voor zorgt dat Topo II $\alpha$  minder actief is omdat het niet kan binden aan het chromatine. In beide gevallen zorgt dit ervoor dat er minder DNA-breuken plaatsvinden na behandeling met doxorubicine. Anderzijds remt C9orf82 (ook wel bekend als CAAP1) het DNA reparatiemechanisme. Afwezigheid van C9orf82 zorgt ervoor dat DNA-schade sneller hersteld wordt. Hierdoor kunnen deze tumorcellen beter omgaan met de DNA-breuken die worden veroorzaakt door behandeling met doxorubicine of etoposide. Wat we gevonden hebben in het lab is ook relevant voor patiënten in de kliniek. Zo laten we zien dat er een correlatie is tussen effectiviteit van doxorubicine-behandeling bij borstkankerpatiënten, en de expressie van Keap1 en SWI/SNF complex subonderdelen SMARCB1 en SMARCA4 in de tumor van deze patiënten. Er zijn verschillende mutaties gevonden in subonderdelen van het SWI/SNF complex, Keap1 en C9orf82 afhankelijk van het tumortype [13-19], en het zou interessant zijn om vooraf te bepalen of patiënten wel baat zullen hebben bij de behandeling met Topo II $\alpha$  remmers zoals doxorubicine of etoposide. Met deze informatie kan dan voorkomen worden dat patiënten onnodig worden behandeld, en kan er gezocht worden naar alternatieve behandelmethodes die niet aangrijpen op Topo II $\alpha$ , zoals de topoisomerase I remmer topotecan of andere anthracyclines die alleen werken via chromatine schade zoals aclarubicine of diMe-Doxo.



**Chromatine schade als voornaamste antitumor mechanisme van anthracyclines**

De anthracyclines doxorubicine, daunorubicine, epirubicine en idarubicine zijn Topo II $\alpha$  remmers die DNA-breken veroorzaken door DNA-Topo II $\alpha$ -anthracycline complexen te vormen, waarbij de katalytische cyclus van Topo II $\alpha$  wordt belemmerd [7]. Als gevolg van deze DNA-schade wordt het DNA-reparatiemechanisme geactiveerd, wordt de celcyclus geremd en wordt celdood geïnduceerd [20]. Lang werd gedacht dat het veroorzaken van DNA-breken door Topo II $\alpha$  remming het voornaamste mechanisme is waarmee deze medicijnen celdood induceren in de tumor. Echter, recentelijk is er een tweede werkingsmechanisme ontdekt, namelijk verwijdering van histonen met als gevolg chromatine schade [9, 21]. In **Hoofdstuk 3** beschrijven we onze bevindingen die erop duiden dat juist de chromatine schade het voornaamste antitumor mechanisme van anthracyclines is. Hiervoor hebben we de biologische activiteit van verschillende anthracyclines bestudeerd; doxorubicine zorgt voor zowel DNA- als chromatine schade, terwijl anthracycline amrubicine en de structureel ongerelateerde Topo II $\alpha$  remmer etoposide alleen DNA-schade veroorzaken. Anderzijds veroorzaken aclarubicine en de nieuw gesynthetiseerde doxorubicine variant ,diMe-Doxo, chromatine schade zonder dat ze ook DNA-schade veroorzaken. De varianten die enkel chromatine schade veroorzaken (aclarubicine en diMe-Doxo) zijn effectief als antikanker medicatie in weefselkweek en muismodellen. Daarnaast vinden wij dat juist de combinatie van DNA- én chromatine schade de oorzaak is van doxorubicine geïnduceerde hartfalen. De varianten die ofwel alleen DNA-breken veroorzaken (etoposide en amrubicine) ofwel alleen chromatine schade veroorzaken (aclarubicine en diMe-Doxo), geen schade aanbrengen aan het hart van muizen. Behandeling van menselijke mini-harten met amrubicine (alleen DNA-schade) of aclarubicine (alleen chromatine schade) hebben geen effect op het contractievermogen van deze mini-harten. Echter, combinatie van deze twee stoffen zorgt voor een afname van de hartfunctie, vergelijkbaar met doxorubicine behandeling.

Andere langdurige bijwerkingen zoals het ontstaan van nieuwe tumoren als gevolg van de therapie, en verminderde vruchtbaarheid zijn ook afwezig of verminderd bij behandeling met anthracycline varianten die slechts één van de twee activiteiten bezitten. We laten hier zien dat het mogelijk is om de hevige bijwerkingen van doxorubicine te scheiden van de antikanker activiteit. Deze varianten zijn werkzaam als antikanker medicijn in verschillende tumor muismodellen, wat impliceert dat deze varianten gebruikt zouden kunnen worden voor patiënten die op het moment uitgesloten worden van behandeling vanwege de cardiovasculaire bijwerkingen, zoals (oudere) patiënten met een zwak hart en/of patiënten die al eerder met anthracyclines behandeld zijn.

**Chemische kenmerken bepalen de biologische activiteit van de anthracyclines**

Naar aanleiding van onze bevindingen beschreven in **Hoofdstuk 3** onderzochten wij of een specifieke deel van de chemische structuur verantwoordelijk is voor de DNA-schade activiteit, zonder te interfereren met de chromatine schade activiteit om zo bij te dragen aan de ontwikkeling van nieuwe anthracycline varianten met minimale bijwerkingen. Om dit te bewerkstelligen hebben we drie sets van anthracycline varianten gesynthetiseerd en getest voor hun activiteiten in weefselkweek. In **Hoofdstuk 4** evalueren we de DNA- en chromatine schade activiteit van tien doxorubicine/aclarubicine hybride varianten, en of tumorcellen in weefselkweek gevoelig zijn voor deze medicijnen. Structureel verschillen de tien varianten op drie punten: de anthraquinone aglycon, de lengte van de suikerketen en de modificatie van het

amine op de eerste suikergroep. Vergelijking van deze varianten laat een duidelijke correlatie zien tussen de efficiëntie van chromatine schade en de cytotoxiciteit in weefselkweek, wat overeenkomt met onze bevindingen in **Hoofdstuk 3**. We vinden dat de chromatine schade (en dus de cytotoxiciteit) sterk wordt verbeterd door *N,N*-dimethylering van de eerste suikergroep, dat het anthraquinone aglycon van doxorubicine iets effectiever is in het doden van tumorcellen in weefselkweek dan het aclarubicine aglycon, en dat de aclarubicine suikerketen beter is dan die van doxorubicine. Deze bevindingen resulteren in de identificatie van drie varianten (3, 8 en 11) (**Hoofdstuk 4**), die effectief tumorcellen doden in weefselkweek vergeleken met doxorubicine. Variant 11 combineert de drie optimale structurele eigenschappen, en is inderdaad de meest cytotoxische variant in dit rijtje. Deze drie (3, 8 en 11) varianten veroorzaken geen DNA-breuken, maar doden tumorcellen door het induceren van chromatine schade, wat het argument versterkt dat chromatine schade het belangrijkste antikanker mechanisme is van anthracyclines.

Onze bevindingen hebben ertoe geleid dat we de structuur-activiteit relatie van doxorubicine verder hebben onderzocht. Om dit te testen hebben we een tweede set met epimeren van de doxorubicine varianten gemaakt en geëvalueerd (**Hoofdstuk 5**). Hieruit concluderen we dat zowel de amine modificatie als de stereochemie van het 3'-amine essentieel zijn voor de biologische activiteit. De oriëntatie van de 4'-hydroxyl groep heeft weinig effect, terwijl varianten met een gedimethyleerd amine in de equatoriale positie een verbeterde cellulaire opname vertonen en effectievere chromatine schade activiteit hebben, met als gevolg een verbeterde cytotoxiciteit.

In **Hoofdstuk 6** beschrijven we de evaluatie van een derde set doxorubicine varianten die we hebben gesynthetiseerd om meer inzicht te krijgen in de mechanische interacties met de 3'-amine groep. Naast diMe-Doxo hebben we drie doxorubicine varianten met een niet-basische 3'-amine substitutie en vier doxorubicine varianten met een cyclische 3'-amine substitutie bestudeerd. De drie niet-basische doxorubicine varianten bleken allemaal goed te zijn in het veroorzaken van DNA-breuken zonder dat ze chromatine schade activiteit hebben, terwijl de vier cyclische doxorubicine varianten juist de tegenovergestelde activiteit vertonen. Ondanks dit verschil in werkingsmechanisme hebben deze doxorubicine varianten allen de capaciteit om, net als doxorubicine, Topo IIα te herlokalisieren. Door middel van ChIP-sequencing van endogeen gelabeld Topo IIα hebben we ontdekt dat de anthracycline (varianten) op verschillende locaties in het genoom Topo IIα op het DNA binden. Dit verschil lijkt te worden bepaald door de specifieke structuur (modificatie op amino suiker) en de biologische activiteit. Daarnaast hebben we een vergelijkbare observatie gedaan voor verschillen in de locatie in het genoom waar deze varianten hun chromatine activiteit hebben (door middel van ATAC-sequencing); varianten die naast chromatine schade ook DNA-breuken veroorzaken doen dit op een andere locatie in het genoom dan de doxorubicine varianten die alleen chromatine schade veroorzaken.

Samenvattend, de modificatie op de 3' positie van het suiker is bepalend voor de biologische activiteit en genomische selectiviteit van anthracycline varianten. Het bestuderen van de effectiviteit en toxiciteit in proefdiermodellen van de meest veelbelovende varianten beschreven in **Hoofdstuk 3 – 6** zal in de toekomst hopelijk bijdragen aan de ontwikkeling van nieuwe behandelingen met verminderde bijwerkingen. Daarnaast laten we zien dat de verschillende varianten selectiviteit hebben voor regio's in het genoom voor zowel Topo IIα remming als chromatine schade. Echter, er is meer kennis nodig over de exacte genoom locatie waar deze varianten werken, en wat de biologische gevolgen hiervan zijn. Uiteindelijk kan dergelijke informatie helpen bij de selectie van specifieke varianten ten opzichte van andere, voor het

verfijnen van de behandeling van bepaalde tumor types.

### **Spelen DNA-sensoren een rol in het celdood mechanisme ten gevolge van chromatine schade?**

Chromatine schade als gevolg van de verwijdering van histonen is het voornaamste mechanisme waarmee anthracyclines tumorcellen doden [22]. Het is echter nog onduidelijk hoe deze chromatine schade precies leidt tot celdood. Onder fysiologische omstandigheden is DNA zeer compact opgevouwen in zogenaamde nucleosomen, zodat onder andere genexpressie gereguleerd kan worden [23]. Lange stukken met eiwitvrij DNA zijn daarom ongebruikelijk in menselijke cellen, en we verwachten dat chromatine schade en ontvouwing van het DNA veroorzaakt door anthracyclines gedetecteerd kan worden door speciale eiwitten in de celkern, die vervolgens de normale situatie kunnen herstellen of celdood initiëren. In **Hoofdstuk 7** beschrijven we drie DNA sensor eiwitten van de PYHIN family (IFI16, IFI16 en MND1) die tot expressie komen in de celkern, en waarvan bekend is dat ze een rol spelen in de reactie op virale infecties [24-26]. We vinden dat de drie DNA-sensoren zich specifiek kunnen herlokalisieren in de celkern als gevolg van behandeling met anthracyclines die chromatine schade activiteit hebben. Verder vinden we dat binding van IFI16 aan DNA verhoogd is na behandeling met doxorubicine (DNA- en chromatine schade) of aclarubicine (enkel chromatine schade), maar niet met etoposide (enkel DNA-schade). Deze data impliceert dat het eiwitvrije DNA als gevolg van de chromatine schade kan worden herkend en gebonden door de DNA-sensoren. Met behulp van massa spectrometrie analyses hebben we een aantal nieuwe interactiepartners van de drie DNA-sensoren geïdentificeerd, waarvan twee tot het ubiquitinerings systeem behoren (deubiquitinerend enzym USP7 en E3-ligase TRIM26), en een ander is DNA helicase XRCC6. Alle drie deze eiwitten zijn beschreven in de context van virale infecties en celdood [27-29]. Het is echter onbekend of, en hoe, de interactie van deze eiwitten met de DNA-sensoren vervolgens leidt tot celdood als gevolg van chromatine schade. Johnstone en collega's hebben aangetoond dat de DNA-sensor IFI16 een interactie kan aangaan met p53 om vervolgens de celcyclus en apoptose signalering te reguleren [30]. Verder is er beschreven dat deze interactie zorgt voor p53-gemedieerde celcyclus regulatie door transcriptie van p21 in U2Os tumorcellen [31]. Aangezien bekend is dat zowel IFI16 als USP7 een interactie aan kunnen gaan met p53 [30, 32], veronderstellen we dat USP7 naar het histonvrije DNA gerekruteerd kan worden via IFI16, om vervolgens p53 te deubiquitineren en een stress reactie te initiëren. Een andere mogelijkheid zou kunnen zijn dat herkenning van het histonvrije DNA resulteert in activatie van het aangeboren immuunsysteem door het rekruteren van TRIM26. Ondanks dat er niet veel bekend is van de functie van TRIM26, is er beschreven dat TRIM26 kan binden aan TBK1 om deze vervolgens te activeren in de context van RNA-virusinfecties. TBK1 kan dan op zijn beurt IRF3 en NK- $\kappa$ B activeren en IFN- $\beta$  expressie induceren [28]. Activatie van het aangeboren immuunsysteem als gevolg van het rekruteren van TRIM26 naar het histonvrije DNA zou wellicht een rol kunnen spelen in de antitumor activiteit van anthracyclines *in vivo*. Echter, meer onderzoek is nodig naar het exacte moleculaire mechanisme waardoor celdood wordt geïnduceerd na herkenning van het histonvrije DNA door de DNA-sensoren, en de rol van de interactie van de sensoren met USP7 en/of TRIM26. Een veelbelovende richting voor verder onderzoek is de rol van p53-gestuurde activatie van het apoptose mechanisme als gevolg van complex formatie van de DNA-sensoren met USP7, TRIM26 of nog onbekende interactiepartners. Het is bekend dat de expressie van eiwitten in de PYHIN family in hematopoëtische

cellen positief gereguleerd wordt door type I en/of type II interferon stimulatie [33]. Wij laten zien dat stimulatie van MelJuSo cellen met IFN $\beta$  of IFN $\gamma$  ook zorgt voor een verhoogde expressie van IFI16, en dat IFN $\beta$  stimulatie deze cellen gevoeliger maakt voor de behandeling met anthracyclines. Wellicht steelt IFI16 een rol in de reactie op DNA-stress in het algemeen, want Fijjuchi en collega's laten zien dat verhoogde expressie van IFI16 in MCF-7 cellen zorgt voor meer celdood door ioniserende bestraling [34].

### **'Small molecules' geneesmiddelen voor de verbetering van kanker immunotherapie**

Terwijl chemotherapie al enkele decennia gebruikt wordt voor de behandeling van kanker, is juist kanker immunotherapie een relatief nieuwe behandelmethode [35, 36]. Kanker immunotherapie behoort tot de zogeheten doelgerichte therapieën, en werk door een systemische CD8<sup>+</sup> T-cel reactie op te wekken tegen de tumorcellen, welke in het gunstigste geval ook uitzaaiingen aanvalt [37]. Er zijn verschillende immuuntherapie strategieën, maar vooral monoklonale antilichaam therapie gericht tegen CTLA-4, PD-1 of PD-L1 heeft recentelijk gezorgd voor een doorbraak in het veld. Deze zogeheten 'checkpoint blokkade' therapieën vertonen indrukwekkende prestaties, maar zijn slechts succesvol bij een deel van de patiënten [36]. Dit wordt over het algemeen veroorzaakt doordat specifieke cellen of andere remmende mechanisme het effect van de T-cellen op de tumor remmen. Om deze remmende mechanismen tegen te gaan zijn verschillende combinatietherapieën getest, waarbij met name combinatietherapieën met 'small molecules' veelbelovend zijn in het verhogen van de effectiviteit van kanker immunotherapie. Een overzicht van deze nieuwe small molecule combinatietherapieën wordt beschreven in **Hoofdstuk 8**.

Concluderend beschrijft dit proefschrift dat de combinatie van DNA- en chromatine schade de oorzaak is van de hevige bijwerkingen die gepaard gaan met de meeste anthracycline behandelingen, zoals doxorubicine. Verder laten we zien dat niet het maken van DNA-schade, maar juist de chromatine schade via het verwijderen van de histonen het voornaamste antitumor mechanisme is van deze anthracyclines. Door verschillende varianten te synthetiseren en te testen hebben we chemische eigenschappen kunnen identificeren die verantwoordelijk zijn voor de biologische activiteit van deze medicijnen. Daarnaast hebben we nieuwe varianten ontwikkeld met een verbeterde cytotoxiciteit in weefselkweek en in muismodellen. Het exacte moleculaire mechanisme waardoor chromatine schade zorgt voor tumor celdood is nog niet volledig bekend, maar wij veronderstellen dat DNA-sensoren hier een rol in spelen. De data beschreven in dit proefschrift illustreert dat het bestuderen van bestaande antikanker medicijnen met behulp van nieuwe inzichten en technieken nog onbetreden wegen kan openen ter verbetering van de huidige kankertherapieën.

### **REFERENTIES**

1. (2018) Latest global cancer data: Cancer burden rises to 18.1 million new cases and 9.6 million cancer deaths in 2018. [www.iarc.fr](http://www.iarc.fr).
2. Lee, E. Y. H. P. & Muller, W. J. (2010) *Oncogenes and Tumor Suppressor Genes*, Cold Spring Harbor Perspectives in Biology. 2.
3. Hortobagyi, G. N. (1997) Anthracyclines in the treatment of cancer - An overview, *Drugs*. 54, 1-7.
4. Camerino B, P. G. (1960) Derivati della parazina II. Sulfonamodopir (in Italian). ,

Gazz Chim Ital 90: 1802–1815.

5. Di Marco, A., Cassinelli, G. & Arcamone, F. (1981) The discovery of daunorubicin, *Cancer Treat Rep.* 65 Suppl 4, 3-8.

6. Arcamone, F., Cassinelli, G., Fantini, G., Grein, A., Orezzi, P., Pol, C. & Spalla, C. (1969) Adriamycin, 14-hydroxydaunomycin, a new antitumor antibiotic from *S. peucetius* var. *caesius*, *Biotechnol Bioeng.* 11, 1101-10.

7. Nitiss, J. L. (2009) Targeting DNA topoisomerase II in cancer chemotherapy, *Nat Rev Cancer.* 9, 338-50.

8. Misteli, T. & Soutoglou, E. (2009) The emerging role of nuclear architecture in DNA repair and genome maintenance, *Nature Reviews Molecular Cell Biology.* 10, 243-254.

9. Pang, B., Qiao, X., Janssen, L., Velds, A., Groothuis, T., Kerkhoven, R., Nieuwland, M., Ovaa, H., Rottenberg, S., van Tellingen, O., Janssen, J., Huijgens, P., Zwart, W. & Neefjes, J. (2013) Drug-induced histone eviction from open chromatin contributes to the chemotherapeutic effects of doxorubicin, *Nature communications.* 4, 1908.

10. Pang, B., de Jong, J., Qiao, X., Wessels, L. F. & Neefjes, J. (2015) Chemical profiling of the genome with anti-cancer drugs defines target specificities, *Nat Chem Biol.* 11, 472-80.

11. Lotrionte, M., Biondi-Zoccai, G., Abbate, A., Lanzetta, G., D'Ascenzo, F., Malavasi, V., Peruzzi, M., Frati, G. & Palazzoni, G. (2013) Review and meta-analysis of incidence and clinical predictors of anthracycline cardiotoxicity, *Am J Cardiol.* 112, 1980-4.

12. Mistry, A. R., Felix, C. A., Whitmarsh, R. J., Mason, A., Reiter, A., Cassinat, B., Parry, A., Walz, C., Wiemels, J. L., Segal, M. R., Ades, L., Blair, I. A., Osherooff, N., Peniket, A. J., Lafage-Pochitaloff, M., Cross, N. C., Chomienne, C., Solomon, E., Fenaux, P. & Grimwade, D. (2005) DNA topoisomerase II in therapy-related acute promyelocytic leukemia, *N Engl J Med.* 352, 1529-38.

13. Chin, L., Meyerson, M., Aldape, K., Bigner, D., Mikkelsen, T., VandenBerg, S., Kahn, A., Penny, R., Ferguson, M. L., Gerhard, D. S., Getz, G., Brennan, C., Taylor, B. S., Winckler, W., Park, P., Ladanyi, M., Hoadley, K. A., Verhaak, R. G. W., Hayes, D. N., Spellman, P. T., Absher, D., Weir, B. A., Ding, L., Wheeler, D., Lawrence, M. S., Cibulskis, K., Mardis, E., Zhang, J. H., Wilson, R. K., Donehower, L., Wheeler, D. A., Purdom, E., Wallis, J., Laird, P. W., Herman, J. G., Schuebel, K. E., Weisenberger, D. J., Baylin, S. B., Schultz, N., Yao, J., Wiedemeyer, R., Weinstein, J., Sander, C., Gibbs, R. A., Gray, J., Kucherlapati, R., Lander, E. S., Myers, R. M., Perou, C. M., McLendon, R., Friedman, A., Van Meir, E. G., Brat, D. J., Mastrogiannis, G. M., Olson, J. J., Lehman, N., Yung, W. K., A. Bogler, O., Berger, M., Prados, M., Muzny, D., Morgan, M., Scherer, S., Sabo, A., Nazareth, L., Lewis, L., Hall, O., Zhu, Y., M. Ren, Y., R. Alvi, O., Yao, J. Q., Hawes, A., Jhangiani, S., Fowler, G., San Lucas, A., Kovar, C., Cree, A., Dinh, H., Santibanez, J., Joshi, V., Gonzalez-Garay, M. L., Miller, C. A., Milosavljevic, A., Sougnez, C., Fennell, T., Mahan, S., Wilkinson, J., Ziaugra, L., Onofrio, R., Bloom, T., Nicol, R., Ardlie, K., Baldwin, J., Gabriel, S., Fulton, R. S., McLellan, M. D., Larson, D. E., Shi, X. Q., Abbott, R., Fulton, L., et al. (2008) Comprehensive genomic characterization defines human glioblastoma genes and core pathways, *Nature.* 455, 1061-1068.

14. Kadoch, C., Hargreaves, D. C., Hodges, C., Elias, L., Ho, L., Ranish, J. & Crabtree, G. R. (2013) Proteomic and bioinformatic analysis of mammalian SWI/SNF complexes identifies extensive roles in human malignancy, *Nature Genetics.* 45, 592-+.

15. Hornick, J. L., Dal Cin, P. & Fletcher, C. D. M. (2009) Loss of INI1 Expression is



Characteristic of Both Conventional and Proximal-type Epithelioid Sarcoma, *American Journal of Surgical Pathology*. 33, 542-550.

16. Gasparini, P., Facchinetti, F., Boeri, M., Lorenzetto, E., Livio, A., Gronchi, A., Ferrari, A., Massimino, M., Spreafico, F., Giangaspero, F., Forni, M., Maestro, R., Alaggio, R., Pilotti, S., Collini, P., Modena, P. & Sozzi, G. (2011) Prognostic determinants in epithelioid sarcoma, *European Journal of Cancer*. 47, 287-295.

17. Lawrence, M. S., Stojanov, P., Mermel, C. H., Robinson, J. T., Garraway, L. A., Golub, T. R., Meyerson, M., Gabriel, S. B., Lander, E. S. & Getz, G. (2014) Discovery and saturation analysis of cancer genes across 21 tumour types, *Nature*. 505, 495-+.

18. Barbano, R., Muscarella, L. A., Pasculli, B., Valori, V. M., Fontana, A., Coco, M., la Torre, A., Balsamo, T., Poeta, M. L., Marangi, G. F., Maiello, E., Castelveter, M., Pellegrini, F., Murgo, R., Fazio, V. M. & Parrella, P. (2013) Aberrant Keap1 methylation in breast cancer and association with clinicopathological features, *Epigenetics*. 8, 105-112.

19. Brennan, C. W., Verhaak, R. G. W., McKenna, A., Campos, B., Noushmehr, H., Salama, S. R., Zheng, S. Y., Chakravarty, D., Sanborn, J. Z., Berman, S. H., Beroukhi, R., Bernard, B., Wu, C. J., Genovese, G., Shmulevich, I., Barnholtz-Sloan, J., Zou, L. H., Vegesna, R., Shukla, S. A., Ciriello, G., Yung, W. K., Zhang, W., Sougnez, C., Mikkelsen, T., Aldape, K., Bigner, D. D., Van Meir, E. G., Prados, M., Sloan, A., Black, K. L., Eschbacher, J., Finocchiaro, G., Friedman, W., Andrews, D. W., Guha, A., Iacocca, M., O'Neill, B. P., Foltz, G., Myers, J., Weisenberger, D. J., Penny, R., Kucherlapati, R., Perou, C. M., Hayes, D. N., Gibbs, R., Marra, M., Mills, G. B., Lander, E., Spellman, P., Wilson, R., Sander, C., Weinstein, J., Meyerson, M., Gabriel, S., Laird, P. W., Haussler, D., Getz, G., Chin, L. & Network, T. R. (2013) The Somatic Genomic Landscape of Glioblastoma, *Cell*. 155, 462-477.

20. Perego, P., Corna, E., De Cesare, M., Gatti, L., Polizzi, D., Pratesi, G., Supino, R. & Zunino, F. (2001) Role of apoptosis and apoptosis-related genes in cellular response and antitumor efficacy of anthracyclines, *Curr Med Chem*. 8, 31-7.

21. Yang, F., Kemp, C. J. & Henikoff, S. (2013) Doxorubicin Enhances Nucleosome Turnover around Promoters, *Curr Biol*. 23, 782-787.

22. Qiao, X., van der Zanden, S. Y., Wander, D. P. A., Borrás, D. M., Song, J. Y., Li, X., van Duikeren, S., van Gils, N., Rutten, A., van Herwaarden, T., van Tellingen, O., Giacomelli, E., Bellin, M., Orlova, V., Tertoolen, L. G. J., Gerhardt, S., Akkermans, J. J., Bakker, J. M., Zuur, C. L., Pang, B., Smits, A. M., Mummery, C. L., Smit, L., Arens, R., Li, J., Overkleeft, H. S. & Neefjes, J. (2020) Uncoupling DNA damage from chromatin damage to detoxify doxorubicin, *Proc Natl Acad Sci U S A*.

23. McGinty, R. K. & Tan, S. (2015) Nucleosome Structure and Function, *Chem Rev*. 115, 2255-2273.

24. Monroe, K. M., Yang, Z. Y., Johnson, J. R., Geng, X., Doitsh, G., Krogan, N. J. & Greene, W. C. (2014) IFI16 DNA Sensor Is Required for Death of Lymphoid CD4 T Cells Abortively Infected with HIV, *Science*. 343, 428-432.

25. Kerur, N., Veettil, M. V., Sharma-Walia, N., Bottero, V., Sadagopan, S., Otageri, P. & Chandran, B. (2011) IFI16 Acts as a Nuclear Pathogen Sensor to Induce the Inflammasome in Response to Kaposi Sarcoma-Associated Herpesvirus Infection, *Cell Host Microbe*. 9, 363-375.

26. Dell'Oste, V., Gatti, D., Gugliesi, F., De Andrea, M., Bawadekar, M., Lo Cigno, I., Biolatti, M., Vallino, M., Marschall, M., Gariglio, M. & Landolfo, S. (2014) Innate Nuclear Sensor IFI16 Translocates into the Cytoplasm during the Early Stage of In Vitro Human Cytomegalovirus Infection and Is Entrapped in the Egressing Virions during the Late Stage, *J Virol*. 88, 6970-6982.

27. Johnson, K. E., Bottero, V., Flaherty, S., Dutta, S., Singh, V. V. & Chandran, B. (2014) IFI16 Restricts HSV-1 Replication by Accumulating on the HSV-1 Genome, Repressing HSV-1 Gene Expression, and Directly or Indirectly Modulating Histone Modifications, *Plos Pathog.* 10.
28. Ran, Y., Zhang, J., Liu, L. L., Pan, Z. Y., Nie, Y., Zhang, H. Y. & Wang, Y. Y. (2016) Autoubiquitination of TRIM26 links TBK1 to NEMO in RLR-mediated innate antiviral immune response, *J Mol Cell Biol.* 8, 31-43.
29. Frost, J. R., Olanubi, O., Cheng, S. K. H., Soriano, A., Crisostomo, L., Lopez, A. & Pelka, P. (2017) The interaction of adenovirus E1A with the mammalian protein Ku70/XRCC6, *Virology.* 500, 11-21.
30. Johnstone, R. W., Wei, W., Greenway, A. & Trapani, J. A. (2000) Functional interaction between p53 and the interferon-inducible nucleoprotein IFI 16, *Oncogene.* 19, 6033-6042.
31. Kwak, J. C., Ongusaha, P. P., Ouchi, T. & Lee, S. W. (2003) IFI16 as a negative regulator in the regulation of p53 and p21(Waf1), *J Biol Chem.* 278, 40899-40904.
32. Sheng, Y., Saridakis, V., Sarkari, F., Duan, S. L., Wu, T. N., Arrowsmith, C. H. & Frappier, L. (2006) Molecular recognition of p53 and MDM2 by USP7/HAUSP, *Nat Struct Mol Biol.* 13, 285-291.
33. Landolfo, S., Gariglio, M., Gribaudo, G. & Lembo, D. (1998) The Ifi 200 genes: An emerging family of IFN-inducible genes, *Biochimie.* 80, 721-728.
34. Fujiuchi, N., Aglipay, J. A., Ohtsuka, T., Maehara, N., Sahin, F., Su, G. H., Lee, S. W. & Ouchi, T. (2004) Requirement of IFI16 for the maximal activation of p53 induced by ionizing radiation, *J Biol Chem.* 279, 20339-20344.
35. Sharma, P. & Allison, J. P. (2015) The future of immune checkpoint therapy, *Science.* 348, 56-61.
36. Ribas, A. & Wolchok, J. D. (2018) Cancer immunotherapy using checkpoint blockade, *Science.* 359, 1350-1355.
37. Koebel, C. M., Vermi, W., Swann, J. B., Zerafa, N., Rodig, S. J., Old, L. J., Smyth, M. J. & Schreiber, R. D. (2007) Adaptive immunity maintains occult cancer in an equilibrium state, *Nature.* 450, 903-7.





## LIST OF PUBLICATIONS

**Sabina Y. van der Zanden**<sup>#</sup>, Dennis P.A. Wander<sup>#</sup>, Merijn B.L. Vriends, Branca C. van Veen, Joey G. C. Vlaming, Thomas Bruyning, Gijsbert A. van der Marel, Jeroen D.C. Codee, Herman S. Overkleeft, Jacques Neefjes. Synthetic (*N,N*-dimethyl)doxorubicin glycosyl diastereomers to dissect modes of action of anthracycline anticancer drugs.

*Manuscript in preparation.*

Thomas P. Brouwer, **Sabina Y. van der Zanden**, Jaap D.H. van Eendenburg, Bert A. Bonsing, Noel F.C.C. de Miranda, Jacques Neefjes, Alexander L. Vehrmeijer. The identification of the anthracycline aclarubicin as an effective cytotoxic agent for pancreas cancer.

*Manuscript in preparation.*

Dennis P.A. Wander<sup>#</sup>, **Sabina Y. van der Zanden**<sup>#</sup>, Gijsbert A. van der Marel, Herman S. Overkleeft, Jacques Neefjes, Jeroen D.C. Codee. Doxorubicin and aclarubicin: shuffling anthracycline glycans for improved cytotoxic agents.

*Journal of Medicinal Chemistry*, DOI: 10.1021/acs.jmedchem.0c01191, (2020).

**Sabina Y. van der Zanden**<sup>#</sup>, Xiaohang Qiao<sup>#</sup> and Jacques Neefjes. New insights into the activities and toxicities of the old anticancer drugs doxorubicin.

*FEBS J.* DOI: 10.1111/febs.15583, (2020).

Xiaohang Qiao<sup>#</sup>, **Sabina Y. van der Zanden**<sup>#</sup>, Dennis P.A. Wander, Daniel M. Borràs, Ji-Ying Song, Xiaoyang Li, Suzanne van Duikeren, Noortje van Gils, Arjo Rutten, Tessa van Herwaarden, Olaf van Tellingen, Elisa Giacomelli, Milena Bellin, Valeria Orlova, Leon G.J. Tertoolen, Sophie Gerhardt, Jimmy J. Akkermans, Jeroen M. Bakker, Charlotte L. Zuur, Baoxu Pang, Anke M. Smits, Christine L. Mummery, Linda Smit, Ramon Arens, Junmin Li, Herman S. Overkleeft and Jacques Neefjes. Uncoupling DNA damage from chromatin damage to detoxify doxorubicin.

*Proceeding of the National Academy of Science*, 117 (26) 15182-15192, (2020).

**Sabina Y. van der Zanden**, Jolien J. Luimstra, Jacques Neefjes, Jannie Borst, Huib Ovaa. Opportunities for small molecules in cancer immunotherapy.

*Trends Immunol.* 41(6):493-511, (2020).

Elmer Maurits<sup>#</sup>, Michel J. van de Graaf<sup>#</sup>, Santina Maiorana, Dennis P.A. Wander, Patrick M. Dekker, **Sabina Y. van der Zanden**, Bogdan I. Florea, Jacques Neefjes, Herman S. Overkleeft, Sander I. van Kasteren. Immunoproteasome inhibitor-doxorubicin conjugates target multiple myeloma cells and release doxorubicin upon low-dose photon irradiation.

*Journal of the American Chemical Society* 142 (16), 7250-7253, (2020).

Marlieke L.M. Jongsma<sup>#</sup>, Jeroen Bakker<sup>#</sup>, Birol Cabukusta, Nalan Liv, Daphne van Elstrand, Job Fermie, Jimmy L.L. Akkermans, Coenraad Kuijl, **Sabina Y. van der Zanden**, Lennert Janssen, Denise Hoogzaad, Rik van der Kant, Ruud H. Wijdeven, Judith Klumperman, Ilana Berlin and Jacques Neefjes. SKIP-HOPS recruits TBC1D15 for a Rab7-to-Arl8b identity switch to control late endosome transport.

*EMBO Journal* 39: e102301, (2020).

Ruud H. Wijdeven<sup>#</sup>, Baoxu Pang<sup>#</sup>, **Sabina Y. van der Zanden**, Xiaohang Qiao, Vincent Blomen, Marlous Hoogstraat, Esther H. Lips, Lennert Janssen, Lodewyk Wesels, Thijn R. Brummelkamp and Jacques Neefjes. Genome-wide identification and characterization of novel factors conferring resistance to topoisomerase II poisons in cancer.

*Cancer Research* 75(19), 4176-4187, (2015).

<sup>#</sup> These authors contributed equally.

## **CURRICULUM VITAE**

Sabina Yasmin van der Zanden was born on October 15th 1989, in Haarlem. She finished her VWO in 2008, at the Rudolf Steiner School in Haarlem. Directly after graduation she started with her Bachelor studies in Biomedical Sciences at the VU university in Amsterdam, which she finished in 2011. During the gap year that followed she worked as a quality officer at Sanquin Amsterdam and went traveling through Latin-America for 5 months. Sabina then went on to continue her studies in September 2012 at the VU university in Amsterdam, with the Master Biomolecular sciences, where she followed both the Molecular Cell biology and Biological Chemistry specialization. In September 2014 she graduated Cum Laude. During her masters, Sabina performed two internships. Her first internship was in the Structural Biology group of prof. dr. Holger Lill at the VU University, where she worked on optogenetic manipulation of bacteria. For her second internship she went to The Netherlands Cancer Institute in Amsterdam, where she worked on a project about bi-directional transport of late endosomes in the Cell biology group of prof. dr. Jacques Neefjes. After finishing her master's degree, Sabina continued to work in the group of professor Neefjes as a PhD candidate, first at the NKI, and after the move in June 2016 at the Leiden University Medical center in Leiden. During her PhD she focused on the working mechanism of the anticancer drugs doxorubicin and its analogs. The results of this research can be found in this thesis.

## ACKNOWLEDGEMENTS

My PhD journey has come to an end. Since science without collaboration is impossible, I would like to thank all co-workers and collaborations for their support and contributed to the work described in this dissertation. But I owe most of my thanks to my doctoral advisor Jacques Neefjes, for the opportunity to work in such an inspiring environment.